CENTRAL LIBRARY
Birla Institute of Technology & Science
PILANI (Rajasthan)

Call No. 621.384/114
R 505R v.1

Accession No. 42093

MASSACHUSETTS INSTITUTE OF TECHNOLOGY
RADIATION LABORATORY SERIES

LOUIS N. RIDENOUR, *Editor-in-Chief*

CRYSTAL RECTIFIERS

MASSACHUSETTS INSTITUTE OF TECHNOLOGY

RADIATION LABORATORY SERIES

Board of Editors

LOUIS N. RIDENOUR, *Editor-in-Chief*

GEORGE B. COLLINS, *Deputy Editor-in-Chief*

BRITTON CHANCE, S. A. GOUDSMIT, R. G. HERB, HUBERT M. JAMES, JULIAN K. KN
JAMES L. LAWSON, LEON B. LINFORD, CAROL G. MONTGOMERY, C. NEWTON, ALB
M STONE, LOUIS A. TURNER, GEORGE E. VALLEY, JR., HERBERT H. WHEA

---

1. RADAR SYSTEM ENGINEERING—*Ridenour*
2. RADAR AIDS TO NAVIGATION—*Hall*
3. RADAR BEACONS—*Roberts*
4. LORAN—*Pierce, McKenzie, and Woodward*
5. PULSE GENERATORS—*Glasoe and Lebacqz*
6. MICROWAVE MAGNETRONS—*Collins*
7. KLYSTRONS AND MICROWAVE TRIODES—*Hamilton, Knipp, and Kuper*
8. PRINCIPLES OF MICROWAVE CIRCUITS—*Montgomery, Dicke, and Purcell*
9. MICROWAVE TRANSMISSION CIRCUITS—*Ragan*
10. WAVEGUIDE HANDBOOK—*Marcuvitz*
11. TECHNIQUE OF MICROWAVE MEASUREMENTS—*Montgomery*
12. MICROWAVE ANTENNA THEORY AND DESIGN—*Silver*
13. PROPAGATION OF SHORT RADIO WAVES—*Kerr*
14. MICROWAVE DUPLEXERS—*Smullin and Montgomery*
15. CRYSTAL RECTIFIERS—*Torrey and Whitmer*
16. MICROWAVE MIXERS—*Pound*
17. COMPONENTS HANDBOOK—*Blackburn*
18. VACUUM TUBE AMPLIFIERS—*Valley and Wallman*
19. WAVEFORMS—*Chance, Hughes, MacNichol, Sayre, and Williams*
20. ELECTRONIC TIME MEASUREMENTS—*Chance, Hulsizer, MacNichol, and Williams*
21. ELECTRONIC INSTRUMENTS—*Greenwood, Holdam, and MacRae*
22. CATHODE RAY TUBE DISPLAYS—*Soller, Starr, and Valley*
23. MICROWAVE RECEIVERS—*Van Voorhis*
24. THRESHOLD SIGNALS—*Lawson and Uhlenbeck*
25. THEORY OF SERVOMECHANISMS—*James, Nichols, and Phillips*
26. RADAR SCANNERS AND RADOMES—*Cady, Karelitz, and Turner*
27. COMPUTING MECHANISMS AND LINKAGES—*Svoboda*
28. INDEX—*Linford*

CRYSTAL RECTIFIERS

By HENRY C. TORREY
ASSOCIATE PROFESSOR OF PHYSICS
RUTGERS UNIVERSITY

And CHARLES A. WHITMER
ASSOCIATE PROFESSOR OF PHYSICS
RUTGERS UNIVERSITY

EDITED BY

S. A. GOUDSMIT LEON B. LINFORD
JAMES L. LAWSON ALBERT M. STONE

OFFICE OF SCIENTIFIC RESEARCH AND DEVELOPMENT

NATIONAL DEFENSE RESEARCH COMMITTEE

FIRST EDITION
THIRD IMPRESSION

NEW YORK AND LONDON
McGRAW-HILL BOOK COMPANY, INC.
1948

CRYSTAL RECTIFIERS

COPYRIGHT, 1948, BY THE
McGRAW-HILL BOOK COMPANY, INC
PRINTED IN THE UNITED STATES OF AMERICA

All rights reserved This book, or parts thereof, may not be reproduced in any form without permission of the publishers

THE MAPLE PRESS COMPANY, YORK, PA.

Foreword

THE tremendous research and development effort that went into the development of radar and related techniques during World War II resulted not only in hundreds of radar sets for military (and some for possible peacetime) use but also in a great body of information and new techniques in the electronics and high-frequency fields. Because this basic material may be of great value to science and engineering, it seemed most important to publish it as soon as security permitted.

The Radiation Laboratory of MIT, which operated under the supervision of the National Defense Research Committee, undertook the great task of preparing these volumes. The work described herein, however, is the collective result of work done at many laboratories, Army, Navy, university, and industrial, both in this country and in England, Canada, and other Dominions.

The Radiation Laboratory, once its proposals were approved and finances provided by the Office of Scientific Research and Development, chose Louis N. Ridenour as Editor-in-Chief to lead and direct the entire project. An editorial staff was then selected of those best qualified for this type of task. Finally the authors for the various volumes or chapters or sections were chosen from among those experts who were intimately familiar with the various fields, and who were able and willing to write the summaries of them. This entire staff agreed to remain at work at MIT for six months or more after the work of the Radiation Laboratory was complete. These volumes stand as a monument to this group.

These volumes serve as a memorial to the unnamed hundreds and thousands of other scientists, engineers, and others who actually carried on the research, development, and engineering work the results of which are herein described. There were so many involved in this work and they worked so closely together even though often in widely separated laboratories that it is impossible to name or even to know those who contributed to a particular idea or development. Only certain ones who wrote reports or articles have even been mentioned. But to all those who contributed in any way to this great cooperative development enterprise, both in this country and in England, these volumes are dedicated.

L. A. DUBRIDGE.

Preface

WITH the development of microwave radar, the crystal rectifier, which had been little used since the invention of the vacuum tube several decades ago, again became important—as important as the magnetron, klystron, or other microwave components.

In the past five years crystal rectifiers have been manufactured, literally by the millions, for use primarily as microwave detectors. A correspondingly large amount of fundamental research and engineering development has taken place in the commercial and governmental laboratories in the United States and in England. As a result the crystal-rectifier unit that has emerged is a compact, stable device which is superior in many applications to the vacuum-tube diode. Its most extensive use up to now has been as a frequency converter in microwave reception, where its performance has not been equaled. It has also been used to a lesser extent as a low-level microwave detector.

The recent development of germanium rectifiers capable of withstanding relatively high inverse voltages holds great promise for applications as second detectors in wideband receivers and in a variety of other circuits where vacuum-tube diodes are ordinarily used.

The purpose of this book is to present the fund of knowledge on crystal rectifiers that has accumulated during the course of World War II. Because of the need in radar systems for high-quality microwave converters, a large fraction of the work was expended for the development of crystal rectifiers for this application. A correspondingly large fraction of the book has, therefore, been devoted to the theory and properties of the crystal converter. Other applications are discussed in Part III as Special Types.

As in every other branch of microwave work, the development of measuring equipment and techniques has taken place simultaneously with that of the crystal rectifier itself. We have, therefore, included detailed discussions of methods of measurement of crystal properties and a description of standard test equipment for production and routine testing.

The techniques for manufacturing converter crystals are discussed in Chap. 10. Special techniques required for the manufacture of other types are described in the appropriate chapters. The procedures presented in detail are drawn largely from the work done at the MIT

Radiation Laboratory and by NDRC contractees, but no attempt has been made to include the details of all of the procedures that have been successfully employed.

Because of the unique nature of war research and development, it is impossible to acknowledge adequately individual contributions to this subject. Much of the work is a result of the joint efforts of many individuals. At the present writing most of the available literature is in the form of reports that, for reasons of security, have not yet been published in scientific journals. Much of the literature referred to will undoubtedly appear later, however, in journal articles, or will be declassified and made available by the United States government. We have therefore given references to some of the more important of these documents.

In England the chief contributors to crystal research and development were the General Electric Company, British Thompson-Houston, Ltd., Telecommunications Research Establishment, and Oxford University; in this country they were the Bell Telephone Laboratories, Westinghouse Research Laboratory, General Electric Company, Sylvania Electric Products, Inc., and E. I. duPont de Nemours and Company. The crystal groups at the University of Pennsylvania and Purdue University, who operated under NDRC contracts, were responsible for much of the fundamental research and development work reported herein.

DuPont and the Eagle-Picher Company developed manufacturing processes and produced in quantity highly purified silicon and germanium oxide, respectively, without which much of the improvement in crystal rectifiers would have been impossible.

We are particularly indebted to our colleagues at the Radiation Laboratory whose contributions and stimulating discussions have been invaluable in writing this book.

The preparation of this manuscript would have been impossible, finally, without the splendid aid of the editorial staff. In addition to those names listed as editors, we wish particularly to emphasize our gratitude to Barbara E. Myers, Marjorie S. Tariot, and Natalie C. Tucker, editorial assistants.

The publishers have agreed that ten years after the date on which each volume in this series is issued, the copyright thereon shall be relinquished, and the work shall become part of the public domain.

HENRY C. TORREY.
CHARLES A. WHITMER.

CAMBRIDGE, MASS.
June, 1946.

Contents

FOREWORD BY L. A. DUBRIDGE v

PREFACE vii

CHAP. 1. INTRODUCTION 1

THE PHENOMENON OF RECTIFICATION 1

1·1. The Nonlinear Element 1
1·2. Detection 2
1·3. Frequency Conversion 4

THE NATURE OF THE CRYSTAL RECTIFIER 5

1·4. The Discovery and Early Use of Crystal Rectifiers 5
1·5. Recent Developments 6

PART I. GENERAL PROPERTIES

CHAP. 2. FUNDAMENTAL PROPERTIES OF THE CRYSTAL RECTIFIER 15

THE PRESENT CRYSTAL CARTRIDGES 15

2·1. Description of the Cartridge 15
2·2. Stability and Handling Precautions 18

ELECTRICAL PROPERTIES 20

2·3. The Voltage-current Characteristic 20
2·4. The Equivalent Circuit 23

MIXER CRYSTALS 25

2·5. Conversion Loss, Noise, and Noise Figure 25
2·6. Optimum Local-oscillator Level 33
2·7. The R-f Impedance of Crystal Rectifiers 35
2·8. The I-f Impedance of Crystal Rectifiers 40

CHAP. 3. PROPERTIES OF SEMICONDUCTORS 45

3·1. Band Theory 45
3·2. Electron Distribution in Semiconductors 48
3·3. Work Functions and Contact Potentials 51
3·4. Electrical Conductivity and Hall Coefficient for Semiconductors 53
3·5. Characteristic Constants of Silicon and Germanium 61
3·6. Effect of Impurity Additions in Silicon and Germanium 64

CHAP. 4. THE SEMICONDUCTOR—METAL CONTACT 68

4·1. Barrier-layer Rectification 68
4·2. Formation and Structure of the Barrier Layer 70
4·3. Diffusion and Diode Theories of Rectification 77
4·4. The D-c Characteristic 82
4·5. Depletion Layers 90
4·6. Rectification at High Frequencies 97

PART II. THE CRYSTAL CONVERTER

CHAP. 5. FREQUENCY CONVERSION 111

5·1. Discussion of the General Problem 111
5·2. The Admittance Matrix 114

THE PHENOMENOLOGICAL THEORY OF CONVERSION 119

5·3. The Admittance Matrix in Terms of Measurable Parameters . . 119
5·4. Transformation of the Matrix to New Variables 121
5·5. Reciprocity 124

CONVERSION LOSS AND MIXER ADMITTANCES 128

5·6. General Definition of Loss; Special Cases 128
5·7. Conversion Loss in the Broadband Case 130
5·8. General Expression for Conversion Loss 136
5·9. Effect of the Image Termination on Conversion Loss 140
5·10. Effect of Image Termination on I-f Impedance 148

THE PHYSICAL THEORY OF CONVERSION 152

5·11. Matrix of a Nonlinear Resistance 153
5·12. Effect of Parasitic Impedances on Conversion Loss 157
5·13. Effect of a Variable Barrier Capacitance 163
5·14. Harmonic Reinforcement 167
5·15. Conversion with a Subharmonic Local Oscillator 170
5·16. Harmonic Generation 173
5·17. Modulation 174

CHAP. 6. NOISE GENERATION 179

THEORY 179

6·1. Shot and Thermal Noise in Crystal Rectifiers 179
6·2. Other Sources of Noise 186

INTERMEDIATE-FREQUENCY AND VIDEO NOISE 187

6·3. Dependence of Noise Temperature on Frequency 188
6·4. Dependence on Temperature 194

MICROWAVE NOISE 195

6·5. The Crystal as a Microwave Noise Generator 195

CHAP. 7. LOSS AND NOISE MEASUREMENTS 198

LOSS MEASUREMENTS 198

7·1. General Considerations 198

7·2. The Heterodyne Method 200
7·3. Impedance Methods 202
7·4. The Incremental and Amplitude-modulation Methods 213

NOISE-TEMPERATURE MEASUREMENTS 218

7·5. General Considerations 218
7·6. The Roberts Coupling Circuit 223
7·7. Narrow-band Coupling Circuit 225
7·8. Use of the Noise Diode in Noise-temperature Measurements . . . 226

MEASUREMENT OF LOSS, NOISE, AND RECEIVER NOISE FIGURE 227

7·9. The Measurement of Receiver Noise Figure 227
7·10. The Measurement of Mixer-crystal Properties 230
7·11. Loss and Noise Temperature as a Function of R-f Tuning 232

CHAP. 8. BURNOUT 236

8·1. General Considerations 236
8·2. Burnout Theory 239
8·3. Burnout Theory 248
8·4. Experiments on Burnout 256
8·5. Burnout Limitations of Standard Crystal Units 260

CHAP. 9. TEST EQUIPMENT 264

STANDARD LOSS TEST SETS 264

9·1. The Conversion-loss Set for the 3-cm Band 265
9·2. The Conversion-loss Set for the 10-cm Band 272
9·3. The Conversion-loss Set for the 1-cm Band 276
9·4. The Mechanical Modulator 280

STANDARD NOISE TEST SETS 283

9·5. The Noise Measuring Set for the 3-cm Band 283
9·6. The Noise Measuring Set for the 10-cm Band 289
9·7. Noise-temperature Measurement of 1-cm Rectifiers 292

BURNOUT 293

9·8. Spike Test 293
9·9. Microsecond Pulse Test 296

FIELD TESTING 297

9·10. D-c Tests 297

CHAP. 10. MANUFACTURING TECHNIQUES 301

PREPARATION OF SEMICONDUCTOR 301

10·1. Purification of the Semiconductor 301
10·2. Addition Agents 306
10·3. Preparation of the Ingot 308
10·4. Polishing, Heat-treatment, and Etching 314

THE CAT WHISKER 316

10·5. Whisker Materials 316
10·6. Fabrication of the Whisker 318

ASSEMBLY AND ADJUSTMENT OF THE CARTRIDGE 323

10·7. The Ceramic Cartridge 323
10·8. The Coaxial Cartridge 326

SOME DESIGN CONSIDERATIONS AFFECTING ELECTRICAL PERFORMANCE . . 328

10·9. R-f Impedance 328
10·10. Conversion Loss and Burnout 329

PART III. SPECIAL TYPES

CHAP. 11. LOW-LEVEL DETECTION 333

PROPERTIES OF CRYSTAL RECTIFIERS AT LOW LEVELS 333

11·1. Rectification at Low Levels 333
11·2. Equivalent-circuit Theory 335
11·3. Effect of Bias on Low-level Properties 340
11·4. Variation of Low-level Properties with Temperature 342

THEORY OF LOW-LEVEL DETECTION 344

11·5. The Figure of Merit of a Video Crystal 344
11·6. Effect of D-c Bias on Figure of Merit 347
11·7. The Effect of Temperature Variation on Crystal-video Receiver Performance . . . . . 34[illegible]

MEASUREMENTS . . . . . [illegible]

11·8. R-f Equipment and Measurements . . . . . 3[illegible]
11·9. Equipment and Methods for Measuring Current Sensitivity, Video Resistance, and Figure of Merit 355

SPECIAL MANUFACTURING TECHNIQUES 357

11·10. Stability Considerations 358
11·11. Processing the Silicon 358
11·12. Fabrication of the Whisker 359
11·13. Adjustment of the Rectifying Contact 359

CHAP. 12. HIGH-INVERSE-VOLTAGE RECTIFIERS 361

THE HIGH-INVERSE-VOLTAGE RECTIFIER AND ITS APPLICATIONS 361

12·1. Preparation of the Ingot 364
12·2. Etching and Surface Treatment 369
12·3. Assembly and Adjustment of the Cartridge 369
12·4. Low-frequency Properties 372
12·5. High-frequency Properties 378
12·6. Silicon High-inverse-voltage Rectifiers 389
12·7. Theory of the Negative-resistance Characteristics 391
12·8. Photoelectric Effects in Silicon and Germanium 392

CHAP. 13. WELDED-CONTACT GERMANIUM CRYSTALS 398

13·1. Construction of Welded-contact Rectifiers 398
13·2. General Properties 400
13·3. Negative I-f Conductance 401
13·4. Loss and Noise Measurements 403
13·5. Theory of Negative I-f Conductance and Conversion Amplification 406
13·6. Applications 415

APPENDIX A The Reciprocity Theorem of Dicke 417

APPENDIX B Skin Effect at a Metal-semiconductor Contact 421

APPENDIX C Spreading Resistance of an Elliptical Contact 427

APPENDIX D Crystal-rectifier Types and Specifications 429

INDEX 435

CHAPTER 1

INTRODUCTION

THE PHENOMENON OF RECTIFICATION

The process of rectification and its applications are well known and extensively treated in the literature. However, within the last five years a wealth of new information on the crystal rectifier has accumulated as a result of its superior performance in microwave receivers. In fact, the use of crystal rectifiers for frequency conversion occurred for the first time during World War II. The purpose of this book is to give an account of the present state of our knowledge of the crystal rectifier and its applications. The applications with which we are chiefly concerned have to do with the use of the rectifier as a nonlinear device in the detection and frequency conversion of r-f signals. As a background for the analysis of the crystal rectifier we shall begin with a brief review of the process of detection and frequency conversion.

1·1. The Nonlinear Element.—Rectification may be defined as an operation on an a-c voltage to produce a unidirectional component. The vacuum-tube diode is a familiar example of a device that performs this function. The unidirectional component arises from the fact that the average resistance to current flow is less in one direction than in the other. In addition to the d-c component in the rectifier output there are also present harmonics of the input signal which arise because of the nonlinear character of the rectifying element. The relative amplitudes of the harmonics depend on the shape of the current-voltage characteristic curve in the operating region. The magnitude of the d-c component also depends on the shape of the characteristic. For example, it is clear that a nonlinear element having the characteristic curve of Fig. 1·1*a*, which is an odd function of the voltage about the origin, will have no output d-c component at all when operated at zero bias. However, if a d-c bias voltage is applied so that the operating point is at A, the application of a small a-c signal will result in a net increase in the direct current over that produced by the bias alone. This occurs because the average current will be greater for the positive swings of the a-c signal than for the negative ones.

Rectifiers that are useful for detection purposes have characteristics similar to that shown in Fig. 1·1*b*. The shape of the characteristic will of course depend on the physical nature of the rectifier. In general, the

important features are a high back resistance and a relatively low forward resistance. At high frequencies other physical characteristics, such as capacitance of the rectifying element, transit time, etc., are important factors. In the vacuum-tube diode, for example, the resistance in the back direction is very high. In the forward direction the current is proportional to the three-halves power of the applied voltage when the voltages are small. For larger voltages there is a region that is approximately linear. As we shall see later, the shape of the crystal-rectifier characteristic may vary widely depending on the nature of the crystal and the way in which it is constructed. We shall postpone the discussion of the crystal-rectifier characteristic and the consideration of the other properties that are of importance in the microwave region.

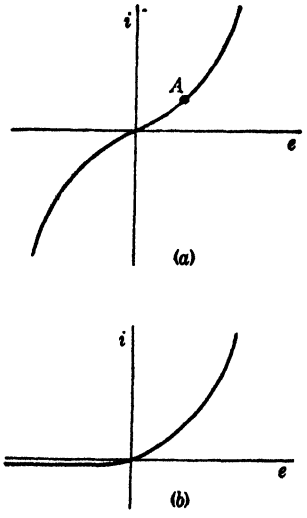

FIG. 1·1.—Nonlinear elements. (a) Nonrectifying element at zero bias; (b) rectifying element.

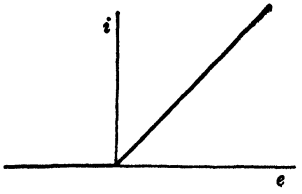

FIG. 1·2.—Ideal rectifier characteristic.

1·2. Detection.—In the use of the rectifier for detection there are two classifications that are of particular interest to us: (1) linear and (2) square-law detection.

Linear Detection.—In linear detection, the rectifier functions essentially as a switch. Let us assume that the rectifier characteristic is ideal—that is, that the resistance in the back direction is infinite, and in the forward direction is small and constant (see Fig. 1·2). It is well known that when a sinusoidal wave is impressed on the ideal rectifier the average current through this rectifier will be proportional to the amplitude of the input wave. The voltage across the rectifier load resistance will then be composed of a d-c component proportional to the amplitude of the input signal plus components of the input frequency and its even harmonics.

Most rectifiers will approximate this ideal performance if the input signal is large enough to make the region of curvature near the origin small compared with the substantially straight part of the characteristic over which the voltage varies. Furthermore, the load resistance is usu-

ally chosen large compared with the rectifier resistance so that the effect on the output voltage of variation of the forward resistance of the rectifier is small.

The efficiency of rectification is defined as the ratio of the d-c voltage across the output load resistance to the peak amplitude of the input signal. It depends on the ratio of load resistance to the internal resistance of the rectifier and the amplitude of the input signal as noted above.

In the detection of amplitude-modulated waves in radio reception a load consisting of a parallel RC combination is commonly used. With proper choice of the values of R and C the output voltage will, to a very close approximation, vary like the envelope of the amplitude-modulated wave. Under these conditions, the rectification efficiency of vacuum-tube diode rectifiers is normally about 70 to 90 per cent. A detailed analysis of linear detectors used in radio receivers may be found in standard textbooks on radio engineering[1] and will not be given here. We will return to a discussion of the use of one of the crystal rectifier types as a linear detector in Chap. 12.

Square-law Detection.—The term *square-law* is applied to a detector in which the d-c, or rectified, output is proportional to the square of the amplitude of the input signal. It can readily be seen that such a response depends on the nonlinearity of the characteristic at the operating point. Over a limited range the current-voltage characteristic of a rectifier can be represented by a Taylor expansion terminating in the squared term

$$i = f(e) = f(e_0) + \frac{df}{de}\,\delta e + \frac{1}{2}\frac{d^2f}{de^2}\,(\delta e)^2, \tag{1}$$

where e_0 is the bias voltage determining the operating point, and δe is the small input signal voltage. The derivatives are evaluated at the operating point e_0. Any rectifier will, therefore, function as a square-law rectifier when the applied signal is sufficiently small, provided that the second derivative of the characteristic does not vanish at the operating point. The linear term is, of course, of no importance as far as rectification is concerned, since it is symmetrical about the operating point.

By means of Eq. (1) we can determine analytically the output of the rectifier for a given input signal. The analysis can be summarized briefly as follows. Let us consider a signal consisting of a single sinusoidal wave, $E \sin \omega t$. In addition to the frequency of the signal, the output will contain d-c and second-harmonic components with amplitudes proportional to E^2. In general, if the signal is composed of a number of sinusoidal components the output will contain, in addition to the frequency components of the signal, the d-c component, second harmonics of each

[1] For example see F. E. Terman, *Radio Engineer's Handbook*, McGraw-Hill, New York, 1943.

frequency component, and sum and difference frequencies formed by every possible combination of frequencies contained in the input signal. The amplitude of the d-c component will be proportional to the sum of the squares of the amplitudes of the signal components. The amplitude of each second-harmonic component will be proportional to the square of the amplitude of the corresponding signal component; the amplitude of the sum and difference frequencies will be proportional to the product of the amplitude of the input components involved in the combination.

As an example, let us consider the square-law detection of an amplitude-modulated wave given by the expression

$$e = E_0(1 + m \sin \beta t) \sin \omega t.$$

For purposes of analysis this wave may be represented by three frequency components, the carrier and two sidebands, with angular frequencies ω, $(\omega - \beta)$, and $(\omega + \beta)$, respectively. These are represented graphically in Fig. 1·3*a*. The relative amplitudes of the additional components in the output of the detector are shown in Fig. 1·3*b* for the case where $m = 0.5$.

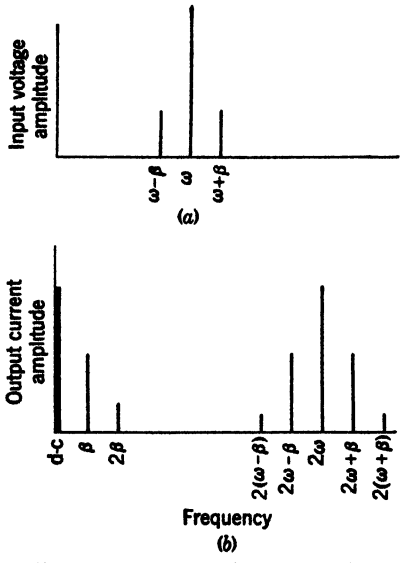

FIG. 1·3.—Frequencies involved in detection. (*a*) Frequencies in detector input (modulation percentage = 50); (*b*) additional frequencies in the detector output.

The square-law detector is a useful device for the measurement of the power of an a-c signal because the rectified output is proportional to the square of the input amplitude. As we shall see later, the crystal rectifier is often employed as a square-law detector in monitoring microwave power. In fact, such a device is serviceable outside the square-law region provided it is calibrated.

It is clear that the magnitude of the various components arising from the square term of Eq. (1) will be proportional to the magnitude of the second derivative of the characteristic at the operating point. Maximum sensitivity will then be obtained by adjusting the d-c bias so that the operating point is also the point of maximum curvature on the characteristic. Other factors of importance in the microwave region, such as capacitance, noise generation, etc., will be discussed in Chap. 11.

1·3. Frequency Conversion.—Heterodyne reception provides a means of converting the carrier frequency of a signal to a new value. This is

accomplished by means of a local oscillator and a nonlinear element. The local oscillator output and the signal are coupled into the nonlinear device, where they generate—among other frequencies—a frequency equal to the difference between the signal and local-oscillator frequencies. Usually, although not always, the local-oscillator power level is large compared with the signal level. The local oscillation may have either a lower or higher frequency than the signal since it is the difference frequency which is usually of interest. Under these conditions the nonlinear element in so far as it functions in the linear region, generates a difference frequency called the intermediate frequency, the amplitude of which is proportional to the signal amplitude and independent of the amplitude of the local-oscillator voltage.

The device that contains the nonlinear element and the means for coupling it to the terminals of the local oscillator and to the input and output terminals is called a *mixer*. The input terminals are used for application of signal power and the output terminals are used for delivery of power at the intermediate frequency. The unit consisting of mixer and local oscillator is called a "frequency converter," and the whole process is referred to as "mixing" or "frequency conversion."

If the signal is an amplitude-modulated wave, the mixer output will consist of a carrier at intermediate frequency plus sidebands which reproduce the original modulation of the signal. In addition, the nonlinear element in the mixer will generate harmonics of the local oscillator and the signal frequencies, sum and difference frequencies of all the applied signals, and these in turn will beat with each other to create still more frequencies and so on, ad infinitum. Fortunately most of these frequencies are so weak that they can be ignored. However, some of them are of importance since their existence results in the diversion of power that otherwise would appear in the i-f signal. An evaluation of the importance of these components in microwave receivers will be given in Chap. 5.

The nonlinear device used in frequency conversion may be any type of detector or demodulator. In radio reception, mixer or frequency-converter tubes have been especially designed for the purpose. In the heterodyne reception of microwave signals the crystal converter is almost universally used at the present time.

THE NATURE OF THE CRYSTAL RECTIFIER

1·4. The Discovery and Early Use of Crystal Rectifiers.—In the early days of the development of radio communication the crystal rectifier was almost universally used as the detector in radio receivers. A typical detector was made by soldering or clamping a small piece of the crystal in a small cup or receptacle. The rectifying contact was made with a

flexible wire cat whisker which was held in light contact with the crystal. Good rectification was obtained only from "sensitive" spots on the crystal and frequent adjustments of the contact point were necessary for good performance.

The development of thermionic tubes made the crystal rectifier obsolete in radio receivers. From about 1925 to 1940 the crystal rectifier was used chiefly as a laboratory device for detecting and monitoring uhf power. A combination of a silicon crystal and a whisker of tungsten or molybdenum was found to be among the most sensitive and was commonly used for this work.

A typical application of the crystal rectifier in early microwave work is described by Southworth and King.[1] A calibrated crystal rectifier was used by them to measure relative gains in an investigation of metal horns for directive receivers of microwaves in the region of 10 to 15 cm. The rectifier was made with a silicon crystal and a whisker of 8-mil tungsten 2 mm long. The crystal was ground into a cylinder 1 mm in diameter and 1 mm long and pressed into a hole bored into the end of a screw. The surface of the crystal was carefully polished so that the contact could slide freely over the surface in seeking a sensitive point. The rectifying contact was adjusted by advancing the mounting screw and tapping the mount until the ratio of back-to-front resistance was in the range of 2 to 5. It was found that with moderate care an adjustment could be maintained fairly constant for several weeks. The d-c output current of the crystal was used as a measure of the absorbed r-f power.

1·5. Recent Developments.—Reception of microwave radar echoes requires a high-gain receiver in which the limit of sensitivity is determined by the masking of the signal by the noise generated in the receiver circuits. The receiver must therefore be designed to introduce a minimum of noise into the input circuit.

One approach to the receiver design problem is to employ low-level detection of the r-f signal pulse, followed by amplification of the resultant video pulse. Because of its relative insensitivity as compared to superheterodyne reception, this method has been used only for beacon receivers where sensitivity is not of prime importance.

Another possible approach is the amplification of the received signal at microwave frequencies. For this purpose amplifier tubes[2] have been designed and constructed at the Radiation Laboratory for amplification at a frequency of 3000 Mc/sec. The best of these are comparable in performance to superheterodyne receivers using crystal mixers. However these tubes are difficult to make and have not been manufactured on

[1] G. C. Southworth and A. P. King, "Metal Horns as Directive Receivers of Ultra-Short Waves," *Proc. I.R.E.*, **27**, 95 (1939).

[2] H. V. Neher, RL Report No. 61-24, July 10, 1943.

a mass-production scale. It is unlikely that an r-f amplifier can compete with crystals at higher frequencies.

The Development of the Mixer Crystal.—The early microwave receivers[1] used mixer tubes especially designed for high-frequency applications, such as the Westinghouse 708A and the British CV58 diode. However, the best of these were noisy, and the noise output increased with frequency. Consequently attention was turned to the crystal rectifier as a possible substitute.

The superior performance of the crystal mixer led to further research and development work, which has continued to this time. The broad general objectives of this work may be put into three general categories, which obviously are mutually dependent:

1. The development of manufacturing techniques for quantity production of high-quality rectifiers for use in the region from 3,000 to 30,000 Mc/sec.
2. Fundamental research on semiconductors, point-contact[2] rectification, and the theory of frequency conversion and noise generation at microwave frequencies.
3. The development of methods and equipment for measuring performance and for laboratory and production testing.

The extent to which these objectives have been achieved will be indicated in the appropriate following chapters. Discussion here will be limited to outlining the salient features of current manufacturing techniques which have produced the crystal rectifier in present use.

The research work has been concerned exclusively with silicon, germanium, or boron, but all of the cartridges manufactured commercially for mixers have used silicon crystals. Extensive research on germanium has resulted, however, in the development of the high-inverse-voltage rectifier and the welded-contact rectifier mentioned later.

Investigation into the possibility of preparing sintered or melted pellets of boron for use as crystal rectifiers begun in 1943, was successful; pellets of pure boron were prepared as well as pellets to which were added selected impurities in varying amounts. Some of the "doped" pellets showed sufficient conductivity to be of interest but exhibited no true rectification. A typical characteristic curve is S-shaped and symmetrical

[1] Crystal mixers were used in some early experimental sets. The crystal and cat whisker were independently mounted in the mixer and the contact was adjustable.

[2] It should be pointed out here that the copper oxide rectifier and selenium rectifier, both developed commercially, are not *point*-contact rectifiers. They are, however, contact rectifiers since the rectifying property is obtained by the contact of a thin film of semiconductor with the metal on which it is deposited. We shall be concerned in this book only with the point-contact rectifier.

about the origin. All of the pellets were poor rectifiers and the project was dropped.

The first mixer crystals made by British Thompson-Houston, Ltd. used commercial silicon of about 98 per cent purity. These crystals exhibited the usual sensitive spots, and exhibited considerable variation in sensitivity from lot to lot.

Crystals of commercial silicon were used in the early rectifiers made at the Radiation Laboratory, and the performance of these units in mixers was comparable to that of the BTH unit.

Much of the research was aimed at perfecting a design of cartridge parts and procedures for assembly and adjustment that would achieve electrical and mechanical stability, uniformity of r-f and i-f impedances, improved sensitivity, and decreased noise output. In general it may be said, however, that the crystals produced at this stage of development left much to be desired; it was common practice then, as a first step in improving performance of radar systems, to replace the crystal rectifier with a new one.

Another important advance in the development was high-burnout crystals of which the British "red-dot" (so-called because of the cartridge identification marking) crystal developed by the General Electric Company, Ltd. was an example. This early high-burnout crystal dissipated relatively large amounts of power without appreciably impairing its performance as a mixer. The most significant feature of its manufacture was the preparation of the silicon crystals. These were obtained from melts made of highly purified silicon powder to which was added a fraction of a per cent of aluminum and beryllium. The crystal surface was then prepared by a carefully controlled process of polishing, etching, and heat treatment.

Now it was already well known from the theory of semiconduction that the conductivity and hence the rectifying properties of silicon are affected by the presence of small amounts of impurities in the crystals. This fact, together with the success of the red-dot procedure stimulated the initiation of research along similar lines at various laboratories. At these laboratories adequate manufacturing procedures were then developed for large-scale production of high-burnout, high-sensitivity rectifiers. These units have a mechanical stability comparable to vacuum tubes, and, under proper operating conditions, a comparable life.

Two important advances in the art will be mentioned here. The first of these was suggested by Seitz[1], who initiated a program in connection with the Experimental Station of E. I. du Pont de Nemours and Company for the development of a method for the production of high-purity

[1] F. Seitz, "Compounds of Silicon and Germanium," NDRC 14-112, U. of Penn., June 1942.

silicon. They succeeded in producing silicon with a spectroscopic purity of better than 99.9 per cent. Other impurities not detectable by spectroscopic analysis, however, such as carbon, were present in larger amounts. Ingots made with this silicon to which is added an appropriate impurity are remarkably uniform in conductivity and rectifying property. Rectifiers using this silicon were high-burnout, low-noise units markedly superior[1] in performance to units made using the same techniques, but made with commercial silicon from other sources.

The second important advance was the discovery that boron was an unusually effective impurity agent in increasing the conductivity of high-purity silicon. In 1943 it was reported[2] that the addition of boron in quantities of the order of 0.001 per cent resulted in a converter of improved sensitivity compared with those utilizing other impurity agents. This crystal was also highly resistant to burnout. As a result, "boron-doping" is now widely used in silicon-crystal manufacture.

A considerable amount of exploratory work has been done on the effect of various impurity agents, but there has as yet been no exhaustive systematic doping program for silicon. Moreover it is not yet understood why certain impurity agents are better than others in improving burnout and sensitivity, nor is the process of noise generation in crystal fully understood. Finally the etching, polishing, and heat treatment of the rectifying surface have been largely empirical developments. The net effect is that the manufacture of high-quality crystals is still something of an art, attained through long experience and careful control of the techniques.

The Development of Special Types.—The term "special types" refers to crystal rectifiers developed for applications other than frequency conversion. They are "special" only in the sense that the principal interest and effort to date have been on the converter application. Among these special types there are three on which considerable work has been done: the *video crystal* for low-level detection, the *high-inverse-voltage rectifier*, and the *welded-contact rectifier*.

The term *video crystal* commonly means a crystal rectifier that is used as a low-level square-law detector of microwave pulses. The video output voltage of the detector is amplified by a video amplifier. Such a receiver is commonly called a *crystal-video receiver*.

The crystal-video receiver was developed somewhat later than the superheterodyne receiver to meet the need for a wideband beacon receiver that would respond to pulses over the range of frequencies encountered

[1] This statement does not apply to units made using the technique developed at the Bell Telephone Laboratories.

[2] H. C. Theuerer, "The Preparation and Rectification Characteristics of Boro-silicon Alloys," BTL Report MM-43-120-74, Nov. 2, 1943.

in interrogating transmitters. The sensitivity of the crystal-video receiver is low compared with that of a superheterodyne receiver, but this is not prohibitive in the beacon application since the signal level for one-way transmission is high compared with the level of echoes at a comparable range. Wideband superheterodyne receivers have been designed for beacon reception and have been used in some beacon sets. However, such receivers are difficult to adjust and are not so light and compact as crystal-video receivers—considerations which are of importance in portable beacons. The crystal-video receiver has therefore found extensive use.

The requirements of the video receiver place limits in particular on the video resistance of the detector. (See Vol. 3.) Video crystals for the first beacon receivers were selected from the mixer crystal production, for not all good mixer crystals are good video crystals. It was soon found that special procedures were essential to produce good video detectors for use in the 3-cm region. These special procedures involved special surface treatment and adjustment for a very small contact area. Since the latter required a small contact force mechanical stability has been difficult to attain. A cartridge of the coaxial type described in the next chapter, is somewhat more stable mechanically than a cartridge of the ceramic type.

In addition to its use as a low-level detector in the crystal-video receiver, the crystal rectifier has also been used extensively in probes and monitors of microwave power. Special types, however, have not been developed for this purpose. Within the range of square-law response the rectified output current of the crystal rectifier may be used directly as a relative power indication. Since, however, the range of square-law response is limited to a few microwatts of r-f power and since the range varies from crystal to crystal, it is desirable to calibrate the detector except for very low-level work. To date no special effort has been made to develop a type having a square-law response over a wide range of input power.

The high-inverse-voltage rectifier was discovered during the course of the research on germanium by the NDRC group at Purdue University. They conducted a systematic investigation of the effect of a large number of impurity agents on the rectifying property of germanium. They found that rectifiers made with tin-doped germanium maintained a very high back resistance for inverse voltages of the order of 100 volts and at the same time exhibited high forward conductance. Other addition agents that produce these properties are N, Ni, Sr, Cu, and Bi. However, the most consistent production of high-inverse-voltage germanium has been obtained with tin; such rectifiers are in general inferior as mixers.

The discovery of the high-inverse-voltage property led to considerable interest in their use in many types of circuit applications at intermediate

frequencies of 30 Mc/sec or less, such as second detectors in wideband receivers, d-c restorers, diode modulators, and switching circuits. As a consequence development has continued.

The general properties of the high-inverse-voltage germanium units are:

1. High back resistance, from 10,000 ohms to more than 1 megohm, for voltages as high as 50 volts.
2. High forward conductance, compared with a diode, in the region of 1 volt, with a sharp break in the characteristic at a few tenths of a volt.
3. Low capacitance (about 0.5 $\mu\mu$f).
4. Small size (about that of a half-watt resistor).

An exploratory investigation by the NDRC group at the University of Pennsylvania has shown that the high-inverse-voltage property can be obtained with silicon by the use of tin, nickel, bismuth, or germanium as alloying agent. At the present stage of development, however, silicon is inferior to germanium for second-detector and d-c-restorer applications.

The welded-contact rectifier was reported by H. Q. North[1] of the General Electric Company during the course of research aimed at the development of germanium crystal rectifiers for microwave-mixer use. It was found that rectifiers having very low conversion loss could be made by using germanium with antimony as a doping agent. However, these crystals are noisier than those that use silicon. Nevertheless some units have a low noise output, but at present the low-noise units constitute but a small percentage of the laboratory production, and no one has as yet discovered how to control this effect properly.

In the course of this research, North found that extremely small and very stable contacts could be obtained by welding the contact point to the crystal surface by passing a current of high density (of the order of 10^7 amp/in^2) for a short time through the contact point. These units have the unique property of showing a conversion gain *greater* than unity when the r-f tuning and d-c bias are suitably adjusted. However, under these conditions the noise increases to such an extent that the rectifiers are no better in over-all mixer performance than the standard type.

Under the conditions of r-f tuning and d-c bias mentioned above, a resonant circuit connected to the i-f terminals of the mixer can be made to oscillate when a source of r-f power at frequencies above 3000 Mc/sec is connected to the r-f terminals of the mixer. Under these conditions a negative resistance has been observed in the current-voltage characteristic. The extent of our present knowledge of these effects will be given in detail in Chap. 13.

[1] H. Q. North, "Final Report on K-band Germanium Crystals," NDRC 14-427, GE Co., Mar. 26, 1945.

PART I
GENERAL PROPERTIES

CHAPTER 2

FUNDAMENTAL PROPERTIES OF THE CRYSTAL RECTIFIER

THE PRESENT CRYSTAL CARTRIDGES

During the course of the war the Army and Navy set up joint Army-Navy[1] specifications for a number of crystal-rectifier types. These specifications standardize the external geometry of the cartridge and specify test equipment, test conditions, and performance limits for production testing. Detailed information on the specifications is given in Appendix D.

For mixer use, specifications have been set up for the microwave bands in the regions of 1, 3, 10, and 30-cm wavelengths. The corresponding rectifier types are designated by the type numbers 1N26, 1N23, 1N21, and 1N25 respectively. As manufacturing techniques were improved, tighter specifications were written, each with a new type number. For example, in the 10-cm region the types specified are 1N21, 1N21A, 1N28, 1N21B, and 1N21C. Similarly, the video crystal type numbers are 1N27, 1N30, 1N31, and 1N32.

With the exception of the 1N26 and the 1N31, all of these types employ the same external geometry in the cartridge, which shall for convenience be called the "ceramic," or 1N21-type, cartridge. The ceramic cartridges of three manufacturers are shown at the top of Fig. 2·1.

The "coaxial," or 1N26-type, cartridge was developed at the Bell Telephone Laboratories for use in the 1-cm region. It is more compact than the ceramic cartridge and is designed to match a coaxial line having a 65-ohm characteristic impedance. The coaxial cartridge has also been used for the 1N31 type, which is a video crystal for use in the 3-cm band. The Western Electric and Sylvania coaxial cartridges are shown in the center of Fig. 2·1.

The pigtail cartridge shown at the bottom of Fig. 2·1 has been designed by Bell Telephone Laboratories for the high inverse-voltage rectifier for second-detector and other diode applications.

2·1. Description of the Cartridges.—The external geometry of the cartridges has, except for the pigtail cartridge, been standardized by the JAN specifications. Detailed drawings showing the dimensions and tolerances are given in Appendix D. The details of the cartridge parts

[1] Hereinafter abbreviated "JAN."

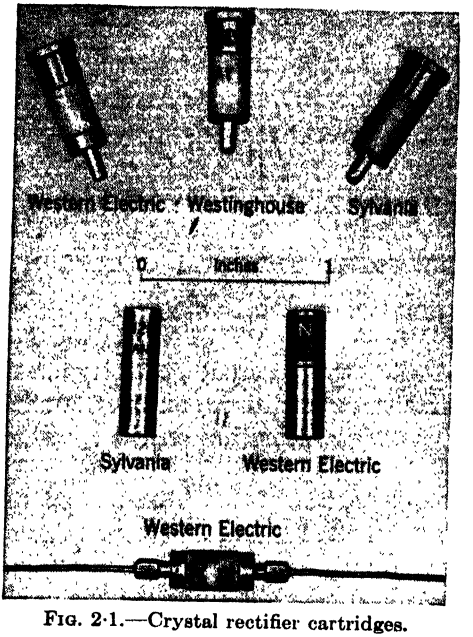

FIG. 2·1.—Crystal rectifier cartridges.

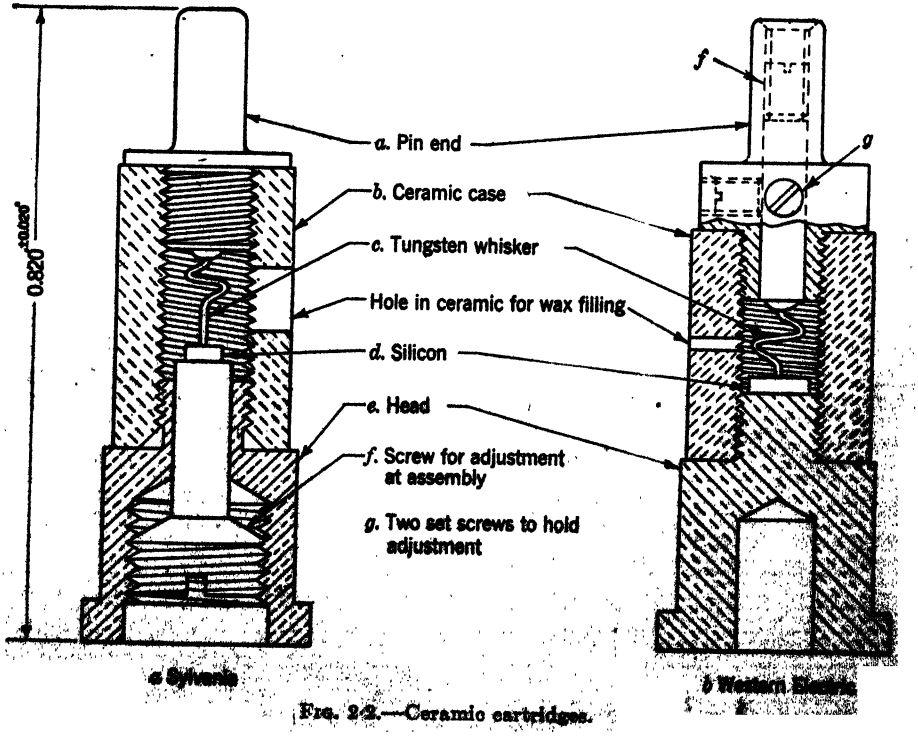

FIG. 2·2.—Ceramic cartridges.

may vary, however, subject to the limitations of the specifications on electrical performance.

The Ceramic Cartridge.—Outline drawings showing the parts of the Western Electric and Sylvania ceramic cartridge are shown in Fig. 2·2. The polarity of the cartridge has been standardized by the JAN specifications as shown by comparison with an equivalent diode in Fig. 2·3. The polarity of the British unit is the reverse of that indicated in Fig. 2·3, the position of the silicon and cat whisker being reversed in the cartridge.

The metals ends are cemented to the ceramic cylinder, and the manufacturer adjusts the rectifying contact once and for all for optimum performance by means of the adjusting screws. The cavity inside the ceramic body is filled with a mixture of Paratac and Opal wax, which increases the mechanical damping and renders the rectifying contact impervious to moisture. The cartridge is mounted in the mixer or crystal holder by means of a spring-finger grip on the pin, and spring fingers or a screw cap on the head. The cartridges are thus as readily replaceable as a tube. The size of the cartridge is convenient for coaxial lines and waveguides normally used for wavelengths greater than about 3 cm.

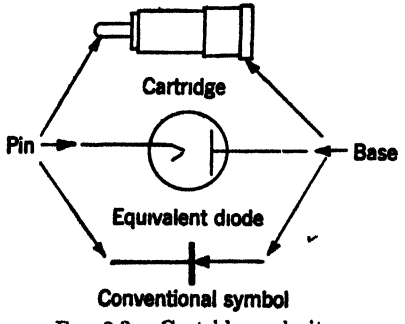

FIG. 2·3.—Cartridge polarity.

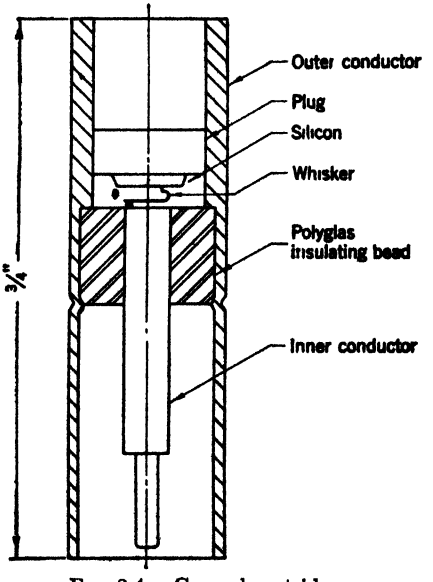

FIG. 2·4.—Coaxial cartridge.

The Coaxial Cartridge.—The coaxial cartridge was designed by the Bell Telephone Laboratories. A Radiation Laboratory design used for laboratory production, and later, with minor changes, put into quantity production by Sylvania Electric Products, Inc., is shown in Fig. 2·4. This cartridge is designed to provide a matched termination for a 65-ohm line, within the variations of impedance occurring in manufacture (see Sec. 2·7). In the usual rectifier mount the pin on the center conductor is held by a spring-finger grip on the center conductor of the

cartridge receptacle, and the outer conductor is pressed against a shoulder on the outer conductor of the receptacle.[1]

The cat-whisker and center-conductor assembly is mounted on a molded insulating bead of polyglas that is pressed into the outer cylinder and secured by a crimp in the outer conductor. The coefficient of expansion of the polyglas bead matches that of the brass outer conductor and thus provides good stability under conditions of changing temperature. The necessity of rigid construction is clear from the fact that the cylindrical cavity containing whisker and crystal is about 0.050 in. long.

The silicon crystal is soldered to a brass plug pressed into the end of the cylinder. Adjustment of the rectifying contact is made by slowly advancing the plug by means of a jig carrying a micrometer screw. The cavity containing the whisker and crystal is, as in the ceramic cartridge, filled with wax.

The Pigtail Cartridge.—The pigtail cartridge is designed to be soldered in place as a circuit element. In the present Bell Telephone Laboratories design the head of the cartridge is replaced by a structure similar to the pin end. The crystal is mounted, like the whisker, on a sliding rod held by set screws after adjustment. The pigtail wires are mounted on fittings pressed onto the pins after assembly and adjustment of the cartridge. The present form of this cartridge is not necessarily the best one, but it was adopted because of lack of time to develop a better one. It is likely that an improved design will soon supersede it.

2·2. Stability and Handling Precautions.—These crystal cartridges have a stability comparable to that of other circuit components. Cartridges stored under tropical as well as normal conditions show no deterioration with time. The JAN specifications provide for a series of rigorous mechanical-design tests to insure long life under conditions that exist in actual applications and during handling. These design tests provide that the electrical performance shall not be impaired more than a small specified amount after being subjected to the following treatment:

1. Immersion in a water bath at 40°C for 15 min followed by immersion for 15 min in water at 25°C.
2. A series of temperature cycles between the limits of −40°C and +70°C. (Specifications for some of the video crystal types impose limits of −55°C and +85°C. The number of cycles specified varies from type to type.)
3. A 30-in. drop onto a hardwood surface. (Some of the video crystal types specify a 10-in. drop.)
4. Application of a torque of 1.5 in-lb about the cartridge axis.
5. An axial-strain test, consisting of the application of a force of 1 lb

[1] See Chap. 9 for a more complete discussion.

applied at the tip of the pin at right angles to the cartridge axis, the head of the cartridge being held in a clamp.

The last two tests are obviously not applicable to a cartridge of the coaxial type.

The crystal rectifier may be impaired in performance in applications where it is required to dissipate excessive amounts of power. This phenomenon is called "burnout."

In a radar system using the same antenna for transmission and reception, a TR switch[1] is used to protect the rectifier from the high-level power of the transmitted pulse. The TR switch is a resonant cavity with loops or irises for coupling r-f power in and out and contains a gas-filled TR tube that is normally nonconducting. Crystal protection is achieved by a gaseous discharge in the TR tube initiated by the transmitted pulse. The ignition takes place in a time that is short compared with the pulse length and provides an effective short circuit at the input terminals of the crystal mixer. The r-f power transmitted through the TR switch during the passage of a transmitted pulse will consist of a "spike," which is transmitted during the preignition time, followed by "leakage power," which lasts for the remainder of the pulse. The TR switch is designed to minimize both these effects.

During the course of the war improvements in TR tubes and associated circuits and in the resistance to burnout of crystal rectifiers made possible a satisfactory crystal life in duplexing systems; the life is limited largely by eventual TR-tube failure or the failure of associated circuits. To insure adequate resistance to burnout, the JAN specifications on the mixer types call for burnout proof tests[2] on each rectifier. Some of the types, in addition, call for a somewhat more rigorous burnout design test on a small fraction of the production. The tests are sufficiently rigorous to insure a long life, comparable to that of conventional vacuum tubes, when the rectifier is properly protected by a TR switch.

Experience has shown that crystal rectifiers may be burned out by improper handling or storage. The discharge of static electricity through the rectifier, static electricity that may have accumulated on ungrounded apparatus or on the operator's body, is sufficient to impair seriously the microwave performance of the rectifier. Damage may also be incurred by a discharge to ground through the rectifier when it is inserted in equipment that is operating at other than ground potential. Damage of this sort may easily be avoided by grounding the apparatus and by holding the cartridge by the base and making bodily contact with the equipment just before inserting the cartridge.

[1] See *Microwave Duplexers*, Vol. 4, Radiation Laboratory Series, for a full discussion.

[2] A "proof test" should not be confused with a "design test." The former merely culls the units with poor burnout characteristics.

The crystal rectifier may also be damaged by exposure of the cartridge to intense r-f fields in the neighborhood of high-power transmitting systems. The manufacturers provide metal containers for storing the cartridges when not in use. One convenient type of container is a lead capsule which can be slipped over the cartridge. This precaution is obviously not necessary for the coaxial cartridge, which is effectively shielded by the outer conductor; this design also minimizes the danger of damage by electrostatic discharge.

ELECTRICAL PROPERTIES

2·3. The Voltage-current Characteristic.—The static rectifier characteristic is of interest on several counts. It is obviously of importance in the theory of point-contact rectification in that an adequate theory must predict quantitatively the features of the current-voltage characteristic. In the second place it has already been pointed out that for low-frequency detection a high back resistance and high forward conductance, together with a sharp curvature at the origin, are desirable. Finally, in the manufacture of rectifiers for microwave use, it is common practice to use the static characteristic as a criterion or guide for the adjustment of the rectifying contact. It should be emphasized, however, that a good static characteristic is not a sufficient condition for a good microwave performance. At sufficiently high frequencies the shunting effect of the capacitance of the barrier at the rectifying contact becomes important. For this reason the size of the contact area must be controlled. Moreover, in microwave applications other factors, such as noise and impedance, are of importance. The measurement of such high-frequency properties is therefore also specified in a production test of the standard types to ensure satisfactory and uniform performance.

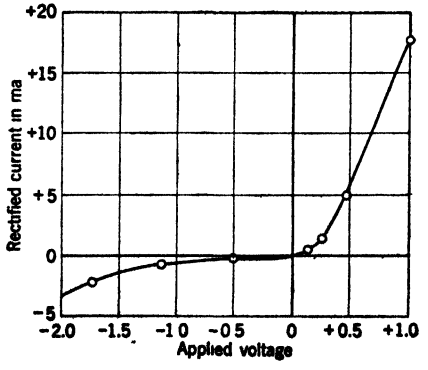

FIG. 2·5.—A typical characteristic curve of a silicon rectifier.

A typical characteristic curve of a silicon rectifier unit is shown in Fig. 2·5. The current increases exponentially in the forward direction for a few tenths of a volt. As the current increases further, the curve approaches a straight line whose slope is determined by the spreading resistance (see Sec. 2·4 and Chap. 4) in the semiconductor. The forward current at 1 volt is 10 to 20 ma for a good mixer crystal.

In the back direction a high-resistance region for voltages of a few volts is followed by a region where the current increases rapidly with

further increase in negative voltage, so rapidly in some cases that it approaches an exponential behavior The standard mixer crystal types have at 1 volt a back resistance of approximately 5000 to 10,000 ohms.

The characteristic curves in the forward direction of several typical rectifiers are shown in larger scale for comparison purposes in Fig 2 6 It is to be noted that the "break" in the characteristic of the crystal rectifiers is much more pronounced than that of the vacuum tube and the forward conductance at about 0 5 volt or more is much larger. The smaller currents obtained with germanium, as contrasted with silicon, at a few tenths of a volt is typical.

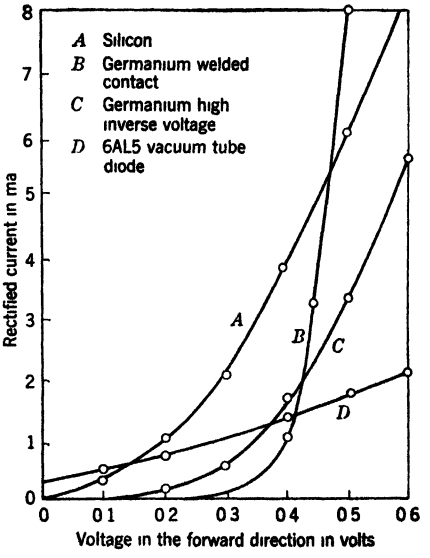

FIG. 2 6 —A comparison of the characteristic curves of several rectifiers.

Characteristic curve B (Fig. 2 6) is typical of the welded-contact rectifier developed recently by North[1] at the General Electric Company. These units use germanium crystals containing 0.2 atomic per cent antimony. The whisker is welded to the crystal by the passage of 250 ma of direct current for a short time in the forward direction. The diameter of the weld on a typical whisker is approximately 0.0002 in. The exponential region of the characteristic is unusually large compared with other rectifiers, and in the forward direction it therefore approaches closely the ideal[2] d-c characteristic,

$$i = A(e^{\alpha E} - 1), \tag{1}$$

where i is the direct current, A and α are constants, and E is the voltage across the barrier. The voltage E is given by

$$E = E' - ir, \tag{2}$$

where E' is the voltage applied to the rectifier and r is the spreading resistance in the semiconductor at the contact point. Figure 2·7 shows the logarithmic characteristic of a typical unit, as observed by Torrey.[3] It should be noted that the coordinates are semilogarithmic; hence a plot

[1] H. Q. North, Final Report, "Welded Germanium Crystals," Contract OEMsr-262, Order No. DIC-178554, Sept. 20, 1945. (This work was done at the Research Laboratory of the General Electric Co.)

[2] See Chap. 4 for a discussion of the theory of the ideal d-c characteristic.

[3] H. C. Torrey, unpublished data at RL.

of Eq. (1) would follow a straight line for appreciable values of E'. From Torrey's curve the following values for the constants of Eq. (1) were obtained:

$$A = 0.0035 \quad \mu a$$
$$\alpha = 29.8 \quad \text{per volt}$$
$$r = 3.2 \quad \text{ohms.}$$

These rectifiers are unique in having an abnormally low value of the spreading resistance and a characteristic which is accurately exponential for forward currents as high as 10 ma.

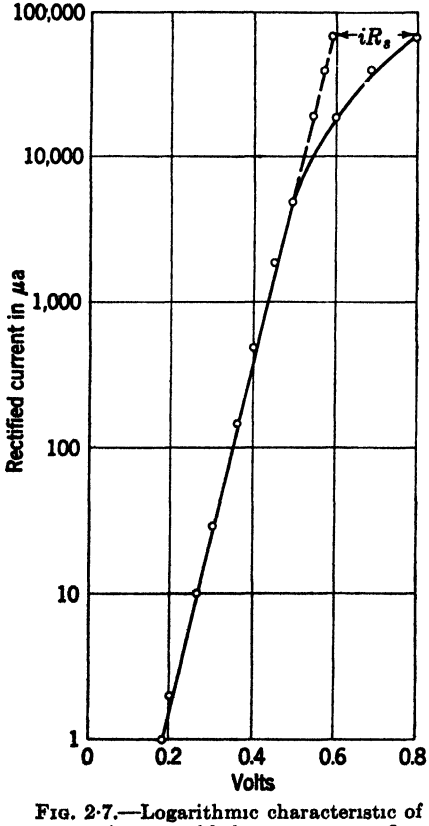

FIG. 2·7.—Logarithmic characteristic of a germanium welded-contact rectifier. Points on the broken curve are calculated for a spreading resistance of 3.2 ohms.

The current-voltage characteristic of a typical germanium high-inverse-voltage rectifier made at Purdue University is shown in Fig. 2·8. The forward current at 1 volt for this particular unit is 8 ma. The crystal in this unit was made from an alloy containing 0.25 atomic per cent of tin.

Outstanding features of the characteristic curve are the high value of the peak back voltage and the negative resistance region exhibited in the back direction for currents exceeding the current at the peak back voltage. This curve is discussed in much more detail in Chap. 12. Recently Theuerer and Scaff[1] have developed a procedure for the heat treatment of ingots of germanium alloyed with 0.1 per cent tin; ingots are obtained in which all but the upper third of the ingot produces rectifiers with peak inverse voltages within a range greater than 50 volts and even approaching 200 volts. In the back direction at about 30 volts these rectifiers have resistances ranging from 10,000 ohms to more than 1 megohm.

The forward currents at 1 volt lie in the range from 5 to 10 ma, and

[1] H. C. Theuerer and J. H. Scaff, "Heat Treatment of Germanium Rectifier Materials," NDRC 14-506, Contract OEMsr-1408, Bell Telephone Laboratories, Aug. 3, 1945.

currents greater than 100 ma may be passed in the forward direction without impairing the rectifying contact.

Figure 2 9 presents a set of characteristic curves for a typical silicon rectifier that show for a crystal of good quality the d-c current in the for-

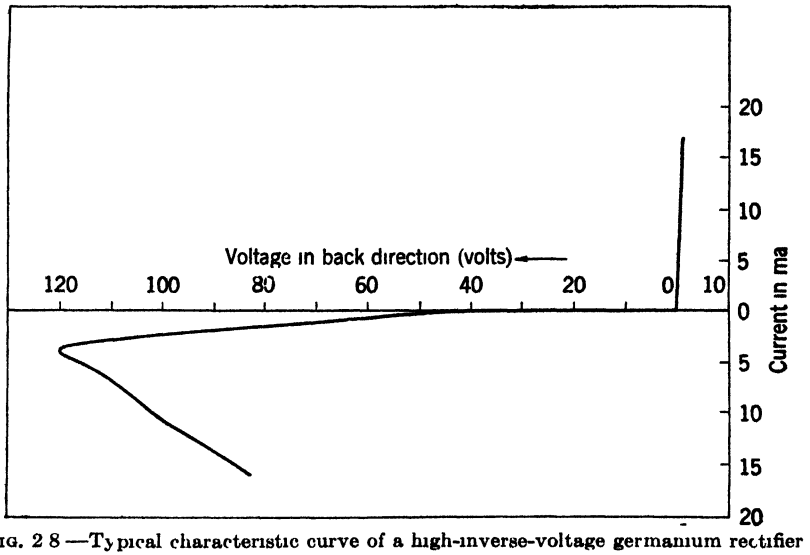

FIG. 2 8 —Typical characteristic curve of a high-inverse-voltage germanium rectifier

ward direction as a function of d-c bias voltage for different levels of 3 2-cm r-f power. The r-f power levels shown in Fig. 2 9 are the actual powers absorbed by the crystal The curves will vary from crystal to crystal, of course, but in general the application of r-f power tends to reduce the curvature of the characteristic as saturation is approached For mixer applications the r-f power is set at a level for which the d-c current in a load of about 100 ohms is from 0 3 to 1.0 ma. (For further discussion see Sec. 2·6.)

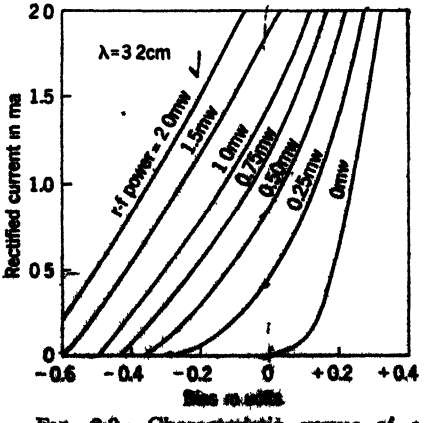

FIG. 2·9.—Characteristic curves of a typical silicon rectifier for different r-f power inputs.

2·4. The Equivalent Circuit.—Only the region in the neighborhood of the point contact need be considered in interpreting point-contact rectification. The other electrical connection to the crystal has such a large cross section that its resistance is always small compared with the forward resistance of the point contact. The simplest equivalent circuit

for a crystal detector that takes into account the known physical parameters at the metal-semiconductor contact is shown in Fig. 2·10. The circuit consists of a nonlinear resistance R shunted by a nonlinear capacitance C, the two in series with a linear resistance r. The term R is the nonlinear resistance of the barrier at the rectifying contact, large in the back direction and small in the forward direction. It becomes increasingly smaller as the current in the forward direction is increased over the exponential part of the d-c characteristic.

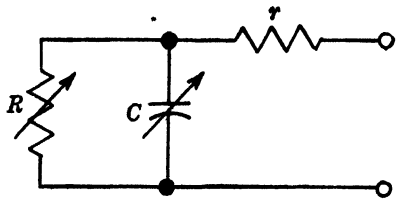

FIG 2 10 -Equivalent circuit of a crystal rectifier

The resistance r is the spreading resistance in the semiconductor resulting from the constriction of current-flow lines in the semiconductor near the contact. If a circular area of contact is assumed, it may be calculated from the known formulas of potential theory that

$$r = \frac{1}{4\sigma a}, \tag{3}$$

where σ is the conductivity of the semiconductor and a is the radius of the circular area of contact. As the current is increased in the forward direction beyond the exponential region, R becomes small compared with r and the characteristic curve approaches a constant slope with a value equal to the reciprocal of the spreading resistance. The bulk resistance of the semiconductor and the resistance of the whisker can be neglected in comparison with r.

The barrier capacitance C arises from the storage of charge in the boundary layer. Since the magnitude of the capacitance depends on the thickness of the barrier layer, which in turn is a function of the applied voltage, the capacitance is nonlinear. Measurements of capacitance vs. bias voltage have been made[1] and indicate this nonlinearity, but the large forward conductance makes a quantitative determination of the effect difficult. At zero bias the barrier capacitance of the standard types of rectifier lies in general in the range from 0.2 to 2.0 $\mu\mu$f. At d-c or low frequencies the capacitance plays no role in the rectification picture, but as the frequency is increased its shunting action reduces the r-f voltage across the barrier. For example, at a frequency of 3000 Mc/sec a capacitance of 1 $\mu\mu$f has a reactance of about 50 ohms. The presence of the spreading resistance makes it impossible to tune out the capacitance with an external reactance. The capacitance of the rectify-

[1] A. W. Lawson, P. H. Miller, L. I. Schiff, and W. E. Stephens, "Barrier Capacitance in Silicon Cartridge Rectifiers," NDRC-14-140, U. of Penn., May 1, 1943.

ing contact therefore plays an important role in the rectification efficiency at high frequencies. ✓

MIXER CRYSTALS

2·5. Conversion Loss, Noise, and Noise Figure.—It is well known that a fundamental limitation on the sensitivity of any radio receiver arises from sources of noise in the circuit elements or from external sources. (For a discussion of the latter situation, see Vol. 24 of this series.) The limitation becomes manifest in different ways. For example, the thermionic vacuum tube is a generator of noise because of, among other reasons, the "shot effect." Since the electrons are emitted by the cathode as randomly distributed discrete particles, the resulting current has a random or statistical fluctuation. As another example, any ohmic conductor has a fluctuation, or noise, voltage developed across it because of the random thermal motion of the electrons within it. Noise from such a source is often called *Johnson noise*. Even in a theoretically perfect receiver (namely, one containing no sources of noise within itself) the minimum detectable signal will still be limited eventually by the Johnson noise in the input impedance.

It is now the generally accepted practice to express the ability of a microwave receiver to detect weak signals in terms of its *noise figure*, precisely defined below. The noise figure indicates quantitatively just how much worse the actual receiver is than an idealized one. In an actual microwave receiver employing a crystal mixer, the output noise will consist of noise originating in the i-f amplifier plus that originating in the mixer. Noise introduced by sources in the video amplifier is so small compared with the amplified noise from the input stages that it may be neglected. In the mixer itself the crystal, driven by a local oscillator, in general generates more i-f noise than a resistor with the same i-f impedance. This is one of its properties that is of importance in the mixer application.

Even if the crystal should generate only Johnson noise (which is approximately the case for occasional units), an additional limitation arises from the fact that in the frequency-conversion process not all of the available power in the r-f signal is converted into power at the intermediate frequency. This *conversion loss* is therefore a second crystal property affecting its mixer performance. Finally, the r-f and i-f impedances of the rectifier are of prime importance in the design of crystal mixers and are functionally related to conversion loss, as is shown in detail in Chaps. 5 and 6.

The definitions to be given here of the quantities involved in the evaluation of crystal-mixer and receiver performance and the analysis of certain relationships between these quantities follow closely those of

Friis,[1] and Roberts,[2] the latter introducing the concept of effective noise figure.

First will be considered any four-terminal network connected to a signal generator and an output circuit as shown in the block diagram of Fig. 2·11. The input and output impedances of the network may have reactive components and may or may not be matched to the generator and output circuits.

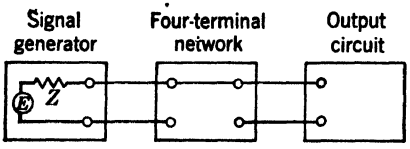

FIG. 2·11.—Block diagram for the analysis of the network noise figure.

Gain of the Network.—The signal generator may be regarded as a voltage source E in series with an impedance $R + jX$. To get the maximum power into a load, the load should have an impedance $R - jX$. This maximum power is by definition the available power from the signal generator, and is given by the expression

$$S = \frac{E^2}{4R}. \tag{4}$$

Similarly, the output terminals of the network can be treated as a new source of signal, having an available power output, which will be called S_0. The power gain G of the network is defined by the relationship

$$G \equiv \frac{S_0}{S}. \tag{5}$$

The gain is by definition independent of the impedance presented to the network by the output circuit but is a function of the generator impedance. It is apparent that for some particular generator impedance the power gain will be a maximum, which will be called G_m. Another useful definition of gain especially apt for a crystal mixer is obtained by matching a signal generator to the crystal mixer at local-oscillator frequency. This gain will be denoted by G_0.

The "loss" of a network is, of course, the reciprocal of the power gain. The term is often used instead of "gain" when the network is a crystal mixer, a situation in which one is almost invariably concerned with conversion gains less than unity.

Noise Figure.—For making measurements of noise power, a practical standard of comparison is the Johnson noise generated in a resistor. The available noise power from a resistor into a "cold," or noiseless, load in an incremental band of frequency df is given by the well-known expression

$$dN = kT\,df, \tag{6}$$

[1] H. T. Friis, "Receiver Noise Figures," *BTL Memorandum* MM-42-160-39, May 13, 1942; *Proc. I.R.E.*, **32**, 419 (1944).

[2] S. Roberts, "Theory of Noise Measurements on Crystals as Frequency Converters," RL Report No. 61-11, Jan. 30, 1943.

where k is Boltzmann's constant, N is the available noise power, and T is the absolute temperature. It is convenient to choose as a standard temperature $T_0 = 290°K$, in which case $kT = 4 \times 10^{-21}$ joule, and kT/e, another quantity frequently encountered, is 0.025 volt.

In so far as noise considerations are concerned, a perfect network is one where there are no noise sources within the network itself. Actually, such networks exist; in such a case the ratio dN_0/S_0 of available output noise power to available output signal power is greater than the ratio dN/S of available input noise power to available input signal power. The noise figure F of the network is then defined for this book by the equation

$$\frac{dN_0}{S_0} = F\frac{kT_0\,df}{S}, \tag{7}$$

in which $kT_0\,df$ is the available input noise power from a resistor. From Eqs. (5) and (7) we obtain

$$dN_0 = FGkT_0\,df. \tag{8}$$

The noise output, noise figure, and the gain are alike in that all are functions of the impedance of the generator. The noise figure is a minimum for some particular value of generator impedance, which in general is not the same as that giving maximum gain.

Effective Noise Figure.—In actual practice networks that have finite bandwidths are of concern. The total available noise output of such a network is given by the integral of Eq. (8),

$$N_0 = kT_0\int_0^\infty FG\,df. \tag{9}$$

Now Eq. (7) can be rewritten in the form

$$\frac{dN_0}{dN} = FG, \tag{10}$$

from which it is seen that FG is at least as great as unity at all frequencies, and the integral in Eq. (9) therefore does not converge. Actually in making measurements of output noise some form of wattmeter which measures the amount of power delivered into some load is used. This quantity will drop to zero outside the pass band of the amplifier, whereas the available Johnson-noise power at the output terminals of the network is independent of frequency. In treating effective noise figure the output-meter gain is introduced and defined as the ratio of the power actually delivered into the meter to the power available from the network. In Eq. (9), G then is defined as the gain of the network-output-meter combination, and is the product of the power gain of the amplifier and that of the output meter. The integral in Eq. (9) then converges.

The effective noise figure F' is now defined by the relation

$$F' = \frac{N_0}{N_0'}, \tag{11}$$

where N_0' is the available output noise power if F were unity at all frequencies, that is,

$$N_0' = kT_0 \int_0^\infty G\, df. \tag{12}$$

In other words N_0' is the noise that would be delivered to the output load if there were no noise sources within the network.

The effective noise figure F' is then given by the expression

$$F' = \frac{N_0}{N_0'} = \frac{\int_0^\infty FG\, df}{\int_0^\infty G\, df}. \tag{13}$$

The effective, or noise, bandwidth B of the network can now be defined as

$$B = \frac{\int_0^\infty G\, df}{G_{\max}}, \tag{14}$$

where $G_{\max}$ is the maximum of the power gain vs. frequency characteristic.

Introducing Eq. (14) into Eq. (13), we obtain for the effective noise figure the expression

$$F' = \frac{N_0}{kT_0BG_{\max}}, \tag{15}$$

which gives F' in terms of measurable quantities. The application of Eq. (15) in the measurement of receiver noise figure is discussed in Chap. 7.

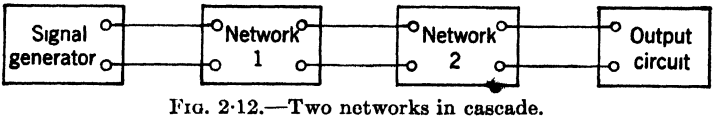

FIG. 2·12.—Two networks in cascade.

Noise Figure of Two Networks in Cascade.—The noise figure for two networks in cascade, shown schematically in Fig. 2·12, can now be obtained in terms of the properties of the two networks.

Applying Eq. (8) to the two networks as a whole, we obtain for the noise output in the incremental frequency band df the expression

$$dN_{0(1+2)} = F_{1+2}G_{1+2}kT_0\, df, \tag{16}$$

where the subscript (1 + 2) indicates that the quantity applies to the

over-all network. The relation,

$$G_{1+2} = G_1G_2, \tag{17}$$

follows directly from the definition of gain. From Eqs. (16) and (17) we obtain

$$dN_{0(1+2)} = F_{1+2}G_1G_2kT_0\,df. \tag{18}$$

Similarly, Eq. (8), applied to network 1, gives

$$dN_{01} = F_1G_1kT_0\,df. \tag{19}$$

The part of the output noise from network 2 originating in the signal generator and network 1 is

$$dN'_{0(1+2)} = dN_{01}G_2 = F_1G_1G_2kT_0\,df. \tag{20}$$

The part of the output noise from network 2 originating within network 2 is

$$dN''_{0(1+2)} = F_2G_2kT_0\,df - G_2kT_0\,df. \tag{21}$$

The second term of the right-hand member of Eq. (21) is subtracted in order not to include for a second time the Johnson noise from the output resistance of network 1.

The addition of Eqs. (20) and (21) gives for the total output noise power the expression

$$\begin{aligned} dN_{0(1+2)} &= dN'_{0(1+2)} + dN''_{0(1+2)} \\ &= F_1G_1G_2kT_0\,df + F_2G_2kT_0\,df - G_2kT_0\,df. \end{aligned} \tag{22}$$

Equating the right-hand members of Eqs. (18) and (22), we obtain

$$F_{1+2} = F_1 + \frac{F_2 - 1}{G_1}\,. \tag{23}$$

Putting Eqs. (23) and (17) into Eq. (13), we have for the effective noise figure

$$F'_{(1+2)} = \frac{\int_0^\infty G_1G_2F_1 + G_2(F_2 - 1)\,df}{\int_0^\infty G_1G_2\,df}. \tag{24}$$

If network 2 has a small bandwidth compared with network 1, G_1 and F_1 may be considered constant over the range of integration; in this case Eq. (24) reduces to

$$F'_{1+2} = F_1 + \frac{F'_2 - 1}{G_1}. \tag{25}$$

In performing the integration indicated in Eq. (24), the factor G_2 in the term $G_2(F_2 - 1)$ is to be regarded as the gain of the network-meter

combination. This accounts for the use of the prime in the right-hand side of Eq. (25).

It must be emphasized that F_2' is a function of the output impedance of network 1, which is considered as a generator for network 2. In applications of this equation, the measurement of F_2' must be made with a signal generator having the same terminal impedance as the output impedance of network 1.

Equation (25) is of particular interest in the evaluation of crystal-mixer performance in superheterodyne receivers. The crystal mixer may be considered as network 1 and the i-f amplifier as network 2. In actual applications since the bandwidth of the mixer is large compared with that of the i-f amplifier, Eq. (25) applies. The term G_1 then becomes the conversion gain of the mixer, that is, the ratio of available output power at the intermediate frequency to the available input power at radio frequency, and F_2' is the effective noise figure of the i-f amplifier. The noise figure F_1 of the crystal mixer may be expressed in terms of *noise temperature.*

Noise Temperature.—It has already been noted that a crystal rectifier, when driven by a local oscillator, in general generates more noise than the Johnson noise produced by an equivalent resistor. The noise temperature[1] t is defined as the ratio of the available noise power output of the crystal to that of a resistor at room temperature (it should be noted that the *available* power does not depend on the value of the resistance); that is,

$$t = \frac{dN_0}{kT_0\,df}, \tag{26}$$

where dN_0 is the available noise power output of the crystal.

Relationships between Noise Figures, Conversion Loss, and Noise Temperature.—Equation (8), substituted in Eq. (26), gives

$$t = FG, \tag{27}$$

whence, from Eq. (25),

$$F'_{\text{rec}} = L(t + F'_{\text{i-f}} - 1), \tag{28}$$

where the conversion loss L is the reciprocal of the conversion gain, F'_{rec} is the over-all effective noise figure of the crystal mixer and i-f amplifier, and $F'_{\text{i-f}}$ is the effective noise figure of the i-f amplifier.

The three properties of the crystal that are involved explicitly or implicitly in Eq. (28) are the conversion loss, the noise temperature, and the i-f impedance. As is shown in Chap. 7, any one of these three quanti-

[1] This quantity is called the "output noise ratio" in the JAN specifications. Although it is not a temperature but a ratio, the term "noise temperature" is commonly accepted and widely used. The name is explained by the fact that the product tT_0 is the temperature a passive resistor would have to have in order to generate as much Johnson noise as the noise output of the crystal in question.

ties can be measured to a good approximation without either of the others being known. This is particularly advantageous both in production testing and in the experimental laboratory.

From Eq. (28) it is seen that noise temperature and i-f amplifier noise figure are additive terms. During the course of World War II, the improvement in these two quantities occurred more or less concurrently. The average noise temperature of present rectifiers is around 1.5 times[1] and preamplifiers have been recently designed having noise figures as low as 1.5 db (about 1.4 times) at 30 Mc/sec, and 1.2 db at 5 Mc/sec.

By means of Eq. (28) we can easily calculate the noise figure of a typical receiver using a crystal mixer. For example, a crystal rectifier such as the 1N21C type, having a conversion loss of 5.5 db and noise temperature of 1.5 times, and an i-f amplifier having a noise figure of 3 db will have an over-all noise figure of 9.5 db (or about 9 times). [The values substituted in Eq. (28) must obviously be expressed numerically, and not in decibels.]

In using Eq. (28) for calculating the receiver noise figure we must remember that the results are accurate only in so far as the r-f and i-f impedances are maintained the same in the combination of mixer and i-f amplifier as they were in the equipment in which the separate quantities were measured.

Another quantity useful in crystal-noise measurements and analysis is the Y-factor. It is defined as the ratio of available output noise power N_0 of an amplifier whose input terminals are loaded by a crystal mixer to the same quantity N_{0s} when the amplifier is loaded by a dummy cartridge containing an ohmic resistor. We can easily obtain an expression for the Y-factor by applying Eq. (15) first to the receiver (mixer and amplifier) and then to the amplifier alone; thus

$$Y = \frac{N_0}{N_{0s}} = \frac{F'_{\text{rec}}G_{\text{rec}}}{F'_{\text{i-f}}G_{\text{i-f}}}, \tag{29}$$

where G_{rec} and $G_{\text{i-f}}$ are the maxima of the respective power gain-frequency characteristics, as used in Eq. (14). As $G_{\text{rec}} = GG_{\text{i-f}}$, in substituting Eqs. (17) and (28) into Eq. (29) we obtain

$$Y = \frac{L(t + F'_{\text{i-f}} - 1)G}{F'_{\text{i-f}}}. \tag{30}$$

Since GL is unity, this reduces to

$$Y = \frac{t - 1}{F'_{\text{i-f}}} + 1. \tag{31}$$

Equation (31) can be rewritten in the form

$$t = F'_{\text{i-f}}(Y - 1) + 1. \tag{32}$$

[1] This is the way t is customarily expressed.

Equation (32) provides a convenient means of measuring noise temperature in terms of the Y-factor and the noise figure of the i-f amplifier. In actual practice care must be taken in the design of the amplifier input circuit to insure that the Y-factor is independent of the i-f impedance of the mixer over the range of normally encountered crystal i-f impedances. Circuits fulfilling this requirement are discussed in Chap. 7.

Another useful relationship can be derived by the combination of Eqs. (28) and (32):

$$F'_{\text{rec}} = LF'_{\text{i-f}}Y. \tag{33}$$

Equation (33) is convenient to use in the statistical study of burnout in that a measurement of conversion loss and Y-factor before and after

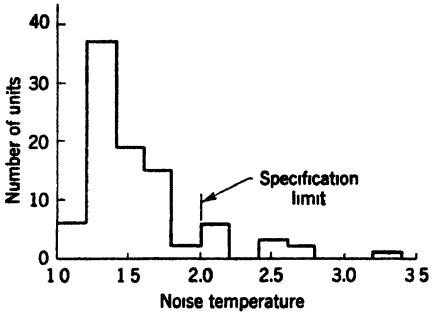

FIG. 2·13.—Typical distribution of noise temperature of 1N21B rectifiers. Random sample selected prior to acceptance tests.

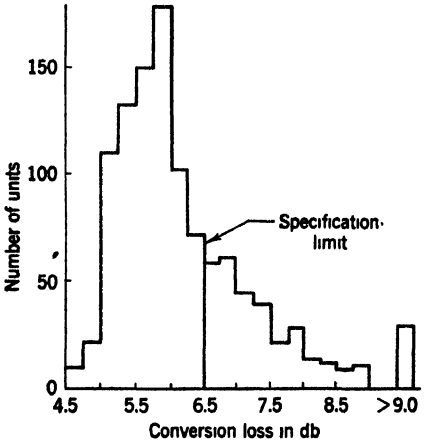

FIG. 2·14.—Typical distribution of conversion loss of 1N21B rectifiers. Random sample selected prior to acceptance tests.

application of specified amounts of power enables one to calculate directly the consequent impairment in receiver noise figure. The deterioration of receiver noise figure expressed in decibels is just the sum of the deterioration in Y-factor and conversion loss expressed in decibels.

Range of Conversion Loss and Noise Temperature in Production Units.—In the manufacture of crystal rectifiers, even by the most carefully controlled methods, a considerable spread in the values of conversion loss and noise temperature is found. Figures 2·13 and 2·14 show typical distributions of random samples taken from the manufacturers' production lines before rejection of units failing to pass the performance tests. These units were type 1N21B rectifiers for 10-cm use. Similar distributions of the Radiation Laboratory rectifier for 1-cm applications, typical of the 1N26 type, are shown in Figs. 2·15 and 2·16. These data were taken with the standard test equipment described in detail in Chap. 9, as prescribed

by the JAN specifications, with the exception of the noise temperatures of Fig. 2·15 which were measured using a radio frequency of 24,000 Mc/sec and an intermediate frequency of 60 Mc/sec. (As indicated in Appendix D, the JAN specifications provide for the measurement of the noise temperature of type 1N26 rectifiers at a radio frequency of 9375 Mc/sec.) Summarized briefly, the test conditions for these measurements consist of a mixer having a fixed r-f tuning, a specified i-f and d-c load, and a specified r-f power level and radio frequency. The d-c bias voltage is that due to the rectified current into the d-c load and is about −0.1 volt.

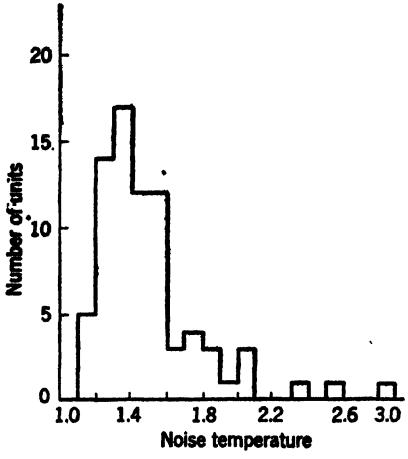

FIG. 2·15.—Typical distribution of noise temperature of 1N26 rectifiers. Random sample of units made at the Radiation Laboratory.

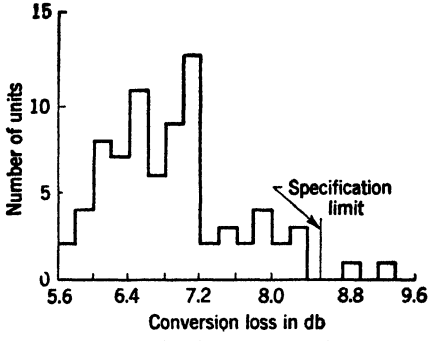

FIG. 2·16.—Typical distribution of conversion loss of 1N26 rectifiers. Random sample of units made at the Radiation Laboratory.

2·6. Optimum Local-oscillator Level.—The conversion loss, noise temperature, and receiver noise figure are all functions of the local-oscillator power level. Figure 2·17 shows the conversion loss and noise temperature of a typical 1N23B rectifier ($\lambda = 3.2$ cm) as a function of rectified current; these curves are obtained by varying the local-oscillator power. The curves are also characteristic of the other frequency bands. The noise-temperature curve is approximately linear over the range of interest. The conversion loss approaches a constant value as the rectified current is increased; above a rectified current of approximately 1 ma there is little change in conversion loss.

The effect of local-oscillator power level on receiver noise figure can be calculated from the data of Fig. 2·17 by means of Eq. (28). The calculated curves for three values of i-f amplifier noise figure are shown in Fig. 2·18. The curves are characterized in general by a broad minimum in the region of 0.3 to 0.8 ma and it is in this range that crystal mixers are ordinarily operated. Since the minimum is broad, the choice of operating level is not critical. It is obvious from the curves that the minimum is

broader for "quiet" crystals and would in fact disappear for a crystal having a noise temperature of unity for all values of rectified current. The shape of the conversion-loss curve makes it clear that even in this

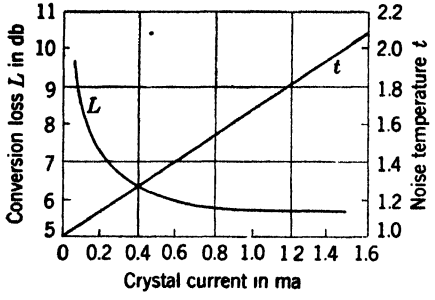

FIG. 2·17.—Conversion loss and noise temperature as a function of rectified current for a typical 1N23B crystal rectifier.

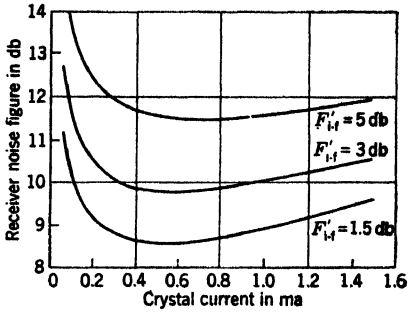

FIG. 2·18.—Receiver noise figure as a function of rectified current for the 1N23B rectifier plotted in Fig. 2·17. The three curves are for different i-f amplifiers, as indicated.

case there would be no point in operating at large values of rectified current. Indeed, for receivers where there is appreciable noise at the intermediate frequency from the local oscillator, it would be disadvantageous. The lower limit of operable range is obviously set by the rapid increase of conversion loss at low local-oscillator power level.

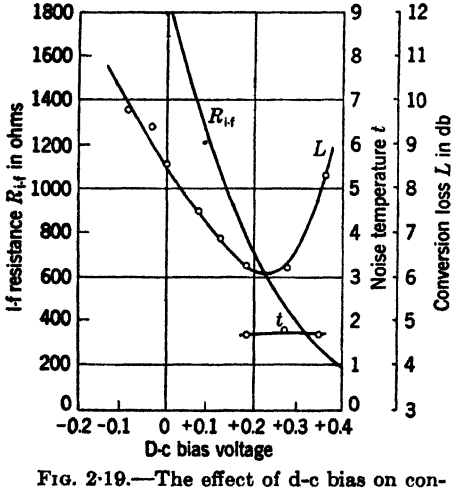

FIG. 2·19.—The effect of d-c bias on conversion loss, noise temperature, and i-f resistance for a germanium rectifier at a radio frequency of 9375 Mc/sec and power level of 0.1 mw.

The effect of d-c bias on silicon crystal-mixer performance has been investigated by R. V. Pound and H. B. Huntington[1] at the Radiation Laboratory and by Sharpless[2] at Bell Telephone Laboratories. The effect of a negative bias (bias in a direction that reduces the rectified current) is always undesirable in that the noise temperature and conversion loss are increased. A small positive bias of about two- or three-tenths of a volt, however, is found to be beneficial in reducing the noise output of noisy crystals. For such units

[1] Unpublished data.

[2] W. M. Sharpless, "The Influence of Direct-current Bias on the 10-cm Performance of Silicon Rectifiers as First Converters," BTL MM-42-160-78, July 24, 1942.

a decrease in receiver noise figure of about 1 db can be obtained with an optimum positive bias. For the present silicon rectifiers the effect is, in general, negligible.

In the case of germanium rectifiers the effect of bias on noise temperature has been found by North[1] to be much more pronounced than for silicon. Typical curves for a germanium rectifier are shown in Fig. 2·19. With zero d-c bias this rectifier has a conversion loss of 6.2 db at a local-oscillator power level of 1 mw (about 1-ma rectified current) and a noise temperature of 4.4 at a rectified current of 0.6 ma. On the other hand the data shown in Fig. 2·19 were taken at a local-oscillator power level of 0.1 mw. It should be noted that the conversion loss at the optimum bias in this latter case is approximately the same as that at the higher local-oscillator level with zero bias, while the noise temperature on the other hand has dropped from 4.4 to about 1.8 at optimum bias.

2·7. The R-f Impedance of Crystal Rectifiers.—The r-f impedance of crystal rectifiers is a property of prime importance in the design of crystal mixers. Impedance mismatches at radio frequency not only result in signal loss due to reflection, but also affect the i-f impedance seen at the i-f terminals of the mixer, an effect that becomes more serious with rectifiers of low conversion loss. To avoid the complexity of tuning the mixer each time a crystal rectifier is changed, a considerable effort has been made to control the spread in values of r-f impedances of production units to a reasonable amount and to design test- and radar-system mixers that will match crystals of average impedance. The procedure has been an empirical one of selecting representative samples, measuring their r-f impedances, and then designing mixers that will match the center of the distribution. Impedance standards have been devised by Roberts[2] and Whitmer[3] which may be inserted in the mixer in place of the crystal and whose r-f impedances may be adjusted to a chosen value at the center of the crystal-impedance distribution. These standards are then used to "pre-tune" test mixers so that their performance is identical. (See Chap. 9.)

With the exception of the 1N25 and 1N26 types, no attempt has been made to specify r-f impedance limits explicitly. A certain amount of implicit limitation is obtained, however, by making performance tests on conversion loss with the standard fixed-tuned mixer. Thus units with a borderline value of conversion loss under matched conditions will be rejected.

[1] H. Q. North, Final Report, "K-band Germanium Crystals," NDRC 14-427, GE Co., Mar. 26, 1945.

[2] S. Roberts, "Conversion Loss Measuring Apparatus for Crystals in the 3-cm Band," RL Report No. 53-28, Aug. 3, 1943.

[3] C. A. Whitmer, unpublished work at RL.

In general the uniformity in r-f impedance of production units is determined by the degree to which the manufacturing procedures can be accurately controlled. The success that has been obtained is demonstrated by Figs. 2·20 and 2·21 in which are plotted on impedance-circle diagrams (Smith charts) the r-f impedances (or admittances, as indicated) of representative samples from different manufacturers.

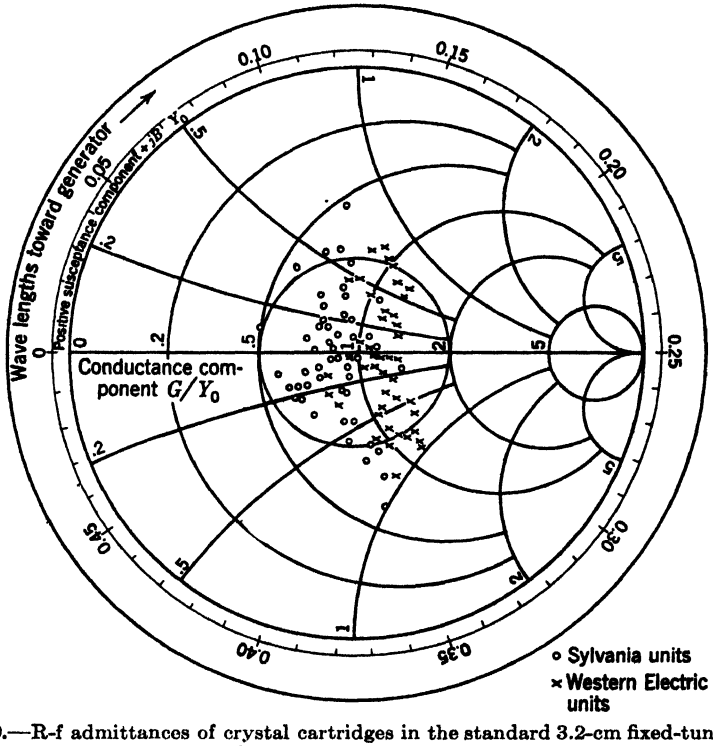

FIG. 2·20.—R-f admittances of crystal cartridges in the standard 3.2-cm fixed-tuned mixer. R-f power level, 0.6 mw.

A block diagram of the equipment used in making these measurements is shown in Fig. 2·22; the equipment is described in detail in Vol. 11 of the Radiation Laboratory Series. The r-f power available to the mixer is adjusted to a specified value by means of the attenuator, which also serves to isolate the oscillator from the mixer. The signal power level is ordinarily very low, but in this case is fixed at local-oscillator level with the result that what is measured is the r-f impedance at that level. Experience has shown, however, that the value at this level is approximately the same as that at signal level. A low-resistance milliammeter is connected to the output (i-f) terminals of the mixer.

The probe is connected to a calibrated crystal or a bolometer, whose output current or power measures the standing-wave maximum and minimum. If a crystal rectifier is used in the probe and its rectified current

is limited to a few microamperes, it is a good enough approximation for these measurements to assume that the electric field in the r-f line is proportional to the square root of the probe current. The standing-wave voltage ratio is then the square root of the ratio of maximum to minimum

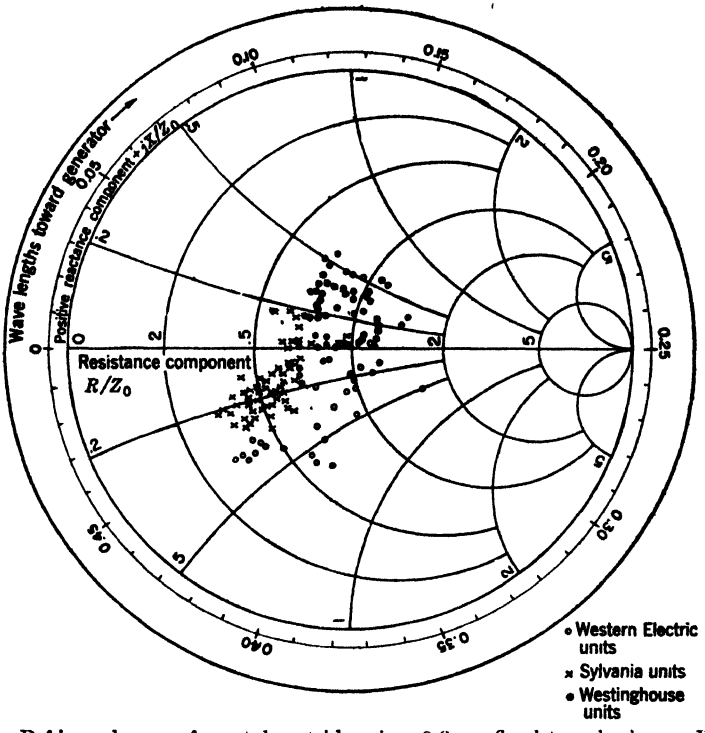

FIG. 2·21.—R-f impedances of crystal cartridges in a 9.8-cm fixed-tuned mixer. R-f power level, 0.5 mw.

probe current. The standing-wave voltage ratio, together with the position of the minimum in the slotted section, (see Vol. 9 of the Series) locates the impedance with respect to a given reference point on the Smith chart. In the measurement of the admittance of a crystal car-

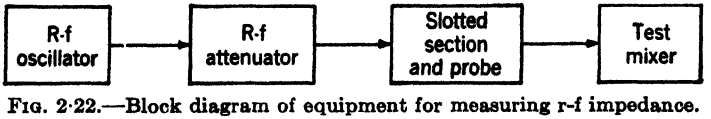

FIG. 2·22.—Block diagram of equipment for measuring r-f impedance.

tridge in a fixed-tuned mixer, the reference point, corresponding to zero admittance, is chosen as the position of the minimum in the slotted section when the cartridge is removed. A shift in the reference point merely rotates the pattern on the Smith chart about the center. The impedance of each point on the chart is therefore the impedance of the combination of mixer and crystal cartridge in units of the line impedance of the slotted section. In Fig. 2·20 the circle shown for a standing-wave

voltage ratio of 2.0 includes all units for which the reflection loss is equal to or less than 0.5 db. A waveguide mixer is the standard type used in the 3-cm region; the crystal is shunted across the guide, and in this case it is consequently convenient to plot admittances. In the 3-cm band it can be seen from the chart that the spread in susceptance is larger than the spread in conductance. In system-mixer design in the 3-cm band the crystal has been so placed in relation to the TR switch that the TR

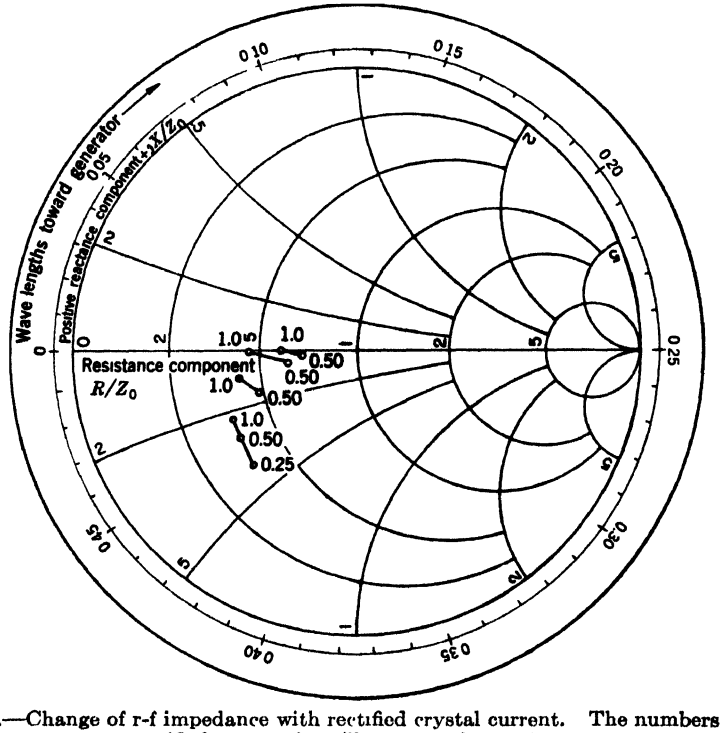

FIG. 2·23.—Change of r-f impedance with rectified crystal current. The numbers indicate rectified current in milliamperes, $\lambda_{r\text{-}f}$ = 9.8 cm.

switch can tune out the susceptance of the crystal; in this case, the mismatch found is caused by conductance alone.

Figure 2·21 shows the impedance distribution in the standard coaxial fixed-tuned test mixer at a wavelength of 9.8 cm. The standard tuning of this mixer has since been changed to the center of this distribution. There is no correlation between the impedance distributions at 10 and 3 cm. This arises in part from the physical differences in the coaxial and waveguide mixers and in part from the difference in frequencies; at the higher frequency the physical dimensions of the elements of the cartridge, which determine the impedance, are a sizable fraction of a wavelength, and the cartridge is a shunt element in a waveguide rather than a series element in a coaxial line.

The effect on r-f impedance of varying the r-f power level is shown in Fig. 2·23. The numbers at each point on the chart give the rectified crystal current in milliamperes for which that particular impedance was obtained. The variation of crystal current over the range from 0.25 to 1.0 ma, the region where mixers are ordinarily operated, does not result in a significant change in r-f impedance.

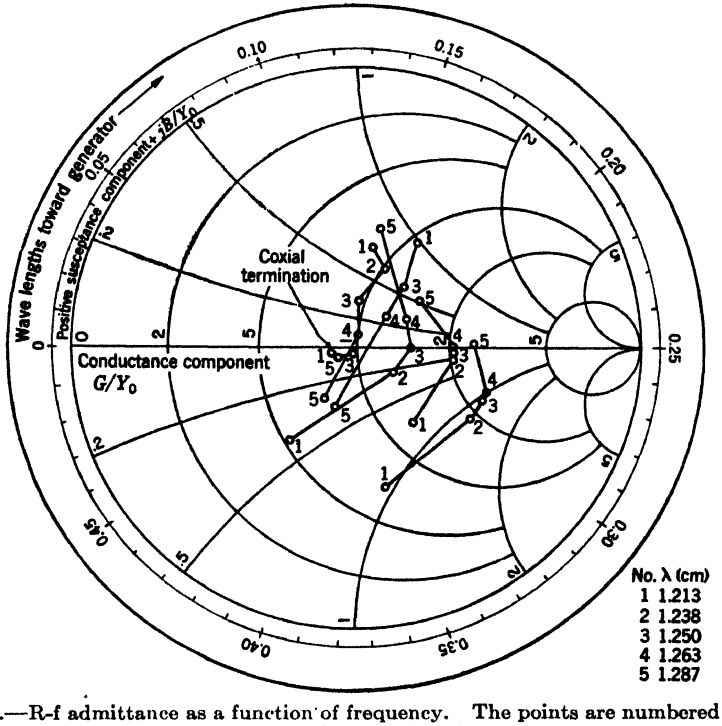

FIG. 2·24.—R-f admittance as a function of frequency. The points are numbered in order of increasing wavelength.

The variation of impedance with frequency for the coaxial-type cartridge (1N26 type), designed for use at 1.25 cm, is shown in Fig. 2·24. It must be remembered that the frequency sensitivity is a function of the crystal cartridge and mixer combined. These measurements were made using a crystal holder shown in cross section in Fig. 2·25. The waveguide-to-coaxial transformer shown is designed to provide a matched termination to standard ¼- by ½-in. waveguide when the coaxial crystal receptacle is terminated in a 65-ohm line. A transformer of this type is employed in many of the mixers used in the 1-cm radar systems.

The r-f impedances shown in Fig. 2·24 were measured over a wavelength range from 1.213 to 1.287 cm, centered at 1.250 cm. The small variation observed over this range for the standard coaxial termination indicates that most of the variation in impedance is in the crystal cartridge itself.

The r-f impedance is a complicated function of cartridge geometry, size and shape of cartridge parts, composition of the semiconductor, and whisker pressure. It is very difficult therefore, in the case of the ceramic cartridge, to adjust the r-f impedance without affecting other properties of the rectifier. In this respect a cartridge of the coaxial type has the advantage of sufficient space in the pin end for the insertion of a coaxial transformer which, within limits, will match a given crystal impedance to a 65-ohm line.

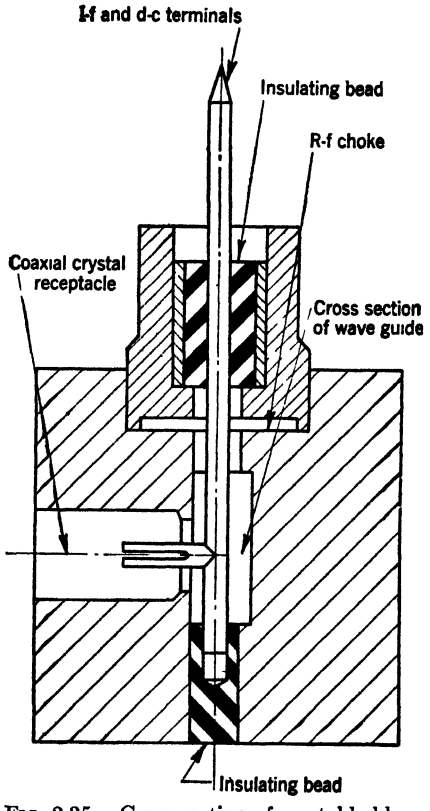

FIG. 2·25.—Cross section of crystal holder for the 1N26 cartridge.

2·8. The I-f Impedance of Crystal Rectifiers.—A matter of prime importance in the design of coupling circuits between the mixer and the i-f amplifier is the i-f impedance that is seen on looking into the i-f terminals of a crystal mixer. The i-f impedance pertinent here is that at the output terminals of the mixer when the rectifier is driven by a local oscillator. The value of the i-f impedance is found to depend on the conditions under which it is measured. It is a function of the local-oscillator power level and depends on the r-f properties of the mixer and the circuit connected to the r-f input terminals of the mixer. Finally, for a given mixer and measuring equipment, the i-f impedance of commercial rectifiers, like other crystal quantities, shows a spread of values occurring even with carefully controlled manufacturing techniques. In this chapter only typical data on some of these effects will be presented. The theoretical treatment will be found in Chap. 5.

Measurement of I-f Impedance and D-c Resistance.—The i-f impedance can be measured with an impedance bridge designed to operate at the desired intermediate frequency. At the Radiation Laboratory a Schering bridge designed by Beers[1] to operate at 30 Mc/sec has been found satisfactory.

The dynamic low-frequency (d-c) resistance is of interest since the theory of frequency conversion predicts that for crystal mixers used

[1] Y. Beers, "A 30-Mc Schering Bridge," RL Report No. 61-19, May 12, 1943.

with low-Q r-f systems, as is the case in crystal test equipment, the i-f and d-c conductances are the same.

The d-c resistance can be easily determined on the assumption that a crystal excited by a local oscillator is equivalent to a d-c generator with an internal resistance. This d-c resistance is determined by measuring (1) the short-circuit current, and (2) the current into a given external load. The d-c resistance R is obviously given by the expression

$$R = r\frac{1}{k-1}, \tag{34}$$

where r is the external load and k is the ratio of short-circuit current to the current when the load r is used. The assumption of equivalence to a generator allows this method to be used with good results when k is not greater than 2.

The d-c resistance may also be measured by means of a bridge operated at low frequency, for instance, 60 cycles. Another method is to apply a low-frequency source of a few volts in series with a resistance of, for example, 100,000 ohms to the i-f terminals. Since the d-c resistance of the mixer is a few hundred ohms, this arrangement provides essentially a constant-current source. The d-c resistance can then be determined by reading the voltage across the i-f terminals with a suitable voltmeter.

A comparison of the i-f and d-c resistances measured at the Radiation Laboratory by Huntington[1] using the foregoing methods shows good agreement for the standard 10-cm test mixer. A similar result has been reported by Smith[2] in which the i-f resistance is measured with the aid of a diode noise source. Other investigators, however, have found a discrepancy between the i-f and d-c resistances, the former running 10 to 35 per cent lower than the latter. A discrepancy of about 25 per cent is found, for example, in the mixer used in the 3-cm standard test equipment. Smith[3] has offered the suggestion that the discrepancy is mainly a function of the r-f apparatus used in the measurement. According to his theory, the i-f voltage applied to the i-f terminals for the impedance measurement modulates the r-f wave reflected by the crystal. Part of the modulated wave is then reflected back again to the crystal by tuning mechanisms or other discontinuities in the r-f line. Part of this is absorbed by the crystal, the remainder being again reflected, and so on. As a result of this process, components from the reflected modulated wave arrive at the crystal in various phases with respect to the applied

[1] H. B. Huntington, unpublished data.

[2] R. N. Smith, "Crystal Noise as a Function of D-c Bias and 30-Mc Impedance Measured with a Diode Noise Source," OSRD Contract, OEMsr-362, Sec. D-1, NDRC Report, Purdue Univ., June 25, 1943.

[3] R. N. Smith, "The Theory of Crystal Mixers in Terms of Measurable Mixer Constants," OSRD Contract, OEMsr-362, Sec. D-1, NRDC Office, Mar. 24, 1944.

i-f voltages, resulting in an i-f voltage which on demodulation has a strong effect on the measured impedance. Smith tested this hypothesis by an experiment in which the crystal is mounted in one end of a long coaxial line containing a sliding double-slug tuner. The d-c and i-f resistances were measured for several positions of the tuner in the r-f line. These positions of the tuner were one-half an r-f wavelength apart, so that the r-f matching conditions were the same in each position; however, the time taken for the modulated wave to travel from the crystal to the tuner is different for each position.

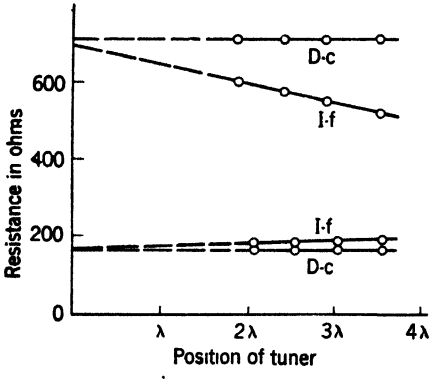

FIG. 2·26.—Effect of r-f apparatus on the measurement of i-f impedance.

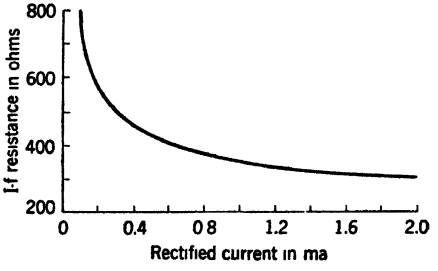

FIG. 2·27.—The dependence of i-f resistance on rectified current.

Measurements were made on several crystals. A typical set of data is shown in Fig. 2·26. The two sets of data are for settings of the tuner corresponding to maximum and minimum d-c resistance. It can be seen that the discrepancy becomes less as the distance between the tuner and crystal is decreased, and that the curves approach the same value when extrapolated back to the crystal position.

A further check on Smith's hypothesis might be made by investigating the discrepancy as a function of intermediate frequency. Such an investigation has not yet been reported.

The I-f Resistance as a Function of Rectified Current.—The effect on i-f resistance of varying the local-oscillator power level is shown for a typical silicon crystal in Fig. 2·27. The crystal mixer was matched to the r-f line and the power level was adjusted by means of a variable attenuator. No d-c bias was used. In the usual region of mixer operation, the variation of i-f resistance is about 100 ohms, from 0.4 to 1.0 ma, which is considerably less than the spread in the resistance of commercial units, as can be seen from Fig. 2·28.

The I-f Resistance Spread of Crystal Rectifiers.—The distribution of i-f resistance in a typical sample of type 1N26 rectifiers in the standard 1.25-cm crystal test equipment is shown in Fig. 2·28. The data shown

were taken at a fixed r-f power level of 1.0 mw, in a fixed-tuned mixer, tuned to match the center of the r-f impedance distribution. The d-c resistance was measured by means of a constant-current source at 60 cycles by the method previously described. In the equipment used the d-c and i-f resistances were the same. The upper and lower limits of the spread encompass about a 2 to 1 range, which is found to be typical of the 3- and 10-cm types under similar experimental conditions.

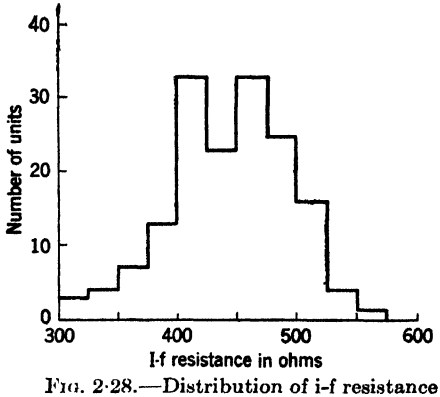

FIG. 2·28.—Distribution of i-f resistance for a representative sample of 1N26 rectifiers in standard test equipment.

The Dependence of I-f Resistance on R-f Matching Conditions.—It has already been mentioned that the i-f resistance depends strongly on the r-f circuit connected to the input terminals of the mixer. The effect becomes more pronounced for the low-conversion-loss units. In fact a method has been developed by Dicke[1] for measuring conversion loss by measuring variation in i-f impedance with known values of r-f impedance presented to the mixer. This so-called "impedance method" of measuring conversion gain is discussed in Chap. 7. It will be sufficient for our purposes here merely to illustrate the nature of the impedance variation by typical data taken by Dicke with the gain-measuring apparatus. In Table 2·1, R_1 is the i-f resistance measured with the mixer matched to the

TABLE 2·1.—DEPENDENCE OF THE I-F RESISTANCE ON THE R-F INPUT IMPEDANCE

R_1, ohms	R_2, ohms	R_3, ohms
613	873	436
570	786	410
780	1056	589
572	777	423

r-f line. The line is supplied with r-f power at local-oscillator power level by a suitably isolated signal generator. The values R_2 and R_3 are obtained by introducing into the r-f waveguide a standard susceptance which produces a voltage standing-wave ratio of 2.38. The effective line length from the susceptance to the crystal is then varied. The values

[1] R. H. Dicke, "A Reciprocity Theorem and Its Application to Measurement of Gain of Microwave Crystal Mixers," RL Report No. 61-18, Apr. 13, 1943.

R_2 and R_3 are the maximum and minimum i-f resistances obtained as the line length is varied. Table 2·1 shows the results for four 1N26 rectifiers.

TABLE 2·2.—THE I-F IMPEDANCE OF A SET OF CRYSTALS IN THREE DIFFERENT MIXERS FOR A HIGH-Q R-F INPUT CIRCUIT

Crystal number	Mixer No. 1 (Rectified current 0.5 ma)		Mixer No. 2 (Rectified current 0.5 ma)		Mixer No. 3 Fixed LO coupling		
	R, ohms	C, $\mu\mu$f	R, ohms	C, $\mu\mu$f	R, ohms	C, $\mu\mu$f	Rectified current ma
1	230	−4.2	1100	+5.1	574	+4 4	0.91
2	280	−1.2	1100	+4.2	644	+3.6	0.73
3	275	−3.3	450	+4.3	370	+3.6	0.80
4	250	−4.4	535	+5.3	328	+4.7	0.96
5	280	−6.6	305	+4 3	280	+2.9	0 67
6	240	−3 6	556	+6 0	416	+4 4	0.90
7	300	−3.7	420	+4.2	376	+3.2	0 72

An effect of this kind becomes more pronounced when the r-f input consists of a high-Q device such as a TR switch. If the TR switch is tuned to signal frequency and if its Q is sufficiently high, it presents quite different admittances at signal and image frequencies (see Chap. 5), both of which affect the i-f admittance. At the crystal, the admittances at signal and image frequencies will depend on the line length from the TR to the crystal; hence the i-f impedance of the crystal mixer may vary from mixer to mixer. The magnitude of this effect can be seen from the data in Table 2·2 that were obtained by Waltz and Kuper[1] at the Radiation Laboratory. In this table, R and C represent the parallel components of resistance and capacitance measured at the i-f terminals with a 30-Mc/sec bridge. The mixers were coupled to the signal generator through a TR switch tuned to the signal frequency. The mixers are of three different designs used in radar systems. The negative sign in the capacitance column indicates an inductance requiring the indicated capacitance to produce resonance. In general it is characteristic of such results that if, in a certain mixer, the resistance of all crystals tends to cluster about some average value, then the reactance components will exhibit marked fluctuations from crystal to crystal; but if the r-f circuits of the mixer are such that the reactance components are constant, the resistance components will fluctuate. The theoretical interpretations of these results will be discussed in Chap. 5.

[1] M. C. Waltz and J. B. H. Kuper, unpublished data.

CHAPTER 3

PROPERTIES OF SEMICONDUCTORS

In this chapter some of the underlying ideas of modern solid state theory are qualitatively reviewed with particular emphasis on the electron theory of semiconductors. A few quantitative results are stated but not derived. The discussion is restricted to those aspects of the subject that bear on the problem of contact rectifiers and that will be of use in the succeeding chapters, especially Chap. 4. The reader who desires a broader and more detailed account is referred to the many excellent texts on solid-state theory.[1]

3·1. Band Theory.—The classification of crystalline materials according to their electrical and optical properties and the detailed study of each of the several classes is enormously facilitated by the *band theory*, which plays a role in the physics of solids that is analogous and of comparable importance to the concept of energy levels in the theory of individual atoms and molecules.

Indeed there is not only an analogy but a direct connection between the electronic energy levels of an individual free atom and the electronic energy bands of a solid material consisting of a collection of atoms forming a crystal lattice. The electronic energy bands of the lattice may be considered to be derived from the atomic energy levels of the free atoms. In some cases there is a one-to-one correspondence between the lattice bands and the atomic levels from which they are derived; in other cases the connection is less distinct.

This connection may usually be traced by imagining the lattice to be formed by bringing together a collection of atoms from a state of remote separation to the final state, namely, the equilibrium separation found in the actual crystal lattice. The reader is referred to the standard works cited for a description of the manner in which this connection between the atomic levels and the lattice bands can be established. It will suffice here to state that, in the lattice, there are a number of allowed values of energy accessible to an electron. These energy states are

[1] See F. Seitz, *The Modern Theory of Solids*, McGraw-Hill, New York, 1940; R. H. Fowler, *Statistical Mechanics*, 2d ed., Cambridge, London, 1936, Chap. 11; A. H. Wilson, *The Theory of Metals*, Cambridge, London, 1936; N. F. Mott and H. Jones, *The Theory of the Properties of Metals and Alloys*, Oxford, New York, 1936; A. H. Wilson, *Metals and Semiconductors*, Cambridge, London, 1939; and N. F. Mott and R. W. Gurney, *Electronic Processes in Ionic Crystals*, Oxford, New York, 1940.

grouped into bands consisting of a large number of closely spaced energy levels, the number of levels of a band being, in fact, of the order of the number N of atoms in the lattice.

Any one of the levels of a band can, by the exclusion principle, accommodate at most a single electron. It follows that a band can accommodate at most a number of electrons equal to the number of levels of the band. A filled band is one in which all of the levels are occupied. These allowed bands are separated by ranges of energy containing no levels (except perhaps a few caused by impurities or lattice imperfections) and therefore not permitted to electrons. A typical lattice will have a few narrow and widely separated bands of low energy filled by electrons and derived from the inner-core energy levels of the constituent atoms. Bands of higher energy derived from the energy levels of the valence electrons of the constituent atoms are relatively broad and closely spaced. They may in fact overlap to some extent. These bands of the valence electrons may be either completely or only partly filled. Finally, at still higher energies, there may be completely empty bands.

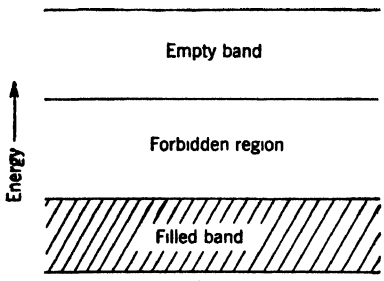

FIG. 3·1.—Electronic energy bands of an insulator or of a semiconductor.

Metals and Insulators.—It is possible on this basis to understand the vast difference in electrical conductivity between metals and insulators A metal, in the band theory, has its uppermost band (or group of overlapping bands) containing electrons (valence band) only partly filled. For such a band there are permitted empty levels adjacent to the highest occupied levels. An applied electric field easily forces the electrons in the highest occupied levels into the adjacent empty levels; these electrons exchange energy with the field, and conduction results.

On the other hand, an insulator has a band structure consisting of a number of filled bands above which are a number of vacant bands (see Fig. 3·1). Conduction is now almost impossible. An electron can conduct only by being accelerated by an applied field, that is, it must exchange energy with the field. One way is to change its energy level in the band. In an insulator all occupied bands are full; all their energy levels are occupied and, by the exclusion principle, will not accept additional electrons. Consequently conduction by this means is impossible. The only alternative is for an electron to be forced by the applied field from a filled band to an empty band. Such a process is, however, highly improbable.[1]

Semiconductors.—It is seen, therefore, how the existence of very good

[1] C. Zener, *Proc. Roy. Soc.*, **A145**, 523 (1934).

conductors (metals) and very poor conductors (insulators) is accounted for by the band theory. It remains to show how semiconductors, that is, materials with intermediate conductivities, can be fitted into the band theory. There are two distinct types of semiconduction, intrinsic and extrinsic; they may both, however, occur in the same semiconductor.

Intrinsic semiconduction occurs in materials that have a band structure similar to that of insulators (see Fig. 3·1) but with the difference that the gap in energy between the highest filled band and the lowest empty band is relatively small. At absolute zero the material is an insulator, but at finite temperatures enough electrons are thermally excited from the filled to the empty band to produce a limited amount of conduction. This conduction is produced not only by the excited electrons but also by the electrons of the nearly filled band. Silicon and germanium both exhibit intrinsic conduction at sufficiently elevated temperatures. Intrinsic conduction is, however, of little importance in crystal rectifiers.

Extrinsic semiconductors also have the band structure of Fig. 3·1. Extrinsic semiconduction occurs because of the presence of extra energy levels as a result of lattice imperfections or of the presence of impurities. These extra energy levels lie in the normally forbidden region between a filled and an empty band and may act either as *donators* or as *acceptors*. An extra level acts as a donator if it is filled at absolute zero. At finite temperatures a donator level may donate its electron to the empty band. Once in the empty band an electron is, of course, in a condition to conduct. An extra level acts as an acceptor if it is empty at absolute zero. At finite temperatures an acceptor level may accept an electron from the filled band and thus leave an empty level in the band. Conduction in the previously filled band is now possible because an electron may be transferred by field excitation into the vacant level. In silicon and germanium as used in rectifiers, conductivity is extrinsic because of the presence of impurities. In silicon as used in rectifiers the impurity levels usually act as acceptors; in germanium, they usually act as donators. In copper oxide (an extrinsic semiconductor) the extra levels act as acceptors and arise from lattice imperfections caused by a stoichiometric deficiency of copper in the lattice. A filled donator level is electrically neutral and an empty donator level has a single positive charge. On the other hand, a filled acceptor level (that is, one that has accepted an electron) has a single negative charge, whereas an empty acceptor level is electrically neutral. The reasons for these statements are given in Sec. 3·6.

The width of the forbidden region (see Fig. 3·1) is several electron volts in the case of insulators, but is only about one volt for silicon and germanium. It has been found that, at least in the case of silicon and germanium, the extra energy levels produced by impurities lie very close

(that is within 0.1 ev) to the band to which they donate or from which they accept electrons. Thus donator levels lie below and very close to the "empty" band, and acceptor levels lie above and very close to the "filled" band. A possible reason for this fact has been suggested by Bethe and is given in Sec. 3·6.

3·2. Electron Distribution in Semiconductors.—It will be shown in Chap. 4 that a knowledge of the electron distribution in semiconductors is vital to the understanding of the rectification process. It was shown in the previous section that conduction is the result either of a few electrons in a normally "empty" band, or of a few vacancies in a normally "filled" band, or in some cases of a combination of the two.

It can be shown that in the first case, that is, the case of a few electrons in the normally empty band, these electrons act as a free classical assembly. Their velocity is zero at the bottom of the band and increases proportionally to the square root of their energy measured from the bottom of the band. Their effective mass, however, may be larger than the normal mass of a free electron. Since they are few in number, they do not form a degenerate gas as do the "free" electrons in metals but obey the classical Maxwell-Boltzmann statistics.

The electrons of a nearly filled band, however, behave in a very different manner. Since almost all of the available energy levels are filled, the electron gas is highly degenerate. The velocity of an electron is zero at the top of the band and increases with decreasing energy in the band. This anomaly is related to the fact that the effective mass of an electron near the top of the "filled" band is negative. In fact, the application of an electric field that would normally accelerate a free electron actually retards an electron near the top of the "filled" band. These electrons thus respond to the field as though they have a positive rather than a negative charge. It has been found convenient to focus attention not on the large number of electrons of the nearly full band but rather on the vacant levels or "holes" as they are called. These holes, few in number, move about in the lattice as the electrons fill them and leave new holes behind. It is shown in works on solid-state theory that these holes act precisely as though they were positively charged electrons with positive mass. It is possible, in fact, to ignore the electrons entirely, that is, to suppose the band to be completely full and to treat the holes as a free classical nondegenerate assembly of positive electrons obeying Maxwell-Boltzmann statistics. The case of a nearly full band then becomes very similar to that of a nearly empty band with the difference that, in a nearly full band, the current carriers (holes) are positively charged with energy (and velocity) increasing from the top to the bottom of the band.[1]

[1] For a more complete treatment of the concept of holes see, for example, F. Seitz, *The Modern Theory of Solids*, McGraw-Hill, New York, 1940, Sec. 68.

A semiconductor that conducts principally by electrons in the nearly empty band is said to be an "n-type" semiconductor; a semiconductor that conducts principally by holes in the nearly filled band is referred to as a "p-type semiconductor.

Both silicon and germanium at room temperature are extrinsic semiconductors, even if highly purified, since there are always present residual impurities that are able to supply more conducting electrons or holes than are obtained by thermal excitation from the "filled" to the "empty" band. At higher temperatures intrinsic conduction becomes predominant, the threshold temperature for intrinsic conduction depending on the impurity content. It should be noted that pure intrinsic conduction takes place by equal numbers of electrons in the "empty" band and holes in the "filled" band. As processed for use in rectifiers, impurities of special types are added to the semiconductor. Impurities of a given type act either as donators or as acceptors, never as both. The impurities normally added to silicon make it p-type, whereas those normally added to germanium make it n-type.

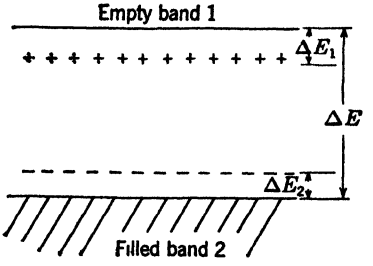

FIG. 3·2.—Band structure of an extrinsic semiconductor showing positions of donator levels (+) and acceptor levels (−).

Figure 3·2 shows the energy level diagram of an extrinsic semiconductor with both acceptor levels (designated by − signs) and donator levels (designated by + signs). It is rarely necessary to consider the case where both types are simultaneously present, but Fig. 3·2 shows both types, and the nomenclature for the various energy gaps can therefore be indicated in one diagram. It is seen that ΔE is the width of the entire "forbidden" region, ΔE_1 is the energy depth of the donator levels below the "empty" band, and ΔE_2 is the elevation in energy of the acceptor levels above the "filled band."

The problem of calculating for any case the equilibrium numbers of electrons in the nearly empty band or of holes in the nearly filled band has been solved by Wilson[1] and by Fowler.[2] Wilson treats the problem as a dissociative equilibrium and Fowler uses the principle of equality of the thermodynamic chemical potentials of a number of groups of electrons in thermal equilibrium. The two methods lead to equivalent results.[3] Wilson's treatment is followed here.

[1] A. H. Wilson, *Proc. Roy. Soc.*, **A133**, 458 (1931) and **134**, 277 (1932).

[2] R. H. Fowler, *Proc. Roy. Soc.*, **A140**, 506 (1933); also, his *Statistical Mechanics*, 2d ed., Cambridge, London, 1936, Secs. 11·6 and 11·61.

[3] Fowler's method is applicable to somewhat more general cases, however, than is Wilson's.

Let us consider first the case of an n-type extrinsic semiconductor with N_1 donator levels per unit volume located at an energy depth ΔE_1 below the nearly empty band. Let the number of electrons excited to the nearly empty band be n_1 per unit volume. The number of bound electrons in the donator levels is then $N_1 - n_1$. Let us consider the equilibrium of the reaction

$$\text{Free electron} + \text{bound hole} \rightleftarrows \text{bound electron.}$$

The mass action law gives

$$\frac{n_1^2}{N_1 - n_1} = K_1, \tag{1}$$

where K_1 is the equilibrium constant of the reaction. From statistical mechanics[1]

$$K = 2\left(\frac{2\pi m_1 kT}{h^2}\right)^{3/2} e^{-\frac{\Delta E_1}{kT}}, \tag{2}$$

where m_1 is the effective[2] electron mass, k is Boltzmann's constant, T the absolute temperature, and h is Planck's constant.

The solution of Eq. (1) is

$$n_1 = \frac{\nu_1}{2} e^{-\frac{\Delta E_1}{kT}} \left[\left(1 + \frac{4N_1}{\nu_1} e^{\frac{\Delta E_1}{kT}}\right)^{1/2} - 1\right], \tag{3}$$

where

$$\nu_1 \equiv 2\left(\frac{2\pi m_1 kT}{h^2}\right)^{3/2}. \tag{4}$$

Two limiting cases are of special interest:

1. Weak ionization of the donators ($n_1 \ll N_1$) as a result of either low temperature ($T \ll \Delta E_1/k$) or high concentration of donators ($N_1 \gg \nu_1$). We obtain from Eq. (3) in this case

$$n_1 \approx \sqrt{N_1 \nu_1}\, e^{-\frac{1}{2}\frac{\Delta E_1}{kT}}. \tag{5}$$

2. Strong ionization of donators ($n_1 \approx N_1$) as a result of either high temperature ($T \gg \Delta E_1/k$) or low concentration of donators ($N_1 \ll \nu_1$). We find in this case from Eq (3),

$$n_1 \approx N_1\left(1 - \frac{N_1}{\nu_1} e^{\frac{\Delta E_1}{kT}}\right). \tag{6}$$

[1] Fowler, *Statistical Mechanics, op. cit.*

[2] It was noted in Sec. 3·2 that the effective electron mass of a lattice electron differs in general from the mass of a free normal electron. See F. Seitz, *Modern Theory of Solids*, McGraw-Hill, New York, 1940, Sec. 68.

Let us consider next the case of a p-type extrinsic semiconductor. The reaction of interest here is

$$\text{Free hole} + \text{bound electron} \rightleftarrows \text{bound hole}.$$

Denoting by n_2 the number of free holes per unit volume, by N_2 the number of acceptor levels per unit volume each at the energy ΔE_2 above the nearly filled band, and putting

$$\nu_2 \equiv 2\left(\frac{2\pi m_2 kT}{h^2}\right)^{3/2}, \tag{7}$$

where m_2 is the effective mass of a free hole, we obtain equations precisely similar to Eqs. (3), (5), and (6), with subscripts 2 instead of 1.

Finally, there is the case of an intrinsic semiconductor. By similar methods we find for the number n_1 of free electrons per unit volume (in the nearly empty band) which in this case is equal to the number n_2 of free holes per unit volume (in the nearly filled band),

$$n_1 = n_2 = \sqrt{\nu_1\nu_2}\, e^{-\frac{\Delta E}{2kT}}, \tag{8}$$

where ΔE is the energy separation of the two bands.

3·3. Work Functions and Contact Potentials.—As will be shown in Chap. 4, the contact potential difference between a metal and a semiconductor is of the greatest importance in the theory of rectification. If two substances are placed in contact it is found that the electrical potential of one substance in general differs from that of the other by an amount characteristic of the two materials. This difference in potential is called the "contact potential difference." The contact potential difference between two metals is almost equal to the difference between their work functions. The work function of a material is the work required to extract an electron from it and remove it to infinity. The contact potential difference between a metal and a semiconductor is also approximately equal to the difference of their work functions, although this approximation is poorer than for the case of a metal-metal contact. For a metal-semiconductor contact, the discrepancy between the contact potential difference and the work function difference is of the order of kT, which is about 0.025 ev at room temperature. The contact potential difference, on the other hand, is generally between 0.2 and 0.5 ev.

The work function χ of a semiconductor depends on the amount and type of impurities present. The various cases can be worked out, using Fowler's methods,[1] with the results:

[1] R. H. Fowler, *Proc. Roy. Soc.*, **A140**, 506 (1933) or *Statistical Mechanics*, 2d ed., Cambridge, London, 1936, Sec. 11·6z.

1. Intrinsic semiconductor:

$$\chi = W_x + \tfrac{1}{2}\Delta E, \tag{9}$$

where χ is the work function and W_x is the difference between the potential energy of an electron at the bottom of the nearly empty band and that of an electron at rest for outside the semiconductor.

2. Extrinsic semiconductor, n-type:
   a. Weak ionization of donators ($n_1 \ll N_1$),

$$\chi_1 \approx W_x + \tfrac{1}{2}\Delta E_1. \tag{10}$$

   b. Strong ionization of donators ($n_1 \approx N_1$),

$$\chi_2 \approx W_x. \tag{11}$$

3. Extrinsic semiconductor, p-type:
   a. Weak ionization of acceptors ($n_2 \ll N_2$),

$$\chi_3 \approx W_x + \Delta E - \tfrac{1}{2}\Delta E_2. \tag{12}$$

   b. Strong ionization of acceptors ($n_2 \approx N_2$),

$$\chi_4 \approx W_x + \Delta E. \tag{13}$$

These various cases are illustrated graphically in Fig. 3·3.

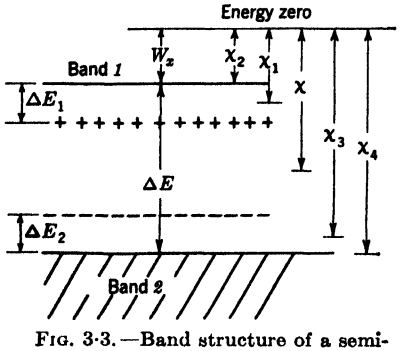

FIG. 3·3.—Band structure of a semiconductor showing work functions (χ, χ_1, χ_2, . . .) that apply in various special cases.

The contact potential difference ϕ_{xm} between a metal and a semiconductor is now defined as the amount by which the electrical potential of the semiconductor must exceed the electrical potential of the metal when they are in contact and in equilibrium. Let χ_m be the work function of the metal, which is closely equal to the difference between the potential energy of an electron at the top of the Fermi distribution in the metal and that of an electron at rest far outside the metal. The expressions for the contact potential difference ϕ_{xm} between the metal and a semiconductor for the various special cases are given by Fowler as:

1. Intrinsic semiconductor:

$$-e\phi_{xm} = \chi - \chi_m - kT \ln \left(\frac{m_2}{m_1}\right)^{3/4} \tag{14}$$

where e in this and subsequent equations stands for the absolute value of the electronic charge.

2. Extrinsic semiconductor, n-type:
   a. Weak ionization of donators ($n_1 \ll N_1$),

$$-e\phi_{xm} = \chi_1 - \chi_m - \frac{1}{2}kT \ln\left(\frac{N_1}{\nu_1}\right). \tag{15}$$

   b. Strong ionization of donators ($n_1 \approx N_1$),

$$-e\phi_{xm} = \chi_2 - \chi_m - kT \ln\left(\frac{N_1}{\nu_1}\right). \tag{16}$$

3. Extrinsic semiconductor, p-type:
   a. Weak ionization of acceptors ($n_2 \ll N_2$),

$$-e\phi_{xm} = \chi_3 - \chi_m + \frac{1}{2}kT \ln\left(\frac{N_2}{\nu_2}\right). \tag{17}$$

   b. Strong ionization of acceptors ($n_2 \approx N_2$),

$$-e\phi_{xm} = \chi_4 - \chi_m + kT \ln\left(\frac{N_2}{\nu_2}\right). \tag{18}$$

When contact is made between a metal and a semiconductor, all of the electronic energy levels of the semiconductor are depressed by the amount $e\phi_{xm}$ relative to those of the metal. This depression is accomplished by the formation of a double layer of charge near the contact surface. This double layer acts as a potential barrier and its presence, as we shall see in Chap. 4, is a prerequisite for rectification. The height of the barrier, in energy, is just $e\phi_{xm}$.

3·4. Electrical Conductivity and Hall Coefficient for Semiconductors.—As will become clear in Chap. 4, there are a number of physical quantities characteristic of an extrinsic semiconductor that are of importance in the theory of rectification and conversion. Among these quantities are: number density, mean free path, mobility of the free electrons (or free holes), and positions of the impurity levels with respect to the energy bands. The mobility and number density may be found by measurements of electrical conductivity and Hall coefficient, as will shortly become evident. By a study of these quantities as a function of temperature the mean free path and the positions of the impurity energy levels may be found.

Derivations of the expressions for conductivity and Hall coefficient for semiconductors may be found in standard works on solid-state theory.[1]

Conductivity.—The expression for electrical conductivity σ_1 of an n-type extrinsic semiconductor with n_1 free electrons per unit volume is

$$\sigma_1 = \frac{4}{3}\frac{e^2 l_1 n_1}{(2\pi m_1 kT)^{1/2}} \tag{19}$$

[1] For example, R. H. Fowler, *Statistical Mechanics*, 2d ed., Cambridge, London, 1936; or F. Seitz, *The Modern Theory of Solids*, McGraw-Hill, New York, 1943.

where l_1 is the mean free path of the electrons, m_1 is their effective mass, and the other symbols have their usual meanings. The corresponding expression for the electrical conductivity of a p-type extrinsic semiconductor is the same as Eq. (19) with subscripts 2 instead of 1 (thus referring to the corresponding quantities for the free holes).

The mobility of a current carrier (electron or hole) is defined as the mean drift velocity in unit electric field. It is given by

$$b_1 = \frac{4}{3}\frac{el_1}{(2\pi m_1 kT)^{1/2}} \tag{20}$$

for the case of electron conduction. A similar expression with subscripts 2 instead of 1 applies in the case of hole conduction.

Comparing Eqs. (19) and (20) we see that

$$\sigma_1 = en_1b_1, \tag{21}$$

and

$$\sigma_2 = en_2b_2. \tag{22}$$

In the case of a composite semiconductor, where current is carried both by electrons and by holes, we have

$$\sigma = e(n_1b_1 + n_2b_2). \tag{23}$$

Hall Effect.—It will be seen from Eqs. (21) and (22) that the conductivity gives the product of the number density of current carriers and their mobility. Measurements of the Hall effect, however, give the number density directly. By combining the two measurements, therefore, the mobility can be determined. The Hall effect occurs when a magnetic field, transverse to the lines of current flow, is applied to a current-carrying conductor or semiconductor. An emf is established in the conductor in a direction orthogonal to both magnetic field and current. Let us suppose that the current flows in the x-direction and that the magnetic field is applied in the z-direction. The emf is then established in the y-direction. When equilibrium is established (with the result that there is no transverse flow of current), the emf is countered by an electric field in the y-direction E_y, arising from charges on the walls of the conductor. This field E_y is found to be proportional to the magnetic induction B_z and to the current density J_x. The proportionality constant,

$$R = \frac{E_y}{J_xB_z}. \tag{24}$$

is known as the "Hall coefficient."

It is shown in works on solid-state theory[1] that R is given, in the case

[1] For example, R. H. Fowler, *Statistical Mechanics*, 2d ed., Cambridge, London, 1936, *loc. cit.*; or F. Seitz, *The Modern Theory of Solids*, McGraw-Hill, New York, 1940, *loc. cit.*

of a simple n-type extrinsic semiconductor, by

$$R_1 = -\frac{3\pi}{8}\frac{1}{en_1}, \tag{25}$$

and, in the case of a simple p-type extrinsic semiconductor, by

$$R_2 = +\frac{3\pi}{8}\frac{1}{en_2}. \tag{26}$$

Since e by definition is the absolute value of the electronic charge, we see from Eqs. (25) and (26) that the sign of the Hall coefficient is negative for electronic conduction and positive for hole conduction.

The importance of the Hall coefficient is due to the fact, evident from Eqs. (25) and (26), that it gives directly the number densities of the current carriers, provided, however, that the carriers are all either electrons or holes. For a composite semiconductor, the Hall coefficient depends also on the mobilities of the carriers. The Hall coefficient of a composite semiconductor is given[1] by

$$R = -\frac{3\pi}{8e}\frac{n_1b_1^2 - n_2b_2^2}{(n_1b_1 + n_2b_2)^2}, \tag{27}$$

where b stands for mobility as before and subscripts 1 and 2 refer, respectively, to electrons and to holes. In the special case where $n_1 = n_2 = n$, which holds for intrinsic semiconductors, Eq. (28) reduces to

$$R = -\frac{3\pi}{8}\frac{1}{en}\frac{b_1 - b_2}{b_1 + b_2}. \tag{28}$$

By combining Eqs. (25) and (21) or Eqs. (26) and (22) we see that the electronic mobility is given directly by the product of Hall coefficient and conductivity for a simple semiconductor,

$$\left.\begin{aligned} b_1 &= -\frac{8}{3\pi}\sigma_1R_1; \\ b_2 &= +\frac{8}{3\pi}\sigma_2R_2. \end{aligned}\right\} \tag{29}$$

Variation with Temperature.—Let us now consider the temperature variations to be expected for σ and R. The simpler case is that of R. At high temperatures the semiconductor is in the intrinsic range and R is given by Eq. (28). The sign of R evidently depends in this case on the relative magnitudes of b_1 and b_2. For silicon and germanium it is found that $b_1 > b_2$; that is, the electron mobility exceeds the hole mobility.

[1] V. A. Johnson, private communication, Purdue Univ. According to Dr. Johnson the ambiguity in the value of R for a composite semiconductor (R. H. Fowler, *op. cit.*, p. 428) has been resolved in favor of Eq. (27).

This result is in accord with the band theory, which predicts a larger effective mass for the holes than for the electrons. In the intrinsic range the variation of R with temperature is dominated by the factor n in Eq. (28). This quantity varies rapidly with temperature according to the exponential law, Eq. (8). Thus the plot of ln $|R|$ vs. $1/T$ in the intrin-

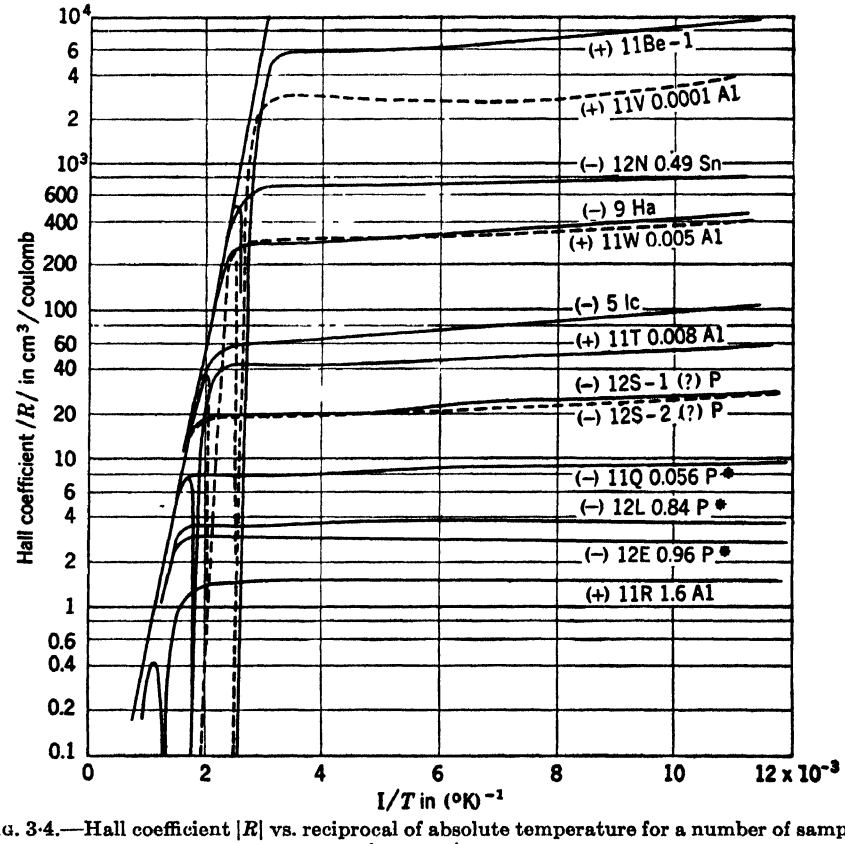

FIG. 3·4.—Hall coefficient $|R|$ vs. reciprocal of absolute temperature for a number of samples of germanium.

sic range should be a straight line with a slope proportional to ΔE, the energy width of the forbidden region between the "empty" and the "filled" bands. The sign of R should be negative in the intrinsic range, since $b_1 > b_2$.

At somewhat lower temperatures the behavior of R as a function of T is governed by the type of impurity present. If at low temperatures the semiconductor is n-type extrinsic, the sign of R, by Eq. (25), should remain negative; but if the semiconductor is p-type extrinsic at low temperatures, the sign of R should reverse and become positive at low temperatures. Where the temperature is sufficiently low to preclude intrinsic excitation, R is given either by Eq. (25) or by Eq. (26). In

these cases n_1 (or n_2) is given by Eq. (3) or its analogue with subscripts 2 instead of 1. At *very low* temperatures the limiting form of Eq. (3) is Eq. (5) or its analogue with subscripts 2 instead of 1. In this latter case the slope of a curve of $\ln |R|$ vs. $1/T$ is proportional to $\frac{1}{2}\Delta E_1$ (or $\frac{1}{2}\Delta E_2$). Figure 3·4 shows a plot of $\log_{10} |R|$ vs. $1/T$ for a number of samples of germanium differing in type and in relative concentration of impurities. Each curve is identified by symbols giving the sign of the carrier at low temperatures, the ingot from which the sample was obtained, and the relative concentration and the type of impurity. Thus the symbol (−) 12N 0.49Sn means that the sample is n-type extrinsic (−) at low temperatures, the ingot number is 12N and the sample contains 0.49 per cent (atomic) of tin (Sn) addition.

The noteworthy features of these curves are:

1. Large slope (the same for all) at high temperatures. This slope, as stated above, is proportional to ΔE.
2. The reversal in sign of R between the intrinsic range and the extrinsic range for all p-type samples at low temperatures. Since $\log_{10} |R|$ is plotted, the reversal of sign is indicated by the sudden decrease and subsequent increase of $\log_{10} |R|$ at a critical temperature. The value of $|R|$ actually passes through zero at this temperature although it is impossible, of course, to show this on the logarithmic plot.
3. The very small slope of the curve of $\log_{10} R$ vs. $1/T$ at low temperatures. In many cases this slope is too small to measure. According to the above discussion it is proportional to ΔE_1 (or to ΔE_2) and its small value indicates that ΔE_1 (or ΔE_2) is very small for all the samples of germanium. In other words, the impurity levels lie very close to the "empty" band (n-type) or to the "filled" band (p-type).

Corresponding curves for two samples of p-type silicon are shown as curves, I (R) and II (R) in Fig. 3·5. Both of these curves, as expected, show a change in sign of R in going from the intrinsic to the extrinsic range. The slope of the curves at low T is much larger than in the case of germanium, indicating that the impurity levels do not lie as close to the bands in silicon as they do in germanium.

The analysis of the dependence of conductivity on temperature is more difficult than in the case of the Hall effect. At high temperatures, where intrinsic conduction is dominant, we see from Eq. 23, since $n_1 = n_2 = n$, that

$$\sigma = en(b_1 + b_2). \tag{30}$$

The dominant factor in Eq. (30) is n, as in the case of the Hall effect. Thus, in the intrinsic range, the slope of $\ln \sigma$ vs. $1/T$ should be the same

as the slope of ln $|R|$ vs. $1/T$, in agreement with experiment. At lower temperatures, where extrinsic conduction is dominant, σ is given by either Eq. (21) or Eq. (22). In germanium n changes little with temperature in the extrinsic range, as we saw from the analysis of the Hall effect. The dominant factor is thus the mobility, which is given by Eq. (20) for n-type extrinsic semiconductors. If the mean free path l is determined by collisions with the lattice as in a pure conductor, l should be inversely proportional to T and b should vary as $T^{-3/2}$. This variation is strong enough to overcome the decrease in n as the temperature decreases, and thus σ increases slowly as the temperature decreases, for the higher

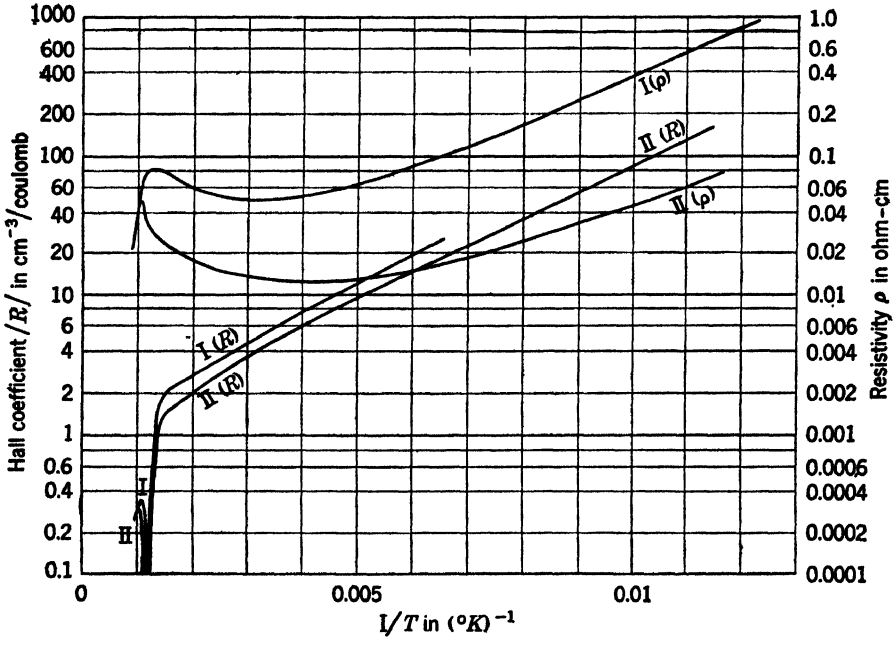

FIG. 3·5.—Resistivity ρ and Hall coefficient $|R|$ for two samples (I and II) as a function of temperature. P-type silicon; aluminum impurity.

temperatures of the extrinsic range. It is found in some samples, however, that σ at very low temperatures begins to *decrease* as the temperature decreases. This is explained by the fact that at low temperatures the mean free path is limited by collisions of the carriers with impurity atoms. Conwell and Weisskopf have shown[1] that the mean free path due to scattering by impurities decreases as the temperatures decrease. Lark-Horovitz and Johnson[2] have applied the theories of lattice scattering and impurity scattering and, in the case of germanium, have been able to

[1] E. Conwell and V. F. Weisskopf, "Theory of Impurity Scattering in Semiconductors," *Phys. Rev.*, **69**, 258 (1946).

[2] K. Lark-Horovitz and V. A. Johnson, "Theory of Resistivity in Germanium Alloys," *Phys. Rev.*, **69**, 258 (1946).

predict the observed temperature dependence of conductivity throughout the extrinsic range. They have used the measured Hall coefficients in conjunction with Eq. (25) to find the value of n and have calculated b from the theory. The agreement of the calculated and observed values of σ is excellent.

In Fig. 3·6 the resistivity $(1/\sigma)$ is plotted logarithmically against $1/T$ for a number of germanium samples. The identification of the samples is the same as for Fig. 3·4. As $1/T$ increases, that is, as the temperature decreases, the curves at first exhibit the large slope of the intrinsic range. At lower temperatures the resistivity decreases with temperature because

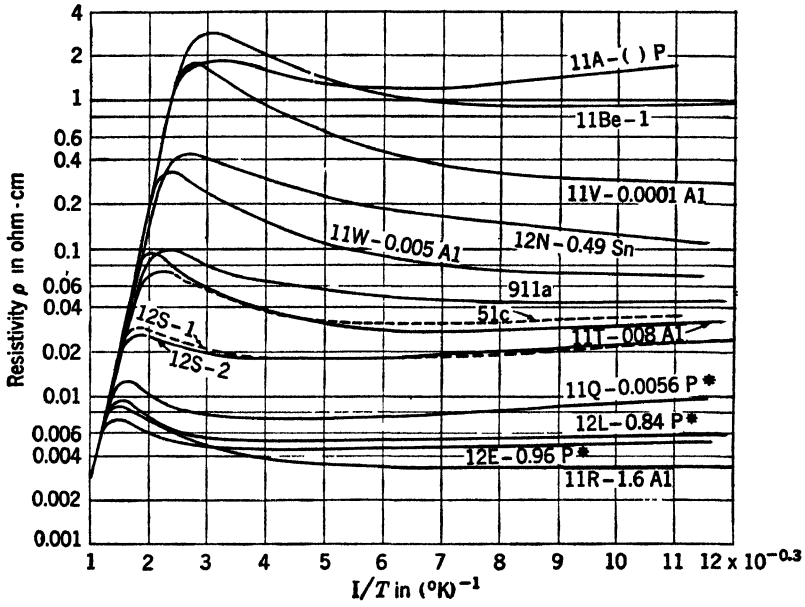

FIG. 3·6.—Resistivity ρ vs. reciprocal of absolute temperature for a number of samples of germanium.

of the dominance of lattice scattering, and at very low temperatures some of the curves begin to rise slowly with temperature because of the dominance (in this range) of impurity scattering.

Figure 3·7 shows the analysis made by Lark-Horovitz and Johnson of the resistivity curves of two samples of n-type germanium with antimony additions. The two samples differ only in the amount of impurity added. The curves for the Hall coefficients of the same two samples are shown in Fig. 3·8. Evidently sample 33E has about one-sixth the concentration of impurity levels found in sample 34E. The calculated curves for the separate effects of lattice and impurity scattering are shown as broken lines; their sum fits the experimental curves within experimental error. By an extension of their analysis, Lark-Horovitz and Johnson have been

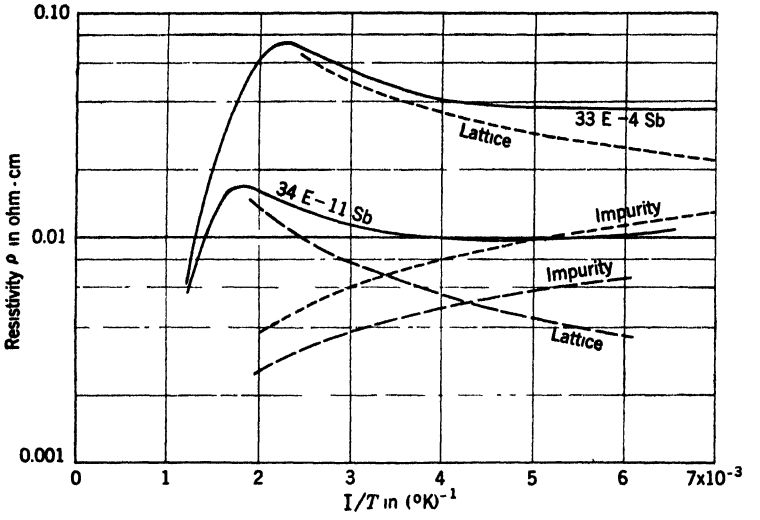

FIG. 3·7.—Analysis of resistivity at low temperatures for n-type germanium. The sum of lattice and impurity curves fit the corresponding experimental curves within experimental error.

——— experimental curves
..... calculated ρ_I, ρ_L for 33E
— — — calculated ρ_I, ρ_L for 34E

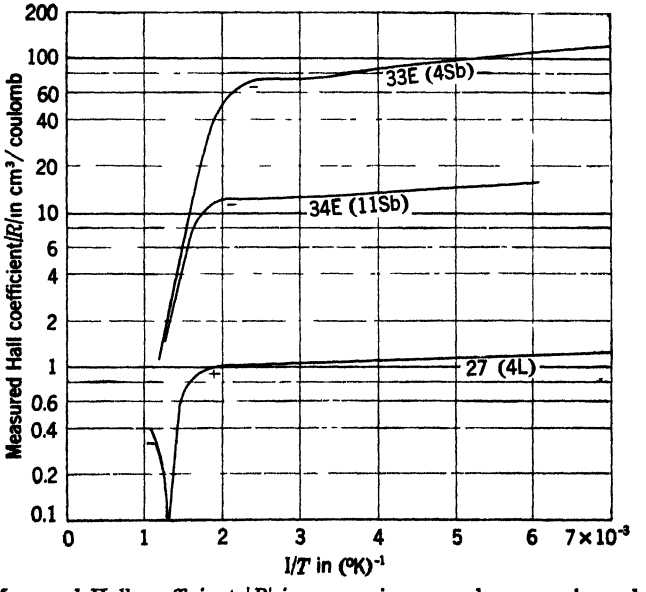

FIG. 3·8.—Measured Hall coefficient $|R|$ in germanium samples vs. reciprocal of absolute temperature.

able to fit the resistivity curves over the whole temperature range, including the intrinsic part.

In Fig. 3·5 the curves marked I(ρ) and II(ρ) show the dependence of resistivity on temperature for two samples of p-type silicon. Again three characteristic regions are shown. The chief qualitative difference between these curves and the corresponding curves for germanium samples is the more rapid increase of resistivity with cooling at low temperatures. As is evident from the curves of the Hall coefficient for the same two samples (Fig. 3·5) this increase is principally a result of the decrease in n_2 with cooling and is little affected (contrary to the case of germanium) by the dominance of impurity scattering at low temperatures.

Measurements of σ and R as a function of temperature for silicon and germanium have been made at Purdue University and at the University of Pennsylvania.[1] The curves reproduced here were provided by the Purdue group.[2]

3·5. Characteristic Constants of Silicon and Germanium. *Impurity Activation Energies.*—Among the physical quantities characteristic of silicon and germanium and of their impurity content are ΔE_1 and ΔE_2, representing, respectively, the depth of donator levels below the nearly empty band in the case of an n-type extrinsic semiconductor, and the height of the acceptor levels above the nearly full band in the case of a p-type extrinsic semiconductor. These quantities may be called the impurity activation energies.

As will be shown in Sec. 4·3, these quantities are of importance in the diffusion (thick-barrier) theory of rectification at all frequencies. They enter also into the diode (thin-barrier) theory of rectification in the case of high (microwave) frequencies, as shown in Sec. 4·6.

The impurity activation energy may be found, as shown in the previous section, from the dependence of Hall coefficient on temperature at low temperatures. In the case of germanium the magnitudes of ΔE_1 and ΔE_2 are so small that they are not easily measured by the slopes of the curves of $\log_{10} |R|$ vs. $1/T$, as is seen from Fig. 3·4. It will suffice for our present purposes, however, to know that ΔE_1 and ΔE_2 are small compared with kT in the case of germanium.

In the case of silicon the impurity activation energy is definite and measurable, as can be seen from the plot of the Hall coefficients in Fig. 3·5. For the two samples (both p-type) plotted there we obtain $\Delta E_2 = 0.081$ ev for sample I and $\Delta E_2 = 0.074$ ev for sample II. Both

[1] K. Lark-Horovitz, A. E. Middleton, E. P. Miller, and I. Walerstein, "Electrical Properties of Germanium Alloys, I. Electrical Conductivity and Hall Effect," *Phys. Rev.*, **69**, 258 (1946); and F. Seitz, "The Electrical Conductivity of Silicon and Germanium," NDRC 14-110, U. of Penn., Nov. 3, 1942.

[2] Private communication.

samples I and II have unknown amounts of aluminum additions, the amounts, however, being sufficient to give conductivities of the magnitudes desired for silicon as used in rectifiers.

Carrier Mobilities.—The mobility of the current carriers enters into the theory of rectification at high frequencies (see Sec. 4·6). Other factors being the same, the higher the mobility, the higher the rectification efficiency.

The mobility can be determined, as explained in Sec. 3·4, by combining data on Hall coefficient and on conductivity. Mobility is influenced both by the lattice and by the impurities. At high temperatures

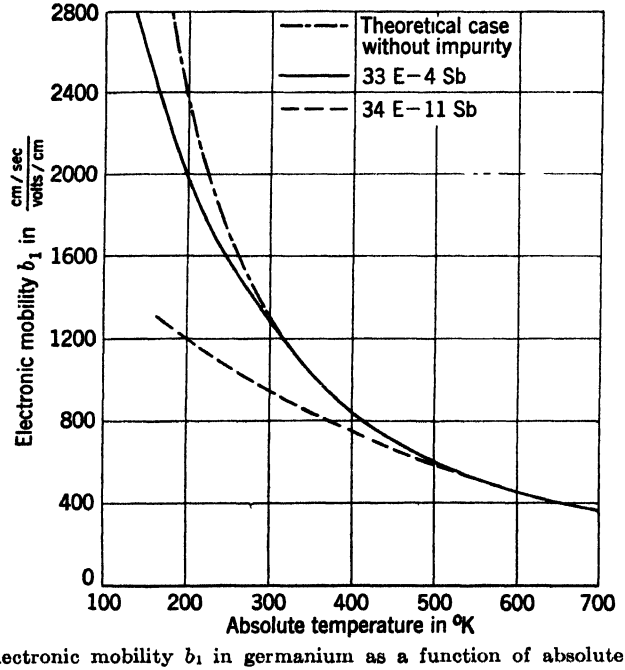

FIG. 3·9.—Electronic mobility b_1 in germanium as a function of absolute temperature.

lattice scattering is predominant and the mobility is proportional to $T^{-3/2}$. At low temperatures the influence of impurity scattering decreases the value of mobility from that given by the three-halves-power law. In Fig. 3·9 the temperature variations of mobility in two samples of germanium (the same samples plotted in Fig. 3·7) are shown and compared with the theoretical three-halves-power law for lattice scattering alone. It will be recalled that these two samples differ only in the amount of impurity. Figure 3·9 shows clearly the effect of impurity concentration on mobility. At high temperatures the three-halves-power law is obeyed for both samples; at low temperatures the departure from the theoretical curves is most pronounced for the sample of greater impurity concentration.

The contribution to mobility from lattice scattering alone may be written as

$$b_1 = \frac{B_1}{T^{3/2}}. \tag{31}$$

for n-type, with a similar expression with subscripts 2 for p-type. Lark-Horovitz and Johnson[1] have obtained for germanium $B_1 = 6 \times 10^6$ and $B_2 = 2 \times 10^6$, where b is measured in $\frac{\text{cm/sec}}{\text{volt/cm}}$ and T is in degrees Kelvin. Making use of Eq. (20) together with the theoretical expression for mean free path due to lattice scattering, it can be shown that

$$\frac{m_2}{m_1} = \left(\frac{B_1}{B_2}\right)^{3/5}, \tag{32}$$

which yields $m_2/m_1 = 1.6$ for germanium.

Only n-type germanium and p-type silicon are used in practical rectifiers. Probably owing in large part to the effectively larger masses of silicon holes over germanium electrons, the carrier mobility in p-type silicon is one-third or less than that in n-type germanium. As has already been mentioned, excellence of a rectifier depends strongly on magnitude of mobility. For this reason alone germanium might be expected to be preferable to silicon. However, other factors enter which mitigate this circumstance.

Mean Free Paths.—The mean free path of the current carriers is an important parameter in the theory of rectification. Besides entering into the mobility, Eq. (20), the magnitude of the mean free path (as compared with the thickness of the rectifying barrier), determines which of the several theories of rectification hold.

Since individual resistivities, the one arising from lattice and the other from impurity scattering, add to give the total resistivity, the corresponding mean free paths add by the reciprocal law

$$\frac{1}{l} = \frac{1}{l_I} + \frac{1}{l_L}, \tag{33}$$

where l_I and l_L are the mean free paths due respectively to impurity and to lattice scattering.

In Fig. 3·10, l_I and l_L are plotted as a function of temperature for three samples of germanium. The plot for l_L is the same for all samples, whereas the values of l_I, of course, depend on the amount of impurity. The total l, experimentally determined, is also plotted in each case. For most samples of germanium useful in rectifiers l will lie in the neighborhood of from 10^{-5} cm to 5×10^{-6} cm.

[1] Private communication.

No such extensive analysis of data is available for silicon at present, but the values of the total mean free path may be found from Hall and resistivity data. For the two samples shown in Fig. 3·5, we find $l = 1.0 \times 10^{-6}$ cm and 2.9×10^{-6} cm for samples I and II respectively. These values may be regarded as typical for samples of silicon useful in rectifiers.

Width of the "Forbidden" Region.—The separation of the nearly full band from the nearly empty band, that is, the width ΔE of the "forbidden" region in Fig. 3·3, is determined by the slopes of the $\log_{10} \sigma$ or $\log_{10} |R|$ curves vs. $1/T$ in the intrinsic regions, as explained in Sec. 3·4. In this way we find $\Delta E = 0.76$ ev in the case of germanium and $\Delta E = 1.1$ ev in the case of silicon.

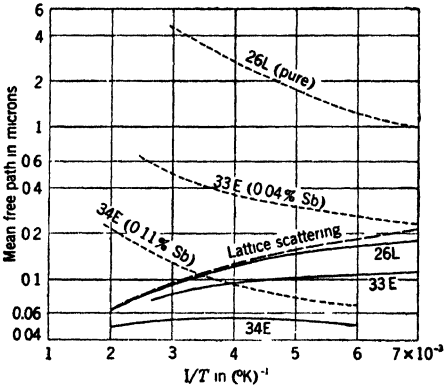

FIG. 3·10.—Electron mean free paths of a typical group of samples of germanium.

..... mean free path due to impurity scattering.
— — — mean free path due to lattice scattering (same for all samples).
——— effective mean free path due to combination of two types of scattering.

Although ΔE does not enter into the theories of rectification, it is probably of importance in the case of high-inverse-voltage rectifiers. It is possible that the existence of voltage peaks and negative resistance in the d-c characteristics of high-voltage rectifiers are ascribable in part to the onset of intrinsic conduction at the high power levels at which these effects occur (see Sec. 12·7).

3·6. Effect of Impurity Additions in Silicon and Germanium.—If it were possible to obtain perfectly pure silicon and germanium, so that even at normal temperatures ($\approx 300°$K) conduction would be purely intrinsic, the conductivity would be very low. By extrapolation of the intrinsic parts of the resistivity curves we find that the intrinsic contribution to conductivity at 300°K is about 10^{-6} mho/cm for silicon and 10^{-2} mho/cm for germanium. In either case the smallest observed conductivity for pure material is of the order of 10^{-2} mho/cm.

In studying the properties of these semiconductors much work has

been done on the effects of various addition agents. It is a striking fact that most impurities have the effect of making silicon extrinsically p-type and germanium extrinsically n-type. There are some notable exceptions to this rule, however. Thus boron, aluminum, gallium, and oxygen produce strong p-type conduction in silicon and weak p-type conduction in germanium, whereas nitrogen, phosphorus, arsenic, and antimony give strong n-type conduction in germanium and at least phosphorus produces n-type conduction in silicon. It is a general rule that elements in the third column of the periodic table tend to produce p-type conduction, and elements in the fifth column tend to produce n-type conduction in both materials.

It is not difficult to understand the reasons for this rule. Silicon and germanium are in the fourth column of the periodic table. They have four valence electrons and form tetrahedral bonds (diamond lattice). An element with three valence electrons and of about the same atomic dimensions would be expected to be able to substitute for a silicon or germanium atom in the lattice, accepting an electron from the filled band in order to complete the tetrahedral bond. A hole would thus be left in the filled band and would then either become bound to the impurity ion or would, as a result of thermal excitation, free itself and wander through the lattice, acting as a free carrier.

On the other hand an atom with five valence electrons (fifth column) would give up an electron as a result of the tetrahedral binding. This electron would either be bound to the ion or free itself to the conduction band.

Other elements may have analogous effects. For example, oxygen, being very electronegative, would be expected to act as an acceptor and produce hole conduction, as in fact it probably does. It probably, however, enters the lattice interstitially rather than substitutionally.

It is a remarkable fact that almost all impurities introduced into pure silicon or germanium give rise to extrinsic conductors of about the same activation energy (different, however, for the two semiconductors). This and the further remarkable fact that this energy in every case is very small (compared with the band separation) was explained by Bethe.[1] He pointed out that the impurity ion will attract the freed electron or hole and bind it in a coulomb field, independent of the ion and dependent only on the dielectric constant of the semiconductor.

Let us, for example, consider the case of a trivalent impurity such as aluminum. If the hole it produces just succeeds in freeing itself, it would have an energy at the top of the normally filled band. If, on the other hand, the hole is bound to the impurity ion, its energy will be

[1] H. A. Bethe, "Theory of the Boundary Layer of Crystal Rectifiers," RL Report No. 43-12, Nov. 23, 1942.

less and the corresponding acceptor level will lie above the top of the filled band by an amount determined by the binding energy of the hole. Classically the hole will describe an orbit about the negatively charged ion and its energy can be determined by the Bohr formula for the energy of the electron in a hydrogen atom. The interaction potential energy in the present case will be $e^2/\epsilon r$, where ϵ is the permittivity of the semiconductor. The Bohr formula must therefore be modified by replacing e (the electronic charge) by $e/\sqrt{\epsilon/\epsilon_0}$. This modification leads to the energy

$$\Delta E_2 = -\frac{R_y \epsilon_0^2}{\epsilon^2 n^2}, \tag{34}$$

where R_y is the Rydberg energy (13.5 volts) and n the quantum number ($n = 1, 2, 3, \cdots$). The acceptor level therefore lies an amount ΔE_2 above the filled band.

According to Eq. (34) there should be an infinite series of levels, $n = 1$ to ∞. This, however, is not actually the case because of the large dimensions of the orbits obtained for $n > 1$. Already for $n = 1$ the radius of the orbit is ϵ/ϵ_0 times the Bohr radius, or 7×10^{-8} cm for $\epsilon/\epsilon_0 = 13$. The radius increases as n^2 and is therefore 3×10^{-7} cm for $n = 2$. With $5 \times 10^{+18}$ impurities per cubic centimeter, their mean distance apart is about 7×10^{-7} cm. A hole that is 3×10^{-7} cm from a certain negative ion is therefore just as near to a neighboring ion and is not subject to the coulomb force of one ion, but rather to the forces of many. This means that the discrete state $n = 2$ does not actually exist but is absorbed in the continuum. An ion, therefore, produces only one level and this is separated from the band by the energy ΔE_2 of Eq. (34) with $n = 1$. The energy ΔE_2 on this basis turns out to be 0.08 ev which is about the value observed in the case of silicon. From this discussion it is evident that the positive ions, instead of producing additional levels ($n = 2, 3, \cdots$), actually raise the upper limit of the filled band. This effect should lower ΔE_2 to perhaps 0.04 to 0.06 ev.

This discussion has been illustrated by an example of a negative ion and positive hole (p-type extrinsic semiconductor). The same arguments apply to the case of a positive ion and an electron except that now the electron level lies just below the conduction band. The estimated value of ΔE_1 is, however, the same as ΔE_2.

Experimentally, ΔE_1 (or ΔE_2) is 0.02 ev or less in the case of germanium and about 0.08 ev in silicon. Bethe's theory thus gives the right order of magnitude although the difference between germanium and silicon is not explained.

This section concludes with remarks concerning the efficiency of various addition agents.

It has been found that although many addition agents will produce

conductivities of the desired order (10 to 100 mho/cm) only a few produce good stable rectifiers. Thus, aluminum and boron have been found to be best for silicon, and phosphorus and antimony are superior for germanium.[1] Boron has the remarkable property (unique among all addition agents) that, in the case of silicon, an extremely small amount ($\approx$ 0.001 per cent) is sufficient to produce the desired conductivity.

Aluminum and beryllium added to silicon in small quantities have the desirable feature of increasing the hardness and toughness of the ingot. Furthermore, they serve to improve the resistance to burnout. Accordingly, the combination boron-beryllium in approximate per cent by weight, 0.002 and 0.02 respectively, added to pure duPont silicon, was found at Radiation Laboratory to produce superior ingots. In this case almost all the conductivity is supplied by the boron.

It is noteworthy that the impurity additions best for silicon are as a general rule worst for germanium; the reverse is also true.[1] Thus silicon, as used for rectifiers, is always p-type (hole conductor), whereas germanium is always n-type (electron conductor).

[1] These remarks do not apply to high-inverse-voltage rectifiers (see Chap. 12).

CHAPTER 4

THE SEMICONDUCTOR—METAL CONTACT

This chapter treats of the process of rectification[1] at the contact between a metal and a semiconductor. The barrier-rectification process will be described qualitatively and it will then be shown how the conditions necessary for rectification are obtained at a metal-semiconductor contact. The *sine qua non* for rectification is the existence of a barrier layer at the contact. The structure of this layer and its modifications are examined in some detail. Finally the special circumstances of rectification at high frequencies are considered.

4·1. Barrier-layer Rectification.—The rectification process in crystals takes place in the immediate vicinity of the metal-semiconductor contact,

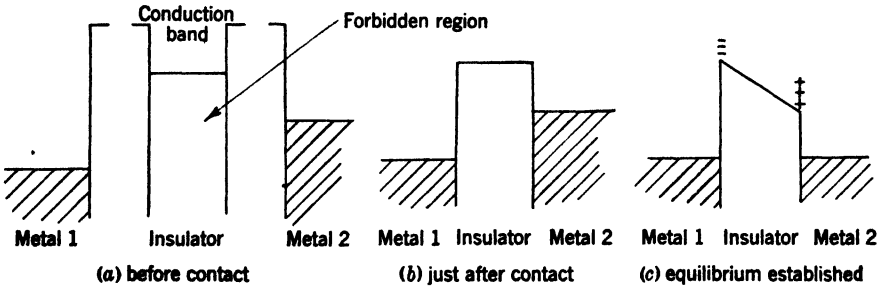

FIG. 4·1.—Formation of a rectifying barrier between two metals of different work function.

in fact, within a few hundred or thousand atomic diameters of the contact surface. In this region there exists a potential barrier or "hump" of potential energy. Rectification is believed to be a result of the asymmetrical distortion of this hump by the applied potential.

Semiconduction is not at all essential for rectification and the only excuse for the use of semiconductors is that the required barrier is easily and naturally formed at a metal-semiconductor contact. Under certain conditions, however, a similar potential barrier may be formed between two metals that differ in surface work function; the barrier will then rectify. Since this process is somewhat easier to understand than metal-semiconductor rectification, a brief sketch of it is given first.

[1] The term "rectification" implies a current-voltage characteristic asymmetrical with respect to the voltage, that is, $|I(+v)| \gg |I(-v)|$. This condition applies also in the case of frequency conversion.

Figure 4·1*a* shows the customary potential-energy diagram[1] of two metals of different work functions not in contact. Let us suppose that between them there is a thin wall of a crystalline insulator with filled and empty electronic bands. Immediately after contact has been made the situation is as shown in Fig. 4·1*b*. There will result a net electron flow from metal 2 to metal 1 because there are more electrons near the top of the barrier in metal 2 than in metal 1. This flow will persist until a surface double layer of charge is established; this double layer depresses the electron levels of metal 2 relative to those of metal 1, bringing the tops of the Fermi distributions of the two metals to the same level. At this point no further net flow occurs and we have a state of equilibrium (Fig. 4·1*c*).

The result of applying an external voltage (smaller in magnitude than the work-function difference) in the direction which raises the

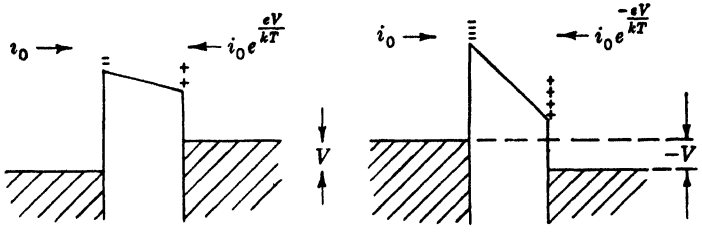

(*a*) Voltage applied in forward direction (*b*) Voltage applied in back direction

FIG. 4·2.—Rectification at a metal-metal contact.

electron levels in metal 2 relative to those of metal 1 is shown in Fig. 4·2*a*; the result of applying a voltage in the opposite direction is shown in Fig. 4·2*b*. In either case there is no change in the height of the barrier as viewed from metal 1 (metal of higher work function) but the height of the barrier, viewed from metal 2 (metal of lower work function), increases linearly with applied voltage V. Thus in neither case will there be a change in the number of electrons flowing from metal 1 across the barrier to metal 2, but the flow from metal 2 to metal 1 (and hence the net current) does vary with voltage. If the energy distribution of electrons (that is, the number of electrons per unit energy range) in metal 2 were constant for energies above the Fermi surface, there would be no rectification, and the contact would be ohmic (current proportional to voltage). This electron distribution, however, is not, in fact, constant, but nearly exponential (Boltzmann law); hence the current is nonlinear with voltage, the barrier is nonohmic, and rectification is possible.

From the above example it can be seen that large net currents flow

[1] F. Seitz, *The Modern Theory of Solids*, McGraw-Hill, New York, 1940, Sec. 26.

when the electron energy levels of metal 2 (low work function) are raised relative to those of metal 1 (high work function) by the applied potential, that is, by making metal 1 anodic and metal 2 cathodic. A voltage so applied is said to be in the "forward" direction; an opposite voltage is said to be in the "reverse" or "blocking" direction.

The simple example given reduces the general problem of rectification to its bare essentials. The more interesting case, however, in which one of the metals is replaced by a semiconductor and the insulating layer is absent, differs only in degree and not in kind from this simple case.

The simple case, however, is not entirely academic in interest. It should be possible to make metal-insulator-metal rectifiers with much smaller spreading resistances than metal-semiconductor rectifiers have, consequently giving greater rectification efficiency at high frequencies (see Sec. 4·6). Attempts thus far to construct workable metal-insulator-metal rectifiers have not been successful, but in view of their possible advantages further research is desirable.

4·2. Formation and Structure of the Barrier Layer.—It was shown in the preceding section how rectification is accomplished with the aid of a barrier layer between materials of different work functions. The nature of the barrier layer formed in the vicinity of a metal-semiconductor contact, will now be examined.

The equilibrium between the electrons of a metal and those of a semiconductor is governed by the equality of the electron chemical potential in the two materials. This condition, it has been noted, requires that all electron levels in the semiconductor be depressed by the amount $e\phi_{xm}$ relative to those of the metal. Expressions for $e\phi_{xm}$ are given by Eqs. (3·14) to (3·18) for the various cases of interest.

In this chapter we shall not be concerned with *intrinsic* semiconduction since, in the case of silicon and germanium, this occurs only at elevated temperatures and would in any case result in poor rectification because of the equal numbers of electrons and holes. For *extrinsic* semiconduction an approximation useful for the present purpose is found by ignoring terms of order kT in $e\phi_{xm}$, since these terms are small compared with the contact potential difference in all cases of interest. Thus, from Eqs. (3·15 to 3·18) we get

(1) n-type extrinsic (all values of n_1),

$$-e\phi_{xm} \approx -e\phi_0 \equiv \chi_2 - \chi_m = W_s - \chi_m; \tag{1}$$

(2) p-type extrinsic (all values of n_2),

$$-e\phi_{xm} \approx -e\phi_0 \equiv \chi_4 - \chi_m = W_s + \Delta E - \chi_m. \tag{2}$$

(See Fig. 3·3 for an explanation of the symbols used.) Terms in ΔE_1

and ΔE_2 have been neglected in Eqs. (1) and (2) since, as Sec. 3·3 made clear, these quantities for normal silicon and germanium are of order kT.

Figure 4·3*a* shows the energy relation for separated metal and semiconductor (n-type). Figure 4·3*b* gives the configuration after contact is made and before equilibrium is established. This situation does not persist long. Electrons begin to flow from the semiconductor into the metal and establish a negative surface charge density on the metal surface. An equal residuum of positive charge resides near the surface of the semiconductor, distributed over a region of thickness D. This positive charge is contributed by the ionized impurity levels. The net effect of the double layer is to lower all electron energy levels in the bulk semiconductor by the amount given by Eq. (1), which can now be taken as the difference in work functions of the metal and semiconductor. Figure 4·3*c* shows the resulting configuration. It is evident that the result of the double layer is to bring the bottom of the conduction band in the bulk semiconductor down to about the level of the top of the Fermi distribution in the metal. Between the metal and bulk semiconductor is a barrier layer of height $e\phi_{xm} = \chi_m - W_x$ and width D. The latter quantity is clearly determined by the positive-charge density in the semiconductor which, in turn, is determined by the density of impurity levels near the surface of the semiconductor.

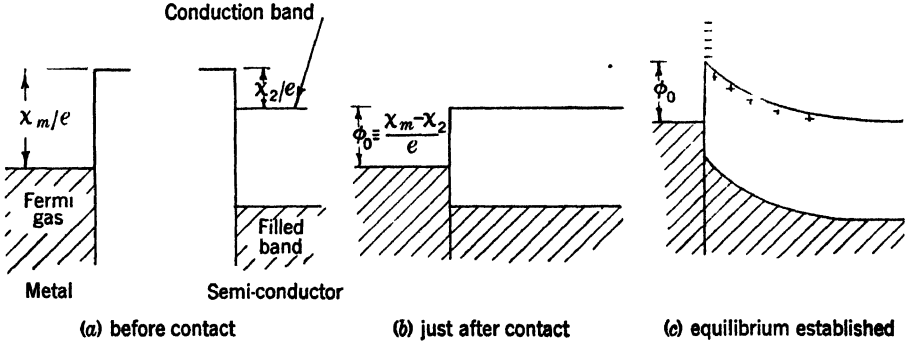

FIG. 4·3.—Formation of a rectifying barrier between a metal and a semiconductor.

For a p-type extrinsic semiconductor the situation is closely similar. Figure 4·4 shows the final configuration in this case. The barrier now impedes the flow of holes and the double layer is reversed in sign.

It should be noted that, in the case of Fig. 4·3 $\chi_m > W_x$, and in the case of Fig. 4·4, $\chi_m < W_x + \Delta E$. If these inequality signs were reversed, no barrier would be erected. In either case the flow of current would be unimpeded and ohmic. Rectification is possible, therefore, only if

$$\chi_m > W_x \qquad \text{for } n\text{-type,} \tag{3}$$

$$\chi_m < W_x + \Delta E \qquad \text{for } p\text{-type.} \tag{4}$$

It is clear that the same metal and the same semiconductor with different types of impurities are capable of satisfying both Eqs. (3) and (4). This deduction is in accord with the observed fact that both silicon and germanium, properly "doped," are capable of giving n-type or p-type rectification in conjunction with the same metal.

Rectification is accomplished in much the same manner as by the barrier between the two metals of different work functions discussed in the preceding section. Figure 4·5a shows the configuration of the metal-semiconductor barrier when a voltage is applied in the forward direction (direction of easy flow). The height of the barrier, viewed from the metal, is still given by ϕ_0, the contact potential difference. Thus the number of electrons traversing the barrier from metal to semiconductor is a constant independent of the applied voltages. On the other hand, the electron levels in the semiconductor have been raised by the amount eV, where $-V$ is the applied voltage; hence the height of the barrier, viewed from the semiconductor, has decreased by eV. The "slack" has been taken up by a decrease in barrier space charge because of a flow of electrons into the barrier. Since the electron energy distribution in the semiconductor is exponential above the bottom of the conduction band, the electron current from semiconductor to metal increases exponentially with V.

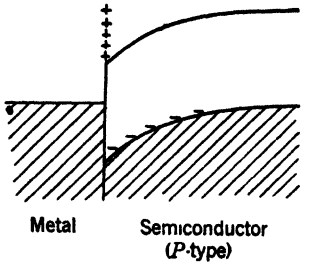

FIG. 4·4.—Barrier between a metal and a p-type semiconductor.

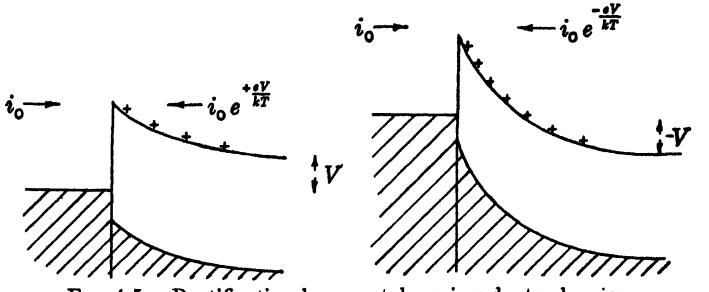

FIG. 4·5.—Rectification by a metal-semiconductor barrier.

Figure 4·5b shows the configuration of the barrier with a voltage applied in the blocking direction. Again the barrier height, viewed from the metal side, and also the electron flow from metal to semiconductor have not been changed by the applied voltage. The barrier height, viewed from the semiconductor, has increased and the electron flow from semiconductor to metal has decreased.

Let us now examine in more detail[1] the structure of the barrier layer.

[1] For the following theory of a natural "dielectric" barrier, see further, H. A.

The shape of the barrier is related to the space charge by Poisson's equation,

$$\frac{dE}{dx} = \frac{e}{\epsilon}(n_+ - n_-), \tag{5}$$

where E is the electric field intensity, ϵ is the permittivity of the semiconductor, e is the electronic charge, and n_+ and n_- are, respectively, the number densities of positive and negative charges. The discussion will be confined to an n-type extrinsic semiconductor. Then n_- is taken to be the number density of free electrons and n_+, the number density of ionized donators. The notation of Fig. 4·5 is used: $e\phi_0$ is the difference of work functions, and the height of the barrier as viewed from the metal. If $e\phi$ is the potential energy of an electron and $-V$ is the applied voltage, then

$$E = \frac{d\phi}{dx}. \tag{6}$$

A potential of order kT/e or larger above the potential of the bulk semiconductor is sufficient to remove nearly all the electrons from the donators and to reduce the electron density to a value small compared with that of the positive charges. Now kT/e is only 0.026 volt at room temperature, very small compared with the potential difference ϕ_0 ($\approx$ 0.5 volt). Therefore, over most of the potential curve of the barrier it may be assumed that $n_+ = N$ and $n_- = 0$, where N is the donator density. Thus the charge density in the barrier is constant and equal to Ne. Poisson's equation then simplifies to

$$\frac{d^2\phi}{dx^2} = \frac{eN}{\epsilon}. \tag{7}$$

Now, Eq. (7) is integrated with the boundary conditions,

$$\begin{aligned} \phi = V, \quad \frac{d\phi}{dx} = 0 \quad &\text{at } x = D; \\ \phi = \phi_0 \quad &\text{at } x = 0; \end{aligned} \tag{8}$$

where D is the thickness of the barrier, that is, the layer in which the charge of the donators is not neutralized by electrons. Thus,

$$\phi = V + \frac{en}{2\epsilon}(D - x)^2 \tag{9}$$

with

$$D = \left[\frac{2\epsilon(\phi_0 - V)}{eN}\right]^{1/2}. \tag{10}$$

Bethe, "Theory of the Boundary Layer of Crystal Rectifiers," RL Report No. 43-12, Nov. 23, 1942.

As an example, if $V = 0$, $\phi_0 = 0.5$ volt, $\epsilon = 13\epsilon_0$, and $N = 5 \times 18^{18}$ cm^{-3}, we find that

$$D = 1.2 \times 10^{-6} \quad \text{cm}, \tag{11}$$

which is comfortably large in comparison with the interatomic distance. The value assumed here for N, 5×10^{18} cm^{-3}, is fairly typical of representative samples of silicon and germanium. The value 13 assumed for ϵ/ϵ_0 is in accord with the spectroscopic data[1] for silicon and cannot be much different in the case of germanium. The value of the potential difference ($\phi_0 = 0.5$ volt) is in approximate accord with measurements of Meyerhof[2] for silicon against tungsten. Variations in these assumed values will not in any case change the result much because of the square-root dependence of D.

It is evident, therefore, that a "natural" barrier layer will be of the order of magnitude of 10^{-6} cm thick in the case of silicon and germanium. As will be seen later, a barrier of almost this thickness is needed in order to account for observed barrier capacitance.

Image Force.—The quantity ϕ gives only the potential of an electron in the electrostatic field of the surface. It does not take into account the image force acting on the electron. Including the image force, the potential[3] is

$$W = \phi - \frac{e}{4\epsilon x}. \tag{12}$$

With the constants as chosen, the maximum of the potential W occurs close to the metal surface, that is, at a distance $x \ll D$. If x^2 is neglected in Eq. (9), the maximum of W is found to lie at

$$x_m = \left(\frac{eD}{8\epsilon\phi_0}\right)^{1/2}, \tag{13}$$

and has a value,

$$W_m = \phi_0 - \left(\frac{2e\phi_0}{\epsilon D}\right)^{1/2} = \phi_0 - \left(\frac{2e^3N\phi_0}{\epsilon^3}\right)^{1/4}, \tag{14}$$

for the case of zero bias ($V = 0$). For the values of the constants as above,

$$x_m = 0.05D = 6 \times 10^{-8} \quad \text{cm},$$
$$W_m = 0.40 \quad \text{volt}.$$

It is seen that x_m/D is small; hence the image force does not seriously affect the potential barrier. This result, however, is intimately con-

[1] J. F. Mullaney, *Phys. Rev.*, **66**, 326 (1944).

[2] W. E. Stephens, B. Serin, and W. E. Meyerhof, *Phys. Rev.*, **69**, 42 (1946).

[3] See, for example, F. Seitz, *The Modern Theory of Solids*, McGraw-Hill, New York, 1940, pp. 162, 163.

nected with the high dielectric constant chosen, which has the effect of increasing the thickness of the barrier layer [Eq. (10)] and reducing the image-force lowering [Eq. (14)]. Indeed, were it not for such a high dielectric constant, rectification by a natural barrier layer would be very poor, if not impossible.

Natural vs. Artificial Barriers.—This conclusion does not, of course, rule out the possibility of an artificial barrier layer. In fact there is reason to believe that the density of donators is somewhat reduced below the bulk value near the surface of the semiconductor in the case of modern silicon rectifiers. The following section treats the possibility of this *depletion layer*. Such a layer would have the desirable property of increasing the thickness of the barrier (as $1/\sqrt{N}$) and reducing the effect—always undesirable—of image force. Furthermore, it is not at all certain that there is not a surface layer of some foreign material, such as oxygen or quartz, between the metal and semiconductor. Such a layer would at least change the work function of the semiconductor and might even be thick enough to provide a substantial barrier. However, as Seitz[1] has pointed out, quartz does not possess any electronic energy bands near the conduction band of silicon, and thus electrons could penetrate only by the "tunnel" effect. A quartz layer as thin as 10^{-7} cm would be practically impenetrable to electrons. On the other hand, a layer 10^{-7} cm thick is negligible compared with the natural layer already present (10^{-6} cm).

It seems reasonable, therefore, to conclude that the barrier layer in silicon and germanium is *natural* in the sense that it consists of the material of the semiconductor, but possibly *artificial* in the sense that the concentration of donator levels may be somewhat less than in the bulk semiconductor.

Capacitance of the Barrier Layer.—When an alternating field is applied to the contact, the barrier is alternately charged and discharged by the flow of electrons from the semiconductor in and out of the barrier. Let us assume that time effects resulting from recombination and ionization of the donators can be neglected. They certainly can be neglected if it is assumed that the donators are completely ionized in the bulk semiconductor. Their neglect is approximately valid in any case at low frequencies. (The high-frequency case will be discussed in Sec. 4·6.) For small amplitudes of the applied voltage the barrier acts as a condenser with capacitance

$$C = -A\frac{dq}{dV}, \tag{15}$$

where A is the area of the contact, q is the total surface charge, and $-V$

[1] F. Seitz and S. Pasternack, "The Principles of Crystal Rectifiers," NDRC 14-102, U. of Penn., June 10, 1942.

is the applied voltage. The surface charge q is given by

$$q = NeD(V), \tag{16}$$

where the thickness D depends on the applied potential $-V$ in accordance with Eq. (10). Then,

$$C = \frac{A\epsilon}{D}, \tag{17}$$

which incidentally is the same as the capacitance of a parallel-plate condenser of area A and thickness D.

This capacitance effectively shunts the nonlinear resistance of the barrier. Its value is not constant with applied potential. In fact, from Eqs. (10) and (17),

$$C \propto \frac{1}{\sqrt{\phi_0 - V}}. \tag{18}$$

Comparison of Theoretical and Experimental Barrier Capacitance.– Measurements of C provide the best experimental data for the barrier thickness D. There are two general methods for measuring C. One is a direct measurement of the impedance of the rectifier. The barrier capacitance is then inferred from the impedance, suitable account being taken of such extraneous effects as the whisker inductance, stray capacitances, etc. These measurements are usually made at frequencies of the order of magnitude of 10 Mc/sec, since it is easier to take account of extraneous impedances at frequencies of this order than at frequencies in the microwave range. A common technique is to measure the impedance of a crystal cartridge just before and then after contact is made between the whisker and semiconductor.

The second method assumes the equivalent circuit of Fig. 2·10 for the rectifier and compares low-level rectification efficiency at audio and at microwave frequencies. From the difference one can compute C. This method is described more fully in Sec. 11·5.

The two methods agree only in order of magnitude, the second method generally giving lower values of contact capacitance than the first. The difference is probably due to relaxation effects in the barrier (see Sec. 4·5).

In one case[1] after the capacitance of a silicon-tungsten contact had been determined by the bridge method at zero bias and at 14 Mc/sec, the diameter of the contact was found to be 1.2×10^{-3} cm. Substitution in Eq. (17), assuming $\epsilon = 13\epsilon_0$, gave $D = 2 \times 10^{-6}$ cm. This value is to be regarded as an upper limit, since the computation assumes that the whole area of the whisker point was in intimate contact with the silicon.

[1] See A. W. Lawson, P. H. Miller, L. I. Schiff, and W. E. Stephens, "Barrier Capacity in Silicon Cartridge Rectifiers," NDRC 14-140, U. of Penn., May 1, 1943.

The value obtained is therefore in satisfactory agreement with the theoretical value of D, viz., 1.2×10^{-6} cm.

Measurements of variation of barrier capacitance with bias do not agree well with the square-root law, Eq. (18). Bridge measurements tend to show a very rapid increase of capacitance in the forward direction. Increases by a factor of 100 have been observed[1] for silicon units when the applied voltage was changed from 0 to 0.5 volt (across the whole unit). It should be noted, however, that it is exceedingly difficult to separate resistance and reactance effects in such measurements. These results must be regarded as tentative. The measured values at zero bias, however, should be fairly reliable, since the barrier resistance in this case is large ($\approx$ 5000 ohms) compared with the barrier-capacitive reactance ($\approx$ 50 ohms). At moderately small ($\approx$ 0.5 volt) inverse voltages, the bridge results show a small decrease in the capacitance, as is to be expected from Eq. (18). At higher inverse voltages ($\approx$ 1.0–2.5 volts) the capacitance increases, but this may be a spurious effect.

The rectification-efficiency method does not agree with the bridge method with regard to variation of capacitance with bias. In general, the former method results in a fairly constant value in the inverse direction and a small rise for silicon crystals in the forward direction. Quantitative comparison with Eq. (18) is difficult, but, for silicon, disagreement is not indicated. In the case of germanium, however, observations[2] using the rectification-efficiency method have shown considerably larger increases of capacitance with forward bias than can be accounted for by Eq. (18). This circumstance is helpful, however, in understanding the negative i-f conductance of welded-contact germanium rectifiers (Secs. 13·5 and 13·6).

4·3. Diffusion and Diode Theories of Rectification.—A qualitative picture of barrier-layer rectification was presented in Sec. 4·1. The quantitative theoretical treatment is considerably affected by the value assumed for the barrier thickness. There are three distinct cases of interest, corresponding to very thin, intermediate, and very thick barriers. A very thin barrier ($\approx 10^{-7}$ cm) offers the possibility of electron transit by means of the well-known quantum-mechanical "tunnel" effect.[3]

The first theory of barrier-layer rectification, developed independently in 1932 by Wilson, by Nordheim, and by others, was based on the tunnel effect.[4] This theory was accepted for a number of years until it was

[1] *Ibid.*

[2] R. N. Smith, "Determination of Crystal Parameters at Microwave Frequencies" (Crystal Rectifier Conference), Columbia U., Sept. 11, 1943.

[3] This effect is closely similar, in general principles, to the propagation of electromagnetic energy through waveguides below cutoff.

[4] See A. H. Wilson, *Proc. Roy. Soc.*, **136**, 487 (1932); and L. W. Nordheim, *Zeits. f. Phys.*, **75**(7–8), 434 (1932).

realized that it predicted rectification in the wrong direction. Furthermore, there was good evidence that the barrier is considerably thicker than 10^{-7} cm for this and other rectifiers.

The defects of the tunnel theory led Mott[1] in 1939 to propose a thick-barrier theory. He supposed (as we did in Sec. 4·1) that electrons were able to surmount the barrier primarily by thermal excitation. His theory was oversimplified by the assumption that the electric-field intensity E was constant in the barrier layer (absence of space charge). Schottky[2] was able to free the theory from this arbitrary assumption. He considered two extreme cases, "exhaustion layers" and "reserve layers." In an exhaustion layer the impurities are considered to be completely ionized in the layer itself, although not necessarily in the bulk semiconductor. The case of an exhaustion layer was discussed in Sec. 4·2. A reserve layer is complicated by the incomplete ionization of impurities and does not concern us here, since, as was pointed out in Sec. 3·7, impurities are 20 to 40 per cent ionized in bulk silicon and nearly completely ionized in bulk germanium. Thus only a small rise in potential energy above the bulk value will in either case shift the equilibrium to complete ionization.

Both Mott and Schottky assume barriers thick compared with the mean free path of the carriers, an assumption in accord with measured values of 10^{-5} to 10^{-4} cm for the barrier thickness in copper-cuprous oxide and in selenium rectifiers. Since collisions occur in the barrier, one is forced to treat the flow of current in the barrier as a statistical problem involving detailed balance.

A barrier of intermediate thickness ($\approx 10^{-6}$ cm), that is, thick enough to reduce the number of electrons penetrating the barrier by the tunnel effect to a value small compared with the number surmounting the barrier by thermal excitation yet still thin enough so that collisions within the barrier can be ignored, is a much simpler problem. In this case there is an analogy to the motion of electrons in a vacuum-tube diode. The carriers must have sufficient energy to surmount the potential barrier (analogous to the work function of the cathode of a diode). They will then fly over the barrier unimpeded and make their next collision in the metal (analogous to the anode of a diode). Because of these similarities the theory of a barrier of intermediate thickness is commonly referred to as the "diode theory."

The Diffusion Theory.—The thick-barrier, or diffusion, theory does not appear to apply to ordinary silicon and germanium mixer rectifiers, since, as we have seen in Sec. 4·2, their barrier thickness is of the order of 10^{-6} cm, which is less than the mean free path of the carriers. The

[1] N. F. Mott, *Proc. Roy. Soc.*, **A171**, 27 (1939).

[2] W. Schottky and E. Spenke, *Wiss. Veroff. Siemenswerke*, **18**, 225 (1939).

barrier thickness of high-inverse-voltage rectifiers has not yet been determined by capacitance measurements, but it is difficult to understand how a high inverse resistance can be maintained at applied potentials of 100 volts or more (as is observed for these rectifiers) by a barrier thinner than 10^{-5} cm.

The fundamental equation governing diffusion theory[1] is

$$j = ebnE \pm bkT\frac{dn}{dx}. \tag{19}$$

The symbols have the following meaning: j is the current density; e, the absolute value of the electronic charge; n, the density of free electrons or holes; E, the electric field intensity; b, the carrier mobility; k, Boltzmann's constant; T, the absolute temperature; and x, the one-dimensional space coordinate. The plus sign holds for electron conduction (n-type extrinsic), and the minus sign for hole conduction (p-type extrinsic). This law is valid if the mean free path is small compared with the distance over which the potential energy changes by an amount kT. The current density j is seen to be composed of two parts: one $ebnE$ gives the ohmic dependence of current on field intensity, and the other $\pm bkT(dn/dx)$ gives the contribution of diffusion resulting from the gradient in carrier density dn/dx.

If $j = 0$, Eq. (19) integrates at once to give the usual Boltzmann law,

$$n = \text{const} \times e^{\pm\frac{e}{kT}\int_0^x E\,dx}. \tag{20}$$

For $j \neq 0$, the equation can still be formally integrated, but, to get a useful result, the dependence of E on n must, in general, be taken into account. For the case of an exhaustion layer, E will be independent of n, but in the case of a reserve layer it has a complicated dependence on n. The latter dependence is given by the Poisson equation [Eq. (5)], in which we can put $n_- = n$. The quantity n_+ depends on n since they are related by the equilibrium of the reaction,

$$\text{Bound electron} \rightleftarrows \text{bound hole} + \text{free electron}.$$

The relation between the number of free electrons n, bound holes n_+, and bound electrons $N - n_+$ (N is the donator density) is given by

$$\frac{nn_+}{N - n_+} = K, \tag{21}$$

where K is the equilibrium constant of the reaction. In the bulk semiconductor, $n_+ = n$, and comparing Eq. (21) with Eqs. (1) and (2)

[1] See N. F. Mott and R. W. Gurney, *Electronic Processes in Ionic Crystals*, Oxford, New York, 1940, Chap. 5, Eq. 30.

we get

$$K = 2\left(\frac{2\pi m_1 kT}{h^2}\right)^{\frac{3}{2}} e^{-\frac{\Delta E_1}{kT}}. \tag{22}$$

Fortunately the complications of a reserve layer do not appear to apply to germanium and silicon.

Since diffusion theory has limited, if any, application to silicon and germanium rectifiers, it will suffice to illustrate it by integrating Eq. (19) for the special case (assumed by Mott) of zero space charge in the barrier. This should apply, then, to an artificial insulating barrier. From Eq. (5) we see that zero space charge implies constant E. Then Eq. (19) is integrated at once to

$$n(x) = \frac{j}{ebE} + \left[n(0) - \frac{j}{ebE}\right] e^{\frac{eEx}{kT}}. \tag{23}$$

At $x = D$ we assume that we pass abruptly to the properties of the bulk semiconductor, so that $n(D) = n(\infty)$. Mott and Schottky assumed[1] that $n(0)$ is given by the number density of electrons in the metal at the potential ϕ_0 above the surface of the Fermi distribution and is independent of j. Putting $j = 0$ and $x = D$ in Eq. (23), we obtain

$$n(0) = n(D)e^{-\frac{eED}{kT}} = n(\infty)e^{-\frac{e\phi_0}{kT}}. \tag{24}$$

Noting that $eED = \phi_0 - V$, substituting Eq. (24) in Eq. (23), and solving for j, we obtain

$$j = [en(\infty)bE]\frac{1 - e^{-\frac{eV}{kT}}}{1 - e^{-\frac{e(\phi_0 - V)}{kT}}}. \tag{25}$$

Since, in general,

$$e^{\frac{e(\phi_0 - V)}{kT}} \gg 1,$$

we obtain finally

$$j = ebn(\infty)E \cdot e^{-\frac{e\phi_0}{kT}}(e^{\frac{eV}{kT}} - 1). \tag{26}$$

The exponential factor dominates the weak dependence of E on V, hence Eq. (26) may be written approximately as

$$j = A(e^{\alpha V} - 1), \tag{27}$$

where A and α are constants. Equation (27) is a general result (in the

[1] It has been shown by R. G. Sachs, "The Diffusion Theory of Crystal Rectifiers," NDRC 14-129, Purdue U., Sept. 10, 1942, that $n(0)$ is not really independent of j and that in certain circumstances a term j/ev should be added to the right-hand side of Eq. (24) where v is the mean thermal velocity of the bulk electrons. This refinement will not be introduced here.

first approximation) of all theories of contact rectification and will be compared with experiment in Sec. 4·4.

The Diode Theory.—If there is assumed a barrier thin compared with the mean free path, collisions in the barrier layer can properly be neglected. The electron distribution is then given by the Maxwell-Boltzmann law based on the bulk properties of the semiconductor. Thus, if we now write n for the number of carriers per unit volume in the bulk semiconductor, we have for dn, the number of carriers per unit volume crossing unit area per second in the $-x$ direction with velocity between v and $v + dv$,

$$dn = n\left(\frac{m}{2\pi kT}\right)^{1/2} e^{-\frac{mv^2}{2kT}} v\, dv. \tag{28}$$

The number of carriers with sufficient kinetic energy η to surmount the barrier is

$$\int_{e(\phi_0 - V)}^{\infty} \left(\frac{dn}{d\eta}\right) d\eta = \frac{1}{2} n\bar{v} e^{-\frac{e(\phi_0 - V)}{kT}}, \tag{29}$$

where

$$\bar{v} \equiv \left(\frac{2kT}{\pi m}\right)^{1/2}$$

is the average velocity.

The current density j_1 from semiconductor to metal is then

$$j_1 = \tfrac{1}{2} ne\bar{v} e^{-\frac{e(\phi_0 - V)}{kT}}. \tag{30}$$

The current density j_2 from metal to semiconductor is constant in this approximation and, since it must equal j_1 when $V = 0$,

$$j_2 = \tfrac{1}{2} ne\bar{v} e^{-\frac{e\phi_0}{kT}}. \tag{31}$$

The net current density from semiconductor to metal is then $j_1 - j_2$, or

$$j = \tfrac{1}{2} ne\bar{v} e^{-\frac{e\phi_0}{kT}} \left(e^{\frac{eV}{kT}} - 1\right). \tag{32}$$

This expression is seen to have the general form of Eq. (27). It resembles Eq. (26) in that the current density is proportional to the factor $e^{-\frac{e\phi_0}{kT}}$ but differs from Eq. (26) in the proportionality factor. In general, $\frac{1}{2}ne\bar{v}$ is considerably smaller than $ebnE$.

We have seen that the natural barrier is of the order of 10^{-6} cm thick. On the other hand it was pointed out in Sec. 3·5 that the mean free path in germanium is in the range from 5×10^{-6} to 1×10^{-5} cm, and in silicon from 1×10^{-6} to 3×10^{-6} cm. Diode theory appears applicable to germanium, therefore, but in the case of silicon it would appear that

neither diode nor diffusion theory could be applied, since the barrier thickness is of the same order as the mean free path. Bethe[1] has pointed out, however, that the mean free path should not be compared with the total thickness of the barrier, but rather with the distance over which the potential energy changes by kT. The reason is that the number of those electrons which are stopped by the barrier should be compared with the number of those stopped by collisions.

Now, if W_m is the potential maximum, the potential energy is

$$eW_m - kT$$

at a distance of about 6×10^{-8} cm on the semiconductor side of the maximum, and at half that distance on the metal side. These distances are small compared with the mean free path. Therefore, practically all electrons moving toward the potential maximum are stopped by the potential rather than by collisions. Diode theory is evidently still applicable. This point has been examined in further detail by Herzfeld[2] who concurs with Bethe on the applicability of diode theory results even to the case where some collisions occur within the total thickness of the barrier.

The derivation of the d-c characteristic on the basis of the diode theory given above assumes special and ideal conditions. The result is considerably modified if proper account is taken of image forces, tunnel effect, and fluctuations in number density of donators and in work function over the surface of the contact. Such effects are considered in the following section.

4·4. The D-c Characteristic.—As we have seen in the preceding section both diffusion and diode theories[3] predict a current-voltage characteristic of the form

$$I = A(e^{\alpha V} - 1), \tag{33}$$

where I is the current, V the voltage applied across the barrier, and A and α are the constants. Both theories agree in (a) assigning to α to the value e/kT or about 40 (volt)$^{-1}$ at room temperature, and (b) making A proportional to $e^{-\frac{e\phi_0}{kT}}$, where $e\phi_0$ is the contact potential difference. The result (a) will now be compared with experiment.

In making this comparison it must be borne in mind that V is not the voltage V_a applied across the rectifier, but is less than V_a by the voltage

[1] H. A. Bethe, "Theory of the Boundary Layer of Crystal Rectifiers," RL Report No. 43-12, Nov. 23, 1942.

[2] K. F. Herzfeld, "Theory of Small Deviations from Pure Diode Behavior," NDRC 14-286, Purdue U., May 5, 1944.

[3] The tunnel theory gives similar results, but with the direction of rectification reversed.

drop Ir in the ohmic resistance r of the semiconductor. The value of r is determined by the size and shape of the contact and by the conductivity σ of the semiconductor. In Appendix C is derived an expression for r for the case of a contact surface in the form of an ellipse. In the special case of a circular contact of radius a this expression reduces to

$$r = \frac{1}{4\sigma a}. \tag{34}$$

The quantity r is commonly referred to as the "bulk resistance" or "spreading resistance," since it is produced by the bulk semiconductor as distinct from the barrier layer and is associated with the spreading of the lines of current flow from the contact into the semiconductor.

Equation (34) is not suited for establishing r since measurements of the contact dimensions are difficult and the conductivity is subject to local variations. The voltage drop across r is usually found by assuming a forward characteristic of the form,

$$I = A[e^{\alpha(V_a - Ir)} - 1], \tag{35}$$

and plotting ln $(I + A)$ vs. $V_a - Ir$ in the forward direction, determining A and r by trial to produce a straight line of intercept A. Fortunately, the two corrections are in most cases independent; the addition of A to the current has its largest effect at small currents, whereas the correction due to spreading resistance is most important at large currents where the effective resistance of the barrier decreases and Ir increases more rapidly than V_a.

When the data are analyzed[1] in this way, it is found that invariably ln I follows a straight line (of slope α) up to 0.2 or 0.3 volt, but then makes a rapid transition to a second straight line of different slope (α') and intercept (A'). A typical analysis of this kind is shown in Fig. 4·6. To maintain the slope at the initial value α it must be assumed that r decreases with voltage, which is difficult to explain. On the other hand, if one assumes a larger value of r than that giving the straight line at high values of V, the curve may be made to continue with the slope α to somewhat higher voltages, but it always tends eventually to bend over to a curve with negative slope, as shown by the dashed line in Fig. 4·6. Although it is true that one should expect the line to increase its slope as the contact potential is increased, it is difficult to explain this bending back of the curve. It cannot be explained, for example, by the concept of heating of the contact, since it may be shown that the power absorbed is insufficient to raise appreciably the temperature of the contact.

[1] H. J. Yearian, "Investigation of Crystal Rectifier DC Characteristics," NDRC 14-115, Purdue Univ., Dec. 3, 1942.

At all events, it appears that α or α' is much smaller than the theoretical 40 (volt)$^{-1}$ and one is confronted with the necessity of explaining observed values of the order of 10 (volt)$^{-1}$. Analysis of a large number of characteristics both of silicon and germanium gives values of α (lower

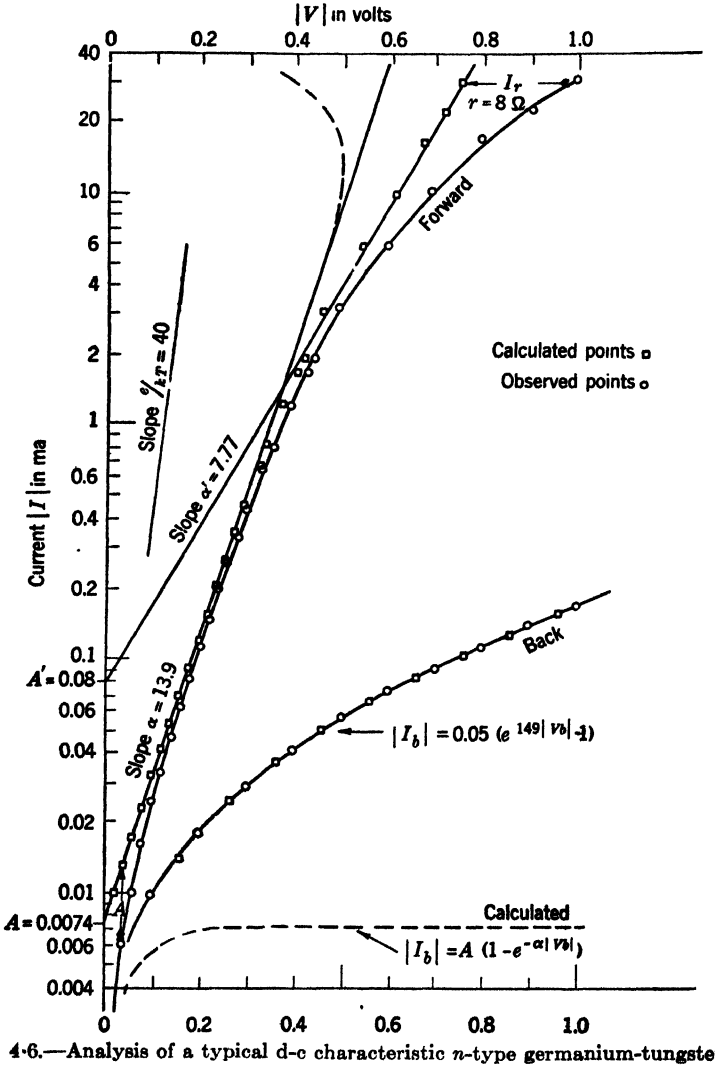

FIG. 4·6.—Analysis of a typical d-c characteristic n-type germanium-tungsten.

slope) ranging from 5 to 35 (volts)$^{-1}$ and values of α' always less than the corresponding values of α.

With the simple characteristic, Eq. (33), the current in the reverse direction would be expected to increase asymptotically to the value A according to

$$|I| = A(1 - e^{-\alpha|V|}). \tag{36}$$

It does not so increase. The reverse currents always continue to increase and attain values at 1 volt of as much as ten times A. The reverse characteristic can often be fitted by an equation of the form of Eq. (36), but the value of constants required for the fit shows no obvious relation to values appropriate to the forward direction.

It must be understood that the above remarks apply only to silicon and germanium rectifiers as ordinarily manufactured for mixer use. High-inverse-voltage and welded-contact types show very different behaviors. Their characteristics are discussed in Chaps. 12 and 13, respectively.

It can be shown on the basis of the Schottky theory of a reserve layer that one can obtain an equation of the form

$$I = A(e^{\frac{1}{3}\frac{eV}{kT}} - 1). \tag{37}$$

The values of α, however, are often found to be less than $\frac{1}{3}(e/kT)$. Furthermore, Eq. (37) does not reproduce observed reverse characteristics. Finally (see Sec. 4·3) one does not expect a reserve layer for silicon and germanium.

As we have seen in Sec. 4·3, the diode theory should be applicable to silicon and germanium rectifiers. Our task, then, is to see how the diode theory can be modified to give the small value of α observed and to account at the same time for the fact that Eq. (36) with constants A and α fitted to the forward characteristic does not at all reproduce the reverse characteristic.

Bethe's Theory of the D-c Characteristic.—Bethe[1] has proposed that theory and experiment can be reconciled by a combination of the following circumstances:

1. The image-force lowering of the barrier was calculated above [Eq. (14)] for the case of zero bias. In general, however, it will be a function of the applied voltage and will then modify the current-voltage characteristic. It is easy to see that the effect is in the right direction to improve agreement with theory.
2. As mentioned above, electrons can leak through the barrier by the tunnel effect. The amount of leakage is strongly dependent on the barrier thickness, and, since the barrier is much thinner near the top, the result is to lower the effective height of the barrier. The amount by which the barrier is lowered depends on the applied potential. The decrease in barrier height becomes smaller as the voltage increases in the positive direction. This effect is also in the right direction to improve agreement with theory.

[1] H. A. Bethe, "Theory of the Boundary Layer of Crystal Rectifiers," RL Report No. 43-12, Nov. 23, 1942.

3. The barrier space charge has been treated as a continuous charge distribution. Actually it is discrete and subject to fluctuations that may be very large. Thus, in a section of barrier consisting of a cube 10^{-6} cm on a side, there will be only 5 charges on the average for a donator density of 5×10^{18} per cm^3 and large fluctuations must be expected in a volume of this size. There will consequently be major fluctuations in barrier thickness which, in combination with image force and tunnel effect, will produce fluctuations in barrier height. The general effect is as though the work function of the surface fluctuated over the contact. Spots of relatively low work function will provide ohmic leaks through the barrier. As we shall see, such an effect will go far toward reconciling theory and experiment.
4. Finally, the unavoidable presence of dirt on the surfaces separating metal and semiconductor serves to produce local fluctuations in work function.

These effects are now considered in turn.

Effect of Image Force.—The effect of image force on the barrier height was found for the special case of zero applied voltage in Sec. 4·3. For the general case, we have only to replace ϕ_0 by $\phi_0 - V$ in Eq. (14). The integral in Eq. (29) now goes from $e(W_m - V)$ to ∞, and Eq. (32) is replaced by

$$j = \tfrac{1}{2}nc\bar{v}e^{-\frac{e(\phi_0-\theta)}{kT}}\left(e^{\frac{eV}{kT}} - 1\right), \tag{38}$$

where

$$\theta = \left[\frac{2e^3N(\phi_0 - V)}{\epsilon^3}\right]^{1/4} \tag{38a}$$

measures the decrease in barrier height due to the image force. It is evident from Eqs. (38) and (38*a*) that the increase of j with V is slower than that given by the factor $e^{eV/kT} - 1$ alone. The image force is thus in the right direction to improve agreement with experiment.

For $V \ll \phi_0$ we may expand θ in a Taylor's series in V/ϕ_0 and retain only linear terms. Thus,

$$\theta \approx \left(\frac{2e^3N\phi_0}{\epsilon^3}\right)^{1/4}\left(1 - \frac{V}{4\phi_0}\right). \tag{39}$$

Introducing this in Eq. (38) we obtain for the total current,

$$I = Ae^{-(1-\beta)\frac{eV}{kT}}\left(e^{\frac{eV}{kT}} - 1\right), \tag{40}$$

or

$$I = A\left[e^{\beta\frac{eV}{kT}} - e^{-(1-\beta)\frac{eV}{kT}}\right], \tag{41}$$

where

$$\beta = 1 - \left(\frac{e^3N}{128\epsilon^3\phi_0^3}\right)^{1/4} = 1 - \frac{x_m}{D}. \tag{42}$$

The quantity x_m is the shift in position of the barrier maximum brought about by image force [see Eq. (13)]. In Sec. 4·2 it was found that $x_m/D = 0.05$ for typical values of the constants.

We see from Eq. (41) that the exponential current increase in the forward direction has the slope $\alpha = \beta \frac{e}{kT}$. To obtain agreement with experiment, we need a value of β of about $\frac{1}{4}$; hence, the theoretical value of β, viz., 0.95, is much too large.

In the reverse direction the agreement with experiment is somewhat better but still leaves much to be desired.

Effect of Penetration of the Barrier.—The tunnel effect with a barrier potential of the form of Eq. (9) which includes the effect of the image force has been treated by Courant.[1] The general result is that the tunnel effect produces about the same barrier-lowering as the image force. Furthermore, the dependence of barrier-lowering on voltage is also about the same for the two effects. For small voltages V, we again obtain an equation of the form of Eq. (40), where the value of β (including both effects), although somewhat smaller than for image force alone, is still much too large to give the correct slope in the forward direction. If the constants are adjusted so as to give a value of β in agreement with experiment in the forward direction, it will certainly lead to erroneous results in the reverse direction, even to predicting the wrong direction of rectification.

It is clear then that image force and tunnel effect will not by themselves secure agreement with experiment.

Fluctuation Effects.[2]—It is convenient to lump together the effects of fluctuations in barrier space charge and of surface contaminations since, as we have seen, these effects have the common result that effective barrier height varies over the contact surface. Besides small variations from the mean, there should be local areas, perhaps as small as 10^{-12} cm^2, where the barrier no longer exists.

Before the effect of a random distribution of contact potentials is

[1] E. Courant, "The Effect of Image Force and the Quantum Mechanical Tunnel Effect on the D-c Characteristics of Crystal Rectifiers," Cornell Univ. Report, Contract OEMsr-429, May 17, 1943.

[2] For a more extensive treatment of fluctuation effects, see V. F. Weisskopf, "On the Theory of Noise in Conductors, Semiconductors, and Crystal Rectifiers," NDRC 14-133, Purdue Univ., May 12, 1943; R. G. Sachs, "Theory of Contact Rectifiers," NDRC 14-168, Purdue Univ., June 15, 1943; and H. J. Yearian, "The Investigation of Crystal Rectifier D-c Characteristics," NDRC 14-115, Purdue Univ., Dec. 3, 1942.

treated, our result for the current-voltage characteristic, Eq. (32), must be somewhat amended. Equation (32) applies only if the voltage V across the barrier is less than the contact potential ϕ_0. For values of $V > \phi_0$, the current no longer increases with V but is constant and equal to its value $\tilde{I}$ for $V = \phi_0$. (It must be remembered here that V is the voltage across the barrier and not the applied voltage $V_a = V - Ir$.) In other words, although the current always increases with applied voltage V_a, it is eventually entirely limited by the spreading resistance r, and the voltage drop across the contact becomes and remains equal to ϕ_0. For a contact of uniform ϕ_0, this effect is of no importance because V does not exceed ϕ_0 at values of current that can be safely passed. If, however, there are spots of small ϕ_0 present at the contact, the current through these spots may reach the critical value at small applied voltages.

If there are spots of low ϕ_0 present, most of the current will tend to pass through them. However, these spots will, if their size is large compared with the mean free path, have a *local* spreading resistance r, associated with each of them which limits the current through them. This local spreading resistance may become very large for a small spot. On the other hand, if the spots of low ϕ_0 are so extremely small that their dimensions are small compared with the mean free path, we can no longer speak of a local spreading resistance and the current through the spots will saturate at the temperature-limited value $\tilde{I}$. Thus, in accordance with Eq. (41) we can write for the current through any given spot

$$I = \tilde{I} e^{-\beta \frac{e\bar{\phi}_0}{kt}} [e^{\beta \frac{eV}{kt}} - e^{-(1-\beta)\frac{eV}{kT}}], \tag{43}$$

if

$$V < \bar{\phi}_0,$$

where $\bar{\phi}_0$ is the effective contact potential of the spot. On the other hand,

$$I = \frac{V}{r_s} \qquad \text{for } V > \bar{\phi}_0 \text{ and } \bar{a} \gg l, \tag{44}$$

$$I = \tilde{I} \qquad \text{for } V > \bar{\phi}_0 \text{ and } \bar{a} \ll l, \tag{45}$$

where $\bar{a}$ is the radius of the spot, l is the mean free path, and V is the voltage applied across the whole barrier.

We now conceive of the contact as being made up of (*a*) fairly large regions of dimensions comparable with the total area of the contact regions where the contact potential is close to some constant value ϕ_0 of the order of 0.5 volt; and (*b*) local small adjacent regions with very different values of ϕ_0. Only those small regions (*b*) of very small ϕ_0 will be effective in modifying the current-voltage characteristic. The spreading resistance of a spot is no longer always given by $1/4\sigma\bar{a}$ since the

current lines may be modified by a cluster of neighboring spots. If s is the number of spots in a cluster, the linear dimension of the cluster will be of the order of $\bar{a}\sqrt{s}$ and the spreading resistance of the cluster is of the order of $1/4\sigma\bar{a}\sqrt{s}$. If one considers the cluster to be made up of s spots in parallel, each one contributes a resistance of order $\sqrt{s}/4\sigma\bar{a}$. Since the current flows mainly through regions whose $\bar{\phi}_0$ is near to or less than V, the clustering is important only at high values of V (where a great number of regions fulfill this condition, and hence the probability of clustering is appreciable).

The current-voltage relation of the rectifier can then be determined by summing the individual currents I_p from each spot.

$$I = \sum_{p_1} \bar{I}_p e^{-\frac{\beta_p e\bar{\phi}_{0p}}{kT}} [e^{\frac{\beta_p e(V - i_p r_p)}{kT}} - e^{-\frac{(1-\beta_p)e(V - i_p r_p)}{kT}}] + \sum_{p_2} I_p, \qquad (46)$$

where r_p is the spreading resistance of the pth element, $\bar{I}_p$ is its thermally limited current, and $\bar{\phi}_{0p}$ is its effective contact potential. The first summation is extended over the elements p for which $V - i_p r_p < \bar{\phi}_{0p}$ and the second, over the remainder. In the second sum I_p is given by Eq. (44) or (45) (whichever is appropriate to the particular spot) or some other intermediate value if $\bar{a} \approx l_p$.

It can be seen that almost any current-voltage dependence, less steep than the one of a single rectifier, can be constructed by a suitable distribution of values $\bar{\phi}_{0p}$ among the elements. Figures 4·7*a* and 4·7*b* illustrate characteristics which are the result of a superposition of rectifier elements. In Fig. 4·7*a* the spots have been assumed small compared with the mean free path and in Fig. 4·7*b* the converse case is shown. In either case a straight $\log_{10} I$ vs. V characteristic results and has the slope of the envelope of the contributing curves. This slope must always be less than the slope of the straight portions of the contributing curves and may be much less, in accordance with the distribution and number of spots of low work function.

Only the forward characteristic has been plotted, but it is clear that almost any shape of reverse characteristic can also be obtained. We would expect the reverse characteristic to be made up of an ohmic part plus an exponential part. This is in accord with analyses of reverse characteristics made by Yearian.[1]

The idea of a "spotty" work function thus does away with the disagreement between theory and experiment. Unfortunately the analysis of a current-voltage characteristic in this way is far from unique. We may postulate certain probability distributions for the number of

[1] H. J. Yearian, "Investigation of Crystal Rectifier D-c Characteristics," NDRC 14-115, Purdue U., Dec. 3, 1942.

spots with given contact potentials ϕ_{0k} and for ϕ_{0p} itself, and proceed to apply them to experimental characteristics. Although such analyses have been made, they are somewhat academic because of lack of uniqueness. The idea of distributed contact potentials has been of value, however, in reconciling the theory of the d-c characteristic with observations. It will be found in Chap. 6 to be useful in the discussion of noise generation by crystal rectifiers.

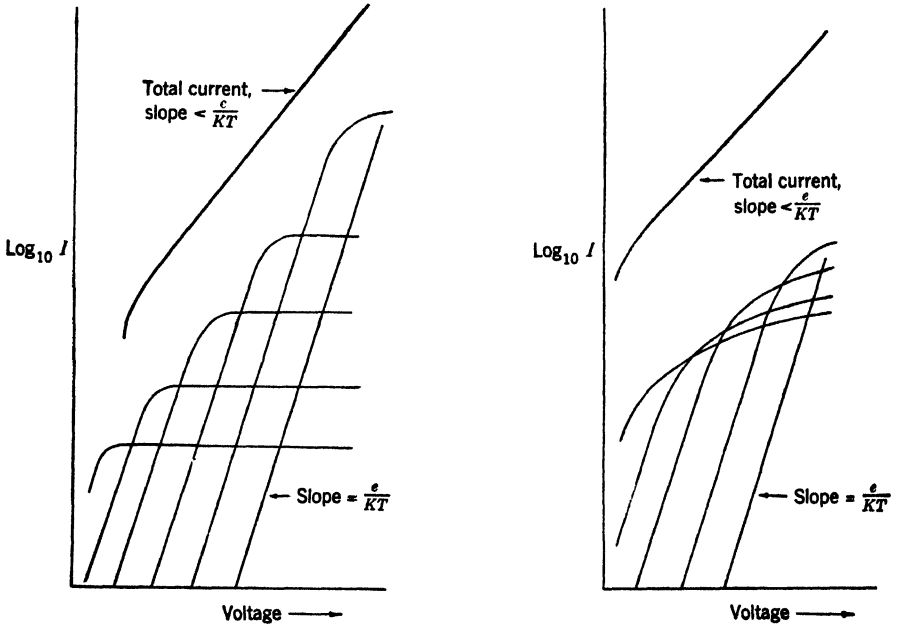

FIG. 4·7.—Current-voltage curves of two typical rectifiers with distributed contact potentials, showing how the total current is the sum of the current contributions (light lines) from individual spots of different contact potentials.

4·5. Depletion Layers.—Up to this point we have confined our attention to the case of a natural barrier which by definition consists of the same material as the bulk semiconductor, with the same density of impurities. There is, however, some reason for believing that the impurity concentration in the barrier may be lower than in the bulk semiconductor for silicon as processed by modern methods for use in rectifiers. Direct experimental evidence for such a "depletion layer" is scanty. Its presence has been inferred, however, from the following arguments.

The theory of high-frequency rectification (Sec. 4·6) shows that rectification (and hence conversion) efficiency is a function of the quantity ωrC, where r is the spreading resistance of the semiconductor and C is the barrier capacitance. The smaller ωrC is, the greater is rectification efficiency. For a natural barrier, this quantity decreases as the number

N of impurity levels per unit volume increases. We cannot increase N indefinitely, however, because the barrier thickness is proportional to $N^{-1/2}$ and a point is reached at which rectification is limited by leakage in the blocking direction as a result of image forces and tunnel effects. The obvious escape from this dilemma is to have an artificial blocking layer, the thickness of which depends only weakly (or not at all) on N; N can then be made large, and r consequently small, without the barrier thickness being affected and, hence, without C being increased and the inverse resistance decreased.

It is well known that rectification by a silicon-metal contact can be greatly improved (for the same contact areas), especially at high frequencies, by a process of heat treatment of the silicon wafer before assembly. A process of this type was first used by the General Electric Company, Ltd. of England in the manufacture of the British "red dot" crystal. It is now universally used in modified form by manufacturers in the United States. This process is fully described in Chap. 10, so it will suffice here to remark that it consists essentially of heating polished silicon wafers in an atmosphere of air at a temperature in the neighborhood of 1000°C for about 1 hr. These wafers are previously cut from an ingot of "doped" silicon (that is, pure silicon plus added impurities or "doping agents").

There is good evidence (reviewed below) that the beneficial effects of heat treatment are ascribable to the formation of a thin surface layer on the silicon wafer, which differs in its electrical properties from the bulk material. In particular, it is found that much larger inverse resistances result from contact with the heat-treated surface than with the original surface. It might be conjectured that a layer of different material (such as quartz) is formed as a result of the heat treatment. As a matter of fact, an oxide surface is certainly formed by heating in air. However, this is always dissolved in dilute hydrofluoric acid before use of the wafer. Furthermore, Fox and Pearsall[1] have shown that the same beneficial effects result from heating in helium or in nitrogen, which are inert with respect to the silicon. Finally, electron-diffraction studies by Lark-Horovitz[2] have revealed no observable difference in crystal structure between the preheat-treated and postheat-treated (and deoxidized) surface. The characteristic diffraction spots of silicon are found in both cases.

The conclusion appears inescapable that a thin layer is formed on the heat-treated surface and that this layer differs only in impurity content

[1] M. Fox and C. S. Pearsall, "Results of Heat-treating Silicon in Various Atmospheres" (Colloquium on Crystal Rectifiers, Vacuum Tube Development Committee), New York, Mar. 27, 1944.

[2] Private communication.

from the interior. The theoretical arguments above then indicate that this is a depletion layer.

For the sake of clarity the case for a depletion layer has perhaps been somewhat oversimplified. Besides (and previous to) heat treatment the surface of the silicon wafers are always highly polished to a mirrorlike finish. It has been conjectured that this polishing produces a flow layer which independently modifies the electrical properties of the surface. High inverse resistance is not obtained by the polishing action, however, and is produced only by the subsequent heat treatment. According to the experience of the Bell Telephone Laboratories,[1] the results of the heat treatment do not depend on the texture of the surface. The function of the smooth surface, these investigators believe, is to facilitate tapping and reduce the noise output of the rectifier.

It has already been mentioned that heat treatment results in an increase of resistance in the blocking direction. That this effect is a property of a surface layer may be demonstrated by etching[2] the surface electrolytically in 24 per cent HF. As the etching proceeds, the inverse resistance of the silicon decreases until it eventually reaches and remains at its value before the heat treatment.

The effect of heat treatment is a somewhat critical function of temperature. Furthermore, increasing the time of heat treatment apparently produces a result similar to that obtained by raising the temperature. Some data bearing on these effects are given in Sec. (10·4). Further evidence of the formation of a thin surface layer of special properties is found by heat-treating, grinding or etching off the surface, and heat-treating again at a different temperature. The properties of the wafer then correspond to the final, and not to the initial, temperature.

It has been mentioned that the heat treatment improves high-frequency performance (rectification and conversion efficiency) for the same contact area. Now contact areas of rectifiers using natural silicon (no heat treatment) must be made very small for good microwave performance. Such rectifiers tend to be mechanically and electrically unstable and are especially susceptible to burnout by leakage power through the TR switch, as well as by accidental exposures to electrical power. The great benefit of the heat-treatment process has accrued from the large contact areas it has made possible and the consequent mechanical and electrical stability with no impairment, in fact, with considerable improvement, in conversion efficiency. It is probably safe

[1] See W. G. Pfann, "Oxidation of Silicon for Point-contact Rectifiers," BTL Report MM-43-120-100, Sept. 22, 1943, for a good account of the experimental effects of heat treatment.

[2] This process actually removes a layer of silicon from the surface and is not to be confused with the previously mentioned removal of the oxide layer by dilute HF (nonelectrolytic).

to say that no innovation in crystal manufacturing technique has contributed so much to improved crystal performance as has the heat-treatment process.

Diffusion and Evaporation of Impurities as Means for the Production of a Depletion Layer.—It was suggested by Bethe[1] that a depletion layer might be formed by passing a large current through a crystal rectifier in the forward direction, the supposition being that the large current would raise the temperature of the contact high enough to cause diffusion of impurities in the barrier layer. At the same time, the direction of the applied voltage is such that it will accelerate positively charged donators (n-type semiconductor) or negatively charged acceptors (p-type semiconductor) into the interior of the semiconductor and will therefore deplete the surface layer of charged impurities. This suggestion was made to explain the observation of Lawson and coworkers[2] that large forward currents have the effect[3] of increasing the reverse resistance at 1 volt.

The suggestion that heat treatment of a silicon wafer produces a depletion layer by a process of diffusion and evaporation of impurities was made by Serin and Stephens,[4] who gave a mathematical treatment of the diffusion and evaporation process which is reproduced here in part. Consider a semi-infinite homogeneous block of semiconductor with a plane face at $x = 0$ and extending in the positive x-direction. Suppose that at time $t = 0$ the block has a uniform concentration N_0 of impurity atoms. The concentration $N(x,t)$ at a distance x from the surface at some later time t is given by the solution of the diffusion equation,

$$\mathfrak{D}\frac{\partial^2 N}{\partial x^2} = \frac{\partial N}{\partial t}, \tag{47}$$

that satisfies appropriate boundary conditions. Here $\mathfrak{D}$ is the diffusion coefficient, assumed independent of the concentration.

The rate of loss of impurity atoms per unit area from the surface is *assumed* to be proportional to the surface concentration. This rate of loss must equal the rate of arrival at the surface by diffusion, if there is to be no piling up of impurity atoms on the surface. Thus, one boundary condition is

$$-\frac{\partial N}{\partial x} + hN = 0 \qquad \text{at } x = 0, \tag{48}$$

[1] H. A. Bethe, "Theory of High-frequency Rectification by Silicon Crystals," RL Report No. 43-11, Oct. 29, 1942.

[2] A. W. Lawson *et al.*, "D-c Burn-out Temperature in Silicon Rectifiers," NDRC 14-113, Univ. of Penn., Nov. 1, 1942.

[3] These experiments were performed on silicon that had not been heat-treated.

[4] B. Serin and W. E. Stephens, "Production and Effects of a Depletion Layer in Doped Silicon," NDRC 14-282, Univ. of Penn., May 29, 1944. See also, B. Serin, *Phys. Rev.*, **69**, 357 (1946).

where

$$h = \frac{K}{\mathfrak{D}}, \tag{49}$$

and K is the ratio of the rate of loss per unit area by evaporation to the surface concentration. The other boundary conditions are

$$\left.\begin{aligned} N(x,0) &= N_0 \qquad \text{for } x > 0, \\ N(\infty,t) &= N_0. \end{aligned}\right\} \tag{50}$$

The problem is formally equivalent to an analogous solved problem[1] in heat flow, namely that of a semi-infinite body initially at a uniform temperature losing heat by radiation into a region at zero temperature. Thus the solution may be written down at once as

$$\frac{N}{N_0} = \operatorname{erf}\left(\frac{x}{2\sqrt{\mathfrak{D}t}}\right) + e^{hx+h^2\mathfrak{D}t}\left[1 - \operatorname{erf}\left(\frac{x}{2\sqrt{\mathfrak{D}t}} + h\sqrt{\mathfrak{D}t}\right)\right], \tag{51}$$

where

$$\operatorname{erf}(u) \equiv \frac{2}{\sqrt{\pi}}\int_0^u e^{-w^2}\,dw. \tag{52}$$

Of especial interest is the solution after sufficient time has passed with the result $N(0,t)/N_0 \equiv \alpha_0 \ll 1$.

Under this condition,

$$\alpha_0 \approx \frac{1}{h\sqrt{\pi\mathfrak{D}t}}, \tag{53}$$

and the solution [Eq. (51)] reduces approximately to

$$\frac{N}{N_0} \approx \operatorname{erf}\left(\frac{\sqrt{\pi}}{2}h\alpha_0 x\right) + \frac{e^{-\frac{\pi}{4}h^2\alpha_0^2 x^2}}{\left(\frac{\pi}{2}h\alpha_0 x + \frac{1}{\alpha_0}\right)}. \tag{54}$$

Figure 4·8 shows a plot of N/N_0 as a function of x in units of $d \equiv 1/h\alpha_0$. In plotting this curve it has been assumed that $\alpha_0 = 0.1$.

The diffusion coefficient may be expressed in terms of atomic parameters by

$$\mathfrak{D} = a\delta^2 e^{-\frac{\epsilon_D}{kT}}, \tag{55}$$

where a is the "jumping" frequency of a substituted impurity atom in the bulk crystal lattice, δ is the distance between adjacent bulk atoms, ϵ_D is the diffusion activation energy, k is Boltzmann's constant, and T is the absolute temperature.

[1] See H. S. Carslaw, *Introduction to the Mathematical Theory of the Conduction of Heat in Solids*, 2d ed., Macmillan, London, 1921, Sec. 25.

It is possible to derive an analogous expression for the evaporation coefficient K. By definition

$$K = -\frac{\frac{dn}{dt}}{N(0,t)}, \tag{56}$$

where dn/dt is the rate of evaporation of impurities and $N(0,t)$ is the volume density of surface impurity atoms. The rate of evaporation is equal to the probability per unit time that an atom will have evaporated, multiplied by the number of impurity atoms per unit area on the surface. Assuming for the probability $ae^{-\frac{\epsilon_K}{kT}}$, where a is the same jumping frequency, and assuming for the surface density of impurities, the number per unit area in the first atomic layer, we obtain

$$-\frac{dn}{dt} = N(0,t)a\delta e^{-\frac{\epsilon_K}{kT}}. \tag{57}$$

From Eqs. (57) and (56), it follows that

$$K = a\delta e^{-\frac{\epsilon_K}{kT}}; \tag{58}$$

hence, by Eqs. (58) and (55),

$$h = \frac{K}{\mathfrak{D}} = \frac{1}{\delta} e^{-\frac{\epsilon_K - \epsilon_D}{kT}}. \tag{59}$$

The thickness d of the depletion layer is thus given by

$$d = \frac{\delta}{\alpha_0} e^{\frac{\epsilon_K - \epsilon_D}{kT}}. \tag{60}$$

This expression is very sensitive to the relative magnitudes of ϵ_K and ϵ_D. Since for silicon $\delta = 2.3 \times 10^{-8}$ cm, for $\alpha_0 = 0.1$,

$$d = 2.3 \times 10^{-7} e^{\frac{\epsilon_K - \epsilon_D}{kT}} \quad \text{cm.} \tag{61}$$

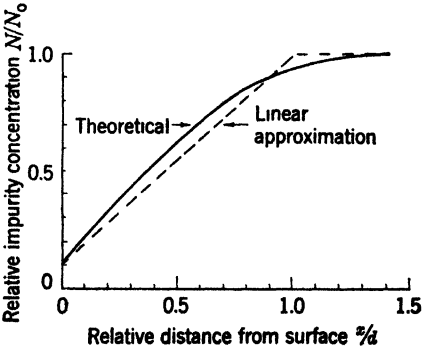

FIG. 4·8.—Impurity concentration as a function of distance from surface.

Hence, for ϵ_K slightly larger than ϵ_D we can obtain values of d in the range from 10^{-6} to 10^{-5} cm. In general it can be said that, to account for a depletion layer of reasonable thickness, we must have $\epsilon_K \approx \epsilon_D$. Directly measured values of ϵ_K and ϵ_D are not yet available to check this conclusion.

Serin and Stephens go on to calculate the barrier shape for various

assumed values of the depletion-layer width d and the natural barrier width D. They did not take into account the tunnel effect and the distribution of contact potentials which, we saw in the preceding section, have marked effects on the d-c characteristic. Thus their comparisons of theoretical with observed effects of heat-treatment on reverse resistance are qualitative at best and will not be given here.

It is obvious, however, what the general trend must be. A depletion layer thickens the barrier and thus reduces the back leakage brought about by tunnel effect and image force, in accordance with observation. One important source of contact potential variation, namely, that of fluctuations in impurity density, must be considerably reduced by a depletion layer. The other source, surface contamination, should not be affected. This latter is probably the more important of the effects, since rectifiers using heat-treated silicon certainly have, in general, no greater positive slopes of their d-c characteristics than untreated rectifiers with natural barriers.

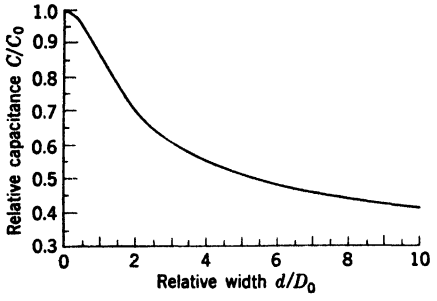

FIG. 4·9.—Barrier capacitance as a function of width of depletion layer d. The quantities C_0 and D_0 are capacitance and width of natural barrier.

The depletion layer must certainly decrease the contact capacitance. Serin and Stephens have calculated this effect and arrive at the result,

$$C = \frac{\epsilon A}{D}, \tag{62}$$

which is observed to have the same form as obtained for a natural barrier. The value of D, however, is now given in terms of the thickness d of the depletion layer and the thickness D_0 that a natural barrier layer would have in the absence of the depletion layer. Specifically,

$$D^2 = D_0^2 + \frac{d^2}{3} \qquad \text{for } d < \sqrt{\tfrac{3}{2}}\, D_0; \tag{63}$$

$$D^3 = \tfrac{3}{2} d D_0^2 \qquad \text{for } d > \sqrt{\tfrac{3}{2}}\, D_0. \tag{64}$$

In Fig. 4·9 the ratio of the contact capacitance C to its value C_0 for $d = 0$ is plotted as a function of d/D_0.

We can now estimate the effect of the depletion layer on the quantity ωCr which, as we noted above, essentially determines the rectification efficiency and conversion loss at microwave frequencies. Let us take the case $d > \sqrt{\frac{3}{2}}\, D_0$. From Eq. (10), $D_0 \propto N_0^{-1/2}$, where N_0 is the concentration of impurities in the bulk semiconductor.

The spreading resistance r is by Eq. (34) inversely proportional to σ, the conductivity, and consequently is by Eq. (19) inversely proportional to n, the bulk electron density, which in turn depends on N_0, the impurity concentration. If the ionization of impurities is nearly complete in the bulk semiconductor, as in germanium (Sec. 3·5), $n \approx N_0$. For the other extreme of weak ionization $n \propto N_0^{1/2}$, see Eq. (5). The case of silicon normally falls somewhere between these extremes. Thus we have the following dependence of D and ωCr on N_0:

1. With no depletion layer (natural barrier), $D = D_0 \propto N_0^{-1/2}$, $\omega Cr \propto N_0^{-1/2}$ (complete ionization), ωCr does not depend on N_0 (weak ionization). (65)
2. With a depletion layer of thickness $D > \sqrt{\frac{3}{2}}\, D_0$, $D \propto N_0^{-1/3}$, $\omega Cr \propto N_0^{-2/3}$ (complete ionization), $\omega Cr \propto N_0^{-1/6}$ (weak ionization). (66)

Thus the effect of the depletion layer, as expected, is to increase the dependence of ωCr on N_0 and to decrease the dependence of the barrier thickness D on N_0. The depletion layer thus makes it possible to improve rectification by a decrease in ωCr consequent to an increase in N_0 without a serious reduction in barrier thickness.

4·6. Rectification at High Frequencies. *General Considerations.*—We have seen (Sec. 2·4) that a crystal rectifier can be represented approximately by the equivalent circuit of Fig. 4·10. The barrier resistance R, which depends on the voltage across it, is shunted by the barrier capacitance C, and this combination is in series with the ohmic spreading resistance r of the bulk semiconductor. At low frequencies, $\omega CR \ll 1$ even where R is the maximum barrier resistance; the capacitance can then be completely ignored and the rectification is determined entirely by the d-c characteristic.

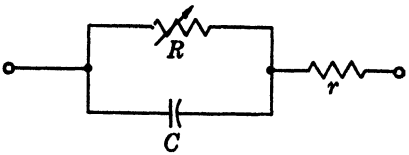

FIG. 4·10.—Equivalent circuit of a crystal rectifier; R is the nonlinear barrier, C the barrier capacitance, and r the ohmic spreading resistance.

At microwave frequencies, however, the capacitive susceptance ωC of the barrier is actually large compared with $1/R$ in the back direction and considerable modification of the rectifying properties should be expected. Measured barrier capacitances range from 0.02 to 1.0 $\mu\mu$f, the smaller values being found in crystals prepared for use in the 1-cm band and the larger values in high-burnout, 10-cm band rectifiers. A capacitance of 1 $\mu\mu$f has a reactance of only 50 ohms at a wavelength of 10 cm; whereas back resistances normally encountered are 5000 ohms or more. Thus the back resistance is effectively shunted by the barrier capacitance at microwave frequencies and may therefore be ignored.

The rectification efficiency and therefore also the conversion loss should depend on the ratio of back-to-forward impedance. At reasonably high forward voltages the barrier resistance R is small compared with the barrier reactance $1/\omega C$ and with the spreading resistance r. The forward resistance is then just r. For any back voltage and for reasonably small forward voltages, R is very large; therefore the impedance of the contact proper is just $-j/\omega C$ and the total back impedance is

$$Z = r - \frac{j}{\omega C}. \tag{67}$$

The "back-to-front" ratio is

$$\frac{Z}{r} = 1 - \frac{j}{\omega C r}. \tag{68}$$

Dimensional considerations alone make it clear that rectification efficiency and conversion loss, both dimensionless quantities, can depend on the crystal parameters only through the factor $\omega C r$. Clearly, the barrier resistance is always negligible; it is either shunted by the barrier capacitance or is small compared with the spreading resistance. Only over a small range of forward voltage does it contribute to the impedance.

The conversion loss L is thus a function of $\omega C r$, obviously an increasing function, and low conversion loss requires a small value of $\omega C r$, certainly less than unity. We can express $\omega C r$ in terms of the properties of the semiconductor by use of Eqs. (34) and (17). We obtain

$$\omega C r = \frac{\pi}{240} \frac{\epsilon}{\epsilon_0} \frac{a}{\sigma D \lambda} \tag{69}$$

where the radius of the contact a, the barrier thickness D, and the wavelength λ are in centimeters; and the conductivity σ is in mho-cm^{-1}. If for example, $\lambda = 3$ cm, $D = 2 \times 10^{-6}$ cm, $\epsilon = 13\epsilon_0$, and $\sigma = 50$ mho/cm, then $\omega C r$ will be less than unity, provided

$$a < \frac{240}{\pi} \frac{D \lambda \sigma \epsilon_0}{\epsilon} = 1.8 \times 10^{-3} \quad \text{cm.} \tag{70}$$

Contacts actually used fulfill this condition by a wide margin. A representative value of a for 3-cm-band crystal contacts is 3×10^{-4} cm. With the above values of ϵ/ϵ_0 and D, such a contact will have a capacitance of 0.1 $\mu\mu$f and the spreading resistance will be 17 ohms.

To improve rectification we need to make the quantity $\epsilon a/\sigma D \lambda$ as small as possible. An obvious solution is to decrease a, the contact radius. Unfortunately very small values of a lead to mechanical and electrical instability. Bethe[1] has suggested a way out of this dilemma

[1] H. A. Bethe, "Theory of High Frequency Rectification by Silicon Crystals," RL Report No. 43-11, Oct. 29, 1942.

by using an elongated, or knife-edge, contact. It can be shown that the parameter a in Eq. (69) is then replaced (approximately) by the short dimension of the contact. Thus a contact of fairly large area, and hence good stability, can be obtained with no sacrifice in conversion loss. This point is discussed more fully in Chap. 8. It was at one time believed that the excellent performance of the British "red dot" crystals was essentially achieved by making these crystals with an elongated contact. This view is no longer held, however. It may be shown theoretically that very large ratios of long-to-short dimensions of the contact must obtain before the beneficial effects become important and the actual dimensions of the "red dot" contacts do not appear to meet this extreme condition. Furthermore, experiments by Fox and Pearsall and by Stephens[1] have shown no significant difference between knife-edge contacts of the "red dot" type and circular contacts, either with respect to conversion loss or stability. Attempts have been made to increase the ratio of long-to-short contact dimensions to a value that would be expected to improve performance, but the techniques for making such a contact are extremely difficult and no success has as yet been attained.

A second escape from the dilemma is to increase the parameter D the thickness of the barrier layer. As we have seen in the preceding section, there is good reason to believe that this is actually accomplished by heat-treatment of the silicon wafers, following the "red dot" techniques or a modification of them. The real value of this formation of a depletion layer is a consequence of the fact that it makes possible an increase in the value of σ by an increase in the impurity content of the semiconductor without a simultaneous decrease in D. This point will not be further treated here, since it was discussed in detail in the preceding section.

An increase in σ without an effect on the other parameters might be attained by an increase in carrier mobility Eq. (3·21). Thus germanium is known (Sec. 3·7) to have about three times the mobility of silicon. Other things equal, germanium should therefore be superior to silicon. It is found, however, that germanium does not yield to heat-treatment in the same manner as silicon, and germanium rectifiers tend to be somewhat "noisier" than silicon rectifiers.

Welding of a small metal-semiconductor contact improves mechanical stability enormously and may also improve electrical stability (resistance to burnout). No one has yet succeeded in welding metal wires to silicon. Welded metal-germanium contacts are discussed in Chap. 13. They have such special and peculiar properties that they cannot be adequately

[1] See M. Fox, "Comparison of Cone and Wedge Tips on Radiation Laboratory Silicon;" and W. E. Stephens, "Comparison of Cone and Wedge Tips on Radiation Laboratory Silicon" (Crystal Rectifier Conference, Vacuum Tube Development Committee), Nov. 19, 1943.

treated by the simple considerations above. It is remarked here only that they have not as yet been brought to the point where they can replace silicon rectifiers to advantage.

The only other parameter is ϵ/ϵ_0, the dielectric constant. As pointed out in Sec. 4·2, a high dielectric constant is necessary for the formation of a natural barrier. The use of an artificial barrier layer lessens the importance of a high dielectric constant. Perhaps something might be gained by using a semiconductor that has a lower dielectric constant and an artificial barrier layer.

Relaxation Effects.—Lawson and others[1] have noted that the rectification efficiency of crystal rectifiers does not decrease with frequency as rapidly as might be expected from the observed values of barrier capacitance and d-c characteristic. It is obviously important to understand the nature of this effect. Once its cause is made clear, some means may be found to enhance it and thereby increase the utility of crystal rectifiers at high frequencies. Lawson ascribes the effect to relaxation processes in the barrier layer. It is reasonable, but not certain, that Lawson's explanation is correct. This section is devoted to an exposition, in modified form, of his theory.[2]

We have seen that the capacitance of the barrier is caused by the flow of electrons into and out of the barrier layer. The charging current is in quadrature with the applied voltage and the barrier layer thus acts as a condenser. In the analysis of the capacitance given here, it has so far been assumed that the electrons remain permanently "free," and can therefore respond without time lag to a sudden change in voltage. The possibility should now be considered that some of the electrons may become trapped by combination with charged impurity atoms. The electrons in the barrier will either be free or bound to impurity atoms. Let us first consider the case for which the frequency f is small compared with the probability B per unit time for ionization of an impurity atom. The free electrons will emerge from the barrier as soon as their potential energy exceeds the potential energy of an electron in the bulk semiconductor. The bound electrons will emerge somewhat later, but, if $B \gg f$ as assumed, their time lag will be small compared with the half period of the wave and they contribute equally to the quadrature component of the current.

If, however, $f \approx B$, the time lag of the bound electrons will be an appreciable part of a half cycle. The current produced by the emergence of the bound electrons will then consist of two components, one in phase

[1] See A. W. Lawson, *et al.*, "High-frequency Rectification Efficiency of Crystals," NDRC 14-153, Univ. of Penn., July 1, 1943; and E. R. Beringer, "Crystal Detectors and the Crystal Video Receiver," RL Report No. 638, Nov. 16, 1944.

[2] A. W. Lawson, *et al.*, "Ionization of Donator Levels in Crystal Rectifiers by Thermal Agitation," NDRC 14-173, Univ. of Penn., July 7, 1943.

and one in quadrature with the voltage. Since the total charging current (quadrature component) is now reduced, it is clear that the effective barrier capacitance is less than at low frequencies ($f \ll B$). Furthermore, there will now be a conductance G shunting the barrier, because of the in-phase component of the current.

At still higher frequencies, $f \gg B$, an electron that had become bound during the discharging part of a cycle may wait for several cycles before again contributing to the current. The charging current (and therefore the barrier capacitance) is thus still further reduced. The in-phase current, and thus the conductance G, should increase with frequency in this region, approaching a constant value in the limit, since the rate of ionization of donators would be nearly constant during a half cycle at very high frequencies ($f \gg B$).

The magnitude of these effects clearly depends on the ratio of free-to-bound electrons at equilibrium. If this ratio is large, the relaxation effects will be relatively unimportant. If the ratio is small, the importance of the effects at microwave frequencies depends on the magnitude of B. We have seen in Chap. 3 that ionization of impurities is 20 to 40 per cent complete in the case of silicon and nearly 100 per cent complete for germanium at thermal equilibrium (room temperature) in the bulk semiconductor. Thus if the surface levels are of the same character in the bulk impurity levels, we should expect no relaxation effects in germanium rectifiers but possible relaxation (depending on the value of B) in silicon rectifiers. It is possible, however, that surface levels exist which are of an entirely different nature from the bulk impurity levels. Any interruption in the periodic structure of the lattice, such as that occurring at the surface, is capable of producing electron levels in the normally forbidden region of the band structure[1] (Sec. 3·1). These surface levels might lie at much greater depths below the conduction band than the impurity levels.[2] If this is the case, we should expect strong relaxation effects in both silicon and germanium.

The magnitude of the relaxation time $1/B$ is of great importance in the theory of the relaxation effects. The value of B may be estimated[3] as follows: The equilibrium of the reaction,

$$\text{Free electron} + \text{bound hole} \rightleftarrows \text{bound electron},$$

[1] F. Seitz, *The Modern Theory of Solids*, McGraw-Hill, New York, 1940, pp. 320 ff.

[2] Some evidence that this is the case for silicon is obtained from studies of photoconductivity by Miller (P. H. Miller and M. H. Greenblatt, "Photoeffects in Pure Silicon," NDRC 14-412, Univ. of Penn., Mar. 20, 1945), who found that the threshold for photoconductivity in silicon is about 0.5 ev; whereas the band separation in silicon is known to be 1.1 volts (Sec. 3·5). His results might be explained by the hypothesis of surface levels lying 0.5 volt below the conduction band.

[3] N. F. Mott and R. W. Gurney, *Electronic Process in Ionic Crystals*, Oxford, New York, 1940, p. 108.

is governed by the mass action law,

$$\frac{n^2}{N-n} = 2\left(\frac{2\pi mkT}{h^2}\right)^{3/2} e^{-\frac{\Delta E}{kT}}, \tag{71}$$

where

n = number density of free electrons,
N = number density of impurity levels,
ΔE = depth of an impurity level below the conduction band.

The right-hand member of Eq. (71) is the equilibrium constant of the reaction [see Eqs. (3·1) and (3·2)].

This result determines the number of free electrons at equilibrium. For a nonequilibrium (and electrically neutral) state, application of detailed balancing gives

$$\frac{dn}{dt} = B(N-n) - An^2, \tag{72}$$

where B is the probability per unit time for an electron transition from the bound to the free state and An^2 is the number of transitions per unit time in the opposite direction. Now A may be formally written as

$$A = \sigma u, \tag{73}$$

where σ is the capture cross section of an empty donator level and u is the mean thermal velocity of an electron in the free state. From Eq. (72) equilibrium occurs when

$$\frac{n^2}{N-n} = \frac{B}{A}. \tag{74}$$

Comparing this with Eq. (71) and inserting Eq. (73), we get

$$B = \frac{2\pi m(kT)^2}{h^3}\,\sigma\sqrt{6\pi}\; e^{-\frac{\Delta E}{kT}}, \tag{75}$$

where we have introduced for u the expression,

$$u = \left(\frac{3kT}{m}\right)^{1/2}. \tag{76}$$

The quantity B may be estimated from Eq. (75) by taking $\sigma = 10^{-15}\ \mathrm{cm}^2$, whence

$$B = 1.5 \times 10^{11} e^{-\frac{\Delta E}{kT}} \quad \mathrm{sec}^{-1}. \tag{77}$$

There is some experimental evidence that B_0, the coefficient of $e^{-\Delta E/kT}$ in this expression, may be as low as $10^{10}\ \mathrm{sec}^{-1}$. This latter value is based on the rate at which electrons must be freed thermally from trapping

centers in rock salt in order to explain the observed temperature dependence of photoconductivity.[1]

A better estimate of B may be had by treating the problem with the aid of quantum mechanics. In this way Seitz[2] has obtained 10^{10} sec^{-1} as an upper limit for B_0, and Lawson[3] concludes that B_0 is about 2×10^9 sec^{-1}, if $\Delta E < k\theta_D$, where θ_D is the Debye temperature of silicon. If $\Delta E > k\theta_D$, he finds that B_0 may be as small as 10^6 sec^{-1}. Since these estimates are of the order of, or smaller than, microwave frequencies, it is clear that a considerable relaxation effect must be anticipated.

In Lawson's treatment of relaxation theory the assumption is made that the time for the inverse process, that is, electron capture by an ionized donator, is short compared with the microwave period. The truth of this assumption may be investigated by calculating the time for the attainment of equilibrium, starting from an electrically neutral semiconductor with completely ionized donators. The relaxation time for this process is found by integrating Eq. (72). It is

$$\tau = \frac{n_0}{(2N - n_0)B}, \tag{78}$$

where n_0 is the equilibrium value of n. If $B = 10^{10}$ sec^{-1} and $n_0/N = 0.2$ (a typical value for silicon), we obtain $\tau = 1.1 \times 10^{-11}$ sec which, although less than microwave periods in use, cannot be regarded as negligibly small.[4] Lawson's results must therefore be interpreted with caution, although there is no doubt that his theory is qualitatively correct.

These considerations will now be applied to the following problem. We assume a barrier layer containing N impurity levels per unit volume located at an energy depth ΔE below the conduction band. In the bulk semiconductor, there are n_0 free electrons per unit volume. The barrier layer is assumed to have, before an alternating voltage is applied, a uniform space-charge density eN. It is assumed that there is an abrupt transition from the charged barrier layer to the neutral bulk semiconductor. An alternating sinusoidal voltage[5] $V_0 \cos \omega t$ is applied to the barrier; this causes the potential of the bulk semiconductor to vary sinusoidally with the time. When the potential rises, electrons flow

[1] N. F. Mott and R. W. Gurney, *op. cit.*, p. 136.

[2] F. Seitz, "Transition Probability for Excitation from Bound Levels" (Crystal Rectifier Conference), Columbia Univ. Sept. 11, 1943.

[3] A. W. Lawson *et al.*, NDRC Report 14-173, Univ. of Penn., July 7, 1943.

[4] In the case of surface levels n_0/N might be much smaller than 0.2 and hence τ much shorter than 10^{-11} sec.

[5] In this section *voltage* (and the synonomous term *potential*) is defined for convenience as the potential energy of an electron divided by the absolute value of the electronic charge. It thus has the opposite sign of the conventional voltage. This fact must be borne in mind in interpreting the results.

into the barrier and neutralize a part of its volume. In accordance with the above discussion, the equilibrium free-electron density is assumed to be established immediately. When the voltage wave recedes, electrons pour out of barrier. It is assumed, and easily justified, that the free electrons will slide down the potential hill in a time short compared with the period of the wave. The bound electrons will leak out of the barrier at the rate $B(N - n)$. Once having escaped from the impurity ions, these electrons will also be assumed to depart instantaneously. A small decrease ΔV in potential exposes a fraction $(df/dV)\,\Delta V$ of the volume f of the barrier to the electron-stripping process and charges this part of the barrier by the amount $en_0(df/dV)\,\Delta V$ at once and by the amount

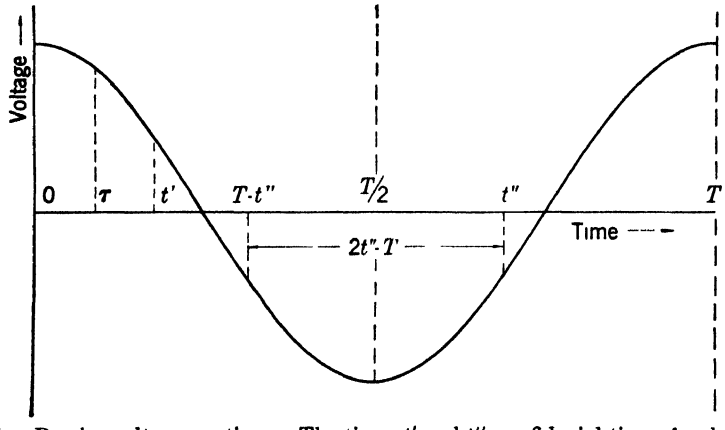

FIG. 4·11.—Barrier voltage vs. time. The times t' and t'' are fiducial times for downswing and upswing respectively, and τ is time in general.

$eN(df/dV)\,\Delta V$ eventually, if sufficient time elapses before the potential rises again for the donators to become ionized completely.

Figure 4·11 shows the form of the voltage wave $V_0 \cos \omega t$. At $t = 0$, the potential begins to recede. The current at time $0 < t' < \frac{1}{2}T$ (where T is the period of the voltage wave) is in two parts.

1. That due to the free electrons that depart in the interval t' to $t' + dt'$. This current is given by

$$i_1 = -en_0 \frac{df}{dV}\frac{dV}{dt'},$$

$$= en_0 V_0 \frac{df}{dV}\,\omega \sin \omega t'. \tag{79}$$

The sign has been chosen so that a positive current increases the positive charge on the barrier.

2. That due to the evaporating bound electrons. These electrons come continuously from the part of the barrier exposed during the interval 0 to t'. If τ is some generic time in this interval, the

contribution from a small interval $d\tau$ at τ is

$$di_2 = -e(N - n_0)Be^{-B(t'-\tau)} \frac{df}{dV} \frac{dV}{d\tau} d\tau. \tag{80}$$

Integrating this from 0 to t', we obtain

$$i_2 = e(N - n_0) \frac{df}{dV} V_0 \frac{B\omega}{B^2 + \omega^2} (\omega e^{-Bt'} + B \sin \omega t' - \omega \cos \omega t'). \tag{81}$$

Let us now consider the currents flowing in the time interval

$$\tfrac{1}{2}T < t'' < T.$$

This current is also composed of two parts.

1. The current flowing into the volume $(df/dV)\, dV$ flooded by the advancing wave during the small interval dt'' at t''. The amount of charge in this part of the barrier is that remaining after removal of the free electrons at $t = T - t''$ and the subsequent evaporation from the donators during the interval $2t'' - T$. The current is this charge divided by dt'', and is

$$\begin{aligned} i_3 &= -e\{n_0 + (N - n_0)[1 - e^{-B(2t''-T)}]\} \frac{df}{dV} \frac{dV}{dt''} \\ &= e\{n_0 + (N - n_0)[1 - e^{-B(2t''-T)}]\} \frac{df}{dV} V_0\omega \sin \omega t''. \end{aligned} \tag{82}$$

2. The current still emerging from the part of the barrier not yet submerged by the advancing voltage wave. This part of the barrier was exposed during the time $0 < \tau < T - t''$. The contribution to the current is found by integrating Eq. (80) from $\tau = 0$ to $\tau = T - t''$. We obtain

$$\begin{aligned} i_4 = e(N - n_0) \frac{df}{dV} V_0 \frac{B\omega}{B^2 + \omega^2} [\omega e^{-Bt''} - Be^{-B(2t''-T)} \sin \omega t'' \\ - \omega e^{-B(2t''-T)} \cos \omega t'']. \end{aligned} \tag{83}$$

Collecting terms, we find, after some simplifications, for $0 < t < \frac{1}{2}T$,

$$\begin{aligned} i = eN \frac{df}{dV} V_0\omega \sin \omega t + e(N - n_0) \frac{df}{dV} V_0 \frac{\omega^2 B}{\omega^2 + B^2} (e^{-Bt} - \cos \omega t) \\ - e(N - n_0) \frac{df}{dV} V_0 \frac{\omega^3}{\omega^2 + B^2} \sin \omega t; \end{aligned} \tag{84}$$

and for $\frac{1}{2}T < t < T$,

$$\begin{aligned} i = eN \frac{df}{dV} V_0\omega \sin \omega t + e(N - n_0) \frac{df}{dV} V_0 \frac{\omega^2 B}{\omega^2 + B^2} (e^{-Bt} - e^{-B(2t-T)} \cos \omega t) \\ - e(N - n_0) \frac{df}{dV} V_0 \frac{\omega^3 + 2B^2\omega}{\omega^2 + B^2} (e^{-B(2t-T)} \sin \omega t). \end{aligned} \tag{85}$$

The current is easily seen to be continuous at $t = 0$ and $t = \frac{1}{2}T$. The current of each cycle is a reproduction of the current of the preceding

cycle. Thus i may be developed in a Fourier series. The constant term of this series vanishes, as is required by the condition that i be a charging and not a conduction current. The physically interesting term of the Fourier series is the first harmonic. Putting

$$i = \sum_{-\infty}^{+\infty} \tfrac{1}{2} I_n e^{jn\omega t}, \tag{86}$$

we find

$$I_1 = -(G + j\omega C)V_0, \tag{86a}$$

where

$$G = \omega e N \frac{df}{dV} \frac{N - n_0}{N} F_1\left(\frac{\omega}{B}\right)$$

$$C = eN \frac{df}{dV}\left[1 - \frac{N - n_0}{N} F_2\left(\frac{\omega}{B}\right)\right].$$

The functions $F_1(x)$ and $F_2(x)$ are given by

$$F_1(x) = \frac{x}{2(1 + x^2)}\left[1 + \frac{1}{2\pi}(1 - e^{-\frac{2\pi}{x}})\frac{2x^3}{1 + x^2}\right] \tag{87}$$

$$F_2(x) = \frac{x^2}{2(1 + x^2)}\left[1 + \frac{1}{2\pi}(1 - e^{-\frac{2\pi}{x}})\frac{x(x^2 - 1)}{1 + x^2}\right]. \tag{88}$$

Remembering the sign conventions adopted (I has the conventional and V_0, the unconventional sign) it is clear from Eq. (86a) that the barrier acts at the (angular) frequency ω as a capacitance C and a conductance G in shunt (with each other and with the nonlinear resistance of the barrier). Both C and G are functions of the frequency. Since $F_2(0) = 0$, at $\omega = 0$

$$C = C_0 \equiv eN \frac{df}{dV}.$$

This C_0 is the barrier capacitance as calculated in Sec. 4·2, assuming no relaxation. As the frequency increases, $F_2(\omega/B)$ increases monotonically (see Fig. 4·12), becoming unity at $\omega = \infty$. Thus C decreases with frequency, approaching the value $\frac{n_0}{N} C_0$ at $\omega = \infty$. For weak equilibrium ionization of impurities, the capacitance may become very small at high frequencies.

Since $F_1(0) = 0$, we have $G = 0$ at $\omega = 0$. As the frequency increases, G increases monotonically, approaching the value

$$G(\infty) = \frac{3}{2}\frac{N - n_0}{N} BC_0.$$

The curves $F_1(x)$, $F_2(x)$, and $G(x)/G(\infty)$ are shown in Fig. 4·12.

The conversion loss of a crystal rectifier may be calculated as a

function of frequency by using Eqs. (86*a*), (87), (88), and the methods developed in Chap. 5. This calculation will not be carried through explicitly here. The general qualitative result is that the conversion loss increases less rapidly with frequency for $f > B$ and more rapidly for $f < B$ than it does for the case of $B = \infty$, that is, no relaxation. For values of B of the order of 10^8 or 10^9 sec, the conversion loss at microwave frequencies is considerably less (1 to 10 db) than should be expected for the case of no relaxation.

These results must be accepted with some reservation. We have seen that Lawson's assumption of instantaneous attainment of equilibrium from a state of excess ionization (more precisely, attainment of equilibrium in a time short compared with the period of the wave) is

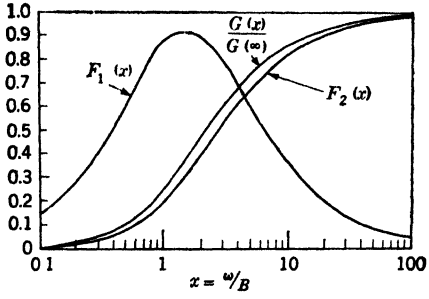

FIG. 4·12.—Frequency variation of shunt capacitance C and shunt conductance G.
$C(x) = C_0[1 - \alpha F_1(x)], G(x) = \alpha\omega C_0 F_1(x), G(\infty) = \frac{3}{2}\alpha B C_0, \alpha \equiv \frac{N - N_0}{N}$.

not really valid. An improved theory, discarding this assumption, should not, however, alter the general qualitative picture. A second defect of the Lawson theory is the assumption of an abrupt transition from the bulk semiconductor with its equilibrium distribution of free electrons to the barrier region where no free electrons are present. Actually, the transition must take place smoothly over a region of thickness $\approx D(kT/e\phi_0)^{1/2}$, where D is the barrier thickness, and ϕ_0, the barrier height. The potential energy will change by about kT in this region. The assumption of an abrupt transition should be valid, therefore, if the amplitude V_0 of the voltage wave is large compared with kT/e. In the case of low-level rectification (video detection), however, $V_0 \ll kT/e$ and the theory must be considerably modified.

At all events, it is clear that barrier relaxation plays an important role in high-frequency rectification and conversion. It undoubtedly deserves more attention than has been paid to it so far. The crucial parameter is the depth of the impurity levels ΔE_1, since the value of the relaxation constant B depends strongly on the value of ΔE_1 by Eq. (77). The value of ΔE_1 could perhaps be controlled to some extent by the type of impurity used, or possibly by surface treatment, if the surface levels play a role in relaxation processes.

PART II
THE CRYSTAL CONVERTER

CHAPTER 5

FREQUENCY CONVERSION

5·1. Discussion of the General Problem.—In this chapter there will be considered in some detail the theory of *mixing* in a nonlinear element. Mixing may be broadly defined as the conversion of a signal from one frequency to another by combining it with a local-oscillator voltage in a nonlinear device. The nonlinear device is essential to the mixing process. By the principle of superposition, the addition of two frequencies in a *linear* device never results in additional (beat) frequencies and only the two original frequencies will exist in the Fourier spectrum of the resulting disturbance. If, however, the device is nonlinear, it will generate the sum and difference frequencies of the applied signals. These newly created frequencies will, in turn, beat with each other and with the originally applied signals to create still more frequencies, and so on *ad infinitum*. The spectrum of the output voltage from such a nonlinear device may, therefore, be exceedingly complex.

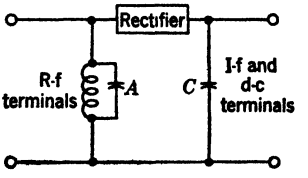

FIG. 5·1.—Transformation from a two-terminal to a four-terminal mixer.

The most common and, at the same time, most important mixing process in microwave receivers is the conversion of a signal at a microwave frequency to one at a relatively low frequency, say 30 Mc/sec. This process takes place in a "mixer," which consists of a two-terminal nonlinear device, such as a crystal rectifier, having associated linear circuits designed to provide separate terminals for high frequencies (signal and local-oscillator waves) and for the low frequencies (i-f and d-c). Figure 5·1 shows one method by which the separation may be accomplished. The tuned circuit A offers a high impedance to the local-oscillator and signal frequencies and a low impedance to intermediate frequencies and d-c; the capacitance C has the opposite effect. The reader is referred to Vol. 24 of the Radiation Laboratory Series for details of mixer structure. For the present we need know only that there are provided separate terminal pairs at high and low frequency.

To the high-frequency terminals is applied the local-oscillator microwave of frequency[1] ω at a level of about 1 mw. The mixer is nonlinear

[1] In this chapter "frequency" will be used loosely to denote the angular frequency $2\pi f$, where f is the usual frequency denoting the number of oscillations per unit time.

at this level and generates harmonics $n\omega$ ($n = 2, 3, \ldots$) of the local-oscillator frequency. In addition the microwave signal of frequency α is also applied to the high-frequency terminal but at such a relatively low level (usually less than 1 μw) that there is negligible generation of its harmonics. To be specific, it will be assumed henceforth that $\alpha > \omega$. No loss of generality results from this assumption. The function of the mixer is to convert the signal frequency α to the intermediate frequency $\beta \equiv \alpha - \omega$ as a result of beating α with ω. Many other beat frequencies are generated, however. The "sum frequency" $\alpha + \omega$ is generated with almost equal efficiency. The frequencies $\alpha - \omega$ and $\alpha + \omega$ beat with ω and $n\omega$ to create additional frequencies. These in turn are partially converted to further beat products; the resulting spectrum is thus complicated. Beats between two low-level frequencies, such as α and β, can be ignored, however, since the conversion loss for such a process is very large. Thus the spectrum consists of the following frequencies.

At low level.....	$\alpha \equiv \omega + \beta$	(signal)
	β	(intermediate frequency)
	$\gamma \equiv \omega - \beta$	(image)
	$n\omega \pm \beta$	(harmonic sidebands)
At high level.....	ω	(local oscillator)
	$n\omega$	(harmonics of the local oscillator)

The image frequency $\omega - \beta$ is of special importance in the theory of mixers; it is denoted here by a special symbol γ.

From the following discussion, which treats the relative importance of these frequencies, it is apparent that many of them can be excluded from further consideration. The image and the harmonic sidebands can be called "parasitics," since power consumed at these frequencies is taken from the available signal power and the result is to lower conversion efficiency of the signal to the intermediate frequency. By terminating the parasitics reactively we can insure their minimum power dissipation. There is another effect of the parasitics which should be considered in mixer design, namely, the phase relationship they bear to the signal, depending on their termination. By proper choice of reactive termination of the parasitics we can insure that the intermediate-frequency voltages produced by beating of the parasitics with ω or $n\omega$ add in phase to the direct product of the beat between $\omega + \beta$ and ω. These two considerations should be kept in mind in the following discussion of the relative importance of the various parasitics.

Let P_s be the power available from the signal source and let G be the conversion gain from signal to intermediate frequency (G is the reciprocal of the conversion loss L and is usually between 0.1 and 0.3).

Then the power available at intermediate frequency is GP_s. This power must be compared with the power available at intermediate frequency as a result of beating of parasitics with the local-oscillator frequency or its harmonics. The first step is to estimate the efficiency of production of the various parasitics. As a convenient rule of thumb, adequate for an order-of-magnitude calculation, it may be assumed that the conversion gain as a result of beating any frequency with the nth harmonic $n\omega$ of the local oscillator to form the sum or difference frequency is about G^n. Falkoff[1] has shown that this is roughly true for the case $n = 2$.

First there must be considered the effect of the image sideband $\gamma = \omega - \beta$. This frequency is generated as a result of the direct beat between signal $\omega + \beta$ and the second harmonic 2ω, and also as a result of the beat between β and ω. The first process gives G^2P_s as the power available at γ, according to our rule, and the second method also gives G^2P_s, since the power available at β is GP_s and the second beating with ω adds another factor of about G. The power at γ is then of the order of G^2P_s and, by beating γ with ω to produce β, another factor of G is added, with the result that the power available at β by the indirect path through γ is of order G^3P_s.

Next, let us consider the upper harmonic sideband $2\omega + \beta$. This sideband is produced by the direct beat between the signal $\omega + \beta$ and ω. Its available power is thus about GP_s. The intermediate frequency β can be produced by beating $2\omega + \beta$ with 2ω with a conversion gain of about G^2. Thus the available power at intermediate frequency by the indirect path through $2\omega + \beta$ is about G^3P_s.

It might be concluded from these arguments that the parasitics $2\omega + \beta$ and $\omega - \beta$ are of comparable importance. This is not true, however. One must consider not only the power but also the phase at intermediate frequency. If the i-f voltage produced by one of the indirect paths is in phase with that of the direct beat of $\omega + \beta$ with ω, the effect of the parasitic is greatly enhanced. Now the phase at intermediate frequency is determined by the phase of the parasitic, which can be controlled to a certain extent by adjusting the impedance terminating the parasitic at the mixer terminals. This control is more effective at the image frequency $\omega - \beta$ than at the harmonic sideband $2\omega + \beta$ because of the shunting effect of the barrier capacitance of the crystal. This capacitance cannot be completely tuned out because of the series spreading resistance (see Fig. 5·12). Let us consider a typical case. Assuming the capacitive reactance of the barrier equal to 50 ohms at $2\omega + \beta$ and 100 ohms at $\omega - \beta$, and taking 30 ohms for the spreading resistance, we find that the impedance that can be presented to the barrier is restricted

[1] D. L. Falkoff, RL Report No. 958, Mar. 11, 1946.

to a range of 13.4 in absolute value in the case of $\omega - \beta$ and to a range of only 4.6 for $2\omega + \beta$. A second reason for the greater importance of $\omega - \beta$ is that the i-f impedance of the mixer depends strongly on the termination to $\omega - \beta$ but only weakly on that to $2\omega + \beta$. The converse is true for the r-f impedance, but the i-f impedance is, in general, the more critical factor in receiver design.

So far only the parasitics $\omega - \beta$ and $2\omega + \beta$ have been considered. A similar analysis applied to the other second harmonic sideband $2\omega - \beta$ and to higher harmonic sidebands shows that they are relatively ineffective. The available i-f power as a result of the intervention of these parasitics is of order G^5P_s or less.

It must be concluded that the image $\omega - \beta$ is the most important parasitic and that special attention should be paid to its termination in mixer design. Care should be taken to insure a nondissipative termination at the harmonic sideband $2\omega + \beta$, but it does not seem likely that the particular choice of this termination is of much consequence. The remaining parasitics may be ignored, to a good approximation, except that in the case of very low loss mixers it should be insured that their terminations are reactive.

These considerations allow us to ignore all parasitics in the theory except $\omega - \beta$, provided that it is consistently assumed that $2\omega + \beta$ is reactively terminated.

The mixing process considered above is not the most general that could have been imagined. There might, for example, be the case of a signal at $\omega + \beta$ and beating oscillator at ω/n, i.e., a subharmonic of ω. The result would be lower conversion efficiency to β for the same local-oscillator power (and hence the same noise output), but in the case of extremely high frequencies, where it is impractical or inconvenient to provide an oscillator at ω, this circumvention may be used to advantage. The case of a subharmonic oscillator will be considered again in Sec. 5·15, but for the present the discussion is confined to an oscillator at ω.

Another possibility not hitherto mentioned is "harmonic reinforcement," which amounts to enhancing the effect of the second harmonic of the local oscillator by correct adjustment of its termination or by deliberately injecting second-harmonic power from some external source. Only the first method has been resorted to in practice. The result is to increase the effectiveness of the parasitics $2\omega + \beta$ and $\omega - \beta$. Harmonic reinforcement will be considered briefly in Sec. 5·14.

5·2. The Admittance Matrix.—The principal objectives in this chapter are to derive expressions for conversion loss and for terminal impedance of a mixer; to show how conversion loss is related to properties of the mixer that are simple to measure; to examine the effect of the image-frequency termination on conversion; and to show how conversion

efficiency is related to the physical structure of the mixer and, in particular, the physical properties of crystal rectifiers.

These tasks are enormously facilitated by the circumstances that signal, image, and intermediate frequencies are at such low levels that the relations among their voltages and currents are linear. It is true that conversion results from the nonlinearity of the mixer, but this nonlinearity affects only the local-oscillator wave and its interactions with the low-level components; interactions among the low-level components themselves are linear to a high degree of accuracy. The mixer, in fact, can be regarded as a linear network with separate terminals at the signal frequency, at the image frequency, and at the intermediate frequency. Physically, the signal and image terminals are identical, but conceptually they may be regarded as distinct, since they can be separately loaded by the use of sharply resonant tuned circuits.

Using subscripts α, β, and γ to refer, respectively, to signal, intermediate frequency, and image, we can denote by i_α, i_β, and i_γ the complex current amplitudes and by e_α, e_β, e_γ the complex voltage amplitudes at the three frequencies. We may write the linear relations between these quantities as

$$\left.\begin{aligned} i_\alpha &= y_{\alpha\alpha}e_\alpha + y_{\alpha\beta}e_\beta + y_{\alpha\gamma}e_\gamma^*, \\ i_\beta &= y_{\beta\alpha}e_\alpha + y_{\beta\beta}e_\beta + y_{\beta\gamma}e_\gamma^*, \\ i_\gamma^* &= y_{\gamma\alpha}e_\alpha + y_{\gamma\beta}e_\beta + y_{\gamma\gamma}e_\gamma^*, \end{aligned}\right\} \tag{1}$$

or, in matrix form, as

$$\begin{pmatrix} i_\alpha \\ i_\beta \\ i_\gamma^* \end{pmatrix} = \mathsf{Y} \begin{pmatrix} e_\alpha \\ e_\beta \\ e_\gamma^* \end{pmatrix}, \tag{2}$$

where

$$\mathsf{Y} \equiv \begin{pmatrix} y_{\alpha\alpha} & y_{\alpha\beta} & y_{\alpha\gamma} \\ y_{\beta\alpha} & y_{\beta\beta} & y_{\beta\gamma} \\ y_{\gamma\alpha} & y_{\gamma\beta} & y_{\gamma\gamma} \end{pmatrix} \tag{3}$$

is the so-called "admittance matrix" of the mixer. The asterisk (*) denotes complex conjugate; it will later (Sec. 5·3) be shown that the image current and voltage must appear as complex conjugates in these relations.

The admittance matrix defines all the conversion properties of the mixer. In the general form, Eq. (3), it consists of nine complex quantities ($y_{\alpha\alpha}$, etc.), eighteen quantities in all, but it will be shown presently that the number of independent quantities is much smaller—in the simplest possible case there are only four independent quantities in the admittance matrix. An immediate reduction in the number of independent quantities is achieved on the basis of symmetry by introducing the assumption that the mixer is a "low Q" device. By this is meant

that there are no sharply resonant circuits in the mixer[1] that can discriminate between signal $(\omega + \beta)$ and image $(\omega - \beta)$, which are close together in frequency since $\omega \gg \beta$. This assumption is valid in the case of most practical mixers and will be adopted throughout this chapter. On the basis of symmetry between signal α and image γ we may then write

$$\begin{aligned} y_{\gamma\beta} &= y^*_{\alpha\beta}, & y_{\gamma\alpha} &= y^*_{\alpha\gamma} \\ y_{\beta\gamma} &= y^*_{\beta\alpha}, & y_{\gamma\gamma} &= y^*_{\alpha\alpha}. \end{aligned} \tag{4}$$

Conjugate signs on the right are necessary because the image current and voltage enter into Eq. (2) as complex conjugates.

If it is further assumed that there is no resonant circuit in the mixer capable of discriminating between intermediate frequency and direct current, it is implied also that $y_{\beta\beta}$, the i-f self-admittance, is real. This is expressed by writing

$$y_{\beta\beta} = g_{\beta\beta}, \tag{5}$$

in conformity with a general rule adopted here that g and b with appropriate subscripts stand, respectively, for the real and imaginary parts of an admittance element. The general form for a "low Q" mixer is then

$$\mathrm{Y} = \begin{pmatrix} y_{\alpha\alpha} & y_{\alpha\beta} & y_{\alpha\gamma} \\ y_{\beta\alpha} & g_{\beta\beta} & y^*_{\beta\alpha} \\ y^*_{\alpha\gamma} & y^*_{\alpha\beta} & y^*_{\alpha\alpha} \end{pmatrix}. \tag{6}$$

The number of independent quantities has thus been reduced to nine. Conditions (4) and (5) for a "low Q" mixer are introduced here as a result of a plausibility argument. They are justified rigorously in Sec. 5·3.

A further reduction is possible from the fact that we have at our disposal the origin of time. This fact would be of no help if only a single frequency were involved. In the present case there are three frequencies and the relative phases depend on the time t. Let us suppose that the time origin is shifted, making

$$t = t' + t_0, \tag{7}$$

where t' is the new time variable and t_0 is a constant. It is clear that relations between the complex voltage amplitudes corresponding to the old and the new time zeros are

$$\left.\begin{aligned} e'_\alpha &= e_\alpha e^{j(\omega+\beta)t_0}, \\ e'_\beta &= e_\beta e^{j\beta t_0}, \\ e'_\gamma &= e_\gamma e^{j(\omega-\beta)t_0}, \end{aligned}\right\} \tag{8}$$

[1] This does not imply of course that such circuits are not attached to the mixer terminals.

where a primed quantity is measured in the new time scale. Similar relations hold for the current amplitudes. Substituting these relations in Eqs. (2) and (6), we obtain for the admittance matrix Y′ in the new time scale

$$\mathsf{Y}' = \begin{pmatrix} y_{\alpha\alpha} & y_{\alpha\beta}e^{j\omega t_0} & y_{\alpha\gamma}e^{2j\omega t_0} \\ y_{\beta\alpha}e^{-j\omega t_0} & g_{\beta\beta} & y^*_{\beta\alpha}e^{j\omega t_0} \\ y^*_{\alpha\gamma}e^{-2j\omega t_0} & y^*_{\alpha\beta}e^{-j\omega t_0} & y^*_{\alpha\alpha} \end{pmatrix}. \tag{9}$$

Since t_0 is arbitrary, it can be chosen to make either $y'_{\alpha\beta}$, $y'_{\beta\alpha}$, or $y'_{\alpha\gamma}$ real, in any case reducing by one the number of independent quantities, leaving eight in all.

A further reduction in the number of independent quantities is possible by attaching to the mixer's r-f terminals an ideal (dissipationless) transformer. Such a transformer is characterized by two parameters which, for example, might be the position of the r-f terminals along a transmission line and a susceptance across these terminals. These two parameters can be chosen to reduce the number of independent quantities to six.

This is as far as we can go on purely theoretical grounds. A still further reduction is possible, however, on empirical grounds. The admittance matrix of a linear *passive* circuit is well known to be symmetrical about its main diagonal. If this situation exists in the present case we have

$$y_{\alpha\beta} = y_{\beta\alpha}, \tag{10a}$$

and

$$y_{\alpha\gamma} = y^*_{\alpha\gamma}, \tag{10b}$$

and it is said that *reciprocity holds*. Experimentally reciprocity is found to hold for all silicon converters tested but not, in general, for germanium converters.

Reciprocity cannot be completely divorced from choice of time zero. Thus if $t_0 \neq 0$ in Eq. (9), reciprocity could hold, for example, in the form of Eq. (6) for Y but not for Y′. If it is supposed that the time zero has been chosen to make $y_{\alpha\gamma}$ real, Eq. (10*a*) alone expresses the condition of reciprocity; the second equation (10*b*) is redundant. Since Eq. (10*a*) is a relation between complex quantities, reciprocity imposes two conditions and reduces the number of independent quantities to four. The two conditions may be written

$$|y_{\alpha\beta}| = |y_{\beta\alpha}|, \tag{11}$$

and

$$\arg(y_{\alpha\beta}) = \arg(y_{\beta\alpha}). \tag{12}$$

It is an experimental fact that when reciprocity fails, as it does for many germanium crystals, the failure is in Eq. (11) and not in Eq. (12).

Although there is no theoretical explanation for this, Eq. (12) will in the greater part of this chapter be assumed generally true on empirical grounds. This equation expresses what is called *weak reciprocity*, whereas Eqs. (11) and (12) together may be called *full reciprocity*. Weak reciprocity (alone) reduces the number of independent quantities in our

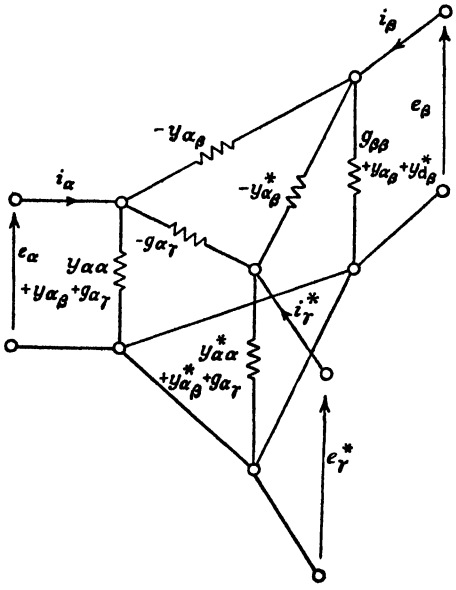

FIG. 5·2.—Equivalent linear network of a crystal mixer for which reciprocity holds.

matrix to five. It is shown in Sec. 5·5 that these five quantities can be chosen so as to make the matrix real, that is,

$$\mathsf{Y} = \begin{pmatrix} g_{\alpha\alpha} & g_{\alpha\beta} & g_{\alpha\gamma} \\ g_{\beta\alpha} & g_{\beta\beta} & g_{\beta\alpha} \\ g_{\alpha\gamma} & g_{\alpha\beta} & g_{\alpha\alpha} \end{pmatrix}, \tag{13}$$

and it is also shown that, if weak reciprocity does not hold, Y cannot be written in real form, whether Eq. (11) holds or not. It is shown in Sec. 5·7 that the assumption of weak reciprocity greatly simplifies the analysis of the effect of image termination on conversion loss.

If full reciprocity holds, conversion loss can be determined by means of impedance measurements (see Sec. 7·3). Also, if full reciprocity holds, the mixer can be represented as a linear passive network.

This network is shown in Fig. 5·2. That it indeed represents Eqs. (2) and (6) with reciprocity can be verified in the usual way by supposing the network to be driven from one of the terminal pairs with opposite pairs short-circuited, and then considering the driving-point admittance and the currents flowing through the short-circuited terminals. This process must be repeated for each terminal pair.

THE PHENOMENOLOGICAL THEORY OF CONVERSION

The elements of the admittance matrix define all the conversion properties of the mixer. Dicke and Roberts[1] have devised a phenomenological theory of mixers that makes it possible to determine all of these elements from simple measurements at the mixer terminals without any knowledge or assumptions about the internal structure of the mixer. The necessary measurements are at local-oscillator level and do not require the presence of a signal. This theory will now be developed. A physical theory of mixers giving the elements of the admittance matrix in terms of the physical constitution of the mixer is presented in Secs. 5·11 to 5·14.

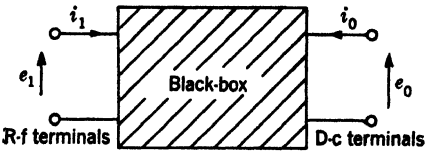

FIG. 5·3.—A mixer conceived as a "black-box" with r-f and d-c terminals.

5·3. The Admittance Matrix in Terms of Measurable Parameters.—The mixer is conceived as a "black-box" with r-f and d-c terminals as shown in Fig. 5·3. Two approximations are made which hold well for practical mixers. It is assumed that the mixer is "low Q" in the sense indicated in Sec. 5·2 and that no harmonic voltages appear at the r-f terminals. The latter assumption does not exclude the presence of harmonics inside the mixer.

The essential idea of this "black-box" theory is that under the above conditions r-f (at local-oscillator level) and d-c voltages can be applied to the appropriate mixer terminals and the effects of the small currents and voltages at signal and image frequencies regarded as small variations of the local-oscillator current and voltage; similarly the i-f current and voltage can be regarded as small variations of the d-c current and voltage.

Let us, accordingly, suppose that the black box of Fig. 5·3 has voltages and currents at its two terminal pairs given by the following scheme.

	R-f terminals	D-c terminals
Voltage	Re $(e_1 e^{j\omega t})$	e_0
Current	Re $(i_1 e^{j\omega t})$	i_0

The following notation will be used.

$y \equiv i_1/e_1$ = r-f admittance of the mixer at local-oscillator level.
$|e_1|$ = absolute value of e_1.
e_1^* = complex conjugate of e_1.

[1] R. H. Dicke and S. Roberts, "Theory of Radar Mixers," RL Report No. 61-5, July 15, 1942; and R. H. Dicke, "A Reciprocity Theorem and Its Application to the Measurement of Gain of Microwave Crystal Mixers," RL Report No. 61-18, Apr. 13, 1943. See also R. N. Smith, "The Theory of Mixers in Terms of Measurable Mixer Constants," NDRC 14-259, Purdue U., Mar. 24, 1944.

The currents flowing at the terminals will be functions of the voltages of the form[1]

$$i_0 = i_0(e_0, |e_1|), \tag{14a}$$
$$i_1 = e_1 y(e_0, |e_1|). \tag{14b}$$

Differentiating Eq. (14) with respect to e_0, e_1, and e_1^*, we obtain

$$\left.\begin{aligned} di_0 &= \frac{\partial i_0}{\partial e_0} de_0 + \frac{1}{2}\frac{e_1^*}{|e_1|}\frac{\partial i_0}{\partial |e_1|} de_1 + \frac{1}{2}\frac{e_1}{|e_1|}\frac{\partial i_0}{\partial |e_1|} de_1^*, \\ di_1 &= e_1 \frac{\partial y}{\partial e_0} de_0 + \left(y + \frac{1}{2}|e_1|\frac{\partial y}{\partial |e_1|}\right) de_1 + \frac{1}{2}\frac{e_1^2}{|e_1|}\frac{\partial y}{\partial |e_1|} de_1^*. \end{aligned}\right\} \tag{15}$$

If there is added to Eqs. (15) the complex conjugate of the second of these equations they will have the form of a three-terminal-pair network. If the time zero is chosen so that de_1 is real, Eqs. (15) have the form of a two-terminal-pair network. It is usually more convenient, however, to choose the time zero so that e_1 is real.

There is now introduced the signal voltage e_α and the image voltage e_γ as differentials of the local-oscillator voltage e_1. The physical r-f voltage will be

$$\text{Re}\,[(e_1 + de_1)e^{j\omega t}] = \text{Re}\,(e_1 e^{j\omega t}) + \text{Re}\,(de_1 e^{j\omega t}). \tag{16}$$

If we then put

$$de_1 = e_\alpha e^{j\beta t} + e_\gamma e^{-j\beta t}, \tag{17}$$

the r-f voltage is seen to be composed of three parts:

$$\left.\begin{array}{ll} \text{Re}\,(e_1 e^{j\omega t}) & \text{(local oscillator)} \\ +\text{Re}\,(e_\alpha e^{j(\omega+\beta)t}) & \text{(signal)} \\ +\text{Re}\,(e_\gamma e^{j(\omega-\beta)t}) & \text{(image).} \end{array}\right\} \tag{18}$$

It has been assumed that these are the only voltages appearing at the r-f terminals. That is, harmonic voltages at these terminals, although not necessarily inside the mixer, are neglected.

In a similar way the i-f voltage e_β can be introduced as a differential of the d-c bias voltage e_0 at the d-c terminals. The voltage at these terminals will then be

$$e_0 + de_0, \tag{19}$$

where

$$de_0 = \text{Re}\,(e_\beta e^{j\beta t}) \qquad \text{(i-f voltage).} \tag{20}$$

In the same manner the currents at signal, image, and intermediate frequencies are introduced as differentials of the local-oscillator current i_1 and the d-c current i_0:

[1] It is clear that the direct current i_0 and the r-f admittance y are independent of the time origin and therefore depend on the absolute value of e_1 but not on its phase.

$$di_1 = i_\alpha e^{j\beta t} + i_\gamma e^{-j\beta t}; \tag{21}$$
$$di_0 = \mathrm{Re}\,(i_\beta e^{j\beta t}). \tag{22}$$

Using Eqs. (17), (20), (21), and (22) and separating the different time factors, we obtain from Eq. (15)

$$\left.\begin{aligned}
i_\alpha &= \left(y + \frac{1}{2}|e_1|\frac{\partial y}{\partial |e_1|}\right)e_\alpha + \frac{1}{2}e_1\frac{\partial y}{\partial e_0}e_\beta + \frac{1}{2}\frac{e_1^2}{|e_1|}\frac{\partial y}{\partial |e_1|}e^*,\\
i_\beta &= \frac{e_1^*}{|e_1|}\frac{\partial i_0}{\partial |e_1|}e_\alpha + \frac{\partial i_0}{\partial e_0}e_\beta + \frac{e_1}{|e_1|}\frac{\partial i_0}{\partial |e_1|}e_\gamma^*,\\
i_\gamma^* &= \frac{1}{2}\left(\frac{e_1^2}{|e_1|}\frac{\partial y}{\partial |e_1|}\right)^* e_\alpha + \frac{1}{2}\left(e_1\frac{\partial y}{\partial e_0}\right)^* e_\beta + \left(y + \frac{1}{2}|e_1|\frac{\partial y}{\partial |e_1|}\right)^* e_\gamma^*.
\end{aligned}\right\} \tag{23}$$

These equations are observed to have the same form as Eq. (1). As expected, the symmetry relations [Eqs. (4) and (5)] for a "low Q" mixer hold. Comparing coefficients of Eqs. (1) and (23) we find

$$y_{\alpha\alpha} = y + \frac{1}{2}|e_1|\frac{\partial y}{\partial |e_1|}, \tag{24a}$$
$$y_{\alpha\beta} = \frac{1}{2}e_1\frac{\partial y}{\partial e_0}, \tag{24b}$$
$$y_{\alpha\gamma} = \frac{1}{2}\frac{e_1^2}{|e_1|}\frac{\partial y}{\partial |e_1|}, \tag{24c}$$
$$y_{\beta\alpha} = \frac{e_1^*}{|e_1|}\frac{\partial i_0}{\partial |e_1|}, \tag{24d}$$
$$g_{\beta\beta} = \frac{\partial i_0}{\partial e_0}. \tag{24e}$$

Let us choose the time zero so that e_1 is real; Eqs. (24) then become

$$\begin{gathered}
g_{\beta\beta} = \frac{\partial i_0}{\partial e_0}, \qquad y_{\beta\alpha} = \frac{\partial i_0}{\partial e_1},\\
y_{\alpha\beta} = \frac{1}{2}e_1\frac{\partial y}{\partial e_0}, \qquad y_{\alpha\alpha} = y + \frac{1}{2}e_1\frac{\partial y}{\partial e_1},\\
y_{\alpha\gamma} = \frac{1}{2}e_1\frac{\partial y}{\partial e_1}.
\end{gathered} \tag{25}$$

We note that the local-oscillator admittance is now given by

$$y = y_{\alpha\alpha} - y_{\alpha\gamma}. \tag{26}$$

5·4. Transformation of the Matrix to New Variables.—All the parameters on the right-hand side of Eq. (16) are directly measurable except for the r-f voltage e_1. In principle e_1 could be found by measuring the r-f power P and the mixer conductance g. It is more convenient, however, to transform Eqs. (25) to new independent variables P and V, where

$$P = \tfrac{1}{2}ge_1^2 \tag{27a}$$

is the r-f power delivered to the mixer and

$$V = e_0. \tag{27b}$$

Although V is identical with e_0, it is distinguished with a new symbol to avoid explicit statement of what is held constant in partial differentiation. Thus $\partial/\partial e_0$ implies that e_1 is held constant; $\partial/\partial V$ implies that P is held constant. The transformation from e_1 to P is useful since P is directly measurable, whereas e_1 is not. In fact, the value of e_1 is somewhat arbitrary, since it depends on the definition of the line impedance.[1]

If X is some dependent variable, then we have the general partial differential relations

$$\frac{\partial X}{\partial e_0} = \frac{\partial X}{\partial V}\frac{\partial V}{\partial e_0} + \frac{\partial X}{\partial P}\frac{\partial P}{\partial e_0}, \tag{28}$$

$$\frac{\partial X}{\partial e_1} = \frac{\partial X}{\partial V}\frac{\partial V}{\partial e_1} + \frac{\partial X}{\partial P}\frac{\partial P}{\partial e_1}. \tag{29}$$

Substituting Eqs. (27*a*) and (27*b*) in Eq. (28), we have

$$\frac{\partial X}{\partial e_0} = \frac{\partial X}{\partial V} + \frac{P}{g}\frac{\partial g}{\partial e_0}\frac{\partial X}{\partial p}. \tag{30}$$

If $X = g$ in Eq. (30),

$$\frac{\partial g}{\partial e_0} = \frac{1}{D}\frac{\partial g}{\partial V}, \tag{31}$$

where

$$D = 1 - \frac{P}{g}\frac{\partial g}{\partial P}. \tag{32}$$

Substituting Eq. (31) in Eq. (30), we obtain

$$\frac{\partial X}{\partial e_0} = \frac{\partial X}{\partial V} + \frac{P}{D}\frac{1}{g}\frac{\partial g}{\partial V}\frac{\partial X}{\partial P}. \tag{33}$$

Substituting Eqs. (27*a*) and (27*b*) in Eq. (29) yields

$$\frac{\partial X}{\partial e_1} = \left(\sqrt{2gP} + \frac{P}{g}\frac{\partial g}{\partial e_1}\right)\frac{\partial X}{\partial P}. \tag{34}$$

If $X = g$ in Eq. (34),

$$\frac{\partial g}{\partial e_1} = \frac{\sqrt{2gP}}{D}\frac{\partial g}{\partial P}. \tag{35}$$

[1] It should be noted here that y and its derivatives are always measured in terms of the characteristic admittance g_0 of the r-f transmission line. Since, in the case of a waveguide, there is no unique definition of g_0, the actual value of y in ohms is somewhat ambiguous. This, however, occasions no real difficulty. The properties of the mixer with which we shall be concerned are its terminal impedances and its conversion loss. The latter is a pure number and so is independent of the units used; the former will always be given in terms of g_0 at the r-f end, and will be independent of g_0 at the i-f end.

Substituting Eq. (35) in Eq. (34) yields, finally,

$$\frac{\partial X}{\partial e_1} = \frac{\sqrt{2gP}}{D}\frac{\partial X}{\partial P}. \tag{36}$$

Equations (33) and (36) make it possible to transform Eqs. (25) at once to the new independent variables P and V. The following abbreviations will be used:

$$\left.\begin{aligned} G_V &\equiv \frac{\partial i_0}{\partial V}, & g_V &\equiv \frac{1}{g}\frac{\partial g}{\partial V}, & b_V &\equiv \frac{1}{g}\frac{\partial b}{\partial V}, \\ G_P &\equiv \frac{\partial i_0}{\partial P}, & g_P &\equiv \frac{1}{g}\frac{\partial g}{\partial P}, & b_P &\equiv \frac{1}{g}\frac{\partial b}{\partial P}. \end{aligned}\right\} \tag{37}$$

The transformed Eqs. (25) become ($y_{\beta\alpha}$ is now real because of the choice of time zero)

$$g_{\beta\beta} = G_V + \frac{Pg_VG_P}{D}; \tag{38}$$

$$y_{\beta\alpha} = g_{\beta\alpha} = \frac{\sqrt{2gPG_P}}{D}; \tag{39}$$

$$y_{\alpha\beta} = g_{\alpha\beta} + jb_{\alpha\beta}, \tag{40}$$

where

$$g_{\alpha\beta} = \frac{1}{2}\frac{\sqrt{2gP}}{D}g_V, \tag{41}$$

and

$$b_{\alpha\beta} = \frac{1}{2}\sqrt{2gP}\left(b_v + \frac{P}{D}g_Vb_P\right); \tag{42}$$

$$y_{\alpha\alpha} = g_{\alpha\alpha} + jb_{\alpha\alpha}, \tag{43}$$

where

$$g_{\alpha\alpha} = g + \frac{Pg}{D}g_P = \frac{g}{D}, \tag{44}$$

and

$$b_{\alpha\alpha} = b + \frac{Pg}{D}b_p; \tag{45}$$

$$y_{\alpha\gamma} = g_{\alpha\gamma} + jb_{\alpha\gamma}, \tag{46}$$

where

$$g_{\alpha\gamma} = \frac{Pg}{D}g_P = g\left(\frac{1}{D} - 1\right), \tag{47}$$

and

$$b_{\alpha\gamma} = \frac{Pgb_P}{D}. \tag{48}$$

In the preceding set of equations the quantity D is given by Eq. (32).

Equations (38) through (48) give all the elements of the mixer matrix

in terms of directly measurable quantities. In Sec. 5·7 these equations are used to derive expressions for conversion loss and mixer admittances.

5·5. Reciprocity.—In Sec. 5·2 reciprocity was defined and its importance in mixer theory pointed out. Reciprocity has been tested experimentally with the aid of the expressions derived in the preceding section. Before describing these tests the general subject of reciprocity will be discussed in more detail.

In Sec. 5·2 it was shown that the equations expressing reciprocity depend on the choice of time zero. Equations (10) express reciprocity provided the time zero is chosen to make $y_{\alpha\gamma}$ real. A more general expression, valid for any time zero, is obtained by applying the condition of symmetry about the main diagonal of the mixer matrix to the general expression, Eq. (9), for the matrix. We obtain

$$y_{\beta\alpha} = y_{\alpha\beta}e^{2j\omega t_0}, \tag{49}$$

$$y^*_{\alpha\gamma} = y_{\alpha\gamma}e^{4j\omega t_0}, \tag{50}$$

where t_0 is an arbitrary constant. Eliminating t_0 between Eqs. (49) and (50), we obtain the two conditions

$$|y_{\alpha\beta}| = |y_{\beta\alpha}|, \tag{51}$$

and

$$\arg y_{\alpha\beta} = \arg y_{\beta\alpha} + \arg y_{\alpha\gamma}. \tag{52}$$

We observe that Eq. (51) is identical with Eq. (11). Equation (52) expresses the general condition of *weak reciprocity* and reduces to Eq. (12) when $\arg y_{\alpha\gamma} = 0$. A statement of weak reciprocity alternative to Eq. (52) is $\operatorname{Im}(y_{\alpha\beta}y^*_{\beta\alpha}y^*_{\alpha\gamma}) = 0$.

Dicke[1] has shown that *full reciprocity* holds if the following conditions are satisfied:

1. The phase of the electric field is constant over the rectifying barrier, that is, the metal-semiconductor junction of the crystal rectifier.
2. There exists a time zero with respect to which the electric field at the barrier is an even function of time.

To these conditions must be added a third not explicitly stated by Dicke, although it is implied in his proof:

3. The electric charge on the barrier is a linear function of the barrier voltage.

Condition 3 excludes the possibility of a variable barrier capacitance.

Conditions 1, 2, and 3 together are sufficient for reciprocity and 3 at least is necessary. It appears, however, (see Appendix A) that Condition 2 may be weakened by replacing the word "even" by "even or odd."

[1] R. H. Dicke, "A Reciprocity Theorem and Its Application to the Measurement of Gain of Microwave Crystal Mixers," RL Report No. 61-18, Apr. 13, 1943.

The "reciprocity theorem" of Dicke is given in Appendix A. It is proved there that, under the above conditions, Eqs. (49) and (50) are satisfied when t_0 is the time zero of Condition 2.

Of the three conditions for reciprocity only the first can be expected to hold to a good approximation. The second condition implies either absence of harmonic voltages at the barrier or the existence of certain phase relationships between harmonics and the fundamental. The third condition may be approximately true for silicon rectifiers but it is known that the barrier capacitance of germanium rectifiers is decidedly variable with barrier voltage.

However this may be, it is a fact that full reciprocity is closely fulfilled for silicon crystals and, although it fails for many germanium crystals, weak reciprocity holds for all crystals tested, silicon and germanium. Experimental tests of reciprocity have been made by Smith,[1] who measured the elements of the admittance matrix by means of Eqs. (38) to (48) which give the matrix elements in terms of measurable parameters. To find the form of the reciprocity relations in these variables, we first consider Eqs. (24). The weak-reciprocity condition, Eq. (52), applied to these equations gives, if ϕ is the phase of e_1,

$$\phi + \arg \frac{\partial y}{\partial e_0} = -\phi + 2\phi + \arg \frac{\partial y}{\partial |e_1|},$$

or

$$\arg \frac{\partial y}{\partial e_0} = \arg \frac{\partial y}{\partial |e_1|}. \tag{53}$$

Now any general variation in y is given by

$$dy = \frac{\partial y}{\partial e_0} de_0 + \frac{\partial y}{\partial |e_1|} d|e_1| \tag{54}$$

or, in the new variables, by

$$dy = \frac{\partial y}{\partial V} dV + \frac{\partial y}{\partial P} dP. \tag{55}$$

According to Eq. (53) $\partial y/\partial e_0$ and $\partial y/\partial |e_1|$ have the same phase. It follows then from Eq. (54) that all variations in y without regard to cause must have the same phase. Hence, from Eq. (55),

$$\arg \frac{\partial y}{\partial V} = \arg \frac{\partial y}{\partial P}. \tag{56}$$

This is the form that the weak reciprocity condition takes in the new variables. If we put $y = g + jb$ and use the abbreviations of Eq. (37),

[1] R. N. Smith, "The Theory of Mixers in Terms of Measurable Mixer Constants," NDRC 14-259, Purdue U., Mar. 24, 1944.

Eq. (56) becomes

$$\frac{b_V}{g_V} = \frac{b_P}{g_P}. \tag{57}$$

Full reciprocity holds if, in addition to Eq. (52), Eq. (51) is also satisfied. That is,

$$|y_{\beta\alpha}|^2 = g_{\alpha\beta}^2 + b_{\alpha\beta}^2. \tag{58}$$

Now Eq. (42) becomes, with use of Eq. (57),

$$b_{\alpha\beta} = \frac{1}{2}\sqrt{2g}P\frac{b_V}{D}. \tag{59}$$

Using Eqs. (59), (39), and (41), we find that Eq. (58) becomes

$$4G_P^2 = g_V^2 + b_V^2,$$

or

$$[illegible] \tag{60}$$

Equations (57) and (60) are the general reciprocity conditions in the new variables, although Eq. (57) alone expresses the weak-reciprocity condition. Smith has tested Eqs. (57) and (60) experimentally. The results of his test of Eq. (60) are given in Fig. 5·4, in which $|\partial y/\partial V|$ is plotted against $2g(\partial i_0/\partial P)$ for a number of crystal rectifiers, both silicon and germanium. All but three of the points fall, within experimental error, on a straight line whose slope is not quite 45°. According to Smith, the small departure of the slope from 45° can probably be ascribed to a systematic error in the measurement of r-f power. It is interesting to note that the only three points which do not fall along this line represent germanium crystals. Apparently some germanium crystals obey the reciprocity condition, Eq. (60), whereas others fail; on the other hand, *all* silicon units tested obey Eq. (60).

Smith also tested the weak-reciprocity condition, Eq. (56), with the same crystals shown in Fig. 5·4. The result was that all these crystals, including the ones that fail Eq. (60), satisfy Eq. (56) within experimental error. The weak reciprocity condition appears to have more universal validity than the general condition. So far, however, attempts to weaken the general physical conditions 1, 2, and 3 as stated above so that they will imply Eq. (56) but not necessarily Eq. (60) have failed. In Sec. 7·3 some additional evidence will be presented showing that full reciprocity is satisfied by silicon units but not always by germanium units.[1]

[1] Smith's results have since been confirmed by Apker's extensive measurements. See L. Apker, "Note on Reciprocity Failure in Crystal Mixers," NDRC 15-931-16. GE Co., Mar. 9, 1945; and "Theory of a Double Mixer for Spectrum Analyzer Applications," NDRC 15-931-16, GE Co., Apr. 3, 1945.

It will now be shown that weak reciprocity is the necessary and sufficient condition for the admittance matrix of the mixer to be reduced to the real form of Eq. (13). Equations (24) are made use of and it is assumed, first, that the matrix is real; then it is shown that this implies weak reciprocity. Equation (24*d*) makes it clear that e_1 is real, thus fixing the choice of time zero. With e_1 real, it is easily seen from Eqs. (24*b*) and (24*c*) that both $\partial y/\partial e_0$ and $\partial y/\partial|e_1|$ are real. Excluding the possibility that $\partial y/\partial e_0$ and $\partial y/\partial|e_1|$ have opposite signs,[1] it follows that

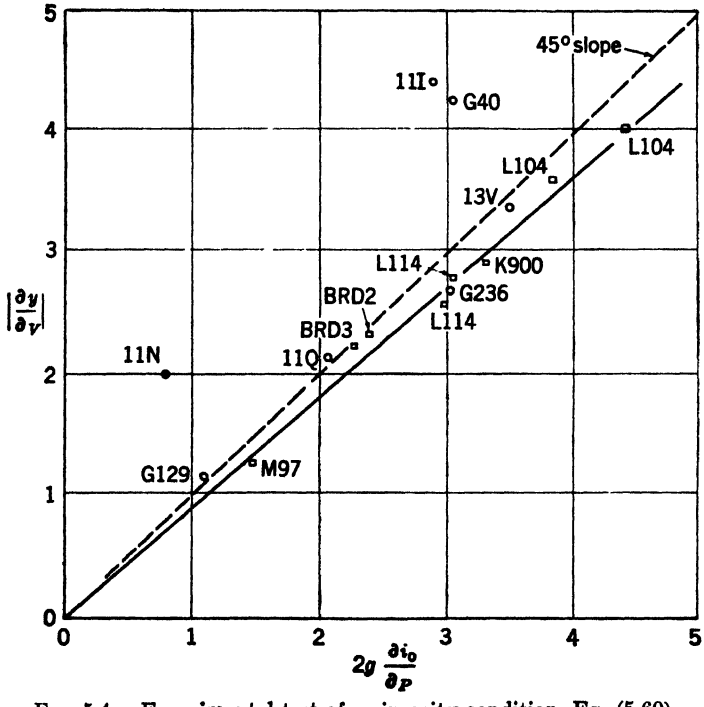

FIG. 5·4.—Experimental test of reciprocity condition, Eq. (5·60).

these quantities have the same phase, in accordance with the weak reciprocity condition Eq. (53). Thus the necessity is proved.

To prove the sufficiency of weak reciprocity, it should be noted that, if $\partial y/\partial e_0$ and $\partial y/\partial|e_1|$ have the same phase in accordance with the weak reciprocity, Eq. (53), and if e_1 is made real by choice of time zero, then $\partial y/\partial e_0$ and $\partial y/\partial|e_1|$ become real together at the appropriate r-f terminals position. From Eqs. (24) the only remaining complex element is y_{aa},

[1] This possibility is excluded on physical grounds. An increase in either local-oscillator voltage or d-c bias must always increase the barrier conductance of a crystal rectifier, as is evident from the form of the current-voltage characteristic (see Fig. 2·5). These effects—of the same sign—could not be transformed into effects of opposite sign at the r-f terminals. Thus $\partial y/\partial e_0$ and $\partial y/\partial|e_1|$, if they are real, must have the same sign.

which can be made real by adding a susceptance at the r-f terminals to cancel the imaginary part of y [see Eq. (24a)]. The addition of susceptance does not affect any parameter of the matrix other than $y_{\alpha\alpha}$. The whole matrix thus becomes real.

It is noteworthy that, if the time zero is chosen to make e_1 real and positive, and if the r-f terminals are located where $\partial y/\partial e_0$ and $\partial y/\partial|e_1|$ are real and positive, and if $y_{\alpha\alpha}$ is made real by addition of a susceptance, every element of the matrix is not only real, but real and positive. In this case the r-f terminals are said to be at the "standard position." The standard position has a periodicity of one-half wavelength along the r-f transmission line.

CONVERSION LOSS AND MIXER ADMITTANCES

5·6. General Definition of Loss; Special Cases.—Following Friis,[1] conversion loss is defined as the ratio of the available input (signal) power to the available output (i-f) power. This definition makes conversion loss depend on the r-f load admittance (i.e., the internal admittance of the signal source) as well as on the properties of the mixer (i.e., the mixer admittance matrix). In some respects this is unfortunate, since it is desirable, for specification purposes, to be able to assign to a crystal converter a number characterizing its conversion efficiency. It is possible, however, to define special r-f load admittances in terms of the elements of the admittance matrix. The corresponding values of conversion loss are then characteristic of the mixer.

For example, let us suppose that the r-f circuit attached to the r-f mixer terminals is broadly tuned in the sense that it presents the same load admittance to the image frequency as to the signal frequency. This is called the "broadband case." Under this condition, there may be defined at least two special values of the conversion loss that depend only on the mixer matrix. The first, denoted here by L_0, is the conversion loss when the load admittance, common to signal and image, is adjusted to match (i.e., to be the complex conjugate of) the admittance y of the mixer to the local-oscillator wave. Now L_0 is not the minimum loss in the broadband case. It will presently be shown, however, that a unique minimum loss usually exists[2] in the broadband case, and it is denoted by L_2. In the next section it will be seen that L_0 and L_2 are nearly equal. In *acceptance testing* of mixer crystals, it is L_0 that is measured and specified.

[1] H. T. Friis, "Receiver Noise Figures," BTL Report MM-42-160-39, May 13, 1942; and *Proc. I.R.E.*, **32**, 419 (1944).

[2] This minimum will always exist provided there is excluded the possibility of negative i-f conductance. Crystals exhibiting negative i-f conductance under certain r-f tuning conditions have recently been made by H. Q. North, however. Such cases are excluded from the present discussion and are treated separately in Chap. 13.

Other values of loss would not require definition were it not for the fact that few microwave receivers actually operate under conditions of broadband r-f tuning. In microwave receivers, the signal is fed to the mixer through a TR (transmit-receive) switch. This resonant cavity presents (approximately) a match to the mixer at signal frequency. In the case of a narrow-band TR switch (the usual case), however, the impedance at the exit window of the TR switch at the image frequency is a good approximation to a short circuit. If the mixer is matched at signal frequency to the conductance g_0 of the line connecting it with the TR switch then, under usual conditions, the TR switch will present an admittance g_0 to the signal (frequency ω_0) and an admittance

$$y = g_0\left[1 + jQ\left(\frac{\omega}{\omega_0} - \frac{\omega_0}{\omega}\right)\right]$$

to neighboring frequencies ω. Here Q is the "loaded Q" of the TR switch, a typical value of which is 250. If the signal frequency is, let us say, 3000 Mc/sec and the intermediate frequency 30 Mc/sec, the image frequency will be 2940 Mc/sec and $y(Q = 250)$ for the image will be $g_0(1 - j10)$—which is a fair approximation to a short circuit. The approximation will not be as good at higher signal frequencies for the same intermediate frequency. If we travel down the line from the TR switch to the position where the admittance matrix of the mixer becomes real (the standard mixer terminals), the short circuit will be transformed at this point to some general susceptance which can be made nearly a short circuit or nearly an open circuit by proper "line-stretching."

Thus it is necessary to examine the separate dependences of conversion loss on signal load and on image load admittance. There are two reasons for this. We wish to see, first, how the specified loss L_0 compares with the loss under operating conditions and, second, what benefit, if any, can be derived from the fact that we have at our disposal two load admittances instead of only one.

In treating this problem (see Secs. 5·8 and 5·9) the image termination will be assumed fixed at some arbitrary value, and the dependence of loss on signal load admittance alone will be studied. It will be shown that the loss has a unique minimum value in general (see the preceding footnote) as a function of signal load admittance. This value of loss is designated by L_m. The dependence of L_m on image termination is then studied (see Sec. 5·9). At the standard r-f terminal position, that is, the position for a real admittance matrix, the loss L_m has special values L_1 for short-circuited image terminals, and L_3 for open-circuited image terminals. The lesser of L_1 and L_3 is shown to be the *smallest possible value* of loss under *any* conditions of r-f tuning. It is also shown that, for some crystals, a value of image load admittance, real at the standard r-f

terminals, exists such that L_m is a maximum with respect to the image termination. This *maximum* loss, when it exists, is called L_4. If L_4 does not exist, it is shown that the greater of L_1 and L_3 is the largest possible value of L_m. Expressions are derived giving all five special values of loss, L_0, L_1, L_2, L_3, and L_4, in terms of the elements of the admittance matrix.

Table 5·1 lists the various special values of loss together with their definitions, for easy reference.

TABLE 5·1.—SPECIAL VALUES OF CONVERSION LOSS

A Symbol	*B* Signal load admittance	*C* Image load admittance	*D* Other special conditions or circumstances
L	Arbitrary	Arbitrary	None
L_0 (measured by standard test sets)	Same as C	Same as B	Mixer matched to local-oscillator wave
L_2	Same as C	Same as B	R-f load admittance adjusted to minimize loss
L_m	Adjusted to minimize loss	Arbitrary	None
Special values of L_m:			
L_1	Adjusted to minimize loss	Short circuit at standard r-f terminals	If $L_1 < L_3$, L_1 is smallest possible L
L_3	Adjusted to minimize loss	Open circuit at standard r-f terminals	If $L_3 < L_1$, L_3 is smallest possible L
L_4	Adjusted to minimize loss	Adjusted to maximize loss	L_4 exists only when L_1 or L_3 is not the greatest possible value of L_m

5·7. Conversion Loss in the Broadband Case.—Expressions are now derived for L_0 and L_2 in terms of the elements of the admittance matrix.

Let us consider a mixer with terminations as illustrated in Fig. 5·5.

It will be assumed that the weak reciprocity condition, Eq. (52), holds and that the mixer matrix has been made real by, let us say, the method described in Sec. 5·5. The behavior of the mixer is then described by Eqs. (2) and (13):

$$\left.\begin{aligned} i_\alpha &= g_{\alpha\alpha}e_\alpha + g_{\alpha\beta}e_\beta + g_{\alpha\gamma}e_\gamma^*, \\ i_\beta &= g_{\beta\alpha}e_\alpha + g_{\beta\beta}e_\beta + g_{\beta\alpha}e_\gamma^*, \\ i_\gamma^* &= g_{\alpha\gamma}e_\alpha + g_{\alpha\beta}e_\beta + g_{\alpha\alpha}e_\gamma^*. \end{aligned}\right\} \tag{61}$$

In Fig. 5·5 we have a current source of peak strength A and internal conductance g_a attached to the signal terminals. The same conductance g_a will be considered to load the image terminals. The available input signal power is, then,

$$P_i = \frac{A^2}{8g_a}. \tag{62}$$

To find the available output power we first find the i-f conductance g_β of the mixer. We have, from Fig. 5·5 (suppressing A),

$$\left.\begin{aligned} i_\alpha &= -g_a e_\alpha, \\ i_\gamma^* &= -g_a e_\gamma^*, \\ i_\beta &= g_\beta e_\beta. \end{aligned}\right\} \tag{63}$$

Substituting Eq. (63) into Eq. (55), we get three homogeneous equations in e_α, e_β, and e_γ^*, the determinant of which must vanish for con-

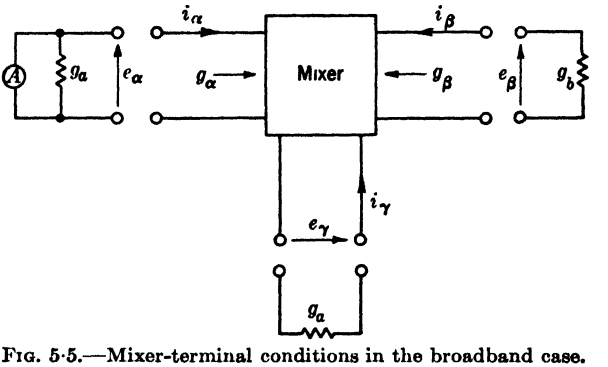

FIG. 5·5.—Mixer-terminal conditions in the broadband case.

sistency. Solving for g_β, we find

$$g_\beta = g_{\beta\beta} - \frac{2g_{\alpha\beta}g_{\beta\alpha}}{g_{\alpha\alpha} + g_{\alpha\gamma} + g_a}. \tag{64}$$

The i-f current i_β flowing into a short circuit ($g_b = \infty$) is next found. In Eq. (61) we put

$$\begin{aligned} e_\beta &= 0, \\ A &= i_\alpha + g_a e_\alpha, \\ i_\gamma^* &= -g_a e_\gamma^*, \end{aligned}$$

and solve for i_β. We get

$$i_\beta = \frac{A g_{\beta\alpha}}{g_{\alpha\alpha} + g_{\alpha\gamma} + g_a}. \tag{65}$$

The available output power will then be

$$P_0 = \frac{i_\beta^2}{8g_\beta}. \tag{66}$$

The conversion loss is given by

$$L = \frac{P_1}{P_0} = \frac{g_{\alpha\beta}}{g_{\beta\alpha}} \frac{(g_{\alpha\alpha} + g_{\alpha\gamma} + g_a)[g_{\beta\beta}(g_{\alpha\alpha}g_{\alpha\gamma} + g_a) - 2g_{\alpha\beta}g_{\beta\alpha}]}{g_a g_{\alpha\beta} g_{\beta\alpha}}. \tag{67}$$

The loss is seen to be a function of the signal generator admittance g_a as well as of the matrix elements $g_{\alpha\alpha}$, etc. It is interesting to notice that, with the exception of the ratio $g_{\alpha\beta}/g_{\beta\alpha}$, all of the mixer parameters in Eq. (67) may be determined by impedance measurements alone. Further, these impedance measurements may be made at either the r-f or the i-f terminals. If full reciprocity holds, $g_{\alpha\beta} = g_{\beta\alpha}$, and the loss may be determined by impedance measurements alone. A discussion of such methods of loss measurement is given in Sec. 7·3.

Minimum Loss L_2.—Let us now minimize L with respect to the signal-generator conductance g_a. As there will be occasion to repeat this process later it will be given here in general form. Let a function of a variable x be defined as

$$f(x) = \frac{(x + a)(x + a - b)}{bx}, \tag{68}$$

where we assume $0 < b < a$. Then, since $a\dfrac{(a - b)}{b} > 0$, f has a unique minimum at

$$x_0 = \sqrt{a(a - b)}, \tag{69}$$

and the minimum value of f is

$$f(x_0) = \frac{1 + \sqrt{1 - (b/a)}}{1 - \sqrt{1 - (b/a)}}. \tag{70}$$

In Eq. (67) we put

$$a = 1 + \frac{g_{\alpha\gamma}}{g_{\alpha\alpha}},$$

$$b = \frac{2g_{\alpha\beta}g_{\beta\alpha}}{g_{\alpha\alpha}g_{\beta\beta}},$$

$$x = \frac{g_a}{g_{\alpha\alpha}};$$

hence,

$$L = \frac{2g_{\alpha\beta}}{g_{\beta\alpha}} f(x). \tag{71}$$

The minimum value of L is then, by Eq. (70),

$$L_2 = 2\frac{g_{\alpha\beta}}{g_{\beta\alpha}} \frac{1 + \sqrt{1 - \eta_2}}{1 - \sqrt{1 - \eta_2}}, \tag{72}$$

where

$$\eta_2 = \frac{b}{a} = \frac{2g_{\alpha\beta}g_{\beta\alpha}}{g_{\beta\beta}(g_{\alpha\alpha} + g_{\alpha\gamma})}. \tag{73}$$

The optimum value of the signal load conductance, which is also the signal conductance of the mixer, is

$$g_a = x_0 g_{\alpha\alpha} = (g_{\alpha\alpha} + g_{\alpha\gamma}) \sqrt{1 - \eta_2}. \tag{74}$$

Substituting Eq. (74) in Eq. (64) we obtain for the i-f admittance of the mixer

$$g_\beta = g_{\beta\beta} \sqrt{1 - \eta_2}. \tag{75}$$

The smallest loss as a function of η_2 is obtained if $\eta_2 = 1$, whence L_2 becomes $2g_{\alpha\beta}/g_{\beta\alpha}$. If full reciprocity holds, $g_{\alpha\beta} = g_{\beta\alpha}$ and the loss can never become less than 2 (3 db), which corresponds to half the signal power being converted to intermediate frequency and the other half to the image frequency. This result is predicated, however, on the assumption that η_2, Eq. (73), is less than unity. If η_2 is greater than unity, the condition $b < a$ leading to the existence of a minimum in $f(x)$, Eq. (68), is not satisfied. There is no minimum loss in this case and conversion with amplification is possible. Crystals exhibiting this property have actually been made; they are discussed in Chap. 13. Such crystals are not suitable for converter use because of excessive noise generation, and thus in the present chapter discussion is limited to the normal case of $\eta_2 < 1$.

Conversion Loss L_0—Mixer Matched to the Local Oscillator.—Under usual conditions of loss measurement (but not, in general, of use) the mixer is not matched to the signal but to the local-oscillator wave. For this case we have

$$g_a = g. \tag{76}$$

Introducing this into our general expression for loss, Eq. (63) and remembering that $g = g_{\alpha\alpha} - g_{\alpha\gamma}$ [Eq. (26)], we obtain

$$L_0 = \frac{4g_{\alpha\alpha}(g_{\beta\beta}g_{\alpha\alpha} - g_{\alpha\beta}g_{\beta\alpha})}{g g_{\beta\alpha}^2}. \tag{77}$$

If we now substitute in Eq. (77) the expressions for the matrix elements in terms of measurable parameters as given by Eqs. (38) to (48), we find

$$L_0 = \frac{2G_V}{PG_P^2} \tag{78}$$

or

$$L_0 = \frac{2\dfrac{\partial i_0}{\partial V}}{P\left(\dfrac{\partial i_0}{\partial P}\right)^2}. \tag{79}$$

Equation (79) is the basis for the incremental method in the absolute calibration of loss-measuring equipment as shown in Sec. 7·4. The

validity of Eq. (79) does not depend on full reciprocity, nor even on weak reciprocity, although the latter was assumed in its derivation. This statement may be verified by assuming a matrix of the general form of Eq. (6), in which no assumptions about reciprocity are made; Eqs. (77), (78), and (79) remain valid even if both reciprocity conditions fail. However, L_0 is not the minimum loss obtainable under broadband r-f tuning conditions. In fact, $L_0 \geqq L_2$, where L_2 is given by Eq. (70).

Since L_0 is the particular value of loss specified to be measured in acceptance testing of crystals, it is well to have an estimate of the amount by which it exceeds the minimum loss L_2. The optimum value of g_a is $x_0 g_{\alpha\alpha}$, as given by Eq. (72). If we put $g_a = Cx_0 g_{\alpha\alpha}$ into Eq. (63), the latter reduces to

$$L = L_2 \frac{(1+C)^2}{4C}\left[1 - \frac{4}{L_2'^2}\left(\frac{1-C}{1+C}\right)^2\right], \tag{80}$$

where

$$L_2' = L_2 \frac{g_{\beta\alpha}}{g_{\alpha\beta}}.$$

Now C is the ratio of the actual signal-generator conductance to the optimum value and $\frac{(C+1)^2}{4C}$ is the usual mismatching factor. In addition to this, however, there is the factor $1 - \frac{4}{L_2'^2}\left(\frac{1-C}{1+C}\right)^2$, which is less than unity, although much closer to unity in general than $\frac{(1+C)^2}{4C}$. The extra factor arises from the circumstance that a mismatch is always somewhat mitigated because the image frequency is also mismatched—a smaller percentage of power being lost, therefore, by image conversion. Equation (80) may be written in the form

$$L = L_2\left[1 + \frac{(1-C)^2}{4C}\left(1 - \frac{4}{L_2'^2}\right)\right]. \tag{81}$$

If we now assume that the mixer is matched to the local oscillator and, hence, $g_a = g$, then

$$\frac{1}{C} = \frac{g_{\alpha\alpha} + g_{\alpha\gamma}}{g}\sqrt{1-\eta_2} = \frac{g_{\alpha\alpha} + g_{\alpha\gamma}}{g}\,\frac{L_2' - 2}{L_2' + 2}. \tag{82}$$

Substituting Eq. (82) in Eq. (81) and using the notation of Eqs. (38) to (48), we obtain

$$L_0 = L_2\left[1 + \frac{\left(\frac{2}{L_2'} - Pg_P\right)^2}{1 - P^2 g_P^2}\right]. \tag{83}$$

Using a result equivalent to Eq. (83) and measuring the parameters involved, Smith[1] found L_0/L_2 for thirteen crystals. He obtained values ranging from 1.00 to 1.04, or a maximum discrepancy of less than 0.2 db. The difference between L_0 and L_2 does not, therefore, seem to be very serious.

The i-f admittance of the mixer is given by Eq. (64). If $g_a = g$, it becomes

$$g_\beta = g_{\beta\beta} - \frac{g_{\alpha\beta}g_{\beta\alpha}}{g_{\alpha\alpha}}. \tag{84a}$$

Using the notation of Eqs. (38) to (48), g_β reduces simply to

$$g_\beta = G_V = \frac{\partial i_0}{\partial V}. \tag{84b}$$

If, instead of allowing g_a to equal g, we assume some general signal generator conductance g_a, we find from Eq. (64) and Eqs. (38) to (48) that[2]

$$g_\beta = G_V + \frac{PG_Pg_V}{\dfrac{g_a + g}{g_a - g} - Pg_P}. \tag{85}$$

This is seen to reduce to Eq. (84) when $g_a = g$.

The admittance g_α of the mixer to the signal frequency depends on the signal-generator conductance g_a, since g_a is the load applied to the image terminals. Substituting

$$\left.\begin{aligned} i_\alpha &= g_\alpha e_\alpha, \\ i_\beta &= -g_b e_\beta, \\ i_\gamma &= -g_a e_\gamma, \end{aligned}\right\} \tag{86}$$

in Eq. (61) and solving for g_α, we arrive at

$$g_\alpha = g + (g + g_a)\frac{g_{\alpha\gamma}(g_{\beta\beta} + g_b) - g_{\alpha\beta}g_{\beta\alpha}}{(g_{\alpha\alpha} + g_a)(g_{\beta\beta} + g_b) - g_{\alpha\beta}g_{\beta\alpha}}. \tag{87}$$

In the notation of Eqs. (38) to (48) this becomes

$$g_\alpha = g\left[1 + (g + g_a)P\frac{g_P(G_V + g_b) - g_VG_P}{(g + g_aD)(G_v + g_b) - g_aPg_vG_P}\right]. \tag{88}$$

For $g_a = g$, this becomes

$$g_\alpha = g\left[1 + 2P\frac{g_P(G_v + g_b) - g_VG_P}{(1 + D)(G_V + g_b) - Pg_VG_P}\right]. \tag{89}$$

[1] R. N. Smith, "The Theory of Mixers in Terms of Measurable Constant Mixers," NDRC 14-259, Purdue Univ., Mar. 24, 1944.

[2] This result was first derived by Smith, *loc. cit.*

5·8. General Expression for Conversion Loss. *Minimization with Respect to the Signal Load Admittance.*—In the preceding section expressions were derived for loss under the restricting condition that the load admittances at signal and image frequencies were the same. These results are now generalized to find the loss with arbitrary load admittances. To make the results as general as possible, no assumptions will, for the present, be made with regard to reciprocity, but the investigation will be based on the general form of the admittance matrix of a low-Q mixer [Eq. (6)].

If an admittance y_c loads the image terminals, we have

$$i_\gamma^* = -y_c^* e_\gamma^*. \tag{90}$$

With the aid of Eq. (90) we eliminate i_γ^* and e_γ^* from Eqs. (2) and (6). This has the effect of reducing the admittance matrix to a 2-by-2 form, in which only signal and i-f quantities appear.

We obtain

$$\begin{pmatrix} i_\alpha \\ i_\beta \end{pmatrix} = \begin{pmatrix} Y_{\alpha\alpha} & Y_{\alpha\beta} \\ Y_{\beta\alpha} & Y_{\beta\beta} \end{pmatrix} \begin{pmatrix} e_\alpha \\ e_\beta \end{pmatrix}, \tag{91}$$

where

$$Y_{\alpha\alpha} = y_{\alpha\alpha} - \frac{y_{\alpha\gamma} y_{\alpha\gamma}^*}{y_{\alpha\alpha}^* + y_c^*}, \tag{92}$$

$$Y_{\alpha\beta} = y_{\alpha\beta} - \frac{y_{\alpha\gamma} y_{\alpha\beta}^*}{y_{\alpha\alpha}^* + y_c^*}, \tag{93}$$

$$Y_{\beta\alpha} = y_{\beta\alpha} - \frac{y_{\alpha\gamma}^* y_{\beta\alpha}^*}{y_{\alpha\alpha}^* + y_c^*}, \tag{94}$$

$$Y_{\beta\beta} = g_{\beta\beta} - \frac{y_{\beta\alpha}^* y_{\alpha\beta}^*}{y_{\alpha\alpha}^* + y_c^*}. \tag{95}$$

Equation (91) represents the two-terminal-pair device of Fig. 5·6. The mixer is driven at the signal terminals by the current source of peak strength A of internal admittance $y_a = g_a + jb_a$. The available power from the signal generator is then

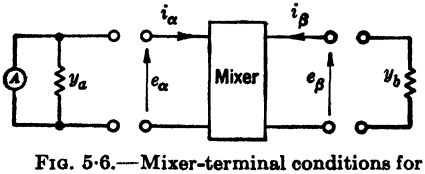

FIG. 5·6.—Mixer-terminal conditions for arbitrary image load considered as part of the mixer.

$$P_i = \frac{A^2}{8g_a}. \tag{96}$$

The i-f admittance y_β of the mixer is found by suppressing A, with the result

$$i_\alpha = -y_a e_\alpha. \tag{97}$$

Substituting this in Eq. (91) and solving for $y_\beta = i_\beta/e_\beta$, we find

$$y_\beta = Y_{\beta\beta} - \frac{Y_{\alpha\beta} Y_{\beta\alpha}}{Y_{\alpha\alpha} + y_a}. \tag{98}$$

Next, we find the i-f current into a short circuit. With

$$A = e_\alpha y_a + i_\alpha, \qquad e_\beta = 0,$$

we find for i_β

$$i_\beta = A \frac{Y_{\beta\alpha}}{Y_{\alpha\alpha} + y_a}. \tag{99}$$

The available output power is

$$P_0 = \frac{|i_\beta|^2}{8g_\beta} = \frac{A^2}{8g_\beta} \frac{|Y_{\beta\alpha}|^2}{|Y_{\alpha\alpha} + y_a|^2}. \tag{100}$$

The loss is then given by

$$L = \frac{P_i}{P_0} = \frac{g_\beta}{g_a} \frac{|y_a + Y_{\alpha\alpha}|^2}{|Y_{\beta\alpha}|^2}, \tag{101}$$

where $y_a = g_a + jb_a$. If one puts

$$Y_{\alpha\alpha} = G_{\alpha\alpha} + jB_{\alpha\alpha}, \tag{102}$$

$$Y_{\beta\beta} = G_{\beta\beta} + jB_{\beta\beta}, \tag{103}$$

and

$$u + jv = \frac{Y_{\alpha\beta} Y_{\beta\alpha}}{G_{\alpha\alpha} G_{\beta\beta}}, \tag{104}$$

Eq. (101) becomes

$$L = \left|\frac{Y_{\alpha\beta}}{Y_{\beta\alpha}}\right| \frac{(G_{\alpha\alpha} + g_a)^2 - uG_{\alpha\alpha}(G_{\alpha\alpha} + g_a) + (B_{\alpha\alpha} + b_a)^2 - vG_{\alpha\alpha}(B_{\alpha\alpha} + b_a)}{G_{\alpha\alpha} g_a \sqrt{u^2 + v^2}}. \tag{105}$$

Equation (105) gives the most general expression for conversion loss. All other loss expressions may be derived from it by specialization. For example, taking y_a and y_c to be equal and real, and assuming weak reciprocity, with the consequence of a real 3-by-3 admittance matrix, we obtain from Eq. (105) the expression [Eq. (67)] for loss in the "broadband" case.

Equation (105) is a convenient starting point for an investigation of the separate effects of signal and image load admittances. Leaving the image load admittance fixed at the arbitrary value y_c, it is first shown that L of Eq. (105) has a unique minimum as a function of signal load admittance.

To minimize L with respect to the signal-load admittance

$$y_a = g_a + jb_a,$$

we first put

$$\frac{\partial L}{\partial b_a} = 0,$$

which, applied to Eq. (105), gives

$$b_a = \frac{v}{2} G_{\alpha\alpha} - B_{\alpha\alpha}. \tag{106}$$

If Eq. (106) is substituted in Eq. (105), and the symbols x, a, and b defined by

$$\left.\begin{aligned} x &\equiv \frac{g_a}{G_{\alpha\alpha}}, \\ a &\equiv 1 - \frac{u}{2} + \frac{1}{2}\sqrt{u^2 + v^2}, \\ b &\equiv \sqrt{u^2 + v^2}, \end{aligned}\right\} \tag{107}$$

Eq. (105) takes the form

$$L = \left|\frac{Y_{\alpha\beta}}{Y_{\beta\alpha}}\right| \frac{(x + a)(x + a - b)}{bx}. \tag{108}$$

The expression involving x here is seen to have the general form of Eq. (68). Accordingly from Eq. (70) we find, for the minimum loss,

$$L_m = \left|\frac{Y_{\alpha\beta}}{Y_{\beta\alpha}}\right| \frac{1 + \sqrt{1 - \epsilon}}{1 - \sqrt{1 - \epsilon}}, \tag{109}$$

where

$$\epsilon = \frac{b}{a} = \frac{2|Y_{\alpha\beta}Y_{\beta\alpha}|}{2G_{\alpha\alpha}G_{\beta\beta} + |Y_{\alpha\beta}Y_{\beta\alpha}| - Re(Y_{\alpha\beta}Y_{\beta\alpha})}. \tag{110}$$

The signal load admittance giving this minimum loss is found from Eqs. (69), (107), (104), and (106). It is

$$\begin{aligned} y_a = G_{\alpha\alpha} &\left\{1 - \frac{\mathrm{Re}\,(Y_{\alpha\beta}Y_{\beta\alpha})}{G_{\alpha\alpha}G_{\beta\beta}} - \left[\frac{\mathrm{Im}\,(Y_{\alpha\beta}Y_{\beta\alpha})}{2G_{\alpha\alpha}G_{\beta\beta}}\right]^2\right\}^{1/2} \\ &- j\left\{B_{\alpha\alpha} - \frac{1}{2}G_{\alpha\alpha}\left[\frac{\mathrm{Im}\,(Y_{\alpha\beta}Y_{\beta\alpha})}{G_{\alpha\alpha}G_{\beta\beta}}\right]\right\}. \end{aligned} \tag{111}$$

With the signal load admittance [Eq. (111)], the i-f admittance of the mixer, found by substituting Eq. (111) into Eq. (98), is

$$\begin{aligned} y_\beta = G_{\beta\beta} &\left\{1 - \frac{\mathrm{Re}\,(Y_{\alpha\beta}Y_{\beta\alpha})}{G_{\alpha\alpha}G_{\beta\beta}} - \left[\frac{\mathrm{Im}\,(Y_{\alpha\beta}Y_{\beta\alpha})}{2G_{\alpha\alpha}G_{\beta\beta}}\right]^2\right\}^{1/2} \\ &+ j\left\{B_{\beta\beta} - \frac{1}{2}G_{\beta\beta}\left[\frac{\mathrm{Im}\,(Y_{\alpha\beta}Y_{\beta\alpha})}{G_{\alpha\alpha}G_{\beta\beta}}\right]\right\}. \end{aligned} \tag{112}$$

If an i-f load admittance y_b, equal to the conjugate of y_β [Eq. (112)], is placed across the i-f terminals, it may be shown from Eq. (91) in the usual way that the signal admittance y_α of the mixer is the conjugate of y_a, as given by Eq. (111). The mixer will then be matched to the signal and i-f external circuits.

The expression for L_m, Eq. (109), is seen to be a function of two parameters, ϵ, as given by Eq. (110), and the factor $|Y_{\alpha\beta}/Y_{\beta\alpha}|$. Each of these parameters depends on the elements of the 3-by-3 admittance matrix and also on the image load admittance y_c. The next task is to study the dependence of L_m on y_c, but first a simplification is introduced without which the mathematical problem would be hopelessly complicated. Weak reciprocity is assumed to hold. Since no exception has been found to it in large numbers of crystals tested, this assumption is well justified. The assumption of weak reciprocity greatly simplifies the problem. One immediate consequence is that one of the two parameters, namely $|Y_{\alpha\beta}/Y_{\beta\alpha}|$, becomes independent of image load admittance. To see this, the ratio of Eq. (93) to Eq. (94) is taken, putting

$$y_{\alpha\beta} = |y_{\alpha\beta}|e^{j\phi_{\alpha\beta}}, \text{ etc.}$$

We obtain

$$\left|\frac{Y_{\alpha\beta}}{Y_{\beta\alpha}}\right| = \left|\frac{y_{\alpha\beta}}{y_{\beta\alpha}}\right| \frac{e^{j(\phi_{\alpha\beta}+\phi_{\beta\alpha})}(y^*_{\alpha\alpha} + y^*_c) - |y_{\alpha\gamma}|e^{j(\phi_{\alpha\gamma}+\phi_{\beta\alpha}-\phi_{\alpha\beta})}}{e^{j(\phi_{\alpha\beta}+\phi_{\beta\alpha})}(y^*_{\alpha\alpha} + y^*_c) - |y_{\alpha\gamma}|e^{-j(\phi_{\alpha\gamma}+\phi_{\beta\alpha}-\phi_{\alpha\beta})}};$$

but, by weak reciprocity, Eq. (52),

$$\phi_{\alpha\gamma} + \phi_{\beta\alpha} - \phi_{\alpha\beta} = 0, \tag{113}$$

with the result

$$\left|\frac{Y_{\alpha\beta}}{Y_{\beta\alpha}}\right| = \left|\frac{y_{\alpha\beta}}{y_{\beta\alpha}}\right|, \tag{114}$$

and is independent of y_c.

If, in addition to Eq. (113), we assume full reciprocity, then, from Eqs. (114) and (51),

$$\left|\frac{Y_{\alpha\beta}}{Y_{\beta\alpha}}\right| = 1. \tag{115}$$

Now weak reciprocity appears to be well established experimentally, so we are not unduly restricting ourselves by assuming Eq. (114), as is done in the following discussion. The loss is now a function of y_c only through the dependence of ϵ on y_c. This dependence is not only on the complex variable y_c, but also on y_c^*. Thus ϵ is a general function of the two variables g_c and b_c and the relationship is given by Eq. (110).

The assumption of weak reciprocity guarantees that the 3-by-3 matrix can be put into real, positive form by the addition of reactive transformers at the r-f terminals.[1] It is assumed henceforth that this has been done. One consequence is that Eq. (114) becomes

$$\left|\frac{Y_{\alpha\beta}}{Y_{\beta\alpha}}\right| = \frac{g_{\alpha\beta}}{g_{\beta\alpha}}. \tag{116}$$

A second consequence is that the dependence of ϵ on g_c and b_c is much

[1] This is proved in Sec. 5·5.

less complicated than in the general case. This dependence of ϵ and the consequent dependence of L_m on image load admittance is studied in the following section.

5·9. Effect of the Image Termination on Conversion Loss.—The conversion loss L_m, minimized with respect to the signal load admittance, is given in consequence of Eqs. (109) and (116) by

$$L_m = \frac{g_{\alpha\beta}}{g_{\beta\alpha}} \frac{1 + \sqrt{1 - \epsilon}}{1 - \sqrt{1 - \epsilon}}, \tag{117}$$

where ϵ is given by Eq. (110).

The assumption of a real 3-by-3 matrix (a consequence of weak reciprocity) simplifies the expression for ϵ to

$$\epsilon = \epsilon_1 \frac{[(\chi + 1 - \theta)^2 + \psi^2][(\chi + 1)^2 + \psi^2]}{[(\chi + 1)(\chi + 1 - \theta^2) + \psi^2][(\chi + 1)(\chi + 1 - \epsilon_1) + \psi^2] + \epsilon_1\theta^2\chi^2}, \tag{118}$$

where there have been introduced the abbreviations

$$\left.\begin{aligned} \epsilon_1 &\equiv \frac{g_{\alpha\beta}g_{\beta\alpha}}{g_{\alpha\alpha}g_{\alpha\gamma}}, \\ \theta &\equiv \frac{g_{\alpha\gamma}}{g_{\alpha\alpha}}, \\ \chi &\equiv \frac{g_c}{g_{\alpha\alpha}}, \\ \psi &\equiv \frac{b_c}{g_{\alpha\alpha}}. \end{aligned}\right\} \tag{119}$$

The loss L_m depends on image termination $y_c = g_c + jb_c$ through the dependence of ϵ on χ and ψ. This dependence is rather complicated, and to see how L_m depends on image termination we must first study the functional dependence

$$\epsilon = \epsilon(\chi,\psi).$$

We find at once as special cases of Eq. (118) the values of ϵ for short-circuited and for open-circuited image terminals.

1. Short-circuited image terminals.

$$y_c = \infty \qquad \text{(i.e., either } \chi = \infty \text{ or } \psi = \infty\text{, or both)},$$
$$\epsilon = \epsilon_1 = \frac{g_{\alpha\beta}g_{\beta\alpha}}{g_{\alpha\alpha}g_{\beta\beta}}. \tag{120}$$

2. Open-circuited image terminals.

$$y_c = 0 \qquad \text{(i.e., both } \chi = 0 \text{ and } \psi = 0\text{)},$$
$$\epsilon = \epsilon_3 \equiv \frac{\epsilon_1}{1 - \epsilon_1} \frac{1 - \theta}{1 + \theta}. \tag{121}$$

Let us first examine the dependence of ϵ on ψ (i.e., on b_c) holding χ (i.e., g_c) constant. We note that ϵ is a function of ψ^2. Differentiating ϵ with respect to ψ^2 and holding χ constant we obtain

$$\frac{\partial\epsilon}{\partial(\psi^2)} = \frac{[(\chi+1)^2+\psi^2][(\chi+1)(2\theta-\theta^2-\epsilon_1)-\theta^2(1-\epsilon_1)]}{D^2}, \tag{122}$$

where D is the denominator of Eq. (118). According to Eq. (122), $\partial\epsilon/\partial(\psi^2)$ does not change sign as ψ varies $(-\infty < \psi < +\infty)$; hence ϵ is monotonic in ψ^2 for constant χ. Now the loss L_m is monotonic in ϵ by Eq. (117); hence L_m, considered as a function of b_c, holding g_c constant, has one, and *only one*, stationary value (either a maximum or a minimum) in the range $-\infty < b_c < +\infty$, and this occurs at $b_c = 0$. The two possibilities are illustrated in Fig. 5·7.

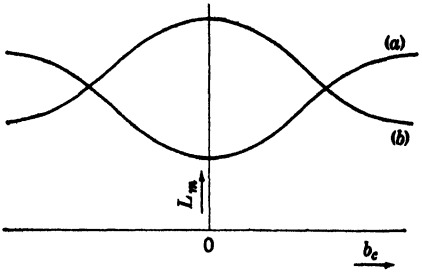

FIG. 5·7.—The loss L_m as a function of image load susceptance. The value of b_c has a stationary value at $b_c = 0$, either a minimum (*a*) or a maximum (*b*).

Which of the two possibilities holds is determined by the sign of $\partial\epsilon/\partial(\psi^2)$, which is observed to be the same as the sign of the factor in the numerator of Eq. (122):

$$(\chi+1)(2\theta-\theta^2-\epsilon_1)-\theta^2(1-\epsilon_1). \tag{123}$$

If this is positive we have a maximum and, if negative, a minimum.

The upper and lower bounds of L_m over the (g_c,b_c)-plane can now be determined by investigating the behaviour of ϵ as a function of g_c, with $b_c = 0$. From Eq. (118) for $b_c = 0$ (i.e., $\psi = 0$), we have

$$\epsilon = \epsilon_1 \frac{(\chi+1-\theta)^2}{(\chi+1-\theta^2)(\chi+1-\epsilon_1)}. \tag{124}$$

The possible stationary values of ϵ are found by putting $\partial\epsilon/\partial\chi = 0$ in Eq. (124). Only one such possibility is found, occurring at

$$\chi = (2\theta+1)(1-\theta)\frac{\epsilon_1 - \dfrac{\theta(\theta+2)}{2\theta+1}}{\theta(2-\theta)-\epsilon_1}. \tag{125}$$

For this point to fall on the positive real axis, we must obviously have $\chi > 0$ or[1]

$$\frac{\theta(2+\theta)}{2\theta+1} < \epsilon_1 < \theta(2-\theta). \tag{126}$$

[1] Condition Eq. (126) with one of the inequality signs reversed also gives $\chi > 0$, provided that $\theta > 1$ or, from Eq. (119), that $g_{\alpha\alpha} < g_{\alpha\gamma}$. From Eq. (26) we see that the conductance g of the crystal to the local-oscillator wave would be negative in this case. Thus for any practical case $\theta < 1$ and Eq. (126) is the only physically possible condition for $\chi > 0$.

The point given by Eq. (125) must always correspond to a minimum in ϵ (i.e., a maximum in L_m), as can be verified by examining the second derivative of Eq. (124). Further, if the surface $L_m(g_c,b_c)$ is considered, the maximum along the real axis ($b_c = 0$) must also be a maximum in the orthogonal direction (g_c = constant).[1] The proof follows from the fact that, when χ is given by Eq. (125), Expression (123) is always positive; hence we have Condition b of Fig. 5·7. Since this maximum in L_m, when it exists [i.e., when Eq. (126) is satisfied], is the only stationary value of L_m over the (g_c,b_c)-plane, it is an upper bound on L_m. When the maximum does not exist, L_m is bounded by its values at $y_c = 0$ and $y_c = \infty$. In any case, the lower bound for L_m is the lesser of its values at $y_c = 0$ and $y_c = \infty$.

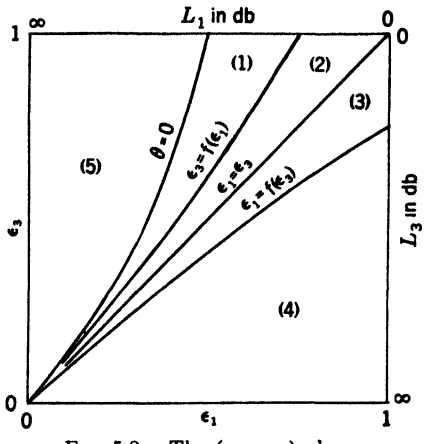

FIG. 5·8.—The $(\epsilon_1 - \epsilon_3)$-plane.

The value of ϵ at the maximum for L_m will be called ϵ_4, and the corresponding maximum loss, L_4. Substituting Eq. (125) into Eq. (124), we find

$$\epsilon_4 = \epsilon_1 \frac{4\theta(1-\theta)(\epsilon_1 - \theta)}{(\epsilon_1 - \theta^2)^2}. \tag{127}$$

It is easy to verify from Eq. (127) that $\epsilon_4 < \epsilon_1$ and $\epsilon_4 < \epsilon_3$. We can translate the condition in Eq. (126) for existence of the maximum loss into relations between ϵ_1 and ϵ_3 by use of Eq. (121). Thus we find that the maximum loss L_4 exists when the following two conditions are satisfied:

$$\epsilon_3 < f(\epsilon_1), \tag{128}$$

$$\epsilon_1 < f(\epsilon_3), \tag{129}$$

where

$$f(x) \equiv \frac{x}{3+x}\left(1 + \frac{2}{\sqrt{1-x}}\right). \tag{130}$$

By Eqs. (120) and (121) these conditions on ϵ_1 and ϵ_3 are conditions imposed on the elements of the admittance matrix.

When the matrix for any crystal is known, the value of ϵ_1 and ϵ_3 can be found from Eqs. (120) and (121). The crystal can then be represented as a point on the (ϵ_1,ϵ_3)-plane. This plane can be partitioned into regions by the curves $\epsilon_1 = f(\epsilon_3)$, $\epsilon_3 = f(\epsilon_1)$, and $\epsilon_1 = \epsilon_3$, as is shown in Fig. 5·8 (where the line $\theta = 0$ or $\epsilon_3 = \epsilon_1/1 - \epsilon_1$ has also been drawn). It is not possible for a crystal point to fall in Region 5, since such a crystal would have a negative value of θ which is excluded by definition (see Sec. 5·5)

[1] That is, there is never a saddle point.

of the standard r-f terminal position. If a point falls in Regions 2 or 3, the maximum L_4 exists; if in 1 or 4, L_4 does not exist and L_m is bounded by L_1 and L_3 (corresponding to ϵ_1 and ϵ_3, that is, to short-circuited and open-circuited image terminals, respectively). If a point falls in Regions 1 or 2, $L_3 < L_1$ and, if in 3 or 4, $L_1 < L_3$. If a point falls on $\epsilon_1 = \epsilon_3$ then of course $L_1 = L_3$ and it may also easily be shown that $L_2 = L_4$; that is, if $L_1 = L_3$, the maximum loss L_4 occurs when the image termination is the same as the signal termination. A point falling on $\epsilon_3 = f(\epsilon_1)$ has $L_1 = L_4$ and a point falling on $\epsilon_1 = f(\epsilon_3)$ has $L_3 = L_4$. The forms of the surfaces $L_m(g_c,b_c)$ corresponding to the four regions, as well as the special case $\epsilon_1 = \epsilon_3$, are shown in Figs. 5 9 *a*, *b*, *c*, *d*, and *e*.

The expression for L_4 obtained by substituting Eq (127) in Eq. (117) can be simplified to

$$L_4 = \frac{g_{\alpha\beta}}{g_{\beta\alpha}} \frac{\epsilon_1(1 - \theta)}{\theta(\epsilon_1 - \theta)}. \tag{131}$$

If Eq. (121) is solved for θ in terms of ϵ_1 and ϵ_3, the above result becomes

$$L_4 = 2\frac{g_{\alpha\beta}}{g_{\beta\alpha}} \frac{\left(\dfrac{1}{\epsilon_1} + \dfrac{1}{\epsilon_3} - 1\right)}{1 - \left(\dfrac{1}{\epsilon_1} - \dfrac{1}{\epsilon_3}\right)^2}. \tag{132}$$

If L_0 [Eq. (77)] is written similarly in terms of ϵ_1 and ϵ_3, we obtain

$$L_0 = 2\frac{g_{\alpha\beta}}{g_{\beta\alpha}} \left(\frac{1}{\epsilon_1} + \frac{1}{\epsilon_3} - 1\right). \tag{133}$$

From Eqs. (132) and (133),

$$L_4 = L_0 \frac{1}{1 - \left(\dfrac{1}{\epsilon_1} - \dfrac{1}{\epsilon_3}\right)^2}. \tag{134}$$

Now $1/\epsilon_1 - 1/\epsilon_3$ cannot become larger than $\frac{1}{3}$ in the Regions 2 and 3 of Fig. 5·8 (where L_4 exists). Consequently,

$$L_0 \leqq L_4 \leqq \tfrac{9}{8}L_0, \tag{135}$$

or, L_4 never exceeds L_0 by more than 0.5 db.

From Eq. (73) we find for η_2 in terms of ϵ_1 and ϵ_3,

$$\eta_2 = \epsilon_1 + \epsilon_3 - \epsilon_1\epsilon_3. \tag{136}$$

Thus, from Eq. (72),

$$L_2 = 2\frac{g_{\alpha\beta}}{g_{\beta\alpha}} \frac{1 + \sqrt{(1 - \epsilon_1)(1 - \epsilon_3)}}{1 - \sqrt{(1 - \epsilon_1)(1 - \epsilon_3)}}, \tag{137}$$

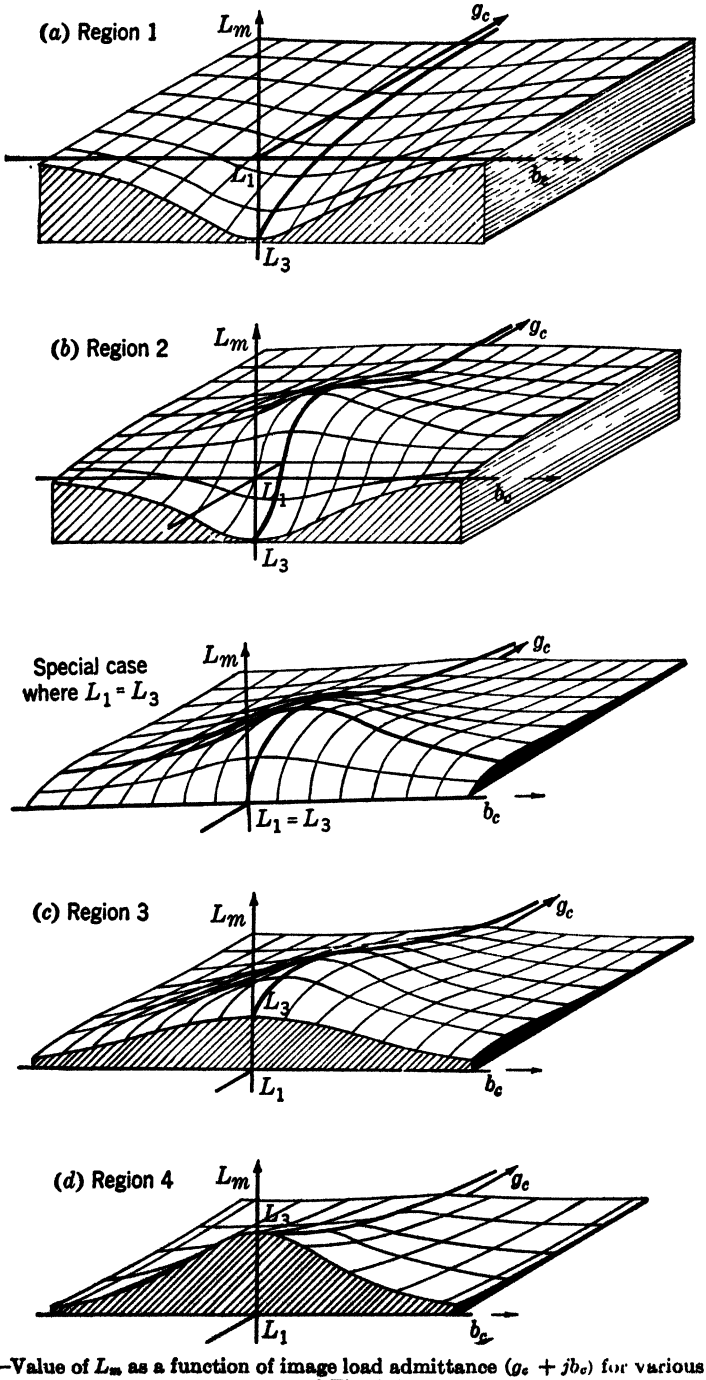

FIG. 5·9.—Value of L_m as a function of image load admittance $(g_c + jb_c)$ for various regions of Fig. 5·8.

and it may be shown that

$$L_2 = 2\frac{\left(\frac{g_{\alpha\beta}}{g_{\beta\alpha}}\right)^2 + L_1L_3}{L_1 + L_3}. \tag{138}$$

It can easily be shown that L_0 may be written in either of the two forms, Eq. (72) or Eq. (117), provided we replace η_2 and ϵ by η_0 and ϵ_0, where

$$\eta_0 = \frac{4\epsilon_1\epsilon_3}{(\epsilon_1 + \epsilon_3)^2}\eta_2, \tag{139a}$$

$$\epsilon_0 = \frac{8\epsilon_1\epsilon_3\eta_2}{(\epsilon_1 + \epsilon_3 + \eta_2)^2}. \tag{139b}$$

Furthermore, L_4 may also be written in these forms by putting

$$\eta_4 = \frac{4\epsilon_1\epsilon_3\eta_2(2\epsilon_1 - \eta_2)(2\epsilon_3 - \eta_2)}{[(4 - \eta_2)(\epsilon_1 + \epsilon_3)^2 - \eta_2^2]^2}, \tag{140a}$$

$$\epsilon_4 = \frac{8\epsilon_1\epsilon_3\eta_2(2\epsilon_1 - \eta_2)(2\epsilon_3 - \eta_2)}{(2\epsilon_1^2 + 2\epsilon_3^2 - \eta_2^2)^2}. \tag{140b}$$

The latter equation is, of course, just Eq. (127) expressed symmetrically in terms of ϵ_1 and ϵ_3.

To recapitulate, there have been defined the following losses (see Table 5·1).

- L_0 (mixer matched to local oscillator, same termination at signal and image frequencies)
- L_1 (mixer matched to signal, image short-circuited at r-f terminals)
- L_2 (minimum loss with same termination at signal and image frequencies)
- L_3 (mixer matched to signal, image open-circuited at r-f terminals)
- L_4 (mixer matched to signal, image impedance adjusted to give maximum loss when this occurs at other than open-circuited or short-circuited image)

The r-f terminals have been so chosen that the mixer matrix elements are all real and positive. The five defined quantities are then given by

$$L_j = \left(\frac{g_{\alpha\beta}}{g_{\beta\alpha}}\right)\frac{1 + \sqrt{1 - \epsilon_j}}{1 - \sqrt{1 - \epsilon_j}}, \qquad j = 0, 1, 3, 4, \tag{141}$$

where ϵ_0 is given by Eq. (139*b*), ϵ_1 by Eq. (120), ϵ_3 by Eq. (121), and ϵ_4 by either Eq. (127) or Eq. (140*b*); and/or by

$$L_j = 2\left(\frac{g_{\alpha\beta}}{g_{\beta\alpha}}\right)\frac{1 + \sqrt{1 - \eta_j}}{1 - \sqrt{1 - \eta_j}}, \qquad j = 0, 2, 4, \tag{142}$$

where η_0 is given by Eq. (139*a*), η_2 by Eq. (73) or Eq. (136), and η_4 by Eq. (140*a*). The quantities L_0 and L_4 may be expressed more directly in terms of measurable quantities by Eqs. (77), (78), (79), and (133) in the case of L_0, and by Eq. (131) in the case of L_4. All of the characteristic loss values L_0–L_4 are then completely determined, except for the constant reciprocity factor $g_{\alpha\beta}/g_{\beta\alpha}$, by two characteristic functions ϵ_1 and ϵ_3 of the mixer matrix elements. Relations among these losses are given by Eqs. (77), (141), and (145).

To see how the values of the characteristic losses run for actual crystal rectifiers, computations have been made for six silicon and seven germanium units. The results are given in Table 5·2. The first column gives the identification; in Columns 2 to 6 are the data obtained for these units at the 10-cm band by Smith [1] The quantities in Columns 2 to 6 are defined by Eqs. (26) and (37). The complete mixer matrix may be obtained from these quantities through Eqs. (38) to (48). (Through proper choice of r-f terminals $b = b_V = b_P = 0$.) The values of θ, ϵ_1, and ϵ_3 were then computed from these data and are given in the next three columns. The five losses were next computed; they are given in Columns 10 to 14. The quantity L_4 is given wherever it exists. In Column 15 is given the ratio of the image conductance for maximum loss L_4 to the local-oscillator conductance of the mixer. Finally, in Column 16 the quantity $g_{\alpha\beta}/g_{\beta\alpha}$, which is a factor in all expressions for loss [Eqs. (141), (142)], is given in decibels.

Any loss equation can be written

$$L_j = \frac{g_{\alpha\beta}}{g_{\beta\alpha}} L_j'. \tag{143}$$

As will be shown later (see Sec. 7·3), the quantity L_j', the so-called "impedance loss," may be determined by impedance measurements at either the r-f or i-f terminals of the mixer, whereas it is impossible to determine $g_{\alpha\beta}/g_{\beta\alpha}$ in this manner. We can find L_j' from the table by subtracting Column 16 from Columns 10 to 14. The departure of $g_{\alpha\beta}/g_{\beta\alpha}$ from unity measures the extent of failure of full reciprocity. In fact, the crystals of Table 5·2 are the same as those represented in Fig. 5·4, used to test reciprocity. It will be recalled that, on plotting $|y_{\alpha\beta}|$ *vs.* $|y_{\beta\alpha}|$ in Fig. 5·4, it was found that the best straight line fitting all crystals except G40, 11I, and 11N did not have a slope of exactly 45°, and it was mentioned that this could perhaps be attributed to a systematic error in the measurement of r-f power. Such an error will account for the predominance of negative signs in Column 16. This possibility was not taken into account in computing the losses of Table 5·2; had it been

[1] The authors are indebted to Dr. R. N. Smith for his kindness in furnishing these data.

TABLE 5·2.—DATA ON THE CONVERSION PROPERTIES OF A NUMBER OF SILICON AND GERMANIUM RECTIFIERS

1	2	3	4	5	6	7	8	9	10	11	12	13	14	15	16
Crystal	P, mw	G_P, volt^{-1}	G_V, volt^{-1}	G_P, mw^{-1}	G_V, mho	θ	ϵ_1	ϵ_3	L_0, db	L_1, db	L_2, db	L_3, db	L_4, db	g_c/g	$g_{\alpha\beta}/g_{\beta\alpha}$, db
L114 Si	0.41	1.43	2.46	0.69	4.00×10^{-3}	0.283	0.334	0.280	9.8	9.3	9.75	10.2	...	....	−0.65
L104 Si	0.27	1.89	3.6	1.39	1.73	0.376	0.630	0.771	5.55	5.9	5.4	4.3	...	....	−0.2
K900 Si	0.47	1.39	2.5	0.72	1.90	0.338	0.565	0.643	6.2	6.4	6.1	5.5	...	....	−0.5
BRD3 Si	0.58	1.10	2.17	0.43	2.40	0.249	0.435	0.463	8.35	8.4	8.35	8.0	8.4	....	−0.1
BRD2 Si	0.66	1.13	2.2	0.425	3.05	0.281	0.433	0.428	8.6	8.4	8.6	8.5	8.6	0.71	−0.1
M97 Si	0.68	0.71	1.23	0.46	2.68	0.313	0.244	0.169	11.9	11.0	11.8	12.8	...	....	−0.6
G129 Ge	0.64	0.55	1.16	0.54	0.65	0.346	0.490	0.466	8.3	8.0	8.3	8.3	8.3	0.21	+0.2
G236 Ge	0.38	1.45	2.55	1.70	1.37	0.646	0.744	0.625	5.4	4.3	5.2	5.6	...	....	−0.6
G40 Ge	0.39	1.44	4.0	1.85	1.40	0.722	0.852	0.931	5.4	4.9	5.3	3.8	5.4	1.7	+1.4
13V Ge	0.30	1.72	3.3	1.74	1.49	0.522	0.706	0.755	5.3	5.1	5.2	4.5	5.3	2.1	−0.2
11I Ge	0.49	1.31	4.0	1.30	1.90	0.637	0.789	0.805	6.6	6.1	6.6	5.9	6.6	1.5	+1.8
11Q Ge	0.59	1.00	2.08	0.40	10.2	0.236	0.136	0.0974	15.4	14.6	15.3	16.1	...	....	+0.2
11N Ge	0.87	0.38	1.9	0.31	0.71	0.270	0.548	0.69	10.6	11.1	10.4	9.4	...	....	+4.0

done, the values for the losses would have been slightly increased (≈ 0.2 db) but their relative values would not have been significantly altered.

A crystal mixer is sometimes used as a modulator, in which a low-level signal at a frequency low compared with microwave frequencies is impressed on the i-f terminals of the mixer. By beating with a microwave local oscillator at high level (≈ 1 mw) this low-frequency signal is converted to sidebands of the local oscillator. The conversion loss to either sideband can be shown to be given by

$$\begin{aligned} L_j'' &= \frac{g_{\beta\alpha}}{g_{\alpha\beta}} L_j' \\ &= \left(\frac{g_{\beta\alpha}}{g_{\alpha\beta}}\right)^2 L_j, \qquad j = 1, 2, 3, 4. \end{aligned} \tag{144}$$

Now all significant departures of $g_{\alpha\beta}/g_{\beta\alpha}$ from unity observed so far are such that $g_{\alpha\beta} > g_{\beta\alpha}$. Thus, for certain (germanium) units it is possible [from Eq. (144)] to obtain a very low loss from i-f to signal. For example, units G40, 11I, and 11N have values of L_3'' equal, respectively, to 1.0, 2.3, and 1.4 db, whereas the corresponding values of L_3 are 3.8, 5.9, and 9.4 db. Such effects do not appear to occur in silicon rectifiers.

It will be seen from Table 5·2 that L_0 and L_2 do not differ by more than 0.2 db for any crystal; that L_4, when it exists, is practically the same as L_0; that the variation in loss amounts to 0 to 1.8 db over the image-admittance plane; and that large variations in loss as a function of image admittance occur about as often for poor crystals as for very good ones.

The same crystals of Table 5·2 are plotted on an (ϵ_1,ϵ_3)-diagram in Fig. 5·10. The germanium units are represented by encircled crosses, and the silicons by circles. It is interesting, but perhaps not significant, that the silicon points fall very nearly on a straight line, while the germanium points are considerably scattered.

5·10. Effect of Image Termination on I-f Impedance.—The i-f impedance of the mixer is a quantity of considerable importance in receiver design. The noise figure of the receiver is determined by the conversion loss, the noise temperature of the crystal, and the noise figure of the i-f amplifier. It has already been noted (Sec. 2·5) that conversion loss and crystal noise temperature depend on the r-f load admittance of the mixer. Similarly, the amplifier noise figure depends on the i-f impedance of the mixer.

In designing an amplifier of low noise figure, some definite value of mixer impedance must be chosen. It is important, once this value has been set, that we be able to rely on the mixer impedance not to vary much from one crystal to another or from one mixer to another. In practice it is found that the i-f impedance of crystals made by one manu-

facturer are reasonably uniform in the same mixer, but that differences occur between products of two manufacturers. Such differences are not very great and can be corrected by specification limits on i-f impedance. More serious, however, are variations in i-f impedance for the same crystal from one mixer to another. Such variations are caused principally by the fact that the terminations to the image frequency differ in different mixer designs. Thus, if mixer A happens to short-circuit

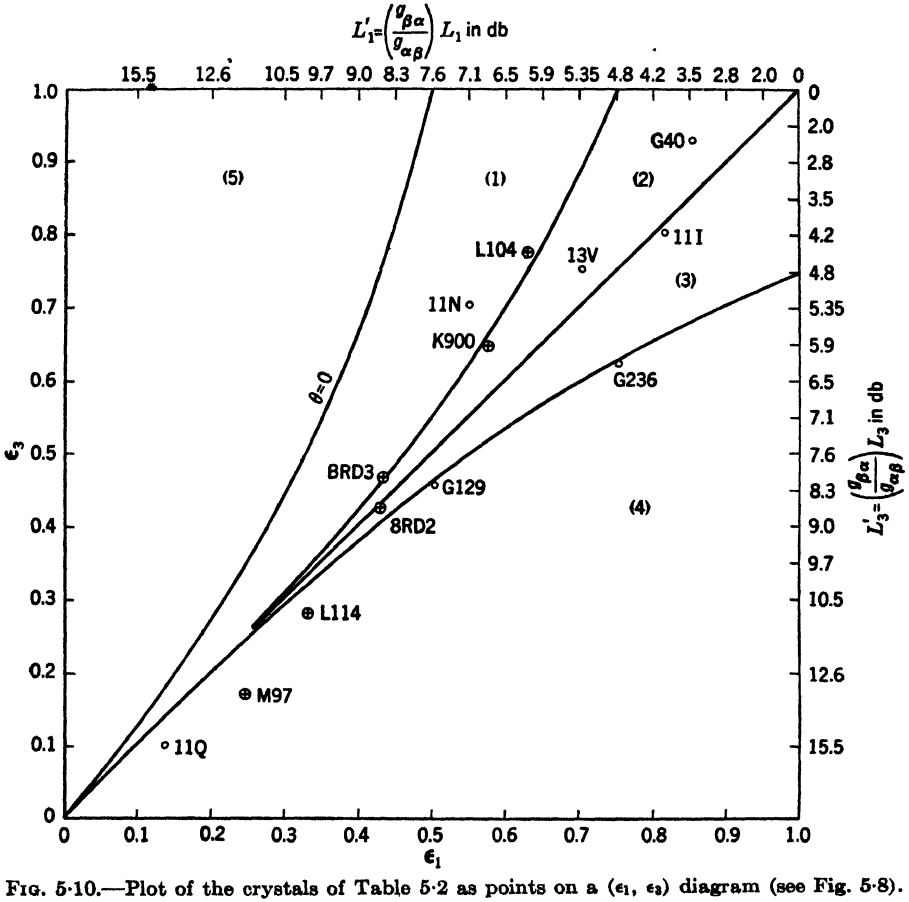

FIG. 5·10.—Plot of the crystals of Table 5·2 as points on a (ϵ_1, ϵ_3) diagram (see Fig. 5·8).

the image, and mixer B to open-circuit the image, the i-f impedances of the same crystal in the two mixers will be very different; the two values of i-f impedance may be in a ratio of as much as 3 or 4 in the case of a low-loss crystal. Variations of this magnitude actually occur and are very serious from the point of view of receiver noise figure.

The effect of variation of image load impedance on i-f impedance must depend, obviously, on the conversion loss of the mixer. For low-loss crystals there is only a small decoupling between the r-f circuit and

the i-f circuit and we must expect such effects to be severe. Variations in signal load admittance are of course equally effective in producing variations in i-f impedance but are unimportant in practice, since mixers are uniformly designed to match the signal. The relation between conversion loss and terminal impedance has been utilized in actual loss measurements, as will be described in Sec. 7·3.

As an example of the dependence of i-f impedance on image terminations, the i-f impedances of the thirteen crystals of Table 5·2 will now be calculated for (*a*) image terminals short-circuited, (*b*) image terminals open-circuited, and (*c*) the case of equal signal and image load admittance adjusted to equal the local-oscillator admittance g of the mixer. It is assumed that in Cases (*a*) and (*b*) also the signal load admittance is g.

Let the i-f admittance of the mixer be y_β, and the image load admittance be y_c. The terminal currents and voltages are then related by

$$\left.\begin{aligned} i_\beta &= y_\beta e_\beta, \\ i_\alpha &= -g e_\alpha, \\ i_\gamma &= -y_c e_\gamma. \end{aligned}\right\} \tag{145}$$

Substituting Eqs. (145) in Eqs. (2) and (13) and eliminating the currents and voltages, we obtain

$$\begin{vmatrix} g_{\alpha\alpha} + g & g_{\alpha\beta} & g_{\alpha\gamma} \\ g_{\beta\alpha} & g_{\beta\beta} - y_\beta & g_{\beta\alpha} \\ g_{\alpha\gamma} & g_{\alpha\beta} & g_{\alpha\alpha} - y_c^* \end{vmatrix} = 0.$$

Solving for y_β, we arrive at

$$\begin{aligned} y_\beta &= g_{\beta\beta} - \frac{g_{\alpha\beta}g_{\beta\alpha}(3g + y_c^*)}{g(3g_{\alpha\alpha} - g) + y_c(g_{\alpha\alpha} + g)} \\ &= g_{\beta\beta} - \frac{g_{\alpha\beta}g_{\beta\alpha}}{g_{\alpha\alpha} + kg}, \end{aligned} \tag{146}$$

where

$$k = \frac{y_c - g}{y_c + 3g}. \tag{147}$$

From Eqs. (146) and (147) we get for the three special cases:

$$\left.\begin{array}{ll} (a) \quad y_c = \infty, & \\ \text{(image short-circuited)} & g_\beta = g_{\beta\beta} - \dfrac{g_{\alpha\beta}g_{\beta\alpha}}{g_{\alpha\alpha} + g} \equiv \dfrac{1}{R_1}; \\ (b) \quad y_c = 0, & \\ \text{(image open-circuited)} & g_\beta = g_{\beta\beta} - \dfrac{g_{\alpha\beta}g_{\beta\alpha}}{g_{\alpha\alpha} - \dfrac{g}{3}} \equiv \dfrac{1}{R_3}; \\ (c) \quad y_c = g, & \\ \text{(intermediate case)} & g_\beta = g_{\beta\beta} - \dfrac{g_{\alpha\beta}g_{\beta\alpha}}{g_{\alpha\alpha}} \equiv \dfrac{1}{R_2}. \end{array}\right\} \tag{148}$$

To calculate the i-f impedances of the crystals of Table 5·2, we substitute for $g_{\alpha\alpha}$ etc., their values in terms of measurable mixer parameters, as given by Eqs. (38) to (48), obtaining

$$y_\beta = \frac{\partial I}{\partial V} + \frac{k}{k+D} P g_V G_P. \tag{149}$$

The three special cases (*a*), (*b*), and (*c*) are then given by letting k equal, respectively, 1, $-\frac{1}{3}$, and 0.

TABLE 5·3.—I-F RESISTANCE OF A NUMBER OF CRYSTALS FOR IMAGE SHORT-CIRCUITED (R_1), MATCHED (R_2), AND OPEN-CIRCUITED (R_3)

Crystal No.	R_1, ohms	R_2, ohms	R_3, ohms
L114	207	250	297
L104	350	570	764
K900	347	530	830
BRD3	313	420	560
BRD2	250	330	430
M97	320	370	415
G129	1100	1540	2100
G236	415	730	1350
G40	316	710	1750
13V	380	670	1230
11I	265	530	1080
11Q	92	98	104
11N	930	1410	2300

It is evident that $R_\beta \equiv 1/g_\beta$ is smallest when the image is short-circuited, and largest when the image is open-circuited.

The values of R_1, R_2, and R_3 of Eqs. (148), as computed from the data of Table 5·2 for the 13 reference crystals, are given in Table 5·3.

The case of a general reactive image termination follows easily from the special cases considered. Since the mixer acts as a linear network connecting the image circuit to the i-f circuit, it is clear that y_β traverses a circle in the y_β-plane as the line between the mixer and a fixed image termination is "stretched." The circle will be a circle of "constant reflection coefficient" with respect to the conductance $g_0 \equiv 1/\sqrt{R_1R_3}$. This circle is shown in Fig. 5·11.

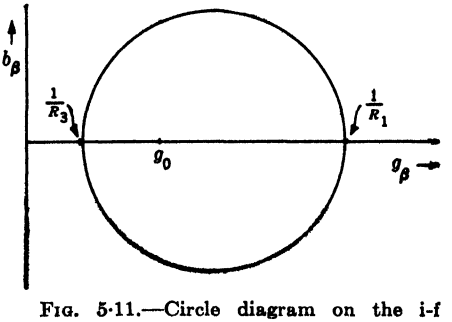

FIG. 5·11.—Circle diagram on the i-f admittance plane. For a general reactive image termination, the i-f admittance falls on the circle whose intercepts are $1/R_3$ and $1/R_1$ as given by Eq. (148).

If a resonant cavity (TR switch) tunes the r-f circuit, the signal will, in general, see a near match (for example, g) but the image will see an admittance determined by the loaded Q of the cavity and the line length from the cavity to the reference terminals of the mixer. As this line length is varied, the i-f admittance will traverse a circle for which the intercepts on the real axis will be given by Eq. (146), with

$$k = \frac{-1}{1 \pm 2\sqrt{1 + \left(\frac{f}{Q\Delta f}\right)^2}}, \tag{150}$$

where f and Δf are the local-oscillator and intermediate frequencies, respectively, and Q is the loaded Q of the TR switch. As an example, if

$$\begin{aligned} f &= 3000 \text{ Mc/sec}, \\ \Delta f &= 30 \text{ Mc/sec}, \\ Q &= 300, \end{aligned}$$

then the values $k = +0.90$ and $k = -0.32$ give the intercepts. This is to be compared with $k = 1$ and $k = -\frac{1}{3}$ for $Q = \infty$. Thus in actual practice the image tuning has an important effect on the i-f impedance.

THE PHYSICAL THEORY OF CONVERSION

The theory of conversion, as developed to this point, is *phenomenological* in that the properties of the mixer are derived from measurements at its terminals and no assumptions are made as to the internal structure of the device. This theory gives all the information required by the system designer but is insufficient to aid in the development and improvement of crystal rectifiers. A different viewpoint will be adopted now and the theory of mixers will be based on the physical properties of crystal rectifiers by a consideration of, first, the mixing action of a simple nonlinear resistance, and second, of the modification of this action by the addition of impedance elements connecting the nonlinear resistance to the terminals of the actual mixer. Later there will be considered modifications of these results caused by the nonlinear capacitance of the barrier.

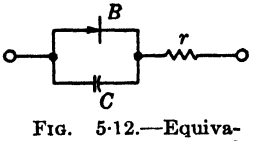

FIG. 5·12.—Equivalent circuit of a crystal rectifier.

Some of these impedances, such as the barrier capacitance and the spreading resistance of the semiconductor, are intrinsic properties of the rectifier; others are introduced by the mixer designer as transformers from the cartridge to the mixer terminals. The latter type of impedance is, of course, always designed to be purely reactive. Let us consider for the moment impedances of the first type.

The equivalent circuit of a crystal rectifier is represented in Fig. 5·12.

In addition to the barrier capacitance C there are other reactive elements. Unlike C, these are either negligible or may be tuned out externally. This equivalent circuit was discussed in Chap. 2, where it was noted that C is not a true capacitance but probably depends on the frequency as well as on the voltage across it. At a fixed frequency, however, a close enough approximation to actuality can for most purposes be arrived at by assuming the circuit of Fig. 5·12 with C having some average value. In Fig. 5·12, B is the nonlinear resistance of the barrier, C is the barrier capacitance, and r is the spreading resistance of the semiconductor and may include other losses in the cartridge, such as whisker resistance. Except in unusual circumstances these are small in comparison with the spreading resistance.

5·11. Matrix of a Nonlinear Resistance.—In considering the mixing action of a nonlinear resistance, let the current-voltage characteristic be given by

$$i = f(e). \tag{151}$$

The current and voltage are assumed to be composed of the following parts:

(*a*)	i_0	e_0	d-c
(*b*)	$\sum_n i_n e^{jn\omega t}$	$\sum_n e_n e^{jn\omega t}$	LO and its harmonics
(*c*)	$\mathrm{Re} \sum_\mu i_\mu e^{jb_\mu t}$	$\mathrm{Re} \sum_\mu e_\mu e^{jb_\mu t}$	signal, image, i-f, and harmonic sidebands. (152)

In (*b*), the summations extend over all integer values of n from $-\infty$ to $+\infty$, not including 0. In (*c*), b_μ includes the frequencies $\omega + \beta$ (signal), $\omega - \beta$ (image), β(i-f), and $n\omega \pm \beta$ (harmonic sidebands).

It is now assumed that the terms in (*c*) are very small compared with the terms in (*b*) and (*a*), and can be considered, as before, to be variations of them. The general variational equation is then

$$\delta i = \frac{di}{de}\,\delta e, \tag{153}$$

where δi and δe are now identified with the current and voltage terms in Eq. (152). For di/de, we may use a Fourier expansion;

$$\frac{di}{de} = \sum_{n=-\infty}^{+\infty} y_n e^{jn\omega t}. \tag{154}$$

Equation (153) has the character of a "mathematical mixer," since, by substitution of Eqs. (151), (152), and (154) into Eq. (153), we obtain *linear* relations among the coefficients of the various frequency com-

ponents. These linear relations are obtained by equating coefficients of $e^{jb_\mu t}$ for the same b_μ. In this way, we find

$$i_{\beta+n\omega} = \sum_{m=-\infty}^{+\infty} y_{n-m} e_{\beta+m\omega}. \tag{155}$$

These equations may be written in matrix form

$$\begin{pmatrix} \cdot \\ \cdot \\ \cdot \\ i_{\beta+2\omega} \\ i_{\beta+\omega} \\ i_\beta \\ i_{\beta-\omega} \\ i_{\beta-2\omega} \\ \cdot \\ \cdot \\ \cdot \end{pmatrix} = \begin{pmatrix} & \cdot & \cdot & \cdot & \cdot & \cdot & \\ & \cdot & \cdot & \cdot & \cdot & \cdot & \\ & \cdot & \cdot & \cdot & \cdot & \cdot & \\ \cdots & y_0 & y_1 & y_2 & y_3 & y_4 & \cdots \\ \cdots & y_{-1} & y_0 & y_1 & y_2 & y_3 & \cdots \\ \cdots & y_{-2} & y_{-1} & y_0 & y_1 & y_2 & \cdots \\ \cdots & y_{-3} & y_{-2} & y_{-1} & y_0 & y_1 & \cdots \\ \cdots & y_{-4} & y_{-3} & y_{-2} & y_{-1} & y_0 & \cdots \\ & \cdot & \cdot & \cdot & \cdot & \cdot & \\ & \cdot & \cdot & \cdot & \cdot & \cdot & \\ & \cdot & \cdot & \cdot & \cdot & \cdot & \end{pmatrix} \begin{pmatrix} \cdot \\ \cdot \\ \cdot \\ e_{\beta+2\omega} \\ e_{\beta+\omega} \\ e_\beta \\ e_{\beta-\omega} \\ e_{\beta-2\omega} \\ \cdot \\ \cdot \\ \cdot \end{pmatrix}. \tag{156}$$

Since di/de is real, we must have

$$y_{-n} = y_n^*; \tag{157}$$

the admittance matrix is Hermitian. The matrix will be symmetrical (i.e., reciprocity holds) if also $y_{-n} = y_n$, but this implies, with Eq. (157), that all y_n are real.

It may be shown that y_n will be real if, and only if, di/de is an even function of the time, which implies that e is an even function of time. If reciprocity holds in the admittance matrix of the barrier layer [Eq. (156)], it will also hold for the final admittance matrix of the mixer. Thus, a *necessary* condition for reciprocity is that a time zero can be found such that e, the voltage across the barrier layer, is an even function of the time. This agrees with one of Dicke's conditions for reciprocity (see Sec. 5·5).

If, following the discussion at the beginning of this chapter, harmonic sideband voltages are neglected and Eq. (157) made use of, Eq. (156) reduces to

$$\begin{pmatrix} i_\alpha \\ i_\beta \\ i_\gamma^* \end{pmatrix} = \begin{pmatrix} y_0 & y_1 & y_2 \\ y_1^* & y_0 & y_1 \\ y_2^* & y_1^* & y_0 \end{pmatrix} \begin{pmatrix} e_\alpha \\ e_\beta \\ e_\gamma^* \end{pmatrix}, \tag{158}$$

where

$$\left.\begin{aligned} i_\alpha &= i_{\beta+\omega}, & e_\alpha &= e_{\beta+\omega}, \\ i_\beta &= i_\beta, & e_\beta &= e_\beta, \\ i_\gamma &= i_{\beta-\omega}^*, & e_\gamma &= e_{\beta-\omega}^*. \end{aligned}\right\} \tag{159}$$

The terms i_α, i_β, i_γ and e_α, e_β, e_γ are the complex currents and voltages at signal, intermediate, and image frequencies, respectively.

As an example, let us now apply Eq. (158) to the case of a nonlinear resistance whose current-voltage characteristic has the typical exponential form found approximately in most crystal rectifiers [see Eq. (4.33)]; viz,

$$i = A(e^{\alpha e} - 1). \tag{160}$$

This gives

$$\frac{di}{de} = \alpha A e^{\alpha e}. \tag{161}$$

Now let us neglect harmonics of the local-oscillator voltage and let us take the voltage e as

$$e = e_0 + e_1 \cos \omega t. \tag{162}$$

The Fourier expansion of Eq. (161) is then[1]

$$\frac{di}{de} = \alpha A e^{\alpha e_0} \sum_{n=-\infty}^{+\infty} I_n(\alpha e_1) e^{jn\omega t}, \tag{163}$$

where $I_n(x)$ is the modified Bessel function $[I_n(x) = j^{-n} J_n(jx)]$. Comparing this with Eq. (154) we see that

$$\left.\begin{aligned} y_0 &= \alpha A e^{\alpha e_0} I_0(\alpha e_1), \\ y_1 &= y_1^* = \alpha A e^{\alpha e_0} I_1(\alpha e_1), \\ y_2 &= y_2^* = \alpha A e^{\alpha e_0} I_2(\alpha e_1). \end{aligned}\right\} \tag{164}$$

The admittance matrix is now real, and we can at once apply the theory of Secs. 5·7, 5·8, and 5·9 to find the characteristic losses and impedances of the nonlinear resistance assumed. Omitting the arguments of the Bessel functions we have, from Eq. (77),

$$L_0 = \frac{4I_0(I_0^2 - I_1^2)}{I_1^2(I_0 - I_2)}. \tag{165}$$

From Eqs. (117), (120), (121), and (164),

$$L_j = \frac{1 + \sqrt{1 - \epsilon_j}}{1 - \sqrt{1 - \epsilon_j}} \; (j = 1, 3), \tag{166}$$

where

$$\epsilon_1 = \frac{I_1^2}{I_0^2},$$

$$\epsilon_3 = \frac{I_1^2}{I_0^2 - I_1^2} \frac{I_0 - I_2}{I_0 + I_2}.$$

[1] See, for example, S. A. Schelkunoff, *Electromagnetic Waves*, Van Nostrand, New York, 1943, p. 55, Eq. (7–4).

Also, from Eqs. (72), (73), and (164),

$$L_2 = 2\frac{1 + \sqrt{1 - \eta_2}}{1 - \sqrt{1 - \eta_2}}, \tag{167}$$

where

$$\eta_2 = \frac{2I_1^2}{I_0(I_0 + I_2)};$$

and, from Eqs. (131) and (164),

$$L_4 = \frac{I_0 I_1^2 (I_0 - I_2)}{I_2(I_1^2 - I_0 I_2)}. \tag{168}$$

It will be recalled that L_0 is the loss when the mixer is matched to the local oscillator; L_1 and L_3 are the minimum losses (as a function of the signal-generator admittance) for short-circuited and open-circuited image terminals, respectively; L_2 is the minimum "broadband loss" (mixer terminated in the same admittance at signal and image frequencies and this admittance chosen to minimize the loss); and L_4 is the loss minimized with respect to the signal-generator admittance and maximized with respect to the image admittance (see Table 5·1, Sec. 5·6).

It is interesting to note that for the simple exponential case the loss is independent of the d-c bias voltage e_0 and of the coefficient A in Eq. (160). This will not, of course, be true for the mixer impedances. In the case of actual crystal rectifiers, conversion loss does depend on d-c bias, but the dependence is weak for small bias ($\approx$ 0.2 volt).

Equation (160) gives a fair representation of the low-frequency current-voltage characteristic of the barrier layer of an actual crystal rectifier (as pointed out in Sec. 4·4). We saw, however, in Sec. 2·4 that there are other impedance elements inseparably associated with a crystal rectifier. One of these is the capacitance of the barrier, which will modify conversion at high frequencies. This capacitance cannot be tuned out because of the series ohmic spreading resistance of the semiconductor. At sufficiently low frequencies the barrier capacitance may be neglected, and so Eq. (160) gives the current-voltage relationship of the rectifier if the spreading resistance is sufficiently low.

Although Eq. (160) does not represent the reverse characteristic well, it may still be used with confidence since, at high frequencies, the reverse barrier resistance is effectively short-circuited by the barrier capacitance; and, in any case, the precise form of the reverse characteristic is unimportant, provided only that the reverse resistance is high (i.e., greater than 5000 ohms)—a condition satisfied by most crystals.

In Fig. 5·13, L_1, L_2, and L_3 have been plotted, as calculated from Eqs. (165–168) as functions of αe_1. There have been omitted L_0 and L_4, since they differ insignificantly from L_2 in this case. The plot may be

regarded as representing loss as a function of local-oscillator voltage e_1 for the same crystal (fixed α) or, alternatively, as a plot of loss for fixed e_1 as a function of excellence α of the rectifier.

It is evident from the figure that the relative magnitude of the three values of loss are in the order $L_2 > L_1 > L_3$. This is not a general result for a nonlinear resistance. It is possible, for example, to have

$$L_1 > L_2 > L_3$$

for certain current-voltage characteristics.

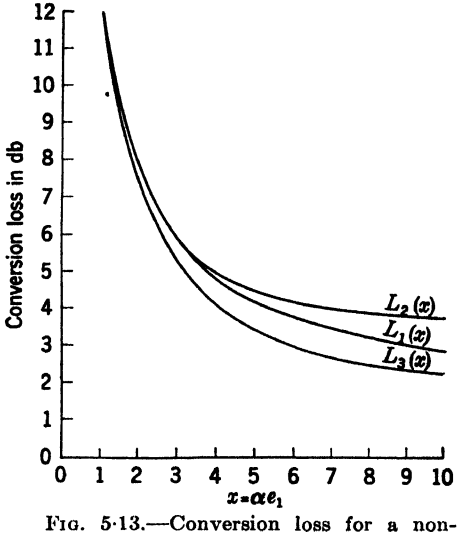

FIG. 5·13.—Conversion loss for a nonlinear resistance with current (i)-voltage (e) characteristic: $i = A(e^{\alpha e} - 1)$.
L_1 = loss for signal matched, image short-circuited.
L_2 = minimum loss with signal impedance = image impedance.
L_3 = loss for signal matched, image open-circuited.
e_1 = local-oscillator voltage amplitude.

Actual crystal rectifiers fail to conform to Fig. 5·13 in many respects. For one thing, it is known that loss depends on d-c bias and must, as shown later, also depend on the factor A. Furthermore, according to Fig. 5·13, L_2 approaches 2 and L_1 and L_3 approach unity at high local-oscillator voltages, whereas, for actual rectifiers, the loss approaches values several decibels in excess of these theoretical limits. Finally, losses of actual rectifiers are considerably greater, for the same αe_1, than is indicated by Fig. 5·13.

In the following section are introduced the barrier capacitance and spreading resistance and it is shown that these parameters will bring the calculated losses into fair agreement with those of actual rectifiers.

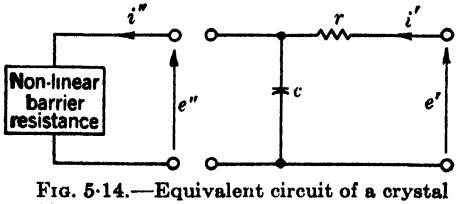

FIG. 5·14.—Equivalent circuit of a crystal rectifier showing the parasitic elements c and r forming a network connecting the barrier to the external circuit.

5·12. Effect of Parasitic Impedances on Conversion Loss. Following the preceding discussion, the equivalent circuit of the rectifier is taken to be as shown in Fig. 5·14.

Other impedances are associated with a crystal cartridge, such as the whisker inductance and end-to-end capacity; these are reactive, however, and are applied to the right-hand terminals of Fig. 5·14, and may accordingly be tuned out externally. They will therefore be regarded

as part of the reactive transformer to the mixer terminals, to be considered in the next section.

In this section it will be assumed that the barrier capacitance is a true constant capacitance. This assumption is contrary to theory and experiment, which agree in finding C to depend on barrier voltage and, to some extent, on frequency. In Sec. 5·13 the modification in the theory required by variability of the capacitance will be examined, but for the present this effect will be neglected. This neglect is probably justified for our qualitative theory of ordinary crystals.[1]

As seen from Fig. 5·14 we may regard the action of C and r on the barrier as the result of applying a linear four-pole network to the barrier terminals. The voltages e' and e'' and the currents i' and i'' as shown in Fig. 5·14 are composed of sums of the voltages and currents at the three frequencies of interest: signal, image, and intermediate. The four-pole network acts separately and independently on each frequency and the effect is precisely as though three separate four-pole networks were imagined attached to three terminal pairs of the barrier, one pair for each frequency. These terminal pairs are physically identical but may be separated conceptually.

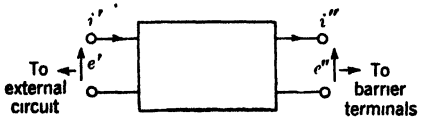

FIG. 5·15.—Typical parasitic four-pole showing current-voltage notation.

Figure 5·15 shows a typical four-pole network; the double-primed quantities are the barrier current and voltage and the single-primed are the current and voltage at the opposite terminals of the four-pole. Figure 5·16 shows the "three four-poles" connected to the "three terminal pairs" of the barrier.

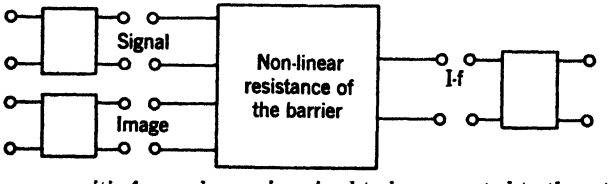

FIG. 5·16.—Three parasitic four-poles are imagined to be connected to three terminal pairs of the barrier.

Since the four-pole networks are linear and passive, we have, at any frequency,

$$\left.\begin{aligned} e'' &= ke' + li', \\ i'' &= me' + ni', \end{aligned}\right\} \tag{169}$$

where $kn - lm = 1$.

[1] However, as we shall see, the nonlinearity of the barrier capacitance can in special cases produce spectacular effects which have actually been observed for certain special rectifiers. They will be described fully in Chap. 13.

The transformation to the far terminals of the four-poles is effected by taking Eq. (169) for e'' and i'', substituting in the general mixer equations for the nonlinear barrier resistance,

$$\begin{pmatrix} i''_\alpha \\ i''_\beta \\ i''^*_\gamma \end{pmatrix} = \begin{pmatrix} y_0 & y_1 & y_2 \\ y_{-1} & y_0 & y_1 \\ y_{-2} & y_{-1} & y_0 \end{pmatrix} \begin{pmatrix} e''_\alpha \\ e''_\beta \\ e''^*_\gamma \end{pmatrix}, \tag{170}$$

and solving for the currents i'_α, etc., in terms of the voltages e'_α, etc. This procedure has been carried out by Peterson and Llewellyn,[1] who give in Table I of their paper the lengthy transformation equations. They have shown that, if the parasitic impedances do not discriminate between signal and image, and if the i-f four-pole is nonreactive, the admittance matrix after transformation has the form applicable to a "low Q" mixer [see Eq. (6)] with the result,

$$\begin{pmatrix} i'_\alpha \\ i'_\beta \\ i'^*_\gamma \end{pmatrix} = \begin{pmatrix} y_{\alpha\alpha} & y_{\alpha\beta} & y_{\alpha\gamma} \\ y_{\beta\alpha} & y_{\beta\beta} & y^*_{\beta\alpha} \\ y^*_{\alpha\gamma} & y^*_{\alpha\beta} & y^*_{\alpha\alpha} \end{pmatrix} \begin{pmatrix} e'_\alpha \\ e'_\beta \\ e'^*_\gamma \end{pmatrix}. \tag{171}$$

They also show that the transformed admittance matrix is symmetrical about the main diagonal (i.e., reciprocity holds) provided a time zero can be chosen such that the barrier voltage is an even function of time. This agrees with one of Dicke's conditions for reciprocity (see Sec. 5·5).

The coefficients k, l, m, and n appropriate to the parasitic four-pole shown in Fig. 5·14 are easily obtained by applying Eqs. (169) to this network. We find, for signal or image frequency,

$$\left.\begin{aligned} k &= 1, & l &= -r, \\ m &= -j\omega C, & n &= 1 + j\omega Cr; \end{aligned}\right\} \tag{172}$$

for intermediate frequency,

$$\left.\begin{aligned} k &= 1, & l &= -r, \\ m &= 0, & n &= 1. \end{aligned}\right\} \tag{173}$$

The small differences between the frequencies of the signal, image, and local oscillator and, also, the capacitive terms at intermediate frequency have been neglected in Eqs. (172) and (173).

If we assume that the barrier voltage is given by Eq. (162), then reciprocity holds and $y_n = y_{-n} = g_n$ and is real. Making use of the transformation equations of Peterson and Llewellyn[2] we obtain for the transformed matrix elements

[1] L. C. Peterson and F. B. Llewellyn, *Proc. I. R. E.* **33**, 458 (1945).
[2] *Loc. cit.*

$$\Delta' y'_{\alpha\alpha} = r^2(g_0 - g_2)[g_0(g_0 + g_2) - 2g_1^2] + r(2g_0^2 - g_1^2 - g_2^2) + (1 + \mu^2)g_0 + \frac{\mu^2}{r} + j\mu\left(g_0 + \frac{1}{r}\right),$$

$$\Delta' y'_{\alpha\beta} = \Delta' y'_{\beta\alpha} = g_1[1 + r(g_0 - g_2) - j\mu],$$

$$\Delta' y'_{\alpha\gamma} = r(g_0 g_2 - g_1^2) + g_2, \tag{174}$$

$$\Delta' g'_{\beta\beta} = r^2(g_0 - g_2)[g_0(g_0 + g_2) - 2g_1^2] + 2r(g_0^2 - g_1^2) + g_0(1 + \mu^2),$$

where

$$\mu = \omega C r,$$

and

$$\Delta' = r^3(g_0 - g_2)[g_0(g_0 + g_2) - 2g_1^2] + r^2(3g_0^2 - 2g_1^2 - g_2^2) - rg_0(3 + \mu^2) + 1 + \mu^2.$$

We are now in a position to find numerical values of the crystal-cartridge matrix for assumed barrier characteristics. To find the characteristic losses and impedances, however, we must first transform the matrix to real form.

Transformation of the Matrix to Real Form.—The transformation to real form is accomplished by adding an appropriate reactive four-pole transformer to the r-f terminals. This transformation becomes unique if the final impedance level is specified. The conversion loss, however, is independent of the impedance level and the choice of the latter will be based on considerations of simplicity in the final equations.

Equation (171) represents a mixer with three terminal pairs. To the two pairs of r-f terminals are now added a pair of identical four-pole transformers. This conceptual process corresponds to adding physically a single four-pole transformer to the single physical r-f terminal pair.

The four-pole transformer is represented by equations similar to Eq.(169):

$$\left.\begin{aligned} e_\alpha &= ae'_\alpha + bi'_\alpha, \\ i_\alpha &= ce'_\alpha + di'_\alpha \end{aligned}\right\} \tag{175}$$

with $ad - cb = 1$. The unprimed quantities refer to the new mixer terminals. The same Eqs. (175) apply to the image frequency with γ substituted for α. The corresponding equations for the i-f terminals are trivial, since no transformation is made there:

$$\begin{aligned} e_\beta &= e'_\beta, \\ i_\beta &= i'_\beta. \end{aligned} \tag{176}$$

Employing an analysis similar to that used in the case of the parasitic four-poles, we obtain for the final matrix (unprimed quantities)

$$\left.\begin{aligned}
\Delta y_{\alpha\alpha} &= (ay'_{\alpha\alpha} - c)(d - by'_{\alpha\alpha})^* + ab^*|y'_{\alpha\gamma}|^2,\\
\Delta y_{\alpha\beta} &= y'_{\alpha\beta}(d - by'_{\alpha\alpha})^* + b^*y'_{\alpha\beta}y'_{\alpha\gamma},\\
\Delta y_{\beta\alpha} &= y'_{\beta\alpha}(d - by'_{\alpha\alpha})^* + b^*y'_{\beta\alpha}y'_{\alpha\gamma},\\
\Delta y_{\alpha\gamma} &= y'_{\alpha\gamma},\\
\Delta y_{\beta\beta} &= \Delta g'_{\beta\beta} + 2[by'_{\alpha\beta}(by'_{\beta\alpha}y'_{\alpha\gamma})^* + y'_{\beta\alpha}(d - by'_{\alpha\alpha})^*]
\end{aligned}\right\} \tag{177}$$

where

$$\Delta = |d - by'_{\alpha\alpha}|^2 - |by'_{\alpha\gamma}|^2.$$

These transformation equations, (177), are general and apply even if the four-pole transformer is dissipative. It can be shown that weak and full reciprocity are independently preserved by the transformation equations.

As a simple method of effecting the desired transformation to real form we take the structure of the four-pole to consist of a susceptance $-b'_{\alpha\alpha}$ canceling the imaginary part of $y'_{\alpha\alpha}$, followed by a length ϕ (in units of $\lambda/2\pi$) of transmission line of characteristic conductance g_0. It can easily be shown by applying Eqs. (175) to this structure that the coefficients a, b, c, and d are given by

$$a = \cos\phi, \qquad b = \frac{-j\sin\phi}{g_0}, \tag{178}$$

$$c = -j(b'_{\alpha\alpha}\cos\phi + g_0\sin\phi), \qquad d = -\frac{b'_{\alpha\alpha}}{g_0}\sin\phi + \cos\phi.$$

If now we choose g_0 and ϕ by putting

$$g_0 = \sqrt{g'^2_{\alpha\alpha} - g'^2_{\alpha\gamma}}, \tag{179}$$

$$\tan\phi = \left(\frac{b'_{\alpha\beta}}{g'_{\alpha\beta}}\frac{g'_{\alpha\alpha} + g'_{\alpha\gamma}}{g'_{\alpha\alpha} - g'_{\alpha\gamma}}\right)^{1/2}, \tag{180}$$

the transformed matrix is real. Substituting Eqs. (178), (179), and (180) in Eq. (177) we find

$$\Delta = 1,$$

$$\left.\begin{aligned}
g_{\alpha\alpha} &= g'_{\alpha\alpha}, \qquad g_{\alpha\beta} = g'_{\alpha\beta}\sec\phi,\\
g_{\alpha\gamma} &= g'_{\alpha\gamma}, \qquad g_{\beta\alpha} = g'_{\beta\alpha}\sec\phi,\\
g_{\beta\beta} &= g'_{\beta\beta} + \frac{2b'_{\alpha\beta}b'_{\beta\alpha}}{g'_{\alpha\alpha} - g'_{\alpha\gamma}}
\end{aligned}\right\} \tag{181}$$

In obtaining these results $y'_{\alpha\gamma}$ has been taken to be real. This assumption does not involve any restriction of generality or any assumption about reciprocity, as we can see by Eq. (9), which shows that a time zero may always be selected to cancel the phase factor of $y'_{\alpha\gamma}$. In the event that weak reciprocity holds, as assumed here, this same time zero makes e_1 an even function of the time (see Sec. 5·5).

We are now in a position to assume a current-voltage characteristic

of the barrier and to calculate the characteristic losses and impedances of our mixer.

Choosing Eq. (160) for the barrier characteristic, we see that the admittance matrix of the barrier has the form of Eq. (164). The matrix Y′ is given by Eq. (174) and the final real matrix Y is given by Eq. (181).

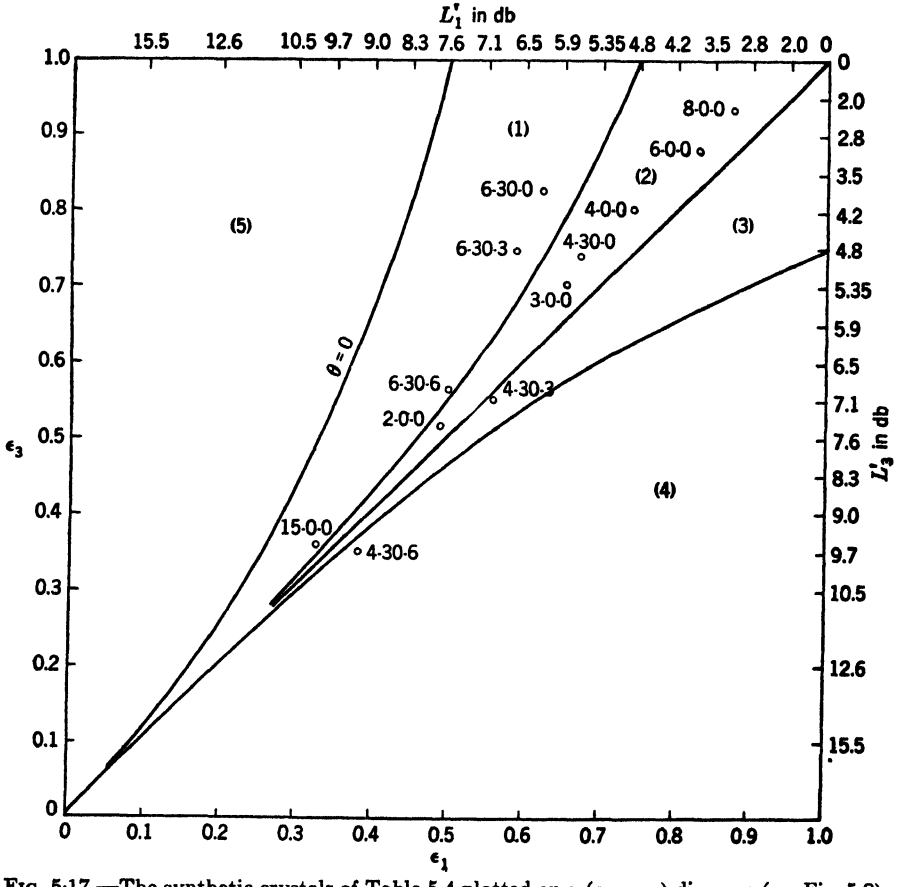

FIG. 5·17.—The synthetic crystals of Table 5·4 plotted on a (ϵ_1 — ϵ_3) diagram (see Fig. 5·8).

As a numerical example let us take

$$e_0 = 0$$
$$\alpha A = 500\ \mu\text{mhos}.$$

Table 5·4 lists the characteristic losses obtained for various assumed values of αe_1, r, and C. In Fig. 5·17 these synthetic crystals have been plotted as points on an (ϵ_1,ϵ_3)-diagram, explained in Sec. 5·7. It is interesting to note that at low local-oscillator drive ($\alpha e_1 = 4$) the barrier capacitance is the principal factor limiting performance, whereas at a higher value of αe_1 (6) the spreading resistance is the main factor. The

general distribution of the synthetic crystals on the (ϵ_1,ϵ_3)-diagram is closely similar to that for the silicon crystals, plotted in Fig. 5·10.

TABLE 5·4.—CHARACTERISTIC CONVERSION LOSSES (L_j) FOR SYNTHETIC CRYSTAL RECTIFIERS*

αe_1	r, ohms	C, $\mu\mu$f	$\mu = \omega Cr$	L_0, db	L_1, db	L_2, db	L_3, db	L_4, db
4.0	0	0	0	5.00	4 85	4.97	4.13	5.02
4.0	30	0	0	5.67	5.70	5.65	4.90	5.75
4.0	30	0.3	0.17	7.15	6.91	7.15	7.05	7.15
4.0	30	0.6	0.34	9.46	9.18	9.44	9.64	....
6.0	0	0	0	4.22	3.78	4.12	3.03	4.23
6.0	30	0	0	5.61	6.24	5 29	3.82	....
6.0	30	0.3	0.17	6.10	6.60	5.91	4.84	....
6.0	30	0.6	0.34	7.42	7.60	7.41	6.94	....

* For definitions of L_0, L_1, etc., see Table 5 1. Other quantities are—

r = spreading resistance,
C = barrier capacitance,
ω = 2π frequency,
e_1 = local-oscillator voltage amplitude,
α = exponential factor of d-c characteristic [see Eq. (160)].

5.13. Effect of a Variable Barrier Capacitance.[1]—In Secs. 5·12 and 5·13 there have been explicitly introduced the parasitic impedance elements C and r of the equivalent circuit of a crystal rectifier and their effect on the mixing properties of the rectifier determined. The approximation was made that the barrier capacitance is a constant, independent of the voltage across it. This assumption is known to be untrue; it will now be abandoned and the theory generalized by permitting the barrier capacitance to vary with applied voltage. Variability of the barrier capacitance can produce interesting and striking effects, which will be considered in some detail in Chap. 13. In this section the admittance matrix of the general barrier with nonlinear capacitance will be derived. The result will throw some light on the general problem of reciprocity. We shall see that reciprocity can never hold exactly in the general case. A qualitative explanation will be given of the experimental fact that reciprocity violations are almost always in the direction of causing the loss from signal to intermediate frequency to exceed the loss from intermediate frequency to signal.

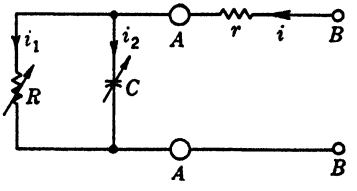

FIG. 5·18.—Equivalent circuit of a crystal rectifier with variable barrier capacitance.

The equivalent circuit here is that of Fig. 5·18. The resistance R

[1] See H. C. Torrey, "Theory of the Negative I-f Conductance of North's Welded Contact Germanium Rectifiers," RL Report No. 55, May 22, 1945.

is the nonlinear resistance of the barrier, C its nonlinear capacitance, and r the linear spreading resistance; r may include other linear losses of the cartridge (for example, whisker and wax). The current i through the rectifier will be composed of these two parts:

$$i_1 = f(e), \tag{182}$$

$$i_2 = \frac{dQ}{dt}. \tag{183}$$

Here e is the barrier voltage; $f(e)$ is the low-frequency dependence of current on voltage, and Q is the charge on the barrier. Thus the total current is

$$i = f(e) + \frac{dQ}{dt}. \tag{184}$$

As in Sec. 5·11, i and e are taken to be composed of frequencies 0, ω, and $n\omega$ ($n = 2, 3, \ldots$), where ω is the local-oscillator (angular) frequency, and it will again be assumed that the components at signal, i-f, image, and harmonic sidebands are small enough to be considered as variations of i and e.

Thus,

$$\delta i = \mathrm{Re} \sum_{\mu} i_\mu e^{jb_\mu t}, \tag{185}$$

$$\delta e = \mathrm{Re} \sum_{\mu} e_\mu e^{jb_\mu t}, \tag{186}$$

where b_μ includes the frequencies β and $n\omega \pm \beta$, ($n = 1, 2, 3, \ldots$), that is, signal, i-f, image, and harmonic sidebands.

The variational equation that replaces Eq. (153) is

$$\delta i = \frac{\partial i}{\partial e}\,\delta e + \frac{\partial i}{\partial e'}\,\delta e', \tag{187}$$

where $e' \equiv de/dt$. The second term on the right must be included since i is now an explicit function of e', inasmuch as Eq. (184) may be written in the form

$$i = f(e) + e'\frac{dQ}{de}. \tag{188}$$

This gives[1]

$$\frac{\partial i}{\partial e} = f'(e) + \frac{d}{dt}\left(\frac{dQ}{de}\right), \tag{189}$$

$$\frac{\partial i}{\partial e'} = \frac{dQ}{de}. \tag{190}$$

[1] The use of $f'(e)$ to indicate differentiation with respect to the argument should be distinguished from the use of the primes elsewhere to indicate differentiation with respect to the time.

Now $f'(e)$ and dQ/de are functions of e and hence may be expanded in Fourier series with fundamental frequency $\omega/2\pi$. If we substitute these expansions, together with Eqs. (185), (186), and the corresponding expression for $\delta e'$ [Eq. (191)] into Eq. (187), we shall find linear relationships among the various frequency components, similar to Eqs. (155) and (156). The required expression for $\delta e'$ may be obtained by differentiating Eq. (186);

$$\delta e' = \frac{d}{dt}(\delta e) = \mathrm{Re} \sum_{\mu} j e_\mu b_\mu e^{jb_\mu t}. \tag{191}$$

As noted above, b_μ includes the frequencies β and $n\omega \pm \beta$. Whenever β appears in the coefficients of Eq. (191), it will be neglected in b_μ, since in practice $\beta \ll \omega$.

Now dQ/de is in fact the capacitance of the barrier; it is the quantity that must be compared with experimental determinations of the barrier capacitance. We may write its Fourier expansion as

$$\frac{\partial i}{\partial e'} = \frac{dQ}{de} = \sum_{n=-\infty}^{+\infty} C_n e^{jn\omega t}. \tag{192}$$

If we let the expansion of $f'(e)$ be given by

$$f'(e) = \sum_{n=-\infty}^{+\infty} g_n e^{jn\omega t}, \tag{193}$$

then, from Eqs. (189), (192), and (193),

$$\frac{\partial i}{\partial e} = \sum_{n=-\infty}^{+\infty} (g_n + jn\omega C_n) e^{jn\omega t}. \tag{194}$$

Substituting Eqs. (192) and (194), together with Eqs. (185), (186), and (191), into Eq. (187) and equating coefficients of the same $e^{jb_\mu t}$, we find linear relations among the coefficients, of the general form

$$\begin{pmatrix} \cdot \\ \cdot \\ \cdot \\ i_{\beta+2\omega} \\ i_{\beta+\omega} \\ i_\beta \\ i_{\beta-\omega} \\ i_{\beta-2\omega} \\ \cdot \\ \cdot \\ \cdot \end{pmatrix} = \begin{pmatrix} & \cdot & \cdot & \cdot & \cdot & \cdot & \\ & \cdot & \cdot & \cdot & \cdot & \cdot & \\ & \cdot & \cdot & \cdot & \cdot & \cdot & \\ \cdots & y_{+2\ 0} & y_{+2+1} & y_{+2+2} & y_{+2+3} & y_{+2+4} & \cdots \\ \cdots & y_{+1-1} & y_{+1\ 0} & y_{+1+1} & y_{+1+2} & y_{+1+3} & \cdots \\ \cdots & y_{0-2} & y_{0-1} & y_{0\ 0} & y_{0+1} & y_{0+2} & \cdots \\ \cdots & y_{-1-3} & y_{-1-2} & y_{-1-1} & y_{-1\ 0} & y_{-1+1} & \cdots \\ \cdots & y_{-2-4} & y_{-2-3} & y_{-2-2} & y_{-2-1} & y_{-2\ 0} & \cdots \\ & \cdot & \cdot & \cdot & \cdot & \cdot & \\ & \cdot & \cdot & \cdot & \cdot & \cdot & \\ & \cdot & \cdot & \cdot & \cdot & \cdot & \end{pmatrix} \begin{pmatrix} \cdot \\ \cdot \\ \cdot \\ e_{\beta+2\omega} \\ e_{\beta+\omega} \\ e_\beta \\ e_{\beta-\omega} \\ e_{\beta-2\omega} \\ \cdot \\ \cdot \\ \cdot \end{pmatrix}, \tag{195}$$

where

$$y_{mn} = g_n + jm\omega C_n. \tag{196}$$

If we neglect harmonic sideband voltages as before, this reduces to

$$\begin{pmatrix} i_\alpha \\ i_\beta \\ i_\gamma^* \end{pmatrix} = \begin{pmatrix} g_0 + j\omega C_0 & g_1 + j\omega C_1 & g_2 + j\omega C_2 \\ g_{-1} & g_0 & g_1 \\ g_{-2} - j\omega C_{-2} & g_{-1} - j\omega C_{-1} & g_0 - j\omega C_0 \end{pmatrix} \begin{pmatrix} e_\alpha \\ e_\beta \\ e_\gamma^* \end{pmatrix}. \tag{197}$$

Now because of the reality of $f'(e)$ and dQ/de in Eqs. (192) and (193) we must have

$$g_{-n} = g_n^*,$$

and

$$C_{-n} = C_n^*. \tag{198}$$

If, further, a time zero can be found such that e, the barrier voltage, is an even function of the time, then, using this time zero, we have $g_{-n} = g_n$ and $C_{-n} = C_n$; hence with Eq. (198) we see that C_n and g_n are real. The existence of this time zero, however, does not make the admittance matrix of Eq. (195) or of Eq. (197) symmetrical. Indeed reciprocity now certainly fails if this time zero exists. The admittance matrix of Eqs. (197) is observed by Eq. (198) to have the symmetry required by a low-Q mixer, as it should according to our assumptions.

Some light is thrown on the general problem of reciprocity failure by Eq. (197). It should be noted that if g_n and C_n can be made simultaneously real by proper choice of time zero (and this should be at least approximately possible), then the reciprocity factor

$$\left|\frac{y_{\alpha\beta}}{y_{\beta\alpha}}\right| = \left|\frac{g_1 + j\omega C_1}{g_{-1}}\right| \geqq 1.$$

It appears from the experimental work of Smith[1] and Apker[2] that for normal crystals the reciprocity factor $\left|\frac{y_{\alpha\beta}}{y_{\beta\alpha}}\right|$, in the present case

$$\left|\frac{g_1 + j\omega C_1}{g_{-1}}\right|,$$

is greater than or equal to unity. Exceptions to this rule have been found by Apker[3] in the case of welded-contact germanium rectifiers for special bias points [not those bias points, incidentally, which give

[1] R. N. Smith, "The Theory of Mixers in Terms of Measurable Mixer Constants," NDRC 14-259, Purdue Univ., Mar. 24, 1944.

[2] L. Apker, "Note on Reciprocity Failure in Crystal Mixers," NDRC 15-931-16, GE Co., Mar. 9, 1945; and "Theory of a Double Mixer for Spectrum and Glyzer Applications," NDRC 15-931-16, GE Co., Apr. 3, 1945.

[3] Private communication.

rise to negative i-f conductance (see Chap. 13)]. The theory of variable capacitance given here does not, of course, exclude such a possibility.

It is noteworthy that weak reciprocity [Eq. (52)] holds for the matrix of Eq. (197) in either of the extreme cases, $\omega C_1 \ll g_1$, $\omega C_2 \ll g_2$ or $\omega C_1 \gg g_1$; $\omega C_2 \gg g_2$; on the other hand full reciprocity fails by a considerable factor in the latter case. As noted above, weak reciprocity always holds experimentally although full reciprocity fails for many germanium crystals.

The subject of the effects of variable capacity is discussed further in Chap. 13, where the admittance matrix of Eq. (197) is made use of in explaining these effects.

5·14. Harmonic Reinforcement.—The phenomenological theory of mixers developed in Sec. 5·3 *et seq.* is based, among other things, on the assumption that harmonic voltages are zero at the terminals of the mixer. It does not appear feasible to attempt a generalization of this theory, which includes harmonic voltages at the mixer terminals. In the physical theory discussed in Sec. 5·11 and the following sections, there have been given general results, which hold if harmonics are present, but absence of harmonic voltages has been assumed, even at the barrier, when numerical examples were given. An adequate mathematical treatment of harmonic effects is, in fact, very difficult; here only a simple numerical example will be given which will at least indicate the qualitative nature of such effects.

Let us assume the low-frequency case, in which the current is a function of the voltage of the form

$$i = f(e). \tag{199}$$

Values of conversion loss will be calculated under the two conditions (*a*) short-circuited harmonics, and (*b*) second harmonic open-circuited, other harmonics short-circuited. The value of loss for other reactive terminations of the second harmonic presumably lie somewhere in between. Case *a* has been treated above (Sec. 5·11). We must now consider Case *b*. The voltage e will be given by

$$e = e_0 + e_1 \cos \omega t + e_2 \cos 2\omega t, \tag{200}$$

and the current by

$$i = \sum_{n=0}^{\infty} i_n \cos n\omega t. \tag{201}$$

The problem, then, is to choose e_2 so that $i_2 = 0$, that is, so that the second harmonic is open-circuited.

If we choose $f(e)$ as in Eq. (160) then

$$i = A\left\{e^{\alpha e_0}\left[\sum_{-\infty}^{+\infty} I_n(\alpha e_1)e^{jn\omega t}\right]\left[\sum_{-\infty}^{+\infty} I_m(\alpha e_2)e^{2jm\omega t}\right] - 1\right\}, \tag{202}$$

where the I's are modified Bessel functions of the first kind,

$$I_n(x) = j^{-n}J_n(jx).$$

The second-harmonic current i_2 is given by

$$\begin{aligned} i_2 &= Ae^{\alpha e_0} \sum_{\substack{n,m \\ (2m+n=\pm 2)}} I_n(\alpha e_1)I_m(\alpha e_2)e^{j\omega t(2m+n)} \\ &= Ae^{\alpha e_0}\left[e^{2j\omega t}\sum_{-\infty}^{+\infty} I_{2(1-m)}(\alpha e_1)I_m(\alpha e_2)\right. \\ &\qquad \left. + e^{-2j\omega t}\sum_{-\infty}^{+\infty} I_{-2(1+m)}(\alpha e_1)I_m(\alpha e_2)\right]. \end{aligned} \tag{203}$$

Since $I_{-m} = I_{+m}$,

$$i_2 = 2Ae^{\alpha e_0}\cos 2\omega t \sum_{-\infty}^{+\infty} I_{2-2m}(\alpha e_1)I_m(\alpha e_2). \tag{204}$$

The condition that $i_2 = 0$ is (if $\alpha e_1 = x$, $\alpha e_2 = -y$)

$$\begin{aligned} &I_2(x)I_0(y) + [I_2(x) + I_6(x)]I_2(y) + [I_6(x) + I_{10}(x)]I_4(y) + \cdots + \\ &\quad = [I_0(x) + I_4(x)]I_1(y) + [I_4(x) + I_8(x)]I_3(y) + \cdots +. \end{aligned} \tag{205}$$

As an example, let us take $x = 4$. By a method of successive approximations we find

$$y = 1.582, \tag{206}$$

and obtain for the Bessel functions

$I_0(y) = 1.731$,	$I_0(4) = 11.3019$,
$I_1(y) = 1.066$,	$I_1(4) = 9.7595$,
$I_2(y) = 0.384$,	$I_2(4) = 6.4222$,
$I_3(y) = 0.096$,	$I_3(4) = 3.3373$,
$I_4(y) = 0.019$,	$I_4(4) = 1.4163$,
$I_5(y) = 0.003$,	$I_5(4) = 0.5047$,
$I_6(y) = 0.0004$,	$I_6(4) = 0.1545$,
	$I_7(4) = 0.0413$,
	$I_8(4) = 0.0098$,
	$I_9(4) = 0.0021$,
	$I_{10}(4) = 0.0004$

Using these values, we find for the Fourier expansion of $di/de = f'(e)$,

$$f'(e) = \alpha A e^{\alpha e_0} \sum a_n e^{jn\omega t} = \sum g_n e^{jn\omega t}, \tag{207}$$

where

$$\begin{aligned} a_0 &= 6.929, & a_3 &= -1.717, \\ a_1 &= 4.355, & a_4 &= -0.778, \text{ etc.} \\ a_2 &= 0, \end{aligned}$$

In calculating conversion loss, the second-harmonic sidebands are assumed to be open-circuited, whereas other harmonic sidebands are short-circuited. The general admittance matrix, Eq. (156), then reduces to

$$\alpha A e^{\alpha e_0} \begin{pmatrix} G_{\alpha\alpha} & G_{\alpha\beta} & G_{\alpha\gamma} \\ G_{\alpha\beta} & G_{\beta\beta} & G_{\alpha\beta} \\ G_{\alpha\gamma} & G_{\alpha\beta} & G_{\alpha\alpha} \end{pmatrix}, \tag{208}$$

where

$$\left.\begin{aligned} G_{\alpha\alpha} &= a_0 - \frac{(a_1 + a_3)^3}{2(a_0 + a_4)} - \frac{(a_1 - a_3)^2}{2(a_0 - a_4)} = 3.97, \\ G_{\alpha\beta} &= a_1 - a_2 \frac{a_1 + a_3}{a_0 + a_4} = 4.35, \\ G_{\alpha\gamma} &= a_2 - \frac{(a_1 + a_3)^2}{2(a_0 + a_4)} + \frac{(a_1 - a_3)^2}{2(a_0 - a_4)} = 1.81, \\ G_{\beta\beta} &= a_0 - \frac{2a_2^2}{a_0 + a_4} = 6.93. \end{aligned}\right\} \tag{209}$$

From these we find [see Eqs. (123*a*), (126), and (143)]

$$\begin{aligned} \epsilon_1 &= 0.689, & \epsilon_3 &= 0.821, \\ \epsilon_2 &= 0.947, \end{aligned}$$

which gives [see Eqs. (141) and (142)]

$$\left.\begin{aligned} L_1 &= \text{loss for short-circuited image} = 5.5 \text{ db}, \\ L_2 &= \text{double sideband loss} = 5.0 \text{ db}, \\ L_3 &= \text{loss for open-circuited image} = 3.9 \text{ db}. \end{aligned}\right\} \tag{210}$$

These values should be compared with the corresponding values for $\alpha e_1 = 4$ and for all harmonics short-circuited (as found in Sec. 5·11), viz.,

$$\begin{aligned} L_1 &= 4.8_5 & &\text{db}, \\ L_2 &= 5.0 & &\text{db}, \\ L_3 &= 4.1 & &\text{db}. \end{aligned}$$

The result of open-circuiting the second harmonic does not therefore produce significant changes in conversion loss, for the example chosen. It seems unlikely that the general case will differ greatly in this respect.

This lends support to the assumption, generally made, that a good approximation to the performance of the mixer is obtained by assuming short-circuited harmonic voltages.

The preceding conclusions with regard to the effect of open-circuiting the second harmonic are perhaps open to objection for the following reasons. The rectified current will be different for the two cases of a short circuit and an open circuit at the second harmonic. In ordinary crystal rectifiers the conversion loss is only a slowly varying function of crystal current, once the latter quantity is sufficiently large. For the example chosen here, however, this is not true. Perhaps the comparison would be fairer if the values of Eq. (210) were compared with the losses for short-circuited harmonics at the *same rectified current.* The rectified current, assuming zero d-c bias, for the example given here (open-circuited second harmonic) is easily calculated. It is

$$i_0 = A(a_0 - 1) = 5.93A$$

when a_0 is given by Eq. (207).

Using the value of αe_1 that gives this value of i_0 for the case of all harmonics short-circuited, we find in this case

$$\begin{aligned} L_1 &= 5.4 \quad \text{db}, \\ L_2 &= 5.3 \quad \text{db}, \\ L_3 &= 4.7 \quad \text{db}. \end{aligned}$$

On comparing these with Eq. (210) we again find no significant difference, except for L_3, where there is an apparent improvement of 0.8 db on open-circuiting the second harmonic.

5·15. Conversion with a Subharmonic Local Oscillator.—The problem of constructing a stable tunable c-w oscillator that will provide sufficient power for use as a local oscillator becomes very difficult at frequencies above 30,000 Mc/sec (1-cm wavelength). An alternative is to use the harmonic power of a lower-frequency oscillator. This harmonic power can be generated by a crystal rectifier. One method is to use two crystals, one for generating the harmonic power, and the other for mixing. A second possibility is to use only one crystal which performs both functions. The latter alternative seems preferable from the point of view of economical circuit design. A possible disadvantage, however, is that the fundamental power required to generate sufficient harmonic power for low mixer conversion loss is large and may be expected to produce considerable excess noise output at the intermediate frequency.

Experiments designed to test the feasibility of a "harmonic mixer" of the second type were made by Falkoff.[1] This work was exploratory in nature and was performed at frequencies lower than those for which

[1] D. L. Falkoff, RL Report No. 958, Mar. 11, 1946.

a harmonic mixer is needed because of the relative availability of components. The work was terminated by the end of the war before it could be extended to the high frequencies of interest.

Figure 5·19 shows a block diagram of the Falkoff apparatus. The local oscillator was at a wavelength of 6.4 cm and the signal at about

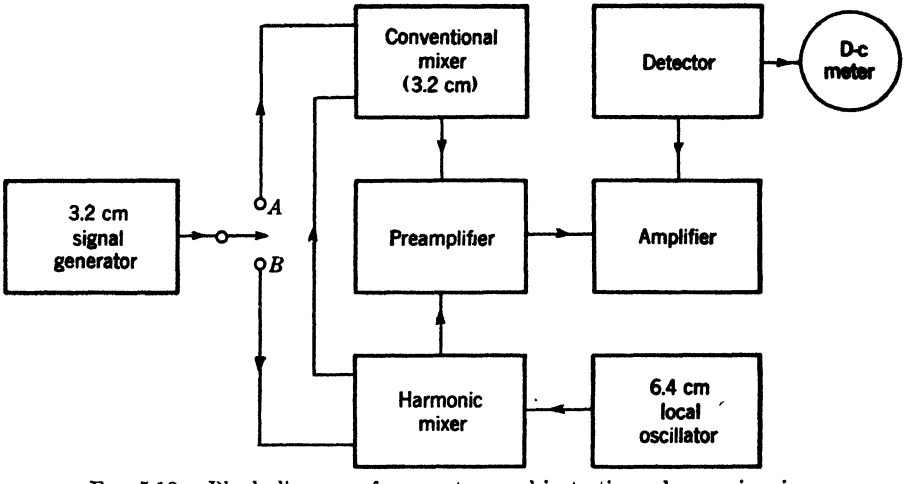

FIG. 5·19.- Block diagram of apparatus used in testing a harmonic mixer.

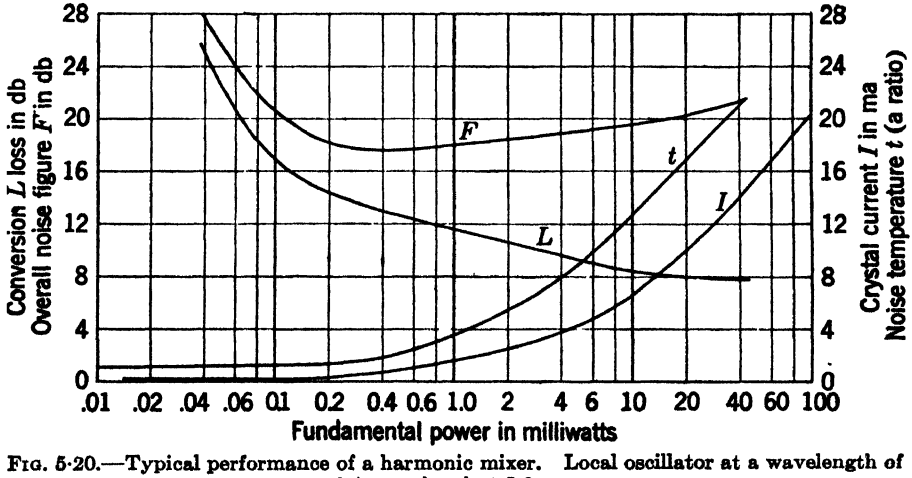

FIG. 5·20.—Typical performance of a harmonic mixer. Local oscillator at a wavelength of 6.4 cm, signal at 3.2 cm.

3.2 cm. A direct comparison of conversion with the harmonic mixer and conversion with a conventional mixer at 3.2 cm was made. (The same signal generator was used for both mixers. At switch position A it was coupled to the conventional mixer, at B to the harmonic mixer.) It was found that sufficient second-harmonic power was available from the harmonic mixer to provide local oscillations for the 3-cm mixer. A

noise diode (not shown) made possible a direct measurement of the noise temperature of the harmonic mixer.

Typical results for the harmonic mixer and commercial 1N23B crystals are shown in Fig. 5·20. These data were taken with the harmonic mixer matched to the external circuits at both 3.2-cm and 6.4-cm wavelengths.

Some noteworthy features of these results are

1. The lowest noise figure occurs at about 0.5 mw of 6.4-cm power, which is about the optimum local-oscillator level for conventional mixers.
2. The noise temperature increases linearly with the 6.4-cm power up to 30 or 40 mw. This is not apparent from the figure because the input power is plotted on a logarithmic scale. Above 40 mw, the noise temperature departs from linearity in the direction of lower values of noise temperature.
3. The conversion loss decreases slowly with 6.4-cm power above 1 mw, approaching a constant value of about 8 db when the 6.4-cm power exceeds 10 mw.
4. The noise figure changes slowly, generally remaining below 20 db over a range of local-oscillator power from 100 μw to 10 mw.

Falkoff found that the lowest conversion loss did not occur for matched harmonic (3-cm band) power out of the harmonic mixer, but that the lowest loss was obtained when the 3-cm output power was decreased by mistuning by a factor of about 2 from the matched condition. This lowest loss was about 2 db less than that for the case of matched 3-cm power.

An effect probably of importance, but not investigated by Falkoff, is that of *selective tuning* at the 6.4-cm terminals of the harmonic mixer. To see why this effect might be important, the mixing process in a second-harmonic mixer might be considered. Let us take the local-oscillator frequency as $\frac{1}{2}\omega$ and the signal frequency as $\omega + \beta$. Thus the signal, beating with the second harmonic ω of the local oscillator, is converted to the intermediate frequency β. However, the signal also beats with the fundamental frequency of the local oscillator and is thereby converted to $\frac{1}{2}\omega + \beta$, a sideband of the local-oscillator frequency $\frac{1}{2}\omega$, and this conversion process should be more efficient than the conversion to intermediate frequency. Consequently, it should be of the utmost importance to insure that power at $\frac{1}{2}\omega + \beta$ is not dissipated by transmission along the matched local-oscillator line. A filter circuit inserted in this line to reflect the $\frac{1}{2}\omega + \beta$ wave would seem most desirable. It would also serve the purpose—if arranged as a bandpass filter passing only $\frac{1}{2}\omega$—of suppressing the noise sidebands of the local oscillator. If

such a filter were to be inserted in the $\frac{1}{2}\omega$-line, its position should be chosen with care to insure optimum phase of the $(\frac{1}{2}\omega + \beta)$-sideband in the mixer. The parasitic $\frac{1}{2}\omega + \beta$ should play a much more important role in the harmonic mixer than does the image frequency in a conventional mixer.

5·16. Harmonic Generation.—In the previous section one solution of the problem of providing local oscillations at very high frequencies—the "harmonic mixer"—was examined. An alternative scheme is to use two crystals—one to generate harmonic power at the desired local-oscillator frequency, and the other to act as a conventional mixer in which this harmonic power beats directly with a signal to produce the desired intermediate frequency.

In the experiments of Falkoff described in the previous section, it was found that the output of 3.2-cm power, converted from 6.4-cm power by the multiplying crystal, ranged from 11 db to 14 db below the input 6.4-cm power, and was ample to provide local oscillations for a conventional 3.2-cm mixer. The efficiency of harmonic generation decreases with increasing fundamental frequency, however. Montgomery[1] has found that the best harmonic-generation crystals (germanium welded-contact rectifiers) produce second-harmonic power about 17 db down from a fundamental at 3.2 cm, with an input power of 30 mw. Although harmonic generation of millimeter waves from a fundamental of 1.2 cm has been studied, no absolute power measurements at the harmonics have been made, and the efficiency is not known in this most interesting case.

Montgomery has, however, made extensive comparisons[2] of the relative harmonic generation from the 1N26 (silicon 1-cm mixer crystal) rectifier and from the welded-contact germanium rectifier of H. Q. North (see Chap. 13), finding that the germanium rectifiers at their optimum d-c bias were slightly superior to the 1N26 crystals in the production of 1.6-cm waves from a fundamental at 3.2 cm. Their superiority was much greater in the generation of the third harmonic (0.4 cm) from a fundamental at 1.2 cm. Figure 5·21 shows the relative performance in this case. The notations "bias," "open-circuited," and "short-circuited" refer to the d-c bias conditions. It was found that the optimum bias for the germanium crystals was critical. The ordinate of this plot is the open-circuit direct voltage obtained from a crystal used as a rectifier of the harmonic power.

Recently North[3] has improved the harmonic generation of his crystals,

[1] D. Montgomery, RL Report No. 818, Oct. 23, 1945.

[2] *Loc. cit.*

[3] H. Q. North, "A Comparison of Silicon and Germanium Microwave Crystals as Harmonic Generators of 4 mm. and 6 mm. Waves," GE Report, Jan. 15, 1946.

in particular the generation of the third harmonic from a 1.2-cm fundamental, by going to welded contacts of very small dimensions. He used whisker deflections of only 0.00012 cm and a welding current of 50 ma as contrasted with 0.0005 cm and 250 ma for the normal case (see Sec. 13·1). These small-contact, welded rectifiers produced 10 to 20 db more output (0.4-cm) power than conventional 1N26 rectifiers at the same input (1.2-cm) power.

5·17. Modulation.—Crystal rectifiers are sometimes used as modulators, i.e., as agents to produce sidebands of a carrier. Crystal modulation falls into two categories: (1) conversion of a low-frequency signal to high-frequency sidebands of a local oscillator; (2) conversion of a pure high-frequency carrier to sidebands. In the first case, the mixer is

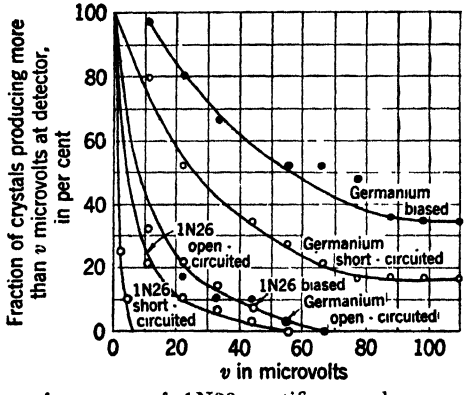

FIG. 5·21.—Relative performance of 1N26 rectifiers and germanium welded-contact rectifiers in the generation of 0.4 cm power from a fundamental at 1.2 cm.

driven by a high-frequency local oscillator and, in the second, by a low-frequency (modulation-frequency) oscillator. The first case is just the inverse of the familiar mixer problem we have been considering up to now, and the second involves some new principles. The first type of modulation has been used by Apker in his double-mixer spectrum analyzer[1] while the second type has been employed by Pound[2] in one of his methods of frequency stabilization of oscillators.

As was shown in Sec. 5·9, modulation of the first type may be treated with the same mathematical theory used for ordinary mixers. If $L_{\alpha\beta}$ is the conversion loss from a high-frequency α signal sideband to a low beat frequency β, the conversion loss for the reverse process is just $L_{\beta\alpha} = |y_{\beta\alpha}/y_{\alpha\beta}|^2 L_{\alpha\beta}$, where $|y_{\beta\alpha}/y_{\alpha\beta}|$ is the reciprocity factor discussed in Sec. 5·9. In all silicon rectifiers observed so far, the experimental value

[1] See L. Apker, E. Taft, and J. Dickey, "Theory of a Double Mixer for Spectrum Analyzer Applications," OEMsr-931 Report 931-17, GE Co., Apr. 2, 1945.

[2] R. V. Pound, "An Improved Frequency Stabilization System for Microwave Oscillators," RL Report No. 837, Oct. 26, 1945.

of $|y_{\beta\alpha}/y_{\alpha\beta}|$ is close to unity, whereas, for germanium rectifiers, this quantity is often found to be much less than unity. The process of modulation is, therefore, in the case of germanium, often considerably more efficient than the inverse process of mixing. Observed values of $|y_{\beta\alpha}/y_{\alpha\beta}|$ for germanium have been found[1] to range between 1 and $\frac{1}{3}$.

The second type of modulation, employing a low-frequency local oscillator, is somewhat simpler in theory than the mixing process considered above. The greater simplicity arises from the fact that all frequencies connected by linear relationships are of the same order, and that, in practice, there is no impedance transformation involved. The theory of this process will now be outlined.

The modulator is shown schematically in Fig. 5·22. Let γ = voltage reflection coefficient at the r-f terminals. It will be assumed that the

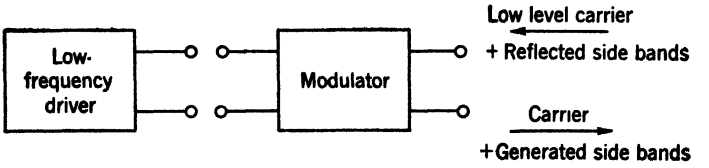

FIG. 5·22.—Block diagram of a modulator whose function is to convert a low-level carrier into sidebands.

carrier is at a sufficiently low level so that the r-f admittance of the modulator is completely controlled by the low-frequency driver. Then

$$\gamma = \sum_{n=-\infty}^{+\infty} \gamma_n e^{jn\beta t}, \tag{211}$$

where β is the modulation frequency.

Let the incident r-f current wave be given by

$$I = \sum_{n=-\infty}^{+\infty} I_{\omega+n\beta} e^{j(\omega+n\beta)t}, \tag{212a}$$

and the reflected current wave by

$$I' = \sum_{n=-\infty}^{+\infty} I'_{\omega+n\beta} e^{j(\omega+n\beta)t}. \tag{212b}$$

By definition of the reflection coefficient,

$$I' = \gamma I. \tag{213}$$

[1] Values greater than one have recently been found by L. Apker (private communication) in the case of welded-contact germanium crystals at special bias points.

The incident and reflected voltage waves will be denoted by V and V'; their Fourier representations are similar to Eq. (212), with $V_{\omega+n\beta}$ and $V'_{\omega+n\beta}$ replacing $I_{\omega+n\beta}$ and $I'_{\omega+n\beta}$, respectively. We have then

$$V' = -\gamma V = -\gamma Z_0 I, \tag{214}$$

where Z_0 is the characteristic impedance of the transmission line attached to the r-f terminals.

Substituting Eq. (211) into Eqs. (213) and (214), we obtain

$$I'_{\omega+n\beta} = \sum_{m=-\infty}^{+\infty} \gamma_{n-m} I_{\omega+m\beta}, \tag{215}$$

$$V'_{\omega+n\beta} = -Z_0 \sum_{m=-\infty}^{+\infty} \gamma_{n-m} I_{\omega+m\beta}. \tag{216}$$

For the present, sidebands at frequencies other than $\omega \pm \beta$ are neglected. Equations (215) and (216) may then be written

$$\begin{pmatrix} I'_{\omega+\beta} \\ I'_{\omega} \\ I'_{\omega-\beta} \end{pmatrix} = \Gamma \begin{pmatrix} I_{\omega+\beta} \\ I_{\omega} \\ I_{\omega-\beta} \end{pmatrix}, \tag{217}$$

$$\begin{pmatrix} V'_{\omega+\beta} \\ V'_{\omega} \\ V'_{\omega-\beta} \end{pmatrix} = -Z_0\Gamma \begin{pmatrix} I_{\omega+\beta} \\ I_{\omega} \\ I_{\omega-\beta} \end{pmatrix}, \tag{218}$$

where Γ is the "scattering matrix,"

$$\Gamma = \begin{pmatrix} \gamma_0 & \gamma_1 & \gamma_2 \\ \gamma_{-1} & \gamma_0 & \gamma_1 \\ \gamma_{-2} & \gamma_{-1} & \gamma_0 \end{pmatrix}. \tag{219}$$

Let us consider now the special case where a pure carrier at frequency ω is incident, and pure sidebands $\omega \pm \beta$ are generated with no carrier. Evidently, in this case,

$$\left.\begin{aligned} \gamma_0 &= 0, \\ I'_{\omega+\beta} &= \gamma_1 I_\omega, \\ I'_{\omega-\beta} &= \gamma_{-1} I_\omega, \\ V'_{\omega+\beta} &= -Z_0\gamma_1 I_\omega, \\ V'_{\omega-\beta} &= -Z_0\gamma_{-1} I_\omega. \end{aligned}\right\} \tag{220}$$

The incident power is

$$P_\omega = \tfrac{1}{2} Z_0 |I_\omega|^2, \tag{221}$$

and the reflected power in the sideband $\omega + \beta$ is

$$P'_{\omega+\beta} = \tfrac{1}{2} Z_0 |\gamma_1|^2 |I_\omega|^2. \tag{222}$$

The conversion loss to this sideband is then

$$L_{\omega,\omega+\beta} = \frac{1}{|\gamma_1|^2}. \tag{223}$$

Similarly, the conversion loss to the other sideband is

$$L_{\omega,\omega-\beta} = \frac{1}{|\gamma_{-1}|^2}. \tag{224}$$

These expressions for conversion loss hold also in the general case in which other sidebands are not neglected. Thus,

$$L_{\omega,\omega+n\beta} = \frac{1}{|\gamma_n|^2}. \tag{225}$$

If we assume that a time zero can be chosen such that the driving voltage (at frequency β) is an even time function, we have $\gamma_{-n} = \gamma_n^*$, and the sidebands are symmetrically generated. In this case,

$$\gamma_1 = \frac{1}{\pi}\int_0^\pi \gamma \cos \beta t d(\beta t).$$

Since $|\gamma| \leqq 1$, it is apparent that $|\gamma_1| \leqq 2/\pi$, and so the conversion loss to the first-order sidebands is greater than $\pi^2/4$ or 3.9 db. An ideal modulator thus has a loss of 3.9 db to either first-order sideband.

As an example, let us neglect reactive effects in the crystal and modulator, and take the crystal current-voltage characteristic to be

$$I = A(e^{\alpha V} - 1),$$

which, as noted above [Eq. (160)], is an approximate representation of the d-c characteristic of an actual rectifier. The r-f admittance will then be

$$\frac{dI}{dV} = A\alpha e^{\alpha V}.$$

Let us assume for simplicity that $Z_0 = A\alpha = 1$, then

$$\gamma = \frac{e^{\alpha V} - 1}{e^{\alpha V} + 1},$$

and

$$\gamma_1 = \frac{1}{\pi}\int_0^\pi \frac{e^{\alpha V_0 \cos \phi} - 1}{e^{\alpha V_0 \cos \phi} + 1} \cos \phi \, d\phi,$$

where $V = V_0 \cos \beta t$ is the low-frequency driving voltage. If $\alpha V_0 \gg 1$,

$$\gamma_1 \approx \frac{2}{\pi}\left(1 - \frac{2 \ln 2}{\alpha V_0} - \frac{5.41}{\alpha^2 V_0^2} \cdots\right).$$

Assuming a value $\alpha V_0 = 10$, we find

$$\gamma_1 = \frac{2}{\pi}(0.856)$$

and $L = 1/|\gamma_1|^2 = 5.4$ db, or 1.5 db above the theoretical minimum loss.

Measurements by R. V. Pound,[1] at the 3-cm band on a 1N23B rectifier gave L $\approx$ 6 db, which agrees well with the example given here.

In this example, all even-order sidebands are suppressed, and the third-order sidebands are down about 10 db below the first-order sidebands.

[1] Private communication.

CHAPTER 6

NOISE GENERATION

THEORY

Little is known about the origin of noise in crystal rectifiers. The spreading resistance of the semiconductor must produce thermal (Johnson) noise and the barrier, acting as a diode (Sec. 4·3), would be expected to produce shot noise of the type unlimited by space charge. Both sources of noise will be treated here (see Sec. 6·1). To account for certain observations, there must exist other sources of noise. Some hypotheses concerning the nature of these sources are made in the following pages (see Sec. 6·2), but it may be that other, potent sources have been overlooked and that some of those considered here are really relatively unimportant.

The "noisiness" of a crystal rectifier is measured by its noise temperature, defined as the ratio of the noise power available from the rectifier to the noise power available from a resistor, $kT_0\,\Delta f$, at the reference temperature $T_0 = 290°\text{K}$ (see Sec. 2·5).

If a crystal rectifier is not excited by the passage of current through it, its noise temperature (at 290°K) is observed to be unity, as required by thermodynamics. An excited crystal rectifier is not in thermodynamic equilibrium and its noise temperature cannot be predicted by any simple considerations. With d-c excitation, t is usually greater than unity, but at small voltages in the forward direction it may become less than unity. In use, mixer crystals are excited by high-frequency currents from the local oscillator at a power level of about 1 mw. Measurement of many thousands of production samples under this condition have given values of t ranging from 1.0 to 3.0. Burned-out crystals may have values of t up to 10 or 20. In no authentic case has a value less than 1.0 been observed.

The treatment of the theoretical problem of crystal noise with local-oscillator excitation has so far met with no success. The following discussion is therefore limited to direct-current excitation.

6·1. Shot and Thermal Noise in Crystal Rectifiers.—In this section are considered only shot noise produced by the barrier and thermal noise caused by the ohmic spreading resistance.[1]

[1] The treatment is based on the work of V. F. Weisskopf. See his "On the Theory

The barrier of a silicon or germanium rectifier was shown in Sec. 4·3 to be somewhat analogous to a temperature-limited vacuum-tube diode. The mean free path of the electrons is larger than the barrier width and the electrons fly over the barrier practically unimpeded by collisions or space charge. The discreteness of electronic charge and the random arrival of electrons at the metal (or, in the case of the reverse current, at the bulk semiconductor) give rise to random current fluctuations commonly referred to as "shot noise." Noise of this type was considered for the case of a temperature-limited diode by Schottky, who showed that the mean square noise current produced by this effect is given by

$$\overline{i^2} = 2eI\,\Delta f \tag{1}$$

in the frequency band f to $f + \Delta f$. Here e is the electronic charge and I is the diode current.

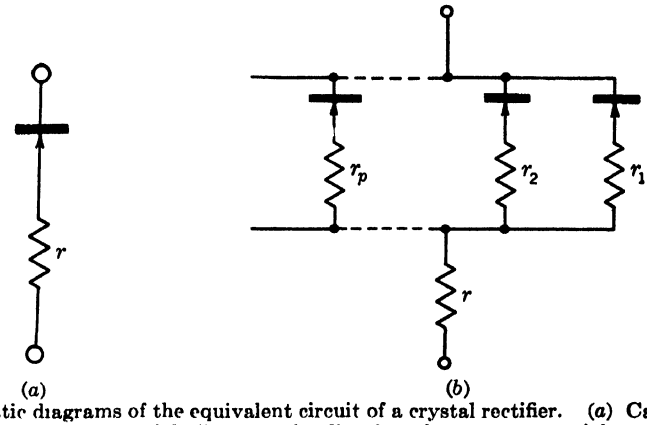

FIG. 6·1.—Schematic diagrams of the equivalent circuit of a crystal rectifier. (a) Case of a uniform contact potential; (b) case of a distributed contact potential.

If this formula could be expected to hold for the case of the crystal-rectifier barrier, then

$$I = I_1 + I_2, \tag{2}$$

where I_1 and I_2 are the electron currents from semiconductor to metal and from metal to semiconductor respectively (since I_1 and I_2 are equally effective in producing shot-noise fluctuations).

Equation (1) should hold for the barrier proper. To obtain the total noise from the rectifier there must now be included the contribution from the spreading resistance. Here, ideal contacts of uniform contact potential must be distinguished from actual contacts which, as noted in Sec. 4·4, probably consist of distributed contact potentials. This

of Noise in Conductors, Semiconductors and Crystal Rectifiers," NDRC 14-133, May 15, 1943.

distinction is necessary for the following reason. In the case of the ideal uniform contact, the spreading resistance may be lumped together and assumed to be in series with the barrier as shown in Fig. 6·1*a*. As was seen in Sec. 4·4, however, for a distributed contact potential, the current flows mostly through local spots of relatively low contact potential. Each of these spots has in series with it its own local spreading resistance r_k, which is not shared by the other spots. The barrier then consists of a number of these series elements all in shunt with each other. Finally the spreading resistance r of the entire contact is in series with this combination. The situation is shown schematically in Fig. 6·1*b*.

To calculate the total available noise power the following theorems concerning the total noise output of a combination of noise sources are utilized. The proofs are fairly obvious.

THEOREM 1. If a number of noise sources of differential (dynamic) resistance ρ_k are connected in parallel, the mean squares of the noise currents are additive; hence

$$\overline{i^2} = \sum_k \overline{i_k^2} \qquad \text{(parallel)}, \tag{3}$$

and the total available noise power P can be expressed in terms of the individual noise powers P_k in the form,

$$\left.\begin{aligned} P &= \rho \sum \frac{P_k}{\rho_k} \\ \frac{1}{\rho} &= \sum_k \frac{1}{\rho_k} \end{aligned}\right\} \qquad \text{(parallel)}. \tag{4}$$

THEOREM 2. If a number of noise sources are in series, the mean squares of the emf's are additive;

$$\overline{V^2} = \sum_k \overline{V_k^2} \qquad \text{(series)}, \tag{5}$$

and the total available noise power is given by

$$\left.\begin{aligned} P &= \frac{1}{\rho} \sum_k P_k \rho_k, \\ \rho &= \sum_k \rho_k \end{aligned}\right\} \qquad \text{(series)}. \tag{6}$$

In addition there is needed the result of Nyquist[1] that the available noise power from an ohmic resistance is $kT\,\Delta f$. This well-known result

[1] H. Nyquist, *Phys. Rev.*, **32**, 110 (1928).

is usually proved by thermodynamic arguments. Recent proofs[1] based on kinetic theory have clearly shown that thermal noise has the same nature and origin as shot noise. Weisskopf also derives the noise power of a nonohmic resistance in which the electrons gain more energy than kT from the field in one free path. A resistance of this type is said to be "overloaded." It is possible that the local spreading resistance of some barrier spots of low contact potential would be of this character.

The simple case of a uniform contact potential is discussed first.

Uniform Contact Potential.—The noise power P_B available from the barrier alone is given by the mean square current of Eq. (1), with I defined by Eq. (2), multiplied by one-fourth the differential resistance R of the barrier. Thus,

$$P_B = \tfrac{1}{2}eIR\,\Delta f. \tag{7}$$

This must be combined with the noise power $kt\,\Delta f$ available from the spreading resistance r according to Theorem 2 above. Then the total available noise power is

$$P = \frac{\frac{1}{2}eIR^2 + kTr}{R + r}\,\Delta f. \tag{8}$$

The noise temperature t is the ratio of P to $kT_0\,\Delta f$; hence,

$$t = \frac{\frac{e}{2kT_0}IR^2 + r\left(\frac{T}{T_0}\right)}{R + r}. \tag{9}$$

The electron currents traversing a barrier of uniform contact potential are given by Eq. (4·41), which may be written here as

$$I' = A[e^{+\frac{e\beta V}{kT}} - e^{-\frac{e(1-\beta)V}{kT}}]. \tag{10}$$

Here I' is the net current and is composed of the difference between the metal-semiconductor current and the current in the opposite direction. The sum of these two currents will be I of Eq. (1); hence

$$I = A[e^{\frac{e\beta V}{kT}} + e^{-\frac{e(1-\beta)V}{kT}}]. \tag{11}$$

In these equations V is the voltage applied to the barrier and β is a parameter determining the amount of barrier lowering resulting from image force and tunnel effect. The height of the barrier above the potential of the bulk semiconductor would be $\phi_0 - V$ without these effects and is $\beta(\phi_0 - V)$ as a result of their inclusion.

[1] C. J. Bakker and G. Heller, *Physica* **6**, 262 (1939); P. R. Weiss and S. A. Goudsmit, RL Report No. 191, Jan. 18, 1943; V. F. Weisskopf, *loc. cit.*

The differential resistance R of the barrier is given by

$$R = \left(\frac{dI'}{dV}\right)^{-1}. \tag{12}$$

From Eqs. (10), (11), (12), and (7) the following expression is obtained for the available noise power from the barrier:

$$P_B = \frac{1}{2} kT\,\Delta f \frac{1 + e^{-\frac{eV}{kT}}}{\beta + (1 - \beta)e^{-\frac{eV}{kT}}}. \tag{13}$$

In the special case of $V = 0$, this reduces, as required by thermodynamics, to $kT\,\Delta f$. When V is large and negative,

$$P_B = \frac{1}{2}\frac{kT}{1 - \beta}\Delta f, \tag{14}$$

and when V is large and positive,

$$P_B = \frac{1}{2}\frac{kT}{\beta}\Delta f. \tag{15}$$

These formulas hold provided V is less than the contact potential ϕ_0. When $V > \phi_0$ the barrier no longer contributes noise.

Since β is a number slightly less than unity, the noise temperature $P_B/kT\,\Delta f$ of a barrier of uniform contact potential should be about $\frac{1}{2}$ in the forward direction ($V \gg kT/e$), unity at $V = 0$, and should become large in the reverse direction. Furthermore, although β has been treated as a constant, it actually should decrease slowly with increasing voltage. Thus the barrier-voltage noise temperature for forward voltage should, starting from unity at zero voltage, first decrease and later increase with voltage. In the reverse direction it should increase rapidly to very large values.

These predictions are only qualitatively in accord with experiment. Before comparing them with the facts there will be discussed the more realistic but complicated case of a barrier with distributed contact potential.

Distributed Contact Potential.—The total noise power P_B of the barrier region must now be found by using Theorems 1 and 2 to sum the contribution of the rectifying elements of different contact potential with their associated spreading resistances.

Let us first consider voltages $V < kT/e$. In this case the local spreading resistances are usually small compared with the barrier resistance, and by Theorem 1, Eq. (7) continues to hold. An alternative expression is obtained by summing contributions of the form of Eq. (13)

for the spots of different contact potential. With the aid of Theorem 1, the following expression is obtained:

$$P_B = \frac{1}{2} kT\,\Delta f \sum_k \frac{R}{\rho_k}\left[\frac{1 - e^{-\frac{eV}{kT}}}{\beta_k + (1 - \beta_k)e^{-\frac{eV}{kT}}}\right], \tag{16}$$

where ρ_k and β_k are, respectively, the differential resistance and the value of β for the kth spot, and $R = \left(\sum_k \frac{1}{\rho_k}\right)^{-1}$ is the total differential barrier resistance.

If the voltage V is large compared with kT/e, three different possibilities can be considered:

1. No overloading; mean free path l of electrons short compared with the radius a of a spot, that is, $l \ll a$.
2. Overloading, $l \ll a$.
3. Overloading, $l > a$.

In the first case, the local spreading resistances are ohmic and each contributes a noise power $kT\,\Delta f$. In the second, they are nonohmic and their noise power, according to Weisskopf, is $(l/a)ei_k\,\Delta f$, where i_k is the current through the kth spot. In the third case no collisions are made in the local-spreading resistances; their noise power is accounted for by the barrier shot noise.

The detailed analysis of each case is rather involved and will not be given here. Weisskopf derives limits for the barrier noise power in each case, expressing them in terms of the equivalent temperature θ of the barrier, defined by

$$k\theta \equiv eIR, \tag{17}$$

where R is the differential barrier resistance, equal to dV/dI. The total current I may now be taken as the *net* current since for $V \gg kT/e$, $I_1 \gg I_2$ [see Eq. (2)]. If θ is assumed to be constant, we obtain on integration

$$I = Ae^{eV/k\theta}, \tag{18}$$

where A is an integration constant. It was pointed out in Sec. 4·4 that a formula of this type holds for the barrier if $V \gg kT/e$, and that the slope of the curve, for *log* I vs. V, is experimentally always smaller than e/kT by a factor of about 2 or 4. Thus θ is larger than T by the same factor.

The limits on P_B for the various possibilities are given by Weisskopf as

$$\tfrac{1}{2}kT\,\Delta f < P_B < \tfrac{1}{2}k(T+\theta)\,\Delta f \qquad \begin{pmatrix}\text{no overloading}\\ a \gg l\end{pmatrix} \tag{19a}$$

$$\tfrac{1}{2}kT\,\Delta f < P_B < \tfrac{1}{2}k\theta\,\Delta f \qquad \begin{pmatrix}\text{overloading}\\ a \gg l\end{pmatrix} \tag{19b}$$

$$P_B = \tfrac{1}{2}k\theta\,\Delta f \qquad \begin{pmatrix}\text{overloading}\\ a < l\end{pmatrix}. \tag{19c}$$

From Eqs. (17) and (19c) P_B can be expressed as $\frac{1}{2}eIR\,\Delta f$. That this is the same as Eq. (7) is not surprising, for when $a < l$, only diode shot noise is contributed by the barrier.

Overloading should take place, according to Weisskopf, if

$$\theta > \frac{T}{\alpha}\frac{a}{l}, \tag{20}$$

where α is a number about equal to 2.

The ratio a/l should be expected to increase with voltage in the forward direction because of the tendency of spots to cluster at high voltages (see Sec. 4·4).

The total noise power of the rectifier is obtained by combining P_B with the noise power of the series spreading resistance r of the whole barrier. Thus by Theorem 2,

$$P = \frac{RP_B + rkT\,\Delta f}{R + r}. \tag{21}$$

It is evident from the preceding discussion that the general expression, Eq. (7), should hold even for the distributed-contact-potential case for voltages $V < kT/e$, and for any voltage in the severely overloaded case ($a < l$).

A test of this relation [Eq. (7)] was made by Smith.[1] Figure 6·2 shows experimental and theoretical noise temperatures plotted as a function of d-c bias for a number of silicon and germanium cartridges. There should be noted the different current scales in the forward and reverse directions.

For most of the units the actual noise is larger than the theoretical. However, in the cases of Nos. 6 and 8 the observed noise in the reverse direction is less than the calculated noise over most of the range. In the forward direction Nos. 6, 7, and 8 (all germanium) definitely have less than theoretical noise over part of the range. The neglect of the local spreading resistance in this range may perhaps explain the fact that the observed noise is smaller than the calculated noise in the reverse direction. Excess noise, on the other hand, must be presumed to result from fluctuation effects such as those considered in the following section.

[1] R. N. Smith, "Crystal Noise as a Function of D-c Bias and 30 mc Impedance Measured with a Diode Noise Source," NDRC 14-167, Purdue Univ., June 25, 1943.

The frequency spectrum of shot noise should be uniform from zero frequency to an upper limit determined by the mean time of flight τ of an electron. Intermediate frequencies in current use are well below $1/\tau$ (which should correspond to about 10^{13} cps). The noise at high frequencies should be reduced by barrier capacitance, but this capacitance should be ineffective at the intermediate frequencies now in use.

6·2. Other Sources of Noise.—Noise produced by processes other than the shot effect originates from the current fluctuations that are created by causes other than the discrete nature of the charges. Fluctuation noise should have a frequency spectrum extending from zero to some upper limit determined by the mean duration of a current fluctua-

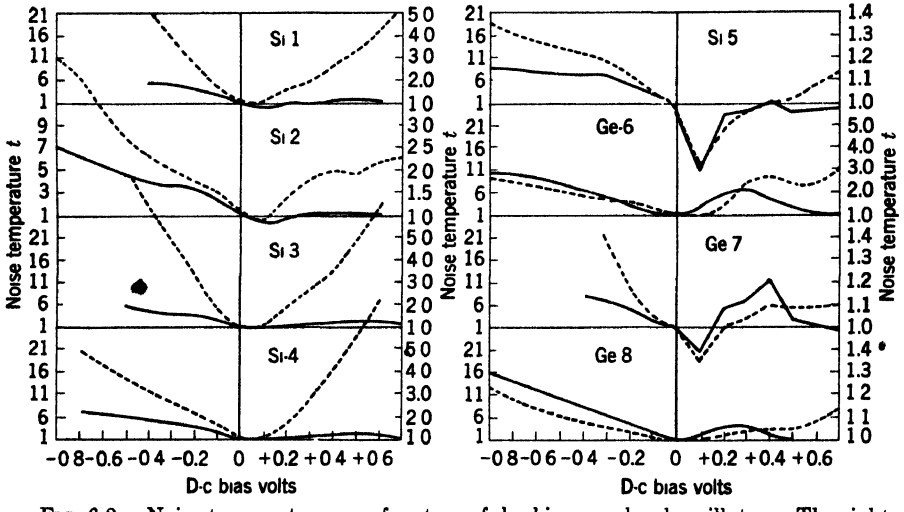

FIG. 6·2.—Noise temperature as a function of d-c bias—no local oscillator. The right- and left-hand ordinate scales apply to positive and negative bias respectively. The broken lines show the experimental data and the solid lines, the values given by Eq. (9).

tion. Hurwitz[1] showed that mean-square fluctuation noise current and mean-square shot noise current are additive and hence give the total mean-square noise current.

Two possible sources of fluctuation noise have been suggested. Weisskopf[2] considers the effect of the motion of ions on the contact surface. The contact potential is strongly affected by the presence of surface ions, whose motion should cause the contact potential to change in the region of the motion. Such changes would strongly modulate the current passing through these regions. A mechanism of this sort is suggested by the fact that double layers of varying strength must be assumed to exist on the surface of the crystal in order to explain the

[1] See V. F. Weisskopf, "On the Theory of Noise in Conductors, Semiconductors and Crystal Rectifiers," NDRC 14-133, May 16, 1943.

[2] *Op. cit.*

variation of contact potential. The ions concentrated on the surface are not strongly bound to specific places and may easily be loosened by thermal vibrations. They would then move to another place of low potential energy. Weisskopf estimates that the ratio of fluctuation noise of this type to shot noise should be about $10^4 K e^{-\frac{\epsilon}{kT}}$, where K is the fraction of the contact area in which fluctuations occur and ϵ is the activation energy for the surface motion of an ion. This ratio can be larger than unity for reasonable values of ϵ.

Another and different source of fluctuation noise has been suggested by Schiff.[1] He has attributed excess noise to an instability of the contact. It is assumed that the "whisker" makes contact with the semiconductor only at a number of spots, each of which is small compared with the contact dimensions. Each spot is assumed to have its own local spreading resistance. Schiff, using the theory given in Sec. 8·2, derives an expression for the temperature of a spot caused by the flow of current through its spreading resistance. He then shows that this temperature is an increasing function of the radius of the spot. Any spot is then unstable; for any small fluctuation that decreases the size of a spot decreases its temperature. The resulting contraction of the silicon and whisker still further decreases the area of the spot. This process continues until the spot contact cools to the temperature of the bulk crystal or pulls completely apart. Likewise, a disturbance that increases the spot size increases the temperature and thus results in thermal expansion and a further increase in size. This continues until the size becomes so large that the temperature no longer depends on it. Such instability would produce noise with a frequency spectrum from an upper limit of the order of magnitude of the reciprocal of the thermal relaxation time of one of the small contacts down to nearly zero frequency. This upper frequency would be well above the intermediate-frequency range. It is not clear, however, that this process would continue indefinitely; it is possible that some spot would tend to grow at the expense of others until the whole contact reached a stable configuration.

INTERMEDIATE FREQUENCY AND VIDEO NOISE

The intermediate frequencies most commonly used in microwave radar are 30 and 60 Mc/sec. Consequently most of the Radiation Laboratory data on crystal noise are obtained from experiments at these frequencies. Experiments by the University of Pennsylvania group[2] have made available additional data for video and audio frequencies;

[1] L. I. Schiff, "Noise in Crystal Rectifiers," NDRC 14-126, Univ. of Penn., Mar. 10, 1943.

[2] P. H. Miller, M. N. Lewis, L. I. Schiff, and W. E. Stephens, "Noise Spectrum of Silicon Rectifiers," NDRC 14-256, Univ. of Penn., Mar. 20, 1944.

these are discussed in Sec. 6·4. The effect of r-f tuning on noise temperature is discussed in Sec. 7·10. The dependence of noise temperature on rectified current was discussed in Chap. 2 (see Fig. 2·17).

6·3. Dependence of Noise Temperature on Frequency. *Dependence of Intermediate-frequency Noise on Excitation Frequency.*—Noise temperatures measured at intermediate frequencies customarily used in radar equipment (about 30 Mc/sec) with r-f excitation in the 1-, 3-, and 10-cm bands do not agree; in some cases the difference may be as large as 1 or 2, or in rare cases even greater. The difficulty in establishing identical experimental conditions may explain the differences observed in particular units for different microwave frequencies, but this explanation can-

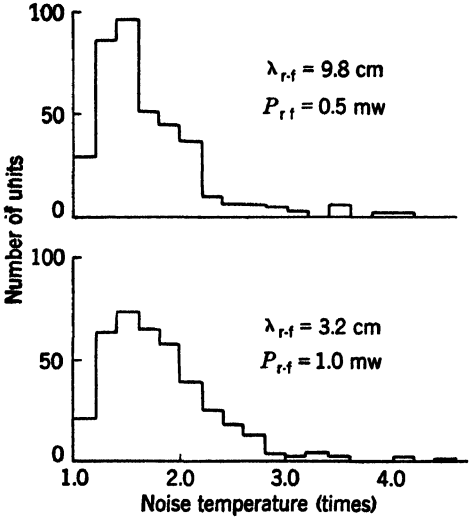

FIG. 6·3.—A comparison of noise-temperature distributions for 1N23 rectifiers for r-f wavelengths of 9.8 and 3.2 cm. Random sample of 1N23 rectifiers.

not as yet be confirmed with data at hand. Measurements made with the standard test equipments (see Chap. 9) are illustrated in Figs. 6·3 and 6·4 for a representative sample of commercial 1N23 units selected prior to acceptance tests. Briefly, the experimental conditions require: (1) fixed r-f power level, (2) fixed-tuned mixer, (3) i-f coupling circuit making the noise temperature measurement independent of i-f resistance, and (4) intermediate frequency, 30 Mc/sec. Figure 6·3 shows the distribution of noise temperature for r-f excitation at 9.8 and 3.2 cm with r-f power levels of 0.5 and 1.0 mw, respectively. The rectified current for a given unit is therefore not ordinarily the same in the two cases, but the average values are approximately the same. Figure 6·4 shows the distribution of the difference in noise temperature of individual units in the 10- and 3-cm bands.

Similar data for the 3- and 1-cm bands are shown in Figs. 6·5 and 6·6. The 3-cm measurements were made using standard test equipment, with the r-f power level adjusted for each unit to give the same rectified current as that obtained at a constant power level of 1 mw in the 1-cm

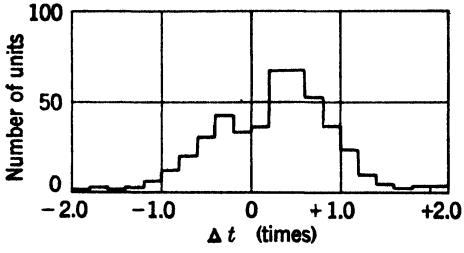

FIG. 6·4.—Difference in noise temperature of 1N23 rectifiers. $\Delta t = t_1 - t_2$, where t_1 is the noise temperature for $\lambda_{r\text{-}f} = 3.2$ cm and t_2 is for $\lambda_{r\text{-}f} = 9.8$ cm.

equipment. The intermediate frequency for the 1-cm measurements was 60 Mc/sec.

The Spectrum of Video Noise.—The noise output of crystal rectifiers at intermediate frequencies of 30 and 60 Mc/sec is approximately the

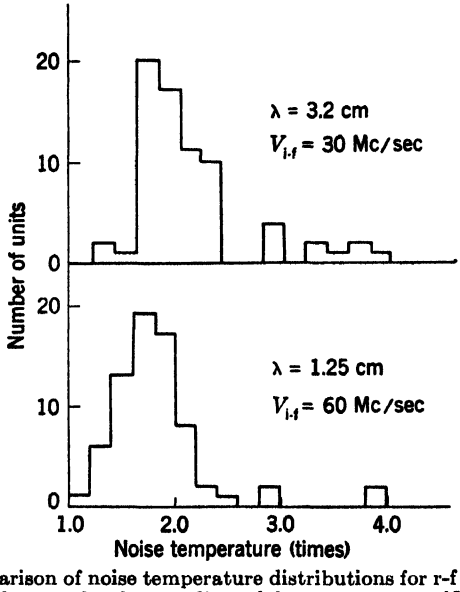

FIG. 6·5.—A comparison of noise temperature distributions for r-f wavelengths of 3.2 cm and 1.25 cm. The r-f power level was adjusted for the same rectified current at the two wavelengths. A random sample of 1N26 rectifiers was used.

same, as can be seen from Fig. 6·5. At lower frequencies, however, the noise temperature increases until at audio frequencies it is orders of magnitudes greater than at intermediate frequencies. The noise spectrum of silicon rectifiers in the range from 15 to 300 kc/sec with d-c and

r-f excitation has been investigated by Miller *et al.*[1] No data are available in the range from 1 to 30 Mc/sec. A block diagram of the apparatus and a circuit diagram of the input circuit used by Miller for the frequency

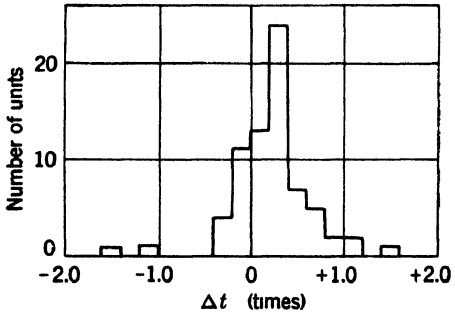

FIG. 6·6.—Difference in noise temperature of 1N26 rectifiers. $\Delta t = t_1 - t_2$, where t_1 is the noise temperature for $\lambda_{r\text{-}f} = 3.2$ cm, $\nu_{i\text{-}f} = 30$ Mc/sec and t_2 is the noise temperature for $\lambda_{r\text{-}f} = 1.25$ cm, $\nu_{i\text{-}f} = 60$ Mc/sec. Data are for the same units plotted in Fig. 6.5.

range from 15 to 300 kc/sec are shown in Fig. 6·7. The dynamic impedance R_2 of the crystal, the input resistor R_1, and the load resistance of the diode R_D are connected in parallel to the grid of the first amplifier tube. The rest of the circuit is for applying d-c bias to the crystal. The

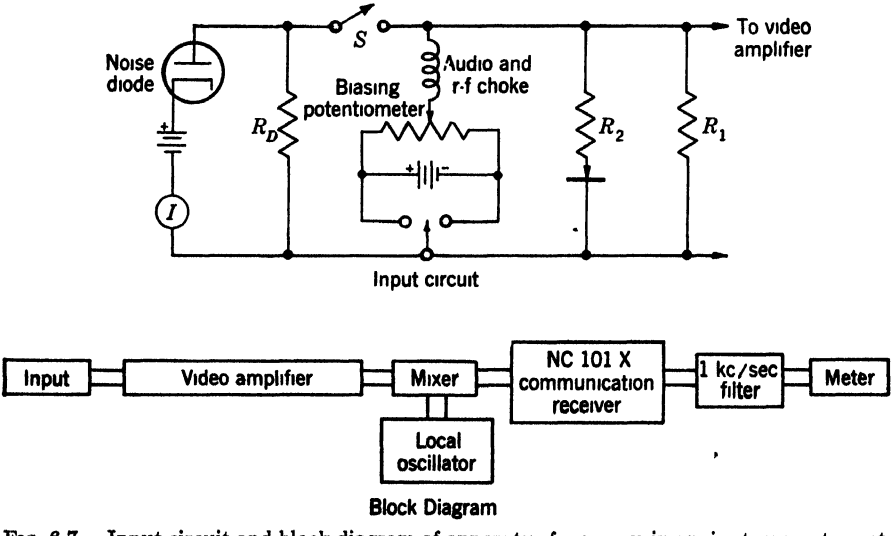

FIG. 6·7.—Input circuit and block diagram of apparatus for measuring noise temperature at low frequencies.

noise diode is a noise-current generator whose mean-square noise current is given by Eq. (1).

[1] P. H. Miller, M. N. Lewis, L. I. Schiff, and W. E. Stephens, "Noise Spectrum of Silicon Rectifiers," NDRC 14-256, Univ. of Penn., Mar. 20, 1944.

It follows from Theorem 1 (Sec. 6·1) that the mean-square voltage applied to the grid of the input tube, with switch S open, is

$$\overline{V_i^2} = 4kT_0\,\Delta f\left(\frac{R_1R_2}{R_1+R_2}\right)^2\left(\frac{t_1}{R_1}+\frac{t}{R_2}\right). \tag{22}$$

When S is closed and the crystal removed, the mean-square input voltage is

$$\overline{V_{iD}^2} = 4kT_0\,\Delta f\left(\frac{R_1R_D}{R_1+R_D}\right)^2\left(\frac{t_1}{R_1}+\frac{eI}{2kT_0}\right). \tag{23}$$

At temperature T_0, t_1 is unity and t_1/R_1 is much smaller than either of the additive terms in Eqs. (22) and (23) and can therefore be neglected to a good approximation.

Let G be the voltage gain of the amplifier. With the crystal removed and S open, the square of the amplifier output voltage is given by

$$V_a^2 = G^2\overline{a^2}\,\Delta f, \tag{24}$$

where $\overline{a^2}$ is the equivalent mean-square input voltage that would represent the noise generated in the amplifier.

The square of the output voltage is then

$$V^2 = G^2(\overline{V_i^2}+\overline{a^2}\,\Delta f) = G^2\,\Delta f\left[\frac{4kT_0R_1^2R_2}{(R_1+R_2)^2}\,t+\overline{a^2}\right], \tag{25}$$

with S open, and

$$V_D^2 = G^2(\overline{V_{iD}^2}+\overline{a^2}\,\Delta f) = G^2\,\Delta f\left[\frac{2eIR_1^2R_D^2}{(R_1+R_D)^2}+\overline{a^2}\right], \tag{26}$$

with S closed.

Combining Eqs. (24), (25), and (26) leads to

$$t = \left(\frac{R_1+R_2}{R_1+R_D}\right)^2\frac{R_D^2}{R_2}\,\frac{eI}{2kT_0}\,\frac{(V^2-V_a^2)}{(V_D^2-V_a^2)}. \tag{27}$$

The value of t is calculated from Eq. (27) from measurements of I and of V_a^2, V^2, and V_D^2 with a square-law output meter. For the data in Figs. 6·8 and 6·9, $R_1 = R_D = 1000$ ohms. If R_2 is assumed to be 1000 ohms also, then Eq. (27) reduces to the expression

$$t = 20I\,\frac{V^2-V_a^2}{V_D^2-V_a^2}, \tag{28}$$

where the diode current I is expressed in milliamperes and the voltages in volts. For values of R_2 ranging from 250 to 4000 ohms, the assumption that $R_2 = 1000$ ohms introduces a maximum error of about 36 per cent. It is estimated that absolute values of t are accurate to about 50 per cent.

The remainder of the apparatus is shown in the block diagram of Fig. 6·7. The video amplifier has a voltage gain of about 10^4 and has a flat response to 1 Mc/sec. The 1000-cps filter has a bandwidth of about 100 cps. A silicon rectifier, especially selected for negligible harmonics, was used for the mixer; the local oscillator was crystal-controlled at a frequency of 7 Mc/sec. A noise frequency f from the input circuit mixes with the local oscillator to give an output frequency of $7 + f$ Mc/sec. If the communications receiver is tuned to $7 + f$ Mc/sec, then the input frequencies of $7 + f$ Mc/sec $\pm$ 1000 cps will give a 1000-cps output voltage and be measured on the meter.

Typical results in the frequency range from 15 to 300 kc/sec are shown in Figs. 6·8 and 6·9. In Fig. 6·8 is plotted the relative noise temperature at a frequency of 30 kc/sec as a function of d-c bias voltage in the back direction. The absolute noise temperatures are indicated for each curve. Curve A shows for comparison the noise from a carbon microphone, and Curves B and C are for silicon rectifiers. From these curves and others measured, it appears that the noise temperature varies roughly as the square of the bias voltage in the back direction, or, over the range for which the back resistance is approximately constant, as the square of the current in the back direction. Similar results are obtained for other frequencies.

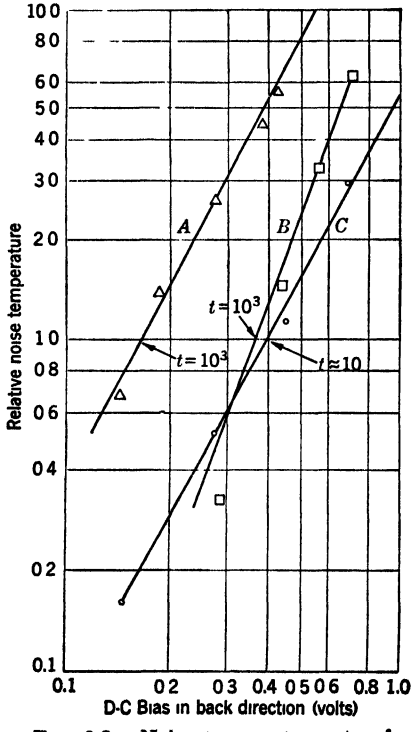

FIG. 6 8.—Noise temperature at a frequency of 30 kc/sec as a function of d-c bias in the back direction. (A) Carbon Microphone, (B) and (C) silicon rectifiers.

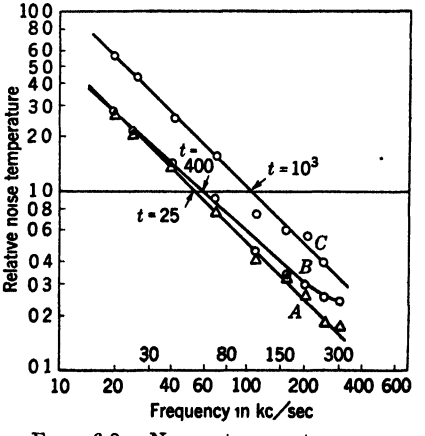

FIG. 6 9.—Noise temperature as a function of frequency for a commercial silicon rectifier. (A) Forward d-c bias of 0 5 ma; (B) excitation by 10-cm r-f power; (C) back d-c bias of 0.01 ma.

In Fig. 6·9, the relative noise temperature of a silicon crystal is plotted as a function of frequency under the following conditions: for Curve A, a d-c forward biasing current of 0.5 ma, Curve B, excitation by 10-cm r-f power at a level which gives a rectified current of 0.5 ma, and Curve C, a back d-c biasing current of 0.01 ma. The approximate absolute value of the noise temperatures are indicated on the figure for each curve. This particular crystal has a noise temperature of 1.6 at 30 Mc/sec.

It is seen from the curve that (a) the noise with back bias is many times larger than with forward bias, and (b) the noise temperature varies inversely as the frequency for both d-c bias and r-f excitation in the frequency range investigated.[1] This relationship is typical of all the crystal rectifiers measured by Miller, as well as for carbon microphones[2] and thin metal resistors[3] measured by others. Miller and Greenblatt[4] have also made measurements in the audio range from 50 to 10,000 cps with an audio amplifier and appropriate filters. In Fig. 6·10 is shown a typical noise temperature-frequency curve for a crystal biased with 0.3 volt in the back direction. It can be seen from the curve that the inverse-frequency law is valid down to frequencies as low as 50 cps. It was also found that in the audio-frequency range the noise temperature with d-c excitation varies as the square of the current in the back direction, in agreement with the results previously given for the frequency range from 15 to 300 kc/sec.

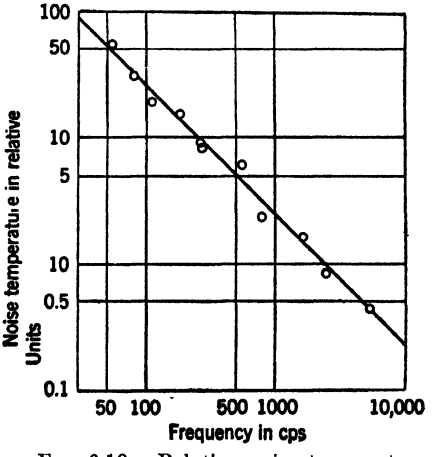

FIG. 6·10.—Relative noise temperature of a silicon crystal as a function of frequency in the audio-frequency range, for a d-c bias of 0.3 volt in the back direction.

The experimental difficulties of measuring noise at audio frequencies make it difficult to assign an absolute value to the noise temperature; for the crystal used in obtaining Fig. 6·10 the value of the noise temperature, calculated for a crystal resistance of 300 ohms, is about 14,000 at a

[1] In a private communication to the authors Miller states that unpublished work in the 300- to 1000-kc/sec range indicates that the inverse relationship is valid at least to 1000 kc/sec.

[2] C. J. Christensen and G. L. Pearson, "Fluctuations in Carbon Contacts," *Bell System Tech. J.*, **15**, 197 (1936).

[3] J. Bernamont, "Fluctuations de Potential d'un Conducteur Metallique," *Ann. phys.*, Series 11, **7**, 71 (1937).

[4] P. H. Miller and M. H. Greenblatt, "Crystal Audio Noise," NDRC 14-387, U. of Penn., Jan. 5, 1945.

frequency of 1000 cps. Since the resistance at a back voltage of 0.3 volt is probably of the order of several thousand ohms, the true noise temperature may be as much as ten times this value. Extrapolation of the curve of Fig. 6·8 to a frequency of 1000 cps gives a noise temperature of about 100,000 with a biasing current of 0.01 ma in the back direction.

Measurements made by the Pennsylvania group on a representative sample of commercial rectifiers indicate that something like 5 per cent of the units tested have a noise temperature at 1000 cps of less than 700, for 10-cm excitation and 0.5 ma rectified current.

Since both Johnson noise and diode noise are independent of frequency, the large increase in noise observed at low frequencies must be the result of some other mechanism, one that could account for the inverse dependence on frequency observed in the range from 50 cps to 0.5 Mc/sec. No adequate hypothesis for such a mechanism has as yet been suggested.

6·4. Dependence on Temperature.—Little is known about the way in which noise temperature varies with the ambient temperature of the rectifier. It was seen in the earlier part of this chapter that the theory of generation of diode noise in the crystal barrier and Johnson noise in the spreading resistance predicts less noise than is in most cases observed with d-c excitation. The mechanism of the generation of the excess noise is as yet unknown.

The only data available are measurements by Lawson, Miller, and Stephens,[1] who used aluminum-doped silicon rectifiers made in the laboratory. With d-c excitation, measurements of the 30-Mc/sec noise temperature were made at room and liquid-air temperatures. A forward-bias voltage was used and adjusted for each crystal to give the same d-c current at the two temperatures; both the dynamic d-c resistance, obtained from the slope of the characteristic curve, and the spreading resistance increase with decreasing temperature, the low-temperature bias therefore being always the larger. The crystals used were unfilled in order to avoid changes arising from contraction of the wax filler at the low temperature. The data listed in Table 6·1 are for those units that survived a cooling cycle with less than 2 per cent change in noise temperature. The observed values of noise temperature, in terms of the standard temperature of 290°K, are listed in Column 7 of Table 6·1. The last column lists the value calculated for diode and Johnson noise alone; use was made of Eq. (9) and the data for spreading resistance and barrier resistance obtained from an analysis of the d-c curve and listed in Columns 5 and 6 of Table 6·1. It can be seen that although the diode and Johnson noise in general decrease with decreasing temperature, the observed noise temperature does not show a significant trend in either direction; it would

[1] A. W. Lawson, P. H. Miller, and W. E. Stephens, "Noise in Silicon Rectifiers at Low Temperatures," NDRC 14-189, U. of Penn., Oct. 1, 1943.

TABLE 6·1.—CALCULATED AND OBSERVED DEPENDENCE OF NOISE TEMPERATU
AMBIENT TEMPERATURE

Crystal	Temperature, °K	Bias voltage, volts	D-c current, ma	Barrier resistance, ohms	Spreading resistance, ohms	t observed	t (calculated for Johnson and diode noise only)
1	300	0.28	0.77	35	30	2.1	0.8
	80	0.69	0.77	70	380	1.7	0.4
2	300	0.32	0.77	60	60	6.8	1.0
	80	1.24	0.77	50	400	6.4	0.3
3	300	0 30	0.77	60	40	9.0	1.0
	80	0.90	0.77	90	300	5.4	0.5
4	300	0.18	0.58	60	40	1.7	0.8
	80	0.75	0.58	160	360	3.2	0.8
5	300	0.21	0.60	50	50	1.6	0.8
	80	0.62	0.58	120	300	1.8	0.6
6	300	0.28	0.59	105	45	2.1	1.2
	80	0 70	0.59	85	380	3.6	0.4
7	300	0.27	0.58	60	80	1.9	0.9
	80	0.84	0.56	0	530	3.0	0.3
8	300	0.20	0.58	45	65	2.3	0.8
	80	0.52	0.58	50	230	2.7	0.3
9	300	0.17	0.58	30	80	2.7	0.9
	80	0.65	0.58	90	290	2.6	0.5
10	300	0.20	0.58	40	70	2.0	0.7
	80	0.58	0.58	40	280	1.5	0.2

therefore appear that the excess noise for d-c excitation does not decrease as the temperature drops. As yet no investigation of this effect has been made with r-f excitation.

MICROWAVE NOISE

6·5. The Crystal as a Microwave Noise Generator.—There is little quantitative information on crystal-noise generation at microwave frequencies. What information is available concerns the use of the crystal rectifier with d-c excitation as a microwave noise source for noise-figure measurements. In this application the available noise power under given

conditions of excitation must be known; this power may be expressed conveniently in terms of the noise temperature at the specified radio frequency. As a noise source, the crystal is placed in a conventional crystal holder such as is used for mixer-crystal testing. The d-c bias is applied at the i-f terminals of the mixer and the r-f noise power is then available at the r-f terminals. The incoherence of the instantaneous noise voltages makes matching the crystal to the r-f line with conventional r-f transforming devices difficult, but crystals that match approximately in the standard holders can be chosen from commercial production. If

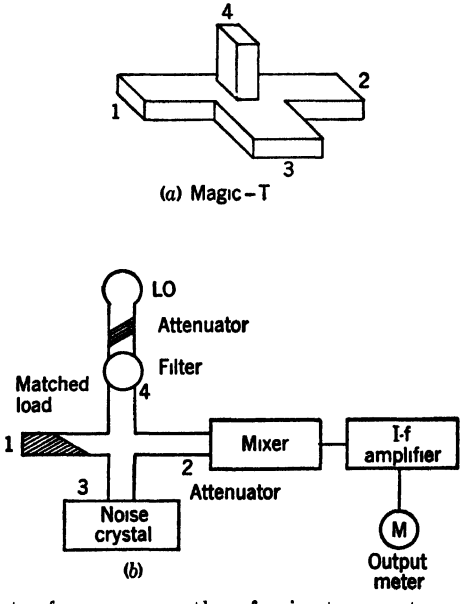

FIG. 6 11.—Apparatus for measuring the r-f noise temperature of a crystal rectifier.

the crystal is mismatched, 5 to 10 db of attenuation can be placed between it and the r-f output terminals whenever it is desired that the noise-generator impedance be the characteristic impedance of the r-f line. The measured noise temperature in the mismatched case, however, will be less than the true value since not all of the available output noise power will be measured.

Like low-frequency noise, the microwave noise power output is much larger with d-c bias in the back direction rather than in the forward direction. With a bias current of 3 to 4 ma in the back direction, the 3-cm noise temperature of a random sample of 1N23 crystals lies in the range from twenty-five to forty times; the r-f noise temperature of 1N26 crystals at 1.25 cm lies in the range of about ten to twenty times. One method of measuring the r-f noise temperature utilizes the "magic T," shown in Fig. 6·11. The properties of this device are discussed in detail in Vol. 16 of the Radiation Laboratory Series; the particular property of

interest in this application is that when Arms 1 and 2 are terminated with matching loads, Arms 3 and 4 are completely decoupled. In the apparatus shown in Fig. 6·11 the local oscillator is connected to Arm 4, and the crystal to be tested to Arm 3; local-oscillator power therefore does not enter the noise-crystal circuit. Half of the output power of the crystal is absorbed in the matched load in Arm 1, but this is compensated for by the fact that both noise sidebands are converted to intermediate frequency by the mixer. The i-f output terminals are connected to an i-f amplifier and output meter. A noise diode, not shown in the figure, may be connected to the input terminals of the i-f amplifier for calibrating the output meter.

The measurement consists essentially in ascertaining two quantities: (1) The noise temperature t_x of the mixer crystal with the noise source replaced by a matched load. This is preferable to turning off the noise source since the r-f impedance of the noise crystal changes markedly with d-c bias. (2) The noise temperature of the mixer crystal t'_x with the noise source on. In the latter case the available noise power at the input terminals of the i-f amplifier will be

$$N_i = kT_0 t_x \Delta f + kT_0 t G_x \Delta f, \tag{29}$$

where t is the r-f noise temperature to be measured and G_x is the conversion gain of the mixer crystal. The first term of the right-hand member is the available noise power from the mixer crystal and the second term is the converted noise power from the noise crystal. The noise temperature t'_x is then

$$t'_x = \frac{N_i}{kT_0 \Delta f} = t_x + tG_x, \tag{30}$$

from which

$$t = \frac{t'_x - t_x}{G_x}. \tag{31}$$

The measurement of t'_x, t_x, and G_x is accomplished by the methods discussed in Chap. 7. The standard noise set described in Chap. 9 can be conveniently used by connecting its mixer to Arm 2 of the magic T of Fig. 6·11.

This method may also be used for the calibration of a noise source employing a reflex velocity-modulated tube, such as that described in Sec. 7·11.

Alternatively, the r-f noise power from the noise crystal may be measured with the microwave radiometer reported by Dicke.[1] This instrument is described in Vol. 24, Chap. 5 of the Radiation Laboratory Series. This method has been used to calibrate 1-cm crystal noise sources for use in noise-figure measurements.

[1] R. H. Dicke, "The Measurement of Thermal Radiation at Microwave Frequencies," RL Report No. 787, Aug. 22, 1945.

CHAPTER 7

LOSS AND NOISE MEASUREMENTS

LOSS MEASUREMENTS

7·1. General Considerations.—The initial sections of this chapter treat the problem of conversion loss measurement. A difficulty arises from the need for apparatus that will satisfy two incompatible requirements. *First*, there is needed for the research laboratory an apparatus that can measure conversion loss under general tuning conditions in order properly to evaluate the capabilities of experimental crystals. The flexibility demanded of such an apparatus entails using a multiplicity of control knobs. They become even more numerous when facilities are provided for noise-temperature measurements to evaluate the over-all performances of the crystals under the same conditions that obtain for conversion-loss measurements.

Second, the apparatus must at the same time be simple enough for manipulation by unskilled personnel in acceptance testing of production units; in other words, it should have a minimum of control knobs. But here another problem is encountered. Since the measurements must be standardized, a uniform method of measurement must be devised that makes it possible for values obtained at one station to be reproduced at another. In addition, measuring conditions should as far as possible simulate those prevailing in system receivers. But since the latter conditions vary so much from one system to another, it is impossible to satisfy this requirement and at the same time achieve uniformity and simplicity. Conversion loss, as we have seen in Chap. 5, depends on the internal impedance of the signal source and not only on the value of this impedance at signal frequency but also on its value at image frequency and, to some extent, at harmonic frequencies. Now it happens that some system receivers are designed to match the mixer to both input (signal) and output (i-f) circuits while others are designed to match the input but to mismatch the output circuit in order to improve the noise figure of the amplifier. The termination at intermediate frequency does not directly affect conversion loss, but, transformed through the mixer, it affects the signal impedance of the mixer and thus the matching signal source impedance on which the conversion loss depends. Again, some systems are provided with broadband TR tubes which do not reflect[1] the

[1] The same result is sometimes achieved in balanced mixers with narrow-band TR tubes by taking advantage of the phase selective properties of the magic T or its coaxial equivalent (see *Microwave Mixers*, Vol. 16, Radiation Laboratory Series).

image frequency; other systems have sharply resonant TR tubes which reflect most of the image frequency power. Furthermore, the latter case shows in practice a distressing lack of uniformity in the phase of the reflected image wave. Finally, some, but not all, system designers have incorporated harmonic filters in the r-f circuit in order to take advantage of harmonic reinforcement. As a result of this lack of uniformity in system design, two crystals of the same conversion loss in one receiver may have different conversion losses in another. Actually such differences are not likely to exceed one or two decibels and are not very serious from the point of view of system efficiency. From the crystal manufacturer's point of view, however, a difference of one decibel between two measuring stations is a serious matter. Failure to meet the conversion-loss test specification limit as tested by the standard apparatus may force the manufacturer to reject a sizable fraction of his crystal production. These rejected units, however, may actually have less conversion loss than some of the accepted units in some particular system receiver.

There does not appear to be any simple way out of this dilemma. The compromise finally adopted involves the measurement for production testing of that particular value of the conversion loss denoted in Chap. 5 by L_0. This value is defined as the conversion loss when the source impedance is the same at both signal and image frequency and is chosen to match the local-oscillator power (rather than the signal power) to the mixer. We saw in Chap. 5 that in practice L_0 differs insignificantly from L_2, the loss when the impedances to signal and image are equal, and this common impedance is adjusted to make the loss a minimum. As explained in Sec. 5·6, L_0 is always greater than the conversion loss minimized independently, both with respect to the signal impedance and with respect to the image impedance. Thus the system designer is assured that a crystal satisfying the test specification limit on L_0 will have a loss less than or equal to this limit in a well-designed receiver with either a sharply or a broadly tuned r-f circuit. The amount by which L_0 exceeds the system receiver loss for the same crystal will vary in practice from zero to about two decibels, the amount depends on the crystal and on the receiver design.

The measurement of L_0 can be made with a simple apparatus that is readily aligned and standardized and gives remarkably uniform results. This method is described fully in Sec. 7·4 and the standardized test set utilizing this method is described in Secs. 9·1, 9·2, and 9·3.

No signal in the ordinary sense is employed in this simplified measurement. Its function is simulated by a variation in local-oscillator power. This variation may take the form of an incremental change in power or of an amplitude modulation of the local-oscillator wave.

Before discussing the simplified method we shall treat other methods

more suited to the research laboratory, namely the conventional heterodyne method (Sec. 7·2) and the impedance method (Sec. 7·3). These have the advantage over the simplified method of greater flexibility, making it possible to study conversion loss as a function of image-tuning and other parameters.

Conversion loss may be determined indirectly by measuring the elements of the mixer admittance matrix. As explained in Chap. 5, this can be accomplished by measuring the local-oscillator mixer admittance y, the direct current i_0, their derivatives with respect to absorbed local-oscillator power P, and the direct voltage V. Although this method is tedious and suitable only to the research laboratory, it is very general, giving not only the conversion loss with arbitrary image-tuning but also the mixer admittances. It also determines the extent of reciprocity failure and therefore the loss when the mixer is used as a modulator rather than as a demodulator. (See Secs. 5·3 to 5·9, for details.)

7·2. The Heterodyne Method.—The most obvious and direct method of loss measurement is the heterodyne method. This method is some-

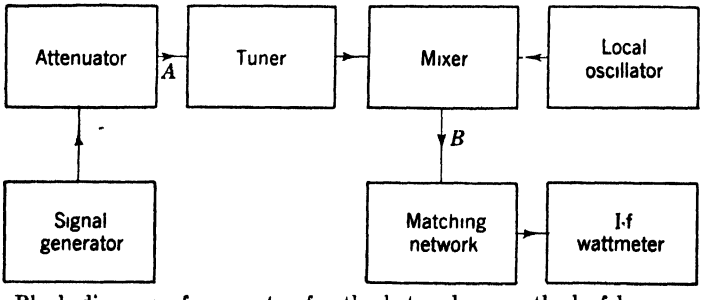

FIG. 7·1.—Block diagram of apparatus for the heterodyne method of loss measurement.

times said to be the only really reliable one since it is the only one that simulates system receiver conditions. Actually, as we have seen in the preceding section, the simulation is at best imperfect because of the variety of conditions one meets in system receivers. We must realize that in any direct measurement of loss the value obtained applies only to the special circumstances of the measurement.

The apparatus used in the heterodyne method of loss measurement, reduced to bare essentials, is shown schematically in Fig. 7·1.

A signal generator feeds signal power to the mixer which converts the power to the "intermediate frequency" by beating with the local oscillator frequency. The converted power is then measured with an i-f wattmeter. Both the available power from the signal generator at A and the available intermediate frequency power at B must be measured, their ratio being the conversion loss. The available signal power is a

property only of the apparatus and not of the crystal to be measured; once it is determined it needs to be remeasured only occasionally as a check on the constancy of the signal generator.

The mixer must be approximately matched to the i-f wattmeter since the *available* i-f power is desired. On the other hand, the available signal power is independent of the tuning at the r-f terminals. This tuning can be adjusted so that the measured loss conforms to the various special cases treated in Chap. 5.

The signal power available at A should be in the range of 1 to 10 μw for best results. A power higher than this leads to trouble from nonlinearity since the mixer is linear only when the signal power is small compared with the local oscillator power ($\approx$ 1 mw). Signal power less than 1 μw is difficult to measure accurately. The power available at A may be measured by breaking the connection at A and feeding the signal into an r-f wattmeter (bolometer). If this is not available as a standard piece of test equipment, it can be easily constructed. A thermistor element such as a Wollaston wire or a Western Electric bead thermistor is used as one arm of a d-c bridge. The bridge is balanced with no r-f power applied to the sensitive element. After application of r-f power, balance is restored by decreasing the direct-current power in the sensitive element. The r-f power is then just equal to the difference in d-c power. Care must be taken to insure a good r-f match to the sensitive element.

The intermediate-frequency wattmeter may be a bolometer of a similar nature. Because a continuous indication is desirable for rapid measurement, it is convenient to calibrate the i-f wattmeter in terms of the off-balance indication of the bridge. For accurate measurement a good match from the mixer to the i-f wattmeter is desirable.

As an alternative to the i-f bolometer, an amplifier followed by a calibrated (preferably square-law) detector may be used as a wattmeter. Such a detector has the advantage of being free from undesirable thermal effects. It is not easy, however, to maintain a constant amplifier gain at usual intermediate frequencies ($\approx$ 30 Mc/sec), although the difficulty is much reduced if the intermediate frequency is in the audio range. But then the problem arises of maintaining the two high-frequency oscillators at a small frequency separation. One solution is to use only one oscillator with audio-frequency amplitude modulation (see Sec. 7·4). The two modulation sidebands then replace the signal. This method has the disadvantage that no discrimination between signal and image is possible, with the result that the loss can be measured only under the condition of equal impedance at signal and image.

The i-f amplifier gain can be maintained at some constant level by making frequent reference measurements of "standard crystals." Maintaining gain by this method is difficult if variable tuned measurements

are wanted, because it means returning to some standard tune each time a check measurement is made.

There is no such difficulty with fixed-tuned measurements, for which the mixer is permanently tuned at input and output at some standard impedance level. This level is determined by finding the mean of the impedance spreads of a large number of crystals of the type to be measured. The circumstance that the actual absorbed i-f power rather than the available power is measured, however, introduces error.

In the heterodyne method one must take care to maintain frequency stability of the oscillators. The usual AFC techniques can be employed to maintain constant frequency difference. If highly resonant r-f circuits are to be used, however, absolute frequency stability should be maintained. A satisfactory method is to use one of the frequency stabilization schemes devised by Pound (see Vol. 16 of the Radiation Laboratory Series).

To study conversion loss as a function of image impedance, a filter must be used in the signal generator lead. A high-Q transmission cavity such as a TR tube might, for example, be inserted at A in Fig. 7·1. The phase of the image wave reflected by the cavity can then be altered by a line stretcher between the mixer and the cavity. Proper account must be taken of the signal transmission loss in the cavity. A difficulty encountered in such an arrangement is that local-oscillator power is also reflected by such a bandpass filter, and large variations in rectified crystal current occur when the phase of the reflected image wave is altered by the line stretcher. A more satisfactory method is to use a band-rejection filter that reflects only the image frequency; a sidearm can be attached at A (Fig. 7·1) and terminated by a single window cavity tuned to the image frequency. The line length between this cavity and the main line is then adjusted to pass an off-resonant frequency through the main line without reflection while the image frequency is reflected. The phase of the reflected image wave can then be varied by adjusting the line length between this sidearm and the mixer. A device of this type was employed by Beringer (see Sec. 7·7) in his investigation of the effect of image impedance on loss and noise temperature.

7·3. Impedance Methods.—It is well known that the transmission loss of a four-terminal linear passive network can be determined from a number of measurements of the impedance at one terminal pair with known loads attached to the opposite pair. Any linear four-terminal device is completely specified by its admittance matrix, that is, by the two self-admittances and the two transfer admittances. If the device is passive the two transfer admittances are equal and give reciprocity. In such a device only three (complex) quantities are needed to define the properties of the device; the loss may be measured by not more than three independ-

ent measurements of impedance. If reciprocity does not hold, however, the four characteristic parameters determining the properties of the network cannot all be determined by impedance measurements. The reason is that impedance measurements determine only the product of the transfer admittances whereas the loss depends on their ratio also.

We have seen (Chap. 5) that a crystal mixer can be regarded as a linear network which, however, is not generally passive. The conversion loss of the mixer cannot therefore be determined in general by impedance measurements alone. Reciprocity failure has so far been observed only in germanium rectifiers, however; the impedance method can still be used, therefore, for silicon crystals, although not with perfect confidence. The impedance method is worth using when possible because the method is easy, quick, and capable of high precision.

If at least weak reciprocity (equality in phase of the transfer admittances) can be generally assumed, and no exception has yet been observed, the impedance method still has some general utility. As noted in Sec. 5·8, if weak reciprocity holds, conversion loss L can be expressed as

$$L = \frac{g_{\alpha\beta}}{g_{\beta\alpha}} L', \tag{1}$$

where $g_{\alpha\beta}/g_{\beta\alpha}$, the so-called "reciprocity factor," is the ratio of the signal–i-f to the i-f–signal transfer admittance. The quantity L', the so-called "impedance loss," depends only on the product of $g_{\alpha\beta}$ and $g_{\beta\alpha}$, not on the ratio, and can therefore be determined by impedance measurements. Thus by measuring the dependence of L' on image-tuning in this way, the variation of L with image impedance can be determined at least to within a constant factor.

An early application of the impedance method to crystal mixers was made by Marcum,[1] who measured r-f impedance with open-circuited and closed-circuited i-f terminals. Dicke[2] also devised a version of the impedance method involving the measurement of i-f impedance with three different r-f loads. Later R. V. Pound modified and improved Marcum's method.

The Dicke Method.—This method has the advantages of being simple, quick, and capable of high precision. Figure 7·2 shows a block diagram of the apparatus used.

An r-f oscillator buffered by a matched attenuator feeds a slotted section of waveguide into which may be inserted a standard susceptance consisting of a metal wire encased in a polystyrene plug. The slotted

[1] J. I. Marcum, "Operation of Crystal Rectifier Units at Microwave Frequencies," Westinghouse Research Report SR-158, Dec. 4, 1942.

[2] R. H. Dicke, "Reciprocity Theorem and Its Application to Measurement of Gain of Micro-Wave Crystal Mixers," RL Report No. 61-18, Apr. 13, 1943.

section is followed by a line stretcher whose purpose is to vary the electrical distance between the susceptance and the crystal. Next comes the crystal mixer, provided with a tuner for matching it to the waveguide. The d-c terminals of the mixer which also serve as the i-f terminals are connected to a 60-cps bridge.

The measuring procedure is as follows:

1. The mixer is matched to the guide and the r-f power is either adjusted to some standard value or adjusted to give the desired rectified current. *The r-f power* is about 1 mw (ordinary local oscillator level).

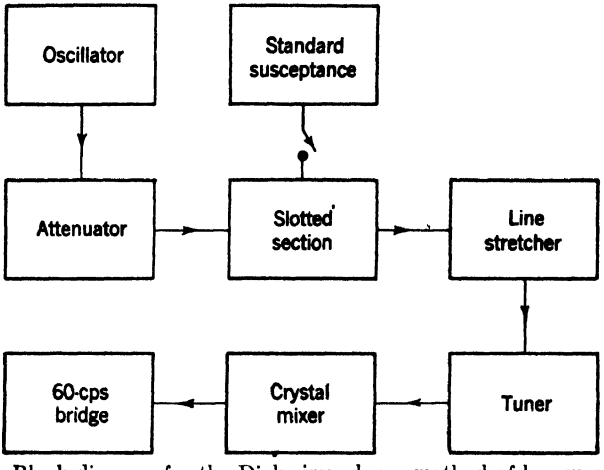

FIG. 7·2.—Block diagram for the Dicke impedance method of loss measurement.

2. The dynamic conductance of the mixer at 60 cps is measured with the bridge. This quantity we denote by g_0.
3. The standard susceptance is placed in the slotted section and the attenuator adjusted to give the original crystal current.
4. The line stretcher is adjusted to maximize the 60-cps conductance. This value g_1 of the conductance is measured.
5. The line stretcher is adjusted to minimize the 60-cps conductance. This minimum conductance g_2 is measured.

The (impedance) conversion loss may then be found from these data, g_0, g_1, and g_2, together with the value ρ of the standing-wave voltage ratio introduced in the guide by the standard susceptance.

In particular the value of L_0', the impedance conversion loss when image and signal are terminated alike and the mixer is matched at local-oscillator level, is given by

$$L_0' = 2\frac{\rho - 1}{\rho + 1}\frac{g_0(g_1 - g_2)}{(g_1 - g_0)(g_0 - g_2)}. \tag{2}$$

Equation (2) will be derived now, and it will be shown how the conversion loss under other conditions of tuning may be determined from the same data.

Equation (5·64) gives the i-f conductance g_β of the mixer when the r-f load admittance common to signal and image is a real conductance g_a. If the r-f load admittance is not purely real, the i-f admittance remains real provided the r-f admittance is the same at signal and image. Using an analysis similar to that employed in deriving Eq. (5·64) we find for g_β, in this more general case,

$$g_\beta = g_{\beta\beta} - \frac{2g_{\alpha\beta}g_{\beta\alpha}(g_{\alpha\alpha} - g_{\alpha\gamma} + g_a)}{(g_{\alpha\alpha} + g_a)^2 + b_a^2 - g_{\alpha\gamma}^2}, \tag{3}$$

where

$$y_a = g_a + jb_a \tag{4}$$

is the r-f load admittance. Equation (3) is easily seen to reduce to Eq. (5·64) if we put $b_a = 0$. Now if the standard susceptance is inserted and the line is stretched between the susceptance and the crystal, the r-f load admittance y_a will traverse a circle in the admittance plane. This circle has its center on the real axis which it intersects at $g_a = \rho g$ and $g_a = \frac{1}{\rho} g$, where g is the guide conductance and ρ the standing-wave voltage ratio introduced by inserting the susceptance (see Fig. 7·3). The equation of the circle is

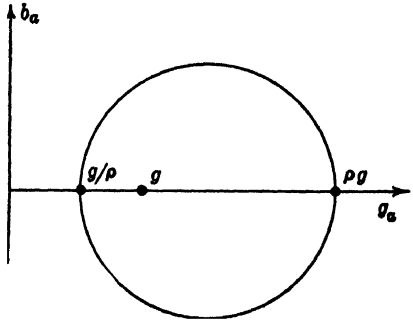

FIG. 7·3.—Diagram showing circle traversed by the r-f load admittance as the line is stretched: g = line conductance; ρ = standing-wave ratio.

$$\left[g_a - \frac{1}{2}\left(\rho + \frac{1}{\rho}\right) g\right]^2 + b_a^2 = \frac{1}{4}\left(\rho - \frac{1}{\rho}\right)^2 g^2. \tag{5}$$

If Eq. (5) is solved for b_a and substituted in Eq. (3), we see that the resulting expression for g_β can be expressed as a fraction containing g_a linearly in both numerator and denominator. Consequently g_β as a function of g_a has no stationary values, and the greatest and least values of g_β occur at the extreme values of g_a, that is, at $g_a = \rho g$ and $g_a = g/\rho$. Furthermore, $b_a = 0$ at both these points. Thus we obtain from Eq. (3) for g_1 and g_2 respectively the maximum and minimum values of g_β as the line is stretched,

$$g_1 = g_{\beta\beta} - \frac{2g_{\alpha\beta}g_{\beta\alpha}}{g_{\alpha\alpha} + g_{\alpha\gamma} + \rho g}, \tag{6}$$

$$g_2 = g_{\beta\beta} - \frac{2g_{\alpha\beta}g_{\beta\alpha}}{g_{\alpha\alpha} + g_{\alpha\gamma} + g/\rho}. \tag{7}$$

The i-f conductance g_0, when the standard susceptance is removed, is found by replacing ρ by unity in either of these results,

$$g_0 = g_{\beta\beta} - \frac{2g_{\alpha\beta}g_{\beta\alpha}}{g_{\alpha\alpha} + g_{\alpha\gamma} + g}. \tag{8}$$

Because, under this condition, the mixer is matched to the oscillator conductance g, we have from Eq. (5·26),

$$g = g_{\alpha\alpha} - g_{\alpha\gamma}. \tag{9}$$

Equations (6) to (9) inclusive may now be solved for $g_{\alpha\alpha}$, $g_{\beta\beta}$, and $g_{\alpha\beta}g_{\beta\alpha}$ with the results

$$g_{\alpha\alpha} = \frac{1}{2}(\rho - 1)\frac{1 + c}{\rho - c}g, \tag{10}$$

$$g_{\beta\beta} = g_0 + (g_1 - g_2)\frac{c(\rho + 1)}{(\rho - c)(1 + c)}, \tag{11}$$

$$g_{\alpha\beta}g_{\beta\alpha} = (g_1 - g_2)\frac{c(\rho^2 - 1)}{2(\rho - c)^2}g, \tag{12}$$

$$c \equiv \frac{g_1 - g_0}{g_0 - g_2}. \tag{13}$$

Equations (9) to (13) inclusive give the elements of the admittance matrix of the mixer in terms of the guide conductance g, the standing-wave ratio ρ, and simple impedance measurements at the d-c terminals of the mixer. Only the product $g_{\alpha\beta}g_{\beta\alpha}$ is determined in this way. As mentioned above, the ratio $g_{\alpha\beta}/g_{\beta\alpha}$—the reciprocity factor—cannot be found by impedance measurements. Substituting these results into our formula (Eq. (5·77)) for the conversion loss L_0 we obtain

$$L_0 = 2\frac{g_{\alpha\beta}}{g_{\beta\alpha}}\frac{\rho - 1}{\rho + 1}\frac{g_0(g_1 - g_2)}{(g_1 - g_0)(g_0 - g_2)}, \tag{14}$$

which with Eq. (1) gives Eq. (2) for the impedance loss, L_0'.

The values obtained for $g_{\alpha\alpha}$, etc., may now be substituted into Eqs. (5·141) and (5·142) to give the losses under various conditions of image tuning.

The great advantage of impedance methods is that no difficult r-f power measurements are required, whereas all other methods involve measurement of r-f power. This suggests that the impedance technique may be used to measure r-f power instead of loss. For example Eq. (51), which is derived in the next section, gives L_0 in terms of the r-f power P. Eliminating L_0 between Eqs. (14) and (51), a result is obtained for P in terms of the reciprocity factor ρ and of quantities all determined by simple low-frequency measurements, capable of high precision. Of course, full reciprocity ($g_{\alpha\beta} = g_{\beta\alpha}$) must be assumed in such measurements, but this

assumption appears to hold for silicon crystals. This method of r-f power measurement, suggested by Dicke, has not yet been exploited but appears to have some value. To the authors' knowledge all other absolute power measurements are calorimetric, that is, they involve the transformation of r-f power into heat.

A special case of interest arises when the standing-wave voltage ratio ρ becomes very large. In this case g_1 and g_2 are the i-f conductances when the r-f terminals are respectively short-circuited and open-circuited. From Eqs. (6) and (7) we find for $\rho = \infty$,

$$\frac{g_2}{g_1} = 1 - \frac{2g_{\alpha\beta}g_{\beta\alpha}}{g_{\beta\beta}(g_{\alpha\alpha} + g_{\alpha\gamma})}, \tag{15}$$

Now in Sec. 5·7 it was shown that the loss L_2 (loss minimized with respect to the r-f load impedance, which is the same at signal and image) is given by Eq. (5·72)

$$L_2 = 2\,\frac{g_{\alpha\beta}}{g_{\beta\alpha}}\,\frac{1 + \sqrt{1 - \eta_2}}{1 - \sqrt{1 - \eta_2}}, \tag{16}$$

where η_2 is given by Eq. (5·73). Comparing this expression for η_2 with Eq. (15) we see that

$$L_2 = 2\,\frac{g_{\alpha\beta}}{g_{\alpha\beta}}\,\frac{1 + \sqrt{g_2/g_1}}{1 - \sqrt{g_2/g_1}}. \tag{17}$$

Thus the (impedance) loss L_2' may be found from only two measurements of i-f conductance, the third measurement (g_0) being unnecessary. In practice the oscillator power in this method is introduced into the guide by a loosely coupled probe, and the impedance is changed from a short circuit to an open circuit by the motion of a plunger terminating the waveguide. This method was suggested by F. B. Llewellyn and has been used to some extent at the Bell Telephone Laboratories. It has the disadvantage of requiring an oscillator capable of putting out a large amount of power, since the oscillator must be loosely coupled to the guide. Also it is difficult to keep the absorbed local-oscillator power constant as the plunger is moved. Furthermore, the method determines only L_2 and gives no information about the loss under more general conditions of tuning.

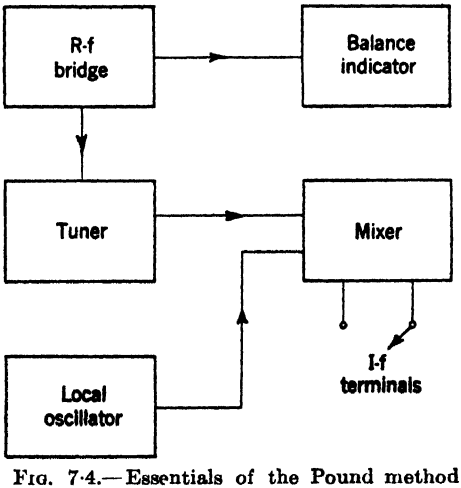

FIG. 7·4.—Essentials of the Pound method of loss measurement.

The Pound Method.—The impedance conversion loss may equally well be determined from r-f impedance data. The essentials of the Pound method are illustrated in Fig. 7·4. An r-f bridge is connected to the signal terminals of the mixer. With the i-f terminals short-circuited, the tuner T is adjusted to balance the bridge. This operation is equivalent to matching the mixer to the bridge circuit with the result that the mixer does not reflect signal power. The i-f terminals are then open-

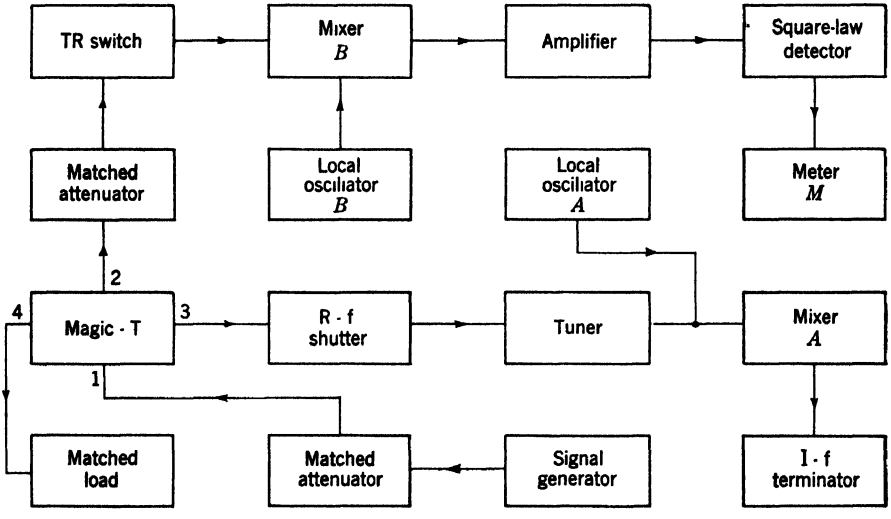

FIG. 7·5*a*.—Block diagram of apparatus used in the Pound method of loss measurement.

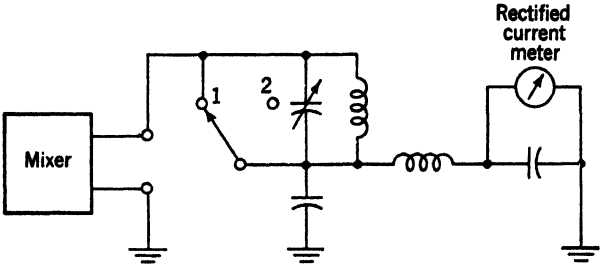

FIG. 7·5*b*.—Diagram of the i-f circuit in the Pound method of loss measurement.

circuited and the off-balance reading of the balance indicator is recorded. The (impedance) conversion loss is then directly obtained from this one datum.

A more detailed diagram of Pound's apparatus is shown in Fig. 7·5. The test mixer is mixer A and the r-f bridge is the magic T with its associated circuits in Arms 1, 2, and 4. There is no direct cross coupling between opposite arms of the magic T. Thus if Arms 3 and 4 are terminated in matched loads, no power from the signal generator will go up Arm 2, the indicating arm of the bridge, and the balance-indicating

meter M will read zero. If Arm 3 is mismatched, half the signal power reflected by Arm 3 goes up Arm 2 and the other half is absorbed in Arm 1. The reading of meter M is therefore proportional to the signal power reflected by Arm 3.

The crystal to be tested is placed in mixer A and the procedure is as follows:

1. The power of the local oscillator A is adjusted to give the desired crystal current.
2. The i-f terminals are short-circuited (Switch Position 1 in Fig. 7·5*b*) and the tuner T is adjusted until meter M reads zero. This matches the signal to the mixer.
3. The i-f termination is switched to a parallel tuned circuit (Switch Position 2 in Fig. 7·5*b*) and the circuit is tuned with the variable condenser for maximum reflected signal power as indicated by meter M. As will be shown later, this operation is equivalent to open-circuiting the i-f terminals.
4. The conversion loss is then given by the formula

$$L_m = \frac{g_{\alpha\beta}}{g_{\beta\alpha}} \frac{\sqrt{\rho} + 1}{\sqrt{\rho} - 1}. \tag{18}$$

The loss given by Eq. (18) is that obtained when the internal impedance of the signal source is adjusted to make the loss a minimum. The image termination is held fixed in making this adjustment. In Eq. (18) $g_{\alpha\beta}/g_{\beta\alpha}$ is the usual reciprocity factor (not determined by the measurement) and ρ is the standing-wave ratio in Arm 3. The value of ρ is found directly from the reading of meter M. This reading, d, is proportional to the reflected signal power in Arm 3 and thus to the square of the magnitude of the reflection coefficient, $|\gamma|^2$, which is the ratio of reflected to incident power. The reading d_0, corresponding to complete reflection, is found by short-circuiting Line 3 with the r-f shutter. Thus,

$$\frac{d}{d_0} = |\gamma|^2 = \left(\frac{\rho - 1}{\rho + 1}\right)^2. \tag{19}$$

By adjusting the gain of the amplifier, d_0 is conveniently made full scale.

The TR tube in Arm 2 is not essential, but it acts as a bandpass filter, passing the signal frequency and reflecting other frequencies. Thus no power from local oscillator A is admitted to mixer B, and conversely no power from oscillator B is admitted to mixer A. In practice it is convenient to tune oscillators A and B on opposite sides of the signal and to control their frequencies relative to the signal with conventional AFC circuits.

Formula (18) will now be derived. In Chap. 5 it was shown that the

properties of the mixer network are determined by the equations [Eq. (5·91)]

$$\left.\begin{aligned} i_\alpha &= Y_{\alpha\alpha}e_\alpha + Y_{\alpha\beta}e_\beta \\ i_\beta &= Y_{\beta\alpha}e_\alpha + Y_{\beta\beta}e_\beta \end{aligned}\right\}. \tag{20}$$

The subscripts α and β denote, respectively, the signal and intermediate frequencies, i_α and i_β are the complex currents and e_α and e_β the complex voltages at the mixer terminals. The coefficients $Y_{\alpha\alpha}$, etc. depend on the image-frequency termination according to Eqs. (5·92) to (5·95).

In the present case the i-f termination is purely reactive so that

$$i_\beta = -jBe_\beta, \tag{21}$$

where B is the susceptance loading the i-f terminals.

The signal admittance,

$$Y_\alpha = \frac{i_\alpha}{e_\alpha}, \tag{21a}$$

of the mixer is found by substituting Eq. (21) in Eq. (20). We obtain

$$Y_\alpha = Y_{\alpha\alpha} - \frac{Y_{\alpha\beta}Y_{\beta\alpha}}{Y_{\beta\beta} + jB}. \tag{21b}$$

Under the conditions of measurement, the signal is matched to the mixer when the i-f terminals are short-circuited. That is, Y_α is equal to the conductance g_0 of the waveguide or transmission line when $B = \infty$. Thus

$$Y_{\alpha\alpha} = g_0 = G_{\alpha\alpha}, \tag{21c}$$

where $G_{\alpha\alpha}$ is the real part of $Y_{\alpha\alpha}$.

For some general value of B we have from Eqs. (21b) and (21c),

$$\frac{Y_\alpha}{g_0} = 1 - \frac{Y_{\alpha\beta}Y_{\beta\alpha}}{G_{\alpha\alpha}(Y_{\beta\beta} + jB)}, \tag{22}$$

and the magnitude of the reflection coefficient in line 3 is

$$|\gamma| = \left|\frac{\dfrac{Y_\alpha}{g_0} - 1}{\dfrac{Y_\alpha}{g_0} + 1}\right|, \tag{23}$$

or

$$|\gamma|^2 = \frac{|Y_{\alpha\beta}Y_{\beta\alpha}|^2}{[2G_{\alpha\alpha}G_{\beta\beta} - \mathrm{Re}(Y_{\alpha\beta}Y_{\beta\alpha})]^2 + [2G_{\alpha\alpha}(B + B_{\beta\beta}) - \mathrm{Im}(Y_{\alpha\beta}Y_{\beta\alpha})]^2}. \tag{24}$$

Clearly $|\gamma|^2$ as a function of B is a maximum when

$$B = \frac{\mathrm{Im}(Y_{\alpha\beta}Y_{\beta\alpha})}{2G_{\alpha\alpha}} - B_{\beta\beta}, \tag{25}$$

and the maximum value of $|\gamma|$ is

$$|\gamma|_m = \frac{|Y_{\alpha\beta}Y_{\beta\alpha}|}{2G_{\alpha\alpha}G_{\beta\beta} - \mathrm{Re}(Y_{\alpha\beta}Y_{\beta\alpha})}. \tag{26}$$

The standing-wave ratio at maximum reflection is

$$\rho = \frac{1 + |\gamma|_m}{1 - |\gamma|_m}. \tag{27}$$

Substituting Eq. (26) in Eq. (27) we obtain

$$\rho = \frac{1}{1 - \epsilon}, \tag{28}$$

where

$$\epsilon = \frac{2|Y_{\alpha\beta}Y_{\beta\alpha}|}{2G_{\alpha\alpha}G_{\beta\beta} + |Y_{\alpha\beta}Y_{\beta\alpha}| - \mathrm{Re}(Y_{\alpha\beta}Y_{\beta\alpha})}. \tag{29}$$

Now in Chap. 5 it was shown that the conversion loss L_m (signal generator impedance adjusted to give minimum-loss, arbitrary-image termination) is given by [see Eq. (5·109)]

$$L_m = \frac{|Y_{\alpha\beta}|}{|Y_{\beta\alpha}|}\frac{1 + \sqrt{1 - \epsilon}}{1 - \sqrt{1 - \epsilon}},$$

where ϵ is the same as in Eq. (29). Thus,

$$L_m = \frac{|Y_{\alpha\beta}|}{|Y_{\beta\alpha}|}\frac{\sqrt{\rho} + 1}{\sqrt{\rho} - 1}. \tag{30}$$

In Sec. 5·8 it was shown that the factor $|Y_{\alpha\beta}|/|Y_{\beta\alpha}|$ is independent of the image termination if, and only if, weak reciprocity holds. Assuming weak reciprocity we obtain, using Eq. (5·116),

$$L_m = \frac{g_{\alpha\beta}}{g_{\beta\alpha}}\frac{\sqrt{\rho} + 1}{\sqrt{\rho} - 1}, \tag{31}$$

which is the desired result.

Comparing Eq. (25) with Eq. (5·112) for the characteristic i-f admittance of the mixer, we see that the required value of B for maximum signal reflection is just that needed to tune out the i-f susceptance of the mixer. If B is now considered as part of the mixer, with the result that the i-f admittance is real, the tuning to give maximum signal reflection is then equivalent to open-circuiting the i-f terminals.

This method of measuring loss has the great advantage of requiring only one meter reading. Only the fraction of reflected power is required, the result being independent of phase. It is reasonably quick and is capable of high precision. Figure 7·6 shows a plot of the impedance loss

$L'_m = \dfrac{\sqrt{\rho}+1}{\sqrt{\rho}-1}$ as a function of the reading of Meter 2. The abscissa is the ratio of the meter reading with a crystal reflecting the signal to the reading when complete reflection is produced (by closing the r-f shutter). This ratio is equal to the fraction of reflected power [see Eq. (19)].

It should be noted that L_m depends on image termination. The image termination that applies to this measurement is of course the particular one in the experimental apparatus. With the arrangement illustrated in Fig. 7·4, the image is matched, that is, it is not reflected back to the crystal. The loss L_m can be studied as a function of image impedance, by using a filter circuit in Arm 3 (see Fig. 7·5*a*). This filter always transmits the signal without reflection but may reflect the image. The phase of the image reflection can then be varied by inserting a line stretcher between the filter and the mixer. As an example, a bandpass filter such as a TR tube may be inserted in Arm 3. By this technique, Pound found that the largest and smallest values of L_m as a function of the electrical distance between this cavity and the mixer differed by about 1.5 to 2.0 db for a number of crystals tested.

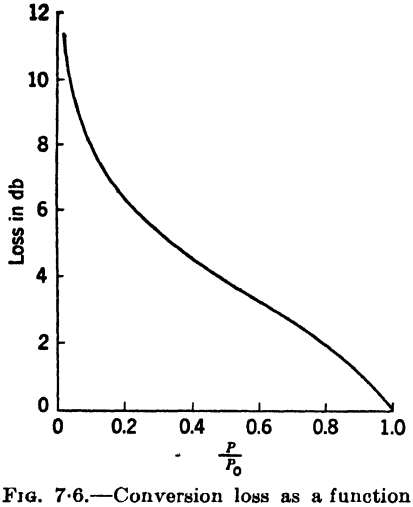

FIG. 7·6.—Conversion loss as a function of the fraction of reflected power.

Before leaving the subject of loss determination by impedance measurements it would be well to discuss how far results of this type of measurement agree with corresponding results obtained using more conventional methods. Provided care is taken to compare losses of the same definition, there is excellent agreement in the case of all silicon crystals and of some germanium crystals, but for other germanium crystals large discrepancies are found. Fifty silicon and germanium crystals were measured for L_0 using both the Dicke impedance method and the Roberts amplitude-modulation method. In no case was a discrepancy larger than 0.2 db found for the silicon units, but some of the germanium units indicated impedance losses as much as 3 db less than the corresponding directly measured values. It is reasonable to attribute this discrepancy to the reciprocity factor $g_{\alpha\beta}/g_{\beta\alpha}$ since other measurements have shown this factor often to be greater than unity in the case of germanium. In no case was the impedance loss found to be greater than the directly measured loss.

7·4. The Incremental and Amplitude-modulation Methods. *The D-c Incremental Method.*—We now come to the methods of loss measurement found to be most satisfactory in production testing. As explained in Sec. 7·1, the quantity measured is L_0. By Eq. (5·79), L_0 is given by

$$L_0 = -\frac{2\dfrac{\partial I}{\partial V}}{P\left(\dfrac{\partial I}{\partial P}\right)^2}, \tag{32}$$

where I is the direct (rectified) current, V the direct (bias) voltage and P the absorbed local-oscillator power. These quantities are all easily measurable. The partial derivatives are not easy to measure directly since it is difficult to maintain one variable (V or P) constant while the

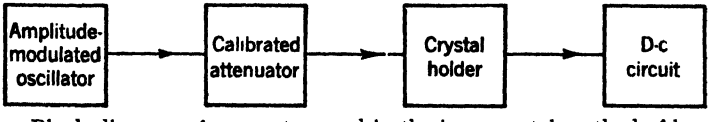

FIG. 7·7a.—Block diagram of apparatus used in the incremental method of loss measurement.

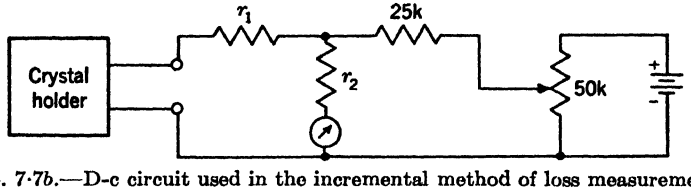

FIG. 7·7b.—D-c circuit used in the incremental method of loss measurement.

other is varied. The equation for L_0 can be so transformed, however, as to make measurement of the partial derivatives unnecessary in order to obtain a fair approximation to L_0.

A schematic diagram of the circuit used in the measurement of L_0 is shown in Fig. 7·7. The crystal is loaded by the resistance $r_1 + r_2$, which is usually adjusted to about 400 ohms. The current supplied by the battery balances out the crystal current at some standard r-f power level P and makes the current in the microammeter zero. The resistance r_1 develops a d-c bias voltage V across the rectifier at the r-f power level P. The r-f power is then increased by dP, producing a change in rectified current which is indicated by the meter. The change in bias voltage dV is then the product of the resistance,

$$\frac{1}{g_b} = r_1 + r_2, \tag{33}$$

by the change in current, or

$$dV = -\frac{1}{g_b}\,dI. \tag{34}$$

Now any change in direct current dI is given by

$$dI = \frac{\partial I}{\partial V}\,dV + \frac{\partial I}{\partial P}\,dP. \tag{35}$$

Eliminating dV and solving for $\partial I/\partial P$ gives

$$\frac{\partial I}{\partial P} = \frac{g_b + \dfrac{\partial I}{\partial V}}{g_b}\frac{dI}{dP}. \tag{36}$$

Substituting this in Eq. (32) we obtain

$$L_0 = \frac{g_b}{2P_0\left(\dfrac{dI}{dP}\right)^2}\cdot\frac{4g_b\dfrac{\partial I}{\partial V}}{\left(g_b + \dfrac{\partial I}{\partial V}\right)^2}. \tag{37}$$

In Eq. (37) we may take P_0 to be the average power, $P + \frac{1}{2}dP$. Now $\partial I/\partial V$, by Eq. (5·84b), is the i-f conductance of the converter under the conditions of measurement. If g_b is equal to $\partial I/\partial V$, the factor

$$\frac{4g_b\dfrac{\partial I}{\partial V}}{\left(g_b + \dfrac{\partial I}{\partial V}\right)^2} \tag{38}$$

is unity and the loss is given by

$$L_0 = \frac{g_b}{2P_0\left(\dfrac{dI}{dP}\right)^2}. \tag{39}$$

This method is ordinarily used in fixed-tuned measurements and g_b is chosen to be equal to the mean i-f conductance of the type of crystal to be measured. For any one crystal the Factor (38) is generally less than unity but the error involved in using Eq. (39) instead of Eq. (37) is less than $\frac{1}{2}$ db if

$$\frac{1}{2}g_b < \frac{\partial I}{\partial V} < 2g_b.$$

For routine measurements the Factor (38) is usually dropped, but it must be included in accurate work.

The loss is obtained from Eq. (39) by measurement of g_b, P_0, dP, and dI. The change in current dI is directly indicated on the microammeter and g_b is accurately measured with a bridge. The r-f power P_0 is measured with a bolometer and is a property of the apparatus only. It can be maintained constant by reference to standard crystals. The change in power dP is produced by a change in attenuation between the crystal

and the r-f oscillator. The attenuator must be carefully calibrated for this purpose.

The d-c incremental method outlined here is not well adapted to rapid production testing. It is used rather to establish an absolute calibration of standard crystals. These crystals are then used to calibrate the actual production test apparatus, which is of the amplitude-modulation type.

The Amplitude-modulation Method.—In the amplitude-modulation method an r-f oscillator is matched to the mixer at local-oscillator level ($\approx$ 1 mw). The output of the oscillator is then modulated in amplitude at some low audio frequency β. The modulation envelope is detected by the crystal which develops a voltage at the frequency β across an output load. The conversion loss L_0 may then be found from this voltage if the percentage modulation and the power of the oscillator are known. This method was developed independently by Smith[1] and Roberts.[2] The particular form now in general use is that of Roberts and is the one described here.

The amplitude-modulation method is similar to the d-c incremental method in that no signal power is used, its function being exercised by a variation in power of the local oscillator. It is well known, however, that a sinusoidal amplitude-modulated wave is equivalent to a sinusoidal carrier plus two sinusoidal symmetrically located sidebands. The carrier in our present case can be conceived as the local-oscillator wave, and the two sidebands as two signals, each separated in frequency from the local oscillator by the modulation frequency β, which plays the role of intermediate frequency. Each signal sideband is the image of the other.

The problem of deducing the relation between L_0 and observable quantities in this measurement can be simply handled. But to make the result unambiguous, especially with reference to the precise definition of the modulation coefficient and to questions of coherence of the beat products from the two sidebands, we must go back to the fundamental mixer equations [Eq. (5·61)], reproduced here.

$$\left.\begin{aligned} i_\alpha &= g_{\alpha\alpha}e_\alpha + g_{\alpha\beta}e_\beta + g_{\alpha\gamma}e_\gamma^* \\ i_\beta &= g_{\beta\alpha}e_\alpha + g_{\beta\beta}e_\beta + g_{\beta\alpha}e_\gamma^* \\ i_\gamma^* &= g_{\alpha\gamma}e_\alpha + g_{\alpha\beta}e_\beta + g_{\alpha\alpha}e_\gamma^*. \end{aligned}\right\} \tag{40}$$

Here the subscripts α, β, and γ denote, respectively, the signal frequency, intermediate frequency, and image frequency; i_α, etc. are the complex current amplitudes; e_α, etc. the complex voltage amplitudes at the terminals of the mixer; $g_{\alpha\alpha}$, etc. are the elements of the admittance matrix

[1] R. N. Smith, "Measurement of Conversion Gain with a Modulated Oscillator," NDRC 14-144, Purdue Univ., Apr. 20, 1943.

[2] S. Roberts, RL Reports No. 53-23, July 3, 1943, and No. 53-28, Aug. 3, 1943.

of the mixer. In our present case both signal and image waves are incident on the crystal and there is perfect symmetry between them, giving

$$\left.\begin{aligned} i_\alpha &= i_\gamma^* \\ e_\alpha &= e_\gamma^*. \end{aligned}\right\} \tag{41}$$

and

The fact that the signal current and voltage are complex conjugates of the corresponding image quantities may be seen at once if we consider the vector representation of an amplitude-modulated wave. The voltage (or current) of the carrier is a constant (real) vector and the two sidebands are vectors of equal magnitude rotating with respect to the carrier in opposite directions. The frequency of the rotation equals the modulation frequency β (see Fig. 7·8).

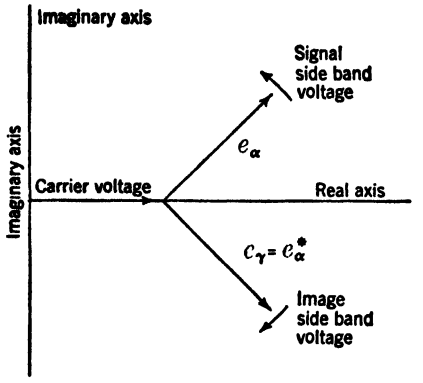

FIG. 7·8.—Vector representation of an amplitude-modulated wave.

The choice of time zero required to make the carrier voltage real also gives a real admittance matrix, provided weak reciprocity holds. Thus Eq. (40) reduces to

$$\left.\begin{aligned} i_\alpha &= (g_{\alpha\alpha} + g_{\alpha\gamma})e_\alpha + g_{\alpha\beta}e_\beta \\ i_\beta &= 2g_{\beta\alpha}e_\alpha + g_{\beta\beta}e_\beta. \end{aligned}\right\} \tag{42}$$

The "intermediate frequency" is now the modulation frequency β, and since the output of the mixer is loaded by a conductance g_b, we have

$$i_\beta = -g_b e_\beta. \tag{43}$$

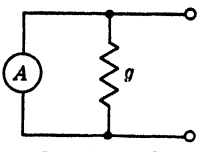

FIG. 7·9.—Oscillator represented as a constant current generator (A) with internal conductance (g).

The oscillator is represented by Norton's theorem as a constant current generator with an internal conductance g as illustrated in Fig. 7·9.

The impedance offered by the mixer to the carrier must be distinguished from that offered to its sidebands. Under the conditions of measurement the carrier (which replaces the local oscillator) is matched to the mixer. The internal conductance g of the oscillator is thus given by Eq. (5·26);

$$g = g_{\alpha\alpha} - g_{\alpha\gamma}. \tag{44}$$

The conductance offered by the crystal to the sidebands will not, however, be g because of the fact that the sidebands are at a low level with

respect to the carrier. The sidebands will not, therefore, be matched to the mixer.

If A_α is the magnitude of the current generated at the sideband frequency α, and A_0 is the corresponding quantity for carrier, we have the usual expression for amplitude modulation

$$A_\alpha = \tfrac{1}{2} m A_0, \tag{45}$$

where m, defined by this expression, is the so-called "modulation coefficient" of the oscillator. The current A_α is equal to the current i_α in the mixer plus the current ge_α in the conductance g, or

$$A_\alpha = i_\alpha + ge_\alpha. \tag{46}$$

Eliminating A_α, i_α, e_α, $g_{\alpha\gamma}$, and i_β from Eqs. (42) to (46), inclusive, we obtain

$$\frac{1}{2}\, mA_0 = -e_\beta \left(\frac{g_b g_{\alpha\alpha} + g_{\alpha\alpha} g_{\beta\beta} - g_{\alpha\beta} g_{\beta\alpha}}{g_{\beta\alpha}} \right). \tag{47}$$

The i-f load conductance g_b is normally chosen to equal the mean i-f conductance, g_β, of a large group of the type of crystal to be measured. For any particular crystal, however, g_b will differ in general from g_β. Let us put

$$g_b = n g_\beta, \tag{48}$$

where by Eq. (5·84a)

$$g_\beta = \frac{g_{\alpha\alpha} g_{\beta\beta} - g_{\alpha\beta} g_{\beta\alpha}}{g_{\alpha\alpha}} \tag{49}$$

is the i-f conductance of the mixer when the mixer is matched to the local oscillator as in the present case.

Substituting Eqs. (48) and (49) in Eq. (47) we obtain

$$\frac{m^2 |A_0|^2}{4} = g g_b |e_\beta|^2 \frac{(1+n)^2}{4n} \left[\frac{4 g_{\alpha\alpha} (g_{\alpha\alpha} g_{\beta\beta} - g_{\alpha\beta} g_{\beta\alpha})}{g g_{\beta\alpha}^2} \right]. \tag{50}$$

Comparing Eq. (50) with Eq. (5·77) we see that the expression in the square brackets on the right of Eq. (50) is just L_0. Solving for this we get

$$L_0 = \frac{4n}{(1+n)^2} \frac{m^2 P}{g_b E_\beta^2}, \tag{51}$$

where we have put $P \equiv |A_0|^2/8g$ as the available power from the carrier and $E_\beta \equiv |e_\beta|/\sqrt{2}$ as the rms modulation voltage across the load g_b.

It must be noted that m is the modulation coefficient referred to the available power of the oscillator and not to the power actually sent into the crystal at the sideband frequencies.[1]

[1] See L. C. Peterson and F. B. Llewellyn, *Proc. I.R.E.*, **33**, 458 (1945).

The expression $4n/(1 + n)^2$ appearing on the right side of Eq. (51) is identical to the Factor (38) appearing in the expression for L_0 in the incremental method. It is replaced by unity in production testing.

The amplitude-modulation method may be used either as an absolute or as a relative method.

As a relative method standard crystals (standardized by the incremental method) are used to establish the basis of measurement. Since m^2, P, and g_b are constants of the apparatus they need not be measured directly. The power P is adjusted to give the correct rectified current of the standard crystals. The modulation in production testing is usually provided by applying a 60-cycle voltage to the grid of the oscillator. This voltage is then so adjusted that the correct readings for the standard crystals are obtained on the output a-c voltmeter. The dial of this voltmeter is usually calibrated in decibels so that the loss L_0 can be directly read from this meter.

If the amplitude-modulation method is used as an absolute method one must measure g_b, P, and m^2: It is easy to measure g_b with a bridge; P is determined with an r-f bolometer employing a thermally sensitive element such as a Wollaston wire or a thermistor bead. The modulation coefficient m is difficult to measure if the modulation is applied electronically. The modulation may be applied mechanically by the device in Fig. 9·18 by which the coefficient m may be measured with great precision. A cardboard disk,[1] one side of which is covered with a resistive coating of carbon, is mounted eccentrically on a motor-driven axle (see Fig. 7·9). The disk is arranged to penetrate somewhat into the waveguide or transmission line between the oscillator and crystal holder. Because of the eccentric mounting the amount of penetration varies over one revolution of the axle. Since the power transmitted is attenuated by an amount depending on the degree of insertion of the disk, the transmitted wave is modulated in amplitude as the disk is turned by the motor. The modulation may be made sinusoidal by proper mounting and shaping of the disk. The envelope of the transmitted wave can be accurately determined by measuring the transmitted power into a linear matched load as a function of angular position of the disk. The modulation coefficient is then found from the envelope. Details of this method are given in Chap. 9.

NOISE-TEMPERATURE MEASUREMENTS

7·5. General Considerations.—The measurement of noise temperature calls, like loss measurement, for two distinct types of measuring equipment, namely, easily manipulated equipment adapted to accurate and rapid routine measurement as in production testing, and equipment

[1] The material of the disk is the same as that used in making carbon rheostats.

for the research laboratory capable of measuring the noise temperature of crystals with possibly widely varying properties.

By definition, the noise temperature is the ratio of the available noise power of the crystal to that of a resistor at a standard temperature, chosen, for convenience, to be 290°K [see Eq. (2·26)]. The available noise power from a resistor at this temperature in a bandwidth of 1 Mc/sec is 4.0×10^{-15} watt, and consequently a high-gain amplifier is required for the measurement. The output power of the amplifier is measured with a wattmeter.

With the amplifier-meter combination the Y-factor can be measured. In Chap. 2 the Y-factor was defined as the ratio of the available output noise power N_o of an amplifier loaded by a crystal mixer to the available output noise power N_{os} when loaded by a standard resistor. In Eq. (2·32) there was derived for the noise temperature, in terms of the Y-factor, the expression

$$t = F'_{\text{i-f}}(Y - 1) + 1. \tag{52}$$

The application of this equation is limited by the fact that both the Y-factor and the i-f noise figure are functions of the i-f impedance of the crystal; the input impedance of the amplifier changes when the standard resistor is replaced by a crystal of different impedance. Roberts'[1] analysis, presented in this section, yields an expression for the noise temperature of a crystal in terms of the Y-factor and of the i-f admittance of the crystal if a narrowband amplifier is used. This method is not adapted to routine testing, however, since it requires a separate measurement of the i-f impedance. Roberts[2] has therefore designed a nondissipative circuit for coupling the crystal and the amplifier which makes Y independent of the crystal conductance to a first approximation for the range of i-f conductances ordinarily encountered in commercial crystals. Such a circuit for use with a narrowband amplifier is discussed in Sec. 7·6, and test sets incorporating it are described in Chap. 9.

The noise temperature can also be measured by an application of Eq. (2·28). In this equation the over-all noise figure of a crystal-mixer–amplifier combination is given by

$$F'_{\text{rec}} = L(t + F'_{\text{i-f}} - 1), \tag{53}$$

where L is the conversion loss of the crystal, t is its noise temperature, and $F'_{\text{i-f}}$ is the effective noise figure of the i-f amplifier. To calculate t requires measuring F'_{rec}, $F'_{\text{i-f}}$, L, and the i-f resistance (which enters implicitly); hence, this procedure is not adapted to routine testing. In development

[1] S. Roberts, "Theory of Noise Measurements on Crystals as Frequency Converters," RL Report No. 61-11, Jan. 30, 1943.

[2] *Loc. cit.*

work on crystals, however, it is frequently desirable to measure all these quantities in assessing the quality of the unit. Methods for their measurement in one test set are therefore included in Sec. 7·10.

We will now proceed to the derivation of an expression for the Y-factor as a function of the i-f impedance of the crystal. An equivalent circuit for the input to the i-f amplifier is shown in Fig. 7·10. The crystal is represented by the noise-current generator i_1 of conductance g_1. The noise-current generator i_2 represents the noise generated by the input conductance g_2 of the amplifier. The susceptance b is the total input susceptance of both the mixer and amplifier.

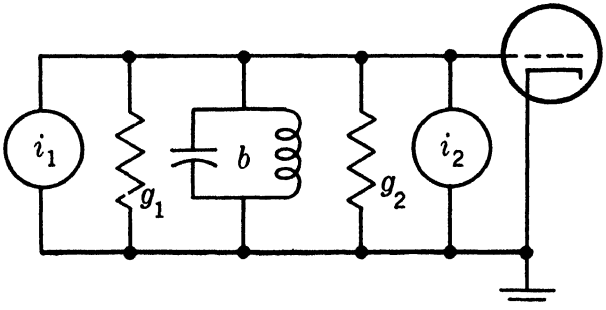

FIG. 7·10.—Equivalent circuit for a crystal rectifier coupled to the amplifier for the noise-temperature measurement.

If t is the noise temperature of the crystal, then the available noise power of the crystal in the incremental frequency range df is $kT_0t\,df$, and the mean-square noise current of the crystal noise generator is

$$\overline{di_1^2} = 4kT_0tg_1\,df. \tag{54}$$

Similarly, the mean-square noise current associated with the input conductance of the amplifier is

$$\overline{di_2^2} = 4kT_0g_2\,df. \tag{55}$$

Then the mean-square noise voltage applied to the grid of the input tube is

$$\overline{de^2} = \frac{\overline{di_1^2} + \overline{di_2^2}}{|y|^2} = \frac{4kT_0(tg_1 + g_2)\,df}{(g_1 + g_2)^2 + b^2}. \tag{56}$$

The output noise power, measured by the output meter of the amplifier, is given by

$$dN_o = u(g_2\,\overline{de^2} + vkT_0\,df), \tag{57}$$

where u is the actual power gain of the amplifier and v is a constant for the amplifier. The quantity $vkT_0\,df$ is the noise power at the grid of the input tube equivalent to that part of the output noise generated in

the amplifier itself. The first term of Eq. (57) is the contribution to the output power from the actual power input to the amplifier, $g_2\,\overline{de^2}$.

Combining Eq. (56) and (57), we obtain

$$dN_o = ukT_0\left[\frac{4g_2(tg_1 + g_2)}{(g_1 + g_2)^2 + b^2} + v\right]df, \tag{58}$$

and

$$N_o = kT_0\int_0^\infty u\left[\frac{4g_2(tg_1 + g_2)}{(g_1 + g_2)^2 + b^2} + v\right]df. \tag{59}$$

For an amplifier whose bandwidth is small compared with that of the input circuit it can be assumed that b, g_1, g_2, and t are constant over the range of integration, hence Eq. (59) may be written,

$$N_o = kT_0\,\frac{4g_2(tg_1 + g_2)}{(g_1 + g_2)^2 + b^2}\int u\,df + kT_0\int uv\,df, \tag{60}$$

where the integration is to be carried out over the pass band of the narrowband amplifier.

To obtain the Y-factor an expression is required for the noise-power output N_{os} when the crystal is replaced by a standard resistor of conductance g_s. The susceptance b is tuned out for this measurement. Hence, setting $b = 0$, $t = 1$ and replacing g_1 by g_s in Eq. (60), we obtain

$$N_{os} = kT_0\,\frac{4g_2}{g_s + g_2}\int u\,df + kT_0\int uv\,df. \tag{61}$$

Also from Eqs. (2·12) and (2·13) we have

$$N_{os} = F'_s kT_0\int G_s\,df, \tag{62}$$

where F'_s and G_s are, respectively, the effective noise figure and gain of the i-f amplifier with a signal generator of the same conductance as the standard resistor. The quantity G_s is the ratio of the power delivered to the output meter to the available input power from the signal generator.

We now need an expression for G_s in terms of u, g_s, and g_2. The output-meter reading S_o is proportional to the input power,

$$S_o = ug_2e_1^2. \tag{63}$$

With an i-f signal generator of conductance g_s and short-circuit current i_1, the available power from the signal generator is

$$S_1 = \frac{i_1^2}{4g_s}. \tag{64}$$

With this signal generator connected to the input terminals the input voltage is

$$e_1 = \frac{i_1}{g_s + g_2}. \tag{65}$$

Combining Eqs. (63), (64), and (65) we obtain

$$G_s = \frac{S_o}{S_1} = u\frac{4g_sg_2}{(g_s + g_2)^2}. \tag{66}$$

The substitution of Eq. (66) in Eq. (62) gives

$$N_{os} = F'_s kT_0 \frac{4g_sg_2}{(g_s + g_2)^2}\int u\,df. \tag{67}$$

Combining Eqs. (60), (61), and (67) we obtain

$$Y = \frac{N_o}{N_{os}} = \frac{1}{F'_s}\left\{\frac{(tg_1 + g_2)(g_s + g_2)^2}{g_s[(g_1 + g_2)^2 + b^2]} - \frac{g_2}{g_s} - 1\right\} + 1. \tag{68}$$

If the susceptance b is tuned out for each measurement, t can be calculated from measurements of Y and g_1. If the r-f terminals of the mixer are terminated with the same impedance at signal and image frequencies, the variation in crystal susceptance from crystal to crystal is small and can be tuned out approximately with a fixed adjustment.

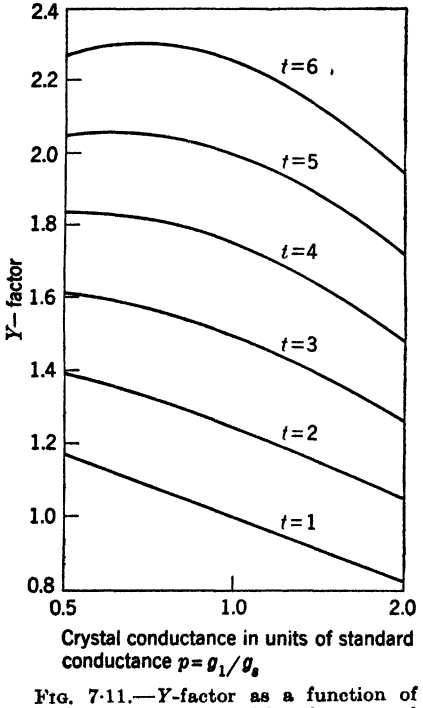

FIG. 7·11.—Y-factor as a function of crystal conductance, with the crystal coupled directly to the amplifier, for various values of t.

To investigate the effect of variation in crystal conductance on the Y-factor, let us write Eq. (68) in simplified form by putting $g_1 = pg_s$ and $g_2 = mg_s$. Assuming $b = 0$, we obtain

$$Y = \frac{1}{F'_s}\left[\frac{(tp + m)(1 + m)^2}{(p + m)^2} - m - 1\right] + 1. \tag{69}$$

If the crystal conductance is equal to the standard conductance, then $p = 1$ and Eq. (69) reduces to Eq. (52).

Figure 7·11 presents Eq. (69) graphically for different values of t; Y is plotted as a function of p for values of p from 0.5 to 2. Values of

$F_s' = 4$ (6 db) and $m = 1$ were used in plotting the graph. An inspection of Fig. 7·11 gives an idea of the errors to be encountered if the dependence of Y-factor on crystal conductance is ignored. For example, a crystal with a noise temperature of 2 and a conductance of $0.5g_s$ has a larger Y-factor than a crystal with a noise temperature of 3 and a conductance of $2g_s$. The range from $0.5g_s$ to $2g_s$ plotted in Fig. 7·11 is sufficient to cover the distribution of i-f resistance in commercial rectifiers.

7·6. The Roberts Coupling Circuit.—A nondissipative coupling circuit designed by Roberts[1] makes the Y-factor independent of crystal impedance to a first approximation, provided that (1) variations in crystal susceptance are small enough to permit the susceptance to be tuned out with a fixed adjustment, and (2) the bandwidth of the i-f amplifier is sufficiently small. The coupling network also serves a useful function as an impedance transformer which matches the crystal to the amplifier.

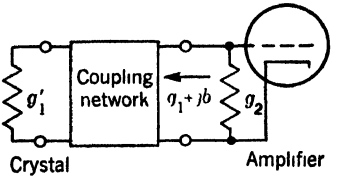

FIG. 7·12.—Block diagram of input coupling network for noise-temperature measurements.

The coupling network is shown in block diagram in Fig. 7·12. The crystal conductance g_1' is connected to the input terminals of the coupling network; the input terminals of the amplifier, having a conductance g_2, are connected to the output terminals of the network. The admittance presented by the output terminals of the network is $g_1 + jb$, in accordance with the notation of the preceding section.

Considering g_1 and b as the only variables in Eq. (68), we may write

$$\frac{dY}{dg_1'} = \frac{\partial Y}{\partial g_1}\frac{dg_1}{dg_1'} + \frac{\partial Y}{\partial b}\frac{db}{dg_1'}. \tag{70}$$

If Y is to have a stationary value for $g_1' = g_s$, then it is necessary that

$$\left(\frac{dY}{dg_1'}\right)_{g'_1 = g_s} = 0. \tag{71}$$

We see from Eq. (68) that $\partial Y/\partial b = 0$ when $b = 0$. If, also,

$$\left(\frac{dg_1}{dg_1'}\right)_{g'_1 = g_s} = 0,$$

it is evident from Eq. (70) that the condition of Eq. (71) is satisfied.

The two conditions that the network must satisfy, therefore, are (1)

$$b = 0 \qquad \text{when } g_1' = g_s,$$

[1] S. Roberts, "Theory of Noise Measurements on Crystals as Frequency Converters," RL Report No. 61-11, Jan. 30, 1943.

and (2)

$$\left(\frac{dg_1}{dg_1'}\right)_{g'_1=g_s} = 0.$$

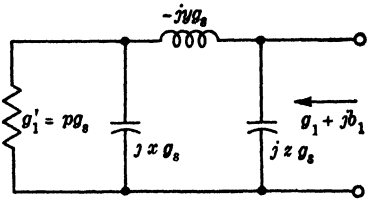

FIG. 7·13.—Input coupling network for a narrowband amplifier.

Both these conditions can be obtained with a simple Π-network, such as that shown in Fig. 7·13; the network also serves as an impedance transformer for matching the crystal to the amplifier. Let us express the admittances of the elements of the network in units of g_s as shown in Fig. 7·13, and let n be the impedance stepup ratio of the network.

Then

$$g_1 = \frac{g_1'}{n} = g_s \frac{py^2}{p^2 + (y - x)^2}, \tag{72}$$

and

$$b = g_s\left[\frac{xy(y - x) - p^2y}{p^2 + (y - x)^2} + z\right]. \tag{73}$$

From Eq. (73) we see that $b = 0$ for $g_1' = g_s$ (or $p = 1$), when

$$z = \frac{y - xy(y - x)}{1 + (y - x)^2}. \tag{74}$$

The second condition of the preceding paragraph is satisfied when

$$\left(\frac{dg_1}{dp}\right)_{p=1} = 0,$$

or

$$(y - x)^2 = 1. \tag{75}$$

Combining Eqs. (75) and (72) and setting $p = 1$, we obtain

$$y = \sqrt{\frac{2}{n}}. \tag{76}$$

Then,

$$\left.\begin{aligned} x &= y \pm 1, \\ z &= y \pm \tfrac{1}{2}y^2. \end{aligned}\right\} \tag{77}$$

Substituting Eqs. (76) and (77) into Eqs. (72) and (73), we obtain

$$\left.\begin{aligned} g_1 &= \frac{g_s}{n}\frac{2p}{p^2 + 1}, \\ b &= \pm\frac{g_s}{n}\frac{1 - p^2}{1 + p^2}. \end{aligned}\right\} \tag{78}$$

For the circuit of Fig. 7·12 and for a stepup ratio of n, Eq. (68) becomes

$$Y = \frac{1}{F'_s}\left\{\frac{(tg_1 + g_2)\left(\frac{g_s}{n} + g_2\right)^2}{\frac{g_s}{n}[(g_1 + g_2)^2 + b^2]} - \frac{g_2 n}{g_s} - 1\right\} + 1. \tag{79}$$

Substituting the values for g_1 and b from Eq. (78), and assuming the standard conductance matched to the amplifier ($g_2 = g_s/n$), we obtain

$$Y = \frac{1}{F'_s}\left[\frac{4\left(\frac{2tp}{p^2+1} + 1\right)}{\left(\frac{2p}{p^2+1} + 1\right)^2 + \left(\frac{1-p^2}{1+p^2}\right)^2} - 2\right] + 1, \tag{80}$$

where $p = g'_1/g_s$. When $p = 1$, Eq. (80) reduces to Eq. (52). Figure 7·14 shows graphically the relation between Y and p for values of p from 0.5 to 2, for an amplifier for which $F'_s = 4$ times. If the crystal conductance is in the range $0.5g_s < g'_1 < 2g_s$, the greatest error that can result from using Eq. (52) is about 11 per cent of $t - 1$ for the particular amplifier constants chosen in Fig. 7·14. Thus for a noise temperature of 2, the maximum error is approximately 0.1, about the same as the experimental error of measurement. The method is therefore an excellent one for routine testing and has been used in the standard test equipment described in Chap. 9.

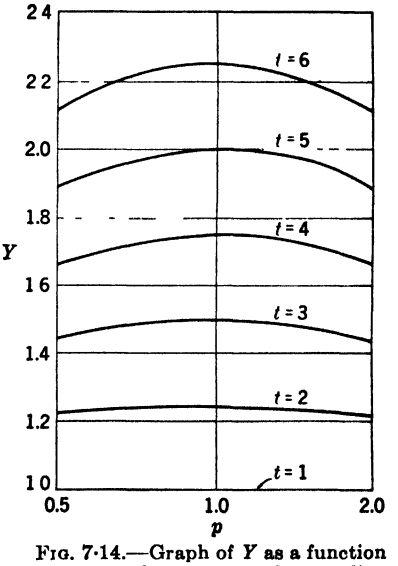

FIG. 7·14.—Graph of Y as a function of crystal conductance for the coupling circuit of Fig. 7·13. $p = \frac{g'_1}{g_s}$, where g_s is the standard conductance and g'_1 is the crystal conductance.

7·7. Narrowband Coupling Circuit.—It can be shown by a similar analysis that Y can be made independent of p to a good approximation through the use of an input circuit with a bandwidth narrow compared with that of the amplifier. The analysis shows that, for the narrowband coupling circuit, g_2 must be very large compared with g_s. Sherwood and Ginzton[1] have used this method, employing as a coupling circuit a high-Q parallel-tuned circuit with the crystal connected to a tap on the inductance coil. For such a circuit, it can be shown that the product of band-

[1] E. Sherwood and E. Ginzton, "Techniques for Testing Radar Crystal Converters and Some Results," Sperry Gyroscope Co. Report 5220-106, Mar. 6, 1943.

width and i-f crystal resistance is constant; the crystal noise voltage applied to the grid is therefore independent of the crystal conductance, provided the crystal conductance is not so large that the bandwidth of the input circuit exceeds that of the amplifier. Circuits designed by Sherwood and Ginzton were suitable for a range of i-f resistance from about 250 to 2000 ohms. The method has not been used extensively for crystal-testing, hence further details will not be given here.

7·8. Use of the Noise Diode in Noise-temperature Measurements.— It was pointed out in Chap. 6 that the mean-square noise current generated in a temperature-limited diode is given by

$$\overline{i^2} = 2eI\,\Delta f, \tag{81}$$

in the frequency band f to $f + \Delta f$, where e is the electronic charge and I is the diode current. If the diode is connected to a load resistance R, the mean-square noise voltage across the resistor arising from the diode noise is

$$\overline{e_1^2} = 2eIR^2\,\Delta f. \tag{82}$$

The mean-square noise voltage arising from Johnson noise is

$$\overline{e_2^2} = 4kT_0R\,\Delta f; \tag{83}$$

hence the total mean-square noise voltage across the resistor is

$$\overline{e^2} = \overline{e_1^2} + \overline{e_2^2} = 4kT_0R\,\Delta f\left(1 + \frac{eIR}{2kT_0}\right). \tag{84}$$

The available noise power from the resistor is

$$P = \frac{\overline{e^2}}{4R} = kT_0\,\Delta f\left(1 + \frac{eIR}{2kT_0}\right). \tag{85}$$

It is clear, then, that the effect of the diode current is to make the resistor noisier by an amount that can be calculated from a measurement of the diode current. The noise temperature of the "noisy" resistor is

$$t = \frac{eIR}{2kT_0} + 1 = 20IR + 1, \tag{86}$$

when $T_0 = 290°\text{K}$, and I is the diode current expressed in amperes.

The noise diode thus provides a source of variable, known noise temperature or a means of adding known amounts of available noise power to the input circuit of an amplifier. Its use for absolute measurement is applicable to intermediate frequencies, where R can be accurately determined. It has been used with some success, however, as an r-f noise source for relative noise-figure measurements.

An example of the application of the noise diode is the calibration of noise-temperature apparatus such as the standard sets described in Chap. 9. In this application the standard resistor is inserted in the equipment and the noise diode is connected. The output meter can then be calibrated directly in terms of noise temperature by means of Eq. (86).

A second application of the noise diode is the measurement of noise figures of i-f amplifiers, accomplished as follows. With the noise diode off and a resistor connected to the input terminals of the amplifier, the output noise power is given [see Eq. (2·15)] by

$$N_o = kT_0F'_{\text{i-f}}G_{\text{i-f}}\,\Delta f, \tag{87}$$

where $F'_{\text{i-f}}$ is the effective noise figure and $G_{\text{i-f}}$ is, as usual, the ratio of the power measured by the output meter to the available input power.

With the noise diode on, the available input-noise power from the diode current is, from Eq. (82),

$$P = \frac{\overline{e_1^2}}{4R}, \tag{88}$$

so that

$$P = \frac{eIR}{2kT_0}\,kT_0\,\Delta f = 20IRkT_0\,\Delta f. \tag{89}$$

The total amplifier output power is then

$$N = kT_0G_{\text{i-f}}\,\Delta f(F'_{\text{i-f}} + 20IR). \tag{90}$$

From Eqs. (88) and (90),

$$\frac{N}{N_o} = 1 + \frac{20IR}{F'_{\text{i-f}}}, \tag{91}$$

whence

$$F'_{\text{i-f}} = \frac{20IR}{\dfrac{N}{N_o} - 1}. \tag{92}$$

It is customary practice to adjust I so as to make $N = 2N_0$; then

$$F'_{\text{i-f}} = 20I_1R, \tag{93}$$

where I_1 is the diode current required to double the noise output.

Diode noise generators are included in the standard test equipment described in Chap. 9, and details of construction will be given there.

MEASUREMENT OF LOSS, NOISE, AND RECEIVER NOISE FIGURE

7·9. The Measurement of Receiver Noise Figure.—It has been shown in Eq. (2·15) that the effective noise figure of a network is given by

$$F' = \frac{N_o}{kT_0BG'}, \tag{94}$$

where N_o is the output-noise power measured by the output meter and G' is the power gain of the network-meter combination at the maximum of the gain-frequency characteristic. The bandwidth B is defined by the relation

$$B = \frac{\int_0^\infty G\,df}{G'}. \tag{95}$$

Applying these equations to a microwave receiver, we see that, with no signal input, the output-noise power is given by Eq. (94). If a signal generator of available power N' is connected to the input terminals of the receiver, the output-noise power of the receiver is

$$N_2 = F'kT_0BG' + N'G', \tag{96}$$

whence

$$\frac{N_2}{N_o} = 1 + \frac{N'}{F'kT_0B}, \tag{97}$$

from which

$$F' = \frac{N'}{kT_0B}\,\frac{1}{\dfrac{N_2}{N_o} - 1}. \tag{98}$$

If the available noise power of the signal generator is adjusted so as to double the output-noise power,

$$F' = \frac{N'}{kT_0B}. \tag{99}$$

If a c-w signal generator is used, the determination of noise figure by means of Eq. (99) involves a measurement of only N' and B.

The effective bandwidth B can be determined by measuring the frequency-response curve of the i-f amplifier if the latter's bandwidth is less than that of the mixer, as it is in receivers employing the usual crystal mixer. For this purpose a variable i-f generator is used with an internal impedance equal to the i-f impedance of the crystal mixer.

The input power N' is supplied by a signal generator provided with a variable attenuator. The noise figure that is measured is the noise figure for the particular generator impedance used in the measurement.

Since the noise figure of a good receiver may be as low as 7 or 8 db, it is necessary to measure input powers as low as 10^{-14} watt for a bandwidth of 1 Mc/sec. The smallest microwave power that can be measured with good laboratory apparatus to an accuracy of a few tenths of a decibel is about 1 μw. Hence a c-w signal generator must be equipped with a calibrated attenuator of about 80-db maximum attenuation. Such equipment can be built, but it is difficult to maintain and is not practical for general use.

A noise generator employing the 417A klystron as a diode has been developed for use in the 10-cm band by Waltz and Kuper.[1] In this application the reflector is connected to the cavity to prevent oscillations, and the tube is operated at a high voltage to insure saturation and low transit time. The output-noise power is proportional to the cathode current, but Eq. (81) does *not* apply because of transit-time effects. Since the load conductance is not known with any certainty, calibration is required for absolute measurements. The range of available power is sufficient to measure noise figures up to about 30 db, and the bandwidth is approximately 2.5 Mc/sec. With a cavity voltage of about 1500 volts, the output power is constant to about 1 db when the cavity is tuned over the range from 9 to 11.5 cm. This device is found to hold its calibration over long periods of time and is suitable for general field use; a correction must be made, however, when the bandwidth of the receiver being measured is greater than that of the noise source.

In the 3-cm range similar noise sources have been constructed, using the type 723A tube. Since the output noise is a critical function of voltage and frequency, such use is restricted to the laboratory, where they may be calibrated *in situ* by a method such as that described in Sec. 6·5. For a more detailed account of noise sources the reader is referred to Vol. 11 of the Radiation Laboratory Series.

Another useful r-f noise generator is a crystal excited by d-c bias in the back direction, as discussed in Sec. 6·5. The crystal can be calibrated for a given d-c bias by the methods described in that section. This noise source has the advantage that the output-noise power is independent of the frequency and proportional to the bandwidth; the bandwidth therefore cancels out in the noise-figure measurement. If $t_{r\text{-}f}$ is the r-f noise temperature of the crystal for a given d-c bias, then the available noise power is

$$N' = kT_0Bt_{r\text{-}f}. \tag{100}$$

Equation (98) then becomes

$$F' = \frac{t_{r\text{-}f}}{\dfrac{N_2}{N_o} - 1}. \tag{101}$$

The ratio N_2/N_o can be conveniently measured with a square-law output meter connected to the terminals of the receiver, such as a bolometer or a crystal operated in the square-law region.

For a more complete discussion of noise-figure measurements the reader is referred to Vols. 18 and 23 of the Series.

[1] M. C. Waltz and J. H. B. Kuper, "Simplified Measurement of Receiver Sensitivities," RL Report No. 443, Sept. 17, 1943.

7·10. The Measurement of Mixer-crystal Properties.—It is often desirable in the course of crystal development to measure the various mixer-crystal quantities under very general conditions. A convenient method is to use a crystal as an r-f noise source and a noise diode as an i-f noise source with the apparatus shown in Fig. 6·11. With such equipment it is possible to measure the i-f resistance, loss, and noise temperature of the receiver crystal, the i-f noise figure, and the over-all receiver noise figure. The method is applicable to receivers for which the output power is a function of the i-f resistance at the input terminals. The input circuit of such an i-f amplifier is shown in Fig. 7·15. The diode noise source is connected through a blocking condenser to the crystal mixer. It functions as a constant-current noise generator with the conductance of the crystal or the standard resistance cartridge used for calibration, as the case may be. The single-tuned circuit of resistance R_1 can be tuned to resonance with the variable condenser C; this is done with each measurement, hence the input impedance is a pure resistance. The input conductance of the amplifier can be adjusted with the resistance R_2. Filters, represented by L_2 and L_3, serve to decouple the power supply and the d-c terminal of the mixer at intermediate frequency.

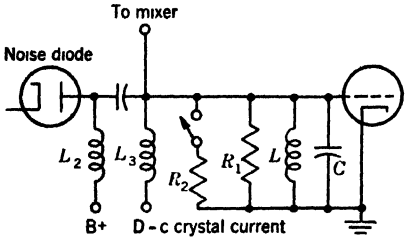

FIG. 7·15.—Input circuit for the laboratory measurement of mixer crystal properties.

Measurement of Crystal I-f Resistance.—For this measurement the r-f noise source is turned off. Let P_1 and P_2 be the available input noise power with the i-f noise source turned off and on, and with a resistor cartridge of resistance R in the mixer. Then, from Eq. (85),

$$P_2 - P_1 = 20IRkT_0\,\Delta f. \tag{102}$$

The difference in output noise power of the amplifier with the noise diode on and off is

$$N_2 - N_1 = \Delta N = 20IRkT_0G_{\text{i-f}}\,\Delta f = F(R). \tag{103}$$

The gain $G_{\text{i-f}}$ is the ratio of the power measured by the output meter to the available input power, and is therefore a function of R. Equation (88) also applies when the resistor is replaced by a crystal, R in this case being the i-f crystal resistance. To determine the i-f resistance of the crystal, the output meter is calibrated by measuring ΔN for a series of resistor cartridges with various values of R, keeping I constant at a predetermined value. With the crystal inserted, ΔN is read for the given value of I, and R determined from the calibration curve.

Measurement of Receiver Noise Figure.—The receiver noise figure is measured by means of the r-f noise source, as described in the previous section.

Measurement of Conversion Loss.—The conversion loss of the crystal is calculated from noise-diode measurements and the known values of R and F'_{rec}.

With the noise diode off and the crystal in the mixer, the output-noise power is

$$N_3 = kT_0G_{rec}F'_{rec}\,\Delta f = kT_0G_{i\text{-}f}G_xF'_{rec}\,\Delta f, \tag{104}$$

where G_x is the conversion gain of the crystal.

With the noise diode on, the output-noise power is

$$N_4 = N_3 + 20IR_xkT_0G_{i\text{-}f}\,\Delta f, \tag{105}$$

where R_x is the i-f resistance of the crystal.

Combining Eqs. (104) and (105), we obtain

$$\frac{N_4}{N_3} - 1 = \frac{20IR_x}{G_xF'_{rec}}, \tag{106}$$

whence

$$L_x = \frac{\left(\dfrac{N_4}{N_3} - 1\right)F'_{rec}}{20IR_x}. \tag{107}$$

Measurement of Noise Temperature.—Once the receiver noise figure, conversion loss, and noise figure of the i-f amplifier are known, the noise temperature can be calculated from the relation

$$F'_{rec} = L_x(F'_{i\text{-}f} + t - 1). \tag{108}$$

The noise figure of the i-f amplifier $F'_{i\text{-}f}$ depends on the input conductance; it can be measured as a function of R by means of the noise diode and the standard resistor cartridges. With a resistor cartridge in place and the noise diode off, the noise output of the amplifier is

$$N_1 = kT_0G_{i\text{-}f}F'_{i\text{-}f}\,\Delta f. \tag{109}$$

Combining Eqs. (109) and (103) we obtain

$$\frac{N_2}{N_1} - 1 = \frac{20IR}{F'_{i\text{-}f}}, \tag{110}$$

whence

$$F'_{i\text{-}f} = \frac{20IR}{\dfrac{N_2}{N_1} - 1}. \tag{111}$$

By means of Eq. (111) $F'_{i\text{-}f}$ may be evaluated as a function of R. The noise temperature t is then calculated from Eq. (108):

$$t = \frac{F'_{rec}}{L} - (F'_{i\text{-}f} - 1). \tag{112}$$

7·11. Loss and Noise Temperature as a Function of R-f Tuning.—The conversion loss was seen in Chap. 5 to depend on the internal impedance of the signal source at signal and image frequencies, and, to a lesser extent, at harmonic frequencies. Moreover, the theory shows that the i-f conductance depends strongly on the relative phase at the crystal of the waves of these frequencies which have been reflected at the r-f terminals. The effect of r-f terminating impedance on noise temperature is also of practical importance. An experimental investigation has been made by E. R. Beringer[1] at the Radiation Laboratory in which the conversion loss, i-f resistance, and noise temperature were measured in an apparatus so designed that the impedance of the source at signal and image frequency could be controlled independently over a range of values. The data for typical 1N23B rectifiers are given in this section. A similar investigation on the welded-contact germanium rectifiers is discussed in Chap. 13.

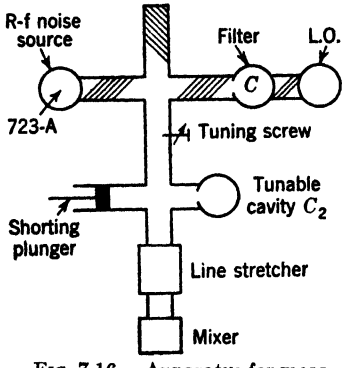

FIG. 7·16.—Apparatus for measuring crystal properties as a function of image and signal source impedance.

The methods used in the measurement of these quantities are in general those described in the preceding section. A diagram of the apparatus is shown in Fig. 7·16. The local oscillator and r-f noise source are connected to opposite arms of a magic T, connected as shown to a second magic T. The filter cavity removes the noise sidebands of the local oscillator at signal and image frequencies. The r-f noise source is a 723A tube connected as a diode, with the cavity tuned to signal frequency. The resistance-strip attenuators in the arms of the magic T have sufficient attenuation to terminate them approximately with the characteristic line impedance. The second magic T functions as a rejection filter at the image frequency. The tunable cavity is tuned to the image frequency. By adjusting the tuning plunger in the opposite arm, approximately 75 per cent reflection was obtained at the image frequency, with essentially no reflection at signal or local-oscillator frequencies. The phase of the reflected wave can be varied by means of the line stretcher L. In addition, the tuning screw may be used to

[1] Unpublished.

tune the signal independently. The amplifier input circuit was that shown in Fig. 7·15.

Results for a randomly selected sample of 1N23B crystals are shown in Table 7·1. These data were taken with a signal frequency of 9423 Mc/sec and an image frequency of 9363 Mc/sec. The tuning screw S was not used; hence the impedance of the source at signal frequency was the line impedance. All measurements were taken with 0.90 ma of rectified current and no d-c bias on the crystal. The first and third row,

TABLE 7·1.—EFFECT ON CRYSTAL PROPERTIES OF THE PHASE OF REFLECTED WAVE AT IMAGE FREQUENCY

For each crystal, the data in the first and third rows are for the phases which give maximum and minimum i-f resistance, respectively; the second row is for a match at both signal and image frequencies

Crystal No.	R	t	L, db	t/R
1	455	1.5	6.8	0.0034
	330	1.9	6.6	0.0058
	210	1.5	7.6	0.0072
2	560	1.4	5.6	0.0025
	325	1.3	6.0	0.0040
	185	1.2	6.8	0.0065
3	610	2.1	5.8	0.0034
	415	1.9	6.4	0.0046
	270	2.0	7.0	0.0074
4	520	1.9	6.5	0.0037
	325	1.8	7.0	0.0055
	218	1.4	7.5	0.0064
5	390	1.6	6.6	0.0041
	282	1.4	6.9	0.0050
	180	1.3	8.0	0.0072

for each crystal, give the data when the image phases are such that the i-f resistance is a maximum and minimum, respectively; the second row gives the results when there is a match at both image and signal frequencies. The variation in conversion loss is about 1 db for variations in R of more than a factor of 2. The noise-temperature variation, however, is less than 25 per cent; in some cases there is no significant change. If we consider the crystal as a noise generator of shunt resistance R, then,

$$kT_0 t\,\Delta f = \frac{\overline{i^2 R}}{4}. \tag{113}$$

from which $\overline{i^2} \propto t/R$. It can readily be seen that with changes in image phase the silicon crystals are much more like a source of constant noise

temperature than of constant noise current. This is also true when both the mage and signal frequencies are mismatched, as shown by the data in Table 7·2. These data were taken by replacing the second magic T (that is, with cavity) of Fig. 7·16 with a sliding tuning screw

TABLE 7·2.—NOISE TEMPERATURE AS A FUNCTION OF SIGNAL AND IMAGE REFLECTION
Measurements were made with the phase adjusted for maximum and minimum i-f resistance and the power-reflection coefficient approximately 0.5.

Crystal No.	R	t
1	530	1.7
	230	1.7
2	610	1.7
	190	1.3
3	790	2.4
	268	2.2
4	595	2.3
	220	2.0
5	460	1.6
	195	1.6

having a power-reflection coefficient of approximately 0.5; with this arrangement both signal and image frequencies are reflected. The two sets of values in the table are for maximum and minimum values of R.

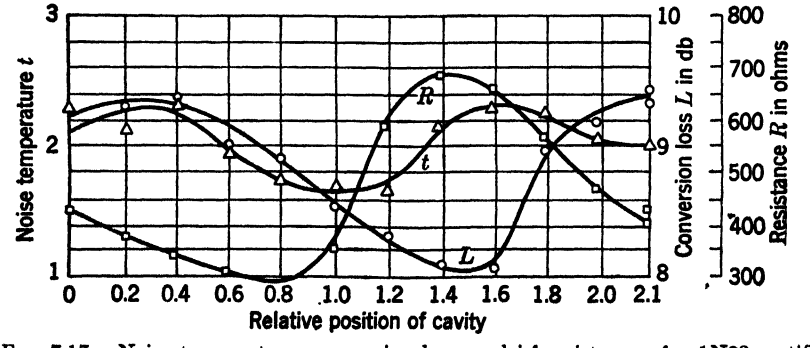

FIG. 7·17.—Noise temperature, conversion loss, and i-f resistance of a 1N23 rectifier as a function of image phase. The phase is varied by changing the line length between the mixer and reflecting cavity.

Figure 7·17 shows the i-f resistance, noise temperature, and conversion loss for a 1N23 rectifier as a function of image phase. The crystal was matched at signal frequency, and a crystal current of 0.5 ma was used,

with self-bias from the d-c meter resistance (about 100 ohms). The phase was varied by means of the line stretcher; the abscissa is the relative position of the cavity as the effective line length is changed. The distance from cavity to crystal increases as the abscissa increases, and the range covers approximately a complete cycle of image phase at the crystal.

CHAPTER 8

BURNOUT

8·1. General Considerations.—Contrary to widely held opinion, the modern crystal rectifier has been perfected to a point where, handled with reasonable care, it has remarkable endurance and stability, both mechanical and electrical. The precautions to be observed in handling crystals have been discussed in Sec. 2·2.

The present chapter will treat the phenomenon known as "burnout," which may be defined as *a change in the rectifying and converting properties of crystal rectifiers as the result of excessive electrical overloads.* One type of burnout is that caused by accidental static electrical shocks, discussed in Sec. 2·2 also. Here we are primarily concerned with overloads encountered in microwave radar receivers. These overloads may occur as a result of

1. Poor shielding of the crystal output leads, that is, the leads to the amplifier or to the crystal-current meter. A little care in design can eliminate this defect.
2. Failure of the TR switch to protect the crystal in a duplex system. (Duplexing involves using the same antenna and transmission line for pulse radar transmission and reception.) Such failures may result from
   a. Deterioration of the TR tube itself. This is probably the most prevalent cause of crystal burnout. A discussion of TR-tube deterioration may be found in Vol. 14 of the Radiation Laboratory Series. Although it is possible to monitor TR-tube performance so that the tube can be replaced before damage is done to the crystal, it is common practice to wait for crystal failure before changing tubes, since it is simpler to change crystals than TR tubes. The danger is that the noise figure of the receiver may rise by a considerable amount before the damage is suspected.
   b. Failure of the voltage supply for the TR-tube "keep-alive" (a weak discharge, maintained by a high-impedance d-c source, to accelerate ignition).
   c. Occasional generation by the transmitter of considerable power at harmonic frequencies. Some harmonics are not sufficiently attenuated by TR switches and consequently severely overload the crystal.

3. Accidental reception of signals of abnormal power by receivers not protected by TR switches, such as a crystal-video receiver. This case is often unavoidable. Some protection is afforded by the use of electrical shutters in the r-f line which may be closed when the set is not in operation.

The type of electrical overload most frequently encountered arises from Item 2 above. The voltage consists of pulses of electromagnetic energy usually at microwave frequencies. These pulses are often about 1 μsec in duration, but they are considerably distorted in shape by transmission through a TR switch. The TR switch consists of a gas-filled tube in a tuned cavity resonator; it attenuates the transmitted power by virtue of the detuning action of a gaseous discharge which is ignited by the leading edge of the transmitted pulse, but normally the echo is of low power and fails to cause breakdown. Because of time lag in the ignition, a considerable amount of power is transmitted through the TR cavity for a time of perhaps 2 to 3 $\times 10^{-9}$ sec at the start of the pulse. Thereafter the attenuation becomes large and the power dissipated in the crystal for the remainder of the transmitted pulse is rarely more than 50 mw, which is insufficient to damage a crystal. The transmitted pulse, seen at the crystal, therefore consists of a high short pulse called a "spike," followed immediately by a low long pulse called a "flat." The duration of the spike is uncertain, but the transmitted energy in the spike has been measured and is normally in the range of 0.01 to 1.0 erg (0.01 to 1.0 $\times 10^{-7}$ joule) but may sometimes become larger, especially if the "keep-alive" is not operating well.

Considerable illumination was thrown on the relative importance of the so-called "spike" and "flat" by the work of McMillan and Wiesner.[1] They measured the total pulse energy with a bolometer and compared it with that computed from the height and width of the pulse as viewed on an oscilloscope. The actual energy content of the pulse was found often to be much larger by the bolometric method. Later measurements, in which the flat part of the pulse was cancelled by an out-of-phase pulse bypassing the TR switch, revealed the energy difference to be accounted for by the failure to observe the true spike power because of insufficient bandwidth in the video circuits in the oscilloscope. The observed spike energies were compared with d-c pulses of comparable duration and of requisite energy to damage crystals; it was found that TR switches not giving sufficient protection were passing spikes with energy sufficient for burnout although the flat portion of the pulse was still as small as that of a proper TR switch.

The experiments conclusively demonstrated that the spikes were the primary cause of burnout. The question, whether burnout depends

[1] F. L. McMillan and J. B. Wiesner, RL Report No. 53-24, July 3, 1943.

on the shape of the spike or merely on its energy content, still remains. This question has not yet been conclusively answered, although the energy of the spike is believed to be the important factor and its shape relatively unimportant. The basis of this belief is the theory of burnout by short pulses, as outlined in Sec. 8·3, and certain experiments reported in Sec. 8·4. Both theory and experiment agree in assigning to an average crystal a thermal relaxation time of about 10^{-8} sec. For shorter pulses the heat developed does not have time appreciably to diffuse away from its point of origin; the temperature reached is determined entirely by the energy developed per unit volume in the semiconductor and by the thermal capacity per unit volume of the semiconductor. If, then, the spikes are shorter than 10^{-8} sec, their energy content and not their shape should determine the temperature reached in the crystal and thus, presumably, the extent of burnout.

Burnout caused by harmonic leakage through the TR switch and in systems with no TR-switch protection is produced by pulses of the order of 1 μsec in length. In this case the shape of the pulse is certainly of importance, and if the pulse is flat, the temperature attained in the semiconductor is proportional to the pulse *power* rather than to the pulse energy, as will be shown in Sec. 8·2.

Burnout in radar receivers is sometimes observed to consist of a sudden change in the properties of the crystal. Often, however, it consists of a gradual deterioration which may take place over several hundred hours of operation. Why this occurs is not known, but it is reasonable to ascribe it to some process such as diffusion of impurities in the semiconductor or a chemical reaction at or near the contact. Such processes, consuming a great deal of time at room temperatures, would be accelerated by the high temperatures attained during a pulse. It has not yet been definitely determined whether the spike or the flat is responsible for this type of burnout, but the spike seems the more likely. Some experiments[1] have shown that moderate pulse powers in the flat region at normal repetition rates are sufficient to cause a gradual long-time deterioration in some crystals. These powers (1 or 2 watts), however, are considerably in excess of those which crystals protected by a TR switch normally have to handle.

Considerable effort has gone into devising adequate burnout tests for crystals. A type of sieve that would reject all but high-burnout crystals would be desirable. Unfortunately we have no way of telling how much power or energy a crystal can withstand without actually applying power to the point of burnout. The information obtained in this way is of only academic interest since the crystal is destroyed in the

[1] H. B. Huntington, "Crystal Life Test Under Flat Pulses," RL Report No. 543, Apr. 7, 1944.

process. If all crystals of identical type and identical manufacture could be presumed to have identical burnout properties, the problem could be easily solved by factory tests of small samples. Unfortunately this is not the case. There appear to be wide differences in burnout properties in a sample of crystals otherwise (that is, in loss and noise temperature) nearly identical.

The following expedient is nevertheless adopted. Converter crystals are now usually tested by applying to each unit in the forward direction a single d-c pulse of duration 2.5×10^{-9} sec. This pulse is generated by the discharge of a coaxial-line condenser and is applied before any measurements of loss and noise. The energy of the pulse is adjusted so that crystals especially susceptible to burnout will deteriorate to the point where they will fail the other acceptance tests; whereas less susceptible units will not suffer much, if any, deterioration. The obvious limitation of such a test is that it is useless if too weak and, if too strong, it will deteriorate the product and lower rates of production. The technical details of the coaxial-line proof test are given in Sec. 9·7.

For crystals not protected by TR switches, such as video detectors, a different burnout-testing procedure is used. Overloads commonly encountered here consist of microsecond pulses of microwave power. The crystals are tested by applying to them in the forward direction a d-c pulse of 1-μsec duration generated by the discharge of an artificial (lumped-constant) transmission line or pulse-forming network. In the case of video detectors, this is used as a design test and not as a proof test because of the burnout properties peculiar to the video-detector crystal. Specifications for video detectors usually require the video impedance to fall within a certain range and a crystal is deemed "burned out" if, as a result of application of power, its impedance does not fall in this range. Now it happens that video crystals can be manufactured with impedances outside this range and the impedances then brought within the desired range by the application of power. Since this involves a major change in the properties of the crystal it is not thought wise to accept such crystals even though they meet production tests, for a subsequent application of power of the same magnitude might possibly again change the impedance perhaps by enough to take it out of the specified range. Accordingly, such crystals are not proof-tested, but small samples, deemed representative of a large production lot, are exposed to pulsed power and a certain fraction are required not to change their impedance by more than a specified amount as a result of such power. In addition it is required that the "figure of merit" of the same fraction shall not decrease below a specified limit.

8·2. Burnout Theory. *Introduction.*—A number of hypotheses have been made concerning the physical cause of burnout. In general these

may be grouped under two heads, (1) voltage breakdown and (2) temperature effects.

The voltage-breakdown hypothesis, advanced by F. Seitz,[1] assumes that electrons are accelerated by intense fields to the point where they produce secondaries by collision. The secondaries in turn produce tertiaries, and so on, with the result that an avalanche of high-energy electrons rips through a portion of the semiconductor and causes intense local heating. This hypothesis, however, leads to conclusions that are in contradiction to the facts. Higher field intensities exist in the blocking direction than in the conducting direction for the same applied voltage because the voltage is applied mainly across the thin barrier region in the former case and mainly across the relatively thick spreading resistance in the latter. Thus the voltage-breakdown hypothesis would predict the onset of burnout at lower voltage in the blocking direction than in the conducting direction. Since exactly the reverse of this is observed, it seems doubtful that voltage breakdown is an important effect in burnout.

The other suggested cause of burnout is the effect of high temperatures produced by joule heat in the spreading resistance or by dissipation of energy gained by electrons in passing over the barrier. There are a number of possible effects of this type. For example, the diffusion of impurities near the surface will be accelerated by high temperatures, or metal atoms from the cat whisker may diffuse into the barrier region, or chemical reactions between semiconductor or metal with impurities on the contact may take place. Sufficiently high temperatures will melt the semiconductor (silicon melts at 1420°C, germanium at 960°C) and at lower temperatures strains set up by intense temperature gradients may cause rupture or splintering of the semiconductor. Since a crystal rectifier is delicately adjusted in assembly to near-optimum performance, any change in the properties or configuration of the contact region may be expected to produce deterioration of the rectifying and conversion actions.

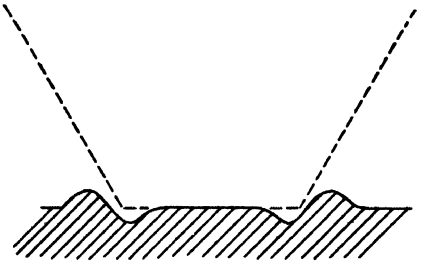

FIG. 8·1.—Profile of the surface of a silicon wafer after severe burnout. The cat whisker (normally as shown by the broken line) has been removed.

It has not as yet been ascertained which of these possibilities is most important. It is at least certain that melting or splintering occurs in severely burned-out units. W. G. Pfann,[1] working at the Bell Telephone Laboratories, disassembled severely burned-out silicon rectifiers and

[1] Private communication.

examined microscopically the silicon surface in the region of the former contact. He found that in the case of crystals burned out by short pulses (1 μsec or less), a ridge is built up just outside the periphery of the contact surface and is often accompanied by a noticeable trough or depression just inside the periphery. Figure 8·1 shows a profile of such a typical surface.

The appearance of this profile strongly suggests that silicon has been removed from the region just inside the contact periphery and deposited just outside the contact. It is reasonable to suppose that this occurs because of whisker pressure on molten silicon near the edge of the contact, and hence the cause of deterioration is correlated with high temperatures. The duration of the electrical disturbance, however, must also play a role, for one would not suppose that the same temperatures would produce the same effects regardless of the exposure time. Moreover, if burnout is at all associated with diffusion effects, the time of exposure is certainly of importance.

The problem of calculating the contact temperature is conveniently divided in two parts. If a constant amount of electric power is steadily applied beginning at time $t = 0$, the temperature will first rise and finally approach a limiting steady-state value. The first and simpler part of the problem is to find this steady-state solution. The more difficult time-dependent case is treated in Sec. 8·3.

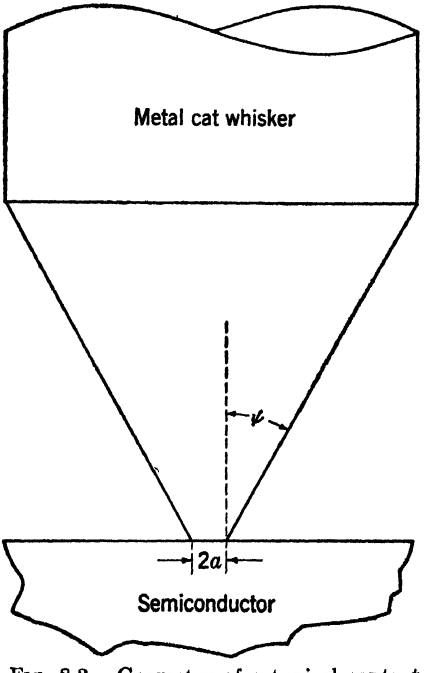

FIG. 8·2.—Geometry of a typical contact rectifier.

The Steady-state Solution.—Let us consider a rectifier of conventional design as illustrated in Fig. 8·2. The contact is assumed to be circular and of radius a; the half-angle of the cone forming the tip of the cat whisker will be denoted by ψ. The subscripts m and s refer to quantities characteristic of the metal and semiconductor respectively.

The case of a static voltage applied across the rectifier is considered first. The thermal-continuity equation for either metal or semiconductor is

$$\nabla \cdot k\nabla\theta + Q = C\frac{\partial\theta}{\partial t}, \tag{1}$$

where θ is the temperature above ambient temperature, k and C are the appropriate thermal conductivity and thermal capacity per unit volume, respectively, and Q is the power dissipated per unit volume. For an ohmic resistance,

$$Q = \sigma|\nabla V|^2, \tag{2}$$

where σ is the electrical conductivity and V the potential.

The equation appropriate to the steady state is obtained from Eq. (1) by putting $\partial\theta/\partial t = 0$. Thus

$$\nabla \cdot k\nabla\theta + \sigma|\nabla V|^2 = 0. \tag{3}$$

It is convenient to regard the temperature as the sum of two quantities θ_1 and θ_2, where θ_1 is the temperature produced by heat generated in the barrier only and θ_2 the temperature produced by dissipation in the spreading resistance.

Let us first find θ_2. From Eq. (3) it follows that

$$\nabla \cdot k\nabla\theta_1 = 0 \tag{4}$$

outside the barrier region. If $\mathbf{j}$ is the thermal current density,

$$\mathbf{j} = -k\nabla\theta_1, \tag{5}$$

and from Eq. (4)

$$\nabla \cdot \mathbf{j} = 0. \tag{6}$$

It is convenient to draw an analogy to the case of the flow of electric current. Thus, if $\mathbf{i}$ is the electric current density, we have

$$\mathbf{i} = -\sigma\nabla V \tag{7}$$

and

$$\nabla \cdot \mathbf{i} = 0. \tag{8}$$

The last two equations may be used to find the electrical resistance,

$$R_{\text{elec}} = \frac{\Delta V}{I}, \tag{9}$$

between two equipotential surfaces of potential difference ΔV where I is the electric current. Similarly, the thermal resistance between isothermal surfaces with temperature difference $\Delta\theta$ is

$$\mathcal{R}_{\text{therm}} = \frac{\Delta\theta}{J}, \tag{10}$$

where J is the total thermal current. Now the contact is nearly an equipotential surface since the electrical conductivity of the metal whisker is large compared with that of the semiconductor. If we assume that the contact is an isothermal surface, the two problems, electrical

and thermal, are formally identical and

$$\sigma R_{\text{elec}} = k\mathcal{R}_{\text{therm}}. \tag{11}$$

By conservation of energy, the heat current J must be just equal to the power P_1 dissipated in the barrier. Let θ_{1_0} be the contact temperature resulting from barrier dissipation only. Then,

$$\theta_{1_0} = \mathcal{R}_{\text{therm}} P_1. \tag{12}$$

The thermal resistance $\mathcal{R}_{\text{therm}}$ includes the thermal resistances $\mathcal{R}_s$ of the semiconductor and $\mathcal{R}_m$ of the whisker. Since these are in parallel,

$$\frac{1}{\mathcal{R}_{\text{therm}}} = \frac{1}{\mathcal{R}_s} + \frac{1}{\mathcal{R}_m}. \tag{13}$$

We now find the contact temperature θ_{2_0} caused only by dissipation in the spreading resistance. We must go back to Eq. (3) which is satisfied by θ_2 in the semiconductor,

$$\nabla \cdot k_s \nabla \theta_2 + \sigma_s |\nabla V|^2 = 0. \tag{14}$$

To solve this equation, a simplifying assumption is made which is not exactly correct but probably a good approximation. It is assumed that θ_2 depends on the coordinates only through an explicit dependence on the potential V. Thus,

$$\theta_2 = \theta_2(V). \tag{15}$$

Combining Eqs. (7), (8), (14), and (15), it is easily shown that

$$\frac{d}{dV}\left(\frac{k}{\sigma}\frac{d\theta_2}{dV}\right) + 1 = 0, \tag{16}$$

which integrates to

$$\theta_2 = AV + B - \int \frac{\sigma}{k} V\, dV, \tag{17}$$

where A and B are integration constants. If these constants can be adjusted to fit the boundary conditions on θ_2, the assumption of Eq. (15) is exact. This may be shown to be true in the limit as the thermal conductivity k_m of the metal whisker approaches either 0 or ∞. For finite k_m it is only approximately the case. For boundary conditions we take

$$\left.\begin{aligned} \theta_2 &= 0 \\ V &= 0 \end{aligned}\right\} \quad \text{at a distance remote from the contact} \tag{18a}$$

$$\left.\begin{aligned} V &= V_0 \\ k_s \frac{\partial \theta}{\partial n}\bigg]_s &= k_m \frac{\partial \theta}{\partial n}\bigg]_m \end{aligned}\right\} \quad \text{at the contact.} \tag{18b}$$

Here **n** is a unit vector normal to the contact surface and the last condition expresses the continuity of heat flow across the contact. In Eq. (17) we integrate from $V = 0$ to $V = V_0$ and assume σ/k independent of temperature and hence of potential. From Eqs. (17) and (18), $B = 0$ and

$$\theta_{2_0} = AV_0 - \frac{\sigma}{2k} V_0^2, \tag{19}$$

where θ_{2_0} is the contact temperature due only to dissipation in the spreading resistance.

It may be shown that Eq. (18*b*) for detailed continuity of heat flow across the contact is not strictly compatible with our assumption, Eq. (15), that θ_2 is a function of the potential only. If, however, the boundary condition is expressed as an integral over the contact surface, the result is compatible with Eq. (15). We get

$$\int_S k_s \frac{\partial \theta_2}{\partial n}\bigg]_s dS = \int_S k_m \frac{\partial \theta_2}{\partial n}\bigg]_m dS. \tag{20}$$

Now, on the left side of Eq. (20), we put

$$\frac{\partial \theta_2}{\partial n} = \frac{d\theta_2}{dV}\frac{\partial V}{\partial n} \tag{21}$$

and we note that the right side of Eq. (20) is just the heat current J_m flowing through the metal. By Eq. (10)

$$J_m = \frac{\theta_{2_0}}{\mathfrak{R}_m}. \tag{22}$$

Thus, substituting Eqs. (21) and (22) in Eq. (20) and putting

$$I = \frac{V_0}{R_s} = \int_S \sigma_s \frac{\partial V}{\partial n}\bigg]_s dS \tag{23}$$

for the electric current when R_s is the (electrical) spreading resistance of the semiconductor, we obtain

$$\frac{k_s}{\sigma_s}\left(\frac{d\theta_2}{dV}\right)_{\text{contact}} \cdot \frac{V_0}{R_s} = \frac{\theta_{2_0}}{\mathfrak{R}_m}. \tag{24}$$

From Eq. (19), it follows that

$$\left(\frac{d\theta_2}{dV}\right)_{\text{contact}} = A - \frac{\sigma_s}{k_s} V_0. \tag{25}$$

Substituting Eq. (25) in Eq. (24) and solving for A, we get

$$A = \frac{\sigma_s}{k_s} V_0 - \frac{R_s}{\mathfrak{R}_m}\frac{\theta_0}{V_0}. \tag{26}$$

Substituting this value of A in Eq. (19), we find

$$\theta_{2_0} = \frac{1}{2}\frac{V_0^2}{R_s}\frac{1}{\dfrac{k_s}{\sigma_s R_s} + \dfrac{1}{\mathcal{R}_m}}. \tag{27}$$

Now V_0^2/R_s is the power P_s dissipated in the spreading resistance and $\sigma_s R_s/k_s = \mathcal{R}_s$ is the thermal resistance of the semiconductor, by Eq. (11). Thus

$$\theta_{2_0} = \tfrac{1}{2}P_s\mathcal{R}_{\text{therm}}, \tag{28}$$

where $\mathcal{R}_{\text{therm}}$ is the total thermal resistance given by Eq. (13).

The contact temperature θ_0 due to heat developed both in the barrier and in the spreading resistance is $\theta_{1_0} + \theta_{2_0}$, or from Eqs. (12) and (28),

$$\theta_0 = \mathcal{R}_{\text{therm}}(\tfrac{1}{2}P_s + P_1). \tag{29}$$

Our work so far has been restricted to the case of a static voltage applied across the rectifier. If this voltage is applied in the forward direction, $P_s \gg P_1$ at voltages required for burnout; hence

$$\theta_0 = \tfrac{1}{2}\mathcal{R}_{\text{therm}}P, \qquad \text{(forward direction)} \tag{30}$$

where P is the total power dissipated. In the blocking direction, P_1 is larger than P_s.

If burnout is caused by high-frequency alternating currents, our result for the static case may be taken over directly since skin effect in the semiconductor is negligible even at the contact. This is proved in Appendix B. In this case, however, barrier dissipation plays only a minor role. In the forward direction Eq. (30) still applies, and in the reverse direction the barrier capacitance shunts most of the current around the barrier into the spreading resistance. Thus, Eq. (30) applies to burnout by microwave power.

The thermal resistance of the semiconductor is obtained directly from Eq. (4·34) by substituting the thermal conductivity k_s for the electrical conductivity σ. We get

$$\mathcal{R}_s = \frac{1}{4k_s a}, \tag{31}$$

where a is the contact radius. The thermal resistance $\mathcal{R}_m$ of the cat whisker is more difficult to estimate. The calculation of temperature has so far been based on the assumption of a steady state, and the time from the beginning of power application to the point where a steady state is nearly attained has not yet been estimated. It will appear later that the contact of average dimensions will reach a nearly steady temperature after a time of about one microsecond. At this time, heat from the contact has not yet penetrated appreciably into the cylindrical part of the whisker stem; hence as far as the contact temperature is concerned

the whisker is properly treated as an infinite cone. In this case, its resistance may be estimated by approximating its surface by a one-sheet hyperbola of revolution asymptotic to the cone. Its resistance then turns out to be

$$R_m = \frac{1}{4k_m a \tan \psi/2}, \tag{32}$$

where ψ is the half-angle of the cone (see Fig. 8·1).

For times of 10^{-4} sec or longer, the resistance of the cylindrical stem of the cone must be added. This will be

$$\mathcal{R}_m]_{\text{stem}} = \frac{l}{\pi q^2 k_m}, \tag{33}$$

if no wax surrounds the whisker and

$$\mathcal{R}_m]_{\text{stem}} = \frac{1}{\pi q}\left[\frac{ln\left(\frac{p}{q}\right)}{2k_m k_w}\right]^{1/2} \tag{34}$$

otherwise.

Here q is the radius of the stem, p the radius of the wax coating, k_w the thermal conduction of the wax, and l the length of the stem. Equation (34) was first derived by Gant[1] under the assumption that the heat conducted by the metal wire to its support is small compared with the heat conducted away from the surface of the wire by the wax filler.

Although for very long times (several seconds) the effect of other parts of the cartridge must also be considered, the discussion will for the most part, be restricted to times of the order of 1 μsec or less. The steady-state solution is then given by Eq. (29) or Eq. (30) with $\mathcal{R}_{\text{therm}}$ given by Eqs. (13), (31), and (32),

$$\mathcal{R}_{\text{therm}} = \frac{1}{4a(k_s + k_m \tan \psi/2)}. \tag{35}$$

Now[2]

$$k_s = 0.2 \frac{\text{cal}}{\text{sec-°C-cm}} \qquad \text{for silicon or germanium}$$

and

$$k_m = 0.4 \frac{\text{cal}}{\text{sec-°C-cm}} \qquad \text{for tungsten.}$$

If we take $\psi = 30°$ and $a = 10^{-3}$ cm,

$$\frac{\theta_0}{P} = \frac{1}{2}\mathcal{R} = 100°\text{C/watt}$$

and is proportionally larger for smaller radii.

[1] D H. T. Gant, ADRDE Research Report No. 226, July 9, 1943.

[2] This value of k_s was determined by measurements made by K. Lark-Horovitz (private communication).

A circular contact has been assumed in these calculations. In Appendix C, it is proved that the semiconductor resistance offered by an elliptical contact of semiaxes a and $b(a > b)$ is

$$\mathcal{R}_s = \frac{K}{2\pi k_s a}, \tag{36}$$

where K is the complete elliptic integral of the first kind with modulus $k = \sqrt{1 - b^2/a^2}$. If $a \gg b$,

$$K \approx \ln \frac{4a}{b}. \tag{37}$$

If the cat whisker in this case is assumed to have the shape of a wedge of half-angle ψ, its resistance can be shown to be about

$$\mathcal{R}_m = \frac{K}{2\pi k_m a \tan \psi/2}. \tag{38}$$

The total thermal resistance can then be made very small by making a large. On the other hand, the rectifying properties of such a contact should be comparable to those of a circular contact of radius equal to the short semiaxis b. In Chap. 4 rectification and conversion efficiency were found to depend on the product ωCR_s, where ω is $2\pi \times$ frequency, C is the barrier capacitance, and R_s is the electrical spreading resistance. The area of the elliptical contact is πab and so its capacitance [see Eq. (4·17)] is

$$C = \frac{\epsilon \pi ab}{D}, \tag{39}$$

where D is the thickness of the barrier layer and ϵ the permittivity of the semiconductor. Thus, for a long thin contact,

$$\omega CR_s = \frac{\epsilon \omega b \ln \dfrac{4a}{b}}{2\sigma D}, \tag{40}$$

and for a circular contact of radius b,

$$\omega CR_s = \frac{\pi}{4} \frac{\epsilon \omega b}{\sigma D}. \tag{41}$$

These quantities are of the same order for the same b even for fairly large ratios of a to b. Thus a long thin contact has the desirable property of being able to withstand larger power dissipation, yet still give good performance as a rectifier or converter. Unfortunately it has not yet been possible to manufacture crystals with such contacts. The difficulty arises from the fact that the eccentricity of the contact ellipse must be very large for the effect to be pronounced. As an example let us con-

sider the elliptical contact with twice the power-handling capacity of a circular contact of radius $\bar{a}$. The supposition is that the two contacts are equally good rectifiers, hence ωCR_s is the same for each. The result is that the elliptical contact must have its long semiaxis $a = 6.6\bar{a}$ and its short semiaxis $b = 0.3\bar{a}$ and thus $a/b = 22$. Such a contact is difficult to construct.

An alternative is to construct a rectifier with a number N of small rectifying contacts. If the separation of neighboring contacts is large compared with the diameter of a contact, the product ωCR_s for the whole rectifier is just the same as for an individual contact. On the other hand, the thermal resistance $\mathcal{R}_{\text{therm}}$ will decrease inversely with N. An improvement in burnout of a factor of 2 could be achieved with only two parallel contacts. This is perhaps easier to construct than a single very long thin contact.

8·3. Burnout Theory. *Contact Temperature as a Function of Time.*—The theory in the preceding section applies to the steady-state solution of the thermal-continuity equation. As will appear later, this solution is not valid if the time elapsed since the application of power is less than 10^{-6} or 10^{-7} sec. Since burnout is now believed to be usually the result of very short pulses of the order of 10^{-9} or 10^{-8} sec in duration, it is obviously important to examine the solution for these cases.

If the time is so short that no heat has appreciably diffused away from the locality where it was generated, the temperature is given by the amount of heat generated per unit volume divided by the thermal capacity C per unit volume, or

$$\theta = \frac{1}{C}\int_0^t Q\,dt, \tag{42}$$

where Q is the rate of generation of heat per unit volume. This result can be directly obtained from the thermal-continuity equation [Eq. (1)] by suppressing the conduction term $\nabla \cdot k\nabla\theta$. Difficulties arise, however, if an attempt is made to apply Eq. (42) to the usual contact between the metal cat whisker and the semiconductor. It turns out that Q becomes infinite at the periphery of the contact because of the crowding of lines of current flow; Eq. (42) would then predict an infinite temperature there, which is, of course, absurd.

The trouble is that it is not right to suppress the conduction term in Eq. (1) near a singularity in Q. At the periphery of the contact there is no time t so short that conduction can be neglected. Equation (42) should hold well, however, at distances from the edge large compared with the radius of the contact. Clearly a separate investigation of the temperature near the periphery is necessary. To do this we must first find out how Q, the heat generated per unit volume, depends on position, especially near the periphery.

The potential distribution in the semiconductor must first be found. The contact area, circular in shape, will be assumed equipotential. It is convenient to introduce spheroidal coordinates in the following way.

Figure 8·3 shows a section through the center of the contact containing the axis of symmetry. The origin of rectangular coordinates (x,y,z) is taken at the center of the contact; the plane $x = 0$ is coincident with the contact surface and the positive x-direction is into the semiconductor. Spheroidal coordinates ξ, ζ and Ω are defined in such a way that Ω is the longitude angle;

$$\frac{x^2}{a^2\zeta^2} + \frac{\rho^2}{a^2(1 + \zeta^2)} = 1 \quad (43)$$

and

$$-\frac{x^2}{a^2\xi^2} + \frac{\rho^2}{a^2(1 - \xi^2)} = 1 \quad (44)$$

define ζ and ξ. Here $\rho^2 = y^2 + z^2$. Equation (44) is the equation of a family of one-sheet hyperboloids of revolution and Eq. (43) is the equation of an orthogonal family of oblate spheroids, a particular member of which, $\zeta = 0$, is a flat disk of radius a coincident with the contact surface. Since the contact surface is equipotential, the potential V will be assumed to depend only on ζ. Laplace's equation for V is[1] then

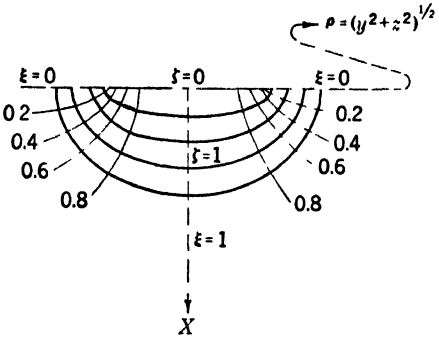

FIG. 8·3.—Section through the contact showing coordinate systems used.

$$\frac{\partial}{\partial\zeta}(1 + \zeta^2)\frac{\partial V}{\partial\zeta} = 0. \quad (45)$$

Integrating, we obtain

$$V = A \tan^{-1}\zeta + B, \quad (46)$$

where A and B are integration constants. If we take $V = V_0$ at $\zeta = \infty$ and $V = 0$ at the contact ($\zeta = 0$), we obtain

$$V = V_0 \frac{2}{\pi} \tan^{-1}\zeta. \quad (47)$$

To find Q we must find ∇V, which is[2] given by

$$\nabla V = \frac{1}{a}\left(\frac{1 + \zeta^2}{\xi^2 + \zeta^2}\right)^{1/2}\frac{dV}{d\zeta}$$
$$= \frac{2V_0}{\pi a}\frac{1}{\sqrt{(1 + \zeta^2)(\xi^2 + \zeta^2)}} \quad (48)$$

[1] See, for example, W. R. Smythe, *Static and Dynamic Electricity*, 1st ed., McGraw-Hill, 1939, Sec. 5·27.

[2] *Ibid.*, Secs. 3·3 and 5·27.

and from Eq. (2), the heat generated per unit volume is

$$Q = \frac{4V_0^2\sigma}{\pi^2 a^2}\frac{1}{(1+\zeta^2)(\xi^2+\zeta^2)}$$
$$= \frac{P}{\pi^2 a^3(1+\zeta^2)(\xi^2+\zeta^2)}, \tag{49}$$

where P is the total power V_0/R_s dissipated in the spreading resistance; $R_s = 1/4\sigma a$. As an auxiliary coordinate r is introduced as the distance from the periphery to some point (x,ρ) in the semiconductor. Evidently,

$$r^2 = x^2 + (\rho - a)^2. \tag{50}$$

Solving Eqs. (43) and (44) for x and ρ, substituting in Eq. (50) and using the approximation, $\zeta \approx 0$ and $\xi \approx 0$, we find

$$r \approx \frac{a}{2}(\zeta^2 + \xi^2). \tag{51}$$

For $\zeta \approx 0$ and $\xi \approx 0$, we find from Eqs. (49) and (51)

$$Q \approx \frac{P}{2\pi^2 a^2 r}. \tag{52}$$

Thus Q is observed to approach ∞ as r approaches zero.

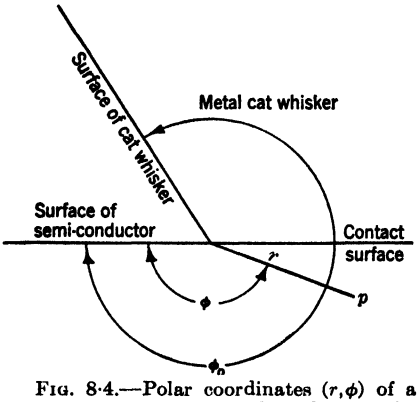

FIG. 8·4.—Polar coordinates (r,ϕ) of a generic point (p) near the edge of the contact.

With this expression for Q we may now solve the thermal-continuity equation for points near the periphery $(r \ll a)$. In this region the curvature of the periphery may be neglected and the edge of the contact may be taken as a straight line. Our coordinates are r and ϕ, the polar angle, as illustrated in Fig. 8·4. The surface of the metal cone makes an angle ϕ_0 with the extension of the surface of the semiconductor.

If it is assumed that k is independent of position, the thermal-continuity equation now becomes

$$k\nabla^2\theta + Q = C\frac{\partial\theta}{\partial t}, \tag{53}$$

where

$$\left.\begin{aligned} &Q = 0 \quad \text{in the metal } (\pi < \phi < \phi_0),\\ &Q = \frac{P}{2\pi^2 a^2 r} \quad \text{in the semiconductor } (0 < \phi < \pi),\\ &\text{and the Laplacian}\\ &\nabla^2 = \frac{\partial^2}{\partial r^2} + \frac{1}{r}\frac{\partial}{\partial r} + \frac{1}{r^2}\frac{\partial^2}{\partial \phi^2}. \end{aligned}\right\} \tag{54}$$

The pulse power P is assumed constant (flat pulse) and dissipation in the barrier layer neglected. The results should apply then either to d-c power in the forward (conducting) direction or to microwave power. Since only order of magnitude is desired, k and C are, for simplicity, assumed to be the same in metal and semiconductor and are independent of temperature, and ϕ_0 is assumed to equal 2π.

These approximations introduce little error. The final result is expressed as the ratio of the temperature at some point on the contact to the equilibrium value of this temperature. This ratio depends only on the thermal diffusitivity, $\kappa = k/C$, which is about the same in silicon and tungsten. Also the assumption $\theta_0 = 2\pi$ is not far from the truth, since the whisker tends to mushroom out at the edge of the contact.

The solution of Eq. (53) is desired that satisfies the boundary conditions:

$$\left.\begin{aligned} &\text{at } \phi = 0 \text{ or } 2\pi, && \frac{\partial\theta}{\partial\phi} = 0; \\ &\text{at } r = \infty, && \theta = 0; \\ &\text{at } t = 0, && \theta = 0. \end{aligned}\right\} \tag{55}$$

The required solution may be found by the usual methods.

For points on the contact surface ($\phi = \pi$) the solution reduces to

$$\theta = \frac{P\sqrt{\pi\kappa t}}{4\pi^2a^2k}\left[f\left(\frac{r^2}{8\kappa t}\right) - \sqrt{\frac{r^2}{\pi\kappa t}}\right], \tag{56}$$

where $\kappa = k/C$ is the thermal diffusivity, and

$$f(x) = e^{-x}[(1 + 2x)I_0(x) + 2xI_1(x)]; \tag{57}$$

$I_n(x)$ is the modified Bessel function of order n, that is, $I_n(x) = j^{-n}J_n(jx)$. For $r^2/8\kappa t \ll 1$,

$$\theta \approx \frac{P\sqrt{\pi\kappa t}}{4\pi^2a^2k}, \tag{58}$$

and for $r^2/8\kappa t \gg 1$,

$$\theta \approx \frac{1}{C}\frac{Pt}{4\pi^2a^2r}. \tag{59}$$

This last result is exactly that given by Eq. (42), since by Eq. (52) $P/(4\pi^2a^2r)$ is one-half the rate of evolution of heat per unit volume in the semiconductor at a distance r from the contact edge. The factor $\frac{1}{2}$ is explained by the fact that the temperature has been evaluated on the contact surface. Since no heat is generated in the metal and an amount Q per unit volume is generated in the semiconductor, the average value $\frac{1}{2}Q$ is effective on the surface.

The general character of the temperature-time relation is now evident. For any point near the edge, but not actually on it, the temperature is proportional to the energy dissipated, namely, $W = Pt$, for sufficiently

short times. As the time increases, the temperature rises less swiftly, eventually becoming proportional to the square root of the time. According to the present solution the temperature should continue to increase without limit. The reason this catastrophe does not occur is that this solution holds only provided the heat evolved in the semiconductor has not had time to diffuse over a distance comparable with the contact dimensions. For longer times ($t > a^2/\kappa$) the neglect of the curvature of the contact periphery is no longer valid. The general qualitative result is then

$$t \ll \frac{r^2}{\kappa}, \qquad \theta \propto Pt = W \tag{60}$$

$$\frac{a^2}{\kappa} \gg t \gg \frac{r^2}{\kappa}, \qquad \theta \propto P\sqrt{t} = \frac{W}{\sqrt{t}} \tag{61}$$

$$t \gg \frac{a^2}{\kappa}, \qquad \theta \propto P. \tag{62}$$

In the last case θ is given by Eq. (30) for $t \approx 1$ μsec.

In Fig. 8·5 the temperature is plotted in units of the steady-state temperature, Eq. (30), as a function of the time for a number of values of r. Equation (35) has been used for $\mathcal{R}_{\text{therm}}$ in Eq. (30) and, in accordance with our present assumption, $k \approx k_s = k_m$ and $\psi = 90°$. This gives, for the steady-state temperature,

$$\theta_0 = \frac{1}{16}\frac{P}{ak}. \tag{63}$$

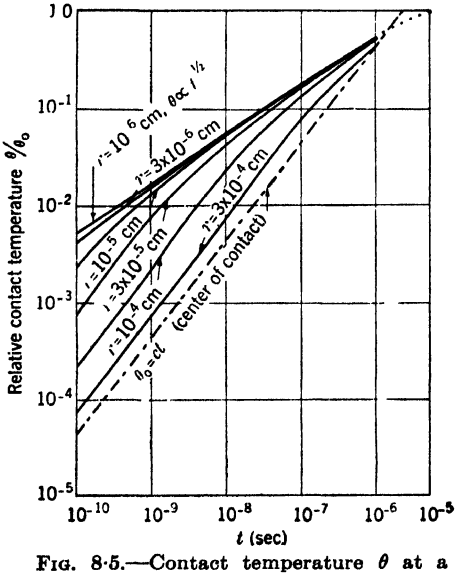

FIG. 8·5.—Contact temperature θ at a point near the periphery as a function of the time since power was applied.

In plotting these curves a has been put equal to 10^{-3} cm, which is appropriate to a fairly large contact, about that used for high-burnout crystals designed for the 10-cm band. It should be noted that θ/θ_0 is proportional to $1/a$. Also, κ has been taken equal to 0.54 cm²/sec, which is the mean of the values of κ for tungsten ($\kappa = 0.62$ cm²/sec) and for silicon ($\kappa = 0.46$ cm²/sec). The ratio θ/θ_0 depends on k and C only through $\kappa = k/C$, hence separate values need not be assumed for them.

The dashed line in Fig. 8·5 is a plot of Eq. (59) for the temperature-time relation at the center of the contact. This equation holds only for

small times ($t \ll a^2/\kappa$), but it has been extrapolated to the equilibrium temperature.

These curves should apply up to times of the order of a^2/κ ($\approx 10^{-6}$ sec in our example) or, equivalently, they apply provided $\theta/\theta_0 \ll 1$. The solution for longer times is probably like that given by the broken line in Fig. 8·5. The temperature should reach an equilibrium value at about 5×10^{-6} sec for a contact of this size (10^{-6} cm radius). For a contact of average size the time required for the steady state is closer to 1×10^{-6} sec.

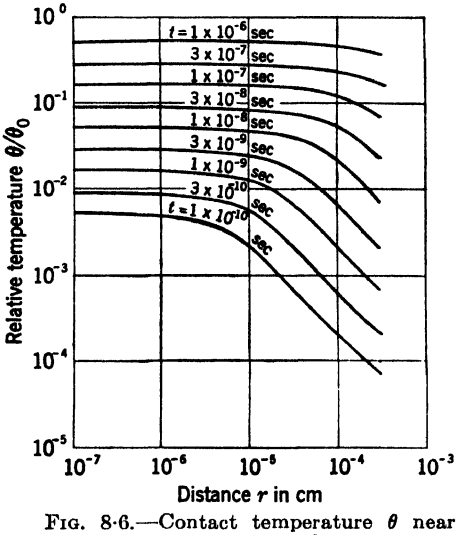

FIG. 8·6.—Contact temperature θ near the periphery as a function of distance r from periphery.

An interesting result of this analysis is that at first the temperature rises much more rapidly at the edge than near the center of the contact. In Fig. 8·6 the temperature is given as a function of the distance r from the edge of the contact for a number of time intervals. For any time interval the temperature is a maximum at the edge and decreases as r increases. As the time increases, the temperature at any point increases and, as a function of r, is fairly constant up to about $r = \sqrt{\kappa t}$, beyond which it starts to drop off.

These results are qualitatively in accord with the observations of Pfann (see Sec. 8·1) and explain why Pfann observed deterioration of only the edge of the contact for short pulses (up to 10^{-6} sec duration), whereas for long pulses (several seconds duration) the whole contact area is affected. The suggestion has been made that edge burnout may be due to skin effect at the contact, but in Appendix B it is shown that the differential heating between edge and center caused by skin effect is negligible at all microwave frequencies. Furthermore Pfann finds the same effects for short d-c pulses (up to 10^{-6} sec).

Tendency to edge burnout is aggravated by the fact that at above 700°C the conductivity of silicon increases rapidly with temperature because of excitation of electrons from the filled band to the conduction band (see Sec. 3·1). These temperatures will be reached first at the edge of the contact, and the resulting increase in conductivity there will increase the flow of current near the edge relative to that at the center of the contact. Since all parts of the contact are effectively in parallel, an increase in conductivity of the edge relative to the rest of the contact

will lead to a relative increase in power dissipation and hence to an increase in temperature at the edge.

It is evident from Fig. 8·6 that pulses of duration 10^{-8} sec or less (such as TR-switch spikes) will cause large temperature differentials between edge and center of the contact. The conventional geometry of the contact is therefore most unfavorable from the point of view of burnout by short pulses. An ideal contact geometry completely eliminating this difficulty is that of a hemisphere of metal whisker embedded in the semiconductor as illustrated in Fig. 8·7. Such a contact might be formed by passing large currents through the rectifier at assembly, thus melting the semiconductor around the whisker tip. Further research is required to learn whether such a process will be successful for silicon. Contacts of this nature have been made by H. Q. North in the case of platinum-germanium contacts (see Chap. 13), but it has not yet been determined whether the expected improvement in short-pulse burnout actually results.

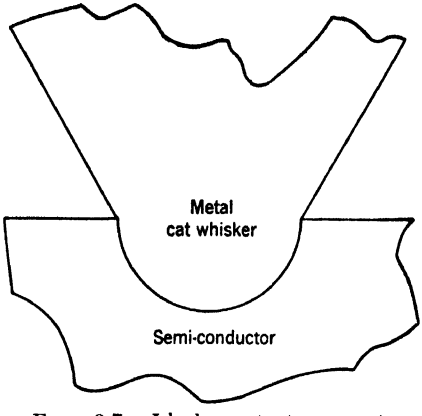

FIG. 8·7.—Ideal contact geometry from the point of view of burnout by short pulses.

Abnormal heating, such as occurs near the edge of the contact, may also occur at other points if the whisker does not make firm electrical contact over the whole surface or if there are surface irregularities where current-flow lines tend to concentrate. It has, in fact, been proved that a smooth, highly polished semiconductor surface is superior to a rough surface with regard to burnout.

Thermal Relaxation Time.—For any point in the semiconductor, except right at the edge of the contact, there always exists a time τ such that for $t \ll \tau$ the temperature is proportional to the total dissipated energy W. Also for sufficiently long intervals after application of continuous power, $t \gg \tau$, the temperature is proportional to the power P (assumed constant). The validity of test specifications for burnout in crystals and for leakage energy and power in TR tubes is uncertain unless the order of magnitude of τ is known. Obtaining an estimate of this quantity is therefore of great importance.

The definition of the relaxation time τ can be made precise by taking τ to be the time required to reach the steady-state temperature if the temperature were to continue to rise at its initial rate. For a point near the periphery we obtain from Eqs. (59) and (63)

$$\tau_p = \frac{\pi^2}{4}\frac{a}{\kappa}r, \qquad (r \ll a), \tag{64}$$

where we have taken $\psi = 90°$. On the other hand for the center point of the contact we have, from Eqs. (42) and (49), since $\zeta = 0$ and $\xi = 1$ at the center,[1]

$$\theta_0 = \frac{Pt}{2\pi^2 a^3 C} \qquad (t \ll \tau). \tag{65}$$

With Eq. (63) this gives for τ at the center,

$$\tau_c = \frac{\pi^2}{8}\frac{a^2}{\kappa}. \tag{66}$$

Evidently,

$$\tau_p = 2\tau_c\left(\frac{r}{a}\right) \qquad (r \ll a). \tag{67}$$

The relaxation time is seen to depend linearly on the distance r from the edge of the contact.

What effective value of r should be used to obtain a value of τ appropriate to the whole contact is difficult to decide. As a guess let us take 10^{-5} cm $< r < 10^{-4}$ cm. Then, if $a = 10^{-3}$ cm and $\kappa = 0.54$ cm^2/sec,

$$\tau_c = 2.3 \times 10^{-6} \text{ sec}, \tag{68}$$

and

$$4.6 \times 10^{-8} \text{ sec} < \tau_p < 4.6 \times 10^{-7} \text{ sec}. \tag{69}$$

It should be noted that τ_p is proportional to the first power, and τ_c to the square, of the contact radius.

The predominant cause of crystal burnout in practice is believed to be the TR-switch spike, which has a duration of about 2 to 3 $\times 10^{-9}$ sec. Since this period is shorter than our lowest estimate or τ_p it is probably the *energy* of the spike rather than its peak power that is effective in burnout. However, this reasoning applies to a contact of large dimensions ($a = 10^{-3}$ cm), appropriate to high-burnout 10-cm band rectifiers. For a 1-cm band rectifier $a \approx 10^{-4}$ cm and τ_p may be smaller than the spike duration.

At present, it is almost universal practice to assess the protection offered by TR tubes by the amount of leakage spike energy. The preceding considerations indicate that this protection may not be adequate for crystals of small contact dimensions. Our estimate of τ_p is, however, only a guess since the effective value of r is unknown. In the next

[1] The factor 2 in the denominator of Eq. (65) is required because θ_0 is the *contact* temperature. In the metal whisker no heat is developed; in the semiconductor the heat-developed Q is given by Eq. (49); at the contact the mean value $Q/2$ applies.

section some experiments are described which indicate that the effective relaxation time for 1N21 rectifiers (contact radius 2 or 3 $\times$ 10^{-4} cm) is about 10^{-8} sec.

In the case of crystals designed for use as video detectors, no TR switch is used; burnout is caused by pulses of the order of 10^{-6} sec; hence the theory of the steady-state temperature applies, and it is the *power* rather than the *energy* of the pulse that is important.

8·4. Experiments on Burnout.—In this section some experiments are described which throw light on the nature of burnout and make possible an estimation of some of the constants involved in the theory outlined in Secs. 8·2 and 8·3.

Burnout by Continuous D-c Power.—In 1942 some careful work was done by Lawson and his collaborators at the University of Pennsylvania[1] on burnout as a result of the application of continuous d-c power under carefully controlled conditions.

A silicon cube about 5 mm on a side cut from an ingot obtained from the Bell Telephone Laboratories was plated with iron on one side and mounted on a lead matrix with the plated side in contact with the lead. Next, the surface opposite the plated side was ground and polished to a mirror finish, then etched with hot NaOH solution before each burnout test. Following this, the cube of silicon with its mounting was placed inside a bell jar on a table. A short straight piece of 7-mil tungsten wire was carefully pointed and mounted in a pin vise and arrangements made to press the point with a controlled and known force against the silicon surface. No tapping was used. The d-c characteristic, especially in the forward direction, was found to be remarkably reproducible when different points were pressed with the same force on different parts of the surface. Furthermore, it was found that the area of the contact surface, as determined by microscopic measurements of the diameter of the squashed point after removal, was definitely related to the force with which the point had been pressed against the surface. The radius of the point could then be ascertained from a knowledge of this force and of the force-area relationship.

A fairly definite although rather artificial criterion for burnout was established. It was discovered that the resistance R_1 of the rectifier at 1 volt in the reverse direction depended on the amount of overload power P previously applied in either direction. This resistance R_1 at first increased with the overload, reached a maximum, and thereafter decreased sharply. A contact was deemed "burned out" when this final sharp decrease occurred. It was later established that the conversion

[1] A. W. Lawson *et al.*, "DC Burnout Temperature in Silicon Rectifiers," NDRC 14-113, Univ. of Penn., Nov. 1, 1942.

efficiencies of cartridge rectifiers that had been "burned out" in this way were definitely deteriorated.

Three methods were used to find the temperature at the contact at burnout. In the first method the temperature was measured with a thermojunction welded to the cat whisker about 1 mm from the contact. This device did not directly measure the temperature at the contact and had to be calibrated by heating the whole cube of silicon up to a known temperature and comparing this temperature with the emf of the thermocouple. These measurements indicated that the temperature at burnout was 500° ± 100°C.

In the second method the amount of overload power required to reach the burnout point was measured as a function of the base temperature of the silicon block. After each measurement the probe was removed, the silicon surface etched, and a new contact of the same dimensions was formed and tested at a higher base temperature in the forward direction. The power required for burnout was found to decrease linearly with the base temperature of the block (which was raised as high as 300°C). By extrapolation of this straight line it was found that, at a temperature of 490°C, no power would be required for burnout. The presumption is then that 490°C is the burnout temperature of the contact.

The third method made use of the results of the theory of Sec. 8·2. According to Eqs. (29) and (35) the steady-state contact temperature is given by

$$\theta = \frac{\frac{1}{2}P_s + P_1}{4a(k_1 + k_2 \tan \psi/2)}, \tag{70}$$

where P_s is the power dissipated in the spreading resistance, P_1 the power dissipated in the barrier, a the radius of the contact, k_1 and k_2 the thermal conductivities of the semiconductor and whisker, and ψ the half-angle of the conical whisker tip. This equation was applied to burnout by power applied in the forward direction; here $P_1 = 0$ and $P_s = I^2R_s$, where I is the electric current. The equation was also applied to the case of power in the reverse direction, where $P_1 = I^2R_1$ and $P_s = I^2R_s$ and R_1 is the barrier resistance. The spreading resistance R_s was measured from the forward current-voltage characteristic and the barrier resistance in the back direction R_1 was taken to be the difference between the total resistance and R_s. When proper account was taken of Peltier heat (which is abnormally large in semiconductors) the temperature at burnout given by Eq. (70) was found to be the same, within experimental error, irrespective of the direction of the applied overload voltage; it was equal to 470° ± 40°C. The Peltier heat accounted for an increase of 30°C in the calculated temperature for forward burnout and a decrease of the same amount for back burnout. The final result is in good accord with the directly measured burnout temperature. This agree-

ment, however, is somewhat marred by the fact that two errors were made in the calculation. These errors are in opposite directions and it is not unlikely that they almost cancel. One error involved using a value of k_1 one-half the presently accepted value (0.84 watts/cm-°C), and the other error resulted from neglect of the thermal resistance of the cylindrical whisker stem. As shown in Sec. 8·2 this neglect is valid for pulses of 1 μsec duration or less, but in the present case of continuous power the stem resistance cannot be neglected. It can be shown that the two errors would cancel if the stem of the probe had a length of 3.3 mm. The actual length was somewhat longer than this but, if radiation effects are allowed for, the effective length might well have been about 3 or 4 mm.

Some general features of the theory were confirmed in these investigations. For example, from Eq. (27) it is noted that for the same applied forward voltage V_0 the contact temperature is independent of the contact radius. Lawson *et al.* found that burnout occurred at the same forward voltage, 6.6 ± 0.7 volts, regardless of the force pressing the whisker against the silicon and consequently regardless of the contact radius. In the reverse direction, the voltage required for burnout depended on the applied force, as is to be expected, considering the effect of the barrier layer, but the burnout temperature according to Eq. (70) was found to be approximately independent of the force and hence of the contact radius.

Burnout by Short D-c Pulses.—According to the theory of Sec. 8·3 there should exist a time τ such that, for pulse durations small compared with τ, the contact temperature is proportional to the energy W of the pulse and does not depend explicitly on its duration. On the other hand uniform pulses of duration long compared with τ should result in a contact temperature proportional to the power P of the pulse. In Sec. 8·3 we defined τ to be the time required to attain the steady-state temperature if the temperature continued to rise at its initial rate. An alternative definition is obtained on the following basis:
for pulse duration $t \ll \tau$,

$$\theta = AW = APt, \tag{71}$$

and for $t \gg \tau$

$$\theta = BP = \frac{BW}{t}, \tag{72}$$

where A and B are proportionality constants. Let us plot the energy W required to produce a certain definite deterioration of the rectifier against the pulse duration t. The resulting curve should have the general appearance of the solid curve of Fig. 8·8. The required pulse energy W should be constant for small t and proportional to t for long t. The intersection of these two asymptotes of the curve defines a time τ which

can be called the relaxation time of the contact. It is easily seen that the two definitions of τ are equivalent provided the amount of deterioration is determined by the contact temperature and not by the time.

In order to measure τ according to this second definition the following experiment was performed, using an apparatus shown schematically in Fig. 9·35. A coaxial-line condenser of adjustable length l and characteristic impedance Z_0 was charged by a d-c supply to a known voltage V. By means of the switch S the condenser could be quickly connected to the terminals of a crystal rectifier, which would then terminate the coaxial line. If the impedance of the rectifier matches the line impedance Z_0, a single pulse of magnitude $V/2$ and duration $2l/c$, where c is the velocity of light, is applied to the rectifier. The energy dissipated in the rectifier is equal to the potential energy $W = \frac{1}{2}CV^2$ of the condenser before discharge. Here C is the capacitance of the coaxial line. If the rectifier resistance R does not match the line impedance, a succession of pulses each of duration $2l/c$ and of decreasing amplitude results; but if

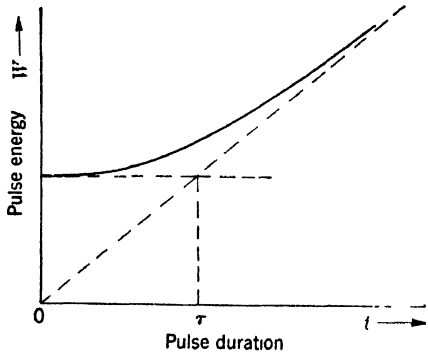

FIG. 8·8.—Pulse energy W required for a given deterioration as a function of pulse duration t.

$$\tfrac{1}{2}Z_0 < R < 2Z_0,$$

90 per cent or more of the total available energy $\frac{1}{2}CV^2$ will be dissipated in the first pulse.

The experimental procedure was as follows:

1. A number of silicon rectifiers of standard type, all made by the same manufacturer, were collected and divided arbitrarily into groups of 10. The loss and noise temperature of each crystal was measured and the noise figure F of a receiver with an amplifier of 5 db noise figure was calculated from these data for each crystal. The mean value of F was found for each group of 10 crystals.
2. The coaxial line charged to a given energy and adjusted to a given length was discharged into one group. After remeasurement of F, the same group was exposed to a pulse of higher energy and again remeasured. This procedure was continued until the average deterioration in F was more than 6 db.
3. The process outlined in (2) was applied to a second group of units with the sole difference that the line length was increased by a factor of approximately 2.

4. The process was repeated with the other groups successively, increasing the line length and therefore the pulse duration by a factor of about 2.

A large amount of data was recorded, but the general result is well represented by the data giving the amounts of energy and power required to produce an average deterioration in F of 3 db. These data are given in Table 8·1.

TABLE 8·1.—PULSE ENERGY W AND POWER P REQUIRED FOR 3-DB DETERIORATION IN NOISE FIGURE AS A FUNCTION OF PULSE DURATION t

T (sec $\times 10^{-9}$)	2.3	3.9	7.0	13.0	26.0
W (ergs)	0.76	0.81	0.61	0.50	1.49
P (watts)	33	21	8.7	3.8	5.7

As is evident from the table, the energy required for 3-db deterioration for short pulses is nearly independent of pulse duration but increases sharply at $t = 2.6 \times 10^{-8}$ sec. On the other hand the required pulse power P decreases with pulse duration at first and becomes roughly constant after $t = 1.3 \times 10^{-8}$ sec. The relaxation time appears, therefore, to be about 1 or 2×10^{-8} sec.

In this experiment, the impedance of the coaxial line was 50 ohms, its capacitance per centimeter of length was about 1 $\mu\mu$f, and a pulse energy of 1 erg corresponded to a charging voltage of 90 volts for the shortest length used. The voltage was applied to the crystal in the forward direction; it may be assumed that, at the high voltages used, the resistance of the crystal is the spreading resistance of the semiconductor, which for the crystals used was between 25 and 50 ohms.

In these experiments only one pulse was applied at each power level. It is known that smaller energies and powers are required for the same deterioration when multiple pulsing is used, but the available data bearing on this point are not extensive. According to reports from England, the energy per pulse required for a given deterioration is less by a factor of 3 to 5 for 10^5 pulses than for a single pulse. The pulse repetition frequency in this work was 100 pps.

It was established at the Radiation Laboratory that after one pulse causing appreciable deterioration the effect of a similar additional pulse is negligible, but that 10^3 additional pulses of the same energy almost doubles the deterioration of the first. After this, still further pulses (10^4) of the same energy may either produce still more deterioration or may have little additional effect, depending on the unit tested.

8·5. Burnout Limitations of Standard Crystal Units.—The following estimates of burnout limitations of standard crystal units must be regarded as crude. As mentioned above, there is a decided lack of

uniformity with regard to burnout among crystals of a given type and closely similar properties. Furthermore, there are inherent difficulties in measuring the absorbed power or energy from microwave pulses. This is especially true for the energy of short pulses (about 10^{-8} or 10^{-9} sec). Such pulses are caused by preignition transmission through a TR tube and their energy content is subject to erratic fluctuations from pulse to pulse since there are fluctuations in the time at which ignition starts. The measured pulse energy is only the average energy of a large number of pulses. A single pulse of abnormal energy, however, may be the sole cause of any deterioration observed. In the case of d-c pulses from a coaxial-line discharge, the amount of pulse energy is less uncertain. Experience shows that multiple d-c pulses have a more drastic effect than a single pulse of the same energy. As a rule of thumb, it may be stated that the amount of energy per pulse required to produce a given deterioration is greater for a single pulse by a factor of 5 or 10 than for a large number, for example 10^5 or 10^6 pulses. This remark applies to d-c pulses but it probably holds as well for microwave pulses.

In Table 8·2 are some burnout data for the principal mixer crystal types. The first column gives the RMA number of the crystal type; the second, the wavelength band for which the crystal type was designed; the third, the energy of the single d-c pulse applied according to specifications as a proof test; the fourth, the energy of a single d-c pulse required on the average to produce a noticeable permanent deterioration of a unit; and the fifth, gives in order of magnitude the energy per pulse of a large number (10^5 or 10^6) of pulses, either d-c or microwave, required for a noticeable permanent deterioration of a unit, according to the above-mentioned rule.

TABLE 8·2.—BURNOUT PULSE ENERGIES FOR STANDARD CRYSTAL TYPES

Type	Band, cm	Proof Test, ergs	Burnout limit, ergs	Multiple pulse burnout limit, ergs
1N28	10	5	20	2–4
1N21B	10	2	5	0.5–1
1N23B	3.2	0.3	2	0.2–0.4
1N26	1.25	0.1	0.2	0.02–0 04

Table 8·3 gives the minimum absorbed power (average absorbed power of a single pulse) required to produce a noticeable permanent deterioration for a number of crystal types. These estimates apply specifically to exposure times of one or two minutes to microwave pulses of duration about 1 μsec at a repetition frequency of about 1000 pps. Burnout is not sensitive, however, to either exposure times or repetition frequencies.

TABLE 8·3.—BURNOUT PULSE POWER FOR STANDARD CRYSTAL TYPES

Type	Band, cm	Pulse power, watts
1N25	30	15
1N28	10	5
1N21B	10	2.5
1N23B	3 2	1 5
1N26	1.25	0.5

It is interesting to observe that the microsecond pulse power required for burnout is roughly proportional to the appropriate wavelength, whereas the short-pulse energy required for burnout is roughly proportional to the square of the wavelength. In making this observation the data applying to the 1N28 rectifier are taken to be appropriate to the 10-cm band since the 1N28 has about the same conversion properties as the 1N21B but is designed to have as high a burnout level as possible without regard to impedance considerations. The 1N21B, on the other hand, has the highest burnout level consistent with certain impedance requirements based on the existence of large numbers of fixed-tuned mixers in field use. The crystal types for use at shorter wavelengths are perhaps more comparable to the 1N28 than to the 1N21B in respect to these design considerations.

This dependence of burnout level on wavelength is just that predicted by the theory of Secs. 8·2 and 8·3. According to Eq. (63) the microsecond pulse power required for a given contact temperature is proportional to the contact radius. On the other hand, the product ωCR_s determining the conversion loss is proportional to the ratio of contact radius to wavelength [Eq. (4·69)]. Thus for constant conversion loss we should expect the observed proportionality between burnout power level and wavelength for the several types of rectifiers. Also according to Eq. (59) the short pulse energy required for a given contact temperature at a distance r from the contact periphery is proportional to the square of the contact radius and to r. Now the effective value of r should not depend very strongly on the contact radius with the result that, by arguments similar to the above, we expect the observed proportionality between short-pulse burnout energy and the square of the wavelength for the several crystal types.

The relaxation times τ, for the various crystal types, may be found by dividing the short-pulse energy by the long-pulse power required for burnout. In this way we get the results of Table 8·4.

The relaxation time τ is observed to be about proportional to the appropriate wavelengths (again excluding the 1N21B) in accordance with Eq. (64).

TABLE 8·4.—RELAXATION TIME τ FOR STANDARD CRYSTAL TYPES

Types	λ, cm	τ, sec
1N28	10	6×10^{-8}
1N21B	10	3×10^{-8}
1N23B	3.2	2×10^{-8}
1N26	1.25	6×10^{-9}

As a general rule the increase in receiver noise figure as a result of burnout can be attributed almost equally to increase in noise temperature and to increase in conversion loss. Like all other rules applying to burnout, this one has notable exceptions. Large increases in noise temperature sometimes occur with hardly any change in loss, sometimes even with a decrease in loss. Sometimes just the reverse is found. An almost inevitable accompaniment of an increase in either loss or noise is a decrease in the reverse d-c resistance of the rectifier. This fact has helped make possible a simple "d-c checker" for field use; this essentially measures the back resistance at 1 volt. Crystals are rejected when their back resistance falls below a value appropriate to their type and predetermined by extensive measurements on partially burned out units. The d-c crystal checker is discussed in Sec. 9·10.

The power-handling limitations of video crystal detectors have been determined by measurements at the University of Pennsylvania. The 1N32 unit, designed for use in the 10-cm band, begins to deteriorate in figure of merit at about 10 watts available power. There is probably some self-protection in this case, however. The crystals were matched to the microwave power at very low level (about 1 μw) and the available power was then increased to the point of burnout. Since the r-f impedance of the crystals is dependent on the power level, the power is mismatched at the high level. The amount of mismatch was not determined, hence all one can say is that the absorbed pulse power required for burnout is less than 10 watts.

The 1N31 unit, a video detector designed for use in the 3-cm band, begins to deteriorate in figure of merit and to change appreciably in video impedance at absorbed powers in the range of 0.1 to 0.5 watt, depending on the crystal tested. In this case the amount of self-protection was determined. In the present standard crystal holder (see Chap. 11) a power of 0.5 watt was absorbed when the available power was 1.0 watt for crystals of one manufacturer and 2.5 watts for those of another. The absorbed power for burnout is about the same in each case.

CHAPTER 9

TEST EQUIPMENT

With the advent of large-scale production of crystal rectifiers an urgent need arose for the development of standard test sets both for acceptance testing by the manufacturer and for the correlation of data obtained in the various laboratories engaged in crystal development. The Radiation Laboratory instituted a program for the design and development of standard sets for measuring crystal conversion loss and noise temperature for 1-, 3-, and 10-cm bands. The following were the design objectives:

1. Equipment that would sort out units that are inferior for use in crystal mixers in radar receivers.
2. Equipment that could be duplicated and calibrated so that measurements could be accurately reproduced from set to set.
3. Equipment capable of rapid, simple operation with a minimum number of operations per measurement.
4. Equipment easy to maintain and as foolproof as possible.

The sets that were designed met these requirements satisfactorily and have been used extensively in production testing for the 1-, 3-, and 10-cm rectifier types in current use. For detailed drawings of the r-f parts the reader is referred to the JAN specifications. The d-c "checker" described in the last section of this chapter was developed at the Radiation Laboratory in response to a need for portable test equipment that could be used in the field to sort out crystals that had deteriorated in use.

STANDARD LOSS TEST SETS

The loss sets for the three frequency bands all employ the amplitude-modulation method discussed in Sec. 7·4. The mixer is fixed-tuned to match the line from the r-f oscillator at local-oscillator frequency. Since the modulation frequency is 60 cps, the source presents the same impedance at the local-oscillator frequency and both sideband frequencies. The equipment, therefore, measures the particular conversion loss denoted in Chap. 5 by L_0. The load conductance at the modulation frequency is chosen to equal the mean conductance of the type of crystal to be measured, and a fixed d-c load is chosen. The conversion loss is then given by Eq. (7·51),

$$L_0 = \frac{4n}{(1+n)^2}\frac{m^2P}{g_b\overline{E_\beta^2}}, \tag{7·51}$$

where m is the modulation coefficient referred to the available power of the oscillator [Eq. (7·45)], P is the available power from the r-f oscillator, g_b is the load conductance at modulation frequency, E_β is the rms modulation voltage across the load, and n is the ratio of the load conductance to the i-f conductance of the particular crystal being tested.

To avoid measurement of g_β, the factor $4n/(1 + n)^2$ is assumed to be unity, Eq. (7·51) becoming

$$L_0 = \frac{m^2P}{g_bE_\beta^2}. \tag{1}$$

It has already been pointed out that the error introduced by this approximation is less than 0.5 db if $g_\beta/2 < g_b < 2g_\beta$; this error is in such a direction as to make the unit with extreme conductance seem worse than it really is. Actually most crystals are well within these limits; hence the average error is substantially less than 0.5 db. In any event the approximate value is an upper limit for conversion loss and in acceptance testing the approximation tends to reject borderline units whose i-f conductance differs widely from the mean.

Similarly the fixed tuning at radio frequency discriminates against those crystals that are poorly matched, since the available r-f power is used for P in Eq. (1). The use of fixed tuning at both radio and intermediate frequencies therefore tends to select crystals uniform in both r-f and i-f characteristics and greatly simplifies the test procedure. The r-f tuning must be carefully standardized, however, so that mixers used at the various test stations are tuned accurately alike and do not favor the characteristics of the product of some particular laboratory. For this purpose standard r-f impedances have been developed at the Radiation Laboratory; these can be inserted in the mixer in place of the crystal. The mixer is then tuned for a match at local-oscillator frequency and the tuning adjustments sealed. The Radiation Laboratory served initially as the standardization laboratory, but this function has since been taken over by the laboratories maintained by the Armed Services.

9·1. The Conversion-loss Set for the 3-cm Band.—The conversion-loss set for the 3-cm band, designed by Roberts,[1] was the first of the standard sets to be built.[2] A photograph of the set is shown in Fig. 9·1, and a block diagram in Fig. 9·2. The lower panel carries the r-f oscillator, crystal holder, and circuits for amplitude-modulating the oscillator and for filtering the output of the crystal. The upper panel contains a regulated power supply for the r-f oscillator with a meter for measuring

[1] S. Roberts, "Conversion Loss Measuring Apparatus for Crystals in the 3-cm Band," RL Report No. 53-28, Aug. 3, 1943; also, "1N23 Loss Measuring Set Type 7368," RL Report No. M-171, June 27, 1944.

[2] A limited number of sets were manufactured by J. C. Fonda, Inc., 333 Fourth St., New York, N. Y.

the rectified crystal current. The voltage across the load conductance is measured with the Model 300A Ballantine voltmeter shown at the right in Fig. 9·1. In routine testing the set is calibrated with standard crystals which have in turn been calibrated by the Service Laboratories just

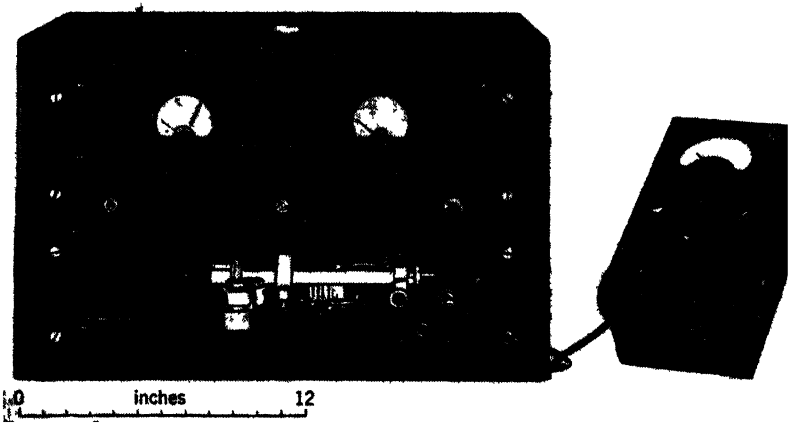

FIG. 9·1.—The conversion-loss set for the 3-cm band.

mentioned. However, the equipment may also be used for absolute calibration by the incremental method, or alternatively, the crystals may be calibrated with a mechanical modulator as described in Sec. 9·4.

R-f Components.—The r-f components are mounted on the front of the lower panel as shown in Fig. 9·3. The 723A oscillator is mounted for convenience in an inverted position. The injector flap and ejector button indicated on the photograph are devices that facilitate insertion and ejection of the crystal into the fairly stiff fingers of the crystal holder. The ejector is a lever arrangement that pushes a plunger against the end of the cartridge pin. These devices are an aid in rapid routine testing.

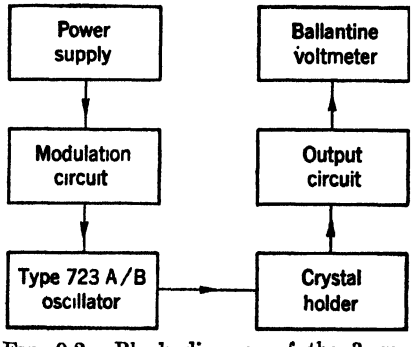

FIG. 9·2.—Block diagram of the 3-cm conversion-loss set.

A cross section of the oscillator mount is shown in Fig. 9·4. The tube socket is mounted on one side of a section of waveguide with an adjusting nut for varying the penetration of the oscillator output antenna through a hole in the waveguide. A choke-type connector is soldered to one end of the waveguide and there is a metal plug in the other end. A resistance strip is inserted parallel to the electric field in the guide through a slot near the closed end of the waveguide and is held by a

clamp. The resistance strip is adjusted in such a way that the oscillator mount matches the characteristic impedance of the waveguide with the oscillator antenna withdrawn. When the oscillator antenna penetrates the waveguide for a small distance, the oscillator is loosely coupled and will deliver the desired 1 mw of power with only a small change in the impedance presented at the waveguide coupling. It can be seen that a tube with low power output will have to be more strongly coupled to give

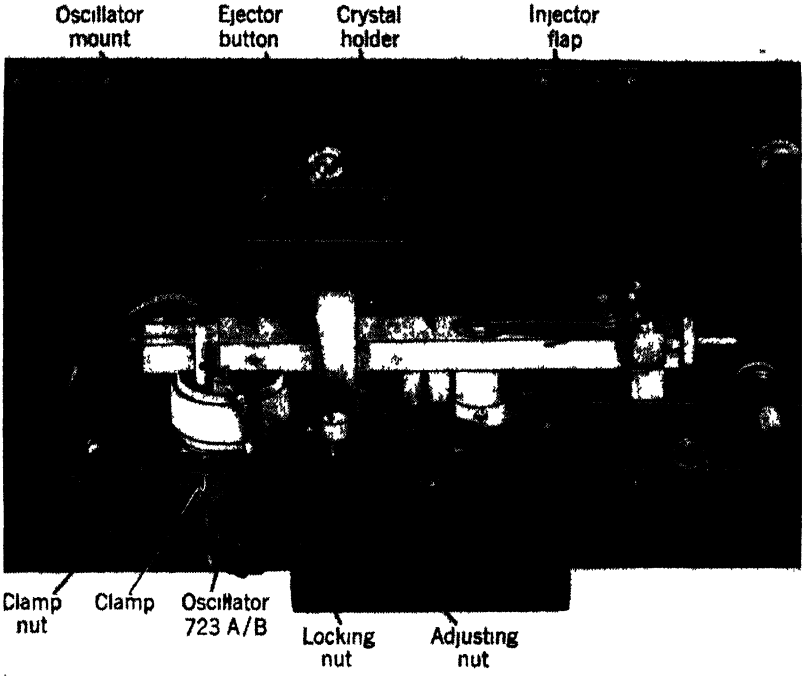

FIG 9 3 —R-f components of the 3-cm conversion-loss set

the desired amount of power; hence the output impedance will be affected to a greater extent. Because the accuracy of the equipment depends on holding close impedance tolerances it is clear that a tube which oscillates weakly should not be used.

The crystal holder is shown in cross section in Fig. 9·5. The crystal cartridge is mounted across the waveguide and is held by spring contact fingers at each end. The contact at the pin end is insulated and provides a terminal for the d-c output of the crystal; an r-f choke and bypass condenser prevent the r-f power from leaking out at this terminal. The crystal holder is interchangeable with the one on the noise measuring set, and for the latter application the capacitance between the output terminal and ground should be 14 $\pm$ 1 $\mu\mu$f.

The tuning adjustments consist of a tuning screw, which may be inserted in either of two positions in front of the crystal, and an adjustable plunger in back of the crystal. These adjustments are set by the standards laboratory at the prescribed fixed tuning and sealed once and for all.

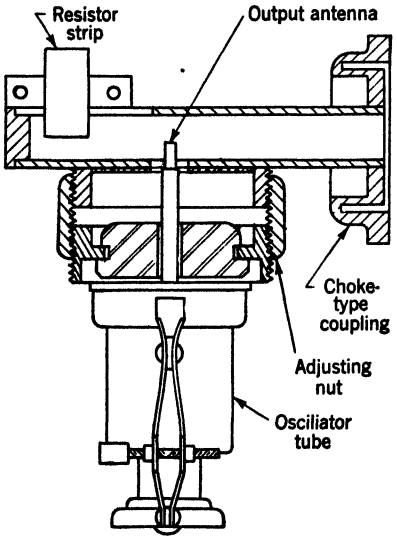

FIG. 9·4.—Oscillator mount.

Circuit Details.—The power supply is a conventional, electronically regulated supply that applies −200 to −300 volts to the cathode of the oscillator, and a reflector voltage from −60 to −150 volts with respect to the cathode. The cavity of the oscillator is connected to ground.

The modulation circuit, a regulator for the modulator voltage, and the crystal-output circuit are all mounted on the r-f panel. The modulation circuit, shown in its most elementary form in Fig. 9·6, is connected between the oscillator tube and power supply. A 60-cps voltage e_1 is applied to the choke L, which also carries the normal d-c cathode current. A fraction of this voltage e_2 is obtained by means of a voltage divider and is applied to the reflector through a filter (C_1,R_6). By choosing the proper ratio

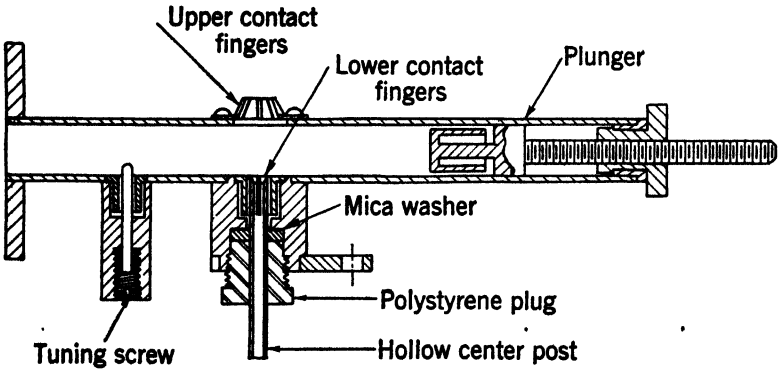

FIG. 9·5.—Crystal holder.

of e_1 to e_2 amplitude modulation can be provided with a minimum of frequency modulation.

A regulator for the modulator voltage is shown in Fig. 9·7. The nonlinear volt-ampere characteristic of a thermistor is utilized for this purpose. As current through the thermistor is increased, the voltage at

first increases until it reaches a maximum and then, as the current is increased still further, the voltage becomes smaller. If the thermistor is operated at its maximum voltage, it is a good voltage regulator because a small change in current causes a negligible change in voltage. The voltage at the maximum for the D162046 thermistor is about 3 volts. Changes in ambient temperature may be expected to change the voltage

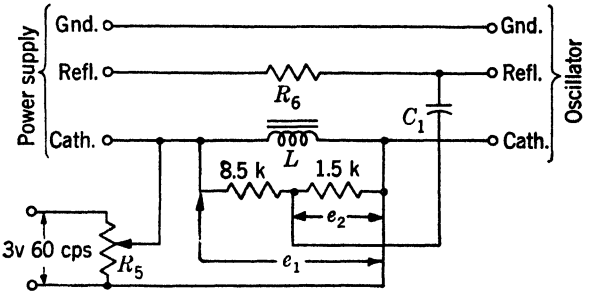

FIG. 9·6.- Modulation circuit.

across the thermistor but this has never caused any noticeable difficulty. The modulation voltage applied to the oscillator is adjusted by means of the rheostat at the output terminals.

The crystal-output circuit is shown in Fig. 9·8. The load consists of a magnetically shielded choke L_1, condenser C, and resistors R_1 and R_2. The circuit is resonant at the modulation frequency of 60 cps at low

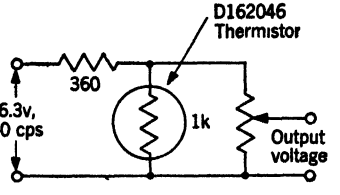

FIG. 9·7.—Regulator for modulator voltage.

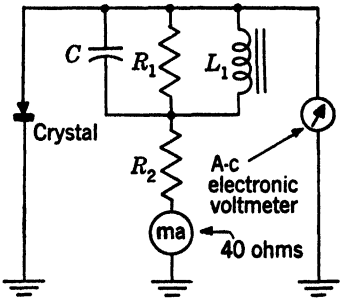

FIG. 9·8.—Crystal output circuit.

level (small currents). The load is designed to have a d-c resistance of 100 ohms and an impedance of $400 + j0$ ohms at the modulation frequency.

Adjustment of R-f Components.—The adjustment of the r-f components is made in the standards laboratory by means of standing-wave measurements with a precision slotted section and a movable probe detector (i.e., a standing-wave machine). A type 723A oscillator is connected to a T-section, on which is mounted a wavemeter. The

T-section is connected to a waveguide attenuator, which is in turn connected to the slotted section. The mixer or oscillator mount to be tuned is connected directly to the flange coupling on the slotted section. The oscillator is tuned to the standard frequency corresponding to 3.200 cm, and the tuning devices on the r-f component are adjusted for a standing-wave ratio as near unity as possible. With precision equipment and careful adjustment the voltage standing-wave ratio can be made 1.01 or less. Such accuracy is needed because small differences in the mixer tuning make appreciable differences in values obtained for the conversion loss of crystals which are at the extremes of the impedance distribution. The inside dimensions of the waveguide for the slotted section, as well as for the other r-f components, should be uniform and accurate.

The standard fixed tuning is established by tuning a standard mixer to match to the characteristic admittance of the waveguide crystals with an r-f impedance at the center of the impedance distribution. Once

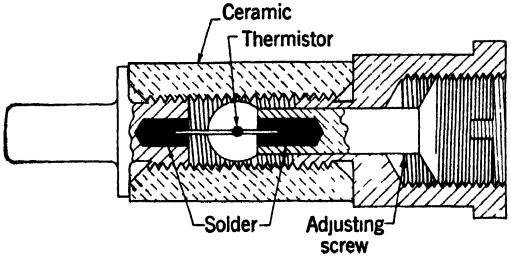

FIG. 9·9.—Standard-impedance cartridge for the 3-cm band.

such a standard mixer is established, a standard-impedance cartridge that matches in the standard mixer is used for tuning other mixers.

The standard-impedance cartridge used for the 3-cm band is shown in Fig. 9·9. It consists of a thermistor mounted in a Sylvania Company ceramic cartridge and is constructed in the following way. One of the leads of an unmounted thermistor bead (Western Electric D-163903) is soldered to the screw that normally carries the silicon crystal. The screw is then inserted in the cartridge and the pin end of the cartridge heated with the result that, as the screw is advanced, the wire on the other end of the thermistor bead dips into the molten solder inside the cartridge on the pin end. The screw is advanced until the bead is centered in the hole in the ceramic. The desired impedance is obtained by adjusting the amount of solder at the two ends of the cartridge and by adjusting the resistance of the thermistor. The resistance is adjusted by connecting the cartridge in one arm of a bridge and adjusting the bridge current. Once the desired combination of these variables is found, a specification of the resistance determines uniquely the impedance of the cartridge. The d-c resistance required to match the various cartridges to the standard 3-cm mixer is in the range of 30 to 50 ohms. The impedance

varies slightly with the orientation of the cartridge in the mixer; therefore both the orientation and resistance must be specified. The 3-cm impedance standard has an admittance in the waveguide, when referred to the plane of the cartridge, of about $1.25 + j\,0.5$ times the characteristic admittance of the waveguide.

It should be emphasized that the primary standard is the standard mixer. The essential function of the standard impedance is to provide a simple means of tuning other mixers so as to be identical with the standard. The use of a stable impedance standard, moreover, provides a means of checking the constancy of the mixer-impedance combination. The impedance standard is also equally useful as a bolometer for the measurements of r-f power required for the *absolute* measurement of conversion loss.

Adjustment and Calibration of the Set.—A wavemeter, mounted on a T-section, is inserted between the oscillator mount and the mixer for adjusting the frequency of the oscillator to the standard value corresponding to 3.200 cm. The equipment is sufficiently stable to require only an occasional check on frequency. Calibration of the equipment is accomplished with secondary-standard crystals provided by the standards laboratory, for which the conversion loss and rectified current are known. The power-level adjustment is made by means of the large adjusting nut on the oscillator mount, and is locked by means of the small locking nut (see Fig. 9·3). This adjustment controls the distance that the output antenna penetrates into the waveguide, thereby varying the coupling of the oscillator to the waveguide. The power level is so adjusted that the value of the rectified current for a given crystal is that in the specifications, 1 mw of available power being obtained by this adjustment.

From Eq. (1) it is seen that the conversion loss of the crystal, in decibels, is given by

$$L(db) = 10 \log_{10} \left(\frac{m^2 P}{g_b} \right) - 20 \log_{10} E_\beta. \tag{2}$$

The decibel scale on the Ballantine voltmeter gives $20 \log_{10} E_\beta^2$ directly. The other constants in Eq. (2) are known, except for m, which is difficult to measure for the modulation method used in the equipment. Accordingly, the conversion loss of the standard crystals are used for calibration. The voltmeter is set on the 0.01-volt full-scale range, and the modulation voltage adjusted so that the term $10 \log_{10} (m^2P/g_b)$ is equal to 20.0. For this setting the output-voltmeter reading on the decibel scale is 20.0 minus the value of conversion loss specified for the standard crystal. This corresponds to a value m of of 1.58 per cent for $P = 1$ mw and $g_b = \frac{1}{400}$ mho. The conversion loss of an unknown crystal in decibels is then just 20.0 minus the reading of the output meter in decibels.

It is desirable to use a set of several standard crystals for the calibration in order to detect any deterioration of an individual unit through handling. To avoid damaging crystals the equipment should be connected to a good ground. The operator should place his hand on the equipment just prior to inserting the crystal cartridge and while he is inserting it in order to avoid burning out the crystal by the discharge of static electricity that may have accumulated on his body.

The Calibration of Standard Crystals.—The standard crystals can be calibrated by the incremental method or by the amplitude-modulation method. Both of these methods are discussed in Sec. 7·4. The latter method utilizes a mechanical modulator for which the modulation coefficient can be accurately measured; this is discussed in detail in Sec. 9·4. For the incremental method, it was shown in Sec. 7·4 that the conversion loss is given by

$$L = \frac{g_b}{2P_0\left(\frac{\Delta I}{\Delta P}\right)^2}, \tag{3}$$

where g_b is the standard load conductance and ΔI is the increment of rectified current in the load resistance r_2 of Fig. 7·7*b* when the available power is increased from P to $P + \Delta P$. The quantity P_0 is the average power, $P + \frac{1}{2}\Delta P$. These quantities can all be measured on the conversion-loss set. For the power measurements a micrometer attenuator, such as is used on the noise set (see Fig. 9·24), is inserted between the oscillator mount and the crystal holder. The attenuator can be calibrated by using the standard-impedance cartridge as a bolometer in one arm of a bridge. The measurement of the current increment ΔI is accomplished with the circuit of Fig. 7·7*b*. The r-f panel of the loss set is provided with a switch that connects the output terminal of the mixer either to the usual load circuit or to a terminal to which the calibrating circuit of Fig. 7·7*b* is connected. In making the measurement at the standard power level of 1 mw the calibrated attenuator is first set for 0.9 mw available power and the current through the output meter is balanced out. The attenuator is then shifted to the 1.1-mw level and the current ΔI through the meter noted. For a load resistance of 400 ohms the conversion loss is given by

$$L = \frac{1}{A(\Delta I)^2}, \tag{4}$$

where A is 20/ma^2 when ΔI is expressed in milliamperes. With precision equipment, an accuracy of 0.1 db can be obtained. For this accuracy an attenuator that matches the waveguide accurately must be used.

9·2. The Conversion-loss Set for the 10-cm Band.—The development of the conversion-loss set for the 10-cm band followed chronologically

that for the 3-cm band and is similar to it in many respects; the differences are chiefly in the r-f components. A photograph of the set, developed at the Radiation Laboratory by Huntington,[1] is shown in Fig. 9·10, and a block diagram in Fig. 9·11. The top panel contains the power supply for the type 707B oscillator; the middle panel contains the modulation circuit and the crystal-output circuit; the bottom panel supports the r-f

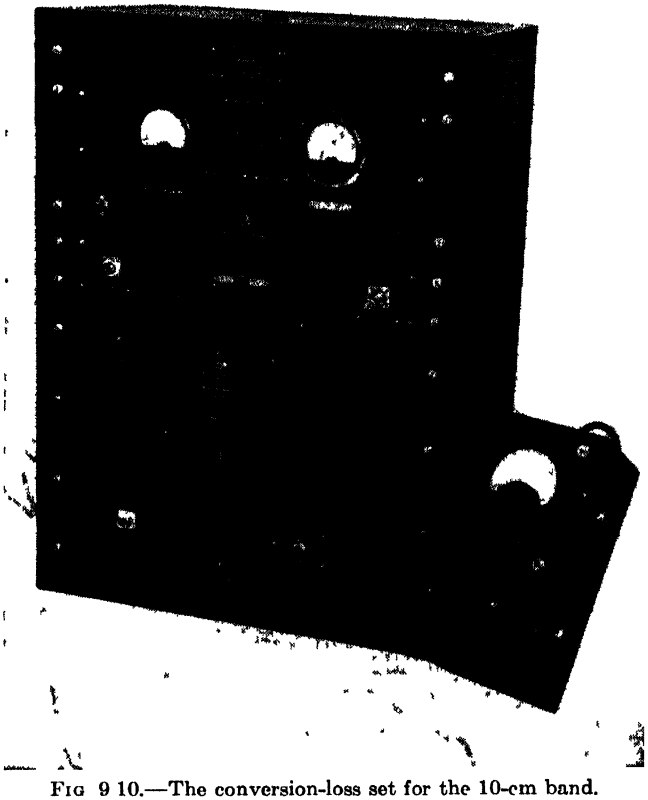

FIG 9 10.—The conversion-loss set for the 10-cm band.

oscillator, attenuator, and mixer. The output modulation voltage is measured, as in the 3-cm set, with a Ballantine voltmeter.

R-f Components.—The r-f oscillator and mixer are mounted on the back of the panel, as shown in Fig. 9·12. The oscillator is mounted in a broadband cavity, designed for a shielded wideband signal generator; it is used here because of its sturdy construction and the case with which it is mounted and tuned. The cavity has two tuning plungers, one for gross and the other for fine adjustment. The tuning knob for the latter

[1] H. B. Huntington, "1N21 Loss Tester Type 7556," RL Report No. M-177, Aug. 21, 1944. The set was manufactured in limited quantities by Photoswitch, Inc., 77 Broadway, Cambridge, Mass.

is accessible from the front of the panel. Power is taken from the cavity by two coupling loops, one of which is connected by means of 50-ohm lossy cable to the waveguide attenuator on the front of the panel and

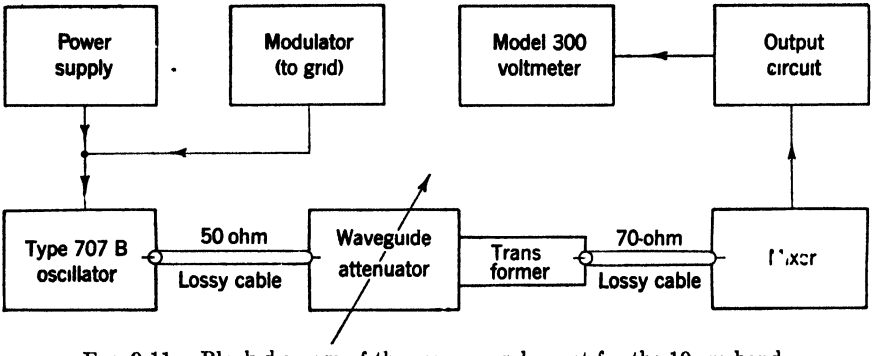

FIG. 9 11 —Block diagram of the conversion-loss set for the 10-cm band

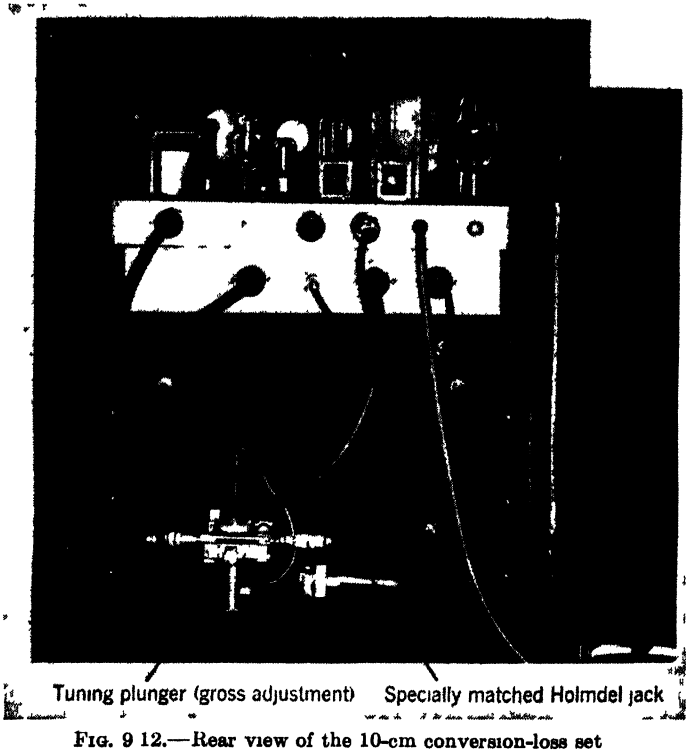

FIG. 9 12.—Rear view of the 10-cm conversion-loss set

supplies the r-f power for the mixer; the other loop is connected to an outlet on the panel and is used for monitoring the frequency, specified for the 1N21 types as 3060 Mc/sec.

The micrometer attenuator is a scaled-up model of the one used in the 3-cm noise set. A resistance strip is mounted in the guide parallel to the electric field so that it can be moved across the guide by a micrometer screw. When it is so moved the attenuator increases to a maximum at the center of the guide where the field is strongest. The total range of attenuator is from 0 to 20 db. The transitions from coaxial line to waveguide are made by probes inserted near the ends of the guide. The output coupling is fitted with a "Holmdel" plug, which matches KS 8086 70-ohm cable with a voltage standing-wave ratio of not more than about 1.07. This mismatch is not serious, since the cable that connects the

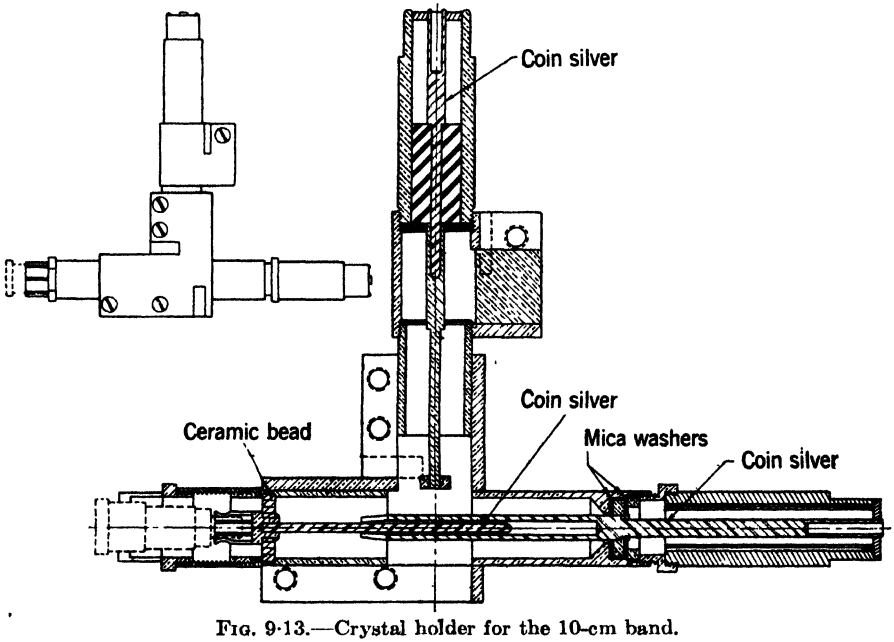

FIG. 9·13.—Crystal holder for the 10-cm band.

attenuator to the mixer supplies about 15 db of attenuation between the two components. The impedance of the r-f source at the input terminals of the mixer is then the characteristic impedance of the KS 8086 cable, approximately 70 ohms. To standardize the impedance accurately, the Holmdel jack that terminates the cable must be especially "tailored" for a match. This "tailoring" consists of inserting a small tuning screw in the outer conductor of the jack, which is then connected to a 70-ohm coaxial-slotted section; the other end of the cable is terminated in a matched load and the tuning screw is adjusted for a match and then soldered in place. (The use of both 50-ohm and 70-ohm cable in the equipment was necessary in order to adapt to this equipment r-f components already designed for other purposes.)

The mixer used in the equipment and shown in Fig. 9·13 was originally

designed by Sharpless[1] at the Bell Telephone Laboratories for conversion-loss measurements by the heterodyne method. It was adapted to the amplitude-modulation method by removing the Holmdel plug that carries the capacity coupling for the local oscillator. A brass plug closes the hole through which this coupling was made.

The crystal terminates one end of a coaxial line, the other end being connected to the i-f output plug. A quarter-wave choke in this plug and a bypass condenser prevent the r-f power from leaking out at this terminal. The capacity seen looking into the i-f terminals is adjusted to the specified value of 15 $\mu\mu$f by adding or removing mica washers in the bypass condenser. The r-f input line is connected to the crystal by a capacity coupling. The two tuning adjustments are the capacitance of this coupling and the length of line between the crystal and the r-f short circuit in the i-f plug. The crystal is held in the crystal receptacle by spring fingers on the inner and outer conductors of the coaxial line.

Circuit Details.—The circuit details are similar in every respect to those for the 3-cm set except that the 60-cps amplitude-modulation voltage is applied to the grid of the type 707B tube. The modulation voltage is regulated by the thermistor circuit of Fig. 9·7. The output circuit is the same as that in Fig. 9·8; the load impedance at 60 cps is $400 + j\,0$ ohms.

Adjustment of R-f Components.—The mixer is tuned by means of a standing-wave machine fitted with a 70-ohm Holmdel jack, into which the mixer is plugged. The standard impedance is a thermistor cartridge which differs from that shown in Fig. 9·9 in the following respects. (1) A thin cylindrical metal sleeve, 0.180 in. long, is placed around the ceramic on the pin end of the cartridge; this sleeve is flush with the end of the ceramic on the pin end and is soldered to the brass fitting on that end. (2) Solder is added to the connections inside the cartridge until there is barely enough space for the thermistor bead between the two balls of solder that are formed. (3) With the above variables properly adjusted, the desired impedance is obtained for thermistor resistances varying from 100 to 110 ohms.

Calibration of the Set.—The calibration of the set is the same as that described in Sec. 9·1. The specified available power is 0.5 mw, and the load resistance at 60 cps is 400 ohms. The constant A in Eq. (4) is therefore 10.0/ma^2 when ΔP is 0.2 mw.

9·3. The Conversion-loss Set for the 1-cm Band.—The conversion-loss set for the 1-cm band was developed at the Radiation Laboratory[2]

[1] W. M. Sharpless, "Manufacturing Electrical Testing Requirements—1N21 Crystal Rectifier," BTL Report MM-43-160-167, Oct. 14, 1943.

[2] C. A. Whitmer, "A Conversion-Loss Set for Testing K-band Crystal Rectifiers," RL Report No. 668, Jan. 16, 1945.

toward the end of the crystal-development work and did not go into production. A block diagram of the set is shown in Fig. 9·14. A mechanical modulator produces the amplitude modulation, and the output circuit is designed for measuring both the i-f resistance and the conversion loss. The set operates at the specified test wavelength of 1.250 cm, and the r-f components, except the modulator and crystal holder, are standard test equipment, described in detail in Vol. 11 of the Radiation Laboratory Series.

R-f Components.—A type 2K33 oscillator, or its equivalent, with a minimum r-f power output of 20 mw is required for the equipment. This provides 1 mw of available power to the crystal and at the same time makes possible the use of at least 6 db of attenuation on each side of the mechanical modulator. The r-f admittance of the modulator differs slightly from that of the waveguide and varies with the rotation of the modulator; for certain orientations of the modulator disk, the modulator may be mismatched to the waveguide by as much as 1.1 in voltage

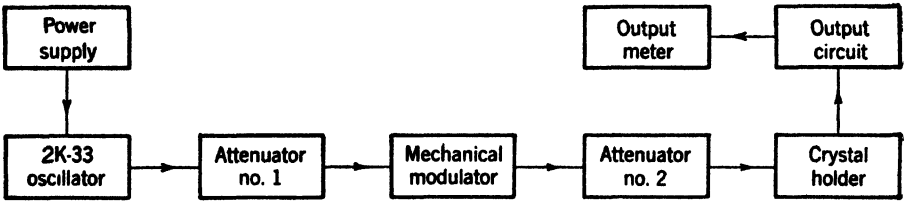

FIG. 9·14.—Block diagram of the conversion-loss set for the 1-cm band.

standing-wave ratio (see Sec. 9·4). The attenuation between the modulator and oscillator is used so that this variation in load impedance will not modulate the oscillator output by an unpredicted amount. Similarly, there should be ample attenuation between the oscillator and mixer so that the characteristic admittance of the waveguide is always presented to the mixer.

The attenuators are "vane" attenuators, varied by varying the projection of a resistance strip through a slot into the waveguide parallel to the electric field.

The mechanical modulator is similar to that described in Sec. 9·4 for the 3-cm waveguide. The attenuating disk, 1 in. in diameter, is rotated by a small motor mounted rigidly to the waveguide. The eccentricity of the disk is set to give a modulation coefficient of about 10 per cent. This value gives a convenient range on the output meter with the specified r-f power and load resistance.

The motor is run at a speed of about 55 rps. Synchronous speed is to be avoided so as to prevent a fixed-phase relation between the modulation voltage produced by the mechanical modulator and that produced by any ripple that may be present in the power supply. The latter should,

of course, be reduced to a minimum to avoid fluctuations in the output voltage. Stray magnetic fields from the motor may produce an undesirable 60-cps modulation of the type 2K33 oscillator, but its effect can be minimized by shielding the motor with sheet iron. By means of a stop, the modulator disk may be quickly set in a rest position at which the same rectified current is obtained as with the modulator running.

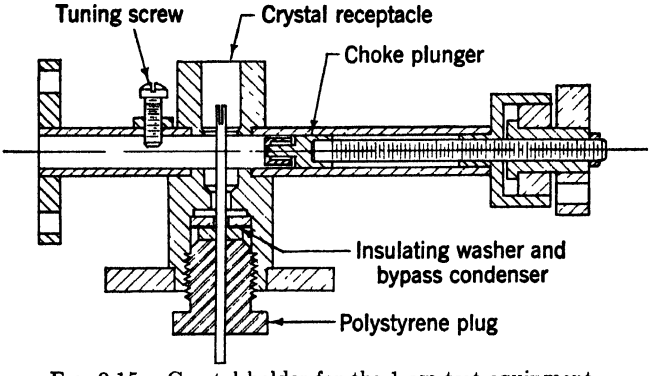

FIG. 9·15.—Crystal holder for the 1-cm test equipment.

The waveguide crystal holder is shown in cross section in Fig. 9·15. The outer conductor of the coaxial cartridge is set against the shoulder in the crystal receptacle; the inner conductor is held by spring fingers on the end of the post that couples the crystal to the waveguide. This post is insulated and provides a terminal for the d-c output of the mixer.

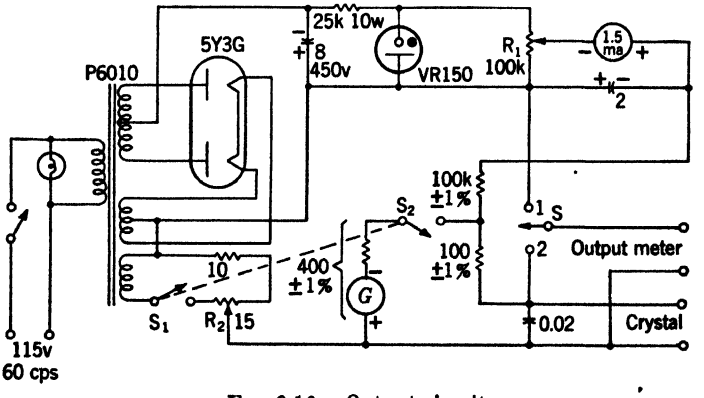

FIG. 9·16.—Output circuit.

An r-f choke and bypass condenser prevent leakage of r-f power at this terminal. The tuning adjustment consists of a tuning screw in front of the crystal and an adjustable choke plunger behind the crystal. A spring device, not shown in Fig. 9·15, is used for seating the cartridge firmly in the crystal receptacle.

Circuit Details.—The output circuit is shown in Fig. 9·16. It provides the specified d-c load of 100 ohms and a-c load of 500 ohms, and also

provides for the measurement of crystal resistance at 60 cps. The circuit is operated in the following way. The switches S_1 and S_2 are ganged in such a way that S_2 is closed when S_1 is open. With S_2 closed, the potentiometer R_1 is adjusted for zero current in the galvanometer G. Under this condition, current from the power supply balances out the rectified current from the crystal in G; the d-c load is then 100 ohms and the a-c load 500 ohms. The rectified current is read on the milliammeter and the a-c voltage is read by closing switch S to position 2.

The circuit provides a variable 60-cps voltage that may be connected to the crystal in series with a resistance of 100,000 ohms by closing switch S_1. Since the i-f resistance of the crystal is in the range from 300 to 600 ohms, essentially a constant-current source is thus provided. The i-f resistance can then be determined by reading the voltage across the crystal with the output meter. With some 2K33 tubes the 60-cps heater supply will produce a 60-cps modulation in the r-f power, which will then introduce an error in the resistance measurement. This situation can be avoided by using an insulated storage battery for the heater supply.

Either the Ballantine model 300 voltmeter or the Hewlett-Packard model 400A voltmeter may be used for measuring the output voltage. The former has a logarithmic meter that can be read more accurately than the Hewlett-Packard in the range needed under actual operating conditions and is therefore preferred for absolute calibration. The Hewlett-Packard meter is perhaps to be preferred once the equipment is calibrated and standard crystals are available. The gain of the meter can be changed in such a way that the indication is in the most sensitive part of the scale for crystals in the acceptable range. A variable gain control makes it possible to set the meter for direct reading of the conversion loss.

Adjustment of R-f Components.—The adjustment of the mechanical modulator is described in Sec. 9·4.

The standard mixer is tuned to match the waveguide when a 65-ohm termination is plugged into the crystal receptacle. The 65-ohm termination for tuning the standard mixer is a coaxial line terminated by a resistance cloth wound around the center conductor in the form of a cone. If the cone is shaped so as to terminate the line in its characteristic impedance, then, for an arbitrary tuning of the mixer, a change in the position of the cone along the line will not shift the position of the minimum of the standing wave in the slotted section. Once this condition is achieved the standard mixer can be fixed-tuned for a standing-wave ratio of unity.

The termination just described is not stable enough for a standard impedance. The standard impedance used for tuning mixers to match the standard one is shown in Fig. 9·17. It consists of a short section of

coaxial line of 65-ohm characteristic impedance; one end of it is identical with the pin end of the cartridge for the 1-cm band, the other end is short-circuited. The outer conductor is slotted longitudinally and rectangular strips of resistance card are inserted on each side so that they make contact with the inner conductor. This device can be matched to the standard mixer by sliding the strips along the slots. Once the correct positions are found, the strips are clamped in the slots and trimmed off flush with the outer surface. Such a termination has the required stability and ruggedness, and the adjustment procedure ensures its having the required impedance.

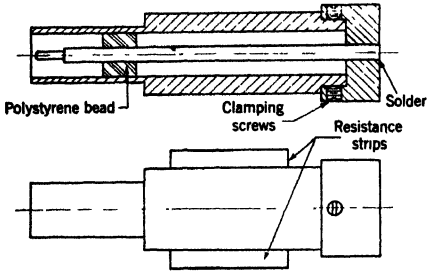

FIG. 9·17.—Standard 65-ohm termination.

The procedure for fixing the tuning of mixers is similar to that described for the other bands.

Calibration of the Set.—The mechanical modulator is calibrated by the method described in Sec. 9·4. Once m is known, the constant term in Eq. (2) can be calculated. To measure the available power P_0, the mixer is replaced by a matched Wollaston wire or thermistor bolometer. Once a set of standard crystals is available, it may be used for checking the calibration of the equipment as described in Sec. 9·1.

If the set is used for the measurement of conversion loss only, the modulator may be run continuously. The measurement then involves setting the potentiometer R_1 (Fig. 9·16) for a null reading of the galvanometer and reading the output voltmeter.

To measure the i-f resistance, the modulator is stopped at the fiducial position and S_1 is closed. The output voltmeter is then read with S closed first to position 1, then to position 2. For readings V_1 and V_2, the i-f resistance is given by

$$R = \frac{V_2}{V_1} \times 10^5 \qquad \text{ohms.} \tag{5}$$

With V_1 fixed at a suitable value, the resistance is obtained from a single reading of the output meter.

9·4. The Mechanical Modulator.—The use of the mechanical modulator for absolute conversion-loss measurements has already been mentioned in Sec. 7·4. The modulator developed by Roberts[1] for the 3-cm band is shown in the photograph of Fig. 9·18. It is essentially a variable attenuator driven by a motor, the attenuation consequently varying

[1] S. Roberts, "A Mechanical Modulator and Precise Method of Calibration for Crystal Conversion Loss Standardization," RL Group Report 53, Jan. 5, 1945.

periodically at a frequency slightly less than 60 cps. The attenuator consists of a thin insulating circular disk, $2\frac{1}{8}$ in. in diameter, which has a uniform resistance coating on one surface and penetrates a slot on the top side of a section of waveguide. The disk introduces more or less attenuation depending on how far it penetrates the waveguide. It is mounted eccentrically on the shaft of the motor, the attenuation therefore varying periodically as the shaft rotates. The mounting hole in the disk is eccentric with respect to the outer edge, and the bushing on which it is mounted is also eccentric. As a result, the eccentricity of the outer edge of the disk with respect to the motor shaft can be adjusted smoothly by rotating the disk on the mounting bushing. By this means the modulation coefficient of the modulator can be set at the

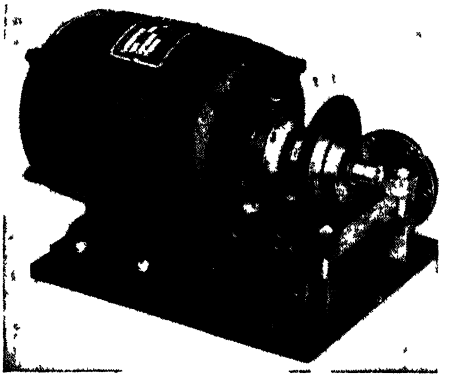

FIG. 9·18.—Mechanical modulator for the 3-cm equipment.

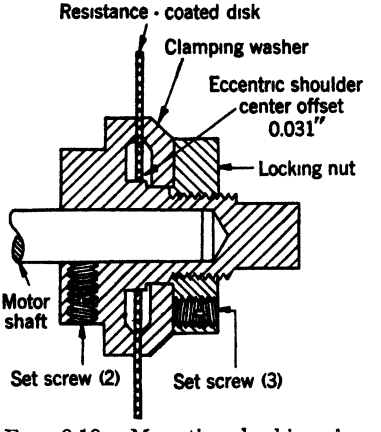

FIG. 9·19.—Mounting bushing for the modulator disk.

desired value. The construction of the bushing and resistor disk is shown in Fig. 9·19.

The average penetration of the disk inside the waveguide is rather critical. If it penetrates too far, the waveform of the modulation tends, because of irregularities in the resistance coating, to be nonsinusoidal. On the other hand, if the penetration is so adjusted that the waveform is nearly sinusoidal, the r-f impedance is affected—that is, the impedance seen on looking into one side of the modulator with a matched termination on the other side is not the characteristic impedance of the waveguide. Furthermore, as has been pointed out in Sec. 9·3, this impedance varies with the rotation of the modulator. It is preferable to adjust the penetration in such a way that the modulation is as nearly sinusoidal as possible and to compensate for the impedance mismatch by the use of attenuators on each side of the modulator. Figure 9·20 shows the variation in power transmission as a function of angle for a typical

modulator. Figure 9·21 shows the standing-wave ratio as a function of angle.

With constant incident power the power transmitted by the modulator is a periodic function of the angular position θ and may be represented by the Fourier series,

$$P = P_1[1 + a_1 \cos(\theta + \phi_1) + a_2 \cos(2\theta + \phi_2) + \cdots +], \qquad (6)$$

where P_1 is the average power and a_i and ϕ_i are constants. The modu-

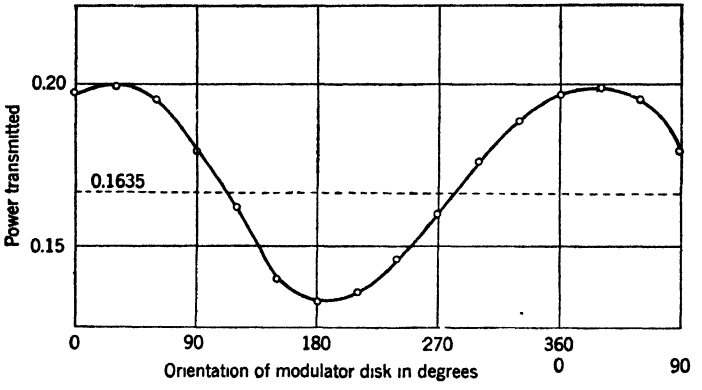

FIG. 9·20.—Transmission characteristic of a mechanical modulator.

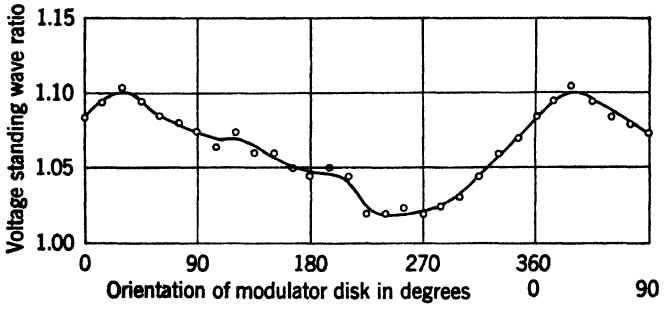

FIG. 9·21.—Standing-wave ratio of mechanical modulator.

lator is adjusted to minimize a_2, a_3, etc., the resultant power, to a good approximation, being given therefore by

$$P = P_1(1 + 2m \cos \theta), \qquad (7)$$

where the modulation coefficient $m = \frac{1}{2}a_1$.

The value of m may be determined by a Fourier analysis of the transmission characteristic given in Fig. 9·20. Instead of integrating to find the coefficients of the fundamental-frequency components, accurate results can be obtained by summations with finite intervals of 30°. Expressed in terms of summations over equally spaced values of θ in the

range from 0° to 360°, the modulation coefficient is

$$m = \frac{\sqrt{(\Sigma P \cos \theta)^2 + (\Sigma P \sin \theta)^2}}{\Sigma P}. \tag{8}$$

The modulation coefficient calculated from the curve of Fig. 9·20 by means of Eq. (8) is 0.100.

STANDARD NOISE TEST SETS

Standard noise sets were developed at the Radiation Laboratory for the 3-cm and 10-cm bands. Acceptance testing in the 1-cm band is

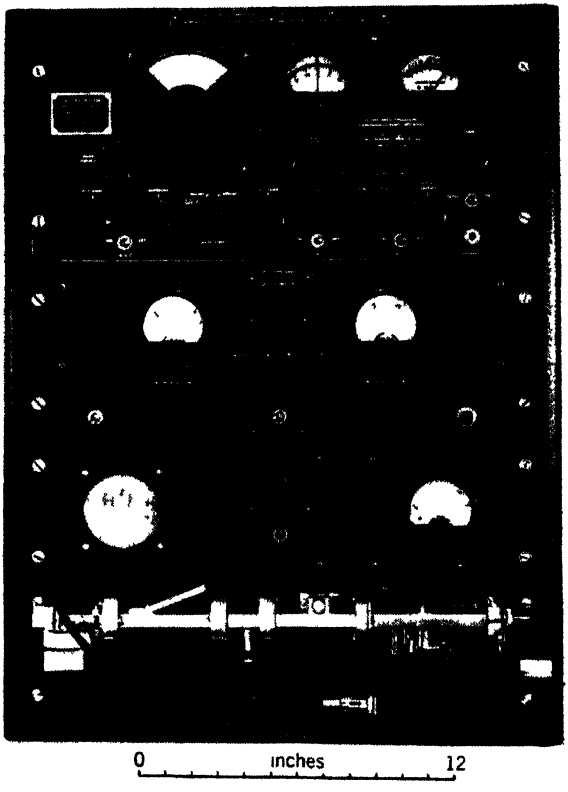

FIG. 9·22.—The standard noise-measuring set for the 3-cm band.

done at present with the 3-cm noise set, using an adapter on the 3-cm crystal holder which makes it possible to plug the 1-cm coaxial cartridge into the holder. Both of the standard sets employ the Roberts coupling circuit described in Sec. 7·6; in both, the noise temperature is measured by comparing the noise power output of the crystal with that of a standard resistor.

9·5. The Noise Measuring Set for the 3-cm Band.—The set for measuring noise temperature in the 3-cm band was developed by Rob-

erts.[1] A photograph of the equipment is shown in Fig. 9·22, and a block diagram in Fig. 9·23. The bottom panel includes the r-f components, input coupling circuit, diode noise source, and preamplifier. The second panel carries a regulated power supply for the preamplifier, and an output

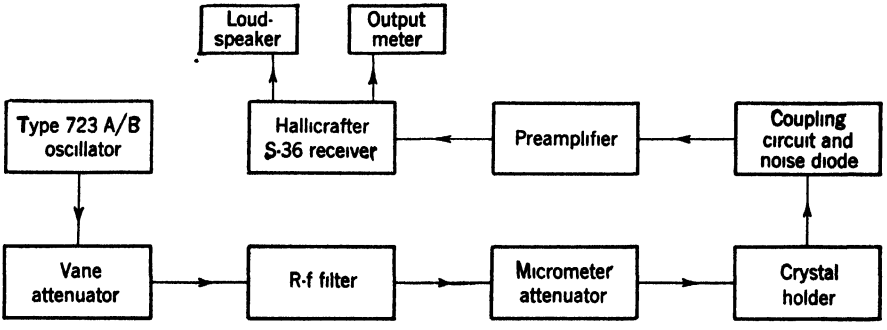

FIG. 9·23.—Block diagram of the noise-measuring set for the 3-cm band

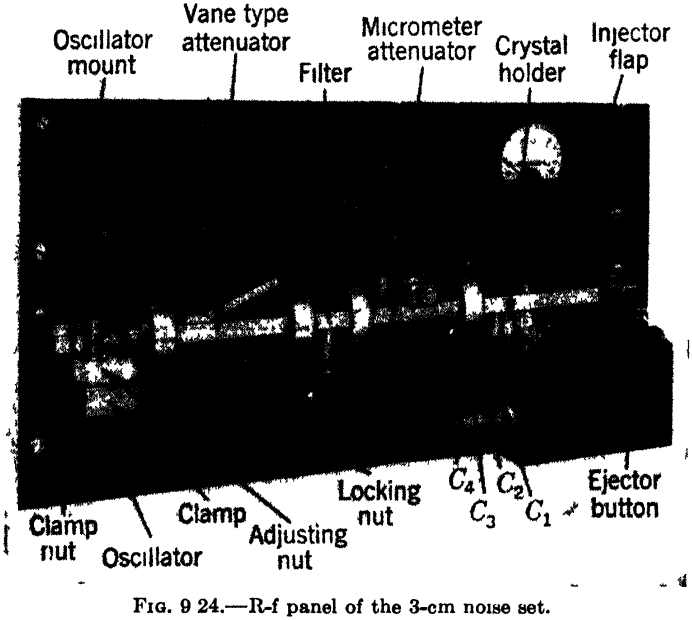

FIG. 9·24.—R-f panel of the 3-cm noise set.

meter and loudspeaker for the Hallicrafter S-36 receiver. The third panel is a power supply for the r-f oscillator; on this panel are mounted meters for measuring the rectified crystal current and the beam current of the oscillator. The top panel is a Hallicrafter S-36 receiver. A type VR-307 voltage regulator mounted on the bottom of the cabinet in the

[1] S. Roberts, "1N23 Noise Measuring Set, Type 7438," RL Report No. M-190, Dec. 21, 1944. This set was manufactured in limited quantities by J. C. Fonda, Inc., New York, N. Y.

rear provides stabilized a-c voltage for the receiver, preamplifier power supply, and the oscillator cathode heater.

R-f Components.—A photograph of the r-f panel is shown in Fig. 9·24. The oscillator and crystal holder are identical with those used in the conversion loss set.

A description of the micrometer attenuator was given in Sec. 9·2. The ends of the resistance strip in the attenuator are tapered; hence the characteristic waveguide impedance is seen on looking in at either end. The purpose of this attenuator is to present the characteristic impedance of the waveguide to the crystal holder at signal and image frequencies as well as at local-oscillator frequency; it is adjusted to a minimum of 5-db attenuation.

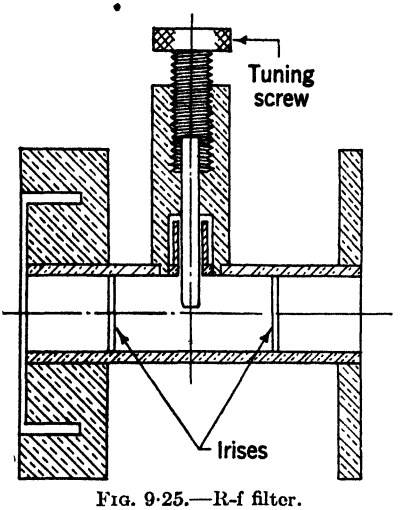

FIG. 9·25.—R-f filter.

The vane-type attenuator operates by moving a resistance-coated card into the waveguide (parallel to the electric field) through a slot in the top of the guide. This attenuator is suitable for varying the attenuation rapidly when a calibration is not required. It is not used in the standard procedure for 3-cm testing but is useful in testing 1N26 rectifiers, where the r-f power level is adjusted for a minimum rectified current of 0.5 ma.

The r-f filter shown in cross section in Fig. 9·25 is a waveguide resonator with iris coupling and a choke-type tuning screw. The Q of this filter is about 1000, and its transmission loss somewhat less than 2 db. It is tuned to the standard test frequency of 9375 Mc/sec; the tuning screw is then sealed. The purpose of the filter is to reject the noise sidebands generated by the oscillator. Without it, the indicated noise temperature is appreciably higher than the true noise temperature of the crystal.

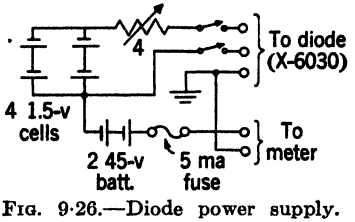

FIG. 9·26.—Diode power supply.

Circuit Details.—The oscillator power supply is identical with that used in the 3-cm conversion loss set. The preamplifier power supply provides a regulated voltage of 105 volts for the preamplifier. A convenient power supply for the noise diode (not included in the equipment) is shown in Fig. 9·26. It is completely shielded.

The input coupling circuit is the Roberts circuit discussed in Sec. 7·6.

A schematic diagram of the coupling circuit and noise diode is shown in Fig. 9·27. The input coupling circuit, which couples the crystal (or the standard comparison resistor R_1) to the preamplifier, is tuned by the capacitances C_2, C_3, and C_4 in the three arms of the coupling network. As was explained in Sec. 7·6, the circuit is so designed that these three tuning parameters can be adjusted for the following conditions: (1) a match of the standard resistance to the preamplifier input resistance, (2) zero susceptance looking in at the output terminals of the network, (3) an output meter reading nearly independent of the input resistance of the crystal.

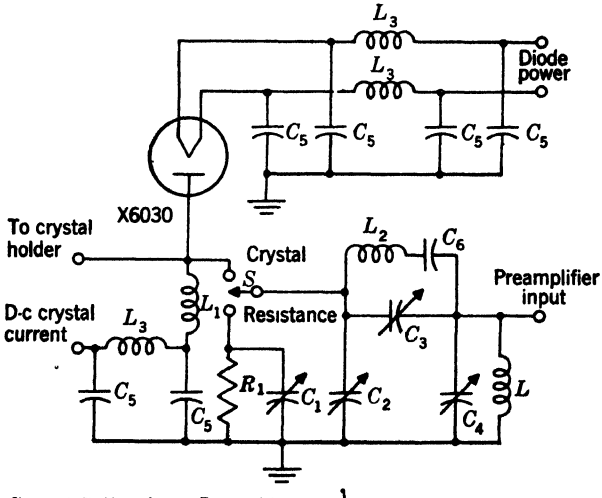

C_1 = 1.5–7 $\mu\mu$f L_1 = 11 turns } #28 wire on ½-in. coil form
C_2 = 5–20 $\mu\mu$f L_2 = 10 turns }
C_3, C_4 = 3–13 $\mu\mu$f L_3 = resonant choke at 30 Mc/sec
C_5, C_6 = 0.001 μf

FIG. 9·27.—Input coupling circuit.

One of the features of the input circuit is the provision for switching from the crystal directly to the standard resistance R_1. The capacitance C_1 is tuned in such a way that with a 300-ohm resistor cartridge in the crystal holder there is no change in output meter reading when switch S is thrown from RES to X'TAL. The combination R_1C_1 then has the same admittance as the circuit connected to the X'TAL terminal of switch S. The conductance is that of the standard resistance R_1, and the capacitative susceptance together with that of C_2 makes up the total susceptance of the input arm of the coupling network.

The tuning of the coupling circuit is accomplished by using as a signal generator a 300-ohm resistor cartridge in the crystal holder, made "noisy" by current from the diode. The condensers C_3 and C_4 are then adjusted for maximum noise output. This matches the 300-ohm resistor cartridge to the input resistance of the preamplifier. The 300-ohm

cartridge is then replaced by cartridges of 150 and 600 ohms and, with the diode off, C_2 is so adjusted that in either case there is essentially no change in output meter reading when switch S is thrown from RES to X'TAL. As a final fine adjustment, cartridges of 150 to 600 ohms are used in the crystal holder with a diode current in each case such that the noise temperature is, for example, 5 times [see Eq. (7-86)]. Capacitance C_4 is then adjusted, making the output meter reading the same for the two resistor cartridges. With proper adjustment, the variation of Y-factor with input resistance is like that shown in Fig. 7·14.

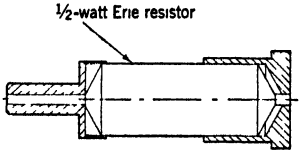

FIG. 9·28.—Resistor cartridge.

The resistor cartridges used in the calibration are shown in Fig. 9·28. These are made from Erie ½-watt resistors, to the ends of which are soldered a base and pin of the same dimensions as the crystal cartridge.

The noise diode is a Sylvania type X6030 tube. It consists of a single tungsten-wire cathode inside a cylindrical anode. It is connected

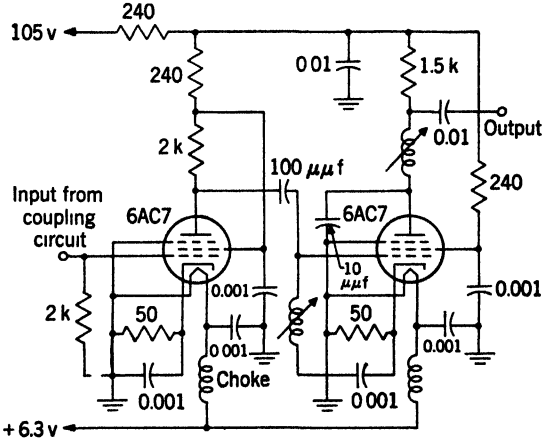

FIG. 9·29.—Preamplifier circuit.

to the crystal-holder terminals through the bypass condensers C_5, and the power supply is decoupled by the chokes L_3, which are resonant at 30 Mc/sec. When the diode is used, the terminal for d-c crystal current is connected to ground by a short-circuiting plug; this connects the plate of the diode to ground for the d-c component.

A schematic diagram of the preamplifier circuit is shown in Fig. 9·29. When used with the coupling network just described, the noise figure of the preamplifier is about 6 db.

The output-meter circuit is built into the Hallicrafter receiver as indicated in Fig. 9·30. The 6SK7 tube indicated in the figure is the

third i-f amplifier of the receiver. This circuit utilizes a crystal rectifier as a detector, giving indications nearly proportional to power. The rectifier connected in parallel with the 200 $\mu\mu$f condenser serves as a d-c return for the output circuit. The output meter is a 200-μa 400-ohm meter. The bandwidth of the equipment is limited by that of the Hallicrafter receiver, which is 80 kc/sec with the selectivity switch turned to BROAD. The intermediate frequency of this receiver is 5.25 Mc/sec, a feature that eliminates the danger of instability from feedback to the 30-Mc/sec input circuit.

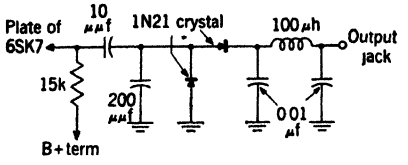

FIG 9·30.—Output-meter circuit.

Calibration and Operation of the Set.—The output meter is calibrated in terms of noise temperature by the method described in Sec. 7·8, using the noise diode. It was shown there that the noise temperature of a resistor R connected to a noise diode is

$$t = 1 + 20IR, \tag{9}$$

where I is the diode current. With the noise diode off, the r-f gain control of the receiver is so adjusted that the output meter reads 100 μa with the standard 300-ohm resistor cartridge in the crystal holder. With the gain fixed at this value, the output meter is read for various values of I corresponding to the range of t values desired. The sensitivity of the output indication is about 20 μa per unit of noise temperature.

For the measurement of crystal noise temperature the available r-f power must be set at the specified value of 1 mw. This is normally done as in the conversion-loss set, by means of the large adjusting nut on the oscillator mount. If calibrated crystals are available, the power level is adjusted for the rectified current specified for the crystals; if not, the set may be calibrated by replacing the crystal holder by a matched bolometer and adjusting the power level to 1 mw. A set of crystals can then be calibrated for checking the power level.

The set is susceptible to interference at the signal and image frequencies and at the intermediate frequency. If interference is present, it can sometimes be recognized by listening to the loudspeaker. Interference cannot always be recognized in this way, however, and hence is especially subtle and troublesome. It may cause an apparent instability and loss of sensitivity or, in other words, an apparent increase in amplifier noise figure. Interference at 30 Mc/sec can sometimes be detected by observing a change in output-meter reading when the bulb of the noise diode tube is touched with the finger. Obviously the set cannot be used as long as there is enough interference to have any effect on the output-meter reading. It is then advisable to operate the set in a well-shielded room.

The set should also be operated in a location relatively free from drafts and with the oscillator tube shielded from air currents. This precaution tends to prevent frequency drift of the oscillator and the consequent change in transmission through the high-Q filter.

9·6. The Noise Measuring Set for the 10-cm Band.—Like the conversion-loss sets, the set for measuring noise temperature in the 10-cm

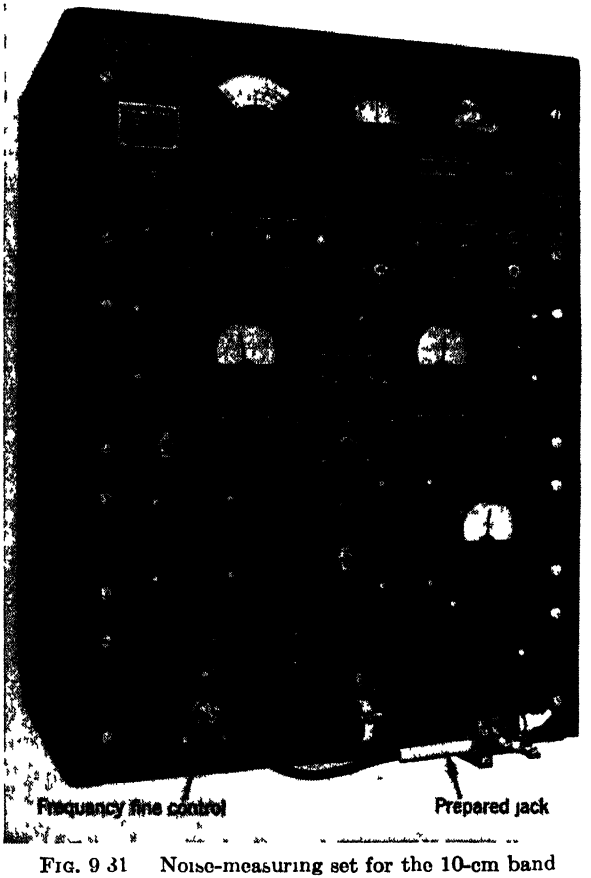

FIG. 9·31 Noise-measuring set for the 10-cm band

band was developed after the 3-cm set; it is therefore in many respects similar in design to the 3-cm set. It was developed by Huntington.[1] A photograph of the equipment is shown in Fig. 9·31; the block diagram is the same as that of Fig. 9·23, except that a type 707B oscillator is used. The bottom panel includes the r-f oscillator, crystal holder, input coupling circuit, noise diode, and preamplifier. The second panel contains a power supply for the preamplifier, a loudspeaker, and the output meter. The

[1] H. B. Huntington, "1N21 Noise Tester, Type 11044," RL Report No. M-191, Jan. 9, 1945. The set was manufactured by Photoswitch, Inc., Cambridge, Mass.

third panel is a power supply for the r-f oscillator and includes a meter for measuring rectified crystal current. The top panel is a Model S-36 Hallicrafter Receiver. The r-f filter is mounted on the bottom of the cabinet in the rear.

R-f Components.—A photograph of the r-f panel is shown in Fig. 9·32. The type 707B oscillator tube, mounted in a broadband cavity as described in Sec. 9·2, can be seen in the lower part of the photograph.

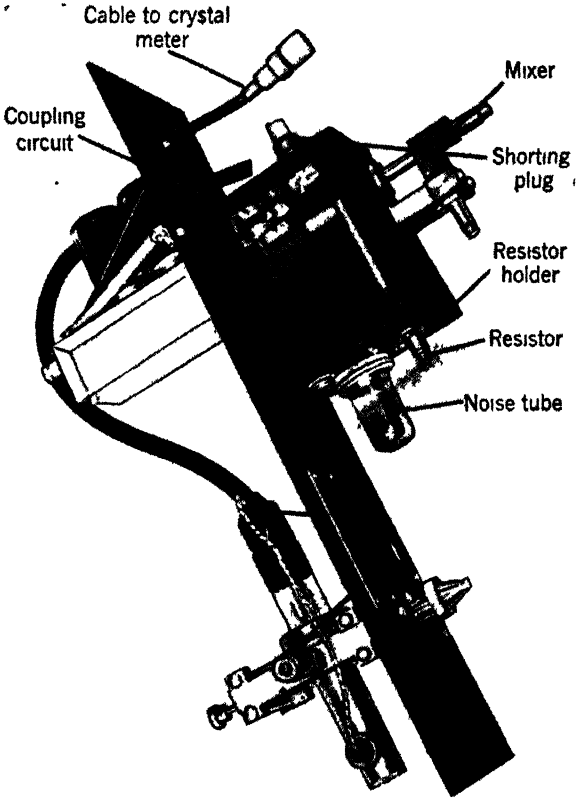

FIG 9 32.—R-f panel of the 10-cm noise set.

The output coupling loop from the cavity is connected to the r-f filter with about 3 ft of 50-ohm lossy cable. The filter is a 721A TR switch. It is tuned to the test frequency of 3060 Mc/sec and has a 0.7-db insertion loss, with about 15 Mc/sec between half-power points. The output loop of the filter is connected to the crystal holder by about 10 ft of 70-ohm lossy cable, which provides about 12 db of attenuation between the filter and crystal holder. As in the loss sets, the cable jack that is connected to the crystal holder is so adjusted that the characteristic impedance of the 70-ohm line is presented at the terminals.

The crystal holder is identical with that used in the conversion-loss set.

Circuit Details.—The power supply for the r-f oscillator is the same as that used in the conversion-loss set. The power output is controlled within limits by a variable resistor between the grid and the cavity of the 707B tube. The power output can be roughly adjusted by means of the coupling loop in the oscillator cavity. The power supplies for the preamplifier and the noise diode are the same as those used in the 3-cm set.

The input coupling circuit is mounted on the r-f panel, as shown in Fig. 9·32. A schematic diagram of the circuit is shown in Fig. 9·33. The circuit is essentially the same as that used in the 3-cm equipment,

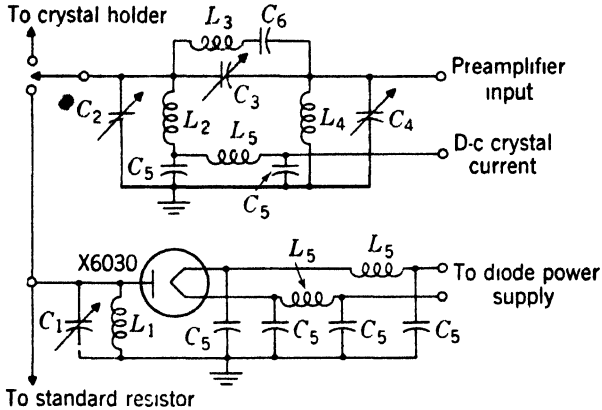

C_1, C_2 = 5–20 $\mu\mu$f
C_3, C_4 = 3–13 $\mu\mu$f
C_5, C_6 = 0.001 μf

L_1 = 20 turns
L_2 = 9 turns
L_3 = 11 turns
} #28 wire on ½-in. coil forms
L_5 = resonant choke at 30 Mc/sec

FIG. 9·33.—Input coupling circuit for the 10-cm noise set.

except that the standard resistor R_1 in the latter is replaced by a resistor holder into which the various resistors used in adjustment and calibration are plugged. The noise diode is connected to the resistor holder as shown in Fig. 9·33. As in the 3-cm set, capacitance C_1 is tuned so that the output-meter reading does not change when switch S is thrown from the crystal holder to the resistor. The equipment is so designed that the transmission line from the crystal to the switch has nearly the same electrical length at 30 Mc/sec as that from the resistor to the switch. The adjustment of C_1 can therefore be made without resistor cartridges in the crystal and resistor holder.

The preamplifier is, with two exceptions, the same as that shown in Fig. 9·29: the grid resistor is 3000 instead of 2000 ohms, and there is a feedback resistor of 22,000 ohms between the plate and control grid of the first tube. The feedback feature is used to compensate for a rela-

tively large variation in capacitative susceptance from crystal to crystal as seen at the 30-Mc/sec terminals of the crystal holder. This variation may be as large as 2.5 $\mu\mu$f and is transformed by the coupling network to an increase in impedance at the grid. The inverse feedback tends to compensate for this effect by decreasing the gain of the first stage as the impedance presented to the grid increases. The effect is attributed to reflections in the crystal holder at image and signal frequencies.

The output-meter circuit is the same as that shown in Fig. 9·30.

The calibration and operation of the 3-cm set, discussed in Sec. 9·5, applies to the 10-cm set, except that the standard resistance is 400 ohms, and the available r-f power is set at 0.5 mw.

9·7. Noise-temperature Measurement of 1-cm Rectifiers.—The JAN specifications for testing the 1N26 rectifier specify that noise-temperature measurements shall be made as specified for the 3-cm rectifier types. They can be made in the standard test set by using an adapter in the crystal receptacle of the crystal holder into which the coaxial cartridge can be plugged. The design of the adapter must be such that it matches the crystal to the 3-cm fixed-tuned crystal holder. It turns out that an adapter which matches one brand of rectifier does not in general match other brands. This is not a surprising fact when one recalls that the impedance of the rectifying contact, and consequently the internal structure of the cartridge that matches the crystal to the 1-cm crystal holder, may differ from brand to brand; with a change in frequency, the impedance transformations effected by the cartridge structure may be different. For example, a quarter-wave transformer at 1 cm is only $\frac{1}{12}$ wavelength at 3 cm.

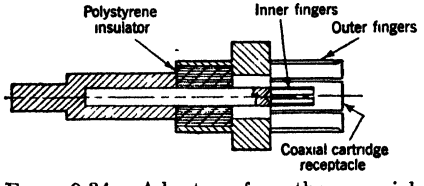

FIG. 9·34.—Adapter for the coaxial cartridge.

The JAN test specifications stipulate that each manufacturer shall design an adapter that will match his own brand of crystal to the 3-cm crystal holder. Such an adapter, suitable for the Sylvania 1N26 cartridge, was designed at the Radiation Laboratory by H. C. Torrey[1] for use with the burnout tester (see Sec. 9·8). This adapter is shown in Fig. 9·34. One end of this adapter has the same dimensions as the ceramic cartridge and plugs into the crystal holder; the other end has spring fingers for the inner and outer conductors of the coaxial cartridge. The center conductor is insulated by means of a polystyrene bead to which the metal parts are force-fitted.

The adapter introduces a certain amount of capacitance in parallel with the crystal. If the equipment is tuned for 3-cm measurements, as it will be if used interchangeably, this additional capacitance increases the

[1] Unpublished data.

indicated noise temperature by about 0.2 units for a 400-ohm crystal in an adapter which introduces 2 $\mu\mu$f capacitance.

The specifications stipulate an r-f power level giving a rectified crystal current of at least 0.5 ma. This adjustment of power level can be conveniently made with the vane attenuator used on the 3-cm equipment.

BURNOUT

9·8. Spike Test.—Most of the standard crystal types designed for mixer use are proof-tested for burnout in the process of manufacture. After assembly, but before any acceptance tests are made, every unit is required to withstand a single d-c pulse generated by the discharge of a coaxial-line condenser. The pulse, of duration about 2.6×10^{-9} sec, is designed to simulate a TR-switch "spike," such as is encountered by crystals in duplex receivers (see Sec. 8·1).

A schematic diagram of the electrical circuit is shown in Fig. 9·35. With the switch S open, the coaxial condenser is charged to some voltage V through the 1-megohm resistor which terminates the line at the open end. With the crystal inserted at X as shown, the switch is quickly closed, the condenser discharging into the crystal. The pulse received by the crystal is not one of exponential decay, as would be the case if the condenser had a lumped capacitance and no inductance. It may be shown from the theory of propagation in transmission lines that, provided the impedance of the crystal is equal to the characteristic impedance of the coaxial line, a single pulse results—of uniform amplitude equal to $V/2$ and duration t_0 equal to twice the line length divided by the velocity of light c,

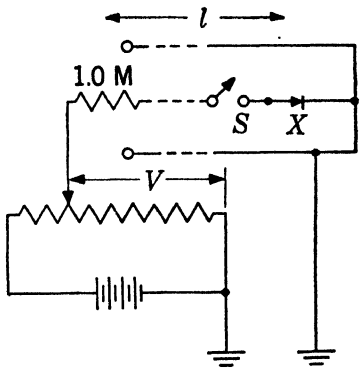

FIG. 9·35.—Circuit for the coaxial line burnout test.

$$t_0 = \frac{2l}{c}. \tag{10}$$

The energy dissipated in the crystal is thus

$$W = \frac{t_0}{Z_0}\frac{V^2}{4}, \tag{11}$$

where Z_0 is the line impedance, and may easily be shown to equal the potential energy of the condenser before discharge.

If the crystal impedance Z does not match the line impedance Z_0, a succession of pulses of decreasing amplitude occurs. If Z is real, each pulse is flat, but if Z has an imaginary part, the pulses are distorted. If,

however, capacitance and inductance of the crystal are small compared with the capacitance and inductance of the line respectively, the distortion is negligible. This is almost certainly the case. Thus we can confine our attention to the case of real Z. Let the ratio of Z, considered real, to Z_0 be denoted by ρ. Then the amplitude V_n of the first few pulses will be given by

$$\left.\begin{aligned} V_1 &= \frac{\rho}{\rho + 1} V_0, \\ V_2 &= \frac{\rho(\rho - 1)}{(\rho + 1)^2} V_0, \\ V_3 &= \frac{\rho(\rho - 1)^2}{(\rho + 1)^3} V_0, \end{aligned}\right\} \tag{12}$$

and the amplitude of the nth pulse will be

$$V_n = \frac{\rho(\rho - 1)^{n-1}}{(\rho + 1)^n} V_0. \tag{13}$$

Thus if ρ is greater than unity, all pulses have the same sign and the initial pulse has a larger amplitude than $V_0/2$. If ρ is less than unity, successive pulses alternate in sign and the initial pulse has less amplitude than $V_0/2$.

It is easily shown from Eq. (13) that the energy W_n absorbed by the crystal load in the first n pulses is given by

$$W_n = W_0 \left[1 - \left(\frac{\rho - 1}{\rho + 1} \right)^{2n} \right], \tag{14}$$

where W_0 is the potential energy of the charged condenser. For example, if $\rho = 2$ or $\frac{1}{2}$, then $W_1 = \frac{8}{9} W_0$, $W_2 = \frac{26}{27} W_0$, etc., whereas if $\rho = 5$ or $\frac{1}{5}$, $W_1 = \frac{5}{9} W_0$, $W_2 = 0.765 W_0$, $W_3 = 0.912 W_0$, etc. Thus even for a considerable mismatch most of the energy is dissipated in a time of the order of t_0. The importance of dissipating most of the available energy in a time less than the thermal relaxation time of the crystal contact has been stressed in Sec. 8·4.

An assembly drawing of the coaxial line as used in these tests is shown in Fig. 9·36. The diameter of the inner conductor is $\frac{3}{16}$ in. and the inner diameter of the outer conductor is 0.436 in. The resulting line impedance Z_0 is 50.5 ohms. In operation the inner conductor is negatively charged and the initial pulse is applied to the crystal in the forward direction. At the high charging voltages used, 30 to 200 volts, the barrier plays no role in the forward direction and the crystal impedance is given by its spreading resistance, which for the various units tested varies from 10 to 70 ohms. The line is terminated at its open end by a

1-megohm resistor encased in a phenol-fiber jacket to take up mechanical shock.

The instrument is operated as follows. A solenoid acting on the steel rod (1) lifts the inner conductor, which slides smoothly and with little friction in the fiber guides (2). The solenoid is then deactivated, dropping the inner conductor about two inches. The charged inner conductor strikes a cap (3) attached to the crystal pin, thus quickly forming electrical connection to the crystal. The crystal and cap are incidentally ejected from the line by the force of this blow. The electrical connection between the inner conductor and the crystal cap is formed by contact between a round surface (4) and a flat surface (5) of a very hard and brightly polished osmium-rhodium alloy. The hardness is required in order to resist the impact, and the polishing is necessary to reduce field emission before physical contact.

There is some question as to whether a good electrical connection can be formed between these contact surfaces in a time of order t_0 (3×10^{-9}

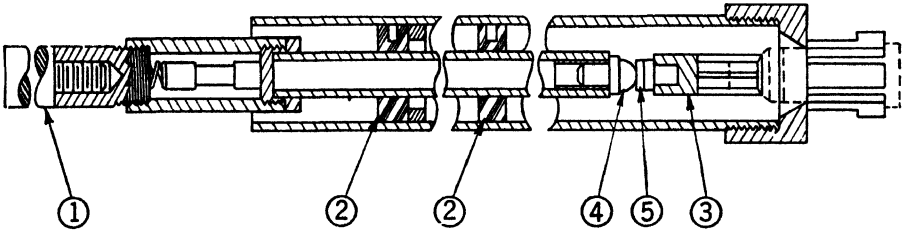

FIG. 9·36. Coaxial line burnout tester.

sec). If there were some straggling at the contact because of field emission, some of the energy would be dissipated at the contact. Experiments conducted in England, however, have indicated that all the available energy is actually dissipated in the load in a device of this type. Another possibility is that a partial electrical connection may be formed between the surfaces prior to physical contact by virtue of the capacitance between the contact surfaces. An elementary calculation reveals, however, that this effect should not appreciably slow contact formation beyond the time t_0 of the fundamental pulse. There is some evidence, on the other hand, that the atmospheric humidity may reduce the effectiveness of the device. This may be due to a bypass of the condenser charge through defective insulation or to a faulty formation of the electrical contact. It is desirable, if possible, to operate the device in a relatively dry atmosphere.

The capacitance of the standard coaxial line is about 25 $\mu\mu$f and the charging voltage, which gives 1 erg of stored energy, is 90 volts. The proof-test energies for the various crystal types are given in Table D·1, Appendix D.

9·9. Microsecond Pulse Tests.—A few crystal types, notably the video detectors 1N32 and 1N27, are tested for burnout by microsecond "d-c pulses" designed to simulate the microwave electrical overloads commonly encountered in their use. The microsecond d-c pulses are formed by the discharge of a pulse-forming network (the lumped constant equivalent of a transmission line). A detailed discussion of such networks will be found in Vol. 5 of the Radiation Laboratory Series. It will suffice here to remark that, like a transmission line, they have a characteristic impedance Z_0 and an effective electrical length l. The analysis of the coaxial-line pulses of the preceding section applies to a pulse-forming network.

In burnout testing with "spikes," the shape of the pulses is not of great importance, since it is the energy of a pulse rather than its power

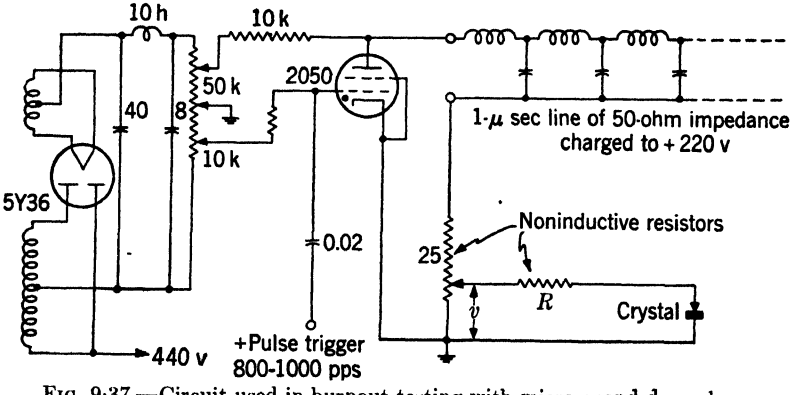

FIG. 9·37.—Circuit used in burnout testing with microsecond d-c pulses.

that is effective in burnout. For burnout testing with microsecond pulses, on the other hand, it is important to ensure that the pulses are flat, so that the pulse power is uniform over the pulse duration. The pulse-forming network must be designed with care to eliminate nonuniformities in the pulse, particularly overshoots near the leading edge.

Figure 9·37 shows the circuit used for testing video detectors. The 50-ohm, 1-μsec pulse-forming network is charged through a 10,000-ohm resistance to about 220 volts. A positive pulse of about 10 volts is coupled to the grid of the thyratron, causing the pulse-forming network to discharge into the 25-ohm resistance and thyratron in series. This series combination matches the impedance of the artificial line. A tap on the 25-ohm resistor leads to a resistance R in series with the crystal rectifier. The advantage of this arrangement over a direct discharge of the line into the crystal is that the termination of the line is nearly independent of the crystal impedance; hence only a single pulse of known amplitude results. The resistance R is chosen to be 25 ohms so that the crystal may be approximately matched to the circuit.

One advantage of a thyratron over a mechanical switch is that multiple pulses may be used with ease. The pulse-repetition frequency is, as indicated, 800 to 1000 pps, and exposure times of 1 min are used in the test.

In the case of video detectors these tests are used as design rather than as proof tests. A similar test employing a 1-μsec pulse is used as a proof test, however, for the 1N25 rectifier, a high-burnout mixer crystal for the 30-cm band. Although the 1N25 rectifier is protected in use by a TR tube and is therefore subject to "spike" burnout, a 1-μsec pulse test is used for it since there is some reason to believe that the coaxial-line tester fails to operate correctly at the high voltages required for this crystal.

FIELD TESTING

9·10. D-c Tests.—It was observed in Sec. 8·4 that a deterioration in the conversion loss and noise temperature of a mixer crystal as a result of burnout or mishandling is almost always accompanied by a decrease in the back resistance of the rectifier. Extensive tests have shown that a simple field test can thus be provided which will distinguish with little error between those crystals that have not deteriorated since passing the manufacturer's acceptance tests and those that have deteriorated to the extent that the receiver noise figure has increased by more than 1 or 2 db.

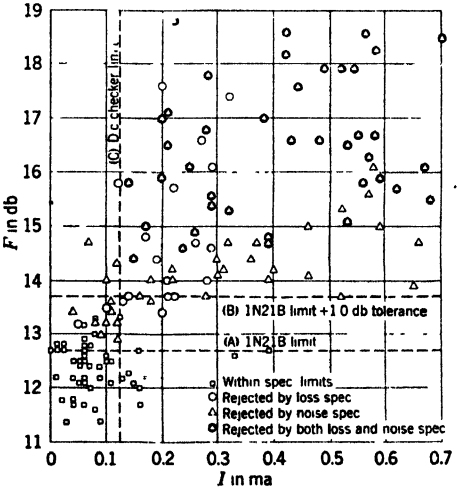

FIG. 9·38.—D-c crystal checker. Calibration chart for 1N21B units; noise figure of receiver (assuming 5-db amplifier) vs. back current at 1.0 volt.

Accordingly, a simple "d-c checker" has been developed, consisting of a small box with a dry cell and a few resistors, which measures the back resistance of the rectifier at 1 volt. It has been found that a somewhat more complete separation of "good" from "bad" units may be made if limits are provided also for forward resistance and for "back-to-front ratio," as measured by a conventional ohmmeter. The checker, therefore, has a simple ohmmeter incorporated in it to measure these quantities.

As an example of the utility of the test of back resistance at 1 volt, the calibration data for the 1N21B mixer crystal (10-cm band) is shown in Fig. 9·38. In this chart each crystal tested is represented as a point. The noise figure of a crystal-mixer receiver with a 5-db amplifier is

plotted vertically, and the reverse current at 1 volt is plotted horizontally. The crystals represented here were deliberately subjected to a sufficient number of microsecond d-c pulses to deteriorate them appreciably, on the average. A horizontal line A is drawn at the 1N21B specification limit corresponding to the acceptance limits on loss and noise, and a second horizontal line B is drawn to indicate the above acceptance limit plus 1 db, a tolerance that is always applied according to specifications on remeasurements.

The vertical line C at 0.125 ma was selected as the test limit for the crystal checker on the basis of these data for the 1N21B rectifier. Although the points are well scattered on the chart, it is apparent that

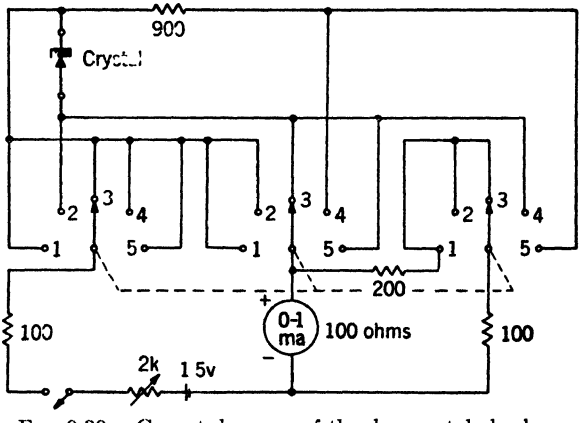

FIG. 9.39.—Circuit diagram of the d-c crystal checker.

the crystals accepted on the basis of the checker limit (i.e., the crystals to the left of line C) are almost all less in noise figure than the specification plus tolerance limit (line B). Also the crystals rejected (points to the right of line C) are almost all greater in noise figure than the limit indicated by line B. Actually the separation is even better than indicated, for, out of 200 1N21B units tested, only 139 are on the chart; the remaining 61 were rejected both by the checker and by noise-figure tests but were too high in reverse current or in noise figure to fall on the chart. Furthermore, it must be remembered that the units represented here had all been partially destroyed in order to provide calibration data. Before these crystals were burned they had been tested both by the checker and by noise and loss measurements. All were less in noise figure than the acceptance limit plus 1.0 db tolerance and all but 2 were correctly indicated as "good" by the check limit of 0.125 ma.

Certain limitations of the checker must be recognized. It has been found to give a reliable test only for units that have at one time passed the test specification limits on loss and noise; hence it cannot be used as a substitute for these tests. Also, separate calibration of the checker is

necessary for each crystal type and the fact that a unit of one type passes the check limit for a second type does not, of course, imply that the unit is an acceptable substitute for units of the second type.

The electric circuit of the checker is shown in Fig. 9·39. In positions 1, 2, and 3 of the ganged five-position switch, the checker is used as an ohmmeter. In position 1, the ohmmeter is short-circuited and the rheostat is adjusted to produce full-scale deflection of the meter. The meter dial has two scales, one reading directly in ohms. In positions 2 and 3 of the switch, the dial reading indicates, respectively, the front and the back resistances of the rectifier. In position 4 the rheostat is readjusted for full-scale deflection. Under this condition 1.0 volt is placed across the crystal unit in the back direction. In position 5 the meter is in series with the crystal and reads on its second scale, calibrated in milliamperes, the back current at 1.0 volt. In calibrating the checker 200 units of each type were used, 100 each from the products of the two leading manufacturers. Whereas, in general, a different limit was required for each type, it was found that for a given type the same limit would usually apply to the products of the two manufacturers. This was found to be true for the 10-cm-band types 1N21, 1N21A, and 1N21B and for the 3-cm types 1N23, 1N23A, and 1N23B. It was not, however, found to be the case for the 1N26, the 1-cm-band unit. The calibration procedure was to measure each unit for conversion loss, noise temperature, back current at 1.0 volt, and front and back ohmmeter resistances. These measurements were made both before and after burning the units with microsecond d-c pulses. From the data for loss and noise, the noise figure F of a crystal-mixer receiver with an amplifier of 5-db noise figure was computed. This noise figure F was then plotted for each crystal against the back current at 1.0 volt and a limit on the latter quantity was selected which would divide the group including burned and unburned units into "good" and "bad" categories determined by the noise-figure acceptance limit plus a 1-db tolerance. It was found that the additional requirement of a "front resistance" less than 500 ohms and a "back-to-front ratio" of more than 10 slightly reduced the number of false acceptances without appreciably increasing the number of false rejections.

The limits on back current at 1.0 volt for the various types are given in Table 9·1 and the calibration results in Table 9·2.

TABLE 9·1.—ACCEPTANCE LIMITS ON BACK CURRENT AT 1.0 VOLT

Type	Acceptance Limit, ma
1N21	0.40
1N21A	0.175
1N21B	0.125
1N23	0.40
1N23A	0.30
1N23B	0.175

TABLE 9·2.—DATA INDICATING RELIABILITY OF THE CRYSTAL CHECKER*

	After burnout	Before burnout
Number tested	600	600
False acceptances, %	2.2	0
False rejections, %	12.6	1.0
Mean error in noise figure of false acceptances, db	0.8	0
Maximum error in noise figure of false acceptances, db	2.1	0

* This table includes crystal types 1N21A, 1N21B, 1N23, 1N23A, and 1N23B.

CHAPTER 10

MANUFACTURING TECHNIQUES

This chapter is limited to a description of representative techniques used in manufacturing crystal rectifiers for mixer applications. The special procedures for making high inverse-voltage rectifiers, low-level detectors, and welded contact rectifiers will be discussed in the chapters devoted to those subjects.

The general processes for making high-quality rectifiers are now well established. At present, these are: (1) purification of the semiconductor, (2) controlled addition of a selected impurity that produces the desired properties, (3) preparation of an ingot from which the wafers used in the cartridge are cut, (4) preparation of the surface of the wafers by a process of polishing, heat treatment, and etching, (5) shaping and pointing the cat whisker, (6) assembly and adjustment, and (7) performance-testing.

No attempt will be made in this chapter to describe in detail the procedures that have been used successfully by all the various manufacturers or to include procedures that the authors regard as obsolete. Those described below may be regarded, however, as representative of the present state of the art. Alternative methods are included in some cases to indicate that no set of techniques is to be regarded as unique.

PREPARATION OF THE SEMICONDUCTOR

10·1. Purification of the Semiconductor.—Because the rectifying property of the semiconductor is affected by minute quantities of impurities, the first step in the manufacture of rectifiers is the purification of the semiconductor. The degree of purification required depends to some extent on the method of preparing the ingot. The process of preparing silicon ingots developed by the Bell Telephone Laboratories (described in Sec. 10·3) uses commercial Electromet silicon, with a purity of 99.8 per cent. The method is such that the upper part of the melt has the required rectifying properties. The lower portion is discarded. Other manufacturers, however, have been able to utilize the whole ingot by using the high-purity duPont silicon.

Purification of Silicon.—The method developed at duPont produces high-purity silicon, excellent for crystal rectifiers, and uniform from lot to lot. The purity is estimated from spectroscopic tests to be not less than 99.9 per cent. Other impurities not detectable by spectroscopic means may be present, but if so they appear to have no adverse

effect on the quality or uniformity of the silicon. In the early stages of development one lot of silicon was found that produced inferior rectifiers. This inferior performance was found to be due to the presence of small quantities of silica. When the silica was dissolved with hydrofluoric acid, the silicon regained its usual excellence.

The process developed by duPont is essentially the reduction of silicon tetrachloride with zinc. The reaction takes place at a temperature (950°C) well below the melting point of silicon but well above the boiling point of zinc, zinc chloride, and silicon tetrachloride. The zinc chloride formed in the reaction and any excess zinc or silicon tetrachloride are carried off as a vapor. The silicon is deposited on the bottom of the reactor chamber in the form of needle-shaped crystals.

A sketch of the general layout of the equipment is shown in Fig. 10·1. The main reactor chamber is a fused silica tube 6 ft long and 8 in. in

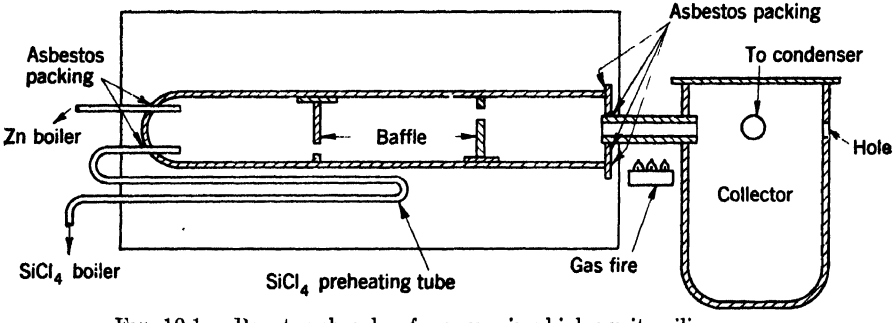

FIG. 10·1.—Reactor chamber for preparing high-purity silicon.

diameter one end of which is fused over and carries two input pipes for introducing the silicon tetrachloride and zinc vapor. A silica plate is clamped to the other end. This plate carries an outlet pipe that feeds a silica pot collector. Zinc chloride and excess zinc settle out in the collector and the excess silicon tetrachloride passes through an outlet near the top to a condenser. The reactor is heated by "globar" heaters (not shown in Fig. 10·1). The whole apparatus is thermally lagged with diatomaceous earth. The joints are packed with a paste made from asbestos mixed to a stiff dough with water.

The zinc, at least 99.9 per cent pure, is bought in slab form. When it is melted in a silica beaker, any oxide present forms a skin on the surface. The molten zinc is poured from beneath this skin into the boiler, from which the zinc vapor is fed to the reactor tube. Because of its low boiling point the silicon tetrachloride is preheated before entering the reactor. This is accomplished by feeding it through long quartz tubes lying within the main heating chamber. The silicon tetrachloride is bought already distilled from an external supplier. Redistillation is unnecessary.

Prior to a run the reactor is heated for 5 hours to a temperature of 950°C; after this the zinc and silicon tetrachloride vapors are introduced.

Since these substances enter the reactor with considerable velocity, baffles are inserted to break up the vapor stream. There are two baffles, each of which is a silica disk fused to a silica base. One disk has a 2-in. hole near its top and the other an identical hole near its bottom. One run takes 24 hr and yields 7 to 8 lb.

During the reaction some silicon is deposited in the outlet pipe. To prevent clogging this silicon is removed at intervals by pushing a silica rod through a hole in the collector and into the outlet pipe.

At the end of a run the end plate is taken off and the silicon removed, the portion near the end plate being discarded. The silicon is washed in HCl and, finally, in distilled water.

The British General Electric Company employs the following procedure[1] for purifying silicon used in the General Electric Company "red-dot" high-burnout crystal. The steps of the procedure outlined below follow the method of Tucker.[2]

1. Commercial silicon powder about 98 per cent pure is crushed so that it will pass through a 200-mesh screen. Then 750 g of the powder are covered with water and HCl is added.
2. After the first violent reaction an excess of HCl is added along with some HNO_3. The mixture is digested for 24 hr.
3. The mixture is diluted, filtered, and washed thoroughly with distilled water.
4. The powder is placed in a platinum pail and a liter of distilled water is added.
5. To the mixture is added about 300 cc of H_2SO_4 and about 200 cc of concentrated HF (about 40 per cent). The HF is added slowly. The mixture is then warmed for 4 hr, and further similar quantities of H_2SO_4 and concentrated HF are added.
6. The mixture is evaporated to fuming; the residue is washed thoroughly with distilled water and then filtered.
7. The material is treated with 700 cc of concentrated HF and left standing for 12 hr.
8. It is then filtered, washed thoroughly, and dried. After undergoing this purification process, the silicon is analyzed and found to be almost spectroscopically pure.

To the authors' knowledge no tests have been made of the comparative excellence of silicon made by this method and the duPont silicon.

[1] This procedure, reported in a memorandum written by H. Guyford Stever on a visit to the GE Co., is the process used as of March 1943.

[2] "Alloys of Iron Research," Part 7, *J. Iron Steel Inst.* (*London*), **115**, 412 (1927).

Germanium.—Two methods have been employed successfully in the production of pure germanium for rectifier use. The first of these methods is the reduction of germanium oxide with hydrogen. At the suggestion of Dr. Karl Lark-Horovitz, the Eagle-Picher Company at Joplin, Mo. developed a method for producing germanium oxide from their standard ore residue. This source of supply made possible the development work on germanium at Purdue University, General Electric Company, and Bell Telephone Laboratories. The same company also supplied germanium tetrachloride for the second method of preparing pure germanium described later.

The procedures used by the various laboratories for the reduction of the oxide are essentially the same. The details of the Bell Telephone Laboratories procedure[1] are as follows. The reduction takes place in a furnace consisting of a 4-in. silica tube 3 ft long which is closed at one end. The other end is sealed to a metal head closed by means of a metal cover that uses a lead gasket. The furnace head carries hydrogen inlet and outlet tubes through which a continuous flow of hydrogen is maintained during the reduction process. The reactor tube is heated by a resistance furnace. A charge of 50 g of germanium oxide is placed in a quartz boat 5 in. long, $1\frac{3}{4}$ in. wide, and 1 in. deep, and the boat placed in a silica shield tube. The furnace tube is then sealed, flushed with hydrogen, and heated at a temperature of 650°C for 3 hr; this is followed by a period of 45 min at 850°C. During the heating cycle the hydrogen flow is maintained at a rate of 5 liters per sec. By this method the germanium dioxide is reduced to germanium with an actual yield of 95 per cent of the theoretical yield. Since some loss probably occurs because of the evaporation of GeO, the yield of 95 per cent probably represents complete reduction.

It has become common practice to test the purity of the product by resistivity measurements on samples taken from various parts of an ingot made from the pure germanium, the resistivity in general increasing with the purity of the sample. Theuerer and Scaff report that the resistivity of germanium made from various lots of Eagle-Picher oxides varies from 4 to 12 ohm-cm.

North[2] reports similar measurements on bulk resistivity with values ranging from 0.5 to 20 ohm-cm. The procedure used by North for reducing the oxide is as follows. The oxide is placed in a fused silica boat within a closed thin-walled iron sleeve which is inserted in an Alundum-tube hydrogen furnace. The iron sleeve is supplied with

[1] H. C. Theuerer and J. H. Scaff, "Development of High Back Voltage Germanium Rectifiers," NDRC Interim Report No. 1, Contract OEMsr-1408, Nov. 21, 1944.

[2] H. Q. North, "K-band Germanium Crystals," NDRC 14-328, GE Co., Mar. 26, 1945.

hydrogen which is carefully dried and purified by passing it through activated alumina, a copper purifier, phosphorous pentoxide, and a liquid-air trap. The reduction process is carried out in 15 hr at a temperature of 650°C; after this, melts of the germanium are made in a graphite boat in the same furnace by heating to a temperature of 1015°C for 20 min.

North's results may be summarized as follows. The bulk resistivity of germanium fused in a hydrogen atmosphere is critically dependent on the amount of water vapor present. If the dew point is as high as 30°F, resistivities as high as 40 ohm-cm are obtained. Moreover, vacuum melts made in the presence of water vapor have yielded resistivities as high as 40 ohm-cm. Regardless of the dryness of the *reducing* hydrogen, germanium *fused* in pure dry hydrogen yields bulk resistivities of 2 ohm-cm and below. Remelting in moist hydrogen raises the resistivity to the range of 10 to 20 ohm-cm. In the development work at General Electric, North found that germanium of a bulk resistivity of 5 to 30 ohm-cm was satisfactory for rectifier use.

In the second method, developed by duPont,[1] high-purity germanium is produced from the tetrachloride in an oxygen-free atmosphere with zinc vapor as the reducing agent. This is similar to their method of producing high-purity silicon. The germanium tetrachloride is obtained from the Eagle-Picher Company.

For this second method the reactor is a 4½-in. silica tube 3 ft long housed in a furnace of insulating brick and heated by means of "globars." The germanium tetrachloride is preheated by passing it through 14 ft of silica tubing, housed within the furnace, before it enters the reactor. Zinc vapor from a silica flask boiler enters the reactor through a jet adjacent to the germanium tetrachloride jet, both of them mounted in one end of the reactor tube parallel to the axis of the tube. During a run the reactor temperature is maintained at 930°C, approximately midway between the boiling point of zinc and the melting point of germanium.

Germanium prepared by this method alloys with zinc at the temperature of the reactor, and the product recovered from the reactor may contain as high as 40 per cent zinc. Most of this residual zinc can be removed by continuing the heating and passing inert gas through the reactor after the reaction has been completed. The product is then broken up by gently hammering it between two blocks of pure zinc and treating it with hydrochloric acid until chemical reaction has ceased. This removes all but about 0.2 per cent zinc, which can be removed by

[1] C. E. Rick and T. D. McKinley, "Sintering or Melting of Boron and Preparation of Hyperpure Germanium," OSRD Progress Report NWP-P-44-3K, Contract OEMsr 1139, Aug. 1 to Sept. 1, 1944.

vacuum melting. Following this hydrochloric acid treatment, the product is treated for 4 hr with concentrated boiling hydrofluoric acid to remove any silica present. It is then washed and dried.

With the apparatus described above, two typical runs yielded a total of 7.2 lb of germanium in a total reaction time of 26 hr. A spectroscopic analysis of the germanium gave an estimated impurity of approximately 0.05 per cent, in addition to the 0.2 per cent zinc mentioned above. Resistivity measurements of melts made from this germanium gave values in the range of 30 to 40 ohm-cm, and the rectification characteristics show that it is at least as good as that prepared by the reduction of the Eagle-Picher germanium dioxide. As yet not enough lots of the duPont germanium have been prepared to determine whether it is superior in uniformity to germanium prepared from the oxide.

There is some question about the validity of the resistivity as an index of purity. Theuerer and Scaff[1] point out that in one melt of duPont high-purity germanium, the top part of which had a resistivity of 120 ohm-cm by the standard potential probe method, there were several sharply defined irregular lines running vertically in the melt where extremely high resistances were found. Along these high-resistance regions ohmic characteristics were found; adjacent to these regions there were observed a negative-resistance characteristic in the forward direction on the oscilloscope and a photo response having considerable sensitivity in the ultraviolet. Similar effects have been observed in a melt of germanium made from GeO_2.

The Purdue University group found that resistivities calculated from spreading resistance may be an order of magnitude lower than those measured directly in a slab of high-resistance germanium, and they suggest that resistivity calculated from spreading resistance is a better indication of purity. However, North[2] reports that consistent results have been obtained with resistivity measurements on large number of ingots treated identically.

10·2. Addition Agents.—To obtain good rectification characteristics a "doping" agent (a specified small quantity of a selected impurity) must be added to the semiconductor, as has been pointed out in Chap. 4. Up to now the particular agent and the proper amount to use has for the most part been decided empirically.

Addition Agents for Silicon.—The mixer crystals that have been manufactured in quantity to date have used either aluminum or boron as an addition agent; in some cases beryllium is also added. Either of these when added to silicon produces a *p*-type crystal.

[1] H. C. Theuerer and J. H. Scaff, BTL Interim Report No. 2, Contract OEMsr-1408, Dec. 16, 1944.

[2] *Op. cit.*

Aluminum was used as a doping agent by the British General Electric Company in the manufacture of red-dot crystals. In this company's procedure 0.25 per cent by weight of aluminum powder and 0.2 per cent by weight of beryllium are added to the silicon. Fox, Pearsall, and Powell[1] found that the amount of aluminum and beryllium added is not too critical. They found that good high-burnout crystals could be made by adding about 0.4 per cent of aluminum and 0.1 per cent of beryllium to the duPont silicon. Both of these addition agents are of the highest purity and are thoroughly mixed in a finely divided state with the silicon. With the Radiation Laboratory procedure of preparing the ingot, the beryllium serves to give a very solid ingot free from cracks and seems to contribute little else of perceptible advantage. On the other hand, Angello[2] reports a method of preparing the melt without the use of beryllium in which nearly all of the melt is useful. Angello used the duPont silicon with 0.5 per cent by weight of 99.9 per cent pure aluminum.

In 1942, during the early days of crystal research, an experimental study of the effect of various doping agents was made by the University of Pennsylvania group.[3] Because of the more recent advances in the melting techniques and in making high-purity silicon, the results of these experiments are now to be regarded as mainly of qualitative interest. Many elements were found which produced good current-voltage characteristics, but the r-f performance was not reported. The Pennsylvania study reported that the addition of 1 per cent of boron to silicon gave the exceptionally high conductivity of 2000 mho/cm, but that no rectification was observed. Theuerer[4] later discovered that the addition of boron to pure silicon in as small a quantity as 0.0005 per cent produces an ingot that is remarkably uniform and excellent for mixer crystals. Because of its excellent properties, combining high burnout and low conversion loss, boron-doped silicon has largely superseded aluminum-doped silicon.

The amount of boron used is not critical and varies with different manufacturers. The Bell Telephone Laboratories have found the range of 0.0015 to 0.005 per cent by weight satisfactory; the Radiation Laboratory procedure uses 0.003 to 0.006 per cent of boron and 0.02 per cent of beryllium, both added in powdered form. To add such small amounts of boron, a master alloy containing 1.0 per cent boron is first made.

[1] Marvin Fox, C. S. Pearsall, and Virginia Powell, "Manufacturing Procedure for the Radiation Laboratory High Burnout Crystals," RL Report No. 501, Dec. 21, 1943.

[2] S. J. Angello, "Westinghouse Crystal Detector Pilot Shop," Research Report SR-176, Apr. 21, 1943.

[3] F. Seitz, "The Electrical Conductivity of Silicon and Germanium," NDRC 14-110, Univ. of Penn., Nov. 3, 1942.

[4] H. C. Theuerer, "Preparation and Rectification Characteristics of Boro-Silicon Alloys," BTL Memorandum MM-43-120-75, Nov. 2, 1943.

This alloy is then used in the appropriate quantity for the doping material. Experiments by C. S. Pearsall at the Radiation Laboratory (unpublished) indicate that gallium in quantities of 0.1 per cent or less is promising as a doping agent. Time did not permit a definitive comparison of rectifier performance with that of boron-doped silicon.

No complete systematic investigation of doping materials in which the best techniques available have been used has as yet been made, and it is possible that such an investigation would uncover other alloys at least as good as the boron-doped silicon. With the present state of knowledge such an investigation is a laborious empirical procedure involving not only the preparation of melts under a variety of experimental conditions but also a statistical analysis of the conversion loss, noise temperature, and burnout characteristics of representative rectifiers made from the melt.

Addition Agents for Germanium.—Investigations of a large number of doping agents for germanium mixer crystals have been made by the Purdue group. Among the elements investigated were nitrogen, phosphorus, vanadium, arsenic, columbium, antimony, tantalum, bismuth, tin, iron, and nickel. Germanium doped with these elements results in an *n*-type semiconductor which shows good d-c characteristics. However, r-f measurements made by the Purdue group in the 10-cm band showed that many of these are inferior, both in conversion loss and noise temperature. Among those doping agents which yield low conversion loss crystals, the most promising ones are antimony and phosphorus.

Extensive development work by North[1] has been carried out with antimony as doping agent. Melts made with 0.2 to 0.5 atomic per cent of antimony have been found satisfactory. These melts exhibit resistivities in the range from 0.003 to 0.01 ohm-cm. The best rectifiers made with these crystals in the 3.2-cm band showed conversion losses as low as 3.8 db with optimum r-f and i-f matching conditions, a typical sampling averaged about 6.5 db. The best noise temperature measured was 1.4, but the average was around four times, at a rectified current of 0.6 ma and with zero d-c bias.

North has also made melts using phosphorus as doping agent. He reports that no better performance has been achieved than with antimony-doped germanium, and that the phosphorus-doped units appear to be more susceptible to burnout.

10·3. Preparation of the Ingot.—The crystals used in the rectifier cartridge are wafers cut from an ingot made by the fusion and recrystallization of a mixture of the pure semiconductor and the appropriate quantity of the doping agent. A good ingot is solid, free from cracks, and

[1] H. Q. North, "K-band Germanium Crystals," NDRC 14-328, GE Co., Mar. 26, 1945.

characterized by uniformity of the required electrical properties, or by a uniform controlled variation of these properties, throughout the ingot.

The procedures used in the preparation of the ingot by various manufacturers differ in the following essential respects:

1. The mechanical details of the furnace.
2. The heating cycle used during the melting and solidification.
3. The atmosphere in which the melt is made. Both vacuum furnaces and furnaces in which a flow of selected gas is maintained are used.
4. The nature of the cooling process. The melt may be cooled in place or may be progressively cooled from top to bottom or vice versa.
5. The crucible material used.

One or two typical procedures that have proved successful will be described. The furnace used by Fox and Pearsall at the Radiation Laboratory is a vacuum furnace of the resistance type (see Fig. 10·2). The furnace is evacuated with a glass oil-diffusion pump (1) and a mechanical pump (2) that are capable of maintaining a pressure of 10^{-4} to 10^{-5} mm of Hg throughout the melting operation. The heating unit (11) is a Norton Company Alundum electric-furnace core No. 8871 cut to a length of 6 in. and wound with about 22 ft of 0.060-in. molybdenum wire. This unit appears also at (7) mounted inside the radiation shield (6) which is a Norton Alundum core of larger size. The beryllia and opaque quartz beakers which are shown at (5) have been superseded, since this photograph was taken, by a beaker made of clear quartz; it is believed that the latter is less likely than the opaque quartz to contain impurities such as TiO_2. These beakers are $1\frac{3}{8}$ in. in diameter, $2\frac{1}{4}$ in. in length, and hold about 50 g of du Pont silicon. The brass portion of the system (12) connecting the diffusion pump to the heating chamber contains a baffle and a liquid-air trap (3). The entire brass portion of the system is water-cooled by means of copper tubing wound on the outside. The heating chamber is divided into two parts, and the photograph shows one part (8) swung open on a hinge. This portion carries a pyrex window (9) through which the progress of melt can be observed. The thermocouple temperature is read on a microammeter (4) and the pressure in the system can be measured on a McLeod gauge (10).

During the evacuation process, the power in the heating coil is gradually increased until after about $1\frac{1}{2}$ hr the melting temperature is reached. The maximum power input is about 1.5 kw at 55 volts. The temperature resulting from this input is somewhat higher than the melting point of silicon. From this point the procedure varies with the doping. For the aluminum-beryllium-doped silicon, the temperature is held constant until the charge is completely molten. The power is then

reduced to about 1 kw at 40 volts and the temperature drops gradually toward the solidification point. With some experience the operator can readily distinguish by visual observation when a further small decrease in temperature will cause solidification. When this point is reached the power is cut off and the freezing takes place within a few minutes. The success of the procedure depends critically on the correct control of the temperature in the neighborhood of the melting point. This is a

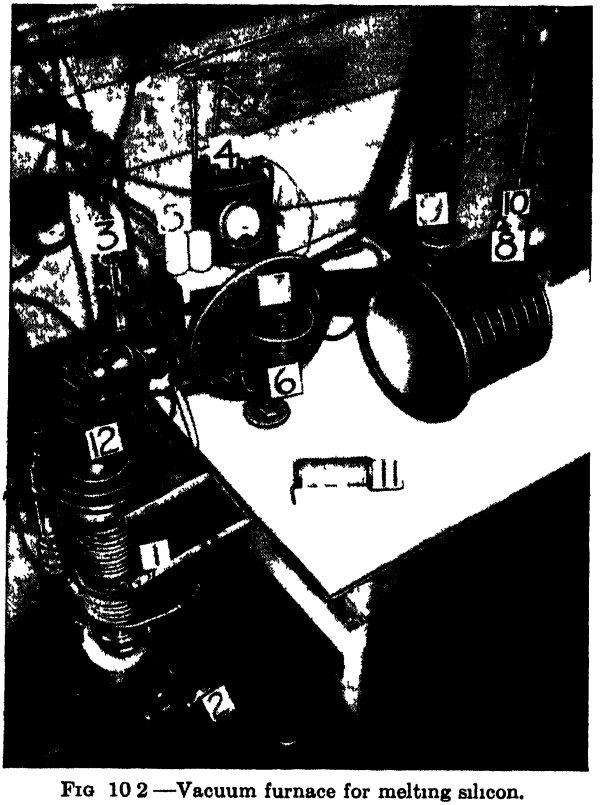

FIG 10 2 —Vacuum furnace for melting silicon.

matter to be learned largely by experience. Cooling the ingot down to room temperature requires about 2 hr.

For melts of silicon doped with boron and beryllium, the heating procedure is the same as that described above. The cooling part of the cycle is altered in the following fashion. After the charge is completely molten the power input to the heating coil is decreased in small steps so that the temperature approaches the freezing point very slowly. Just at the freezing point the power input is held constant so that the solidification takes place slowly throughout the ingot. When solidification is complete the power is again decreased in small steps until the temperature is some 200°C below the freezing point, after which the power is cut off.

The time required for the controlled part of the cooling process requires about $1\frac{1}{2}$ hr.

The ingot obtained by the above process is very solid and free from cracks. Unlike the aluminum-doped ingots, there is no separation of boron or beryllium along the grain boundaries. The slow cooling produces large crystals throughout the ingot. The size of the crystals in a typical ingot can be seen in Fig. 10·3 in which the wafers are cross sections of a typical ingot of boron-beryllium-doped silicon. Wafer (*b*) is unetched; wafer (*c*) is etched to bring out the grain-structure pattern.

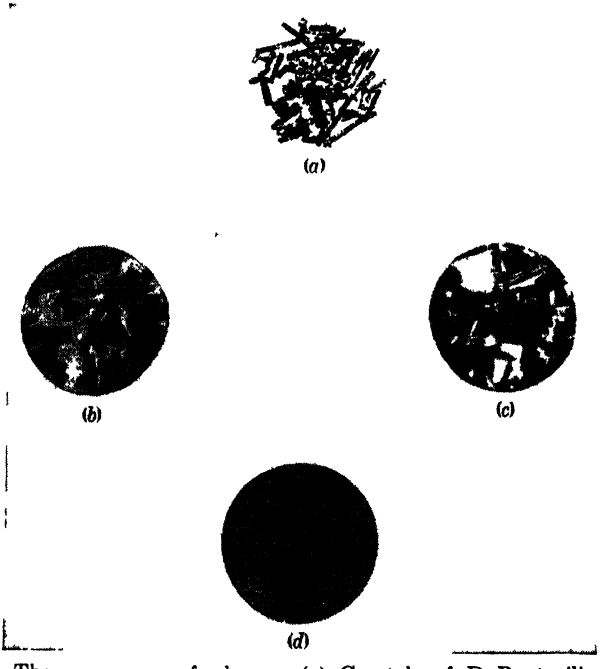

FIG. 10·3.—The processing of silicon. (*a*) Crystals of DuPont silicon. (*b*) Wafer cut from an ingot of boron-beryllium-doped silicon. (*c*) Etched wafer from the same ingot as (*b*). (*d*) A polished wafer from the ingot.

Wafer (*d*) has been polished to a mirror surface with no trace of grain structure. These wafers illustrate a further step in the manufacturing procedure that will be discussed later. A sample of the pure duPont silicon crystals is shown at (*a*) in Fig. 10·3.

The procedure used at the Bell Telephone Laboratories[1] for preparing ingots of silicon involves melting the charge in an induction furnace in an atmosphere of helium. The cooling is accomplished by slowly with-

[1] H. C. Theuerer, "Method of Producing Large Silicon Ingots Suitable for Use in the Manufacture of D-162836, D-163366, and D-164389 Rectifiers," BTL Memorandum MM-43-120-21, Mar. 1, 1943; also, "The Preparation and Rectification Characteristics of Boro-silicon Alloys," BTL MM-43-120-75, Nov. 2, 1943.

drawing the melt from the heat-inducing field. The furnace is a silica tube about 4 in. in diameter. The tube is sealed to a metal head through which the charge is introduced. The head carries an observation window and a gas inlet and outlet for maintaining a flow of helium during the process. A system of pulleys connected to the furnace head makes it possible to raise the furnace through the high-frequency induction coil at a prescribed rate, either manually or by mechanical drive. The solidification then begins at the top of the melt and progresses downward through it as the furnace is raised.

The crucible is a silica cylinder 5 in. tall and $1\frac{3}{4}$ in. in diameter. The crucible fits loosely inside a graphite heater shield in which heat is generated by the high-frequency field. The crucible assembly rests on a

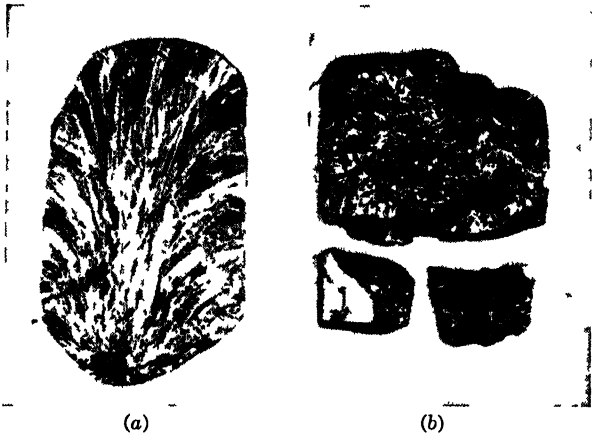

(a) (b)

FIG. 10.4.—Variation in melting practice and its effect on the physical characteristics of the silicon ingot

layer of No. 38 Alundum grain and is surrounded by an Alundum radiation shield. A silica feeding funnel rests in the top of the crucible, because the powdered silicon has a larger volume than the liquid metal. The furnace head carries a silica poker to facilitate feeding the silica powder into the crucible. The poker is inserted through a tubular hole in the head and sealed gas-tight by means of flexible rubber tubing.

After the charge is inserted, approximately 55 min are required to melt the charge and bring the temperature up to 1600°C. The furnace is then raised until the top of the crucible is level with the top of the high-frequency coil. After a period of about three minutes in this position the tube is raised $\frac{1}{8}$ in. at 1-min intervals until it is 7 in. above the starting position. After this process the temperature of the ingot has reached 700°C. It is then allowed to cool to room temperature. It is equally satisfactory to raise the furnace continuously at the rate of $\frac{1}{8}$ in./min by means of the mechanical drive.

The ingots produced by the above process are solid and entirely free from cracks. An etched vertical section through a typical ingot is shown in Fig. 10·4*a*. The fanlike columnar crystal structure results from the temperature gradient established within the melt in the cooling process. The tapering cross section and rounded bottom of the ingot are a result of the expansion of the melt during the freezing process. During the last stages of the process the bottom of the crucible bulges and the crucible is observed to rise in the furnace. Experiments indicate that it is important, for the method described, that the melting time be sufficiently long for devitrification of the silica crucible to take place. Stress relief on freezing then occurs in the crucible rather than in the ingot. With proper choice of the dimensions of the crucible and control of its devitrification, the ingot breaks free of the crucible walls, and a solid ingot free from cracks is obtained.

Figure 10·4*b* shows a fractured ingot obtained at Bell Telephone Laboratories when a melt was cooled by decreasing the power input gradually with the crucible in place in the furnace. It should be noted that fractures of this type have been successfully avoided in using the Radiation Laboratory techniques, but it is not clear which differences in techniques are responsible for the different results obtained in the two laboratories.

The ingots made by the progressive cooling process are $4\frac{1}{2}$ in. tall with a mean diameter of $1\frac{5}{8}$ in. Performance tests show that the upper $2\frac{1}{2}$ in. of these melts are satisfactory for rectifier units. In the lower part of the melt the impedance of the silicon increases and the r-f performance is inferior. About 2500 rectifier units are obtainable from each melt.

The method used by North[1] for making ingots of antimony-doped germanium is as follows. A quartz crucible $\frac{3}{4}$ in. in diameter and 8 in. long is supported vertically in a quartz furnace tube which is evacuated. A liquid-air trap is used and the pressure kept below 10^{-5} mm Hg during the melting and solidification process. The pure germanium charge is placed in the crucible and the antimony is added after the germanium is molten. This is accomplished by means of a small cup containing the antimony which is supported above the crucible in a flexible manner by a sylphon bellows. After the germanium is molten the antimony is shaken into the melt, which is then slowly cooled. Average resistivities of the melts are in the range of 0.003 to 0.1 ohm-cm. In this range the r-f performance is not critically dependent upon resistivity. Higher resistivities increase the spreading resistance and cause higher conversion losses; lower resistivities cause low back resistances and higher losses.

[1] H. Q. North, "K-band Germanium Crystals," NDRC 14-328, GE Co., Mar. 26, 1945.

10·4. Polishing, Heat-treatment, and Etching.—The processing of the semiconductor, following the preparation of the ingot, involves a controlled procedure of polishing, heat-treatment, and etching of the crystal wafer used in the rectifier cartridge. Our present understanding of the effects of these processes, in so far as they are understood at all, has been presented in Chap. 4; the purpose of this section is to describe in detail typical procedures for both silicon and germanium which have been developed as a result of the collective experience of the various laboratories engaged in crystal development. The procedures for silicon are those for boron-doped silicon, developed by Fox, Pearsall, and Powell[1] at the Radiation Laboratory; some of the procedures are direct copies or modifications of those used by other laboratories. The processing of germanium to be described is that used by North[2] at the General Electric Research Laboratories.

Silicon.—The cylindrical ingot is first cut into thin circular wafers about 1 mm thick by means of a Rimlock copper disk whose periphery has a series of closely spaced slots filled with diamond dust. Water is used as a cooling agent. The saw marks are removed by grinding both surfaces of the wafer with No. 600 carborundum on a rotating copper-lapping table wet down with water.

The next step is to polish the side of the wafer that is to be used for the rectifying contact. The polishing process is similar to that used at the Bell Telephone Laboratories by Treuting.[3] Before the polishing operation begins, the wafer is cemented to a copper block with cellulose cement so that it can be held easily. The polishing is done dry on 000 emery paper on a lap rotating at a speed of about 600 rpm. The polishing lap is "worked in" with a steel block and a mixture of light machine oil and kerosene. The polishing starts with a small amount of the oil-kerosene mixture, and as it proceeds, the paper becomes dry. This operation requires from 10 to 15 min. When finished, the polished surface is an extremely good mirror with absolutely no trace of grain-structure pattern. (See Fig. 10·3*d*.) This polishing process differs from earlier techniques where the wet metallographic methods used preserved the grain-structure pattern. Here the intention is to produce a flow layer which erases all evidence of grain structure.

After polishing, the oil is removed by washing the wafer in trichloroethylene. The cellulose cement used to cement the wafer to the metal block is removed from the wafer by immersion in hot concentrated

[1] Marvin Fox, C. S. Pearsall, and Virginia Powell, "Manufacturing Procedure for the Radiation Laboratory High Burnout Crystals," RL Report No. 501, Dec. 21, 1943.

[2] H. Q. North, "K-band Germanium Crystals," NDRC 14-328, GE Co., Mar. 26, 1945.

[3] R. C. Treuting, "Preliminary Development of Improved Burnout Silicon Contact Rectifiers," BTL Report MM-43-120-53, May 18, 1943.

sulfuric acid, and the wafer is afterwards thoroughly washed in distilled water.

After the wafer is cleaned, it is treated by heating in air for about half an hour at a temperature of 900° to 950°C; it is then removed from the furnace and air-quenched. The oxide layer thereby produced on the surface is removed by etching the wafer in 24 per cent hydrofluoric acid for about 30 sec. Experiments by M. Fox at the Radiation Laboratory show that the atmosphere in which the baking takes place need not be air or oxygen. Controlled experiments, using identical techniques, show that the same rectifier performance can be obtained when using atmospheres of CO_2, H_2, He, O_2, or N_2 for the heat treatment of the silicon.

The next step is the plating of the unpolished side of the wafer so that it can be soldered to the mounting in the cartridge. For this purpose nickel-plating done according to the method used by Angello[1] is satisfactory. The unpolished surface is prepared for plating by swabbing it with a mixture of 10 per cent concentrated nitric acid and 90 per cent of 48 per cent hydrofluoric acid applied with a platinum loop. The strength of this solution is adjusted so that the surface reaction proceeds very slowly while the grain-structure pattern becomes more and more sharply defined. If the reaction proceeds too rapidly or for too long an interval, a dark-blue surface layer is formed which interferes with the plating operation. If the etching operation is stopped when small bubbles begin to form all over the surface, a satisfactory etch is obtained. To obtain optimum adhesion of the nickel plate the wafer should be washed and the back surface plated before it dries. In the plating operation the wafer is held in a clamp with bakelite jaws so that only the unpolished side is in contact with the surface of the plating bath. Electrical connection to the wafer is made by a spring contact to the polished surface. The plating bath is:

1. Ammonium nickel sulphate	105 g per liter of water
2. Ammonium chloride	15 g per liter of water
3. Boric acid	15 g per liter of water

A current density of 8- to 10-ma/cm^2 produces an adequate plate in about 5 min at room temperature.

Proper plating of the wafer is important. Poor contact of the crystal with the cartridge may cause excessive noisiness and erratic performance in the rectifier.

After the plated wafer is washed and dried, it is placed on a flat cardboard surface and broken with a knife blade into small pieces of

[1] S. J. Angello, "Westinghouse Crystal Detector Pilot Shop," Research Report SR-176, Apr. 21, 1943.

suitable size for soldering to the cartridge component. It breaks up easily along the grain boundaries, with very little waste material. The advantages of this procedure over that of sawing the wafer into small squares are

1. The resulting pieces are almost free from grain boundaries because the breaks occur along these boundaries.
2. The waste of materials is considerably reduced. With this procedure one obtains 15 to 18 pieces large enough to use per square centimeter of wafer.

The pieces of crystal obtained are now soft-soldered to the cartridge stud or screw by means of a suitable soldering jig. A suitable flux is stainless-steel Soldering Flux No. 6.[1] After the soldering process, the silicon pieces are ground down to the diameter of the stud with a diamond grinding wheel.

The crystal is given a final etch immediately before insertion into the cartridge. The studs on which the crystals are mounted are placed on a platinum screen and immersed in 48 per cent hydrofluoric acid for 5 to 10 sec. This produces a mild electrolytic action. After the studs are washed they are ready for insertion into the cartridge.

Germanium.—In the procedure used by North[2] for antimony-doped germanium, the ingot is cut into wafers 0.020 in. thick and these are ground with 600-mesh Alundum under water on a glass lap. The wafers are then plated with rhodium and cut into squares 0.070 in. on a side. These are soldered to the cartridge studs, which are then mounted, 20 at a time, on a jig for polishing. A wet polishing wheel is used. There are three steps to the polishing process: first, the crystals are ground on a fine stone to bring all the surfaces in the same plane; they are then polished with 600-mesh Alundum on cloth; and, finally, with fine magnesium oxide on cloth to give a high polish.

Heat-treatment and etching appear to be unsuited to antimony-doped germanium. Experiments by North show that heat treatment in air, followed by an etch to remove the oxide, produces a germanium surface which when probed showed almost short-circuit characteristics.

THE CAT WHISKER

10·5. Whisker Materials.—Properties to be considered in the choice of whisker material are its work function and its mechanical properties. It should be a hard metal so that the point is not excessively flattened by the pressure required for good rectifying characteristics; it must be a metal that can be fabricated in wire form and crimped to the desired

[1] Obtained from the Colonial Alloys Co. of Philadelphia, Pa.

[2] *Loc. cit.*

whisker shape; and it should have sufficient elasticity to give mechanical stability for feasible wire sizes.

The work function of the metal is one of the quantities that determine the nature of the barrier at the metal-semiconductor contact, as was explained in Chap. 4. There we saw that, for rectification to occur, the work function of the metal must be less than that of a *p*-type semiconductor; for *n*-type semiconductors the reverse is true. Moreover, the height of the barrier in the semiconductor depends on the difference in work function between the metal and semiconductor.

In the case of silicon, J. A. Becker[1] reports that characteristic volt-ampere curves obtained from various metal-to-silicon point contacts in air do not exhibit differences that can be readily associated with differences in the work functions of the various metals as determined by vacuum thermionic measurements. This is not surprising, for it is well known that work functions are strongly dependent on the presence of absorbed gases or other surface contaminations. It is only when metal contacts are evaporated in vacuum that any reasonable correlation is found between rectification characteristics and metal work function. In the light of present knowledge the whisker material does not play as important a role in the rectification picture as one would expect from theoretical considerations.

For these reasons the choice of whisker material has been an empirical one. For silicon rectifiers, tungsten has been almost universally used. The British-Thomson-Houston Company prefers molybdenum-tungsten, which they have found to be more consistent in quality than pure split-free tungsten. Other manufacturers have found commercial tungsten satisfactory. The mechanical properties of tungsten are well suited to whisker fabrication.

Platinum-ruthenium whiskers have been found to give somewhat higher back resistances than tungsten ones in germanium mixer crystals.[2] The platinum is alloyed with 10 per cent ruthenium, to increase the hardness.

The choice of whisker-wire size is determined largely by the force required on the contact point. In the 10-cm band, where relatively large contact areas are desired and relatively large forces are consequently necessary, 8-mil wires have been used for high-burnout rectifiers. Commercial low-conversion-loss units with good burnout properties are ordinarily made with 5-mil wire in the ceramic cartridge for 10- and 3-cm use. In the coaxial cartridge, where the whisker space is very small and the contact force small, wires 2 *mils* in diameter have been found satisfactory.

[1] Private communication to the Radiation Laboratory, Nov. 9, 1942.

[2] Private communication from H. Q. North.

10·6. Fabrication of the Whisker.—The fabrication of the whisker involves three processes: (1) forming the whisker point, (2) crimping the wire to the desired shape, and (3) soldering or welding the whisker to the metal cartridge component. In actual practice, the order of operations varies from one manufacturer to another. For mechanically formed points, the pointing is usually done before the crimping.

Forming the Whisker Point.—Conical points are now almost universally used in commercial rectifiers. At one time wedge-shaped points were thought to contribute to the high-burnout property, but experiments by Fox and Pearsall at the Radiation Laboratory have shown that for equal areas of contact nothing is to be gained from a knife-edge contact.

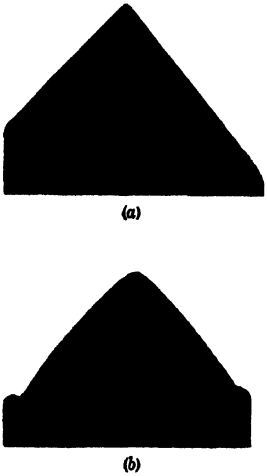

FIG. 10·5.—Effect of electrolytic polishing on contour of ground tungsten points. (*a*) Ground point. (*b*) Ground and electrolytically polished point.

The conical point may be formed either by grinding mechanically on a stone or by an electrolytic method.[1]

In the mechanical method the wire is held against the grinding wheel at an appropriate angle by a rotating pin vise, the axis of rotation being in a plane perpendicular to that of the grinding stone. The included angle of the cone is not critical; an appropriate value is in the neighborhood of 70° to 80°. The diameter of the point of the cone is usually less than 0.0001 in. The contact area will be larger than this, for the point flattens when it is pressed against the silicon. A projection microscope can conveniently be used to inspect the point for flaws.

In some instances large values of noise temperature have been correlated with microscopic irregularities in the geometry of the tungsten point contact. The grinding process may leave irregularities in the form of grinding marks or burrs at the point. An electrolytic polishing process has been used by the Western Electric Company to remove these irregularities. This process, as reported by Pfann[2] gives the point the desired contour and surface smoothness. The process consists of making the point anodic in a solution containing 25 per cent by weight of potassium hydroxide and applying 0.8 volt for 2 sec followed by two successive flashes of 0.2-sec duration at 2.0 volts. A number of points may be connected in parallel and polished simultaneously. The cathode is a

[1] J. R. Woodyard, "Notes on Crystal Detectors," Sperry Research Laboratories Report 5220-110, Apr. 6, 1943; W. G. Pfann, "Electrolytic Pointing of Tungsten Contact Wire in Silicon Rectifiers," BTL Report MM-43-120-73, June 29, 1943.

[2] W. G. Pfann, "Electrolytic Polishing of Tungsten Points in Silicon Rectifiers," BTL Report, Case 24026, Dec. 3, 1942.

copper gauze. After the polishing process the points are washed in a stream of hot water and dried. Figure 10·5 shows a typical point obtained by Pfann before and after the polishing process. Figure 10·6 shows electron microscope photographs taken by the University of Pennsylvania crystal group. Figure 10·6*a* shows a point ground with a carborundum wheel, but not polished. Figure 10·6*b* shows a ground point which has been electrolytically polished. Figure 10·6*c* shows a ground and polished point after it has been pressed with a load of 3 g

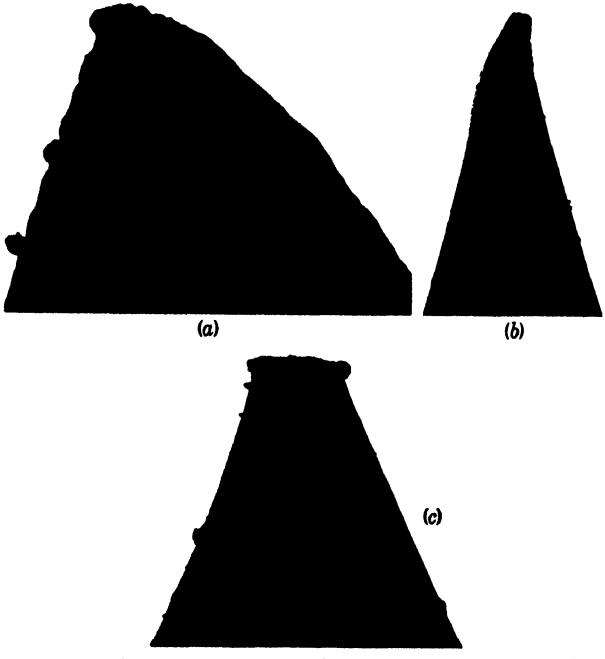

FIG. 10·6.—Electron microscope photographs of tungsten points. (*a*) Ground point, unpolished; (*b*) ground point, electrolytically polished; (*c*) ground and polished point after it was pressed with a load of 3 gm against a silicon surface.

against a polished silicon surface. The angle of the cone of Fig. 10·6*b* and *c* is smaller than usual, but points with larger angles exhibit the same general features.

Pfann[1] has also developed a process for eliminating the mechanical forming of the point by electrolytic pointing as well as polishing. The electrolyte used for the pointing operation is an aqueous solution containing 25 per cent potassium hydroxide by weight with about 0.01 per cent or more of copper in solution. The cathode is a copper gauze that has remained in the electrolyte long enough for a film of oxide to form. The pointing operation is accomplished by placing the whisker wires in a vertical position with their lower ends in the

[1] *Loc. cit.*

electrolyte and applying 1 volt until the current drops to a value between 0.25 and 0.30 ma; for points having a radius of curvature of 0.0003 in. the shutoff current always falls within this range. The pointing process is then followed by polishing flashes as previously described. Figure 10·7*a* shows an electrolytic point made by Pfann, and Fig. 10·7*b* shows for comparison a ground and electrolytically polished point.

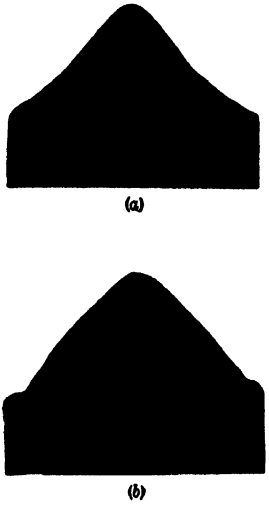

FIG. 10·7.—Point contours. (*a*) Electrolytic point. (*b*) Ground and electrolytically polished point. Radius of curvature at tip is 0.0003 in. in each.

The drop in current at constant voltages arises from the decrease in wetted area as the tungsten is dissolved and from the polarization at the wires. The shaping of the point depends on the formation of a meniscus of a suitable shape about the wire. The potassium hydroxide solution specified produces a satisfactory meniscus for 5-mil wires, and the addition of the copper to the solution produces the required adhesion of the liquid to the wire. Copper gauze is the only cathode material that has been found satisfactory. The concentration of potassium hydroxide is not critical, large changes having little effect on the contour of the point; the value of the shutoff current increases with increase in concentration.

By this procedure as many as 100 wires have been pointed in a single operation, the total time required being about one-half hour. The method provides a means for accurately controlling the length of the whisker assembly. For this purpose the wires are soldered to the cartridge pin and crimped prior to the pointing operation. Since the points always form just below the surface of the solution, uniformity of length can be obtained by uniform mounting of the whisker assemblies in the holder of the electrolytic cell.

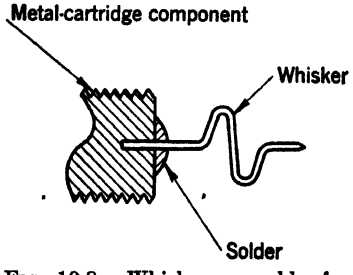

FIG. 10·8.—Whisker assembly for the ceramic cartridge.

The Whisker Shape.—The whisker is bent to the desired shape by means of a crimping jig. The general shape of whisker commonly used for the ceramic cartridge is shown in Fig. 10·8. Details on size and curvature of the loops and the over-all length of the whisker, together with the internal geometry of the cartridge, affect the r-f impedance of the unit in a complicated way; the details of the design have therefore been worked out empirically by the individual manufacturer. The over-

all whisker length used by various manufacturers lies in the range from about 0.1 to 0.15 in. and in production this length is, of course, kept as nearly constant as possible for a given cartridge design. The double-loop structure serves as a spring whose compression provides the contact force; it also provides mechanical stability by maintaining the contact force perpendicular to the crystal surface when the spring is compressed.

The whisker assembly for the Radiation Laboratory coaxial cartridge is shown in Fig. 10·9. The single-loop whisker is commonly used for this type of cartridge, in which it is desirable to keep the whisker size to a minimum. The effects of internal geometry of the cartridge on r-f impedance is pronounced in this type of cartridge; the dimensions of the Radiation Laboratory whisker assembly are therefore included in Fig. 10·9, and those of the remainder of the cartridge in Fig. 10·13. As was mentioned in Sec. 10·5, 2-mil tungsten wire is used for the whisker. Stability of the contact is achieved by making one arm of the loop longer than the other, as shown in Fig. 10·9. This whisker design is similar, except for some modification in dimensions, to that developed earlier at the Bell Telephone Laboratories.

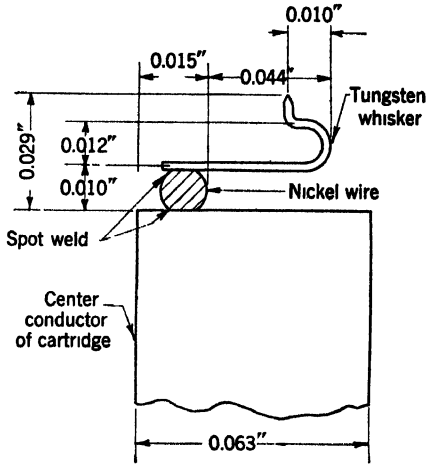

FIG. 10·9.—Whisker assembly for the Radiation Laboratory coaxial cartridge.

Mounting the Whisker.—In the ceramic cartridge it is standard practice to solder the whisker to the cartridge component. Both Bell Telephone Laboratories and Westinghouse Research Laboratories[1] have successfully used a hot-dip method in which the tungsten wire is coated with an alloy of 69 per cent gold, 6 per cent platinum, and 25 per cent silver. The wires are readily wetted by the alloy, which forms a thin adherent coating that can be easily soldered. Nickel-plating the tungsten has also been found satisfactory.

The shank of the whisker is soldered into a hole in the metal end piece of the cartridge (see Figs. 2·2 and 10·10), alignment being maintained during the process by suitable jigs. After soldering, the assembly is inspected for alignment of the whisker axis with the axis of the cartridge. With the excellent crystals now available, "hunting" for a sensitive point is no longer considered good practice.

In the Radiation Laboratory coaxial cartridge, the whisker is spot-

[1] S. J. Angello, Westinghouse Research Report SR-176, Apr. 21, 1943.

welded to the center conductor of the cartridge, a 10-mil nickel wire being used as shown in Fig. 10·9. The nickel wire serves also to separate

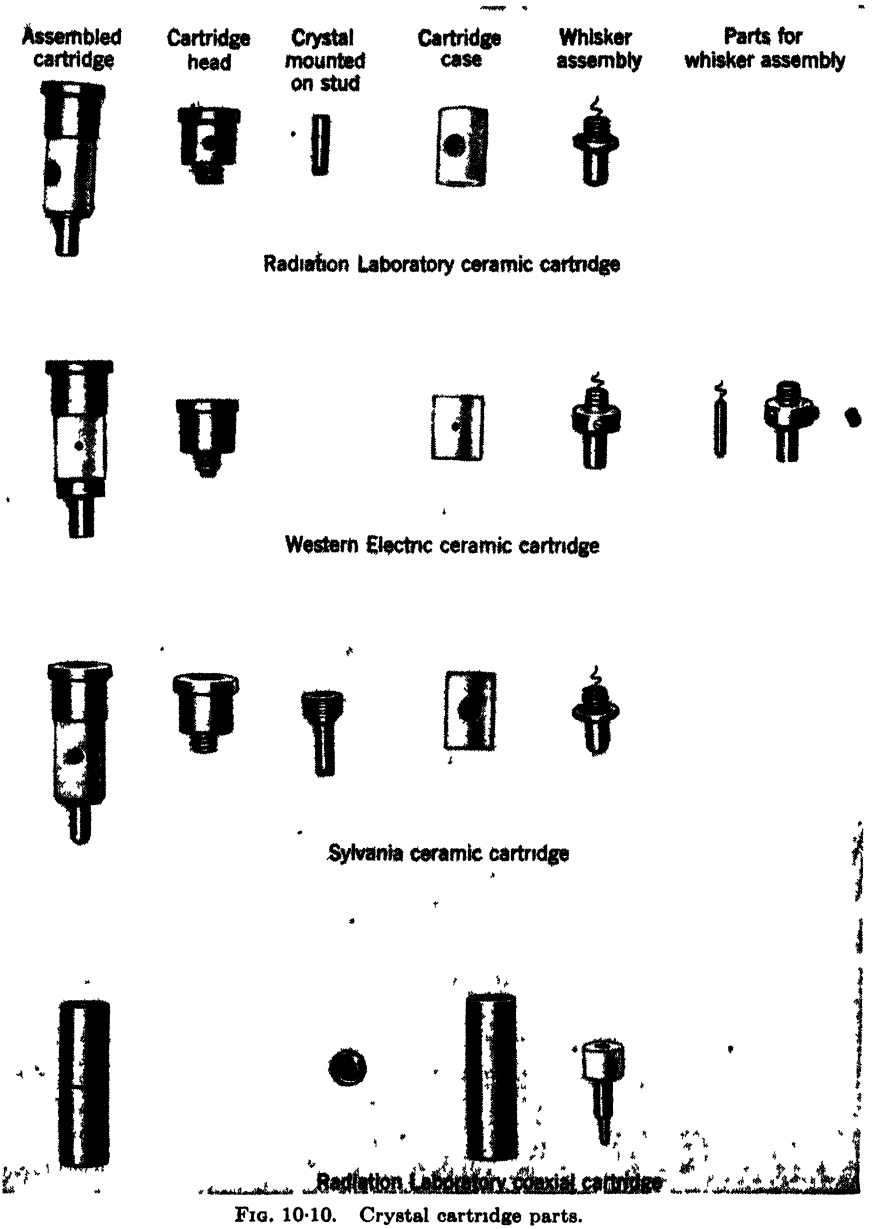

FIG. 10·10. Crystal cartridge parts.

the whisker from the end of the center conductor so that space is provided for the deflection of the spring.

ASSEMBLY AND ADJUSTMENT OF THE CARTRIDGE

10·7. The Ceramic Cartridge.—Cartridge parts for representative ceramic cartridges are shown in the top three rows of Fig. 10·10. The Radiation Laboratory ceramic cartridge shown at the top is similar to that developed and manufactured by the Westinghouse Electric Corporation.[1] The other two cartridges shown in the figure are manufactured by Sylvania Electric Products, Inc. and the Western Electric Company as indicated. All these cartridges meet the JAN specifications on external dimensions but differ in structure because of the different mechanisms used for adjustment of the contact point. Cross sections of assembled cartridges were shown in Figs. 2·2 and 2·4, Sec. 2·1.

The properties required of the cartridge case are, in addition to insulation of the terminals, low loss at microwave frequencies and mechanical strength and rigidity over the temperature range from about −40° to +100°C. It must also be made of a material that can be fabricated with the close dimensional tolerances required (see Fig. D·1). Ceramic materials meet these requirements and are now universally used for the purpose. Specifically, steatite ceramics such as Alsimag[2] 196 or 211 are excellent ceramics for this purpose.

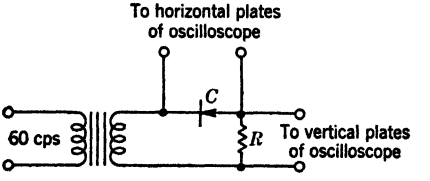

FIG. 10·11.—Circuit used for viewing the rectifier characteristic on an oscilloscope.

The JAN specifications require that the metal parts, usually made of brass, be plated with silver or gold.

The cartridge is assembled by screwing the head and pin tightly into the ceramic case, which is threaded on the inside. A cement such as orange shellac is applied to the parts to make the joint tight.

The adjustment of the Radiation Laboratory cartridge is as follows. After the final etch, the crystal stud is inserted in the cartridge and clamped lightly with the set screw in the side of the cartridge head. The cartridge is then placed in a clamping device where the pressure from a micrometer screw advances the stud toward the whisker point against the mechanical resistance of the set screw. Electrical connections are made to the head and pins of the cartridge so that either the back or the front resistance can be measured in the neighborhood of 1 volt, or the characteristic curve observed on an oscilloscope. For the latter purpose a circuit similar to that shown in Fig. 10·11 is used. A 60-cycle a-c voltage (about 0.5 volt rms) is applied to the primary terminals of a transformer (or Variac), whose voltage output is connected to the recti-

[1] S. J. Angello, Westinghouse Research Report SR-176, Apr. 21, 1943.
[2] Obtained from the American Lava Corp., Chattanooga, Tenn.

fier C in series with the resistor R. A suitable value of R is 10 to 20 ohms.

Once contact is established, the pressure is increased until a predetermined characteristic is observed on the oscilloscope. In this stage the front resistance, measured at a few tenths of a volt, is between 300 and 400 ohms, and the back resistance is about 10,000 ohms. The cartridge is then "tapped"[1] lightly. Judicious tapping causes the front resistance to drop to between 200 to 300 ohms and the back resistance to increase to between 20,000 to 100,000 ohms. (These values are for an applied potential of a few tenths of a volt.) Before tapping, the oscillo-

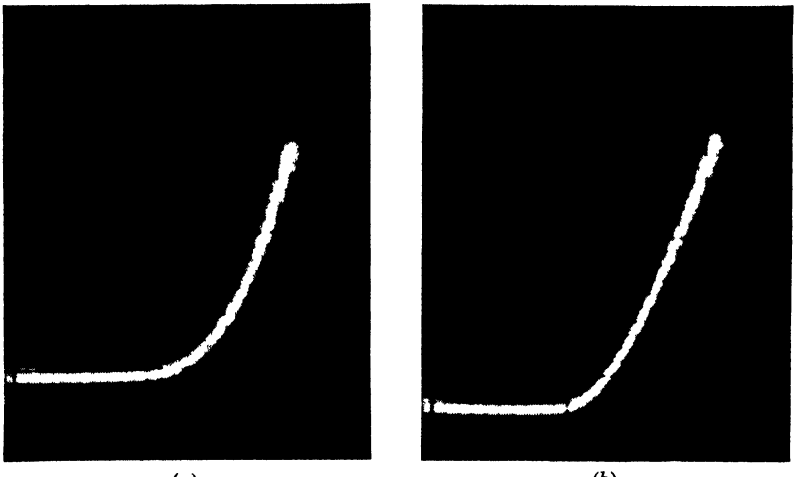

(a) (b)

FIG. 10.12.—D-C characteristic curve as seen on an oscilloscope. (a) Before tapping; (b) after tapping.

scope presentation appears as in Fig. 10·12 at (a). The sloping portion of the curve breaks away gradually from the nonconducting region and the slope of the curve increases with increasing forward voltage. Tapping lightly a few times produces the curve shown in Fig. 10·2 at (b). The break in the curve is more sharply defined and the curve takes on a constant slope with increased voltage. At this stage further tapping has little effect on the characteristic. As a final step the set screw in the cartridge head is screwed in tightly.

The amount of tapping done in the adjusting of the contact is a matter of the operator's judgment and experience. In addition to the changes in the characteristic curve mentioned, tapping has been observed in some cases to decrease the noise temperature of the rectifier. The crystal group[2] at the University of Pennsylvania has conducted controlled experiments where tapping was simulated by taking the contact

[1] "Tapping" means producing mechanical shock by blows of a light mallet.

[2] A. W. Lawson, P. H. Miller, L. I. Schiff, and W. E. Stephens, "Effect of Tapping on Barrier Capacitance," NDRC 14-181, Univ. of Penn., Sept. 1, 1943.

point through one or more loading cycles, and measurements of capacitance were made during the process. They observed that this process in general does not increase the capacitance of the rectifying contact and may even decrease it; from this it is inferred that the net effect of the tapping on contact areas is small. On the basis of the foregoing facts it is difficult to formulate an adequate picture of what happens during the tapping process. The advent of boron-doped silicon and polished surfaces has made the adjustment of a good contact much easier and vigorous and prolonged tapping unnecessary.

After adjustment, the cartridge is impregnated with a viscous wax to provide mechanical stability and at the same time to make it impervious to moisture. A suitable material for this purpose has been developed at the Bell Telephone Laboratories and is commonly used for mixer cartridges by commercial manufacturers in the United States. This material is a mixture of 80 per cent Paratac and 20 per cent Opal wax[1] by weight. The mixture maintains a satisfactory consistency—like that of heavy grease—at least in the temperature range of −40°C to +70°C. At very low temperatures the rectifier is likely to be damaged by the solidification and contraction of the wax, and at temperatures much above 70°C the wax melts. Many other filler materials have been tried but none superior to Paratac and Opal wax has been found for the temperature range from −40° to +70°C.

The wax can be introduced in liquid form through the hole in the side of the ceramic either by vacuum impregnation or by injection with an electrically heated syringe; the hole in the ceramic is sealed by some manufacturers, left open by others. The rectifiers are now ready for r-f performance tests.

The general procedure for assembling and adjusting the commercial rectifiers shown in Fig. 10·10 is similar to that just described, although the adjustment process varies in the amount of tapping, spring deflection of the whisker, and the properties of the d-c characteristic used as the criterion of proper adjustment. The commercial cartridges shown in Fig. 10·10 obviously differ in adjusting mechanism. In the Sylvania cartridge one end of the crystal stud is threaded so as to fit tightly the threaded coaxial hole in the cartridge head. The crystal is advanced toward the whisker by turning the screw and, upon final adjustment, is sealed with a touch of lacquer. In the Western Electric cartridge, the crystal is soldered to the cartridge head and is therefore fixed in position. The whisker is mounted on a movable stud which makes a sliding fit in an axial hole in the pin piece. It is advanced toward the crystal without rotation by a screw in the threaded outer end of the hole. After adjust-

[1] Paratac can be obtained from Stanco Distributors, 28 Broadway, New York, N. Y., and Opal wax from du Pont.

ment the stud is clamped by two set screws in the flange of the pin, and the adjusting screw is backed off.

Bell Telephone Laboratories has established the practice of standardizing the whisker adjustment in terms of spring deflection—that is, the distance the spring is compressed after initial contact is made. The spring deflection is measured by an adjusting device, developed by Theuerer,[1] which utilizes a micrometer caliper for advancing the whisker stud. The relationship between burnout and spring deflection is typified by data reported by Treuting.[2] These data show that, as the spring deflection is increased, the burnout power increases—that is, the r-f power required for a given impairment increases. This result can be predicted from correlations between burnout and apparent point-contact area, the latter increasing with increasing spring deflection. Treuting also found that, as the burnout power increases, the difference between conversion loss at 10 and 3 cm increases, again an effect to be expected from correlations with contact area. From these experiments, Treuting listed the following specifications on spring deflections to be used with boron-doped silicon.

1. A 5-mil whisker with a spring deflection of 2 mils or less yields a rectifier of superior performance in the 3-cm band, with a mean conversion loss between 6 and 8 db. Mean values of conversion loss of 5.5 db were obtained by using very low resistance boron-silicon (obtained with larger boron additions and a higher temperature heat treatment).
2. A 5-mil whisker with a spring deflection of 4 mils yields a unit of superior performance in the 10-cm band, with a mean conversion loss in the neighborhood of 5.5 db and improved burnout characteristics.
3. A 5-mil whisker with a spring deflection of 6 to 8 mils yields a high-burnout unit with an average conversion loss of 6 db under optimum r-f matching conditions, but with marginal values of conversion loss in the fixed-tuned standard mixer.

10·8. The Coaxial Cartridge.—The parts of the Radiation Laboratory coaxial cartridge are shown in Fig. 10·10, and a cross section of the cartridge with dimensions and tolerances, in Fig. 10·13. The metal parts are silver-plated brass. The dimensions of the parts are such that the r-f impedance distribution centers about the standard value of $65 + j0$ ohms, when boron-doped silicon processed according to the procedure described in the preceding sections is used. This impedance is the

[1] H. C. Theuerer, "A Method of Controlling the Contact Area of Silicon Point Contact Rectifiers," BTL Report MM-43-120-94, Oct. 30, 1943.

[2] R. G. Treuting, "Use of Heat-Treated Boro-Silicon in Contact Rectifiers," BTL Report, MM-43-120-95, Sept. 18, 1943.

characteristic impedance of a coaxial line with the same dimensions as the pin end of the cartridge.

To achieve mechanical stability with temperature change, the insulating bead carrying the center conductor and whisker must have the same expansion coefficient as the brass case. In addition it must be a material that can be fabricated accurately to the desired shape, a material that is rigid and does not shrink, and that has a low dielectric loss at frequencies as high as 30,000 Mc/sec. A material that meets all these requirements is Polyglas D+, developed during the war by von Hippel, Kingsbury, and Wesson[1] at the M.I.T. Laboratory for Insulation Research. This material was manufactured during the war in production quantities by the Monsanto Chemical Company and is supplied in the form of a molding powder. It contains a filler of low-thermal-expansion glass of about 96 per cent silica, a binder of poly-2,5-dichlorostyrene, and a moistureproofing agent.

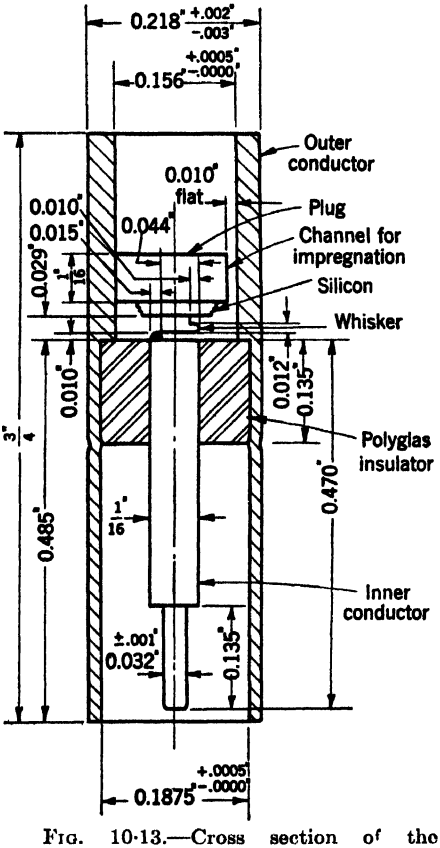

FIG. 10·13.—Cross section of the Radiation Laboratory coaxial cartridge showing the dimensions of the parts.

A bead of this material is molded onto the center conductor at a temperature of around 200°C and a pressure of about 4000 lb/in.^{2} The whisker is then spot-welded to the center conductor and the assembly pressed into place against the shoulder in the outer conductor. The size of the bead is such as to make a tight press fit in the outer conductor. This part of the assembly is completed by crimping the outer conductor at the outer face of the bead, as shown in Fig. 10·13. Prior to insertion of the plug carrying the crystal, the whisker is covered with filler wax. When the plug is inserted any excess of wax is forced out through a channel in the cylindrical face of the plug.

The plug makes a force fit in the outer conductor and is pressed in by a micrometer screw device similar to that previously described. The

[1] A. von Hippel, S. M. Kingsbury, and L. G. Wesson, NDRC Report X, Contract OEMsr-191, October 1945.

adjustment procedure is similar to that for the ceramic cartridge. For 1-cm use the contact area must be kept small, and hence very light contact pressures are used, corresponding to spring deflections of 1 mil or less.

The cartridge designed by North[1] for antimony-doped germanium is shown in cross section in Fig. 10·14. The bead is made of low-loss glass (GE No. 1076) which matches the coefficient of expansion of the silver-plated steel outer and inner conductor. The bead is fused to both outer and inner conductor and the crystal plug is sealed to the outer conductor with low-melting solder or Glyptol. The unit is therefore hermetically sealed and is mechanically stable without the use of filler.

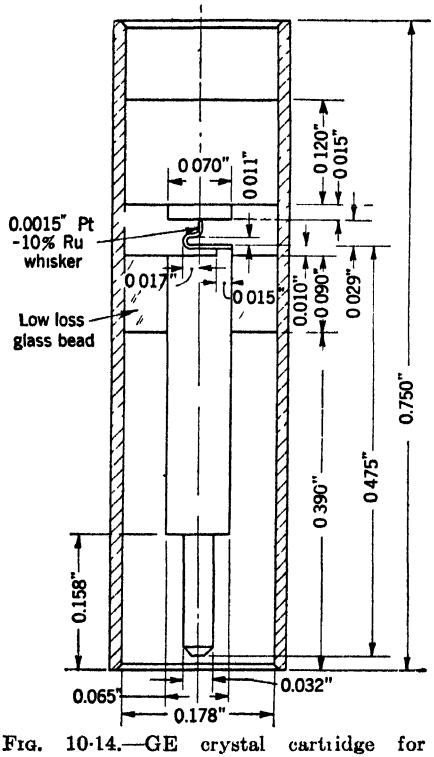

FIG. 10·14.—GE crystal cartridge for germanium crystals.

For use in the 1-cm region, a spring deflection of 0.5 mil is used with a 1.5-mil platinum-ruthenium whisker; this produces a contact force of about 0.4 g. The r-f impedance of these units is such that no matching transformer is needed in the pin end of the cartridge. The polarity of the cartridge is the reverse of that of a silicon rectifier, since antimony-doped germanium is an n-type semiconductor.

SOME DESIGN CONSIDERATIONS AFFECTING ELECTRICAL PERFORMANCE

10·9. R-f Impedance.—The r-f impedance of the crystal cartridge is a complicated function of semiconductor composition, whisker pressure, and cartridge geometry. The first two quantities affect the impedance of the rectifying junction which, together with the impedance of the cartridge parts, make up the network that represents the cartridge as a whole. The whisker pressure and semiconductor are chosen to give best conversion loss and burnout; the external geometry of the cartridge and the tuning of the crystal mixer were standardized early in the development to permit the standardization of r-f radar components. As a result, the designer, in adjusting r-f impedance to a predetermined value,

[1] H. Q. North, "K-band Germanium Crystals," NDRC 14-427, GE Co., Mar. 25, 1945.

has been limited to changes in whisker geometry, internal geometry of the cartridge, and minor changes in whisker pressure that do not appreciably affect loss and burnout. In the case of the ceramic cartridge, a rectifier for the 10-cm band with improved burnout and at the same time good conversion loss when matched at radio frequency can be made by using boron-doped silicon and relatively large contact area. This unit, the 1N28 type, has not been widely used in wartime radars, however, because the r-f mismatch in standard fixed-tuned mixers is too great. The improved burnout obtained with this type makes it highly desirable to choose its r-f impedance as a standard for future applications in this band.

The situation in the coaxial cartridge is a more fortunate one, in that limited final adjustments of r-f impedance can be made by inserting a quarter-wave transformer in the pin end of the cartridge, either as a sleeve on the inner conductor or as a ring pressed into the outer conductor. However, in this case the designer is limited in the transformation obtainable by the space available between inner and outer conductor and by the frequency sensitivity introduced by the transformer. Furthermore, large standing waves in the bead, which would introduce an appreciable loss, are to be avoided if possible. In the Radiation Laboratory coaxial cartridge the bead is a half-wave nontransforming element and the desired r-f impedance is obtained by choosing the geometry of the cartridge as shown in Fig. 10·13. At present writing, the control of r-f impedance is a difficult problem, one which calls for the utmost ingenuity and experience on the part of the cartridge designer.

10·10. Conversion Loss and Burnout.—The attainment of low conversion loss, as we have seen, depends on the nature of the semiconductor and the contact area, the conversion loss for a given semiconductor and given frequency decreasing as the area of contact is decreased; on the other hand we have seen that higher burnout is attained by increasing the contact area. Furthermore, for a given contact the conversion loss increases with increasing frequency. It is at once evident from these facts that a practical compromise between burnout and sensitivity must be arrived at in the design of a rectifier for a given application. With an increase in radio frequency the conversion loss, for a given crystal material, can be maintained only at the expense of burnout, by decreasing contact area. Improvement in both burnout and sensitivity has therefore been attained by improvements in the processing of the semiconductor.[1] As these improvements were made new crystal types were specified, which might well be condensed now to, at most, two types for each frequency band.

[1] The special case of the welded-contact rectifier is discussed in Chap. 13.

At present, extensive measurements of rectifier properties in the microwave region have been confined to wavelengths in the regions at 25-, 10-, 3-, and 1-cm wavelength. On the basis of present knowledge it seems likely that types designed for mixer applications at these wavelengths will also give satisfactory performance at intermediate wavelengths.

PART III

SPECIAL TYPES

CHAPTER 11

LOW-LEVEL DETECTION

The crystal rectifier has been extensively employed as a low-level detector in the crystal-video receiver used in connection with microwave beacons (see Chap. 1). There are many additional applications of crystals as rectifying elements at low power levels in probes and monitors. Here, we shall be largely concerned with their use in the receiver, which must have a minimum sensitivity of about 10^{-8} watt for pulses of 1-μsec duration. This sensitivity has been achieved for microwave frequencies as high as 10,000 Mc/sec.

An analysis of low-level detection involves different properties from those encountered in describing mixer performance. The first part of this discussion is therefore devoted to rectification characteristics of crystals at low r-f power levels, and their relation to the physical parameters of the rectifier. Crystal-video receiver application is treated next and methods of measuring the physical quantities of interest in this application described. Finally, there is an account of the special manufacturing techniques developed for video crystals.

PROPERTIES OF CRYSTAL RECTIFIERS AT LOW LEVELS

11·1. Rectification at Low Levels.—When the rectifier is used as a detector, the output terminals are connected to a d-c circuit, or, for the detection of r-f pulses, to the input stage of a video amplifier. Consider, for example, a d-c circuit consisting of a load resistance and a current meter in series. With r-f power applied, a small change in the d-c circuit resistance causes a small change in the voltage across the crystal and a small change in circuit current. The ratio of the voltage change to the current change defines a *dynamic* output resistance for the crystal, which will be called the "d-c crystal impedance," or "video resistance." We have seen in Chap. 2 that the d-c impedance for an r-f power input in the neighborhood of 1 mw is several hundred ohms (see Fig. 2·27). As the r-f power is lowered toward the microwatt level, the d-c impedance rises to a fixed value of several thousand ohms; this impedance is just the reciprocal of the slope of the current-voltage characteristic at the operating point. In this region of constant d-c impedance the rectified current becomes rigorously proportional to r-f power—that is, the crystal is square law in its response. It is in this square-law region that the rectifier operates in crystal-video receivers.

These facts are illustrated in Fig. 11·1 from data obtained by Beringer.[1] In Fig. 11·1 is plotted on a logarithmic scale the short-circuit current and open-circuit voltage at the output terminals of the rectifier as a function of r-f input power for powers up to about one milliwatt. The variation in d-c impedance is also shown. It can be seen that the square-law behavior breaks down as the power is increased above the

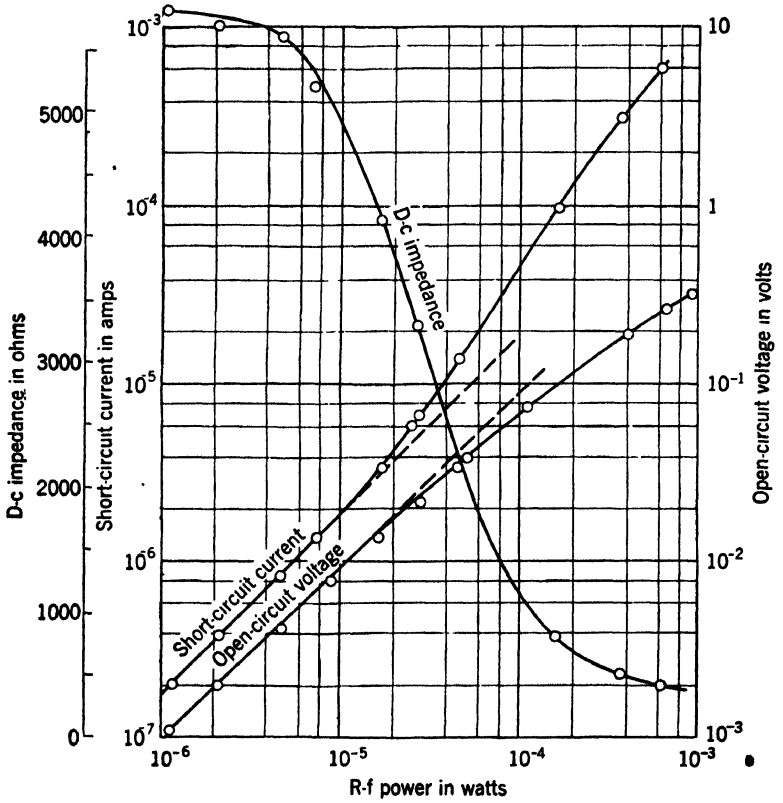

FIG. 11·1.—Rectification properties of a silicon crystal rectifier. The radio frequency is 3300 Mc/sec.

microwatt region; the exact point at which this occurs varies from crystal to crystal but lies in the range from 2 to 10 μw..

Because of the possibility of overloading the crystal it is necessary to apply corrections in the use of the crystal detector as a monitor of r-f power.. The correction clearly depends on the indicating circuit used with the detector. For example, the open-circuit voltage and short-circuit current show opposite deviations from linearity at high power

[1] E. R. Beringer, "Crystal Detectors and the Crystal-video Receiver," RL Report No. 638, Nov. 16, 1944.

level. For this reason crystal probes and monitors must be calibrated for applications beyond the square-law region.

In the microwatt region the characteristics of a crystal rectifier can be represented by a current generator shunted by a resistance equal to the d-c impedance. As the r-f power input is increased, the generator current increases in proportion. As the power level is raised beyond the square-law region, the current increase is more rapid than linear, and the resistance begins to decrease. These two features are characteristic of crystal rectifiers in general, but the relative magnitudes of the effects vary from crystal to crystal.

The current sensitivity is defined as the ratio of short-circuit rectified current to absorbed r-f power—that is, it is the slope of the corresponding curve of Fig. 11·1 in the linear region. This quantity, together with the d-c impedance, is sufficient to determine the performance of the crystal rectifier as a low-level detector as we shall see in Sec. 11·5.

In the 10-cm region, the current sensitivity of production-line crystals ranges from 0.5 to 3.0 μamp/μwatt. (The curve plotted in Fig. 11·1 is not typical in this respect.) The d-c impedances show a wide distribution of values—from 1000 to 20,000 ohms. The specification limits on d-c impedance are given for the various video-crystal types in Appendix D·1.

In the 3-cm region the current sensitivity ranges from 0.5 to about 1.5 μamp/μwatt, when the best manufacturing techniques are used; d-c impedances range as high as 30 to 40 kilohms.

Because of the smaller contact area, good video crystals are in general more susceptible to burnout than mixer crystals. Operational requirements, however, are not so stringent, because the crystal-video receiver is not ordinarily used in applications that require a TR switch for protection. They must have high enough burnout, however, not to be damaged by stray radiation to which they are exposed. The burnout design tests listed in Appendix D for the various video-crystal types are an indication of the amount of energy (or power, as the case may be) that they will dissipate without appreciable impairment.

11·2. Equivalent-circuit Theory. *Current Sensitivity.*—An expression for the current sensitivity, defined in Sec. 11·1, in terms of measurable physical characteristics of the rectifying contact has been derived by Beringer[1] and by Lawson, Miller, Schiff, and Stephens.[2] The predictions of the theory agree only qualitatively with experiment; it has nevertheless proved useful in video-crystal design and will undoubtedly be useful as a basis for a more successful theory as our fundamental understanding of the phenomenon of rectification increases.

[1] *Loc. cit.*

[2] A. W. Lawson, P. H. Miller, L. I. Schiff, and W. E. Stephens, "Behavior of Silicon Crystals at Low Level Powers," NDRC 14-182, Univ. of Penn., Sept. 1, 1943.

The derivation is based on the equivalent circuit of the crystal rectifier shown in Fig. 2·10. The quantity R is the barrier resistance of the rectifying contact, which at the low levels considered here is to a good approximation the d-c impedance of the rectifier. The term r is the spreading resistance in the semiconductor, and C, the barrier capacitance.

The rectifier at low level will be assumed to be a four-terminal network of linear impedances with the r-f signal applied to one pair of terminals and the rectified output appearing at the other pair as shown in Fig. 11·2. Because of the low rectification efficiency in the square-law region, the input and output terminals are effectively independent of the loading at the opposite terminal pair. The only connection between the terminal pairs is the phenomenon of rectification occurring when r-f power is absorbed at the r-f terminals.

FIG. 11·2.—Network representation of the detector crystal.

It will be assumed further that power losses, such as dielectric losses and skin-effect loss in the whisker, are negligible and that the crystal is matched to the r-f generator. The r-f power absorbed by the crystal is then given by

$$P = \frac{V^2}{2}\,\mathrm{Re}\left(\frac{1}{Z}\right), \tag{1}$$

where V is the peak amplitude of the voltage applied to the r-f terminals and Z is the input impedance of the equivalent circuit of the rectifier,

$$Z = r + \frac{1}{\dfrac{1}{R} + jC\omega}. \tag{2}$$

Substituting Eq. (2) in Eq. (1), we obtain

$$P = \frac{V^2}{2}\,\frac{\dfrac{1}{R}\left(1 + \dfrac{r}{R}\right) + \omega^2C^2r}{\left(1 + \dfrac{r}{R}\right)^2 + \omega^2C^2r^2} \tag{3}$$

The voltage V_b across the barrier resistance R is related to V by the expression

$$V_b^2 = \frac{V^2}{\left(1 + \dfrac{r}{R}\right)^2 + \omega^2C^2r^2}, \tag{4}$$

so that

$$P = \frac{V_b^2}{2}\left[\frac{1}{R}\left(1 + \frac{r}{R}\right) + \omega^2C^2r\right]. \tag{5}$$

To obtain the current sensitivity we now need an expression for the rectified current in terms of V_b. This expression may be obtained from the Taylor expansion of the characteristic curve at zero bias. [See Eq. (1·1).] The short-circuit rectified current is given by

$$i = \frac{1}{4} V_b^2 f''(0) - i\frac{r}{R}, \tag{6}$$

where $f''(0)$ is the second derivative of the characteristic curve at the origin. The second term of the right-hand member of Eq. (6) is included to take into account the resistance r in series with the rectifying contact. We have seen that the d-c impedance is the reciprocal of the slope of the characteristic curve,

$$R = \frac{1}{f'(0)}, \tag{7}$$

so that we can write Eq. (6) in the form,

$$i = \frac{V_b^2}{4}\frac{1}{(R+r)}\frac{f''(0)}{f'(0)}. \tag{8}$$

In Chap. 4 [Eq. (4·27)] we derived the expression for the characteristic curve of a rectifier:

$$i = i_0(e^{\alpha V} - 1), \tag{9}$$

from which it is seen that

$$\frac{f''(0)}{f'(0)} = \alpha. \tag{10}$$

We then obtain from Eqs. (10) and (8)

$$i = \frac{V_b^2}{4}\frac{\alpha}{R+r}. \tag{11}$$

The current sensitivity β is obtained by dividing Eq. (11) by Eq. (5):

$$\beta = \frac{i}{P} = \frac{\alpha}{2\left(1+\frac{r}{R}\right)^2}\frac{1}{1+\frac{\omega^2C^2rR^2}{R+r}}. \tag{12}$$

The current sensitivity at zero or very low frequency is obtained by setting ω equal to zero:

$$\beta_0 = \frac{\alpha}{2\left(1+\frac{r}{R}\right)^2}, \tag{13}$$

whence

$$\beta = \beta_0\frac{1}{1+\frac{\omega^2C^2rR^2}{R+r}} \tag{14}$$

A check by Beringer on the validity of Eq. (12) shows only qualitative agreement between measured and calculated values of β. Beringer's results for a good, a medium, and a poor microwave detector crystal are shown in Fig. 11·3. The curves show the calculated variation of β with frequency, and the points plotted are the measured values at frequencies of 600, 3300, and 9300 Mc/sec. Measured values of β at frequencies of

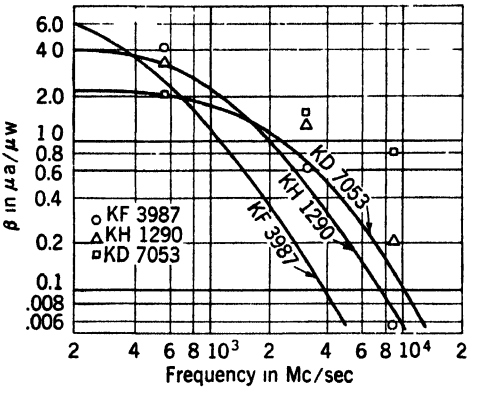

FIG. 11·3.—Variation of current sensitivity with frequency. The points are measured values; the curves are calculated from Eq. (12).

2 kc/sec, 1 Mc/sec, and 10 Mc/sec were identical and served to give the value of β_0. The values of R, r, and C for the three crystals are given in Table 11·1.

TABLE 11·1.—CONTACT PARAMETERS OF THE THREE CRYSTALS USED FOR FIG. 11·3

Crystal No.	R, ohms	r, ohms	C, $\mu\mu$f
KF 3987	4160	45.5	0.75
KH 1290	1770	27.6	0.58
KD 7053	1700	40.2	0.25

The d-c impedance R was measured by the method described in Sec. 11·9. The barrier capacity C was measured at 10 Mc/sec with a twin-T circuit similar to that used in the General Radio 821-A Bridge.[1] The experimental procedure involved a measurement of over-all cartridge capacity and an auxiliary measurement of the residual capacity when the whisker has been backed off from the contact. At zero d-c bias the barrier capacity is very nearly the difference between these two readings. The spreading resistance r was measured by biasing the crystal to a volt or so in the positive direction (to the linear portion of the characteristic) and measuring the differential resistance at that point with an a-c source.

[1] D. B. Sinclair, "The Twin T—A New Type of Null Instrument for Measuring Impedance at Frequencies up to 30 Megacycles," *Proc. I.R.E.*, **28** (No. 7), 310 (1940).

Figure 11·3 shows that both the calculated and measured values of β decrease with increasing frequency, but that the former decrease more rapidly. This discrepancy may be due to a decrease in the effective barrier capacity at microwave frequencies from its low-frequency value. Such an effect would be expected if the time required to ionize the donator levels in the semiconductor were long compared with the period of the applied voltage. This theory has been discussed in Chap. 4 for the case of high-level rectification, but quantitative results for the low-level case have not yet been worked out.

At zero d-c bias, $R \gg r$, so that Eq. (12) reduces to the approximate relation

$$\beta = \frac{\alpha}{2} \frac{1}{1 + \omega^2 C^2 r R}, \tag{15}$$

It is evident from Eq. (15) that β can be increased by increasing α and decreasing C, r, and R. Now C is proportional to the area of contact; R is inversely proportional to the area of contact, and r is inversely proportional to the radius of contact. The product C^2Rr is therefore proportional to the radius of contact. The value of β can therefore be improved by decreasing contact area through the use of light contact pressures. There are two limitations on how far one can go in this direction. The first limitation is mechanical stability. Both the d-c resistance and the current sensitivity are very sensitive to slight changes in contact pressure, and with light pressures mechanical stability is difficult to achieve. On this score the coaxial cartridge design appears to be definitely superior to the ceramic one. The second limitation is an upper limit on R which arises from considerations of receiver design.[1] Further improvement can be achieved if C can be decreased by some means other than decreasing the contact area, but must await further research on the physics of the barrier layer.

We have seen in Chap. 4 that experimental values of α are always less than the theoretical value of 40 volts.$^{-1}$. It was further pointed out there that this discrepancy may be ascribed to fluctuations in barrier space charge or contamination of the contact surfaces producing local fluctuations in the work function over the contact area. The validity of the linear relation between β and α, predicted by Eq. (15), has been investigated by Meyerhof and Stephens.[2] They measured α and β for a group of good video crystals designed for the 3-cm band. The values of β were between 1 and 2 μamp/μwatt; the value of α ranged from 2 to 13 volts^{-1}. This discrepancy did not appear to be explicable in terms of differences in capacity and resistance of the crystals. Whether it is due

[1] See *Radar Beacons*, Vol. 3, Radiation Laboratory Series.

[2] W. E. Meyerhof and W. E. Stephens, "X-band Video Crystals," NDRC 14-274, Univ. of Penn., May 20, 1944.

to an inadequate model for the equivalent circuit or to the difficulty in obtaining good quantitative data on crystal parameters is open to question.

Improvements in current sensitivity to date have been achieved largely by decreasing contact pressure, by an empirical study of doping and surface treatment of the semiconductor, and by adjusting the contact for optimum video performance.

11·3. Effect of Bias on Low-level Properties. *D-c Impedance.*—As we have seen, the d-c, or video, impedance is just the reciprocal of the slope of the characteristic curve at the operating point. With zero d-c bias the values range from about 2000 to 40,000 ohms for silicon crystals and are of the order of 10^6 ohms for germanium welded-contact crystals. At a forward bias of about 0.2 or 0.3 volt the values are reduced to the neighborhood of 100 ohms for silicon and 10^4 ohms for germanium. The latter is a useful value in the crystal-video receiver application, but a forward bias of more than about a tenth of a volt in the case of the silicon crystal reduces the lower limit of the video impedance range below a useful value.

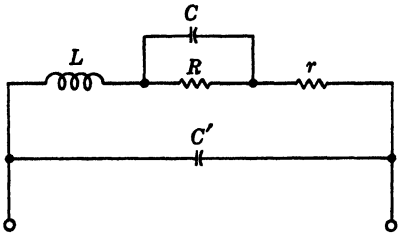

FIG. 11·4.—Equivalent circuit of a rectifier cartridge used for determining barrier capacitance. L—whisker inductance; R—barrier resistance; C—barrier capacitance; r—spreading resistance; C'— residual capacitance of the cartridge.

Capacitance.—It was pointed out in Chap. 4 that, in general, two methods have been used to measure the barrier capacitance. One of these is the direct measurement of the impedance of the rectifier with a suitable impedance bridge at a low frequency ($\approx$ 10 Mc/sec). This method has been used by Beringer, as outlined in the preceding section, and by the Pennsylvania Crystal Group.[1]

The model of the rectifier assumed by Lawson *et al.* is shown in Fig. 11·4. This model differs from that previously used only in the addition of the whisker inductance L and the residual capacitance of the cartridge C'. The latter is the capacitance of the cartridge with the whisker just removed from the crystal and is approximately constant from cartridge to cartridge, having a value in the neighborhood of 0.35 $\mu\mu$f. The whisker inductance L is determined by a measurement of the impedance of a cartridge in which the crystal is replaced by a piece of metal of similar geometry. It has a value in the neighborhood of 0.01 μh. The resistances R and r are determined by an analysis of the d-c characteristic curve. Having determined these constants, one can calculate the capacitance C from the measured impedance of the cartridge.

[1] A. W. Lawson, P. H. Miller, L. I. Schiff, and W. E. Stephens, "Barrier Capacity in Silicon Cartridge Rectifiers," NDRC 14-140, Univ. of Penn., May 1, 1943.

Measurements were made by the Pennsylvania group on silicon crystals with a General Radio 916A Bridge, which measures series resistance and reactance, and with a modified twin-T bridge, which measures shunt conductance and susceptance. With the General Radio bridge a resistance of about 150 ohms is connected in parallel across the cartridge to bring the impedance within the range of the instrument. With both bridges the applied emf must be as small as possible because of the nonlinearity of the barrier resistance. A comparison of results obtained with the two bridges show satisfactory agreement with zero d-c bias applied to the crystal. With a positive d-c bias, however, there is a discrepancy not yet explained in the two values. The observations by the bridge method show that the capacity rises rapidly with forward bias to a value which may be, at a bias of 0.5 volt, as much as 100 times its value at zero bias. It is estimated, however, that the error at this bias may be as large as a factor of 10. This error arises from the fact that, as the positive bias is increased, the voltage across the barrier decreases, and most of the applied voltage is across the spreading resistance. Therefore a small error in determining the spreading resistance introduces a large error in the values obtained for the capacitance. Because of this and the discrepancy between values obtained with the two types of bridge, the results of the bridge measurements can at best be considered qualitatively true. With small values of negative bias, up to about -0.5 volt, the bridge measurements show a small decrease in capacitance, followed by an increase which, at a bias of -2.5 volts, may be as large as ten times the value at zero bias.

The second method of determining capacitance makes use of Eq. (14) of the preceding section. In the use of this equation we must assume that the discrepancy between the measured values of β and the values calculated using the low-frequency value of capacitance is brought about by the variation of capacitance with frequency discussed in the previous section. One then obtains the r-f capacitance in terms of measured values of β at low and at microwave frequencies and the quantities R and r. Meyerhof, Serin, and Vought,[1] using this method, made measurements on silicon and germanium rectifiers. With silicon crystals at a positive bias of 0.2 volt, the r-f capacitance increases to not more than twice its value at zero bias. With germanium crystals the effect is greater; at a forward bias of 0.4 volt the capacitance is about 10 times as great as at zero bias. Like the bridge method, this one is inherently inaccurate because of large errors in the calculated values introduced by errors in measuring the crystal parameters.

[1] W. E. Meyerhof, B. Serin, and R. H. Vought, "X-band Crystal Performance with Bias," NDRC 14-505, Univ. of Penn., July 6, 1945.

Current Sensitivity.—The effect of forward bias on current sensitivity has been investigated by Meyerhof, Serin, and Vought[1] for type 1N31 silicon rectifiers and for the germanium welded-contact rectifiers at a radio frequency of 10,000 Mc/sec. Typical results are shown in Fig. 11·5. The current sensitivity rises to a maximum at 0.1 to 0.2 volts for silicon and 0.3 to 0.4 volts for germanium. The maximum for silicon has a value several times that at zero bias; the current sensitivity for germanium rises from a very small value to a value at the maximum comparable to the maximum value for silicon. The rapid initial rise for germanium may be attributed to the rapid decrease in R, which at zero bias has a value of the order of 10^6 ohms. It is clear that the current sensitivity becomes zero when the forward d-c bias voltage is greater than the contact difference of potential; in this case the barrier resistance and α become zero and the operating point is on the linear part of the d-c characteristic.

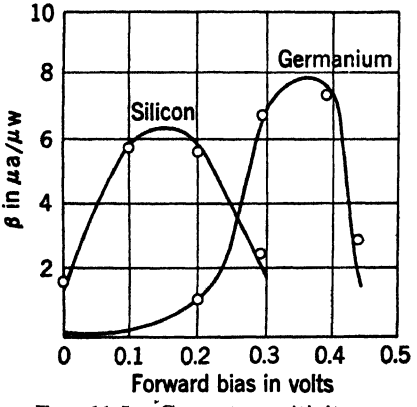

FIG. 11·5.—Current sensitivity as a function of forward bias for a silicon and a welded-contact germanium crystal.

11·4. Variation of Low-level Properties with Temperature.—A variation of R and β with temperature is to be expected on theoretical grounds. We have seen in Chap. 4 [Eq. (4·33)] that the theoretical expression for the current density through the barrier is

$$i = A'e^{-\frac{e\phi_0}{kT}}(e^{\frac{eV}{kT}} - 1), \tag{16}$$

where A' is a constant depending on the conductivity of the semiconductor, ϕ_0 is the effective contact potential difference, V is the potential applied to the barrier, and T is the absolute temperature. The low-level resistance is the reciprocal of the derivative of i with respect to V. With no d-c bias ($V = 0$) this is

$$R = \frac{kT}{eA'}e^{e\phi_0/kT}. \tag{17}$$

Over the temperature range of interest in video-crystal applications (−50° to +70°C), we see that Eq. (17) predicts an approximately exponential increase in R as T decreases. Figure 11.6 shows a typical plot of observed values, obtained by the University of Pennsylvania

[1] *Loc. cit.*

group;[1] R/T is plotted on a logarithmic scale as a function of $1/T$ for an unfilled silicon video crystal over the temperature range from about $-30°C$ to $+70°C$. The expected linear behavior is clearly confirmed.

The main effect of temperature on current sensitivity is probably caused by the change of R with temperature [see Eq. (15)]. Figure 11·7 shows the theoretical variation in R and in β as a function of temperature

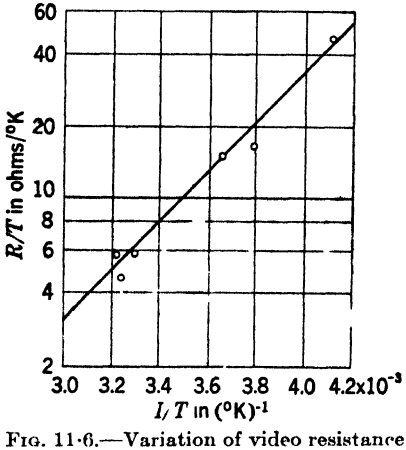

FIG. 11·6.—Variation of video resistance with temperature for a silicon crystal.

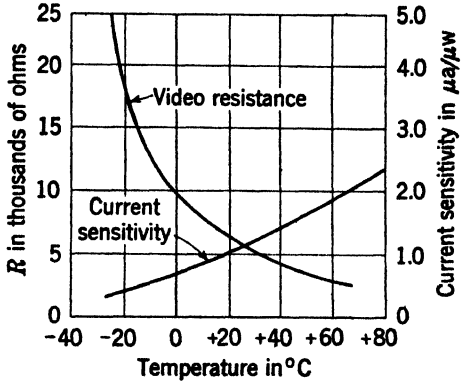

FIG. 11·7.—Theoretical variation of video resistance and current sensitivity with temperature.

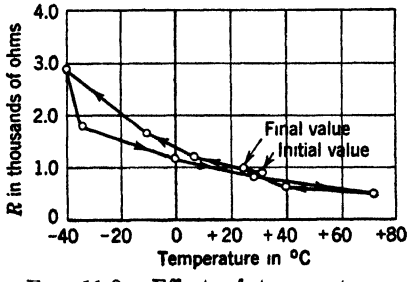

FIG. 11·8.—Effect of temperature cycling on video resistance for an unimpregnated silicon cartridge.

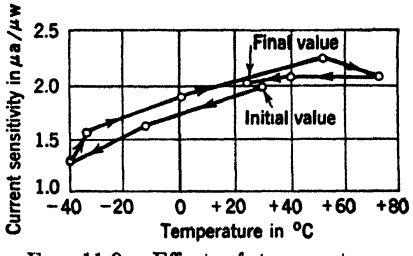

FIG. 11·9.—Effect of temperature cycling on current sensitivity for an unimpregnated silicon cartridge.

for a crystal having a video resistance of about 6000 ohms at room temperature. In general the observed values of β rise with increasing temperature although there are cases where the observed β falls off at higher temperatures, in disagreement with the theory.

Figures 11·8 and 11·9 show observed values of R and β taken around a cycle from $-40°C$ to $+70°C$ by Smith *et al.*[2] These data are for an

[1] A. H. Smith, B. Serin, W. E. Meyerhof, and W. E. Stephens, "Temperature Variation of Low Level Crystal Performance," NDRC 14-308, Univ. of Penn., Aug. 17, 1944.

[2] *Loc. cit.*

unfilled crystal rectifier at a radio frequency of 10,000 Mc/sec. The crystal holder was fixed-tuned to match at room temperature, and the available r-f power was held constant during the experiment. The temperature variation was obtained by enclosing the crystal holder in a thermally insulated box which held either hot water or dry ice in alcohol. The temperature was measured by means of a thermocouple. A temperature cycle required several hours to run for a maximum rate of change of temperature of about 2°C/min.

In general, filled cartridges show a hysteresis effect that in some cases is pronounced at low temperatures. Also some crystals are found to be erratic in performance. These either do not return to the original values after temperature cycling, or the repetition of the cycle does not reproduce the first curves. The hysteresis effect is probably largely attributable to a thermal lag in the filler material, because the effect is much smaller in unfilled crystals. The erratic effects also appear to be largely due to the filler. The differential expansion of the cartridge parts has been measured by the Pennsylvania group and does not appear to be large enough to change the spring deflection more than 0.2 mil for 100°C temperature change. The effect of temperature changes of the filler may be a disturbance of the adjustment (the pressure is small for good video crystals) either by nonisotropic expansion of the filler or by a viscous longitudinal force exerted by the filler on the whisker. Whatever the cause, the erratic effects are most pronounced below room temperature. The temperature-cycling tests outlined in the JAN specifications are sufficient to insure fairly stable video units but do not appear sufficient to insure that the crystal operate in a stable fashion at temperatures much below 0°C. We must remember that even in the absence of erratic or hysteresis effects, there exist the variations of R and β with temperature which appear to be inherent in the rectifying contact.

THEORY OF LOW-LEVEL DETECTION

As with frequency conversion, we are concerned, in low-level detection, with the conversion of microwave power and with the generation of noise by the crystal and amplifier. In the following analysis, introduced by Beringer,[1] an expression will be derived for the output signal-to-noise voltage ratio of a crystal-video receiver. The analysis enables us to define a quantity called the "figure of merit," which expresses quantitatively the excellence of the video-crystal detector in terms of current sensitivity and video resistance.

11·5. The Figure of Merit of a Video Crystal.—The video crystal of a crystal-video receiver is mounted in a crystal holder provided with r-f

[1] E. R. Beringer, "Crystal Detectors and the Crystal-video Receiver," RL Report No. 638, Nov. 16, 1944.

terminals (a coaxial line or waveguide) into which r-f power is coupled, and video terminals from which the output video signal is obtained. The crystal detector and video input circuit of the video amplifier may be represented by the circuit of Fig. 11·10. The crystal is represented by a current generator shunted by the video resistance R of the crystal, the current being a linear function of the r-f power absorbed by the crystal. The quantity C is the combined capacity of the choke system of the crystal holder and the first amplifier tube.

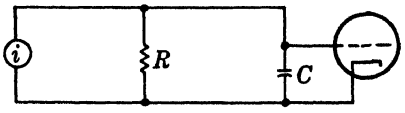

FIG. 11·10.—Equivalent input circuit of the crystal-video receiver.

The rectified current i is given by

$$i = \beta P, \tag{18}$$

where β is the current sensitivity and P is the absorbed r-f power. Disregarding the effect of C on transient signals, one obtains for the signal voltage e on the grid

$$e = \beta PR. \tag{19}$$

The output signal voltage from the amplifier is then

$$E = \beta PRG, \tag{20}$$

where G is the voltage gain of the amplifier.

The output noise of the receiver originates in both the crystal and the receiver. In the absence of feedback and transit-time effects, the receiver noise contribution is often represented by an equivalent noise-generating resistance R_A in series with the grid circuit of the input stage; this resistance does not load the circuit but generates a mean-square noise voltage of $4kTBR_A$. The magnitude of R_A can be deduced from theory; for a high-mu pentode such as the 6AC7, it is about 800 ohms. It can also be measured by a simple procedure, which consists in placing various resistors R_X between the grid and cathode of the first tube and observing the output noise power. The output noise power is proportional to $R_A + R_X$. For some particular value of R_X the output noise power is just double that with the grid connected directly to the cathode; this resistance is then numerically equal to R_A. Values of R_A of 1000 to 1200 ohms have been obtained by Beringer[1] for a typical video amplifier employing a 6AC7 tube in the first stage. In this measurement noise components from the entire pass band of the amplifier contribute to the output noise power, including microphonic and flicker noise in the low-frequency range; consequently R_A will be somewhat higher than the theoretical shot-effect value. In the JAN video-crystal specifications a value of 1200 ohms has been chosen for R_A.

[1] E. R. Beringer, "Crystal Detectors and the Crystal-video Receiver," RL Report No. 638, Nov. 16, 1944.

In the absence of d-c bias the noise generated by a crystal in the microwatt range of r-f power is almost entirely the Johnson noise of a resistance equal to the d-c impedance of the crystal. The total output rms noise voltage $\bar{N}$ of the crystal-video receiver, with no d-c bias, is then given by

$$\bar{N} = G\sqrt{4kTB(R + R_A)}, \tag{21}$$

where G is the voltage gain of the receiver, and B, the effective noise bandwidth, is defined as in Eq. (2·14).

The output signal-to-noise voltage ratio of the receiver is obtained by combining Eqs. (20) and (21):

$$\frac{E}{\bar{N}} = \frac{\beta PR}{\sqrt{4kTB(R + R_A)}}. \tag{22}$$

Equation (22) may be written in the form

$$\frac{E}{\bar{N}} = \frac{P}{\sqrt{4kTB}}\,M, \tag{23}$$

where

$$M \equiv \frac{\beta R}{\sqrt{R + R_A}}. \tag{24}$$

The quantity M, which contains all the crystal parameters appearing in Eq. (23), is a criterion of excellence of the video crystal, since all good

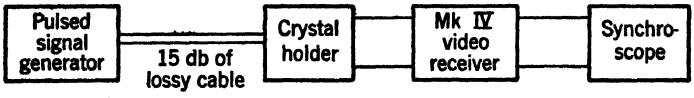

FIG. 11·11.—Block diagram of apparatus for measuring the sensitivity of a crystal-video receiver.

video amplifiers have essentially the same value of R_A. The term M is called the "figure of merit" of the video crystal.

The sensitivity of a crystal-video receiver has been computed by Beringer by means of Eq. (23) and compared with that measured directly by the application of pulsed r-f signals of frequency 3300 Mc/sec to the receiver.

A block diagram of the apparatus is shown in Fig. 11·11. The pulsed signal generator is of the "off-pulsing" type: it is pulsed out of oscillation for 1 μsec at a repetition frequency of 1 kc/sec. This type of signal generator is advantageous for precision work, since the pulse power is very nearly equal to the average power measured with a bolometer. The receiver had an integrated bandwidth of 3 Mc/sec.

The results of the calculation and measurements for several crystals are shown in Table 11·2. The first column gives the figure of merit of the crystal. Column 2 lists the absorbed r-f pulse power calculated by

means of Eq. (23) for $E/\bar{N} = 1$. Column 3 gives the pulse power for "minimum detectable signal"—that is, the smallest immediately seen on an A-scope when its position along the trace is unknown. Column 4 lists the pulse power for the "tangential signal"—that is, the signal which raises the noise by its own width. Both the minimum detectable signal and the tangential signal are somewhat vague in an absolute sense; the latter is of some practical importance, for it is this signal which is commonly regarded as necessary to trigger an electronic switch with a negligible number of spurious events from noise fluctuations. It appears that the minimum detectable signal is about that for which the signal voltage is equal to the rms noise voltage.

TABLE 11·2.—A COMPARISON OF CALCULATED AND MEASURED VALUES OF CRYSTAL-VIDEO RECEIVER SENSITIVITY

Figure of merit	Calculated P for $E/\bar{N} = 1$, watts	Minimum detectable signal, watts	Tangential signal, watts
110	2.0×10^{-9}	2.0×10^{-9}	5.3×10^{-9}
59	3.7	3.7	11.0
115	1.9	2.9	5.0
50	4.4	3.0	10.0
95	2.3	2.6	6.2

11·6. Effect of D-c Bias on Figure of Merit.—The converted noise from d-c bias was seen in Chap. 6 to be very large in the video frequency range. For this reason, the analysis of the preceding section, in which only Johnson noise was assumed in the detector, is not valid when d-c bias is used. Instead, one introduces the video noise temperature of the crystal into the expression for the figure of merit [Eq. (24)], which now becomes

$$M = \frac{\beta R}{\sqrt{Rt + R_A}}, \tag{25}$$

where t is the noise temperature of the biased crystal for a given video amplifier. Since the noise output varies inversely with the video frequency, t will increase rapidly as the low-frequency cutoff of the amplifier is decreased and is therefore a function of the amplifier pass band. As the positive bias is increased from zero, R decreases rapidly, β goes through a maximum, and t increases.

The net effect on M has been investigated experimentally by Meyerhof, Serin, and Vought,[1] using apparatus similar to that shown in Fig. 11·11. The input and biasing circuits are shown in Fig. 11·12. The output of the signal generator consisted of 2-μsec pulses at a repetition frequency of 800 pps, and radio frequency of 10,000 Mc/sec. The pass

[1] *Loc. cit.*

band of the video amplifier was from about 20 kc/sec to 2.8 Mc/sec. Two methods were used to obtain the figure of merit. In the first method, the signal level was decreased until the signal was just equal to noise; the r-f power level was then noted. The figure of merit can then be calculated by means of Eq. (23). In the second method, the signal

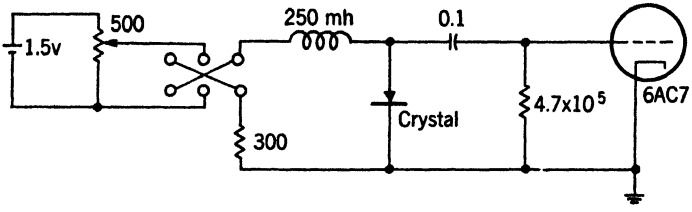

FIG. 11·12.—Input and biasing circuit used for measuring video-crystal receiver performance.

deflection and "average" noise deflection were observed for a standard r-f power input. The two methods correlated on the average with an average difference of about 10 per cent. Typical results for a welded-contact germanium crystal and a 1N31 silicon unit are shown in Fig. 11·13, in which the figure of merit is plotted as a function of bias. The initial rise in M for a welded-contact unit is probably largely accounted for by the large initial increase in β (see Fig. 11·5). The figure of merit at the optimum bias is comparable to that for silicon video crystals. As indicated in the figure, the optimum bias is from 0.2 to 0.3 volt for the germanium welded-contact unit, and zero for silicon.

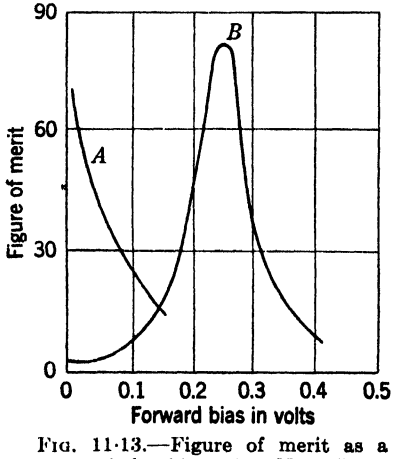

FIG. 11·13.—Figure of merit as a function of d-c bias: A—1N31 silicon rectifier; B—welded-contact germanium rectifier.

11·7. The Effect of Temperature Variation on Crystal-video Receiver Performance.—The variation of the figure of merit with temperature arises from the variation of video resistance and current sensitivity discussed in Sec. 11.14. As the temperature is decreased, β decreases and R increases, so that the two effects tend to cancel each other so far as the figure of merit is concerned. Figure 11·14 shows the variation of the figure of merit over a temperature cycle from $-40°$ to $+70°$C for the same crystal with which the data of Figs. 11·8 and 11·9 were taken. The figure of merit may also increase with increasing temperature, or it may experience little change.

The variation in receiver performance caused by changes in crystal temperature is undesirable in beacon applications. The variations of input signal voltage and input rms noise voltage with temperature has been calculated by Smith *et al.*,[1] for a typical crystal with a figure of merit of 60, a video resistance of 10,000 ohms at room temperature, and typical variations of R and β with temperature. The input signal voltage e is just the product βPR and was calculated for an r-f power of 10^{-8} watt. The rms noise voltage $\bar{n}$ was calculated by means of Eq. (21) by the relation

$$\bar{n} = \frac{\bar{N}}{G}. \tag{26}$$

The results of the calculations are shown in Table 11·3 for temperatures of −40°, +27°, and +70°C. The first two columns of the table list the values of R and β used in the calculations. It can be seen that the signal voltage at 70°C is approximately the same as the noise voltage at −40°C. This means that, if the receiver is set to actuate an electronic triggering circuit for a signal of 10^{-8} watt at high temperature, it may actuate it from noise at low temperatures. It is advisable, therefore, to control the ambient temperature at which the video crystal operates so that it does not go below about 0°C in non-adjustable installations where the set is required to operate over a wide range of temperatures.

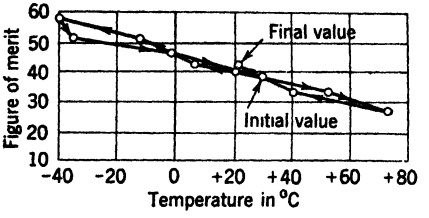

FIG. 11·14.—Effect of temperature cycling on the figure of merit of an unimpregnated silicon crystal rectifier.

TABLE 11·3.—EFFECT OF TEMPERATURE VARIATION ON CRYSTAL-VIDEO RECEIVER PERFORMANCE FOR A TYPICAL VIDEO CRYSTAL

Temperature, °C	R, ohms	β, μa/μw	n, μv	e, μv	$e/\bar{n}$
−40	40–000	0.3	34	120	3.5
+27	10–000	0.6	19	60	3.1
+70	5–000	0.7	15	35	2.3

MEASUREMENTS

We have seen that the performance of a crystal-video receiver can be expressed quantitatively in terms of the figure of merit, which in turn is a function of current sensitivity and video resistance. The following

[1] A. H. Smith, B. Serin, W. E. Meyerhof, and W. E. Stephens, "Temperature Variation of Low Level Crystal Performance," NDRC 14-308, Univ. of Penn., Aug. 17, 1944.

sections are devoted to a description of the equipment and methods developed at the Radiation Laboratory by Beringer[1] for the measurement of these quantities. The equipment is adapted to both laboratory and production testing.

11·8. R-f Equipment and Measurements.—To reduce reflection losses to a minimum the crystal should be matched to the r-f source. In a crystal-video receiver the antenna is usually matched to the r-f line which, in turn, is connected to the crystal holder; the crystal holder then employs matching transformers which match it to the line. In test equipment an r-f signal generator is connected to the line by an attenuator which can be adjusted to provide r-f power to the line at a power level of a few microwatts.

R-f Equipment for the 10-*cm Band.*—Nearly all the measurements in the 10-cm band have been made at an r-f wavelength of 9.1 cm, in accordance with the JAN specifications for testing in this band. A klystron connected to the crystal holder with about 20 db of lossy cable is a suitable signal generator. The crystal is matched to the coaxial line from the signal generator by incorporating into the crystal holder suitable transformers, such as parallel stubs and quarter-wave lines in series. These may be either tunable or fixed-tuned.

Like mixer crystals, video crystals have a distribution in r-f impedance. This distribution is such that for the 1N27 type an approximate match can be obtained by means of a single tuning stub. Such a crystal holder is specified in the JAN specifications. It is shown in cross section in Fig. 11·15. The stub is tuned for maximum rectified current by means of a sliding short-circuiting plug which makes a spring-finger contact with the inner and outer conductors. The pin of the cartridge fits into spring fingers on the center conductor, and the head of the cartridge is held by a copolystyrene washer. The video or d-c connections are made through an r-f choke which makes spring contact with the head of the cartridge.

Recently a fixed-tuned holder has been designed by Beringer to replace the one just described. A cross section of this holder is shown in Fig. 11·16. The crystal cartridge is held by spring fingers at both the head and pin. The cartridge is much easier to insert and remove than in the preceding design, a feature of importance in production testing. The stub is short-circuited for r-f power by the quarter-wave choke mounted on the center conductor of the stub; the video connection to the crystal is made through the center conductor. The center-conductor assembly is insulated by means of the copolystyrene nut on the stub

[1] E. R. Beringer, "Crystal Detectors and the Crystal-video Receiver," RL Report No. 638, Nov. 16, 1944; "Operating Instructions for the Radiation Laboratory X-band Crystal Detector Test Set," Internal Group Report 61, Aug. 10, 1944.

and the copolystyrene sleeve and beads near the r-f input terminals. The sleeve on the center conductor provides essentially an open circuit for video and d-c frequencies and a negligible impedance for r-f frequencies.

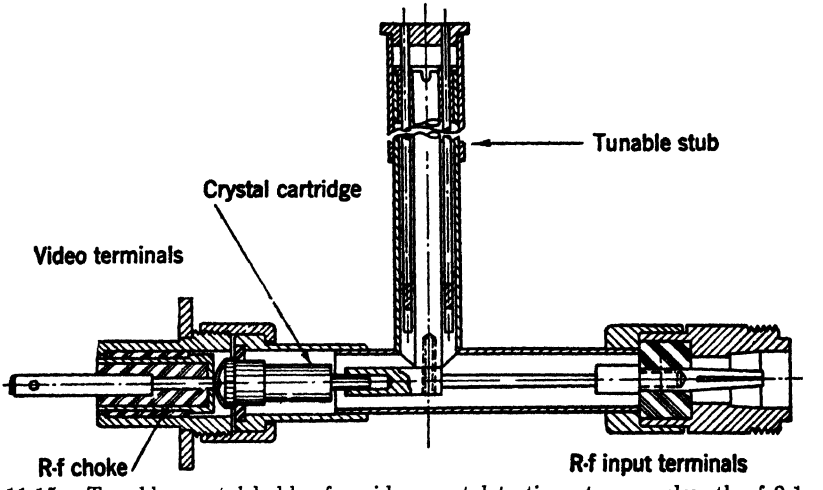

FIG. 11·15.—Tunable crystal holder for video-crystal testing at a wavelength of 9.1 cm.

The tuning is fixed at the center of the r-f impedance distribution. The center is determined by a measurement of the r-f impedance distri-

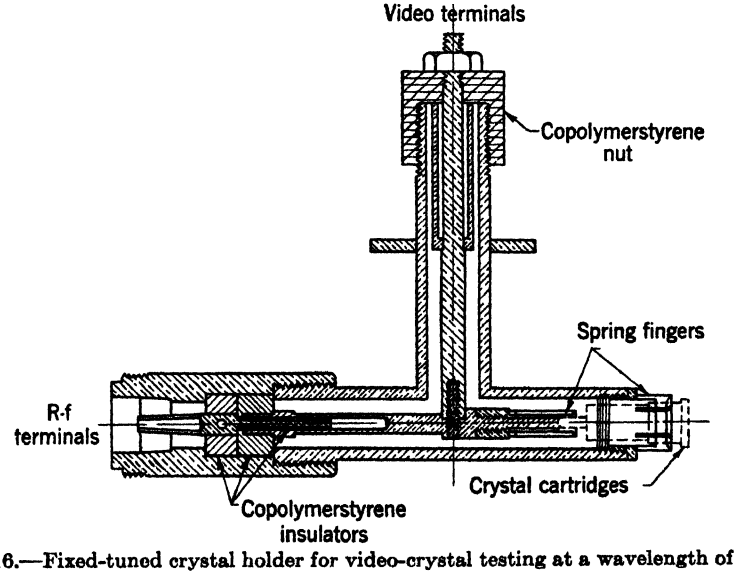

FIG. 11·16.—Fixed-tuned crystal holder for video-crystal testing at a wavelength of 9.1 cm.

bution of a representative sample of rectifier units. Such measurements are made with a standing-wave detector which is inserted between the attenuator and crystal, the method being similar to that described in

Sec. 2·7 for mixer crystals. The power picked up by the probe is so small, however, that a heterodyne standing-wave detector must be used.

The r-f impedance is independent of rectified current in the square-law region. The distribution of r-f impedances of Sylvania 1N27 units is such that, in the fixed-tuned holder, about 70 per cent have a reflection loss of 2 db or less, and 95 per cent have a reflection loss of 3 db or less. The use of the fixed-tuned holder in production testing tends to eliminate borderline units that are poorly matched and hence reflect an appreciable fraction of the available r-f power.

R-f Equipment for the 3-cm Band.—A test set designed by Beringer for the production testing of video crystals in the 3-cm band is shown in

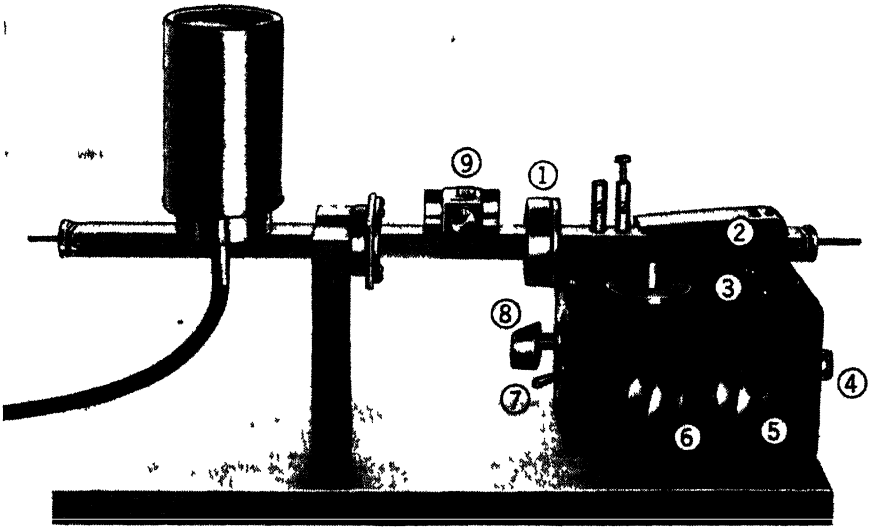

FIG. 11·17.—Test equipment for the production testing of video crystals in the 3-cm band. (1) Waveguide switch; (2) cartridge injector; (3) SW3, (4) d-c output terminals (5) SW1; (6) cartridge ejector; (7) SW2, (8) R_2; (9) variable waveguide attenuator.

Fig. 11·17. Power at 3 cm is provided by a 723-A oscillator tube mounted in the shield can at the left of Fig. 11·17. The waveguide mount for the tube includes a fixed attenuator of approximately 20 db consisting of a tapered piece of IRC resistance strip across the center of the waveguide. The variable attenuator [see (9) Fig. 11·17] has a maximum attenuation of 10 db. It consists of a resistance strip mounted parallel to the narrow side of the waveguide; the position of the strip can be varied from the side to the center of the guide by means of the micrometer screw. The attenuator is connected to the crystal holder with a choke-flange joint. A brass shim, which can be slid across the waveguide between the choke and flange, serves as a waveguide switch (1). A bolometer, not shown in the figure, may be substituted for the crystal holder for measuring the

available r-f power in absolute units. It is convenient in routine testing to calibrate a set of crystals for checking the power level.

The crystal holder is a variable-tuned holder designed for use with the type 1N30 video crystal. It is shown in outline in Fig. 11·18. Two tuning devices are used: the short-circuiting plunger which terminates the waveguide behind the crystal, and the tuning screw inserted in one or the other of the two screw positions. In practice the crystal is matched to the guide by alternately adjusting the tuning of the plunger and the screw for maximum rectified current. The required transformation ratios are extremely high for some of the best video crystals in the 3-cm band, and the distribution in r-f impedance is so large that fixed-

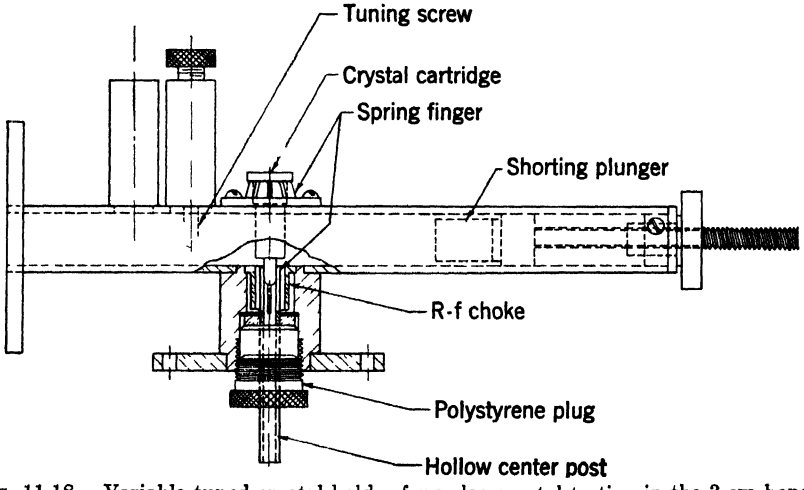

FIG. 11·18.—Variable-tuned crystal holder for video-crystal testing in the 3-cm band.

tuning without considerable reflection loss in the marginal units is difficult to achieve; the large transformation ratios required make the matching structures fairly frequency-sensitive. However, a satisfactory holder with a single tuning adjustment for Sylvania 1N30 units was designed by Beringer. This holder, shown in Fig. 11·19, is similar to that of Fig. 11 18 except that the variable tuning screw is replaced by a fixed one, and a cylinder structure, coaxial with a cartridge, extends from the bottom of the guide about a third of the distance across the guide. With proper choice of dimensions of these tuning devices (and position of the tuning "screw") the admittance distribution is transformed largely into a susceptance spread which can be approximately matched by adjustment of the short-circuiting plunger. A typical frequency-response curve for this holder is shown in Fig. 11·20. All of the holders described heretofore are for the ceramic cartridge. With the advent of the coaxial cartridge it was discovered that additional stability in the high-sensitivity video crystals could be achieved by using the coaxial cartridge. The type num-

ber 1N31 was assigned to this unit; a crystal holder, shown in Fig. 11·21, was consequently designed for it by Beringer and modified by the Pennsylvania group. This holder is fixed-tuned and provides a coaxial

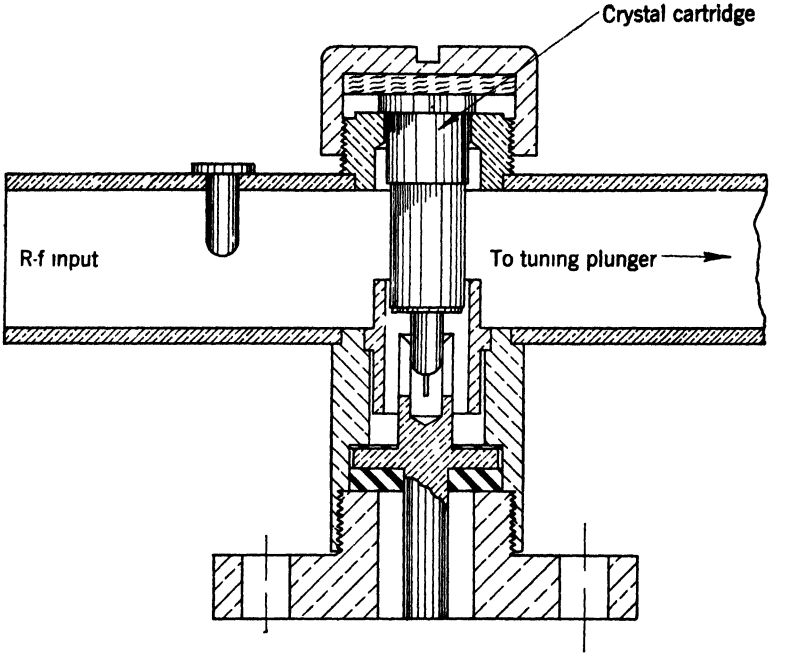

FIG. 11·19.—Video-crystal holder with single tuning adjustment for 1N30 rectifiers.

receptacle for the cartridge; it is coupled to the waveguide by extending the center conductor across the guide. This center conductor also provides the d-c connection to the crystal; it is d-c insulated with a poly-

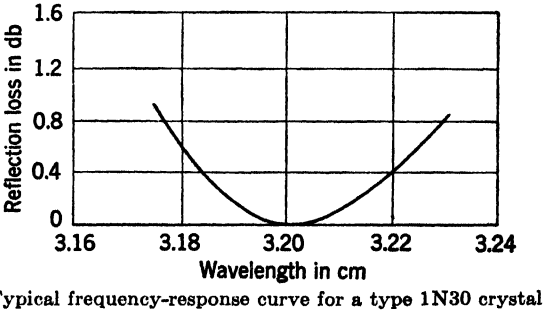

FIG. 11·20.—Typical frequency-response curve for a type 1N30 crystal and holder.

styrene washer and bead. The r-f choke and polystyrene washer provide an r-f short circuit at the surface of the waveguide.

In all of these holders the spring fingers must make good contact with the pin of the cartridge and maintain their stiffness after many

cartridge insertions; this is achieved by using beryllium copper machined to close tolerances and heat-treated. In rapid routine testing the insertion and removal of the cartridge is facilitated by the cartridge injector (2) and ejector (6) in Fig. 11·17. The injector guides the cartridge into the finger structure; the ejector is a cam-driven rod that pushes up against the end of the cartridge pin through the hollow center post of the d-c terminals.

11·9. Equipment and Methods for Measuring Current Sensitivity, Video Resistance, and Figure of Merit.—The circuits for measuring current sensitivity, video resistance, and figure of merit are the same for both the 3- and 10-cm bands; in the equipment shown in Fig. 11·17 it is contained in the black box at the right of the figure, all except the current meter. A schematic diagram of the circuit is shown in Fig. 11·22. The current meter M is a low-resistance meter with a maximum full-scale sensitivity of about 1 microampere. A galvanometer

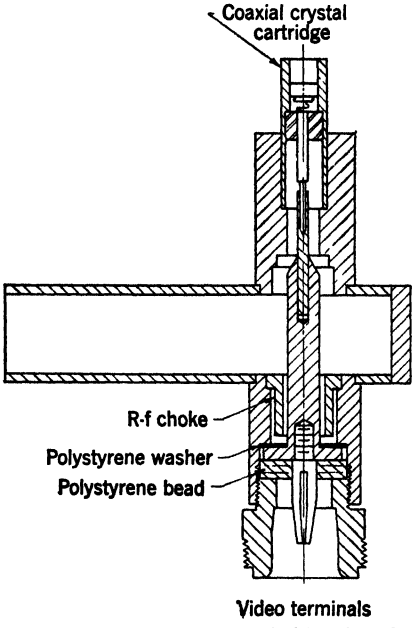

FIG. 11·21.—Video-crystal holder for the type 1N31 rectifier.

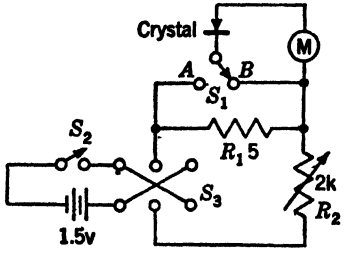

FIG. 112·2.—D-c circuit for video-crystal test equipment.

may be used for this purpose, or a d-c photocell-galvanometer amplifier. A circuit diagram of the latter, designed by S. Roberts and modified by R. Beringer, is given in Vol. 18, Chap. 12 of the Radiation Laboratory Series. It has the advantage of extremely low input impedance (about 5 ohms), fast response, and absolute fixed calibration (it is also useful for measuring crystal-probe currents).

Current Sensitivity.—The current sensitivity is measured by adjusting the r-f power level to a preassigned value in the square-law region (1 to 5 μw) and measuring the rectified current by turning S_1 to position B. Alternatively, a calibrated crystal may be used. For a fixed r-f power level the current sensitivity of the crystal being tested is given by

$$\beta = \beta_s \frac{i}{i_s}, \tag{27}$$

where β_s and i_s are the current sensitivity and observed rectified current for the standard crystal.

Video Resistance.—For the measurement of the video resistance the waveguide switch is closed and S_1 is turned to position A. The circuit provides a low-impedance voltage source in series with the crystal, which may be adjusted by means of the variable resistance R_2. It is calibrated by means of a dummy cartridge in which the ceramic case and the crystal are replaced by a resistor. (See Fig. 9·28 for details of dummy cartridge.) The video resistance of the crystal is then given by

$$R = R_s \frac{i_s}{i}, \tag{28}$$

where R_s and i_s are the resistance and current for the dummy cartridge and i is the observed current for the crystal. If the applied voltage is kept below about 5 mv the currents obtained in the forward and back directions are approximately the same; this can be checked by using reversing switch S_3. For acceptance testing, a voltage of 5 mv for the 5-ohm source is prescribed by the JAN specifications.

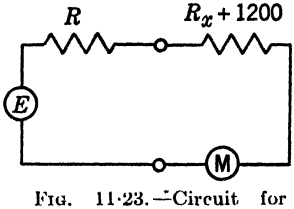

FIG. 11·23.—Circuit for the direct measurement of the figure of merit.

Figure of Merit.—Once the video resistance and current sensitivity are known, the figure of merit can be calculated. In routine testing, however, it is advantageous to be able to obtain the figure of merit directly from the meter reading. A method devised by Beringer makes it possible to do this to a good approximation if the units being tested have known limits of resistance (resistance limits are specified for the various video-crystal types).

Let the equivalent circuit of the crystal, operating at a power level P, be represented by a voltage generator E in series with the crystal resistance R, as shown in Fig. 11·23. If $R_x + 1200$ is the total circuit resistance of the measuring circuit then the current flowing is

$$i = P \frac{\beta R}{R + R_x + 1200}. \tag{29}$$

Let

$$R + 1200 = R_x(1 + \delta).$$

Then

$$i = \frac{P\beta R}{R_x(2 + \delta)}, \tag{30}$$

which may be written in the form

$$i = \frac{P}{2\sqrt{R_x}} \cdot \frac{\beta R}{\sqrt{R + 1200}} \cdot \frac{\sqrt{1 + \delta}}{1 + \frac{1}{2}\delta}, \tag{31}$$

or

$$i = \frac{P}{2\sqrt{R_x}} M \cdot \frac{\sqrt{1+\delta}}{1+\frac{1}{2}\delta}. \tag{32}$$

Let R_1 and R_2 be the resistance limits of the crystals being tested, and let R_x be fixed at the value

$$R_x = \sqrt{(R_1 + 1200)(R_2 + 1200)}. \tag{33}$$

It can be seen then that the rectified current is proportional to the figure of merit multiplied by a correction factor $\sqrt{1+\delta}/(1+\frac{1}{2}\delta)$, which depends on the individual crystal resistance. In actual practice the correction factor is always nearly unity, so that a good approximation is

$$i = \frac{P}{2\sqrt{R_x}} M. \tag{34}$$

For example, if R_1 and R_2 are 30,000 and 10,000 ohms, the value of the correction factor varies from 0.97 to 1.0 over the entire range of values of R.

SPECIAL MANUFACTURING TECHNIQUES

The first video-crystal type was the 1N27 rectifier, designed for a crystal-video receiver in a 10-cm beacon. The upper limit on video resistance was placed at 4000 ohms so that the beacon-triggering circuit would be tripped by 2-μsec interrogation pulses without being tripped by strong 1-μsec search pulses. A lower limit of 60 for the figure of merit gave a satisfactory sensitivity for this particular application. It was found that rectifiers of this type could be selected from the 1N21 mixer-crystal production, with the distribution of figure of merit running from the minimum of 60 to about 100, and with video resistances from about 1000 ohms to the maximum of 4000 ohms. Representative samples from the Sylvania 1N21B units showed somewhat higher figure of merit and resistance, the former ranging from about 60 to 200, with video resistances from about 1000 to 15,000. A considerable fraction of these meet the specifications for the 1N32 type, which is a video crystal for the 10-cm band for applications not requiring pulse discrimination. For this type a lower limit of 100 for the figure of merit and a video resistance in the range from 5000 to 20,000 ohms are specified.

In the 3-cm band the sensitivity of the various mixer-crystal types was insufficient for beacon applications, nearly all of the rectifiers having a figure of merit less than 30. With the development of 3-cm portable beacons an extensive program of research and development was undertaken on video-crystal manufacture, much of it by the University of Pennsylvania group. The fundamental aspects of this work have been discussed in the preceding sections. In the following sections are pre-

sented the techniques developed at the University of Pennsylvania[1] for making the 1N30 type, a high-sensitivity video crystal in the ceramic cartridge. Improvements to date have been achieved largely by using light contact pressures, together with a processing of the silicon and a procedure for adjustment of the contact established largely by empirical methods.

11·10. Stability Considerations.—It was evident from the beginning of video-crystal development for the 3-cm band that improvement in current sensitivity can be obtained by using light contact pressure at the rectifying contact. A spring deflection of about 1 mil is required for good performance in the 3-cm band. With such a light pressure the achievement of mechanical stability has been difficult. This instability is manifested by a change in video resistance and/or current sensitivity (*a*) after mechanical shock, such as the drop test of JAN specifications, (*b*) after temperature cycling, and (*c*) after filling the cartridge.

The stability of the coaxial cartridge is definitely better than that achieved with light pressures in the ceramic cartridge design, and consequently the 1N31 type, utilizing the coaxial cartridge, was specified in the latter stages of the development work. Meyerhof found that the stability of the ceramic cartridge was affected by the size of the crimp in the whisker, a transverse dimension of about 0.065 in. in a 3.5-mil wire being preferable to a smaller loop.

The instability observed during the temperature cycling and the change in characteristics upon filling led to an extensive investigation of various cartridge-filling materials by the University of Pennsylvania group.[2] Among the materials investigated were the silicone greases, vinylite dibutyl pthalate, Paratac mixed with magnesium oxide, beeswax or Acrawax, and polystyrene in various nonvolatile solvents. None of these was found to be as satisfactory as the mixture of Paratac and Opalwax commonly used (see Sec. 10·7) for mixer crystals.

11·11. Processing the Silicon.—The processing of the silicon for video crystals follows the same general procedure as that for mixer crystals. The best units made by the Pennsylvania group used duPont silicon, doped with either of the following:

1. 0.1 per cent Al, 0.015 per cent B, and 0.02 per cent Be.
2. 0.002 to 0.006 per cent B and 0.02 Be.

The percentage of boron is not critical in the range specified. As is the case with mixer crystals, no exhaustive systematic investigation of the relative merits of various doping agents has as yet been made.

[1] W. E. Meyerhof and W. E. Stephens, "X-band Video Crystals," NDRC 14-274, Univ. of Penn., May 20, 1944; W. E. Meyerhof, "Development Research on X-band Video Crystals," NDRC 14-501, Univ. of Penn., Sept. 10, 1945.

[2] A. H. Smith, "Use of Different Fillers in Crystal Rectifiers," NDRC 14-561, Univ. of Penn., Oct. 18, 1945.

After the ingot is made, it is cut into slices and one surface is dry-polished on 0000 emery paper. The low-level characteristics are found to vary somewhat with temperature and time of heat-treatment. Heating in air at a temperature of 975°C for 2 hr appears to yield the highest figure of merit. The polished surface is then etched in 10 per cent hydrofluoric acid, and the back surface then plated for soldering to the cartridge stud. The final electrolytic etch used in the Radiation Laboratory procedure for mixer crystals reduces the figure of merit and is therefore omitted.

11·12. Fabrication of the Whisker.—The shape of the whisker wire and its size influence both the stability and the figure of merit of the video crystal. Experiments by Meyerhof showed that, with 3.5-mil wire, increasing the transverse dimension across the loop from approximately 0.035 to 0.065 in. improves the figure of merit by approximately a

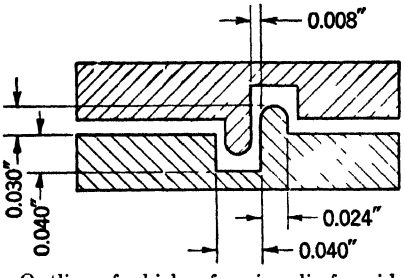

FIG. 11·24.—Outline of whisker-forming die for video crystals.

factor of 2. The largest crimp was also the most satisfactory from the viewpoint of crystal stability. The dimensions of the die for making this crimp in 3.5-mil wire are given in Fig. 11·24.

The conical whisker point is ground on Arkansas stone to make the included angle of the cone between 70° and 90° and the point diameter less than 0.1 mil. Stability is difficult to achieve in the double-loop structure for wires smaller than about 3.5 mils.

11·13. Adjustment of the Rectifying Contact.—The rectifying contact is adjusted in a device that advances the whisker toward the crystal with a micrometer screw, and that is connected to a circuit for measuring the video resistance, similar to that of Fig. 11·22. The contact pressure is increased until the spring deflection is about 1 mil; at this stage the low-level resistance should be less than 2000 ohms. The cartridge is then tapped until the resistance is between 10,000 and 20,000 ohms. Occasionally the resistance is observed to drift immediately after adjustment. Stabilization can sometimes be achieved by additional tapping; otherwise the unit is discarded.

After adjustment the units are impregnated with a Paratac-Opal wax filler by the conventional vacuum-impregnation method. The filling

should take place slowly, since rapid motion of the wax may alter the contact.

As an example of what can be achieved by using these techniques in the laboratory, of the 80 units assembled by Meyerhof, 54 were adjustable, 40 of them meeting the specifications for type 1N30 units—that is, figure of merit greater than 55 in the tunable mixer, and video resistance between the limits of 7000 and 21,000 ohms.

Some of these units were subjected to the JAN design tests, consisting of a 10-in. drop test and a temperature cycle consisting of 2 hr at a temperature of −55°C followed by $\frac{1}{4}$ hr at +70°C. Of 22 units tested, 5 went outside the limits of 5000 to 25,000 ohms, and an additional 6 units shifted more than 40 per cent in resistance during the test. There is still much to be desired therefore in the way of stability even with the best techniques now available. It has been pointed out that the coaxial cartridge is preferable on this score; beyond that, hope for further improvement probably lies in the possibility of discovering new techniques whereby the required small barrier capacitance can be obtained by some means other than the reduction of contact area.

CHAPTER 12

HIGH-INVERSE-VOLTAGE RECTIFIERS

THE HIGH-INVERSE-VOLTAGE RECTIFIER AND ITS APPLICATIONS

The crystal rectifier as a second detector in radar receivers has a number of advantages over the vacuum-tube diode. This application is discussed in detail in Chap. 7, Vol. 23, of the Radiation Laboratory Series. The advantages of the crystal detector discussed there may be briefly summarized as follows:

1. Referring to Fig. 2·6, we see that for voltages greater than a few tenths of a volt the conductance in the forward direction is considerably higher than that for a tube. This characteristic is advantageous in wideband receivers where the diode load resistance is low.
2. The interelectrode capacitance and capacity to ground is very low, a characteristic of importance in both the i-f and video circuits.
3. The crystal detector requires no heater power and can contribute no hum.
4. It requires no more space than a half-watt resistor.
5. It can be equipped with "pigtail" leads and soldered into the circuit, thus requiring no socket.
6. The current-voltage characteristic passes through the origin and reaches an approximately linear region at a low voltage; hence it is more efficient for small input voltages.

Crystal rectifiers available prior to the discovery of the high-inverse-voltage rectifier were, however, inferior to tube diodes in that they conducted in the reverse direction, the resistance decreasing with increasing negative voltage to values of about 1000 ohms at a few volts negative. Moreover, the reverse voltage that may be applied without damaging the crystal is limited. Because of these limitations the use of crystal rectifiers as second detectors in radar receivers was not feasible until the discovery by Benzer,[1] working at Purdue University with Dr. K. Lark-Horovitz, of the high-inverse-voltage property which could be obtained with appropriately doped germanium.

The unusual rectifier properties discovered by Benzer are illustrated by the characteristic curve shown in Fig. 12·1. As can be seen from the

[1] S. Benzer, "The High Voltage Germanium Rectifier," NDRC 14-342, Purdue Univ., Nov. 1, 1944.

figure, a maximum voltage is attained for either polarity of applied voltage, beyond which there exists a negative-resistance region. The second remarkable feature is the high resistance exhibited in the back direction for a large range of applied voltages. At the same time, conductances in the forward direction are comparable with other rectifier types, corresponding to currents of 10 to 20 ma at 1 volt.

The peak back voltage of the crystal, shown in Fig. 12·1, has been greatly exceeded since Benzer's original work. A curve typical of crystals made later at Purdue is shown in Fig. 2·8. In the latter curve the current scale is expanded and the curve has not been extended in the

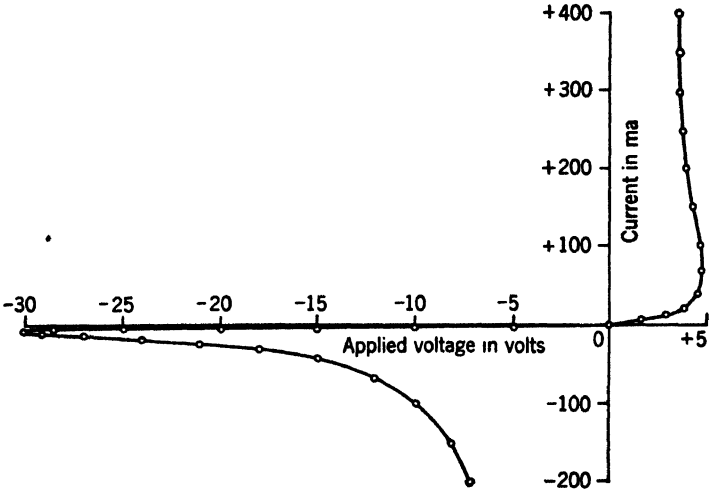

FIG. 12·1.—Characteristic curve of a high-inverse-voltage germanium rectifier.

forward direction to the negative-characteristic region. In the most recent work reported by Scaff and Theuerer[1] at the Bell Telephone Laboratories, a process for making these rectifiers is reported which yields rectifiers with a median value of 7.0 ma forward current at 1 volt, median reverse currents at 1 and 30 volts of 0.002 and 0.036 ma, and a median peak inverse voltage of 200 volts. Occasionally rectifiers have been made with peak inverse voltages as high as 400 volts.

The negative-resistance region in the back direction has been used by Benzer to produce oscillations at frequencies as high as 100 kc/sec. The chief interest up to the present, however, has been in applications requiring the high back voltage and high resistance in the back direction. A more detailed discussion of the properties will be given in the following sections.

[1] J. H. Scaff and H. C. Theuerer, "Final Report on Preparation of High Back Voltage Germanium Rectifiers," NDRC 14-555, BTL, Oct. 24, 1945.

Though most of the work has been done with germanium, investigations at the University of Pennsylvania show that the high-inverse-voltage property can be obtained with properly doped silicon. The results obtained will be discussed in Sec. 12·6.

Following Benzer's discovery, extensive developmental work was carried out on germanium both at Purdue University and at Bell Telephone Laboratories, and several types are now manufactured. Tentative manufacturing specifications are listed in Appendix D; recent improvements in manufacturing techniques already make feasible more stringent specifications. At present, it appears that the Western Electric Type D171561 can be used to advantage in place of vacuum-tube diodes in wideband receivers, and in receivers having a logarithmic response or incorporating d-c feedback loops around individual i-f stages to prevent overloading. In the latter applications detectors are required at the plates of several i-f stages. The relatively large interelectrode capacity of tubes reduces the gain-bandwidth product and makes the design of wideband receivers difficult. In such cases the use of crystal detectors greatly simplifies the design problem.

The high-inverse-voltage rectifiers have also shown great promise in the laboratory for applications in video circuits as clamping diodes, d-c restorers, diode modulators, switching circuits, etc. These applications, in general, require very high back resistance up to at least 5 volts and, depending on the application, up to as high as 50 volts, as well as stability in the current-voltage characteristic under operating conditions. The advantages which the crystal rectifier has over the tube diode in these applications include the following:

1. No filament voltage is required; consequently there is no need for a heater power supply or for the attendant sensitivity of the circuit to fluctuations in heater voltage.
2. There is a relatively high forward conductance.
3. The current-voltage curve passes through the origin.
4. Tests in a diode modulator circuit indicate that the properties of crystals drift less with time when under use than do the properties of diodes.

Among the disadvantages of the crystal in some of these applications are the sensitivity of the current voltage characteristic to temperature and the variation in the characteristics from one crystal to another.

The high-back-voltage crystals also have useful applications as low-frequency rectifiers. The 1N34 "diode," manufactured by Sylvania Electric Products Company, is rated for use at a maximum peak inverse voltage of 50 volts, a peak anode current (sine-wave) of 60 ma maximum, and an average anode current of 22.5 ma. This type is also recom-

mended by Sylvania for use as a second detector or frequency discriminator up to frequencies as high as 100 Mc/sec.

Extensive developmental programs have been carried out under NDRC contracts, first at Purdue University[1] and later at the Bell Telephone Laboratories,[2] to investigate methods for improving the rectifying characteristics and increasing the stability and uniformity of the product, and to develop techniques for the quantity production of the units. As in the case of mixer crystals, no attempt will be made to describe the procedures in detail but rather to describe typical procedures that represent the state of the art at present.

12·1. Preparation of the Ingot.—The germanium used at both Purdue and Bell Telephone Laboratories is prepared from pure germanium dioxide obtained from the Eagle-Picher Company and reduced in hydrogen by the method described in Sec. 10·1.

The ingots are made by melting the pure germanium with a specified amount of the desired doping material, either in a high-vacuum furnace at pressures of the order of 10^{-5} mm Hg, or in an atmosphere of helium. After the charge is liquefied, a temperature gradient is established in the crucible by raising the induction furnace coil at the rate of about $\frac{1}{8}$ in./min. The ingot then solidifies from the bottom upward. Crucibles of quartz or porcelain have been commonly used. Exceptionally good crystals have been made also at the Bell Telephone Laboratories,[3] by using pure graphite crucible and omitting the addition of an impurity. This procedure will be discussed in detail later in this chapter.

Doping Materials and Their Effects on Rectification Characteristics.—An extensive investigation of various doping materials has been made by the group at Purdue University. Nearly all the metallic elements with the exception of the alkali metals and some of the rare elements, have been tried. Also, some compounds have been tried as well as mixtures of two or more elements in varying quantities. The results of this exploratory investigation on single elements may be classified as follows:

1. Elements producing good high-inverse-voltage rectifiers: N, Sn, Ca, Ni, Cu, Sr, Pd, Bi.

[1] See R. M. Whaley and Paul Pickar, "Preparation of High Voltage Germanium Crystals," NDRC 14-341, Purdue Univ., Nov. 1, 1944; R. M. Whaley, "Further Developments in the Preparation and Heat Treatment of Germanium Alloys," NDRC 14-576, Purdue Univ., Oct. 31, 1945; and L. Boyarsky, P. B. Pickar, A W. McDonald, R. N. Smith, R. M. Whaley, and H. J. Yearian, "Production and Performance of Germanium High Back Voltage, High Back Resistance Crystal Rectifiers," NDRC 14-577, Purdue Univ., Oct. 31, 1945.

[2] See J. H. Scaff and H. C. Theurer, *loc. cit.*

[3] Scaff and Theuerer, *op. cit.*

2. Elements that are fair: Mg, Ti, V, Cr, Co, Zn, Cb, Ag, Cd, Ba, Sm, Pr, Ta, Pb, U.
3. Elements that are poor: Be, B, Al, Si, P, Ga, As, Zr, In, Pt, Au, Tl, Th.

Those elements classified as "good" have the best combination of high peak voltage and high forward conductivity. The classification should be interpreted with caution, however, since in many cases only one or two exploratory melts were made and the effect of varying the concentration was not thoroughly investigated. (Note, for example, the results obtained at Bell Telephone Laboratories with arsenic, discussed later in this section.) In some cases, elements classed as "fair" doping agents yielded high peak inverse voltages but relatively low conductivity in the forward direction. It is of interest to note that good high-back-voltage germanium rectifiers are, in general, poor as mixer crystals.

Some compounds containing elements in the "good" classification (such as Bi_2O_3, $BaCl_2$, and SnO) were tried but showed no unusual properties; in general, the best results were obtained with elements.

Some success has been obtained with mixtures of elements such as Pd or Ni with Sr or Ca. Of the various impurities tried in this investigation, however, germanium doped with tin appeared to be the most promising from the viewpoint of rectification characteristics, stability, and uniformity from melt to melt. Consequently the major part of the work at Purdue and at Bell Telephone Laboratories has been done with this element as doping agent. Tests on the amount of tin added showed that, above about 0.1 atomic per cent, the amount of tin added is not critical. With quantities greater than this, tin usually separates out both at internal grain boundaries and at the surface; about 0.1 atomic per cent appears to be the optimum amount.

With tin-doped germanium, the differential cooling described above produces an ingot consisting of a shell of poorly rectifying *p*-type germanium, surrounding a central core of strong rectifying characteristics. In this central core the peak inverse voltage varies from values of 10–50 volts at the top to 100–150 volts at the bottom of the ingot. This effect is reproducible from melt to melt.

The Effect of Heat Treatment of the Ingot.—Interesting effects of heat treatment of the ingot on the rectifying properties have been observed by Scaff and Theuerer.[1] They found it possible to convert, reversibly, *p*- to *n*-type germanium by the proper control of the time and temperature of the heat treatment. If an ingot is heated to 800°C and rapidly cooled, the rectifying characteristics are practically destroyed as a consequence of the conversion of the strongly rectifying *n*-type to the poorly rectifying

[1] *Loc. cit.*

p-type. Typical characteristic curves for the two types are shown for comparison in Fig. 12·2. By a subsequent treatment of the rapidly cooled ingot at 500°C for, let us say, 20 hr, or by slow cooling from 800°C, the p-type germanium is entirely transformed to n-type, and all but the upper one-third of the ingot exhibits peak inverse voltages above 50 volts. Moreover, the shell material converted from p- to n-type exhibits superior peak voltages and back resistance. The treatment is therefore desirable from the standpoint both of quality and quantity.

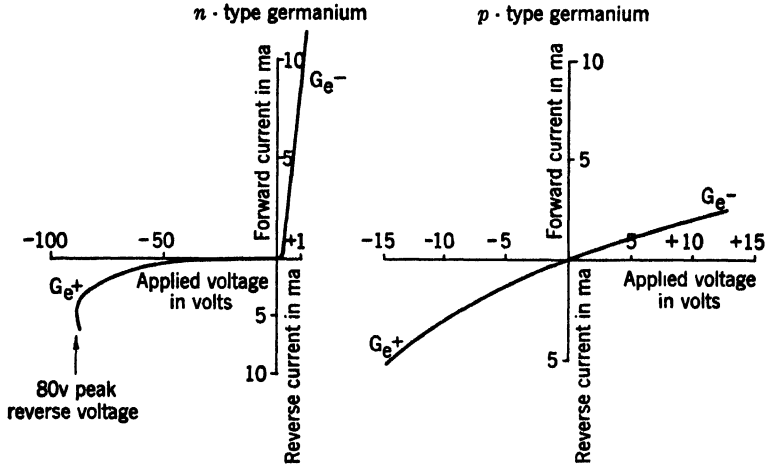

FIG. 12·2.—Typical characteristic curves of n- and p-type germanium.

Some of the conclusions reached by Scaff after a detailed study of the effect are as follows:

1. Since the heat treatment is reversible, the effect cannot be ascribed to chemical change or to the diffusion of impurities. This conclusion is further supported by the fact that the variation in peak inverse voltage from the top to the bottom of the melt, ascribed to variation in impurity in the melt, is not altered after heat cycling.
2. The concentration of impurities in the bottom of the ingot, which is first to solidify and presumably is the purest region, is sufficient for the conversion effect to occur. On the other hand, there appears to be an upper limit to the impurity concentration, as evidenced by the fact that the topmost part of the ingot, which is richest in impurities, is not altered by rapid cooling from 800°C.
3. The rate of conversion from p- to n-type germanium depends on the temperature and appears to be a maximum at about 500°C.
4. Equivalent results are obtained if the heat treatments are conducted in either a vacuum or helium atmosphere.

5. Ingots prepared by fusing pure germanium in a graphite crucible without the addition of tin are n-type, with exceptionally high peak voltages and back resistances. Heat-treating effects in this material are completely analogous to those observed with tin-doped germanium.

Scaff concludes from these experiments that the formulation of p-type germanium by rapid cooling results in the retention of an impurity in solution, whereas the production of the n-type material by subsequent reheating at a lower temperature is caused by precipitation of the impurity from solution.

For a nonmetallic doping agent, i.e., arsenic, analysis at Bell Telephone Laboratories revealed a 20-fold variation in impurity concentration between lots having good and poor rectification characteristics. Specifically, germanium producing good high-back-voltage characteristics contained 0.0004 per cent arsenic, whereas the poor material contained 0.0085 per cent. After a treatment that presumably removed the residual arsenic, the ingot exhibited p-type rectification, which could not be converted to n-type, by either heat treatment or fusion in a graphite crucible. This finding strongly suggests that the arsenic, which is a donator impurity, is responsible for the n-type rectification. This conclusion is further supported by the fact that subsequent remelting of the ingot with 0.001 per cent antimony, also a donator impurity, produced all n-type material, having peak inverse voltages from 20 to 100 volts. Although somewhat lower in peak voltage, the ingot was otherwise similar to those prepared without additions of impurities in graphite crucibles in a dry helium atmosphere. It appears that probably even lower concentrations would improve the high-back-voltage property.

A theory consistent with these observations, proposed by Scaff, postulates that the arsenic originally present in germanium is responsible for the n-type rectification and that an acceptor impurity, perhaps oxygen, is also present, which tends to produce p-type material. In the regions where n-type rectification is exhibited the donators are in excess; in the p-type regions, acceptors are in excess. It is assumed then that the acceptors are activated by heat treatment at 800°C and are retained in this state by rapid cooling; subsequent conversion to n-type germanium by heating at 500°C results in deactivation of the acceptors by their precipitation from this unstable solid solution. Oxygen is suggested as a likely candidate for the acceptor impurity. Thermal transformations are known to occur in germanium oxide near 500°C. Furthermore, the effect of the graphite crucible in producing the n-type material already mentioned may be due to the reducing nature of the graphite. Attempts to eliminate oxygen completely have not been successful to date.

Further experiments at Purdue University[1] have yielded additional interesting results. In these experiments, nitrogen was added as an impurity and graphite crucibles were used. The crucible and germanium charge were given a preliminary outgassing at 700°C before nitrogen was admitted, and the furnace region was evacuated to a pressure of approximately 10^{-5} mm Hg. Similar results were obtained with commercial nitrogen and with nitrogen purified by passing it (1) through a P_2O_5 drying tube, (2) over hot fresh copper turnings to remove oxygen, and finally (3) through a liquid-air trap to remove water vapor and carbon dioxide. Nitrogen was admitted to the vacuum system during the melting operation. Various pressures were tried and it was found that the rectification characteristics were independent of pressure in the range from 2 mm to 1 atmosphere; a pressure of about 0.1 mm was found insufficient to produce usable alloys. During the melting of the germanium powder a copious amount of brown smoke was produced which ceased after the germanium melted to form a regulus. Spectroscopic analysis of powder condensed from the smoke showed the presence of germanium only; hence the smoke may have been either an oxide or a nitride.

Rectifiers made from the nitrogen-germanium ingots exhibited peak back voltages from 100 to 200 volts, forward currents at 1 volt from 5 to 20 ma, and back resistances at 4 volts from about 50,000 to 400,000 ohms.

Ingots of nitrogen-germanium made in quartz or porcelain crucibles had *p*-type high-resistance regions in the portions adjacent to the bottom and sides of the crucible where solidification first takes place. This phenomenon was never observed when graphite crucibles were used. It was found that nitrogen-germanium ingots made in graphite crucibles respond to heat-treatment in a manner similar to that reported by Scaff. Heating the ingot either in vacuum or in an atmosphere of nitrogen at a temperature of 650°C converted some of the *n*-type region to *p*-type material, whereas subsequent treatment at 500°C reconverted it to *n*-type.

In further experiments on heat treatment, Whaley[2] found that germanium-tin alloys prepared in vacuum and subjected to heat-treatment at the same temperature and for the same lengths of time as those used in the Bell Telephone Laboratories experiments showed no changes resulting from the treatment. With ingots prepared in an atmosphere of helium, however, the results obtained duplicated those reported by Scaff, both for the germanium-tin alloy and for pure germanium melted in a graphite crucible. These experiments suggest that an acceptor impurity present in the helium may be taken up by the germanium in the

[1] R. M. Whaley, "Further Developments in the Preparation and Heat Treatment of Germanium Alloys," NDRC 14-576, Purdue Univ., Oct. 31, 1945.

[2] *Loc. cit.*

melting process. As far as can be ascertained no further work has been reported that will definitely establish a theory of the role of impurities in the rectifying properties of germanium.

12·2. Etching and Surface Treatment.—The ingot is cut into wafers; one side of each is copper-plated for soldering to the cartridge mounting stud. The rectifying face is ground to a smooth surface on glass charged with water and 600 aloxite or alumina. The polishing procedure used with mixer crystals is not necessary and has been omitted in both the Purdue and the Bell Telephone Laboratories procedures. An investiga-

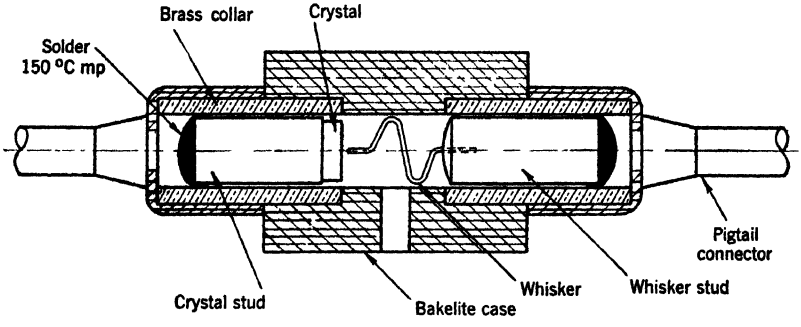

FIG. 12·3.—Bell Telephone Laboratories design of molded bakelite cartridge for the germanium rectifier.

tion by the Purdue group of various etchants showed no significant difference in d-c characteristics produced by the following:

1. Chemical etch: 4 cc HF; 2 cc HNO_3; 200 mg $Cu(NO_3)_2$ in 4 cc H_2O.
2. Electrolytic etch: 1 gm stannyl chloride in 50 cc H_2O.
3. Electrolytic etch: 5 cc concentrated HNO_3 in 50 cc H_2O.
4. Electrolytic etch: 3 cc concentrated HCl; 1 cc concentrated HNO_3 in 10 cc H_2O.
5. Electrolytic etch: 15 gm $CrSO_4 \cdot 5H_2O$ in 50 cc H_2O.

The chemical etch produces a satisfactory result in about one minute. For the electrolytic etches, the germanium is connected as the anode. The application of 2 to 2.5 volts with currents varying from 5 to 15 ma results in a satisfactory etch in 1 to 2.5 min. Because of the relative simplicity of techniques from a manufacturing viewpoint, the Bell Telephone Laboratories use a chemical etch similar to that in the preceding list.

12·3. Assembly and Adjustment of the Cartridge.—The pigtail cartridge used as an interim design by Bell Telephone Laboratories is shown in Chap. 2 (Fig. 2·1). They now have under development a bakelite cartridge that looks promising; a sectional view is shown in Fig. 12·3. The cartridge consists of a bakelite cylinder, in the ends of which are molded two brass collars. The whisker and crystal are

mounted on knurled brass studs which are forced into the collars until the desired contact is made; they are then soldered in place with a low-melting-point solder. The unit is hermetically sealed and hence requires no wax filler for protection from moisture; if a filler is used to increase mechanical stability, a filling hole, as shown, can be provided for introducing it.

No significant difference in rectification characteristics has been found when different whisker materials are used; consequently, as in mixer crystals, tungsten is commonly used.

The adjustment of the rectifying contact is made by the techniques already described; a spring deflection of 2 mils is satisfactory.

As a final step the rectifier is given a stabilizing power treatment. Such a treatment was suggested by observations of Benzer,[1] who discovered that the d-c characteristic in the back direction exhibits a hysteresis effect when traversed for the first time—that is, the characteristic is different for increasing and decreasing voltages; repeated traversals, however, are identical provided the initial maximum voltage is not exceeded. The change of the characteristic results, in general, in higher back resistances. It was further found[2] that relatively high back resistances were not stable when measured before and after the application of voltages approaching the peak back voltage. The resistance measured immediately afterward was frequently as low as one-tenth the initial value, partially or completely recovering to the initial value after standing for about one minute.

Further experimentation[3] showed that the application of power overloads in the form of pulses of about one-second duration are very effective in raising and stabilizing the back resistance. This power treatment can be effected with either direct or alternating current. If direct current is used in the back direction, the pulses are applied to the peak of the characteristic or beyond; in the forward direction, optimum currents range from 0.2 to 0.8 amp. With alternating current, the peak forward current will usually lie somewhere in the range from 0.2 to 1.0 amp. By gradually increasing the applied voltage between pulses an optimum value can be found for a given rectifying contact. Scaff[4] has found

[1] S. Benzer, "The High Voltage Germanium Rectifier," NDRC 14-342, Purdue Univ., Nov. 1, 1944.

[2] L. L. Boyarsky, R. N. Smith, and H. J. Yearian, "Properties of Germanium High-Back Voltage Rectifier Units," NDRC 14-413, Purdue Univ., Mar. 19, 1945.

[3] L. L. Boyarsky, P. B. Picker, A. W. McDonald, R. N. Smith, R. M. Whaley, and H. J. Yearian, "Production and Performance of Germanium High Back Voltage, High Back Resistance Crystal Rectifiers," NDRC 14-577, Purdue Univ., Oct. 31, 1945.

[4] J. H. Scaff and H. C. Theuerer, "Final Report on Preparation of High Back Voltage Germanium Rectifiers," NDRC 14-555, BTL, Oct. 24, 1945.

that the a-c treatment is preferable to d-c treatment in its stabilization effect. The a-c stabilization method adopted at Bell Telephone Laboratories consists of applying 30-volt a-c pulses 0.8 sec long at a frequency of 60 cps. This voltage is applied to the crystal in series with a 50-ohm resistance. The process is repeated until the back resistance measured at 5 volts remains unchanged after the application of 50 volts in the back direction.

The effects of the power treatment may be summarized as follows:

1. Back resistances are increased on the average by an order of magnitude. This increase is general up to voltages of one-half or two-thirds the peak voltage; the resistance in the neighborhood of the peak is not increased by more than a factor of 2.
2. Power-treated units show negligible hysteresis after application of the peak back voltage.
3. Experiments at Purdue with germanium-tin and germanium-nitrogen crystals indicate that forward conductances are usually decreased somewhat by the power treatment; high initial values are decreased by amounts up to 50 per cent while lower values are little changed. Although this effect is undesirable, the change is not a serious one. Experiments at Bell Telephone Laboratories with pure germanium melted in graphite crucibles show that the forward current at 1 volt is somewhat increased by the power treatment (see Fig. 12·4).
4. Power-treated units show somewhat better over-all performance as second detectors than untreated units. Moreover, power-treated units do not show a decrease in peak back voltage in going from direct current to 30 Mc/sec; such a decrease is observed with untreated units.
5. The peak back voltage is, on the average, increased somewhat with germanium-nitrogen materials. With the germanium fused in graphite the change is not significant.

After adjustment and power treatment the cartridges are impregnated with wax. The Paratac-Opalwax mixture used in mixer crystals melts at a temperature less than 90°C, a temperature at which the germanium crystal might be required to operate in some applications. The Bell Telephone Laboratories have used as filler, therefore, a mixture of 20 per cent Acrawax C in Paratac. This wax melts between 95°C and 100°C and does not damage the rectifiers at temperatures as low as −50°C. It appears to be somewhat inferior to the Paratac-Opalwax mixture in shock protection. This is not a serious disadvantage in view of the fact that vibration tests at the Radiation Laboratory indicate that unwaxed cartridges withstand vibration tests required of components permanently wired into actual sets. The chief function of the wax is,

therefore, to protect the unit against moisture. Experiments at Bell Telephone Laboratories with the Paratac-Acrawax mixture show some change in d-c characteristics after prolonged exposure to 100 per cent relative humidity at 90°C. This is not thought to be serious, however, since ordinarily storage at 43°C and 95 per cent relative humidity is considered to be an accelerated tropical test, supplying a water content about twice that of "normal" tropical conditions. The condition of 100 per cent relative humidity at 90°C provides approximately 15 times the water content of the "normal" tropical condition.

Extensive investigations have been made by the group at Purdue[1] in an attempt to improve the protection of the crystal against high humidities at high temperature. They found that, in general, impregnation with wax had the deleterious effect of tending to restore the hysteresis that had been removed by the power treatment. It is to be recalled that this hysteresis is a decrease in back resistance after the application of high back voltage, followed by a gradual return to higher values. It was found that with Paratac-Acrawax filler the hysteresis at 50 volts is negligible, whereas the peak hysteresis in some cases involved resistance changes as large as a factor of 10, followed by restoration usually to the initial value in a matter of a minute or less. Thus, the effect of waxing alone should not impair performance in circuits where the maximum inverse voltage does not approach the peak, or where the maintenance of constant high back resistance is not required.

The Purdue group reports the following as unsatisfactory for moisture protection: coating the surface of the crystal with Pliobond, butyl methacrylate, or silicone. External coating of the cartridge with F125 cement, Pliobond, polystyrene cement, and glyptal were tried. Of these, the F125 cement showed most promise, although it did not always protect against 100 per cent humidity at 90°C. These experiments appear to show that the most satisfactory solution of the problem is likely to be an unimpregnated, hermetically sealed cartridge, such as the one shown in Fig. 12·3.

12·4. Low-frequency Properties.—The properties of interest in the low-frequency application of germanium rectifiers are the peak back voltage, the back resistances at voltages as high as 50 volts, the forward conductance at voltages under 1 volt, and the constancy of these properties under typical operating conditions. These characteristics, at the present stage of development, are best illustrated by a series of distribution curves representing data taken on a large number of rectifiers made in the laboratory by Scaff and Theuerer[2] during the development work

[1] Boyarsky *et al.*, *loc. cit.* (See footnote 3, page 370.)

[2] J. H. Scaff and H. C. Theuerer, "Final Report on Preparation of High Back Voltage Germanium Rectifiers," NDRC 14-555, BTL, Oct. 24, 1945.

on germanium rectifiers at Bell Telephone Laboratories. Figure 12·4 shows the cumulative distribution curves for the forward conductance in four different manufacturing processes. Curves 1 and 2 are for tin-doped germanium and show that the effect of heat treatment tends to decrease the forward conductance; however, the magnitude of the decrease is not serious. Curves 3 and 4 for germanium fused in graphite show a still smaller conductance, which is somewhat improved by the a-c power treatment, as shown by Curve 4. The improvement in other properties for this type of germanium, however, is rather marked, as can be seen in the following curves.

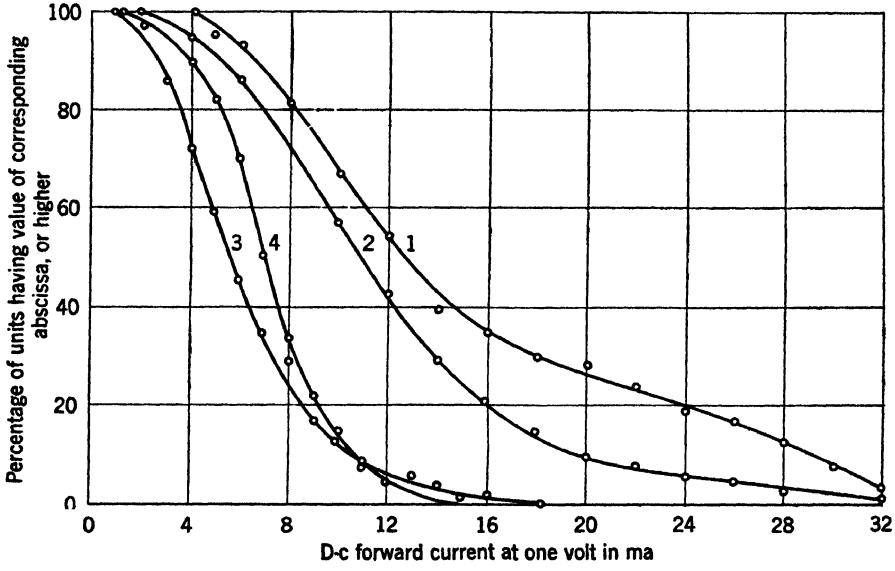

FIG. 12·4.—Cumulative distribution curves of forward conductance obtained at Bell Telephone Laboratories from various germanium ingots. (1) 50-gm germanium + 1 per cent tin ingots. (2) 50-gm germanium + 1 per cent tin ingots, heat-treated. (3) 50-gm germanium ingots, fused in graphite and heat-treated. (4) 50-gm germanium ingots, fused in graphite, heat-treated, and a-c stabilized.

Figures 12·5 and 12·6 show the cumulative distribution curves of back current at 1 volt and 30 volts, respectively, for the same manufacturing processes used in obtaining the data of Fig. 12·4. The superiority in high back resistance obtained by the heat treatment and a-c stabilization of pure germanium fused in graphite is evident from Curve 4, which shows that about 50 per cent of the rectifiers made by this process have back resistances of 0.5 megohm or more for back voltages as large as 30 volts.

Figure 12·7 shows the distribution of peak inverse voltages. It is evident again that the germanium fused in graphite is superior in this property, 50 per cent of the units having peak inverse voltages of 200 volts or greater; some units have been measured with peak inverse voltages of 425 volts.

Temperature Effects.—The d-c characteristic of the germanium rectifier is a function of temperature. This is an intrinsic property to be

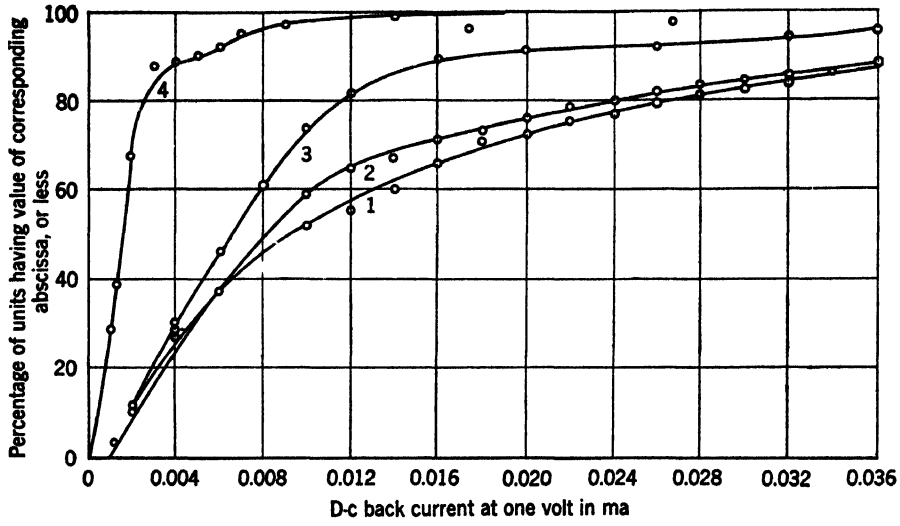

FIG. 12·5.—Cumulative distribution curves of back current at 1 volt obtained at Bell Telephone Laboratories for rectifiers from various ingots. (1) 50-gm germanium + 0.1 per cent tin ingots. (2) 50-gm germanium + 0.1 per cent tin ingots, heat-treated. (3) 50-gm germanium ingots fused in graphite, heat-treated, and a-c stabilized.

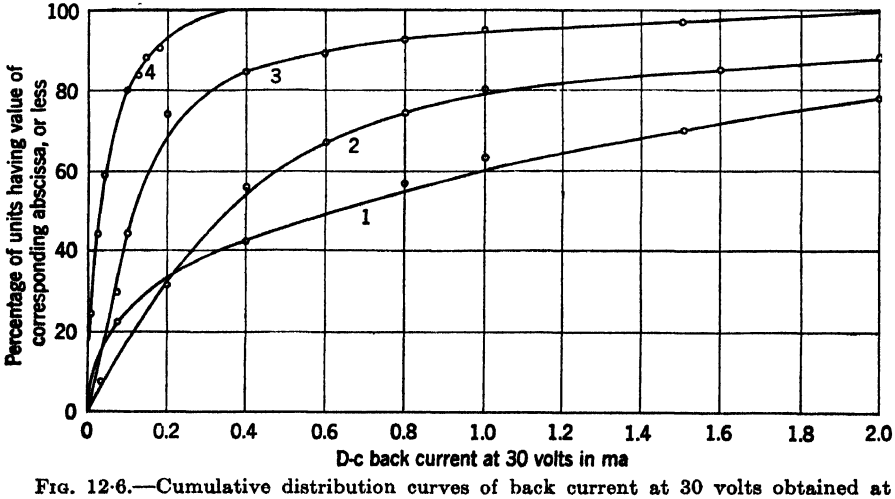

FIG. 12·6.—Cumulative distribution curves of back current at 30 volts obtained at Bell Telephone Laboratories for rectifiers from various ingots. (1) 50-gm germanium + 0.1 per cent tin ingots. (2) 50-gm germanium + 0.1 per cent tin ingots, heat-treated. (3) 50-gm germanium ingots fused in graphite and heat-treated. (4) 50-gm germanium ingots fused in graphite, heat-treated, and a-c stabilized.

expected on the basis of the theory of contact rectification discussed in Chaps. 3 and 4; and it is an effect of considerable practical importance in applications where a constant high back resistance at several volts is

required. The nature of the temperature variation can be seen from Fig. 12·8, where the forward and reverse parts of the characteristic curve of a typical germanium rectifier are plotted for four temperatures ranging

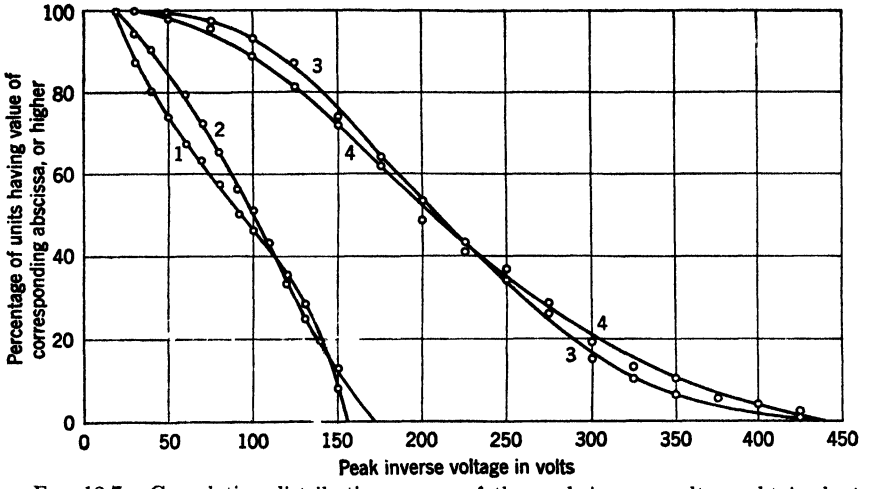

FIG. 12·7.—Cumulative distribution curves of the peak inverse voltage obtained at Bell Telephone Laboratories for rectifiers from various germanium ingots. (1) 50-gm germanium + 0.1 per cent tin ingots. (2) 50-gm germanium + 0.1 per cent tin ingots, heat-treated. (3) 50-gm germanium ingots fused in graphite and heat-treated. (4) 50-gm germanium ingots fused in graphite, heat-treated, and a-c stabilized.

from −40° to +95°C. It is seen that in the forward direction the variation of resistance is small in the vicinity of 1 volt; at a few tenths of a volt, in the exponential region of the characteristic, the forward

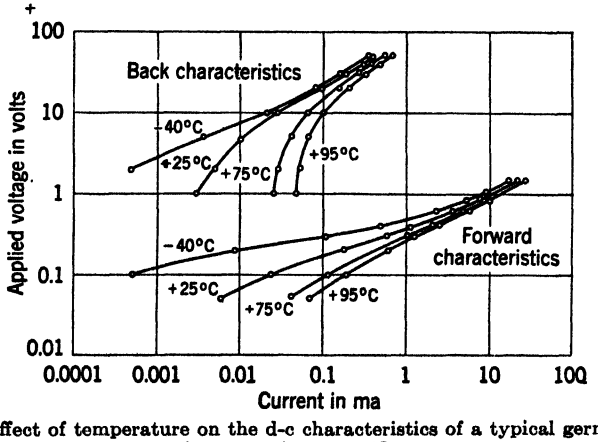

FIG. 12·8.—Effect of temperature on the d-c characteristics of a typical germanium high-inverse-voltage rectifier.

resistance decreases rapidly with increasing temperature; at a voltage of 0.1 volt the resistance at 95°C is an order of magnitude less than that at 25°C. Similarly, in the back direction the resistance at voltages of a

few volts decreases rapidly as the temperature increases, whereas at 30 or 40 volts the change is much less.

Benzer[1] has made a detailed study of the d-c characteristic from 30 volts in the back direction to 1 volt forward over the temperature range from −180° to +145°C, for germanium doped with various impurities such as nitrogen, tin, nickel, and bismuth.

Benzer's results indicate that in the back direction the temperature variation is small for units with low back resistance. For crystals of high back resistance, however, large variations were observed. In general, the back characteristic can be resolved into three current compo-

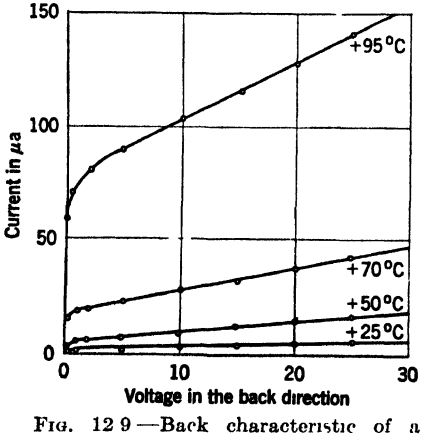

FIG. 12·9—Back characteristic of a germanium rectifier as a function of temperature.

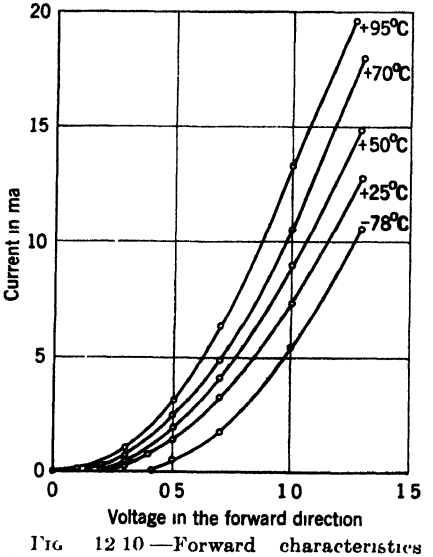

FIG. 12·10—Forward characteristics of a germanium rectifier as a function of temperature.

nents whose relative magnitudes vary from crystal to crystal. One component is exponential, rising to a saturation value at a fraction of a volt. The saturation current tails off into the second component, which is essentially linear. The third component rises more rapidly than linearly as the voltage is increased. The saturation- and linear-current components decrease rapidly with temperature; the third component does not. Figure 12·9 shows the back characteristic as a function of temperature for a rectifier in which the exponential and linear components predominate. At a temperature of −170°C (not shown on the graph) the third component is predominant and shows very little variation up to −78°C. The saturation current varies with temperature according to simple diode theory—that is, a plot of log i vs. $1/T$ is linear.

[1] S. Benzer, "Temperature Dependence of High Voltage Germanium Rectifier D-C Characteristics," NDRC 14-579, Purdue Univ., Oct. 31, 1945.

A plot of the forward characteristic as a function of temperature is shown in Fig. 12·10. Benzer has measured as a function of temperature the constant α in the equation for the forward characteristic (see Sec. 4·4):

$$I = A[e^{\alpha(V_a - Ir)} - 1],$$

where V_a is the potential applied to the rectifier, r is the spreading resistance, and A and α are constants, the latter having the theoretical value of e/kT. As in the case of mixer crystals, the measured value of α at room temperature is less than the theoretical value of about 40 volt^{-1}. With mixer crystals Yearian[1] found that in some cases α was independent of temperature, and for others was approximately proportional to $1/T$ as the temperature was increased. For the high-back-voltage germanium crystals, Benzer found that α decreases even more rapidly than $1/T$ as T is increased. For example a rectifier for which $\alpha = 27$ at 300°K has a value of $\alpha = 6$ at 425°K.

Life Tests.—Varied life tests have been run on germanium rectifiers at both room and elevated temperatures, with the applied power in the form of d-c pulses, continuous d-c, and both low- and high-frequency a-c power.

Tests were conducted by the Purdue group[2] on representative crystals that were connected to a 45-volt d-c source for periods up to 120 hr at a temperature of 90°C. Back resistance, peak back voltage, and forward current were measured before, during, and after the test. These measurements reflect the general changes with temperature already discussed: namely, at high temperatures the back resistance is decreased, more at low voltage than at high, and the forward current is increased. The changes during the test were not great and showed no particular trend up or down; this is also true of the initial and final room-temperature values of resistance.

Tests were also conducted on a number of power-treated units, using in the back direction 50-volt d-c pulses of various shapes ranging from a square pulse 500 μsec long to pulses decaying exponentially with time constants up to several thousand microseconds. In all cases, the pulse is followed by a pulse in the forward direction giving rise to a maximum forward current of from a fraction of a milliampere to 80 ma. The pulses were applied with the crystal at 90°C. The tests were designed to simulate conditions met in d-c restorer and clamping diode circuits. In

[1] H. J Yearian, "Investigation of Crystal Rectifier D-C Characteristics," NDRC 14-115, Purdue Univ., Dec. 3, 1942.

[2] L. Boyarsky, P. B. Picker, A. W. McDonald, R. N. Smith, R. M. Whaley, and H. J. Yearian, "Production and Performance of Germanium High Back Voltage, High Back Resistance Crystal Rectifiers," NDRC 14-577, Purdue Univ., Oct. 31, 1945.

general, the pulses produced no serious changes in crystal characteristics over extended periods of time; none of the units on test failed, and several showed no significant change in their d-c characteristics; most of the units changed by less than 35 per cent in back resistance, the results varying somewhat with the nature of the pulse.

Tests have been conducted at Bell Telephone Laboratories[1] with a group of 100 germanium rectifiers, some unfilled, and others filled with the Paratac-Opalwax or the Paratac-Acrawax mixture. The test consisted in the application of 2-volt a-c power at 60 cps for a period of 2000 hr, with the crystals at 90°C. During the course of the test the units were periodically brought to room temperature and the d-c characteristics measured. The data show that only minor changes in the characteristics were found. In some cases deterioration in back resistance was observed; in others the back resistance was higher than the initial values after 2000 hr. Some of the waxed units exhibited hysteresis effects after an initial period of the treatment; these disappeared after 600 hr of treatment.

12·5. High-frequency Properties.—Because of the interest in the use of high-inverse-voltage rectifiers as second detectors in radar receivers, the investigation of high-frequency properties has been confined for the most part to frequencies of 60 Mc/sec or less. Most of the work has been done at 30 Mc/sec, but enough semiquantitative experiments have been done at higher frequencies in the neighborhood at 60 Mc/sec to indicate that second-detector performance at this frequency is not much inferior to that at 30 Mc/sec. In addition, test methods have been developed and test equipment has been designed by the Purdue group for the measurement of rectification efficiency, over-all detector performance, and i-f impedance in a wideband detector circuit at 30 Mc/sec.

Forward Conductance as a Function of Frequency.—An investigation of the variation in forward conductance as a function of frequency has been made by Yearian.[2] The method consists essentially of a measurement of the rectified current obtained when a sinusoidal voltage wave is applied to the crystal under conditions such that there is no d-c bias. The applied voltage is then symmetrical about the origin of the crystal characteristic and, since the back resistance of the crystals is usually very high, the average value of the current (as read by a d-c meter in series with the crystal) will depend almost entirely on the forward conductance at the applied voltage. Suitable precautions were taken to insure that

[1] J. H. Scaff and H. C. Theuerer, "Final Report on Preparation of High Back Voltage Germanium Rectifiers," NDRC 14-555, BTL, Oct. 24, 1945.

[2] H. J. Yearian, "Dependence of Forward Conductance and Back Resistance of High Back Voltage Germanium on Voltage and Frequency," NDRC 14-581, Purdue Univ., Oct. 31, 1945.

the applied a-c voltage was maintained sinusoidal and that the d-c bias was negligible. Using this arrangement, the rectified current was measured for a-c voltages up to 2 volts at frequencies up to 60 Mc/sec.

Figure 12·11 shows the ratio of the rectified current at an applied rms voltage of 0.8 volt to that for a 60-cps voltage of 0.8 volt as a function of frequency for a typical germanium rectifier. This ratio is unity at 1000 cps but begins to fall off at higher frequencies, with a value of about 0.5 at 30 Mc/sec. A linear plot of the same data shows that at low frequencies the current ratio decreases more rapidly with frequency than at high frequencies; the logarithmic plot of Fig. 12·11, however, indicates that the ratio does not approach a lower limit in the frequency region investigated. The ratio does not, nevertheless, become zero at around 1000 Mc/sec, as is indicated by an extrapolation of the curve; rectification, although very small, is still observed at 3000 Mc/sec.

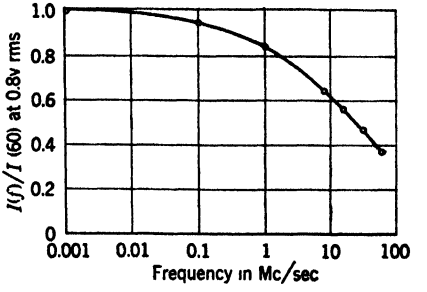

FIG. 12·11.—Rectified current as a function of frequency for a typical germanium high-inverse-voltage rectifier.

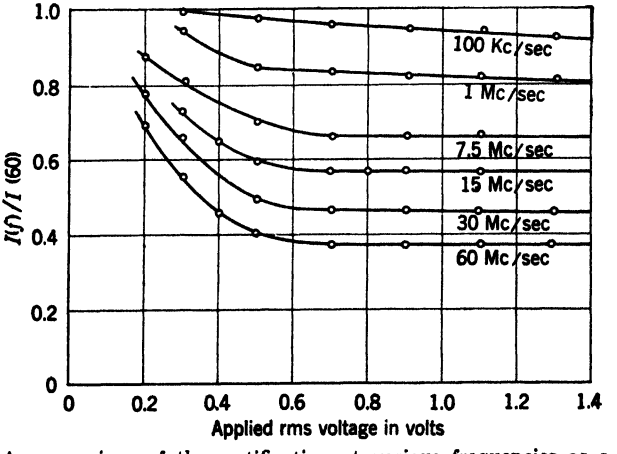

FIG. 12·12.—A comparison of the rectification at various frequencies as a function of applied voltage.

The ratio of the rectified current at a specified frequency to that at 60 cps is not independent of the applied voltage as can be seen from Fig. 12·12, where this ratio is plotted as a function of applied voltage for the various frequencies. It can be seen that the ratio is much larger at lower voltages than at high, approaching unity at zero voltage and decreasing to a constant minimum value for voltages greater than about

0.6 volt rms. In this constant range the data may be represented by the empirical relation

$$I(f) = I(60)\frac{1}{1 + af^{1/2}}, \tag{1}$$

where $I(f)$ is the rectified current at the frequency f and a is a constant for a particular crystal. For the crystal of Fig. 12·11, a has the value of 0.2 $(\text{Mc/sec})^{-1/2}$.

Yearian has interpreted these results to mean that the frequency sensitivity of the rectifier lies in the spreading resistance in series with the rectifying barrier. This conclusion is suggested by the fact that the decrease of rectified current with increasing frequency is much smaller at low voltages where the spreading resistance has little effect on the current; as the applied voltage is increased the voltage swing reaches the linear portion of the characteristic where the effect of the spreading resistance is predominant. To explain the existence of the frequency effect at voltages below 0.2 volt rms, where the main spreading resistance should have little effect on the current, Yearian assumes the multicontact model of the barrier with local spreading resistances in series with small isolated conducting spots. In these local spreading resistances where the current density is very high, it is assumed that the frequency effect is less than in the main spreading resistance.

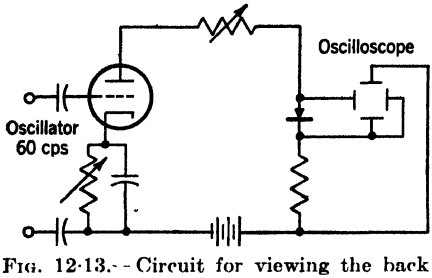

FIG. 12·13.—Circuit for viewing the back characteristic on an oscilloscope.

Dependence of Peak Inverse Voltage on Frequency.—The measurement of the peak inverse d-c voltage of a rectifier is readily accomplished by plotting the d-c characteristic. A convenient and rapid method of determining the peak inverse voltage is by means of a circuit designed by Benzer and shown in Fig. 12·13. The crystal is connected in the plate circuit of a triode in such a way that the plate current is in the back direction in the crystal. The current through the crystal is adjusted by means of the cathode bias and series plate resistors. The horizontal plates of an oscilloscope are connected across the crystal and the vertical plates are connected across a resistor in series with the crystal. A 60-cps voltage applied to the grid of the tube modulates the plate current about its average value and a portion of the current-voltage curve in the back direction is displayed on the oscilloscope. The peak inverse voltage is determined by using a small a-c input voltage and adjusting the plate current until the oscilloscope trace is vertical. The peak inverse voltage is then read on the voltmeter. The circuit can also be used for viewing

the entire back characteristic by properly adjusting the tube plate current and the input signal.

For the measurement of peak back voltages at 30 Mc/sec the circuit of Fig. 12·14*a* has been used by the Purdue group.[1] A 30-Mc/sec source of power is connected to the crystal in series with a large condenser. The distribution of voltage over the current-voltage characteristic is shown in Fig. 12·14*b*. The voltage swings slightly positive for a short time sufficient to replace the charge that leaks off through the back resistance during the remainder of the cycle. Since the back resistance is in general very large compared with the forward resistance, the inverse voltage applied to the crystal $V_{r\text{-}f} + V_{d\text{-}c}$ is approximately equal to twice the value of $V_{d\text{-}c}$. The peak inverse voltage is measured by increasing the power from the 30-Mc/sec source until both $V_{r\text{-}f}$ and $V_{d\text{-}c}$ decrease or at

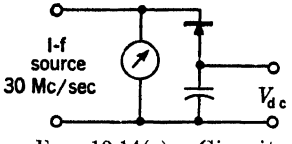

FIG. 12·14(*a*).—Circuit for the measurement of peak inverse voltage at 30 Mc/sec.

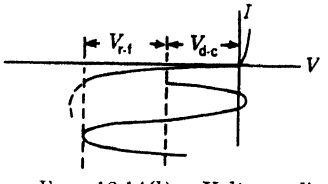

FIG. 12·14(*b*).—Voltage distribution over the crystal characteristic.

least no longer increase. Provided the source of power is sufficiently stable, this will occur when the peak inverse voltage is exceeded and the back resistance suddenly decreases.

Measurements by this method on a large number of germanium rectifiers made without power treatment showed that a majority withstood definitely lower peak inverse voltages at 30 Mc/sec than at direct current, most of them having values of from 40 to 80 per cent of the d-c value. Measurements made at 55 Mc/sec showed a further reduction from the 30-Mc/sec value, although not as much as that from direct current to 30 Mc/sec. At 10 Mc/sec, values were obtained intermediate between the d-c and 30-Mc/sec values.

It was found that the results reported in the preceding paragraphs could be altered by modifying the circuit in such a way that conduction in the forward direction was eliminated during any part of the cycle. This modification was accomplished by connecting to the condenser terminals a d-c voltage, and adjusting it so that $V_{d\text{-}c}$ is maintained equal to or slightly greater than $V_{r\text{-}f}$. With this modification, the peak inverse voltages observed with rectifiers not power-treated are always greater

[1] L. L. Boyarsky, R. N. Smith, and H. J. Yearian, "Properties of Germanium High Back Voltage Rectifier Units," NDRC 14-413, Purdue Univ., Mar. 19, 1945.

than those observed when forward current is observed, and sometimes greater than the d-c peak.

These effects are not observed with germanium rectifiers that have been subjected to the power treatment described in Sec. 12·3. The power-treated units exhibit substantially the same peak inverse voltage at 30 Mc/sec as the d-c value.

The Crystal I-f Impedance at 30 *Mc/sec*—In the application of crystal rectifiers as second detectors, the i-f impedance of the crystal is of importance because of the loading of the amplifier stage which is connected to the detector circuit. The lower the i-f impedance of the detector circuit, the less will be the i-f voltage across it, because of the effect of the internal impedance of the i-f source.

Test equipment has been designed by Smith and Yearian[1] for measuring second-detector properties, including the impedance at 30 Mc/sec. In this method the crystal in series with a condenser is connected to a high-Q sinusoidal source of r-f voltage of about 600 ohms internal resistance, as shown in Fig. 12·14. No load resistor is used. The applied voltage is measured by an r-f voltmeter. The crystal impedance is measured by comparing the decrease in voltage from the open circuit value with the crystal in the circuit to that with a carbon resistor in the circuit.

In general, the i-f impedance measured by the method just described decreases as the measuring voltage is increased, but the way in which the impedance changes as the applied voltage is increased varies widely from crystal to crystal. For a peak applied voltage of 10 volts, the i-f impedance of a representative sample of germanium rectifiers ranged from about 1000 ohms to more that 18,000 ohms, the limit of the measuring equipment. Measurements made at Bell Telephone Laboratories on high-back resistance rectifiers gave values all above the range of the measuring equipment—namely, 18,000 ohms.

The i-f impedance depends on the d-c back resistance of the rectifier, but it is difficult to correlate these quantities quantitatively with measured values of the back resistance because of the nonlinearity of the back characteristic. If a perfect diode (that is, one for which the forward conductance and back resistance are infinite) is assumed, it can readily be shown[2] that the i-f resistance is one-half the load resistance connected to the terminals of the condenser. By means of a Fourier analysis, Yearian[3] has calculated the i-f resistance for various idealized characteristic curves. For example, assuming no load resistor, infinite forward

[1] R. N. Smith and H. J. Yearian, "Test Equipment for Germanium Second Detector Units,' NDRC 14-394, Purdue Univ., Jan. 25, 1945.

[2] See *Microwave Receivers*, Vol. 23, Sec. 7·1, Radiation Laboratory Series.

[3] *Loc. cit.*

conductance, and constant back resistance, the i-f resistance is one-third the back resistance. With finite forward conductance the expression for the i-f resistance becomes, to a close approximation,

$$R = \frac{1}{2\eta + 1} R_b, \tag{2}$$

where R_b is the constant back resistance and η is the rectification efficiency, which in this case will be very nearly equal to unity. As we have seen, the actual crystal rectifier is ordinarily far from linear in the back direction and varies greatly from crystal to crystal. Yearian concludes from his analysis that where the back characteristic has a very rapid

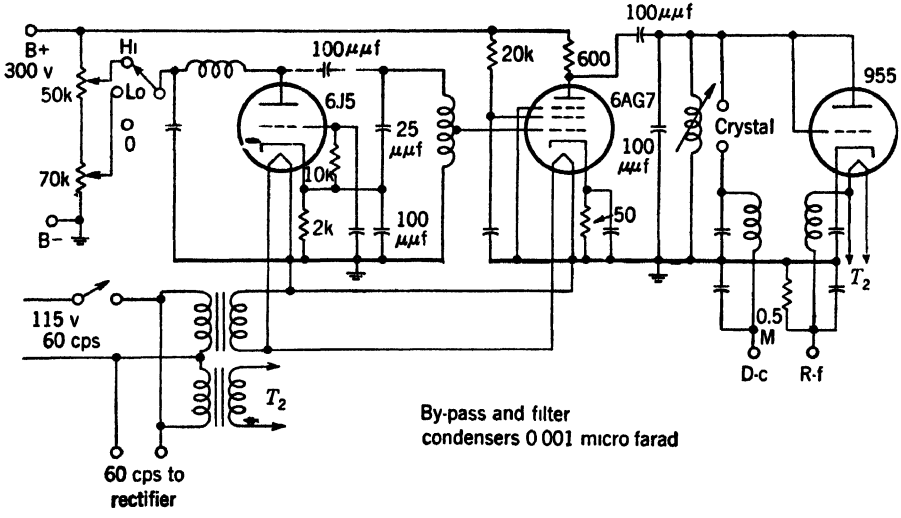

FIG. 12·15.—Impedance tester for measuring the impedance of crystal second detectors at 30 Mc/sec.

increase, or "tail,"—as, for example, the region where the peak inverse voltage is approached—the i-f resistance may be as low as one-eighth of the average back resistance obtained by taking the time average over the i-f cycle of the conductance in the back direction.

Figure 12·15 shows the circuit details for an impedance tester designed by the Purdue group for routine testing of i-f impedance at 30 Mc/sec. The detector circuit is the same as that shown in Fig. 12·14. A 6J5 oscillator drives the 6AG7, which supplies the sinusoidal 30-Mc/sec voltage across the 600-ohm resistor. This voltage is measured by a vacuum-tube voltmeter employing a 955 tube, with a high-impedance d-c meter to measure its output. Standard voltages are chosen as 20 and 10 volts peak with no crystal in place; these are adjusted by the HI and LO controls. The equipment is calibrated by means of standard carbon resistors ranging from 20,000 to 500 ohms. The output inductance on the 6AG7

tube is adjusted on open circuit to maximize the output and should be checked periodically, in consequence of the fairly high Q of the circuit.

Second-detector Performance.—In order to investigate the behavior of germanium crystals as second detectors two types of testing equipment have been used.[1] The first of these is designed to simulate the conditions of operation that would be encountered in the second detector of an actual wideband receiver. The second set was designed for measuring the rectification efficiency of a wideband detector circuit.

The output stage and detector circuit used in the set for measuring over-all performance are shown in Fig. 12·16. It consists of a 30-Mc/sec wideband output stage employing an 807 tube and having a voltage amplification with the detector removed of about 5.2. A load resistor of 1000 ohms and a bypass condenser of 10 $\mu\mu$f is used, which gives a time constant of 0.01 μsec. The inductance is tuned to resonate with the total capacity to ground at a frequency of 30 Mc/sec.

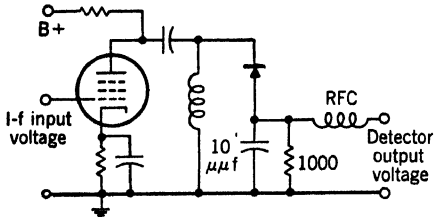

FIG. 12·16.—Wideband i-f output and second detector circuit for measuring over-all detector performance.

The behavior of representative germanium rectifiers in this circuit is shown in Fig. 12·17, where the rectified output voltage $V_{d\text{-}c}$ is plotted as a function of the peak voltage applied to the grid of the tube. Two properties exhibited by the curves are of interest, namely, the sensitivity, or slope of the curve, and the range of linearity, which is defined by the upper and lower limit of applied i-f voltage beyond which the sensitivity decreases below a useful value. It is seen from the curves that the slope is nearly constant over a range from about 0.5 to 5 volts, depending on the crystal. At higher voltages the sensitivity decreases because the back resistance becomes low enough to decrease the efficiency of rectification and at low voltages the forward resistance becomes comparable to the load resistance, which also decreases the rectification efficiency.

The maximum slope is obtained by measurements at medium input grid voltages (about 3 volts). At this level the rectification efficiency of the best crystals approaches that of a perfect diode, since the back resistances are very high at this voltage and the peak voltage in the forward direction is high enough to be in the region of very low forward resistance. Measurements made on a large number of units established maximum slope of 1.2 for the circuit of Fig. 12·16.

[1] L. L. Boyarsky, R. N. Smith, and H. J. Yearian, "Properties of Germanium High Back Voltage Rectifier Units," NDRC 14-413, Purdue Univ., Mar. 19, 1945; and R. N. Smith and H. J. Yearian, "Test Equipment for Germanium Second Detector Units," NDRC 14-394, Purdue Univ., Jan. 25, 1945.

In defining the range of linearity, a standard allowable variation in sensitivity has been arbitrarily chosen to be a factor of 2, the maximum sensitivity being taken as the maximum slope (in this case, 1·2), and the minimum sensitivity being one-half this value. Using this criterion, values of 0.1 and 10.0 peak volts applied to the grid have been established by measurements on a large number of rectifiers as an approximate average of the upper and lower limits of the range of linearity. Once these

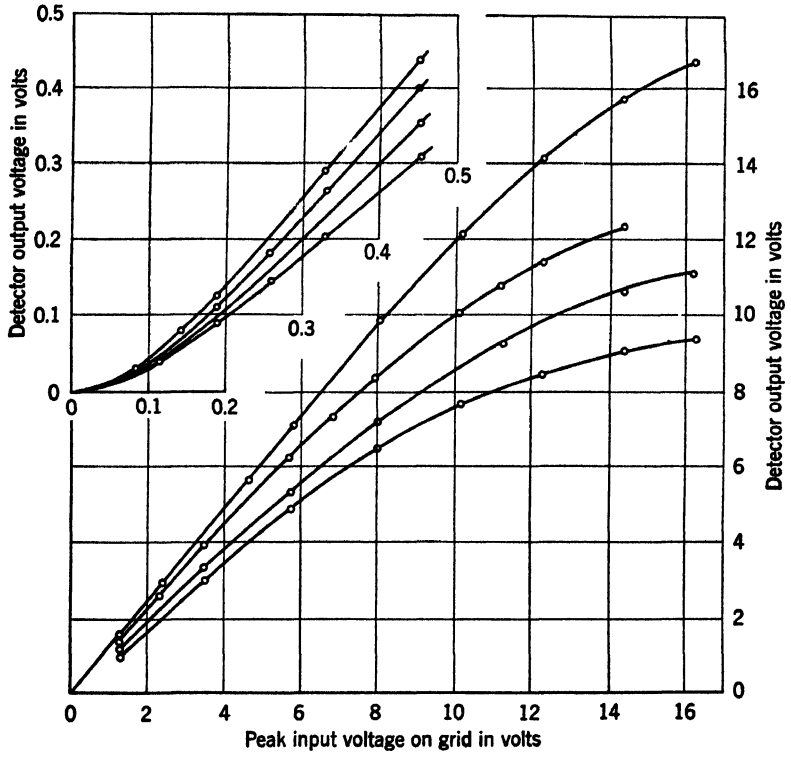

FIG. 12·17.—Detector output voltage for a sample of germanium rectifiers in the circuit of Fig. 12·16.

levels are established, a measurement of the slope at these two levels gives an indication of the performance as a second detector. If the slope exceeds one-half the maximum sensitivity, then the range of linearity will be greater than the standard range, and the sensitivity of the unit will be greater than this half-value throughout the standard range. The sensitivity at the high and low levels can be measured by modulating the 30-Mc/sec carrier at a low frequency, let us say, 60 cps, and measuring the detector output at the modulation frequency.

Figure 12·18 shows the circuit details of the Type B test set designed by the Purdue University group for the routine testing of over-all performance, as outlined in the preceding paragraphs. It was designed

for the purpose of establishing standard levels at which to make measurements and to establish standards of performance at these levels; the tentative specifications listed in Table D-3 of Appendix D are written for this equipment. The set consists of a 6J5 30-Mc/sec oscillator followed by a 6AG7, which decouples the oscillator from the following output stage and provides a variable attenuation for the low-level measurement and a 60-cps modulation for the sensitivity measurement. The output stage and rectifier circuit is that of Fig. 12·16.

The 955 tube serves as an r-f voltmeter which is used to set the output voltage at standard values of HI and LO of 24.7 volts and 0.5 volt respec-

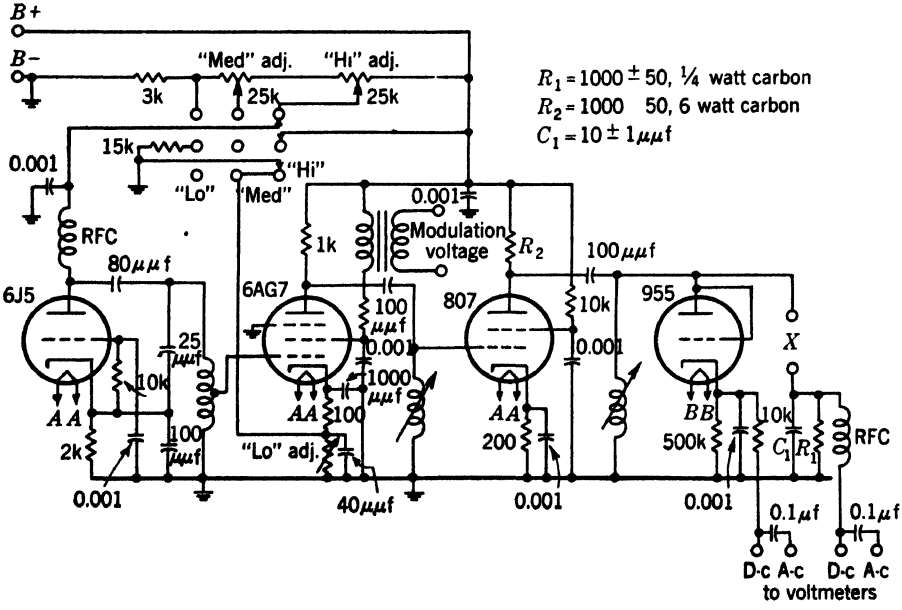

FIG. 12·18.—Type B test set for measuring over-all performance of crystal second detectors for an intermediate frequency of 30 Mc/sec.

tively, corresponding to the limits of 10 volts and 0.1 volt previously established for the peak voltages applied to the grid of the output stage. Provision is also made for measurements at a medium voltage of 7.2 volts. The r-f voltmeter does not read the true 30-Mc/sec voltage with a crystal in the detector circuit because of the distortion introduced by the crystal. The levels are therefore set with a 600-ohm carbon resistor in the crystal holder. The 955 tube with a load of 500,000 ohms serves also for measuring the amount of modulation. With a 500,000-ohm load the time constant is short enough so as not to attenuate the 60-cps rectified modulation. The modulation voltage is standardized at 0.92 peak volt for a reading of 24.7 volts at 30 Mc/sec. For the measurement of these voltages high-impedance a-c and d-c voltmeters are connected to the

appropriate output terminals of the 955 detector circuit. The same meters are switched to the crystal output terminals for the test measurements. The variable inductance in the output circuit of the 807 is tuned to give maximum output voltage with a 600-ohm resistor in the crystal holder. This corresponds closely to the adjustment for maximum output with a good germanium detector in place.

The modulation method is satisfactory for measuring sensitivity at high and medium levels but is impractical at low level. At low level, experiments show good correlation between sensitivity and d-c output voltage for a given type of rectifier; at the standard low-level input, 35 mv d-c output corresponds to a slope of about one-half the maximum value at medium levels. To calibrate the output of the 807 for the low-level test, standard crystals are used which have been checked against primary standards maintained at the standards laboratory; the 955 voltmeter is inadequate at this voltage level. The crystal output voltage is measured with a 20,000-ohm millivoltmeter.

Measurements have been made at Purdue University[1] on representative samples of power-treated units having very high back resistances; these units had been made at Purdue and at the Bell Telephone Laboratories. With the high-level 30-Mc/sec input (24.7 volts) the d-c output voltages average about 10 volts, with variations of not more than a volt or so from crystal to crystal. The 60-cps modulation output voltage varies from about 0.3 to 0.4 volt. With the low-level 30-Mc/sec input voltage, the d-c output voltage is more than 40 mv for the Bell Telephone Laboratories units and somewhat lower for the Purdue units. A comparison of these results with those for rectifiers that have not been subjected to power treatment shows that the power treatment causes an increase in the high-level output voltage of the detector, especially in the a-c output voltage where the increase is by a factor of about two. This fact implies that the range of linearity of the response has been extended to considerably higher input levels by the power treatment. At low level the Bell Telephone Laboratories power treatment also causes a significant increase in the a-c output voltage, but the somewhat more drastic power treatment used in manufacturing the Purdue crystals causes a small decrease of sensitivity at this level. Results obtained with a sample of germanium crystals made by Sylvania Electrical Products Company are comparable to those obtained for the Purdue heat-treated units.

It is evident from these results that the power treatment, which improves the d-c properties, also improves second-detector performance.

[1] L. Boyarsky, P. B. Picker, A. W. McDonald, R. N. Smith, R. M. Whaley, and H. J. Yearian, "Production and Performance of Germanium High Back Voltage, High Back Resistance Crystal Rectifiers," NDRC 14-577, Purdue Univ., Oct. 31, 1945.

Experiments have been performed by Boyarsky and Smith[1] on the effect of bias and detector load on over-all performance, using a set similar to the Type B set but modified so that positive d-c bias could be applied to the crystal detector. With a detector load of 1000 ohms, an optimum bias of about 0.12 volt decreases the lower limit of linearity from about 0.1 volt on the grid of the input stage to about 0.07 volt; for a larger detector load resistance the effect was smaller.

Without bias, the effect of increasing load resistance is to increase both the sensitivity and range of linearity, as would be expected.

Rectification Efficiency.—For routine testing of second-detector crystals the system of measurements just described for the Type B test set is

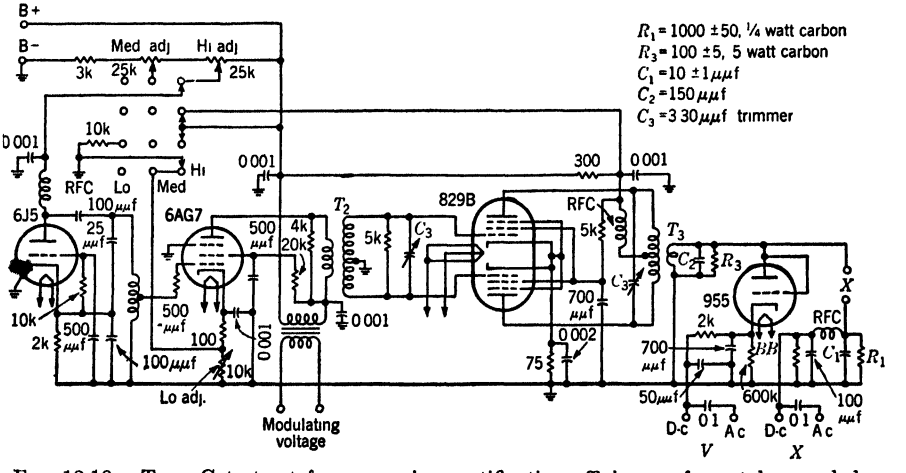

FIG. 12·19.—Type C test set for measuring rectification efficiency of crystal second detectors.

undesirable because it measures over-all performance in a particular kind of a set. Since rectification efficiency is the predominant factor controlling performance in a wideband second-detector circuit, it is preferable to use a test set for measuring this quantity for acceptance testing. Rectification efficiency is defined as the ratio of the d-c output voltage to the peak value of the sinusoidal input voltage. The modulation rectification efficiency, corresponding to the sensitivity measurement of the Type B test set, is defined as the ratio of the rectifier output voltage at the modulation frequency to the peak value of the input modulation voltage. The detailed circuit diagram of the Type C test set designed by the Purdue group[2] for measuring these quantities is shown in Fig. 12·19.

[1] L. L. Boyarsky and R. N. Smith, "Dependence of Performance of Germanium Second Detector Units on Bias and Video Load," NDRC 14-416, Purdue Univ., Mar. 28, 1945.

[2] *Loc. cit.*

The 6J5 and 6AG7 tubes serve the same purpose as in the Type B test set. A push-pull amplifier employing an 829B tube delivers 30-volt peak sinusoidal voltage at a frequency of 30 Mc/sec to the 100-ohm load R_3. The transformers T_2 and T_3 are critically coupled, tuned-primary and tuned-secondary transformers. The internal impedance of the r-f source across R_3 is 50 ohms. The detector output circuit consists of a 10-$\mu\mu$f condenser and a 1000-ohm load resistor as in the previously described set. The 955 r-f voltmeter is the same as that in the Type B test set except that a load resistor of 600,000 ohms is used instead of one of 500,000 ohms.

For high-level measurements, the HI control is adjusted for a reading of 29·1 volts on the d-c meter of the r-f voltmeter, with a 750-ohm carbon resistor in the crystal holder. The 60-cps modulation voltage is adjusted for a reading of 0.50 volt on a high-impedance a-c meter connected to the a-c terminals of the r-f voltmeter The carbon resistor is now replaced by the crystal to be tested and the a-c and d-c voltmeters switched to the "X" terminals The d-c output voltage divided by 29·1 gives the rectification efficiency and the a-c output voltage multiplied by 2 gives the modulation rectification efficiency.

The r-f peak voltage for "medium level" is standardized at 9.0 volts, and the low level is set by means of standard crystals as in the Type B test set.

The theoretical maximum value for the modulation rectification efficiency is about 41 per cent for both the high and medium levels; the value corresponding to one-half maximum sensitivity in the over-all measurement is about 25 per cent. A value of 35 mv for the low-level output voltage corresponds to about one-half maximum sensitivity.

12·6. Silicon High-inverse-voltage Rectifiers.—Following the discovery of the high-inverse-voltage property in appropriately doped germanium an exploratory investigation was carried out on silicon by the crystal group at the University of Pennsylvania.[1]

Ingots were prepared from high-purity du Pont silicon, to which were added small known amounts of various impurities. The ingots were made in a vacuum furnace in quartz crucibles. As in the case of mixer crystals, the addition of 0.02 per cent of beryllium insured a solid ingot free from cracks. The beryllium did not appear to have much effect on the electrical properties of the silicon.

The preparation of the surface was similar to that used for silicon mixer crystals. The ingot is sawed into wafers about 1 mm thick. One side is nickel-plated for soldering to the cartridge stud, and the other side is first wet-ground with 600 carborundum, then polished to a high gloss on 0000 emery paper wet with kerosene. It is then heat-treated in air

[1] M. N. Lewis, J. H. Taylor, R. J. Gibson, Jr., and W. E. Stephens, "High Back Voltage Silicon," NDRC 14-453, Univ. of Penn., June 28, 1945.

at 1050°C for about two hours. The wafer is then broken into small pieces, which are soldered to the cartridge studs. Just before assembly the polished oxidized surface is washed in 24 per cent hydrofluoric acid until the oxide is dissolved off. Omission of the polishing or heat treatment was found to yield inferior rectifiers. The whiskers were made of tungsten and were of conventional design. For high peak back voltage and low forward currents the contact force is made as small as is consistant with stability. Increasing the load increases the forward current but decreases the peak back voltage. In none of the samples tested have both high back voltage and high forward conductance, comparable with the germanium rectifiers, been simultaneously attained.

TABLE 12·1.—RECTIFICATION CHARACTERISTICS OF SOME SAMPLES OF HIGH-INVERSE-VOLTAGE SILICON RECTIFIERS

Doping agent	Amount added, per cent	Beryllium added, per cent	Typical performance		
			Peak back voltages, volts	Back resistance at 15 v, ohms	Forward current at 1 v, ma
Nickel	0.16	0.02	45	30×10^3	2
Nickel	0.6	0.02	40	10	5
Tin	0.4	0.02	60	10	0.05
Germanium	0.5	0.02	60	10	0.25
Germanium	0.75	0.02	40	5	1
Germanium	1.0	0.02	30	2	2
Germanium and nickel	0.3, 0.06	0.02	70	100	0.2
Bismuth	0.02	0.02	40	3	1
Calcium hydroxide	0.1	0.01	80	50	0.1
Aluminum	0.006	0.02	5	...	10
None	.....	0.02	90	30	0.1

Table 12·1 lists the peak back voltage, the back resistance at 15 volts, and forward current, obtained using typical units made with silicon containing various impurities. It is to be noted that tin, nickel, calcium, and bismuth, which are good doping agents for germanium, also produce the high-back-voltage property in silicon. Also, like germanium, the impurities that produce good mixer crystals are inferior for producing the high-back-voltage property. High peak back voltages are observed with pure silicon, but the forward conductance is very low. A typical d-c characteristic curve of a silicon high-inverse-voltage rectifier is shown in Fig. 12·20.

Voltages much greater than the peak back voltage, or sometimes slightly less than that value, may burn out the crystal; if burnout does

not occur, the application of the peak back voltage tends to reduce hysteresis effects. In general, the high-back-voltage silicon made by the Pennsylvania group is not comparable with germanium in ability to withstand power dissipation.

Tests made of the second-detector properties of a typical group of rectifiers showed that they will pass all the requirements of the tentative specifications listed in Appendix D, except the low-level rectification; however, they are also inferior to the germanium rectifier in high-level rectification and sensitivity. It must be remembered, however, that much less work has been done on high-back-voltage silicon than on germanium and it is possible that a comparable amount of research on silicon may alter this situation.

For the high-back-voltage silicon rectifiers, measurements were made of the rectified current as a function of frequency, similar to the experiments on germanium. In these experiments the short-circuited rectified current was measured for 1 volt rms applied to the crystal at frequencies

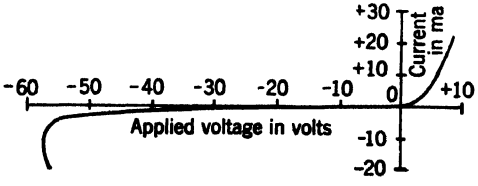

FIG. 12·20.—Typical characteristic curve of a silicon high-inverse-voltage rectifier.

of 60 cps and 30 Mc/sec. The rectified currents for the samples tested were relatively small, ranging from 0.1 to 0.7 ma, but the decrease in rectified current over the frequency range from 60 cps to 30 Mc/sec was less than 10 per cent. It can be seen, by reference to Fig. 12·11, that the high-back-voltage silicon units are much less frequency-sensitive than the germanium rectifiers.

12·7. Theory of the Negative-resistance Characteristics.—There is as yet no satisfactory theory of the high inverse voltages and negative-resistance characteristics displayed by the crystals discussed in this chapter.

A theory has been developed by Benzer[1] that attempts to account for the existence of voltage peaks and negative resistance on the basis of the onset of intrinsic conduction at the high contact temperatures that must exist at the peak voltage and in the negative-resistance part of the characteristic. Although there is little doubt that temperature effects are responsible and that intrinsic conduction has a bearing on the prob-

[1] S. Benzer, "The High Voltage Germanium Rectifier," NDRC 14-375, Purdue Univ., Dec. 26, 1944.

lem, it can be shown that Benzer's theory is inadequate because of the incompatibility of his postulates. A more precise analysis, made by H. C. Torrey,[1] reveals that voltage peaks cannot possibly exist (in the forward direction, at least) if the thermal conduction of the whisker is neglected, as it is in Benzer's theory. This neglect seems very plausible, however, in the case where thermal equilibrium is established after a few seconds of continuous current flow.

Some numerical calculations by Goodman[2] indicate that a voltage peak may perhaps occur if the thermal resistance of the whisker is taken into account, but more work needs to be done before the theory can be considered adequate.

Perhaps the most puzzling question is how it is possible for the barrier to withstand the enormous field intensities that must exist at peak voltages of 100 volts or more. Breakdown by barrier-lowering arising from image forces and tunnel effects would be expected for a barrier of normal thickness (10^{-6} or 10^{-5} cm) at only a few inverse volts. W. E. Stephens[3] has postulated a barrier as thick as 10^{-4} cm for the high-inverse-voltage rectifiers, but it is difficult to see how such a thick barrier could be formed.

12·8. Photoelectric Effects in Silicon and Germanium.—In the course of research on crystal rectifiers interesting photoeffects were observed in both silicon and germanium. These effects are related to the rectifying characteristics of the semiconductor and will undoubtedly contribute to the understanding of semiconduction. In addition they hold promise for practical photoelectric applications.

Photoelectric Effects in Silicon.—The photoconductivity of pure du Pont silicon was observed at the Radiation Laboratory by M. Fox and C. S. Pearsall[4] during the development work on mixer crystals reported in Chap. 10. A detailed investigation of the effect was not made at that time, however. More recently Miller and Greenblatt[5] have reported an exploratory investigation of photoeffects in pure silicon. The samples investigated were pure du Pont silicon needles or melts made from these needles. Both photoconductive and photovoltaic effects were observed. Samples were plated, soldered onto a mount, and a point contact made with a tungsten whisker. Whiskers of molybdenum and platinum were also used, but the whisker material was found to have little influence on the character of the photoeffect.

[1] Unpublished data.

[2] Private communication from B. Goodman.

[3] Unpublished data.

[4] Unpublished data.

[5] P. H. Miller, Jr. and M. H. Greenblatt, "Photoeffects in Pure Silicon," NDRC 14-412, Univ. of Penn., Mar. 20, 1945.

In the photoconductive effect the change in current upon illumination of the contact area was investigated as a function of wavelength and intensity of illumination. Most of the samples investigated were p-type material, and the largest photoconductive effects were observed with the point positive. In the spectral-distribution curve, the maximum response occurs at a wavelength of about 1.5 μ, with an apparent threshold at about 2.1 μ. The wavelength at which the maximum occurs is independent of the silicon, the point material, and the bias voltage, but the change in current upon illumination increases as the bias voltage is increased.

Occasional time-dependent effects were observed. After the initial increase in current when the light is turned on, the current may continue to increase for several seconds. When the light is turned off, there is a sudden decrease, which may be followed by a gradual falling-off in the current. Such effects are difficult to duplicate and are usually found with mechanically unstable contacts.

No change in current as large as 0.5 per cent was observed with doped materials, although in pure materials a change in conductivity as large as a factor of 10 was observed. Only the region in the neighborhood of the point contact was photoconductive.

The increase in current produced by an increase of intensity of illumination was investigated, an incandescent lamp being used as a light source. For low intensities the increase in current is approximately proportional to the light intensity; as the illumination is further increased, the current increase is less rapid than linear.

The investigation of the photovoltaic effect in silicon showed that the region as far as several millimeters from the point contact can be the photosensitive element. The shape of the spectral-distribution curves are similar to those obtained in the photoconductive effect, with a maximum at the same wavelength. The current is usually in the direction of high resistance, although occasionally currents in the opposite direction are found. In a typical sample with zero bias a current of 0.16 μa was observed for an illumination of 1.2×10^{-2} watts/cm^2 at a wavelength of 1.5 μ, the maximum of the spectral-distribution curve. The silicon, when illuminated, acts as a cell having constant internal resistance and an emf that depends upon the wavelength and intensity of illumination. The internal resistance appears to be roughly three times the spreading resistance.

All the experiments described in the preceding paragraphs were on untreated surfaces of crystals. Photoeffects are still observed on polished surfaces but appear to be so complicated and difficult to reproduce that they have not as yet been studied in detail.

Photoelectric Effects in Germanium.—Photoeffects in germanium high-

back-voltage rectifiers were first observed by P. R. Bell at the Radiation Laboratory and led to a detailed study by Benzer[1] of photoeffects in germanium; these studies are summarized in the following paragraphs.

Photoeffects are commonly found in high-resistivity germanium and occur most frequently in the boundary region separating p-type and

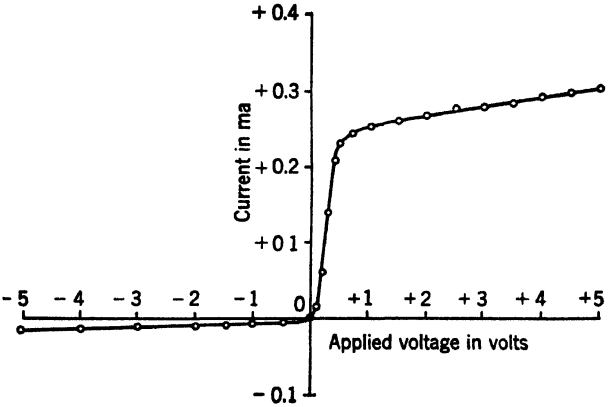

FIG. 12·21.—D-c characteristic of a germanium "photodiode" crystal at 25°C, no illumination.

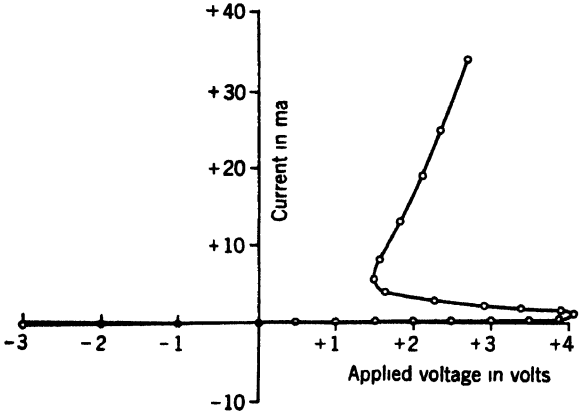

FIG. 12·22.—D-c characteristic of a germanium "photopeak" crystal at 25°C, no illumination.

n-type germanium. The photosensitivity is associated with two unusual types of current-voltage characteristic or a combination of these two types. The first type, illustrated in Fig. 12·21, shows a saturation effect in the forward current; it has been given the descriptive name of "photodiode." The second type, shown in Fig. 12·22, exhibits a voltage peak followed by a negative-resistance region, which becomes positive at larger

[1] S. Benzer, "The High Back Voltage Germanium Rectifier," NDRC 14-342, Purdue Univ., Nov. 1, 1944; and "Photoelectric Effects in Germanium," NDRC 14-580, Purdue Univ., Oct. 31, 1945.

currents. With illumination the peak voltage decreases and may be reduced to practically zero if the illumination is sufficiently intense. This type has been given the name "photopeak."

Figure 12·23 shows the effect of various intensities of white light upon the forward characteristic of a photodiode. The back characteristic is little affected. The effect is reversible and occurs for flashes as short as 10^{-5} sec. It can be seen from Fig. 12·23 that the photocurrent is almost independent of the voltage applied to the rectifying contact in the saturation region. The photocurrent is also proportional to the intensity of illumination over a wide range. For a good photodiode this linear response extends up to illuminations of 1 or 2 lumens/cm^2. Spectral-distribution curves show a maximum response at a wavelength of about 1.3 μ, with a threshold of about 1.6 μ. The number of photoelectrons per incident quantum at the maximum is about 0.9.

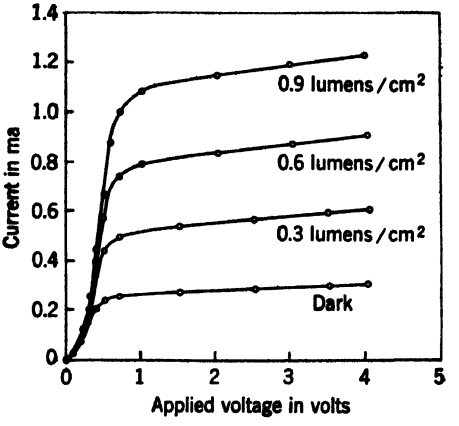

FIG. 12·23.—Effect of white-light illumination on photodiode characteristic.

Photodiode points are also photovoltaic. A given crystal generates an emf proportional to the intensity of illumination, with an internal resistance equal to the slope of the characteristic curve at the origin. This resistance is, in general, large but, by increasing the contact area it may be greatly reduced without affecting the photoelectric properties. The polarity is such that the whisker becomes negative. The spectral-distribution curve is the same as that for the photoconductive effect.

The saturation current of a photodiode is extremely sensitive to temperature. At room temperature a change of 10°C changes the saturation current by a factor of 2.

These photodiode characteristics occur in regions that may be several square millimeters in area. Such a region may be made visible by etching the surface electrolytically. All points within a given region have remarkably similar characteristics. Within this region, a change in whisker force produces large changes in back resistance while the forward saturation current is almost unaffected. When voltage is applied in the saturation direction, a large potential drop is found across the boundaries of the region. With the applied voltage in the back direction, however, the drop across the boundary is much less. These effects are interpreted by Benzer to mean that the photodiode effect is caused by a large barrier

surrounding the sensitive surface element, thus limiting the forward current for any point contact made within the region. The barrier must be a rectifying one, since the back current, with large whisker forces, far exceeds the saturation current.

Benzer found that, if a small spot of light is moved along a line intersecting the sensitive region, the photocurrent rises rapidly to a maximum at the boundary of the sensitive region, then passes through a shallow minimum as the region is traversed. He interprets this result to mean that the barrier, even in the center of the region, lies very close to the surface.

The "photopeak" type of characteristic was reported by Woodyard,[1] who used the negative-resistance region to produce oscillations up to frequencies as high as 1 Mc/sec. Benzer reports[2] that photopeak characteristics with peak voltage as high as 25 volts have been observed, although peaks are usually found at 1 or 2 volts. The current at the peak is usually of the order of 1 ma. At currents well above 1 ma and above the negative-characteristic region, the characteristic is determined by the spreading resistance. For very high-resistivity material, the spreading resistance may be so large that the photopeak appears only as a kink in the characteristic.

Photopeaks are usually found in border regions between p-type and n-type material, but the photopeak region usually has a linear dimension of only a fraction of a millimeter. Unlike the photodiode, the photopeak may vary greatly from one point to another, and it is very sensitive to whisker pressure; the peak voltage decreases as the whisker load is increased.

It has already been mentioned that the peak voltage decreases with illumination. At low intensities of illumination the decrease in peak voltage is proportional to intensity. Sensitivity varies greatly from one unit to another; an illumination of 0.5 lumen/cm^2 is sufficient to remove completely the peak of a sensitive unit, whereas an insensitive one may show little response. Exploration with a small spot of light shows that only light that falls in the immediate region of the point is effective.

A photo response may be obtained for light flashes as short as 10^{-5} sec. The spectral-distribution curve has not been studied in detail, but preliminary experiments indicate that it is similar to that of the photodiode.

The photopeak rectifier has a possible application as a triggering device. If it is biased positively just below the peak voltage, illumination will cause the peak to decrease so that the current jumps to a value

[1] J. R. Woodyard, "Notes on Crystal Detectors," Sperry Research Laboratories Report 5220-110, Apr. 6, 1943.

[2] S. Benzer, "The High Back Voltage Germanium Rectifier," NDRC 14-342, Purdue Univ., Nov. 1, 1944.

limited by the spreading and circuit resistances, a current large enough to actuate a relay. Since the crystal rectifies, an a-c bias can be used; the device then is automatically restored to operating condition when the light is removed.

Like the photodiode, the photopeak is temperature-sensitive, the peak voltage decreasing with increasing temperature. Raising the temperature from 24° to 50°C will, in general, reduce the peak voltage by a factor of about two. Photopeak crystals are not as rugged as photodiode crystals and may be burned out by the passage of too much current through the contact.

The photoeffect mentioned earlier as observed in some high-inverse-voltage germanium rectifiers is of a different nature from those just described. In this effect, illumination causes changes in current at a given applied voltage, as well as a photovoltaic effect when there is no applied voltage. At high back voltage, time lags occur in the responses, and the current during illumination may be less than that in the dark.

In addition to these effects, many interesting combinations of the types just discussed have been observed. Further research work on these effects will undoubtedly shed further light on the theory of semiconduction and the nature of the high-back-voltage phenomenon. On the practical side, the photopeak and photodiode crystals offer excellent prospects for the development of photoelectric cells using these materials.

CHAPTER 13

WELDED-CONTACT GERMANIUM CRYSTALS

It has long been supposed that a simple contact rectifier used as a frequency converter must always have a conversion loss greater than unity, or, in other words, that the available output (i-f) power must always be less than the available input (signal) power. This specious conjecture has no convincing theoretical argument in its favor, however. North, of the General Electric Company, has recently demonstrated[1] that the conjecture is, in fact, false. North has constructed germanium rectifiers with welded contacts that have the remarkable property (under certain bias and r-f tuning conditions) of delivering more power at intermediate frequency than is available from the signal source. Energy conservation is of course not violated since the local oscillator supplies the extra power.

It has been shown that this amplifying ability of North's crystals is associated (although not necessarily concomitant) with the phenomenon of negative i-f conductance which they sometimes exhibit. There is convincing evidence that negative i-f conductance is a result of two factors: (1) the variability of contact capacitance with voltage (a property also of normal rectifiers) and (2) the abnormally low spreading resistance.

Unfortunately, measurements have shown that, because of the great amount of i-f noise power they generate, these remarkable crystals are, when judged by over-all receiver noise figure, inferior to standard types in spite of their amplifying properties. The crystals can be used in such a manner, however, that their i-f conductance is positive. In this condition they behave as normal crystals; their loss, although small, is greater than one and their noise is not excessively large. Used in this way they are comparable to the best of the standard converter types. They are superior to all standard types as *harmonic generators*, especially as generators of millimeter radiation.

13·1. Construction of Welded-contact Rectifiers. *History.*—Welded rectifying contacts appear to have been made first by the Purdue University group,[2] who found that passage of enough forward current through a contact from germanium to platinum-iridium to make the whisker white-hot resulted in a firm bond between whisker and germanium. The

[1] H. Q. North *et al.*, "Welded Germanium Crystals," GE Final Report—Contract OEMsr-262-Order No. DIC178554, Sept. 20, 1945.

[2] Progress Report, Purdue Univ. Contract OEMsr—322, Oct. 26, 1942.

welded contact continued to rectify and was more stable against overloads than an unwelded unit. Measurements showed, however, that microwave performance had deteriorated as a result of the welding. Not much more was done with welded contacts at Purdue.

Later, North,[1] in an attempt to reduce crystal noise temperature, succeeded in welding germanium to platinum contacts with condenser discharges. The conversion loss of the rectifiers suffered in this process and the work was dropped.

The new welded units, unique in the remarkable properties already mentioned and exceptional in other respects, are made by passing large continuous forward currents (about 0.25 amp) through contacts of small dimensions from germanium to platinum-ruthenium.

Techniques.—The techniques of construction are similar to those of North's version of the 1N26 rectifier as described in Sec. 10·3. The only essential difference, in fact, is in the welding process. Pure germanium is fused with 0.2 atomic per cent of antimony. The solidified ingot is cut into wafers about 0.03 in. thick, which are plated on one face with rhodium and then sawed to size for the cartridge. This plated face is soldered to a silver plug and the opposite face is ground and polished to a bright finish, first with 600-mesh alundum on cloth and finally with magnesia on cloth. Faint traces of magnesia are removed with dilute HCl. No etch is used in any part of the process.

The 1N26 structure of Fig. 10·14 is retained. The whisker is a 0.0015-in.-diameter platinum-ruthenium alloy (10 per cent ruthenium). The ruthenium is used solely to lend mechanical strength to the whisker. The whisker tip is carefully pointed to a point radius of less than 0.00002 in. The silver plug holding the germanium is pressed into the cartridge and advanced until electrical contact is just made. It is then further advanced to produce enough spring deflection to give a force on the contact of 150 mg. At this point 250 ma of direct current are passed through the contact in the forward direction for 5 to 10 sec. This treatment results in a secure weld.

Antimony appears to be the only doping agent (of those usable for microwave rectifiers) that will withstand the welding currents. Phosphorus and arsenic, ordinarily good doping agents for germanium microwave rectifiers, are not suitable for welded-contact rectifiers.

Properties of the Weld.—The weld appears to be secure, requiring a tensile force of 500 mg to break it. Microscopic examination of a broken weld reveals that the whisker point penetrates the germanium surface and that the resulting contact is roughly hemispherical in shape with a diameter of about 0.0002 in. The welding current density at the contact

[1] H. Q. North, "Colloquium on Crystal Rectifiers," Columbia Univ., May 1, 1943.

is thus about 7×10^6 amp/in.^{2} The tensile stress sustained by the weld is about 35,000 lb/in.^{2} Once the weld is formed, no change in the d-c characteristic is observed between the unstressed state of the contact and a compressed state of 30,000 lb/in.^{2} A tensile stress of this magnitude, however, causes a marked decrease in back resistance at 1 volt.

13·2. General Properties.—The welded unit is mechanically extremely stable. It may be dropped from heights of 6 ft or more on a linoleum floor with no adverse effects. Since the contact has been treated with 250 ma of direct current in process of manufacture, subsequent current overloads of this magnitude in the forward direction do not cause burnout. When 10 units were tested for short-pulse burnout with the d-c spike tester (Sec. 9·8), 6 were unchanged in noise temperature after 5-erg pulses and 6 were unchanged in conversion loss after 10-erg pulses. These results may be too optimistic, however, because it is possible that these units were not well matched to the coaxial line of the spike tester.

Typical forward d-c characteristics of these rectifiers are shown in Curve B of Fig. 2·6 and in Fig. 2·7. The forward current-voltage characteristic is remarkable in that it is accurately exponential over nearly five decades on a logarithmic current scale; the derivative $d(ln\ I)/dV$ is abnormally large, generally in the range from 25 to 30 volt^{-1}. According to the theory of Sec. 4·4 this exponential property of the forward characteristic would indicate that the contact has a nearly uniform contact potential difference. Further evidence that this is the case is obtained from a study of the reverse characteristic, which is also exponential up to about 0.5 volt. According to Eq. (4·41), the current-voltage characteristic of a contact of uniform contact potential difference should be given by

$$i = A(e^{\beta \frac{e}{kT} V} - e^{-(1-\beta)\frac{e}{kT} V}), \tag{1}$$

where β is a parameter determined by the amount of barrier lowering brought about by image force and tunnel effect. In the forward direction, Eq. (1) gives approximately

$$i = Ae^{\beta \frac{e}{kT} V}, \tag{2}$$

and in the reverse direction,

$$|i| = Ae^{(1-\beta)\frac{e}{kT}|V|}. \tag{3}$$

From Eqs. (2) and (3) it follows that the sum of the exponential coefficients of V in the two directions should be e/kT. This was, in fact, observed to be the case within experimental error for one welded unit measured at Radiation Laboratory. It is not yet known whether it is generally true for all welded units.

The spreading resistance r can, as explained in Sec. 4·4, be found from the forward characteristic in the region of departure from the exponential curve. The values of r thus obtained usually fall in the range from 2 to 4 ohms, which is abnormally low for a contact of small dimensions. The dynamic resistance of the welded rectifiers at zero bias is abnormally large, usually in the range from 2 to 10 megohms. At 1 volt in the reverse direction the resistance is about 10,000 to 20,000 ohms and decreases rapidly at higher inverse voltages.

Because their large dynamic resistance narrows the video bandwidth, the welded units are generally not suitable for use at zero bias as video detectors. Their resistance falls in the desired range (about 10,000 ohms) at an appropriate forward bias, but their large noise output in this condition militates against their use.

13·3. Negative I-f Conductance.—The negative i-f conductance displayed by the welded-contact units under suitable conditions was first observed by Waltz,[1] who measured their admittance at 30 Mc/sec with a bridge. In this work the crystal was excited with about 1 mw of power from a microwave (3-cm) oscillator. Waltz found that the i-f conductance becomes negative, if the r-f load admittance is suitably adjusted, and reaches magnitudes as high as several thousand micromhos. If a tuned circuit is attached to the i-f terminals, the tuned circuit will oscillate at its resonant frequency if the sum of its shunt conductance and the crystal i-f conductance is zero. Oscillations of this type have been observed over a wide range of frequencies extending up into the microwave region, but never exceeding the exciting frequency.

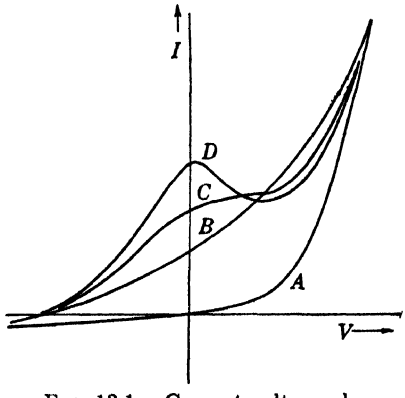

FIG. 13·1.—Current-voltage characteristics of welded-contact rectifiers as affected by r-f power.

The negative i-f conductance can be conveniently displayed on an oscilloscope. The 60-cps current-voltage characteristic is presented on the oscilloscope screen with a circuit of the type shown in Fig. 10·11. With no r-f (microwave) power applied to the crystal the curve looks somewhat like Curve A of Fig. 13·1. If a normal (nonwelded) crystal is used, the application of r-f power of about 1 mw changes the shape of the curve in such a way that it resembles Curve B of Fig. 13·1; in this case the finite current at zero bias is, of course, rectified current. Welded units under similar conditions may also produce a curve of type B, but usually the curve looks like Curve C; there is a range of voltage near zero

[1] M. C. Waltz, private communication.

bias over which the current increases very little. If now the r-f load admittance is correctly adjusted, for about half of the welded units as made by North there is produced a curve of type *D* in which, over a portion of the curve, the current actually decreases with increasing voltage; the dynamic conductance is negative. Now the i-f conductance of the converter is, of course, just the dynamic conductance of this characteristic and is therefore negative. Occasionally two distinct regions of negative i-f conductance are observed. Figure 13·2 shows an actual observed characteristic with two such regions.

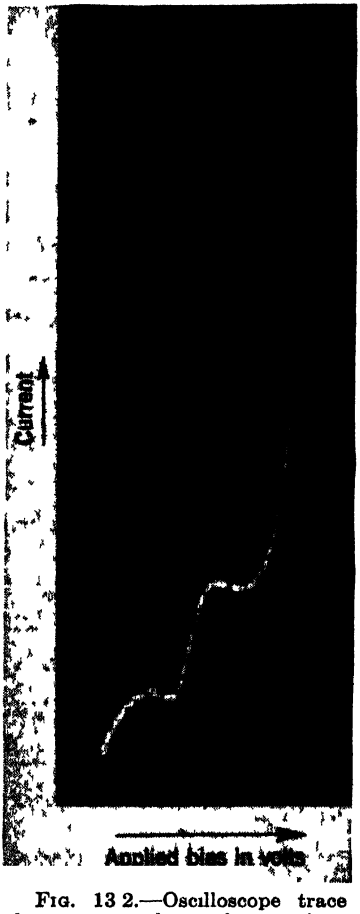

FIG. 13 2.—Oscilloscope trace of a current-voltage characteristic showing two regions of negative conductance (the left-hand one occurs at negative bias).

Curves of type *D* are frequently and easily produced if the microwave oscillations have a wavelength in the 3-cm band. They are found infrequently, however, with 10-cm excitation. If the oscillations are in the 1-cm band, negative conductance is frequently observed, but the characteristic curve rarely has the appearance of Curve *D*. Instead, it presents a peculiar scalloped appearance, with several narrow regions of negative conductance and abrupt transitions to wider regions of positive conductance. It has been found at the General Electric Company that whenever these negative-conductance regions appear with 1-cm-band excitation they are invariably accompanied by parasitic oscillations in the 3-cm band. No parasitic oscillations are observed, however, when the crystal is driven with power in the 3-cm band.

A source of power with zero or negative internal conductance has an infinite available power. According to the usual definition then, the conversion loss of a mixer with negative i-f conductance is zero; the conversion gain is infinite. Actually, of course, unlimited power cannot be extracted at intermediate frequencies because the conductance must change with the power extracted and become positive at sufficiently high power. Actually, the usual definition of conversion loss is not meaningful when applied to the crystals of negative i-f conductance. There is no doubt, however, that these crystals amplify as well as convert.

13·4. Loss and Noise Measurements. *Measurements of Conversion Loss.*—Curious results are obtained when conventional apparatus is employed to measure the "conversion loss" of these welded rectifiers.

Tests made with the 60-cps amplitude-modulation method using a 3-cm oscillator have shown that considerably more 60-cps power can be extracted from the crystal than is available in the modulation sidebands of the oscillator. In one case the ratio of the output power to available input power was as high as 16 db.

A number of North's units were measured for conversion loss by the Pound (impedance conversion loss) method (see Sec. 7·3). It was found that at a proper bias point the indicated conversion loss was unity. A remarkable consequence was that opening and closing the i-f terminals had precisely the same effect on the amplitude of the reflected signal wave as opening and closing the r-f shutter (Fig. 7·5). It appeared that there was a perfect lossless connection through the rectifier between the r-f and i-f sections.

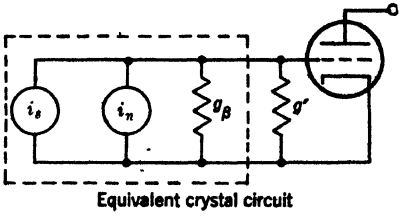

FIG. 13·3.—Equivalent input circuit of the i-f amplifier.

Noise Figure.—The loss measurements, although interesting and significant, are not of themselves sufficient to determine the merit of these crystals as frequency converters. In addition, data on the noise output of the crystals are needed. Independent measurements of conversion loss and noise temperature, however, are possible only when the i-f conductance of the mixer is positive. The significant quantity in any case is the noise figure of the whole receiver including the mixer, and this quantity has a definite measurable value irrespective of the sign of the i-f conductance.

At Radiation Laboratory there was built an apparatus by Beringer[1] and others especially designed to measure the noise figure of a receiver with a welded-contact converter and to assess the relative influence on noise figure of conversion loss (or gain) and of noise generation. It has already been described in Secs. 7·10 and 7·11 and illustrated in Figs. 7·15 and 7·16. Figure 13·3 shows an equivalent circuit of the input to the i-f amplifier. The crystal is represented here, by Norton's theorem, as a conductance g_β, which may have either sign, with two parallel constant-current generators (at i-f); one, i_s, represents the converted signal, and the other, i_n, the converted and generated noise of the crystal. No i-f susceptance is shown, as any such susceptance is tuned out before each measurement.

[1] E. R. Beringer, C. P. Gadsden, and M. C. Waltz, "X-Band Noise Figure Measurements of Welded Contact Germanium Crystals," RL Group Report 52, July 16, 1945.

The conductance g' is made up of two parts; one, the shunt conductance g_1 of the parallel tuned circuit, and the other, g_2, an added conductance which is switched in when measuring the welded units, since otherwise the total conductance would generally be outside the calibrated range of the amplifier noise figure. The method of measurement is described in Sec. 7·10. (The conductances g_1 and g_2 correspond to the resistances R_1 and R_2 of Fig. 7·15.) The quantities determined by the measurements are the over-all noise figure, the noise temperature t, and conversion loss L of the combination of crystal and load conductance g'. Also the conductance g of the crystal and the currents i_s and i_n are determined. These data and a knowledge of the noise temperature t_s of the r-f signal source give all the relevant information. For example, if the i-f conductance g of the crystal is positive, the conversion loss L_x and noise temperature t_x of the crystal itself are given by

$$L_x = L\frac{g_\beta}{g_\beta + g'}, \tag{4}$$

$$t_x = 1 + \left(1 + \frac{g'}{g_\beta}\right)(t - 1). \tag{5}$$

If the i-f conductance g_β of the crystal is negative, these results do not hold and, in fact, the quantities L_x and t_x become nugatory. The conversion and noise generation of the crystal can still be described with the aid of i_s and i_n. Thus, for an ideal amplifier generating no noise, the ratio of signal power to noise power at the amplifier output terminals is

$$\frac{i_s^2}{i_n^2} = \frac{\dfrac{t_s}{L}}{t - \dfrac{g'}{g_\beta + g'}}. \tag{6}$$

The noise figure F is the noise temperature t_s of the signal source when the output signal-to-noise ratio is unity. Thus, writing $F = F_0$ for an ideal amplifier, one obtains

$$F_0 = L\left(t - \frac{g'}{g_\beta + g'}\right). \tag{7}$$

This result, giving the lowest possible noise figure, holds, whatever the sign of g_β, provided of course that $g_\beta + g'$ is positive.

The over-all noise figure can also be computed for a nonideal amplifier with noise figure $N > 1$. The result can be shown to be

$$F = L\left(t - 1 + N\frac{g_\beta}{g_\beta + g'}\right). \tag{8}$$

Beringer[1] and his coworkers first made measurements for the broadband case in which there is no discrimination between signal and image r-f tuning. The apparatus is that shown in Fig. 7·16 with the image filter (magic T with cavity) removed. It was found that the over-all noise figure changed little as a function of the position and amount of insertion of the screw tuner and as a function of the amount of local-oscillator drive and the d-c crystal bias. Although the output noise power changed by as much as 20 db in this adjustment, the noise figure remained within the range of 13 to 18 db. This constancy of noise figure suggests that the ratio of i-f noise power to i-f signal power remains about the same, that is, independent of the i-f conductance. Experiments confirmed this deduction. Table 13·1 shows measured values of i_n as a function of crystal i-f conductance, with bias voltage and crystal current constant. The conductance variation corresponds to different screw insertions.

TABLE 13·1.—CRYSTAL I-F NOISE CURRENT AS A FUNCTION OF I-F CONDUCTANCE FOR DIFFERENT R-F TUNING

g_β	i_n (arbitrary units)
− 62 μmhos	1.7
− 30	2.0
− 8	2.0
+ 770	2.0
+1400	2.0
+3700	2.6

It is seen that i_n is practically constant over wide changes in g_β. Since the noise figure is nearly constant, i_s must also change little.

Thus signal and noise power increase together as the conversion loss decreases, and no improvement in noise figure results. The suggestion has been made that the r-f signal source is seriously mismatched when the screw tuner is deeply inserted to give a negative i-f conductance. If it were possible to decrease the i-f conductance by some other means so that the signal impedance would still be at one's disposal, the noise figure could perhaps be improved. Beringer *et al.*[2] found that the i-f conductance can be made very low, even negative, by reflecting only the image sideband. In this work the arrangement of Fig. 7·16 was employed. A band-reject filter reflected the image frequency, with reflected phase made adjustable by means of the "line stretcher." It was found that no improvement resulted from the reflected image frequency and that the lowest noise figure was obtained with both sidebands matched. Table 13·2 summarizes these measurements. It should be noted that the crystal conversion loss is negative (expressed

[1] *Loc. cit.*
[2] *Loc. cit.*

TABLE 13·2.—CONVERSION AND NOISE PARAMETERS AS A FUNCTION OF INDEPENDENT TUNING OF THE R-F SIDEBANDS

Crystal i-f conductance as produced by		g_β, μ mhos	t	i_n, in arbitrary units	L, db	L_x, db	t_x	F_0, db	F, for 3-db amplifier, db
Signal-frequency reflection	Image-frequency reflection								
Low	low	58	9.9	2.0	5.1	−3.9	79.0	14.6	14.7
High	low	1080	3.9	2.3	5.9	+4.5	4.6	11.5	12.4
Intermediate	low	880	4.2	2.2	7.0	+5.4	5.7	12.9	13.6
(Matched signal)	low	650	4.7	2.1	4.8	+2.7	7.0	11.1	11.7
(Matched signal)	high	4000	1.5	2.4	7.7	+7.3	1.55	8.7	11.7
Low	high	3200	1.7	2.3	10.3	+9.8	1.8	12.3	14.3
(Matched signal)	(matched signal)	1900	2.1	2.0	7.1	+6.3	2.3	9.1	10.9

in db) in the case of i-f conductance minimized by both signal- and image-frequency reflections (first row of the table). For another crystal Beringer was able to produce negative i-f conductance by reflecting the image frequency with the signal frequency matched.

The lowest noise figure obtained (if an amplifier with a 3-db noise figure is assumed) was 10.9 db. Although this figure is well within the limit for 1N23B rectifiers (the best 3-cm-band crystals) it is not spectacular. In fact, the noise figures of many 1N23B crystals, with the same amplifier, are from 8 to 10 db.

Later measurements by North[1] substantiated Beringer's finding that the best performance occurs with a matched signal, corresponding to high i-f conductance. North was able, however, by correct bias adjustments and at relatively low local-oscillator drive, to obtain for some crystals over-all noise figures (again with a 3-db amplifier) as low as 6 or 7 db. These values were obtained for matched signal and image frequencies at relatively high i-f conductance.

It must be said that not all possibilities for using the welded-contact units as converters, under the condition of low or negative i-f conductance, have yet been exhausted. For example, it is possible (although not likely) that at a higher intermediate frequency the noise output may be considerably reduced.

13·5. Theory of Negative I-f Conductance and Conversion Amplification.—The two anomalies of North's crystals, conversion gain and nega-

[1] H. Q. North, *et al.*, "Welded Germanium Crystals," GE Final Report, Contract OEMsr-262—Ordn. No. DIC 178554, Sept. 20, 1945.

tive i-f conductance, are closely associated, if not concomitant. It is clear that a mixer with negative i-f conductance will amplify, since in the linear approximation the available power from its i-f terminals is unlimited. The conversion loss of such a mixer is exactly zero. A conversion loss of unity, however, implies no attenuation between signal and i-f terminals, and a conversion loss in the range from zero to unity implies amplification. Thus it is not necessary for a mixer to have negative i-f conductance in order for it to amplify. For example, the data given in the first row of Table 13·2 should be noted. The crystal referred to has a positive i-f conductance but also has 3.9-db conversion gain.

It can be shown by the methods of Chap. 5 that, under the condition of weak reciprocity and provided the reciprocity factor $g_{\alpha\beta}/g_{\beta\alpha}$ is not less than unity, no possibility of conversion amplification exists unless the i-f conductance becomes negative at some r-f load admittance. The proof is somewhat tedious and will be omitted. By methods similar to those of Sec. 5·10 it can be shown that values of r-f load admittance exist for which the i-f conductance is negative if, and only if,

$$\eta_2 > 1, \tag{9}$$

where η_2 is defined in terms of the elements of the mixer matrix by Eq. (5·73),

$$\eta_2 = \frac{2g_{\alpha\beta}g_{\beta\alpha}}{g_{\beta\beta}(g_{\alpha\alpha} + g_{\alpha\gamma})}. \tag{10}$$

Weak reciprocity is assumed in proving Eq. (10). Measurement[1] of the mixer matrices for a number of welded units showed that weak reciprocity held for all units tested but that full reciprocity failed for all. The data on four of the units are given in Table 13·3. The first row gives

TABLE 13·3.—ADMITTANCE MATRIX ELEMENTS OF WELDED-CONTACT RECTIFIERS

Crystal no.*	D404	D401	D405	D574
e_0, volts	0.15	0.20	0.17	0.23
i_0, ma	0.57	0.67	0.83	0.52
P, mw	1.67	1.00	0.65	0.65
$g_{\alpha\alpha}/g_0$	13.3	14.2	8.42	10.94
$g_{\alpha\beta}/\sqrt{g_0}$	0.201	0.376	0.192	0.170
$g_{\beta\alpha}/\sqrt{g_0}$	0.116	0.206	0.145	0.110
$g_{\alpha\gamma}/g_0$	6.68	7.20	2.42	2.44
$g_{\beta\beta}$	0.0021	0.0073	0.0052	0.0024
$g_{\alpha\beta}/g_{\beta\alpha}$	1.73	1.83	1.32	1.55
η_2	1.11	0.99	0.99	1.07

* In the first column g_0 is the characteristic conductance of the r-f transmission line or waveguide. All conductances g_0, $g_{\alpha\alpha}$, etc. are given in mhos.

[1] By L. Apker, General Electric Company, private communication.

the d-c bias voltage (positive); the second, the crystal current; the third, the available r-f power from the local oscillator; the fourth to eighth, the elements of the mixer matrix [see Eq. (5·13)]; the ninth, the reciprocity factor $g_{\alpha\beta}/g_{\beta\alpha}$; and the tenth, the quantity η_2 of Eqs. (9) and (10). Evidently units D404 and D574 can exhibit negative i-f conductance, but units D401 and D405 cannot (at the particular bias and local-oscillator level stated).

From the theory of Sec. 5·7 it can be seen that the conversion loss, with equal terminations at the two r-f sidebands, can be less than unity only if Eq. (9) holds. Thus conversion amplification is closely associated with negative i-f conductance and the theory of one is essentially the theory of the other.

It will now be shown[1] that negative i-f conductance can result if the rectifier is represented as a nonlinear resistance in shunt with a voltage-variable capacitance, provided that the resistance (e.g., spreading resistance) in series with this combination is sufficiently small.

The linear relations among the currents and voltages at signal, image, and intermediate frequencies have been derived for a rectifier of this type in Sec. 5·11 and are given by Eqs. (5·197). In order to simplify the analysis it is now assumed that a time zero exists making the barrier voltage at local-oscillator frequency an even function of the time. In accordance with the discussion following Eqs. (5·197), this assumption simplifies the equations to the following form:

$$\left.\begin{aligned} i_\alpha &= (g_0 + j\omega C_0)e_\alpha + (g_1 + j\omega C_1)e_\beta + (g_2 + j\omega C_2)e^*, \\ i_\beta &= \qquad g_1 e_\alpha \qquad\qquad + g_0 e_\beta \qquad\qquad + g_1 e^*_\gamma, \\ i^*_\gamma &= (g_2 - j\omega C_2)e_\alpha + (g_1 - j\omega C_1)e_\beta + (g_0 - j\omega C_0)e^*_\gamma. \end{aligned}\right\} \tag{11}$$

The above assumption about the form of the local-oscillator wave is exactly true if harmonic voltages are zero or are correctly phased with respect to the fundamental. In actual fact the assumption is only approximately true, but it is not believed that the qualitative conclusions reached will be affected by failure of the assumption. In Eq. (11) i_α, i_β, and i_γ are the terminal currents at signal, intermediate, and image frequencies, respectively; and e_α, e_β, and e_γ are the corresponding voltages. The quantities g_n and C_n are, respectively, the Fourier coefficients of the dynamic conductance and capacitance of the barrier [see Eqs. (5·192) and (5·193)].

Let us suppose, as an example, that the signal and image voltages are terminated by the same load admittance $y_a = g_a + jb_a$, hence,

$$i_\alpha = -y_a e_\alpha, \tag{12}$$

$$i_\gamma = -y_a e_\gamma. \tag{13}$$

[1] See H. C. Torrey, RL Group Report 53, May 22, 1945.

It can be shown that, if the i-f conductance cannot become negative under this symmetrical sideband condition, it cannot be negative for any possible r-f load admittance.

When i_α, i_γ, e_α, and e_γ are eliminated from Eqs. (11), (12), and (13) and the equations are solved for the i-f admittance of the mixer, viz.,

$$\begin{aligned} y_\beta &= \frac{i_\beta}{e_\beta} \\ &= g_\beta + jb_\beta, \end{aligned} \tag{14}$$

we obtain $b_\beta = 0$, and

$$g_\beta = g_0 \frac{\left[b_a + \omega\left(C_0 - \frac{g_1 C_1}{g_0}\right)\right]^2 + \left[g_a + g_0\left(1 - \frac{g_1^2}{g_0^2}\right)\right]^2 - G^2}{(b_a + \omega C_0)^2 + (g_a + g_0)^2 - g_2^2 - \omega^2 C_2^2}, \tag{15}$$

where

$$G^2 = \omega^2\left(\frac{g_1 C_1}{g_0} - C_2\right)^2 + g_0^2\left(1 - \frac{g_1^2}{g_0^2}\right) - (g_0 - g_2)\left(g_0 + g_2 - \frac{2g_1^2}{g_0}\right). \tag{16}$$

The task is to discover under what conditions, if any, the i-f conductance g_β can become negative. The case of a constant capacitance ($C_1 = C_2 = 0$) is examined first. In this instance Eq. (15) reduces to

$$g_\beta = \frac{(b_a + \omega C_0)^2 + \left[g_a + g_0\left(1 - \frac{g_1^2}{g_0^2}\right)\right]^2 - g_0^2\left(1 - \frac{g_1^2}{g_0^2}\right)^2 + (g_0 - g_2)\left(g_0 + g_2 - \frac{2g_1^2}{g_0}\right)}{(b_a + \omega C_0)^2 + (g_a + g_0)^2 - g_2^2}. \tag{17}$$

It is clear from an examination of Eq. (17) that both the denominator and numerator of the fraction on the right are always greater than or equal to zero for any y_a with positive real part, provided that

$$g_1 \leqq g_0, \tag{18a}$$

$$g_2 \leqq g_0, \tag{18b}$$

and

$$\frac{2g_1^2}{g_0} \leqq g_0 + g_2. \tag{18c}$$

It will now be proved that these conditions [Eqs. (18)] are always satisfied under the assumption of a symmetrical barrier voltage, provided that the d-c characteristic (with no r-f voltage applied) has no point of negative dynamic conductance over the range of the local-oscillator voltage excursion.

The quantities g_n are the Fourier coefficients of $f'(e)$ according to Eq. (5·193), where

$$i = f(e) \tag{19}$$

is the equation of the d-c characteristic. The Fourier development of $f'(e)$ with the assumption of a symmetrical barrier voltage e becomes

$$f'(e) = g_0 + 2g_1 \cos \omega t + 2g_2 \cos 2\omega t + \cdots +; \tag{20}$$

hence

$$g_n = \frac{1}{2\pi} \int_{-\pi}^{+\pi} f'(e) \cos n\omega t \, d(\omega t). \tag{21}$$

Let

$$F(e) \equiv \frac{f'(e)}{\int_{-\pi}^{+\pi} f'(e) \, d(\omega t)}. \tag{22}$$

By hypothesis, $f'(e)$, and so also $F(e)$, is greater than or equal to zero;

$$F(e) \geqq 0. \tag{23}$$

Also from Eq. (22),

$$\int_{-\pi}^{+\pi} F(e) \, d(\omega t) = 1. \tag{24}$$

Now from Eqs. (21), (22), and (24),

$$g_1 = g_0 \int_{-\pi}^{+\pi} F(e) \cos \omega t \, d(\omega t) \leqq g_0 \int_{-\pi}^{+\pi} F(e) \, d(\omega t) = g_0, \tag{25}$$

and

$$g_2 = g_0 \int_{-\pi}^{+\pi} F(e) \cos 2\omega t \, d(\omega t) \leqq g_0 \int_{-\pi}^{+\pi} F(e) \, d(\omega t) = g_0. \tag{26}$$

Thus the first two inequalities [Eqs. (18*a*) and (18*b*)] are demonstrated. To prove the third, it should be noted that from Eq. (26)

$$g_2 = g_0 \int_{-\pi}^{+\pi} F(e)(2 \cos^2 \omega t - 1) \, d(\omega t), \tag{27}$$

or

$$g_0 + g_2 = 2g_0 \int_{-\pi}^{+\pi} F(e) \cos^2 \omega t \, d(\omega t), \tag{28}$$

and that, from Eq. (25),

$$\frac{2g_1^2}{g_0} = 2g_0 \left[\int_{-\pi}^{+\pi} F(e) \cos \omega t \, d(\omega t) \right]^2. \tag{29}$$

Now, it is clear that

$$\int_{-\pi}^{+\pi} F(e) \left[\cos \omega t - \int_{-\pi}^{+\pi} F(e) \cos (\omega t) \, d(\omega t) \right]^2 d(\omega t) \geqq 0,$$

since the integrand is always greater than or equal to zero. This reduces, on expansion, to

$$\left[\int_{-\pi}^{+\pi} F(e) \cos \omega t \, d(\omega t)\right]^2 \leqq \int_{-\pi}^{+\pi} F(e) \cos^2 \omega t \, d(\omega t). \tag{30}$$

From Eqs. (28), (29), and (30) we obtain

$$\frac{2g_1^2}{g_0} \leqq g_0 + g_2, \tag{31}$$

which is the third inequality [Eq. (18c)].

It has thus been proved that the i-f conductance is never negative under the following conditions:

1. Constant barrier capacitance.
2. Local-oscillator voltage at the barrier is an even time function about some time zero.
3. The d-c characteristic (with no r-f power applied) does not have a negative slope within the local-oscillator excursion.
4. The r-f load admittance has a positive real part.

Conditions 3 and 4 apply to all measurements in which negative i-f conductance is observed. Thus negative i-f conductance is caused by failure of Condition 1 or 2, or both. It is conjectured, but not proved, that failure of Condition 2 alone will not lead to negative i-f conductance. Some experimental evidence in favor of this conjecture has been found by Hahn[1] at General Electric Company.

It will now be proved that failure of Condition 1 alone leads, under certain conditions, to negative i-f conductance. To do this we must return to the general expression Eq. (15) for g_β. Let us make N the numerator of the fraction on the right-hand side of Eq. (15) and D its denominator. Then g_β is negative, if either

$$N > 0, \qquad D < 0, \tag{32}$$

or

$$N < 0, \qquad D > 0. \tag{33}$$

Now the equation, $N = 0$, is the equation of a circle in the (g_a,b_a)-plane with the center at $b_a = -\omega[C_0 - (g_1/g_0)C_1]$, and $g_a = -g_0[1 - (g_1^2/g_0^2)]$. This circle is shown as Circle A in Fig. 13·4. Its radius is G [Eq. (16)]. Since $g_1 \leqq g_0$, the center falls in the negative-conductance half of the (g_a,b_a)-plane. All points for which $N < 0$ lie within this circle. Because of the presence of the term $\omega^2[(g_1/g_0)C_1 - C_2]^2$ in Eq. (16) for the radius

[1] See H. Q. North *et al.*, "Welded Germanium Crystals," GE Report, Contract OEMsr-262, Order No. DIC 178554, Sept. 20, 1945.

G, it is possible for this circle to extend into the positive-conductance half of the (g_a,b_a)-plane and thus for N to be negative at a physically realizable value of the r-f load admittance y_a. It must be remembered, however, that y_a is the r-f load admittance presented to the terminals of the barrier, that is, terminals A-A of Fig. 5·18, and not that presented to the rectifier terminals (terminals B-B of Fig. 5·18). Thus y_a includes the series spreading resistance r, whose presence restricts the physically possible values of y_a to points within a circle on the y_a-plane of radius $1/2r$ with center on the real axis at $g_a = 1/2r$. This circle is represented as Circle B

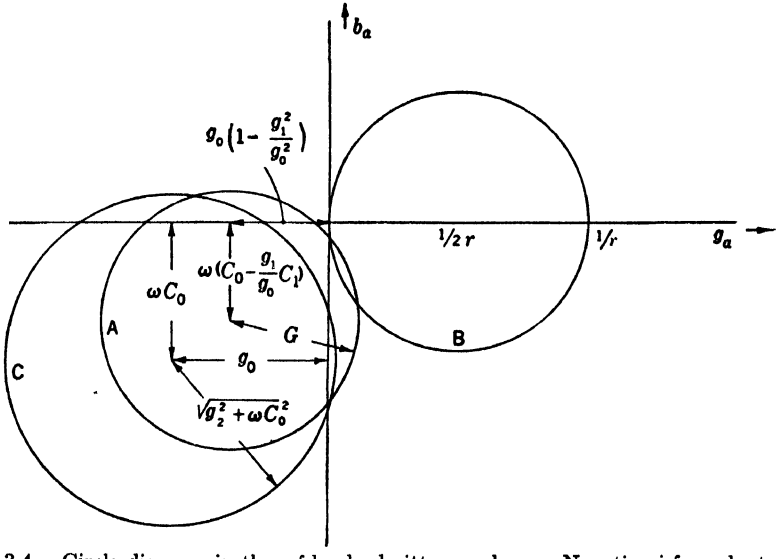

FIG. 13·4.—Circle diagram in the r-f-load admittance plane. Negative i-f conductance is possible if either Circle A or Circle C intersects Circle B.

of Fig. 13·4. Thus N can be negative only if Circle A intersects Circle B and only then becomes negative if y_a falls within the lune common to the two circles.

The equation $D = 0$ is the equation of a circle in the y_a-plane and bounds all values of y_a for which $D < 0$. The circle, $D = 0$, represented as Circle C of Fig. 13·4, has a radius $(g_2^2 + \omega^2 C_2^2)^{1/2}$ and its center falls in the negative-conductance half of the plane at $y_a = -(g_0 + j\omega C_0)$. For sufficiently large values of C_2, Circle C may extend into the positive-conductance half of the y_a-plane and may even intersect Circle B, and thus form a lune containing all the physically possible values of y_a that make $D < 0$.

Thus there are the following possibilities for negative i-f conductance g_β:

1. Circle A but not Circle C intersects Circle B.
2. Circle C but not Circle A intersects Circle B.

3. Both Circle A and Circle C intersect Circle B, but the two lunes thus formed are not coincident.

Since it can be shown the two lunes of Condition 3 can never be coincident, it follows that if either Circle A or Circle C or both of them intersect Circle B, physically possible values of y_a exist for which the i-f conductance is negative.

Condition 1 corresponds to the inequality of Eq. (33). In this case the negative-conductance region of Fig. 13·4 is bounded by points of zero conductance. This is the case commonly observed (Curve D of Fig. 13·1) when the local-oscillator wavelength is in the 3-cm band.

Condition 2 corresponds to the inequality of Eq. (32). In this case the negative-conductance region of Fig. 13·1 is bounded by points of infinite conductance. Such a region has not as yet been observed.

Condition 3 includes both inequalities [Eqs. (32) and (33)]. In this case the negative-conductance region may be bounded by points of zero conductance on one end and infinite conductance on the other. This phenomenon has been observed by Dicke[1] for 1-cm local oscillations.

As a result of this analysis it can be concluded that the qualitative conditions necessary for negative i-f conductance are:

1. Barrier capacitance must be variable with barrier voltage. The variation must be strong, so that C_1 or C_2 is large and Circle A or C has a large radius.
2. The spreading resistance r must be small so that Circle B has a large radius.
3. The constant term C_0 in the Fourier expansion of the barrier capacitance must not be large, since the separation of Circles A and C from Circle B increases with C_0 (see Fig. 13·4).

Now it is an experimental fact that the barrier capacitance of North's welded-contact rectifiers is a strong function of barrier voltage, at least as strong a function as for normal germanium rectifiers. It is also an experimental fact that the spreading resistance of the welded rectifier is abnormally small for a contact radius of 0.0002 in. The small size of the contact is helpful in reducing the magnitude of C_0. Thus it appears that the welded-contact rectifiers meet the qualitative conditions for negative i-f conductance to a higher degree than normal crystals.

Quantitative estimates of the values of r required to give negative i-f conductance have been made by Torrey.[2] Equation (1) was used for $f(e)$, and the values of g_n were then computed as a function of bias voltage by using values of the constants A and β appropriate to the welded rectifiers. The barrier capacitance was assumed to vary with barrier

[1] R. H. Dicke, private communication.
[2] H. C. Torrey, unpublished.

voltage according to Bethe's Eq. (4·18) corrected for values of voltage in the neighborhood of the contact potential difference. With $C_0 = 0.2$ $\mu\mu f$, C_1 and C_2 were computed. It was found that negative i-f conductance of the type corresponding to the inequality of Eq. (32) could occur if the spreading resistance r is less than 10 ohms, and of the type corresponding to the inequality of Eq. (33) if r is less than 3 ohms. As noted above, the spreading resistance of the welded units usually falls in the range from 2 to 4 ohms and is therefore sufficiently low to satisfy the theoretical conditions for negative i-f conductance.

Subsequent measurements[1] of dependence of contact capacitance on voltage revealed that Bethe's formula, Eq. (4·18), does not hold well for the welded units. These results were obtained by comparison of microwave with audio-frequency low-level rectification efficiency; the equivalent circuit of Fig. 2·10 was assumed. This method was described in Sec. 11·2. It was found that the barrier capacitance was nearly constant with voltage for bias voltages less than 0.2 volts, but thereafter increased exponentially with voltage. It is expected that, if the calculated values of C_1 and C_2 are corrected in accordance with these results, the upper limit on r for negative i-f conductance will increase.

Hahn[1] has made some interesting experiments which throw light on the problem of negative i-f conductance. He constructed a low-frequency analogue of a crystal rectifier by using a vacuum-tube diode to simulate the nonlinear resistance of the barrier and a circuit employing a reactance tube to simulate the variable capacitance. The experimental circuit was designed to operate at an impedance level fifty times that of the crystal and at a frequency one twenty-thousandth of the microwave frequency (the latter about 10,000 Mc/sec). The circuit included reactive elements to simulate the whisker inductance and the capacitance to ground of the glass bead that supports the inner conductor of the rectifier. Hahn found that, when the variable capacitance circuit was disconnected, the "i-f conductance" of the equivalent rectifier could not be made negative although the other elements of the circuit were adjustable over wide ranges. When the capacitance was caused to vary with voltage in order to simulate (with appropriate scaling) the observed capacitance variation of the crystals, however, negative i-f conductance was definitely obtained. Hahn displayed the current-voltage characteristic of the equivalent rectifier on an oscilloscope and was able to duplicate in every way the corresponding curves of an actual welded rectifier (Fig. 13·1). He also found that the equivalent series spreading resistance had to be sufficiently small before negative i-f conductance appeared.

[1] H. Q. North, *loc. cit.*

He discovered, too, that the value of the whisker inductance was fairly critical for negative i-f conductance. North[1] later showed that an alteration in the shape of the whisker, and therefore of its inductance, affected the i-f conductance. For certain whisker geometries, negative i-f conductance could not be obtained although all other factors were unchanged.

It is reasonable to conclude from this work that the nonlinear capacitance of the barrier is the controlling factor in the appearance of negative i-f conductance, although other elements of the rectifier also have some influence.

13·6. Applications.—Although it has been found that the welded-contact rectifier of North, in its present form at least, cannot to advantage replace the conventional rectifier as a converter or video detector, it still has utility in other applications.

It has been found by D. Montgomery (see Sec. 5·16) that the welded rectifiers are excellent harmonic generators, being superior to conventional types (e.g., the 1N26) in the generation of second and third harmonics of 1.25-cm waves. Their superiority is especially marked as generators of the third harmonic. Later work by North[2] confirmed this result. He also experimented with welded contacts of still smaller areas and found considerable improvement in the generation of 0.4-cm radiation from a fundamental of 1.20-cm wavelength. Beringer[3] has constructed silicon rectifiers that are perhaps not greatly inferior to North's crystals in harmonic generation, but are mechanically and electrically unstable by virtue of their small contact areas. The much greater stability of the welded contact gives it a marked advantage. Some data in regard to harmonic generation by welded and conventional rectifiers are given in Sec. 5·16.

Hennelly[4] has constructed germanium high-inverse-voltage rectifiers with welded contacts. The technique used was similar in most respects to North's, but with the difference that, following the lead of the Purdue group, tin or nitrogen was used instead of antimony as a doping agent. Hennelly found that highest inverse voltages and largest inverse resistances occurred with germanium prepared by vacuum melts with no added donors. The forward currents obtained in this case, however, were low, only about 2 ma at 1 volt. The most satisfactory rectifiers were made with vacuum-melted germanium with 0.2 atomic per cent of tin added. In this case, inverse resistances of 0.5 megohms at −40 volts

[1] H. Q. North, *loc. cit.*

[2] H. Q. North, "A Comparison of Silicon and Germanium Crystals as Harmonic Generators of 4 mm and 6 mm Waves," GE Report, Jan. 15, 1946.

[3] Personal communication.

[4] H. Q. North *et al.*, "Welded Germanium Crystals," GE Final Report, Contract OEMsr-262—Ordn. No. DIC 178554, Sept. 20, 1945.

and 0.25 megohms at −50 volts were obtained. The current at 1 volt forward was about 16 ma (at 25°C) in this case. Characteristic curves obtained for pure germanium melted in dry nitrogen exhibited properties intermediate between those of vacuum melts with no added impurity and vacuum melts with 0.2 per cent tin added. The stability gained from welded contacts is of great value for the high-voltage type, as for other types of rectifiers, and further work along lines initiated by Hennelly is desirable.

The accurate exponential law obeyed by the forward characteristics of antimony-doped welded germanium rectifiers is useful in circuit applications where a logarithmic or exponential response is desired. Kallman has utilized this principle in some d-c bridge circuits. In particular, he designed a double-bridge circuit for indicating the ratio of two direct voltages on a logarithmic scale.

No use has yet been made of the amplifying properties of the welded rectifiers used as converters. It is possible that a lightweight receiver—with no tubes, yet capable of detecting audio modulation of a weak microwave signal close to noise level—might be constructed by keeping these crystals on the verge of oscillation by a suitable feedback arrangement. Some work along these lines was started by Dicke, but inconclusive results had been obtained when the war came to an end.

North[1] has found that welded rectifiers, used as frequency converters in the 3-cm band and biased outside of the negative i-f conductance characteristic, will operate with low loss (3 to 4 db) at reduced local-oscillator drive. The noise output is then comparable to that from a conventional rectifier, and the over-all receiver noise figures obtained are excellent (below 6 db).

[1] Private communication.

APPENDIX A

THE RECIPROCITY THEOREM OF DICKE[1]

It will now be proved that the mixer-admittance matrix in the "low Q" form, Eq. (5·6), is symmetrical about the main diagonal, provided the following conditions are satisfied.

1. The phase of the electric field strength is uniform over the rectifying barrier or barriers of the mixer.
2. A time zero can be, and is, chosen such that the electric field strength at the barrier is an even function of time.
3. The current-density components at the barrier depend only on the components of the electric field intensity (and not, for example, on their time derivatives). This restriction excludes the possibility of a nonlinear barrier capacitance.

The theorem will be proved by establishing Relations (5·49) and (5·50).

The black box of Fig. 5·3 is supposed enclosed in a region R bounded by a surface S intersecting the terminals which for convenience are assumed to be coaxial. Since the voltage applied to the terminals is periodic in time, the field quantities in R may be expressed as a Fourier series in the time

$$\left.\begin{aligned} \mathbf{E}(t) &= \sum_{n=-\infty}^{\infty} \mathbf{E}_n e^{jn\omega t} \\ \mathbf{H}(t) &= \sum_{n=-\infty}^{\infty} \mathbf{H}_n e^{jn\omega t} \\ \mathbf{J}(t) &= \sum_{n=-\infty}^{\infty} \mathbf{J}_n e^{jn\omega t} \end{aligned}\right\} \tag{1}$$

From Maxwell's equations, it follows that

$$\begin{aligned} \operatorname{curl} \mathbf{H}_n - j\omega\epsilon\mathbf{E}_n &= \mathbf{J}_n, \\ \operatorname{curl} \mathbf{E}_n + j\omega\mu\mathbf{H}_n^* &= 0, \end{aligned}$$

where ϵ and μ, the permittivity and permeability, are functions of position, and $\mathbf{E}$, $\mathbf{H}$, and $\mathbf{J}$ are, respectively, the electric field strength, the magnetic field strength, and the electric current density. Let us con-

[1] R. H. Dicke, "A Reciprocity Theorem and its Application to the Measurement of Gain of Microwave Crystal Mixers," RL Report No. 16-18, Apr. 13, 1943.

sider variations of the field quantities obtained by varying the terminal voltages.

Let d_0 denote a change resulting from a variation of e_0 holding e_1 constant, and let d_1 denote a change resulting from a variation of e_1 holding e_0 constant. Thus,

$$\left.\begin{aligned} d_0e_1 &\equiv 0, \qquad d_0e_0 \neq 0, \\ d_1e_0 &\equiv 0, \qquad d_1e_1 \neq 0. \end{aligned}\right\} \tag{2}$$

It is assumed for the whole region *except* the barrier that

$$\mathbf{J} = \sigma\mathbf{E}, \tag{3}$$

where the conductivity σ is a function of position. At a rectifying barrier a tensor relation is assumed to exist between $d\mathbf{J}$ and $d\mathbf{E}$ and the components of the tensor assumed to be functions of $\mathbf{E}$. Thus,

$$dJ^{(k)} = \sum_l \sigma(k,l)(\mathbf{E})\, dE^{(l)}. \tag{4}$$

The tensor will be assumed symmetric, hence

$$\sigma^{(k,l)} = \sigma^{(l,k)}. \tag{5}$$

The superscripts signify cartesian components. Making use of the vector identity,

$$\operatorname{div} \mathbf{A} \times \mathbf{B} = \mathbf{B} \cdot \operatorname{curl} \mathbf{A} - \mathbf{A} \cdot \operatorname{curl} \mathbf{B},$$

we obtain

$$\operatorname{div} (d_0\mathbf{H}_n \times d_1\mathbf{E}_n - d_1\mathbf{H}_n \times d_0\mathbf{E}_n) = d_0\mathbf{J}_n \cdot d_1\mathbf{E}_n - d_1\mathbf{J}_n \cdot d_0\mathbf{E}_n \tag{6}$$

By Eq. (3), the expression on the right of Eq. (6) vanishes everywhere except at the rectifying barrier.

Let us now apply [illegible] to the barrier by forming the following sum (t_0 being a constant):

$$\sum_n e^{2jn\omega t_0} \operatorname{div} (d_0\mathbf{H}_n \times d_1\mathbf{E}_n - d_1\mathbf{H}_n \times d_0\mathbf{E}_n)$$

$$= \sum_n e^{2jn\omega t}(d_0\mathbf{J}_n \cdot d_1\mathbf{E}_n - d_1\mathbf{J}_n \cdot d_0\mathbf{E}_n). \tag{7}$$

Since

$$d_0\mathbf{J}_n = \frac{\omega}{2\pi} \int_{-\frac{\pi}{\omega}}^{+\frac{\pi}{\omega}} d_0\mathbf{J}(\lambda) e^{-jn\omega\lambda}\, d\lambda,$$

and

$$d_1\mathbf{E}_n = \frac{\omega}{2\pi} \int_{-\frac{\pi}{\omega}}^{+\frac{\pi}{\omega}} d_1\mathbf{E}(t) e^{-jn\omega t}\, dt,$$

we have

$$\sum_n e^{2jn\omega t_0}\, d_0\mathbf{J}_n \cdot d_1\mathbf{E}_n = \frac{\omega^2}{4\pi^2}\int_{-\frac{\pi}{\omega}}^{+\frac{\pi}{\omega}}\int_{-\frac{\pi}{\omega}}^{+\frac{\pi}{\omega}} d_1\mathbf{E}(t)\cdot d_0\mathbf{J}(\lambda)\sum_n e^{jn\omega(2t_0-\lambda-t)}\, dt\, d\lambda.$$

Using the relation

$$\sum_{n=-\infty}^{\infty} e^{jna} = 2\pi\delta(a),$$

where $\delta(a)$ is the Dirac δ-function,

$$\delta(a) = 0 \qquad a \neq 0$$
$$\int_{-\infty}^{\infty} \delta(a)\, da = 1,$$

we have

$$\sum_n e^{2jn\omega t_0}\, d_0\mathbf{J}_n \cdot d_1\mathbf{E}_n = \frac{\omega^2}{4\pi^2}\int_{-\frac{\pi}{\omega}}^{+\frac{\pi}{\omega}}\int_{-\frac{\pi}{\omega}}^{+\frac{\pi}{\omega}} d_1\mathbf{E}(t)\cdot d_0\mathbf{J}(\lambda)\delta(2t_0-\lambda-t)\, dt\, d\lambda$$
$$= \frac{\omega}{2\pi}\int_{-\frac{\pi}{\omega}}^{+\frac{\pi}{\omega}} d_1\mathbf{E}(t) d_0\mathbf{J}(2t_0-t)\, dt, \quad (8)$$

where we have integrated over λ holding t fixed.

Substituting Eqs. (6) and (4) into Eq. (7), we find

$$\sum_n e^{2jn\omega t_0}\, \mathrm{div}\,(d_0\mathbf{H}_n \times d_1\mathbf{E}_n - d_1\mathbf{H}_n \times d_0\mathbf{E}_n)$$
$$= \frac{\omega}{2\pi}\int_{-\frac{\pi}{\omega}}^{+\frac{\pi}{\omega}} \sum_{k,l} \sigma^{(k,l)}(2t_0 - \quad$$
$$[d_0E^{(l)}(2t_0-t)d_1E^{(k)}(t) - d_1E^{(l)}(2t_0-t)d_0E^{(k)}(t)]\, dt. \quad (9)$$

Now a new time variable t' is introduced,

$$t = t' + t_0.$$

Thus the right-hand side of Eq. (9) becomes

$$\frac{\omega}{2\pi}\int_{-\left(\frac{\pi}{\omega}\right)-t_0}^{+\left(\frac{\pi}{\omega}\right)-t_0} \sum_{k,l} \sigma^{(k,l)}(t_0-t')[d_0E^{(l)}(t_0-t')d_1E^{(k)}(t_0+t')$$
$$- d_1E^{(k)}(t_0-t')d_0E^{(l)}(t_0+t')]\, dt'.$$

According to Condition 2 for the reciprocity theorem (see Sec. 5·5), there exists a time zero with respect to which $d\mathbf{E}$ is an even function of

time. Let t_0 be this time zero. The preceding expression then vanishes identically; from Condition 1, this result holds over the whole barrier.

The right-hand side of Eq. (9) now vanishes over the entire region R. Integrating Eq. (9) over R and converting to a surface integral over S by the divergence theorem we obtain

$$\sum_n e^{2jn\omega t_0} \int_S (d_0\mathbf{H}_n \times d_1\mathbf{E}_n - d_1\mathbf{H}_n \times d_0\mathbf{E}_n) \cdot d\mathbf{S} = 0.$$

The field quantities vanish everywhere over the surface except at the terminals. At the d-c terminals the only term appearing is that for $n = 0$. At the r-f terminals the only terms appearing are for $n = \pm 1$. The integration over the terminals is straightforward and, in terms of the terminal voltages and currents,

$$2(d_0i_0d_1e_0 - d_1i_0d_0e_0) + \text{Re}\,[e^{2j\omega t_0}(d_0i_1d_1e_1 - d_1i_1d_0e_1)] = 0.$$

From Eq. (2),

$$d_1e_0 = d_0e_1 = 0;$$

hence,

$$2d_1i_0d_0e_0 = \text{Re}\,(e^{2j\omega t_0}d_0i_1d_1e_1). \tag{10}$$

The relations between the variations of the terminal currents and voltages are given by Eq. (5·15). Substituting Eq. (5·24) into Eq. (5·15), we find

$$\left.\begin{aligned} di_0 &= g_{\beta\beta}de_0 + \tfrac{1}{2}y_{\beta\alpha}de_1 + \tfrac{1}{2}y^*_{\beta\alpha}de^*_1 \\ di_1 &= 2y_{\alpha\beta}de_0 + y_{\alpha\alpha}de_1 + y_{\alpha\gamma}de^*_1. \end{aligned}\right\} \tag{11}$$

Substituting Eq. (11) into Eq. (10) we obtain

$$\text{Re}\,[(y_{\beta\alpha} - y_{\alpha\beta}e^{2j\omega t_0})d_1e_1] = 0.$$

Since the phase of d_1e_1 is arbitrary, we have

$$y_{\beta\alpha} = y_{\alpha\beta}e^{2j\omega t_0}, \tag{12}$$

which is the first of the reciprocity relations, Eq. (5·49).

If, instead of defining d_1 and d_0 by Eq. (2), we define them instead by

$$d_1i_0 = d_0i_1 = 0,$$
$$d_1i_1 \neq 0, \qquad d_0i_0 \neq 0,$$

and follow a similar procedure, we obtain

$$y^*_{\alpha\gamma} = y_{\alpha\gamma}e^{4j\omega t_0}, \tag{13}$$

which is the second of the reciprocity relations, Eq. (5·50).

APPENDIX B

SKIN EFFECT AT A METAL-SEMICONDUCTOR CONTACT[1]

The skin depth δ in a conductor of dimensions large compared with δ is given by

$$\delta = \frac{1}{\sqrt{\pi f \mu \sigma}}, \tag{1}$$

where f is the frequency and μ and σ are, respectively, the permeability and conductivity of the conducting material.

For tungsten we may take $\mu = \mu_0$ and $\sigma = 1.8 \times 10^5$ mho cm^{-1}. In this case we have, for

$$f = 3 \times 10^9 \text{ cps}, \qquad \delta = 2.2 \times 10^{-4} \text{ cm};$$
$$f = 1 \times 10^{10} \text{ cps}, \qquad \delta = 1.2 \times 10^{-4} \text{ cm};$$
$$f = 2.4 \times 10^{10} \text{ cps}, \qquad \delta = 0.65 \times 10^{-4} \text{ cm}.$$

In the case of silicon and germanium as used in rectifiers, the conductivity is less than that of tungsten by a factor of 10^{-3} or 10^{-4} and the skin depth is thus greater by a factor of 30 to 100. Now the radius of the rectifying contact varies from 10^{-3} cm to 2×10^{-4} cm. There is thus in general an appreciable skin affect in the cat whisker and practically none in the semiconductor. The above estimations do not apply, however, to the immediate neighborhood of the semiconductor-metal contact. To find the spatial distribution of current at the contact we must solve a boundary-value problem, taking into account the discontinuity in conductivity. In this way it can be determined whether the redistribution of current-flow lines from a decided skin effect in the whisker to a negligible effect in the semiconductor (1) takes place mostly in the metal; (2) takes place mostly in the semiconductor; or (3) is divided about equally between them.

The solution of this problem is presented here. It will appear that Alternative (1) is the correct one; the skin effect at the contact is therefore in general very small.

As a simple model there will be considered two semi-infinite right-circular cylinders, one of metal M, the other of semiconductor S having the same diameter and connected coaxially with a nonrectifying butt joint as shown in Fig. (B·1). Although this model is much simplified it will be shown that the conclusions drawn from it apply to the more general case.

[1] H. C. Torrey, "Colloquium on Crystal Rectifiers, "Vacuum Tube Development Committee Offices, New York, N. Y., June 17, 1944.

The subscripts 1 and 2 denote quantities in the metal and semiconductor, respectively. Then[1] at $z \approx -\infty$,

$$\mathbf{i}_1 = \frac{I_0\left(\sqrt{jP_1}\,\rho\right)}{I_0\left(\sqrt{jP_1}\,a\right)}\,\mathbf{i}_{01}, \tag{2}$$

where

$\mathbf{i}_1$ = current density at radial distance ρ from the axis,

$P_1 = 2\pi\mu_1\sigma_1 f$, (3)

$\mathbf{i}_{01}$ = current density at the surface ($\rho = a$).

A similar result with subscript 2 instead of 1 holds in the semiconductor at $z \approx +\infty$. Then Eq. (2), with appropriate subscripts,

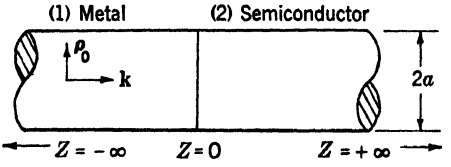

FIG. B·1.—Semi-infinite cylinders of metal and semiconductor in contact.

will serve as the boundary condition on $\mathbf{i}$ at distances remote from the contact.

The current density satisfies the differential equation,

$$\nabla \times \nabla \times \mathbf{i} = -jP\mathbf{i}, \tag{4}$$

and the continuity equation,

$$\nabla \cdot \mathbf{i} = 0. \tag{5}$$

Introducing the radial and axial components of $\mathbf{i}$ by

$$\mathbf{i} = i_z\mathbf{k} + i_\rho\boldsymbol{\rho}_0, \tag{6}$$

where $\mathbf{k}$ and $\boldsymbol{\rho}_0$ are the unit axial and radial vectors, we obtain from Eqs. (4) and (5) the differential equations,

$$\frac{\partial^2 i_z}{\partial\rho^2} + \frac{1}{\rho}\frac{\partial i_z}{\partial\rho} + \frac{\partial^2 i_z}{\partial z^2} - jPi_z = 0; \tag{7}$$

$$\frac{\partial^2 i_\rho}{\partial\rho^2} + \frac{1}{\rho}\frac{\partial i_\rho}{\partial\rho} + \frac{\partial^2 i_\rho}{\partial z^2} - \left(jP + \frac{1}{\rho^2}\right) i_\rho = 0. \tag{8}$$

[1] See, for example, William R. Smythe, *Static and Dynamic Electricity*, McGraw-Hill, New York, 1939, Sec. 11·03.

These equations are to be solved subject to the boundary conditions,

(a) for i_z;

$$\text{at } z = \pm\infty, \qquad i_z = \frac{I_0(\sqrt{jP}\,\rho)}{I_0(\sqrt{jP}\,a)}\, i_0; \tag{9}$$

$$\text{at } z = 0, \qquad (i_z)_1 = (i_z)_2; \tag{10}$$

$$\text{at } \rho = 0, \qquad i_z \text{ is finite}; \tag{11}$$

(b) for i_ρ;

$$\text{at } z = \pm\infty, \qquad i_\rho = 0; \tag{12}$$

$$\text{at } \rho = 0 \text{ or } a, \qquad i_\rho = 0; \tag{13}$$

$$\text{at } z = 0, \qquad \left(\frac{i_\rho}{\sigma}\right)_1 = \left(\frac{i_\rho}{\sigma}\right)_2. \tag{14}$$

The last condition ensures the continuity of the tangential component of the electric field vector across the contact.

By standard methods we find a general solution of Eq. (8) which satisfies Conditions (12) and (13):

In metal:

$$i_{\rho 1} = \sum_n B_{1n} J_1\left(\frac{x_n \rho}{a}\right) e^{+\sqrt{jP_1 + \frac{x_n^2}{a^2}}\cdot z}; \tag{15}$$

In semiconductor:

$$i_{\rho 2} = \sum_n B_{2n} J_1\left(\frac{x_n \rho}{a}\right) e^{-\sqrt{jP_2 + \frac{x_n^2}{a^2}}\cdot z}; \tag{16}$$

where $x_n (n = 1, 2, \cdots)$ are the roots of

$$J_1(x) = 0, \tag{17}$$

and $J_1(x)$ is the usual Bessel function (its subscript is not to be confused with subscripts used to distinguish metal from semiconductor).

To satisfy Eq. (14) we must have

$$\frac{B_{1n}}{\sigma_1} = \frac{B_{2n}}{\sigma_2}. \tag{18}$$

The corresponding solutions for i_z are now found from Eqs. (7) and (5):

$$i_{1z} = f_1(\rho) + \sum \frac{x_n/a}{\sqrt{jP_1 + \frac{x_n^2}{a^2}}} B_{n1} J_0\left(x_n \frac{\rho}{a}\right) e^{+\sqrt{jP_1 + \frac{x_n^2}{a^2}}\cdot z}; \tag{19}$$

$$i_{2z} = f_2(\rho) - \sum \frac{x_n/a}{\sqrt{jP_2 + \frac{x_n^2}{a^2}}} B_{n2} J_0\left(x_n \frac{\rho}{a}\right) e^{-\sqrt{jP_2 + \frac{x_n^2}{a^2}}\cdot z}; \tag{20}$$

where

$$f(\rho) = \frac{I_0(\sqrt{jP}\rho)}{I_0(\sqrt{jP}a)} i_0. \tag{21}$$

As they stand, Eqs. (19) and (20) obviously satisfy Eq. (9). The only remaining boundary condition to be satisfied is Eq. (10). This condition, with Eq. (18), determines B_{1n} and B_{2n}.

Putting $(i_z)_1 = (i_z)_2$ at $z = 0$ in Eqs. (19) and (20), we get

$$f_2(\rho) - f_1(\rho) = \sum_n A_n J_0\left(x_n \frac{\rho}{a}\right), \tag{22}$$

where

$$A_n = \frac{x_n}{a} \frac{B_{1n}}{\sigma_1} \left\{ \frac{\sigma_1}{\sqrt{jP_1 + \frac{x_n^2}{a^2}}} + \frac{\sigma_2}{\sqrt{jP_2 + \frac{x_n^2}{a^2}}} \right\}. \tag{23}$$

The coefficients A_n are now determined from Eq. (22) by use of the well-known orthonormal properties of the Bessel functions. The final result for B_n is

$$\frac{B_{1n}}{\sigma_1} = \frac{B_{2n}}{\sigma_2} = \frac{2}{x_n J_0(x_n)} \frac{\alpha_2 - \alpha_1}{\beta_2 + \beta_1}, \tag{24}$$

where

$$\alpha = \frac{i_0 \sqrt{jP} \cdot a I_1(\sqrt{jP} \cdot a)}{(jPa^2 + x_n^2) I_0(\sqrt{jP} \cdot a)}, \tag{25}$$

and

$$\beta = \frac{\sigma}{\sqrt{jPa^2 + x_n^2}}. \tag{26}$$

Expressions (24), (25), and (26) are now substituted in (20). Putting $z = 0$, and assuming $\sigma_2 \ll \sigma_1$ we obtain for the axial component of current density at the contact,

$$i_c = f_2(\rho) + \bar{i} P_2 a^2 \sum_{n=1}^{\infty} \frac{J_0\left(\frac{x_n \rho}{a}\right)}{J_0(x_n) \sqrt{(x_n^2 + jP_1 a^2)(x_n^2 + jP_2 a^2)}} \tag{27}$$

where $\bar{i}$ is the mean axial current density,

$$\bar{i} = \frac{1}{\pi a^2} \int_0^\infty i_c \cdot 2\pi\rho d\rho.$$

In (27) the root $x_n = 0$ is excluded from the summation.

Now the current density is entirely axial at $\rho = 0$ and $\rho = a$. To estimate the magnitude of the skin effect at the contact, two quantities

from Eq. (27), will be computed, viz., $\left|\frac{i_{c(\rho=0)}}{i_{c(\rho=a)}}\right|^2$ and the phase shift in i_c from $\rho = 0$ to $\rho = a$.

These two quantities give all the relevant information. The first gives the magnitude of the heating effect and the second bears on the question of the validity of one of Dicke's conditions for reciprocity.

The magnitude of both effects will turn out to be small. There can then be used *a fortiori* arguments to show that the effects are even smaller for the case of an actual rectifier including the nonlinearity of the contact resistance and the different geometry.

As an example we take,

$$a = 1.1 \times 10^{-3} \quad \text{cm}$$
$$f = 3 \times 10^{9} \quad \text{cps}$$
$$\sigma_2 = 50 \quad \text{mho/cm.}$$

We then find

$$P_2 a^2 = 1.46 \times 10^{-2}$$
$$P_1 a^2 = 53.1.$$

From Eq. (27),

$$i_c = \bar{i}(1 + 1.28 \times 10^{-3} + j5.01 \times 10^{-3}) \qquad (\rho = a),$$
$$i_c = \bar{i}(1 - 0.959 \times 10^{-3} - j2.43 \times 10^{-3}) \qquad (\rho = 0).$$

The phase shift over the contact is then 7.4×10^{-3} radian, or 0.42°.

If $\Delta|i|^2$ is the difference in the square of the absolute value of the axial currents at $\rho = 0$ and $\rho = a$, we have

$$\frac{\Delta|i|^2}{|\bar{i}|^2} = 2(1.28 + 0.96) \times 10^{-3}$$
$$= 4.5 \times 10^{-3}.$$

The heating effect is, therefore, less than one-half of one per cent.

It is interesting to note that, although the skin effect is small at the contact, it is still much larger there than in the body of the semiconductor, where the differential heating is of the order 10^{-5} or 0.01 per cent.

The effect at the frequency 3×10^9 cps has been computed for about the largest contact it is practicable to use at that frequency. The maximum size of the contact at higher frequencies will be less. The conversion loss is roughly a function of fCr (as we saw in Sec. 4·5), where C is the barrier capacitance and r the spreading resistance. Now, $C \propto a^2$ and $r \propto 1/a$, so the loss is a function of fa. The skin effect, however, depends on fa^2. If we assume that fa (or loss) is kept constant by decreasing a as the frequency is increased, then fa^2, and hence the skin effect, will be less at higher frequencies.

Furthermore, the skin effect for the actual geometry of a rectifier, in which the semiconductor is a semi-infinite cylinder of larger dimensions, will be less than for the geometry of the model assumed. Finally, the effect of the nonlinear resistance can only decrease the skin effect, since the effective conductivity will be less than that of the bulk semiconductor.

It follows from this reasoning that the skin effect is entirely negligible for all point-contact rectifiers at any microwave frequency and the current flow at the contact may be treated with the d-c approximation.

APPENDIX C

SPREADING RESISTANCE OF AN ELLIPTICAL CONTACT

The contact surface between metal and semiconductor is approximated by an ellipse of semidiameters a, b ($a \gg b$) and rectangular axes chosen so that the x-y plane contains the contact surface, the long dimension of the contact being along the x-axis. Ellipsoidal coordinates ξ, ζ, η are now defined by

$$f(\theta) = \frac{x^2}{a^2 + \theta} + \frac{y^2}{b^2 + \theta} + \frac{z^2}{\theta} = 1, \tag{1}$$

where θ stands for any one of the triplet (ξ, ζ, η) and

$$\xi \geqq 0 \geqq \eta \geqq -b^2 \geqq \zeta \geqq -a^2.$$

The confocal ellipsoids, ξ = constant, are the equipotential surfaces of the problem, since for $\xi = 0$, $f(\xi) = 1$ degenerates into the elliptical contact. Laplace's equation for the potential V becomes

$$\frac{\partial}{\partial \xi}\left[\sqrt{(\xi + a^2)(\xi + b^2)\xi}\,\frac{\partial V}{\partial \xi}\right] = 0.$$

Thus,

$$V = A \int_0^{\xi} \frac{d\xi}{\sqrt{(\xi + a^2)(\xi + b^2)\xi}}, \tag{2}$$

where A is an integration constant.

According to Eq. (2), $V = 0$ at the whisker contact, and if $V = V_0$ (the applied potential) at $\xi = \infty$,

$$A^{-1} = \frac{1}{V_0} \int_0^{\infty} \frac{d\xi}{\sqrt{(\xi + a^2)(\xi + b^2)\xi}}.$$

Thus Eq. (2) becomes

$$V = \frac{V_0}{K} \operatorname{sn}^{-1}\left(\sqrt{\frac{\xi}{\xi + b^2}}, k\right), \tag{3}$$

where

$$k = \sqrt{1 - \frac{b^2}{a^2}},$$

and

$$K = \operatorname{sn}^{-1}(1,k)$$

is the complete elliptic integral of the first kind with modulus k. Now if r is the radial distance from the center of the contact, as r becomes large, $\xi \approx r^2$ and

$$V \approx V_0\left(1 - \frac{a}{Kr}\right).$$

The current is thus

$$\begin{aligned} I &= 2\pi r^2 \sigma \frac{\partial V}{\partial r} \\ &= \frac{2\pi\sigma a}{K} V_0, \end{aligned}$$

where σ is the conductivity; and the resistance is

$$R = \frac{K}{2\pi\sigma a}. \tag{4}$$

This result is general.

So far, the condition that $a \gg b$ has not been used. In fact, if $a = b$, then $K = \pi/2$ and $R = 1/4\sigma a$, the well-known result for a circular contact of radius a. If $a \gg b$, $k \approx 1$, and $K \approx \ln (4a/b)$. Thus for a long, thin contact,

$$R = \frac{\ln 4\dfrac{a}{b}}{2\pi\sigma a}. \tag{5}$$

APPENDIX D

CRYSTAL-RECTIFIER TYPES AND SPECIFICATIONS

The specifications on electrical performance of the various crystal types as of September 1945 are listed in Tables D·1, D·2, and D·3. The mechanical tests are summarized in Sec. 2·2.

A summary of the JAN specifications[1] for the mixer and video crystal types is given in Tables D·1 and D·2 respectively. The tentative specifications on the Western Electric high-inverse-voltage types were written jointly by the Bell Telephone Laboratories, Radiation Laboratory, and the NDRC group at Purdue University and have not yet been incorporated in the JAN specifications. The 1N34 rectifier was initiated by Sylvania Electric Products, Inc. and will probably soon be available from other manufacturers.

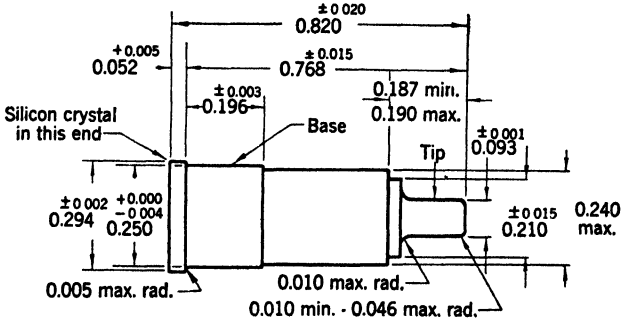

FIG. D·1.—Mechanical design specifications for the ceramic cartridge.

Test methods and equipment that meet the requirements of the JAN specifications for testing mixer and video crystals are described in detail in Chaps. 9 and 11 respectively. Equipment for testing the high-inverse-voltage types listed in Table D·3 was described in Chap. 12.

The mechanical design specifications for the ceramic and coaxial cartridges are shown in Figs. D·1 and D·2, respectively.

Comments on the Specifications.—The wavelengths given in Column 2 of Tables D·1 and D·2 designate the approximate region for which the various types are adapted. Rectifiers passing the tests at a particular

[1] The quantities listed in Columns 4–13 are taken from the JAN specifications. No attempt has been made to include all of the details of these specifications. For complete detailed information the reader is referred to the joint Army-Navy Specifica- into JAN-1A for Electron Tubes.

radio frequency will in general be as good in conversion loss at lower frequencies. The converse may not, however, be true. The types designed for higher radio frequency usually are adjusted for smaller contact area to achieve a smaller barrier shunting capacitance. This at the same time makes for lower burnout. The specifications, moreover, which call for specified r-f and i-f matching conditions in the test equipment, tend to insure uniformity in r-f and i-f rectifier impedances. These considerations make it advisable to use the various types only for the frequency band for which they were tested.

The various mixer types within each band are, with one exception, interchangeable as far as impedance-matching properties are concerned.

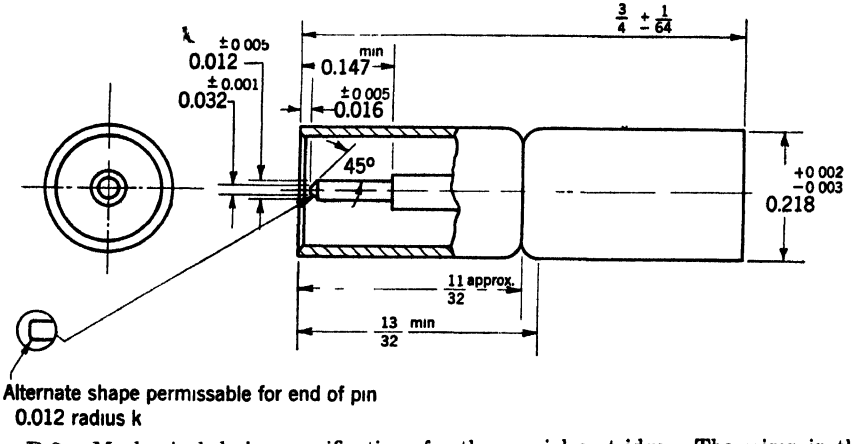

FIG. D·2.—Mechanical design specifications for the coaxial cartridge. The crimp in the cartridge may be omitted if desired.

They differ only in sensitivity and burnout. The one exception is type 1N28, which differs from the 1N21 types in r-f and i-f impedance. The distribution in i-f impedance centers around 250 ohms, compared with 400 ohms for the 1N21 types. The r-f tuning of the test mixer is in each case standardized at the center of the r-f impedance spread of representative samples from the various manufacturers.

Each unit is subjected to the burnout proof test and a small specified representative fraction of the total production to the burnout design test.

The types for which the burnout test value is listed in ergs are tested by subjecting the rectifier to a single video pulse of short duration compared with the thermal relaxation time of the rectifier contact. The value listed in the table is the amount of energy dissipated in the crystal.

The types for which the burnout test value is listed in watts are tested by subjecting the crystal to a number of video pulses of 1-μsec duration, a time long compared with the thermal relaxation time of the crystal.

TABLE D·1.—MIXER TYPES

Type No.	Band λ, cm	Description	P, mw	Max L, db	Max t	B_p	$Z_{i\text{-}f}$, ohms	Z_m, ohms	R_L, ohms	R_c, ohms	Min I	f, Mc/sec
1N21	9–11	obsolete	0.5	8.5	4	.....	.....	..	.....	..	0.4	3060
1N21A	9–11	medium sensitivity low burnout	0.5	7.5	3	0.3 erg	...	.	75–100	300	0.4	3060
1N21B	9–11	high sensitivity medium burnout	0.5	6.5	2	2.0 erg	.....	400	100	400	0.4	3060
1N21C	9–11	most sensitive medium burnout	0.5	5.5	1.5	2.0 erg	.....	400	100	400	0.4	3060
1N23	3–5	low sensitivity low burnout	1.0	10.0	3	0.3 erg	.....	400	100	300	...	9375
1N23A	3–5	medium sensitivity medium burnout	1.0	8.0	2.7	1.0 erg	.....	400	100	300	...	9375
1N23B	3–5	high sensitivity low burnout	1.0	6.5	2.7	0.3 erg	.....	400	100	300	....	9375
1N25	25–30	high burnout	1.25	8.0								
1N25			0.9	....	2.5	6.5 watt	100–400	200	100	200	...	1000
1N26	1–1.5	medium sensitivity low burnout	1.0	8.5	2.5	0.1 erg	300–600	500	100	300	...	24000 9375
1N28	9–11	medium sensitivity high burnout	0.4	7.0	2.0	5.0 erg	.....	...	.....	...	0.4	3060

Key to symbols:

- P R-f power level, using the modulation test method
- L Conversion loss
- t Noise temperature
- B Specification value for burnout proof test
- $Z_{i\text{-}f}$ Resistance at audio frequency seen at the i-f terminals of the mixer
- Z_m Load impedance presented to the i-f terminals of the mixer at the modulation frequency
- R_L D-c load resistance
- R_c Input impedance of the i-f amplifier used in the noise measurements as seen at the terminals of the crystal holder
- f Radio frequency used for testing

The intermediate frequency for the noise measurement is in all cases 30 Mc/sec

The value listed in the table is the maximum available power in the pulse. The test for the 1N25 unit specifies a minimum of 50 pulses. A group burnout test at 26 watts pulse power, not listed in Table D·1, is also specified for the 1N25 unit. The 1N31 and 1N32 types call for a 1-min exposure to video pulses at a minimum pulse-repetition frequency of 800 pps.

TABLE D·2.—VIDEO CRYSTAL TYPES

Type No.	Band λ, cm	Description	Min M	R_a, ohms	Max P, μw	R_v, kilohms	Max E, mv	B_d, w	B_p, ergs	f, Mc/sec
1N27	9–11	for pulse discriminating receivers	60	1200	5	4 (max)	1	....	...	3295
1N30	3–5	ceramic cartridge	55	1200	5	7–21	5	....	0.3	9375
1N31	3–5	coaxial cartridge improved stability	55	1200	5	6–23	5	0.02	...	9375
1N32	9–11	high sensitivity	100	1200	5	5–20	5	0.36	...	3295

Key to symbols:

- M Figure of merit
- R_a Fictitious series resistance in grid circuit of input tube, whose noise contribution is equivalent to the amplifier noise; used to calculate M.
- P R-f power level at which measurement is made
- R_v Video resistance (equivalent to the d-c resistance in the forward direction at low level)
- E D-c voltage used for d-c resistance measurement
- B_d Specification value for burnout design test
- B_p Specification value for burnout proof test
- f Radio frequency used for testing.

TABLE D 3 —HIGH-INVERSE-VOLTAGE RECTIFIERS
(Manufacturer's tentative specifications)

Type No	Description	Input frequency for test	Rectification in test circuit				Detection of 60-cps modulation at high level		Minimum peak back voltage, v d-c	Impedance at 30 Mc/sec, ohms	D-c resistance, megohms	Minimum current at +1 volt, ma
			Low-level test		High-level test							
			Input, volts (peak)	Minimum output, mv d-c	Input, volts (peak)	Minimum output, v d-c	Modulation on input, volts (peak) at 60 cps	Minimum output volts at 60 cps				
W.E. D171561	Second detector	30 Mc/sec	0 5	15	24 7	5	0 92*	0 10	50			
W E D171612	D-c restorer	30 Mc/sec	0 5	15					50	2000	0 1 (at −1 v)	
W E. D172925	D-c restorer	30 Mc/sec	0 5	15						2000	0 06 (at −50 v) 0 25 (at −5 v)	5
RMA No IN34	Crystal diode	60 cps	Input, v rms 30†		Output, v d-c 10†				50		0 025 (at −50 v) 0 2 (at −10 v)	5

* This voltage is the modulation of the 24 7-volt (peak) 30-Mc/sec carrier
† Tested with 500-ohm load resistance, no condenser.

Index

A

Acceptance testing, 128
Acceptors, 47
Addition agents, 67, 306–308, 364
(*See also* particular addition agent)
Admittance matrix, 114–118
in terms of measurable parameters, 119–124
Admittance matrix elements of welded-contact rectifiers, 407
Aluminum, as addition agent, 67
American Lava Corporation, 323
Amplitude-modulation method of loss measurement, 215–218
Angello, S. J., 307, 315, 321
Antimony, as addition agent, 67
Apker, L., 126, 166, 174, 175, 407
Artificial barrier, 75
Attenuator, micrometer, 275
vane-type, 285

B

Back current, at one volt, germanium rectifier, 374
at 30 volts, germanium rectifier, 374
Back-to-front ratio, 297
Back voltage, peak (*see* Peak inverse voltage)
Bakker, C. J., 182
Band theory, 45–48
Barrier capacitance, 24
variable, effect of, 163–167
variation of, with bias, 77
Barrier layer, capacitance of, 75–77
formation and structure of, 70–77
Barrier-layer rectification (*see* Rectification, barrier-layer)
Becker, J. A., 317
Bell, P. R., 394
Bell Telephone Laboratories, 9, 22, 26, 34, 128, 207, 256, 276, 304, 306, 307, 311, 313, 314, 318, 321, 325, 326, 362–365 367–375, 378, 382, 387, 406, 429
Benzer, S., 361–363, 370, 376, 380, 391, 392, 394–396
Beringer, E. R., 100, 232, 334, 335, 338, 340, 344, 345, 349, 353, 354, 403, 405, 406, 415
Bernamont, J., 193
Beryllium, as addition agent, 67
Bethe, H. A., 48, 65, 72–73, 82, 85, 93, 98, 414
Bias (*see* D-c bias)
Boron, as addition agent, 67
for use as crystal rectifiers, 7
Boyarsky, L., 364, 370, 372, 377, 381, 384, 387, 388
British red-dot crystal, 8, 91, 99
British-Thomson-Houston Company, 317
Broadband case, 128
Bulk resistance, 83
Bulk resistivity measurement, 304
Burnout, 236–263
affected by design, 329
caused by harmonic leakage, 238
causes of, 236
by continuous d-c power, 256–258
definition of, 236
edge, 253
by long pulses, theory of, 241–248
by short d-c pulses, 258–260
by short pulses, theory of, 248–256
temperature at, 257
Burnout experiments, 256–263
Burnout limitations of standard crystal units, 260
Burnout test, using coaxial line, 293

Burnout testing, 239, 293–300
with microsecond d-c pulses, 296
Burnout theory, 239–256

C

Capacitance, of barrier (*see* Barrier capacitance)
Cartridge, assembly and adjustment of, 323–328
crystal, present, 15–20
crystal rectifier, 16
description of, 15–18
germanium rectifier, adjustment of, 369–372
assembly of, 369–372
standard-impedance, 270
(*See also* Ceramic; Coaxial; Pigtail; Resistor; etc.)
Cartridge parts, crystal, 322
Cat whisker (*see* Whisker, cat)
Ceramic cartridge, 16, 17, 323–326
Characteristic, d-c, 82–90
of typical germanium rectifier, effect of temperature on, 375
voltage-current, 20–23
Christensen, C. J., 193
Coaxial cartridge, 17, 326–328
Colonial Alloys Company, 316
Conductivity, electrical, 53–61
Contact, long thin, 247
Contact capacitance with voltage, variability of, 398
Contact geometry, ideal, from point of view of burnout by short pulses, 254
Contact potential, 51–53
distributed, 183
uniform, 182
Contact temperature, as a function of time, 248–254
Conversion, frequency, 4, 111–178
phenomenological theory of, 119–152
physical theory of, 152–170
with subharmonic local oscillator, 114, 170–173
Conversion amplification, 398
theory of, 406–415
Conversion loss, 25
affected by design, 329
in broadband case, 130–135
effect of parasitic impedances on, 157–163
Conversion loss, as function of image-impedance, 202
as function of image tuning, 212
as function of r-f tuning, 232–235
general definition of, 128
general expression for, 136–140
image termination on, effect of, 140–148
measurement of, 231
of network, 26
production testing methods of, 213–218
range of, in production units, 32
special definitions of, 128
of welded-contact rectifier, measurement of, 403–406
Conversion loss L_0, mixer matched to local oscillator, 133
Conversion loss measurements, method of, 198–218, 227–235
Conversion-loss test set, for 1-cm band, 276–280
calibration of, 280
for 3-cm band, 265–272
adjustment of, 271
calibration of, 271
for 10-cm band, 272–276
Conversion-loss test sets, standard, 264–283
Conwell, E., 58
Cornell University, 87
Coupling circuit, 286
narrow-band, 225
Roberts, 223–225
Coupling-circuit tuning, 286
Courant, E., 87
Crystal, as microwave noise generator, 195–197
as noise generator, 229
standard, 201
calibration of, 272
Crystal cartridge (*see* Cartridge; type of cartridge)
Crystal checker, d-c, 297
limitations of, 298
reliability of, 300
Crystal holder, 267
fixed-tuned, for video-crystal testing, 351
tunable, for video-crystal testing, 351
variable-tune, for video-crystal testing in 3-cm band, 353

Crystal holder, waveguide, 278
Crystal-output circuit, 269
Crystal properties, effect on, of phase of reflected wave at image frequency, 233
Crystal rectifier (*see* Rectifier, crystal)
Current sensitivity, 335–340, 342
  equipment for measurement of, 349–357
  methods of measurement of, 349–357

D

D-c bias, effect of, on figure of merit of video crystal, 347
  on low level properties, 340–342
  on noise temperature of germanium rectifiers, 35
  on silicon crystal-mixer performance, 34
D-c characteristic (*see* Characteristic, d-c)
D-c crystal impedance, 333
D-c resistance, comparison of, with i-f resistance, 41
  measurement of, 40
Depletion layers, 90–97
Detection, 2–4
  (*See also* Linear; Low-level; Square-law; etc.)
Detector, second (*see* Second detector)
Dicke, R. H., 43, 119, 124, 197, 203, 413, 416, 417
  reciprocity theorem of, 417–420
Dicke method of loss measurement, 203–207
Dickey, J., 174
Diffusion theory of rectification, 77–81
Diode theory of rectification, 78, 81–82
Donators, 47
Doping materials (*see* Addition agent)
Double layer, 53
Du Pont De Nemours Company, E. I., 67, 305

E

Eagle-Picher Company, 304, 305
Electrical performance, design considerations affecting, 328–330
Electrolytic pointing, 319
Electrolytic polishing process, 318
Electron distribution in semiconductors, 48–51
Equivalent circuit (*see* component for which equivalent circuit is given)
Etching, 314–316, 369
Exhaustion layer, 78

F

Falkoff, D. L., 113, 170
Field testing for burnout, 297–300
Figure of merit, 239
  equipment for measurement of, 355–357
  methods of measurement of, 355–357
  of video crystal, 344–347
    effect of d-c bias on, 347
Fixed-tuned measurements, 214
Flat, 237
  and spike, relative importance of, in burnout, 237
Fluctuation effects, 87–90
Fonda Inc., J. C., 265, 284
Forbidden region, width of, 64
Formation, of barrier layer, 70–77
Forward conductance, as function of frequency, 378–380
  of various germanium ingots, 373
Fowler, R. H., 45, 49, 50–54
Fox, M., 91, 99, 307, 314, 315, 318, 392
Frequency, variation of impedance with, 39
Friis, H. T., 26, 128

G

Gadsden, C. P., 403
Gain, conversion (*see* Conversion loss)
Gain of network, 26
Gant, D. H. T., 246
General Electric Company, 11, 21, 35, 126, 166, 173, 174, 304, 308, 313, 314, 398, 402, 411, 415
General Electric Company, Ltd., of England, 91, 303, 307
General Electric crystal cartridge for germanium crystals, 328
Generator of millimeter radiation, welded-contact rectifier as, 398
Germanium, addition agents for, 308
  characteristic constants of, 61
  photoelectric effects in, 393–397
  purification of, 304–306

Germanium crystal rectifier, 10
Germanium crystals, General Electric crystal cartridge for, 328
welded-contact, 21, 398–416
Germanium etching, 316, 369
Germanium heat treatment, 316
Germanium polishing, 316
Germanium rectifiers, noise temperature, effect of d-c bias on, 35
Gibson, R. J., Jr., 389
Ginzton, E., 225
Goodman, B., 392
Goudsmit, S. A., 182
Greenblatt, M. H., 101, 193, 392
Gurney, R. W., 45, 79, 101, 103

H

Hahn, W. C., 411, 414
Hall coefficient, 53–61
Hall effect, 54
Harmonic generation, 173
Harmonic generator, welded-contact rectifier as, 398, 415
Harmonic reinforcement, 114, 167–170
Heat treatment, 91, 314–316
of germanium ingot, effect of, 316, 365
of silicon, 314–316
Heller, G., 182
Hennelly, 415, 416
Herzfeld, K. F., 82
Heterodyne method of loss measurement, 200–202
High-burnout crystals, 8
High-frequency properties, 378–389
High-inverse-voltage rectifier, 10, 64, 361–397
applications of, 363
as low-frequency rectifier, 363
silicon, 389–391
Holes, 48
Huntington, H. B., 34, 41, 238, 273, 289

I

I-f impedance, of crystals, 40–44
effect of, on Y-factor, 220
effect of image termination on, 148–152
of germanium crystal, 382–384
measurement of, 40
I-f resistance, comparison of, with d-c resistance, 41
crystal, measurement of, 230
I-f resistance, dependence of, on i-f matching conditions, 43
as function of rectified current, 42
I-f resistance spread of crystal rectifiers, 42
Image force, effect of, 86
Image-force lowering of barrier, 85
Image frequency, 112
Image impedance, effect of, on conversion loss, 202
Image termination, effect of, on conversion loss, 140–148
on i-f impedance, 148–153
Image tuning, effect of, on conversion loss, 212
Impedance, variation of, with frequency, 39
Impedance conversion loss, 208
Impedance loss, 203
Impedance methods of loss measurement, 202–213
Impedance tester, 383
Impurities, diffusion of, 93–97
(*See also* Addition agents)
Impurity activation energies, 61
Impurity additions, effect of, 64–67
Impurity atoms, with collisions, 58
Impurity level, 47
Incremental method of loss measurement, 213–215
Ingot, germanium, preparation of, 364–369
preparation of, 308–313
Intermediate frequency, 112

J

JAN specifications, 264
Johnson, V. A., 55, 58, 59, 63
Jones, H., 45

K

Kallman, H., 416
King, A. P., 6
Kingsbury, S. M., 327
Klystron, 417A, as noise generator, 229
Kuper, J. B. H., 44, 229

L

Lark-Horovitz, K., 58, 59, 61, 63, 91, 246, 304
Lawson, A. W., 24, 76, 93, 100, 103, 194, 256, 324, 335, 340

Lewis, M. N., 187, 190, 389
life tests of germanium rectifier, 377
Linear detection, 2
Llewelyn, F. B., 159, 207, 217
Llewelyn method of loss measurement, 207
Local oscillator, subharmonic, conversion with, 114, 170–173
Local-oscillator level, optimum, 33
Loss, conversion (*see* Conversion loss)
Low-frequency properties, 372–378
Low-level detection, 333–360
theory of, 344–349
Low-level detectors, measurements on, 349–357
special manufacturing techniques for, 357–360
Low-level properties, dependence of, on bias, 340–342
variation of, with temperature, 342–344
Low-Q mixer (*see* Mixer, low-Q)

Mc

McDonald, A. W., 364, 370, 377, 387
McKinley, T. D., 305
McMillan, F. L., 237

M

Magic T, 196
Manufacturing techniques, 301–330
special, for low-level detectors, 357–360
Marcum, J. I., 203
MIT Laboratory for Insulation Research, 327
Mean free path, 63
Measurement of (*see* quantity to be measured)
Mechanical modulation, 218
Mechanical modulator, 280–283
Meyerhof, W. E., 74, 339, 341–343, 347, 349, 358, 360
Microsecond pulse tests for burnout, 296
Middleton, A. E., 61
Miller, E. P., 61
Miller, P. H., 24, 76, 101, 187, 190, 193, 194, 324, 335, 340, 392
Minimum loss, L_2, in broadband case, 132
Mixer, crystal, as modulator, 148
low-Q, 115, 119
for 10-cm conversion-loss test set, 275
Mixer crystal, 7–9, 25–44
Mixer-crystal properties, measurement of, 230–232
Mixing, 111–114
Mobility, 54
carrier, 62
Modulation, 174–178
mechanical, 218
Modulation circuit, 268
Modulator, mechanical, 280–283
Modulator voltage, regulator for, 268
Montgomery, D., 173, 415
Mott, N. F., 45, 78, 79, 101, 103
Mullaney, J. F., 74

N

N-type semiconductor, 49
Natural barrier, 75
Negative i-f conductance, 398, 401
theory of, 406–415
Negative-resistance characteristics, theory of, 391
Negative-resistance region in back direction, 362
Neher, H. V., 6
Noise, dependence of, on temperature, 194
intermediate frequency, 187–195
dependence of, on excitation frequency, 188
sources of, 186
video, 187–195
spectrum of, 189–194
in welded-contact rectifier, measurement of, 403–406
Noise diode, 286
use of, in noise-temperature measurements, 226
Noise figure, 25–30
effective, 27
of i-f amplifiers, measurement of, 227
receiver, measurement of, 227–235
of two networks in cascade, 28–30
of welded-contact rectifier, 403–406
Noise generation, 179–197
theory of, 179–187
Noise generator, microwave, crystal as, 195–197
r-f, crystal as, 229
using 417A klystron, 229

Noise measuring set, for 3-cm band, 283–289
calibration of, 288
operation of, 288
for 10-cm band, 289–292
Noise temperature, 30, 179
dependence of, on frequency, 188–194
as function of r-f tuning, 232–235
as function of signal and image reflection, 234
measurement of, 218–235
range of, in production units, 32
Noise-temperature apparatus, calibration of, 227
Noise-temperature dependence on ambient temperature, calculated and observed, 195
Noise-temperature measurement, of 1-cm rectifiers, 292
using noise diode, 226
Noise test sets, standard, 283–293
Nonlinear element, 1
Nonlinear resistance of barrier, 24
Nonlinear resistance matrix, 153–157
Nordheim, L. W., 77
North, H. Q., 11, 21, 35, 128, 173, 304, 308, 313, 314, 317, 328, 398, 399, 403, 406, 411, 414–416
Nyquist, H., 181

O

Oscillator mount, 266
Output circuit, of 1-cm conversion-loss test set, 278
Output-meter circuit, 287
Output noise ratio, 30
(*See* Noise temperature)
Output resistance, dynamic, 333

P

P-type semiconductor, 49
Parasitic impedances, effect of, on conversion loss, 157–163
Parasitics, 112
Pasternack, S., 75
Peak inverse voltage, 362, 375
dependence of, on frequency, 380–382
Pearsall, C. S., 91, 307, 308, 314, 318, 392
Pearson, G. L., 193
Penetration of barrier, effect of, 85, 87
Pennsylvania, University of, 8, 24, 61, 75, 76, 93, 100, 101, 103, 187, 190, 193, 194, 256, 263, 307, 319, 324, 335, 339, 340, 341, 343, 354, 357, 358, 363, 389, 391, 392
Peterson, L. C., 159, 217
Pfann, W. G., 92, 318–320
Phenomenological theory of conversion, 119–152
Phosphorus, as addition agent, 67
Photodiode, 394
Photoelectric effects, in germanium, 393–397
in silicon, 392
Photopeak, 395
Photoswitch, Inc., 273, 289
Pickar, P. B., 364, 370, 377, 387
Pigtail cartridge, 18
Polishing, 314–316
Pound, R. V., 34, 174, 178, 208
Pound method of loss measurement, 208–212
Powell, Virginia, 307, 314
Preamplifier circuit, 287
Precautions, handling, 18–20
Preparation of (*see* item prepared)
Production testing methods, of loss measurement, 213–218
Production units, range of conversion loss and noise temperature in, 32
Purdue University, 10, 41, 55, 61, 80, 82, 83, 87, 89, 119, 125, 135, 166, 185, 215, 304, 306, 361, 363–365, 368–372, 376–378, 381–385, 387, 388, 391, 394, 396, 398, 399, 429
Purification of (*see* item purified)

R

Radiometer, microwave, 197
Receiver, crystal-video, 9
Reciprocity, 117, 124–128, 203
experimental tests of, 125–127
full, 118, 124
weak, 118, 124, 139, 203, 216
general condition of, 124
Reciprocity factor, 203
Reciprocity theorem of Dicke, 125, 417–420
Rectification, barrier-layer, 68–72
diffusion theory of, 77–81
diode theory of, 78, 81–82
efficiency of, 3

Rectification, as function of applied voltage, 379
at high frequencies, 97–107
at low levels, 333–335
at metal-metal contact, 68–70
by metal-semiconductor barrier, 72
phenomenon of, 1–5
Rectification efficiency, 388
Rectified current, as function of frequency, 379
i-f resistance as function of, 42
Rectifier, crystal, early use of, 5
electrical properties of, 20–25
equivalent circuit of, 23–25
germanium, 10
nature of, 5–11
properties of, at low levels, 333–344
recent developments of, 6–11
shot and thermal noise in, 179–186
silicon, 8
types and specifications of, 429–433
high-inverse-voltage (*see* High-inverse-voltage rectifier)
high-quality, general processes for making, 301
welded-contact (*see* Welded-contact rectifier)
Rectifying contact adjustment, for low-level detection, 359
Relaxation effects, 100–107
Reserve layer, 78
Resistance, bulk, 83
spreading (*see* Spreading resistance)
Resistor cartridges, 287
R-f components, 277, 285, 290
adjustment of, 269, 276, 279
R-f filter, 285
R-f impedance, affected by design, 328
of crystal rectifiers, 35–40
R-f impedance, effect of varying r-f power level on, 39
R-f matching, dependence of i-f resistance on, 43
R-f oscillator, 273
R-f power, measurement of, 206
R-f power level, effect of, on r-f impedance, 39
R-f terminals, standard position of, 128
R-f tuning, effect of, on conversion loss, 232–235
on noise temperature, 232–235
Rick, C. E., 305
Roberts, S., 26, 35, 119, 215, 219, 223, 265, 280, 284
Roberts coupling circuit, 223–225

S

Sachs, R. G., 80, 87
Scaff, J. H., 22, 304, 306, 362, 364, 366–368, 370, 372, 378
Schelkunoff, S. A., 155
Schiff, L. I., 24, 76, 187, 190, 324, 335, 340
Schottky, W., 78, 85, 180
Second detector, germanium crystal, type B test set for measuring performance of, 386
type C test set for measuring performance of, 388
performance of germanium crystal as, 384–388
Seitz, F., 8, 45, 48, 50, 53, 54, 61, 69, 74, 75, 101, 103, 240, 307
Semiconduction, extrinsic, 47
intrinsic, 47
Semiconductor-metal contact, 68–107
Semiconductors, band theory of, 46–48
composite, 54, 55
electron distribution in, 48–51
N-type, 49
P-type, 49
preparation of, 301–316
properties of, 45–67
purification of, 301–306
thermal resistance of, 243, 245
Serin, B., 74, 93, 95, 341–343, 347, 349
Sharpless, W. M., 34, 276
Sherwood, E., 225
Shot noise, 180
in crystal rectifiers, 179–186
Sidebands, harmonic, 112
Silicon, addition agents for, 306–308
characteristic constants of, 61
etching of, 314–316
heat treatment of, 314–316
photoelectric effects in, 392
polishing of, 314–316
processing of, for low-level detectors, 358
purification of, 301–304
Silicon crystal mixer performance, effect of d-c bias on, 34
Silicon crystal rectifiers, 8
Sinclair, D. B., 338

Skin effect at metal-semiconductor contact, 421–426
Smith, A. H., 343, 349, 358
Smith, R. N., 41, 77, 119, 125, 135, 146, 166, 185, 215, 364, 370, 377, 381, 382, 384, 387, 388
Smythe, W. R., 249
Southworth, G. C., 6
Special types, development of, 9–11
Specifications of crystal rectifiers, 429–433
  comments on, 429
Spenke, E., 78
Sperry Gyroscope Company, 225, 318
Sperry Research Laboratories, 396
Spike, 237
  and flat, relative importance of, in burnout, 237
Spike test for burnout, 293–295
Spreading resistance, 24, 83
  of elliptical contact, 427
  local, 88
Square law, 333
Square-law detection, 3
Stability, 18–20
Stanco Distributors, 325
Standard position of r-f terminals, 128
Stephens, W. E., 24, 74, 76, 93, 95, 99, 187, 190, 194, 324, 335, 339, 340, 343, 349, 358, 389, 392
Stever, H. Guyford, 303
Structure, of barrier layer, 70–77
Sum frequency, 112
Surface levels, 101, 107
Surface treatment, 369
Sylvania Electric Products Company, 323, 363, 387, 429

T

Taft, E., 174
Taylor, J. H., 389
Terman, F. E., 3
Test equipment, 264–300
  (*See also* quantity measured; component tested)
Thermal noise, in crystal rectifiers, 179–186
Thermal relaxation time, 254
Thermal resistance, of cat whisker, 243, 245
  of semiconductor, 243, 245
Theuerer, H. C., 9, 22, 304, 306, 307, 311, 326, 362, 364, 370, 372, 378
Torrey, H. C., 21, 163, 292, 392, 408, 413, 421
TR switch, 129
Treuting, R. C., 314, 326
Tucker, 303
Tuning, standard fixed, 270
Tunnel effect, 85, 87
Type B test set for measuring over-all performance of crystal second detectors, 386
Type C test set for measuring rectification efficiency of crystal second detectors, 388
Types of crystal rectifiers, 429–433

U

Uniform contact potential difference, 400
University of Pennsylvania (*see* Pennsylvania, University of)

V

Video crystal, 9
  figure of merit of, 344–347
  test equipment for production testing of, 352
Video-crystal holder, with single tuning adjustment for 1N30 rectifiers, 354
Video resistance, 333
  equipment for measurement of, 349–357
  methods of measurement of, 349–357
Voltage-breakdown hypothesis, in burnout, 240
von Hippel, A., 327
Vought, R. H., 341, 342, 347

W

Walerstein, I., 61
Waltz, M. C., 44, 229, 401, 403
Weiss, P. R., 182
Weisskopf, V. F., 58, 87, 179, 182, 186
Welded-contact germanium crystals, 21, 398–416
Welded-contact rectifiers, 11, 329
  applications of, 415
  construction of, 398–400
  general properties of, 400

Welded-contact rectifiers, as generator of millimeter radiation, 398
as harmonic generators, 398, 415
measurement of noise in, 403–406
noise figure of, 403–406
Welded contacts, 99, 254
Wesson, L. G., 327
Western Electric Company, 270, 318, 323
Westinghouse Research Laboratory, 203, 307, 315, 321
Whaley, R. M., 364, 368, 370, 377, 387
Whisker, cat, 316–323
fabrication of, 318–322
for low-level detectors, 359
mounting of, 321
Whisker materials, 316
Whisker point, forming of, 318–320
Whisker shape, 320
Whitmer, C. A., 35, 276
Wiesner, J. B., 237
Wilson, A. H., 45, 49, 77
Woodyard, J. R., 318, 396
Work functions, 51–53
fluctuations in, 86

Y

Y-factor, 31
as function of i-f impedance of crystal, 220
Yearian, H J., 83, 87, 89, 364, 370, 377, 378, 380, 381, 382, 384, 387

Z

Zener, C., 46